

# Journal of Engineering and Technology for Industrial Applications



**ISSN 2447-0228**

**August 2024**

**Volume 10 / No 48**

**Editor-in-Chief: J. C. Leite**

**[www.itegam-jetia.org](http://www.itegam-jetia.org)**



**ITEGAM - JETIA**

Journal of Engineering and Technology for Industrial Applications (JETIA)

ISSN 2447-0228 Online



O **ITEGAM-JETIA: Journal of Engineering and Technology for Industrial Applications** is a publication of the Galileo Institute of Technology and Education of the Amazon (ITEGAM), located in the city of Manaus since 2008. JETIA publishes original scientific articles covering all aspects of engineering. Our goal is the dissemination of research original, useful and relevant presenting new knowledge on theoretical or practical aspects of methodologies and methods used in engineering or leading to improvements in professional practice. All the conclusions presented in the articles It should be state-of-the-art and supported by current rigorous analysis and balanced assessment. Public magazine scientific and technological research articles, review articles and case studies.

**JETIA** will address topics from the following areas of knowledge: Mechanical Engineering, Civil Engineering, Materials and Mineralogy, Geosciences, Environment, Information and Decision Systems, Processes and Energy, Electrical and Automation, Mechatronics, Biotechnology and other Engineering related areas.

#### **Publication Information:**

**ITEGAM-JETIA** (ISSN 2447-0228), (online) is published by Galileo Institute of Technology and Education of the Amazon on a every two months (February, April, June, August, October and December).

#### **Contact information:**

Web page: [www.itegam-jetia.org](http://www.itegam-jetia.org)

Email: [editor@itegam-jetia.org](mailto:editor@itegam-jetia.org)

Galileo Institute of Technology and Education of the Amazon (ITEGAM).

Joaquim Nabuco Avenue, No. 1950. Center. Manaus, Amazonas. Brazil.

Zip Code: 69020-031. Phone: (92) 3584-6145.

#### **Copyright 2014. Galileo Institute of Technology and Education of the Amazon (ITEGAM)**

The total or partial reproduction of texts related to articles is allowed, only if the source is properly cited. The concepts and opinions expressed in the articles are the sole responsibility of the authors.

#### **Previous Notice**

All statements, methods, instructions and ideas are the sole responsibility of the authors and do not necessarily represent the view of ITEGAM -JETIA. The publisher is not responsible for any damage and / or damage to the use of the contents of this journal. The concepts and opinions expressed in the articles are the sole responsibility of the authors.

#### **Directory**

Members of the ITEGAM Editorial Center - Journal of Engineering and Technology for Industrial Applications (ITEGAM-JETIA) of the Galileo Institute of Technology and Education of the Amazon (ITEGAM). Manaus-Amazonas, Brazil.

**Jandecy Cabral Leite**, CEO and Editorial Editor-in-Chief

**Ivan Leandro Rodriguez Rico**, Editorial Assistant

**Alison Mendes de Brito**, Information Technology Assistant

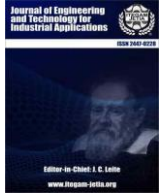
**SUMMARY**

<b><i>DIFFERENCES IN HEMATOXYLIN EOSIN (HE) STAINING RESULTS ON KIDNEY, SKIN AND COLON HISTOLOGY OF MICE (MUS MUSCULUS) BASED ON CUTTING THICKNESS OF 3 MM, 6 MM AND 9 MM</i></b>	<b>5</b>
<i>Eko Naning Sofyanita, Rihanesa Diana Putri, Tristania Shofi Nazhiifah, Utami Purnama Siwi</i>	
<b><i>COMBINING NEURAL AND SEMANTIC FEATURES IN THE ANALYSIS OF BEING SUPPORTIVE IN ONLINE FEEDBACK FROM CUSTOMERS</i></b>	<b>12</b>
<i>Selvi R, Athinarayanan S, Devi V, Gobinath M, Robinson Joel, Shanthakumar P</i>	
<b><i>REAL TIME EMOTION RECOGNITION AND CLASSIFICATION FOR DIVERSE SUGGESTIONS USING DEEP LEARNING</i></b>	<b>18</b>
<i>Sanika Anil Gonjari, Rachana Nandkumar Pawar, Ritika Ajay Pawar, Sharwari Hemant Kshirsagar, Rohini Kokare</i>	
<b><i>SENTIMENT ANALYSIS OF FINANCIAL NEWS USING THE BERT MODEL</i></b>	<b>25</b>
<i>Najeem Olawale Adelayun, Adebisi Abimbola Baale</i>	
<b><i>STATE FUNCTION <math>\Phi (U, E, T)</math>: CONNECTION OF ADVECTION, DISPERSION AND TURBULENCE IN NATURAL STREAMS AT DYNAMIC EQUILIBRIUM</i></b>	<b>32</b>
<i>Julian Daniel Ramos, Alfredo Jose Constain Aragon</i>	
<b><i>APPLICATION OF MACHINE LEARNING FOR THE PREDICTION OF ATMOSPHERIC CORROSION IN THE METROPOLITAN AREA OF MEXICO CITY</i></b>	<b>40</b>
<i>Ernesto Bolaños Rodríguez, Juan Islas, Omar López Ortega, Evangelina Lezama León</i>	
<b><i>METHODOLOGY FOR TARGET FORECASTING OF WATER LEVEL IN HYDROELECTRIC PLANT RESERVOIRS UNDER CONDITIONS OF LOW INFLOW</i></b>	<b>47</b>
<i>César Aristóteles Yajure</i>	
<b><i>SULFURE DIOXIDE EXPERIMENTAL ASSESSMENT OF SULFURE DIOXIDE REMOVAL FROM GAS STREAM FOR INTENSIVE ALGAE CULTURE</i></b>	<b>53</b>
<i>Liset Roche Delgado, Mayra Caridad Morales Perez, Rosa Amalia González Rivero, Arianna Álvarez Cruz, Agustín Andrés García Rodríguez, Juan Pedro Hernández Touse</i>	
<b><i>BROKEN MAGNETS FAULT DETECTION IN PMSM USING A CONVOLUTIONAL NEURAL NETWORK AND SVM</i></b>	<b>59</b>
<i>Benkaihou Said, Özüpak Yildirim, Ridha Djamel Mohammedi</i>	
<b><i>CROP RECOMMENDATION SYSTEM USING MACHINE LEARNING</i></b>	<b>67</b>
<i>Badri Narayan Mohapatra, vandana Kale</i>	
<b><i>DETECTION OF LUNG NODULES USING SUPPORT VECTOR MACHINE</i></b>	<b>73</b>
<i>Jhon Anthony Castro, Marlen Díaz, Rubén Morales</i>	
<b><i>GENERALIZATION OF DATA AUGMENTATION TO REDUCE THE NUMBER OF EPOCHS TO AVERAGE</i></b>	<b>79</b>
<i>Idileisy Torres Rodríguez, Beatriz Pérez, Diamir Rodríguez, Samuel Herrera, Alberto Crispí a</i>	
<b><i>EXPERIMENTAL STUDY OF A NEW HYDROCARBON MIXTURE FOR DOMESTIC RE-FRIGERATOR TO REPLACE R134A</i></b>	<b>84</b>
<i>Anjappa S B, parashurama s, Ramesha D K</i>	
<b><i>ANDROID APPLICATION FOR ACQUIRING IMAGES OF DIABETIC FOOT ULCERS</i></b>	<b>90</b>
<i>Yusely Gonzalez, Gustavo Benitez, Juan Ginori</i>	
<b><i>EFFECT OF NORMATIVE COMMITMENT ON ORGANIZATION PERFORMANCE AT SBC TANZANIA LIMITED (PEPSI) DAR ES SALAAM</i></b>	<b>96</b>
<i>Chacha Alfred Matoka</i>	



---

<i>AVEUGLE AIDERECHOCLOCATION BASED SYSTEM FOR BLINDS</i> <i>NEETHA K, Abirami K A, Andria Raju, Atulya G Nair, Amrutha P</i>	104
<i>AREA AND SPEED EFFICIENT FPGA DESIGN OF S-BOX AES-256 GALOIS FIELD APPROCH BASED ON LOGIC</i> <i>Janshi Lakshmi K</i>	109
<i>TRUST AWARE RECOMMENDATION USING DEEP MATRIX FACTORIZATION MODEL</i> <i>Pradip Mukundrao Paithane</i>	119
<i>QUANTUM MACHINE LEARNING: BRIDGING THE GAP BETWEEN CLASSICAL AND QUANTUM COMPUTING</i> <i>Dr. Krishna Mohan B.H., Padmaja Pulicherla, Purnachandrarao M., Nagamalleswararao P</i>	126
<i>AUTOMATIC LICENSE PLATE RECOGNITION SYSTEM</i> <i>Vishakha Hanumant Jagtap, Rohit Vikas Dhotre, Utkarsh Rajendra Khandare, Harshada Narayan Khuspe, Rohini Kokare</i>	133
<i>DESIGN AND DEVELOPMENT OF IOT-BASED AUTOMATED ATTENDANCE SYSTEM USING FACIAL RECOGNITION</i> <i>George Michael G. Makigod, Edwin R. Arboleda, Janwel Josh B. Sebastian, Luisa Ann Tamayo Ongquit</i>	139
<i>INVESTIGATING THE EFFECT OF TARTARIC ACID ON CONCRETE PRODUCED IN TROPICAL CLIMATES</i> <i>Dele Roger Simeon, Aliu Soyngbe</i>	148
<i>A NOVEL DESIGN EMPLOYING ARBITRARY TREE STRUCTURE FOR ADAPTIVE THRESHOLDING DISCRETE WAVELET PACKET TRANSFORMATION</i> <i>Jency Rubia J, Thangamari P, Srikanth A</i>	158
<i>A REVIEW QUESTIONS CLASSIFICATION BASED ON BLOOM TAXONOMY USING A DATA MINING APPROACH</i> <i>Sucipto Sucipto, Didik Dwi Prasetya, Triyanna Widiyaningtyas</i>	165
<i>EVALUATION OF DAM FOUNDATION GROUTABILITY USING SECONDARY PERMEABILITY INDEX AND ROCK QUALITY DESIGN (CASE STUDY IN JLANTAH DAM, INDONESIA)</i> <i>Dedi Saputra, Yusep M. Purwana, Galuh Chrismaningwang</i>	175
<i>ENVIRONMENTAL EFFECTS OF BIODIESEL ENGINES FUELLED BY WASTE COOKING OIL AND METAL NANO ADDITIVES</i> <i>Sekhar K Ch, Ramya Pakalapati, Balaji Mugada, Anusha Kalluri, Raviteja Surakasi, Iván Leandro Rodriguez Rico</i>	183
<i>SMART INTERSECTION AND IOT: PRIORITY DRIVEN APPROACH TO UBRAN MOBILITY</i> <i>Ayodeji Okubanjo, bashir olufemi odufuwa, Benjamin Olabisi Akinloye, Ignatius Okakwu Ignatius</i>	188
<i>IOT-BASED REAL TIME GREENHOUSE MONITORING AND CONTROLLING SYSTEM</i> <i>Yajie Liu, Md Gapar Md Johar, Asif Iqbal Hajamydeen</i>	194
<i>A BIBLIOMETRIC OF FINANCIAL TECHNOLOGY QR CODE AND QRIS RESEARCH</i> <i>Anisyah Vella, Wihandaru Sotya Pamungkas, Arni Surwanti</i>	201



## RESEARCH ARTICLE

## OPEN ACCESS

## DIFFERENCES IN *HEMATOXYLIN EOSIN* (HE) STAINING RESULTS ON KIDNEY, SKIN AND COLON HISTOLOGY OF MICE (*Mus musculus*) BASED ON CUTTING THICKNESS OF 3 $\mu\text{m}$ , 6 $\mu\text{m}$ and 9 $\mu\text{m}$

\*Eko Naning Sofyanita<sup>1</sup>, Rihanesa Diana Putri<sup>2</sup>, Tristania Shofi Nazhiifah<sup>3</sup> And Utami Purnama Siwi<sup>4</sup>

<sup>1,2,3,4</sup>Medical Laboratory Technology, Department of Health Analyst, Poltekkes Kemenkes Semarang, Indonesia.

<sup>1</sup><http://orcid.org/0000-0002-8355-5305>, <sup>2</sup><http://orcid.org/0009-0007-8176-5046>, <sup>3</sup><http://orcid.org/0009-0001-2247-9003>

<sup>4</sup><http://orcid.org/0009-0006-7179-0830>

Email: <sup>1</sup>[en.sofyanita@gmail.com](mailto:en.sofyanita@gmail.com), <sup>2</sup>[rihannesadianaputri@gmail.com](mailto:rihannesadianaputri@gmail.com), <sup>3</sup>[tristaniashofi@gmail.com](mailto:tristaniashofi@gmail.com), <sup>4</sup>[utamipurnamasiwi@gmail.com](mailto:utamipurnamasiwi@gmail.com)

## ARTICLE INFO

**Article History**

Received: September 12<sup>th</sup>, 2023

Revised: July 08<sup>th</sup>, 2024

Accepted: July 08<sup>th</sup>, 2024

Published: July 18<sup>th</sup>, 2024

**Keywords:**

Microtome,  
*Hematoxylin Eosin*,  
Staining,  
Thickness.

## ABSTRACT

Influencing factors absorption coloring *Hematoxylin Eosin* (HE) is one of them size thickness cutting network, cuts are not appropriate and on time coloring that is not appropriate causes the absorption process color No perfect so that moment observation microscopic view of the cell nucleus and cytoplasm seen more pale and faint . Research objectives This is For now difference results coloring *Hematoxylin Eosin* (HE) on histology kidneys , skin , and colon mice (*Mus musculus*) based on thickness piece 3  $\mu\text{m}$ , 6  $\mu\text{m}$ , and 9  $\mu\text{m}$  microtomes . Research methods This use method Experimental with nine groups treatment that is thickness cutting 3  $\mu\text{m}$  , 6  $\mu\text{m}$  and 9  $\mu\text{m}$  microtome, then preparation done HE staining and observed quality microscopic includes the cell nucleus, cytoplasm and uniformity color. Data collection uses primary data, reading field done with 400x magnification (40x objective). Data processing uses statistical tests Mann Whitney . The results of the *Mann Whitney* test show the preparation kidney ( $p < 0.05$ ) that there is difference in a way significant, preparation skin cuts of 3  $\mu\text{m}$  and 6  $\mu\text{m}$  ( $p > 0.05$ ) that No There is difference significant cuts of 6  $\mu\text{m}$  and 9  $\mu\text{m}$ , 3  $\mu\text{m}$  and 9  $\mu\text{m}$  ( $p < 0.05$ ) that there is difference in a way significant, colon preparation ( $p < 0.05$ ) that there is difference in a way significant. Conclusion of study This is in the kidneys cutting 3  $\mu\text{m}$  microtome results preparation with quality the best coloring compared to with cutting 6  $\mu\text{m}$  and 9  $\mu\text{m}$  microtome, on skin and colon organs cutting 6  $\mu\text{m}$  microtome results preparation with quality the best coloring compared to with cutting 3  $\mu\text{m}$  and 9  $\mu\text{m}$  microtome.



Copyright ©2024 by authors and Galileo Institute of Technology and Education of the Amazon (ITEGAM). This work is licensed under the Creative Commons Attribution International License (CC BY 4.0).

### I. INTRODUCTION

Histotechnics is a method or process of preparing organs, tissues or tissue parts through a series until they become preparations that are ready to be observed or analyzed. The process of making histological preparations has several stages, namely fixation , dehydration , clearing , embedding , blocking , sectioning , staining , mounting , and labeling [1],[2]. Cutting is one of the stages in microtechniques which is very important to produce good preparations. Cutting tissue with a microtome will produce results in the form of thin bands that are translucent to light so that thin slices can help in producing accurate diagnostic results [3].

Of the factors that influence the absorption of *Hematoxylin-eosin* staining is the thickness of the tissue cut. Improper cutting, such as a cut that is too thin and the staining time is not according to the procedure, will cause the color absorption process to be incomplete so that when microscopically observed the cytoplasm looks pale, faint and the boundaries between cells are blurred. Cutting too thick can cause the color intensity to increase, because it is caused by the effect of the optical density of eosin dye which is greater than *hematoxylin* [4],[5]. The absorption process in HE staining is based on an acid-base reaction where the acidic cell nucleus will attract substances that have basic properties which will be blue in color from *hematoxylin*, while eosin has acidic properties

which function to bind protein molecules with a positive charge in connective tissue and cytoplasm [6].

Previous research conducted by [7] stated that the thickness of the light microtome used could vary between 1-10 µm. Shield (2019) explains that the standard thickness of histological tissue sections is 6 µm, which shows good quality results [7],[8]. Explained that cutting histological tissue with a cutting thickness of 6 µm with HE staining showed good quality results with clear cell nuclei and cytoplasm and uniform color [8].

In this study, the organs that can be used to make tissue preparations are the kidneys, skin and colon. Researchers use mice in research because mice have a short life cycle, are easy to breed, and have an anatomical, genetic and physiological structure similar to humans. The criteria for mice that can be used as research objects are mice that are healthy, male, 1-3 months old and have a body weight of around 20-30 grams [9].

Researchers found gaps related to microtome settings for histological tissue cutting because the thickness used in each journal was still different. So the researchers wanted to find differences in HE staining results with microtome cutting thicknesses of 3 µm, 6 µm, 9 µm on histological preparations of the kidneys, skin and colons of mice.

## II. THEORETICAL REFERENCE

### II.1 SUBTITLE

Cutting (sectioning) is part of one of the stages that must be passed before *Hematoxylin Eosin* (HE) staining. The advantage of using a microtome as a tool for cutting biological samples is that it can cut into thin segments for microscopic examination, and is transparent. The disadvantage of a microtome is that if the thickness used is not correct, what will happen is diffusion and poor light penetration by the light microscope [7].

The tissue staining method that is often used routinely is a dye that can stain the nucleus and cytoplasm as well as connecting tissue, namely *Hematoxylin Eosin* (HE) staining. *Hematoxylin* works as a basic dye and *Eosin* works as an acid dye. One of the factors that influence the absorption of *Hematoxylin-eosin* staining is the thickness of the tissue cut. Improper cutting, such as a cut that is too thin and the staining time is not according to the procedure, will cause the color absorption process to be incomplete so that when microscopically observed the cytoplasm looks pale, faint and the boundaries between cells are blurred. Cutting too thick can cause the color intensity to increase, because it is caused by the effect of the optical density of eosin dye which is greater than *Hematoxylin* [4],[5]. The absorption process in HE staining is based on an acid-base reaction where the acidic cell nucleus will attract substances that have basic properties which will be blue in color from *hematoxylin*, while eosin has acidic properties which

function to bind protein molecules with a positive charge in connective tissue and cytoplasm [5],[6].

Previous research states that for light microscopes, the standard cutting used ranges from 1-10 µm [7]. According to [10], histological tissue cutting with a cutting thickness of 3-4 µm with HE staining showed good preparation quality results, the cell nuclei were visible blue, the cytoplasm with connective tissue appeared pink and the color uniformity of the preparations appeared uniform. For explained that cutting histological tissue with a cutting thickness of 6 µm with HE staining showed good quality results with clear cell nuclei and cytoplasm visible and uniform color [7],[8],[10].

## III. MATERIALS AND METHODS

This study analyzed the quality of the results of kidney, skin and colon preparations from mice that were stained with *Hematoxylin-eosin* based on a microtome cutting thickness of 3 µm, 6 µm and 9 µm. This type of research is experimental with a true experimental post test only control group design. The research was conducted from August 2022 to April 2023. This research was carried out at the Animal Testing Laboratory, Faculty of Medicine, Diponegoro University. This research population used kidney, skin and colon preparations from mice (*Mus musculus*) and the samples used were kidney, colon and skin preparations from mice (*Mus musculus*) involving 9 treatment groups, namely microtome cutting thickness of 3 µm, 6 µm and 9 µm. The number of sample preparations used was 15 preparations from kidney, skin and colon from mice determined using the Federer formula.

The tools used in this research were a microtome, glass jar, cutting board, scalpel, tweezers, pin, tissue cassette, base mold, pencil, label paper, ruler, surgical scissors, microtome knife, 1 set of painting containers, jar with lid, microscope, object glass, deck glass, water bath, stopwatch. The materials used in this research were kidney organs, skin and colons of mice, paraffin, xylol, graded alcohol (70%, 80%, 96%, 100%), distilled water, NaCl 0.9%, NBF 10%, chloroform, paper filter, cotton, *Hematoxylin Eosin* (HE) dye solution, immersion oil, entelan (Canadian balsam).

## IV. RESULTS AND DISCUSSIONS

### IV.1 RESULTS

This research uses samples kidney, skin, colon originating from experimental mice (*Mus musculus*), which were then dissected and continued with microtechnical stages until it became a ready-to-read preparation for further microscopic observation by the validator and author. Each reader assessed 5 visual fields in each preparation.

#### IV.1.1 Field of View Assessment Results Data

Table 1: Tabulation of Data from Field of View Assessment Results of Kidney, Skin and Colon Tissue Preparations from Mice (*Mus musculus*) Assessment criteria preparation kidney with a 3 µm cut getting an average total yield of 8.97%, a 6 µm.

Variable	Code	Preparations Preparation								
		Kidney			Skin			Colon		
		Average Score	Total Average	Quality Preparations	Average Score	Total Average	Quality Preparations	Average Score	Total Average	Quality Preparations
3µm cutting	3A	9	8.97%	GOOD	5.2	5.26%	NOT GOOD	7.2	7.02%	GOOD
	3B	9		GOOD	5		NOT GOOD	7		GOOD
	3C	8.8		GOOD	5.6		NOT GOOD	7.2		GOOD
	3D	9		GOOD	5.6		NOT GOOD	6.8		NOT BAD
	3E	9		GOOD	5.2		NOT GOOD	6.4		NOT BAD

	3F	9		GOOD	5,6		NOT GOOD	8		GOOD
	3G	9		GOOD	5.2		NOT GOOD	6.4		NOT BAD
	3H	9		GOOD	5		NOT GOOD	7		GOOD
	3I	9		GOOD	5		NOT GOOD	7.2		GOOD
6 μm cutting	6A	7.5	8.07%	GOOD	5	5.57%	NOT GOOD	8.8	8.73%	GOOD
	6B	7.5		GOOD	5		NOT GOOD	8.6		GOOD
	6C	8		GOOD	5,6		NOT GOOD	8,6		GOOD
	6D	8.2		GOOD	5		NOT GOOD	8,8		GOOD
	6E	8.1		GOOD	5,6		NOT GOOD	8,8		GOOD
	6F	8.7		GOOD	5,4		NOT GOOD	9		GOOD
	6G	8		GOOD	6		NOT GOOD	8,8		GOOD
	6H	8		GOOD	7		GOOD	8,8		GOOD
	6I	8.7		GOOD	5,6		NOT GOOD	8,4		GOOD
9 μm cutting	9A	4.9	4.65 %	NOT BAD	5	5.0%	NOT GOOD	5,6	5.22%	NOT BAD
	9B	4		NOT BAD	5		NOT GOOD	5		NOT BAD
	9C	4		NOT BAD	5		NOT GOOD	6,2		NOT BAD
	9D	4		NOT BAD	5		NOT GOOD	5,2		NOT BAD
	9E	5		NOT BAD	5		NOT GOOD	5		NOT BAD
	9F	5		NOT BAD	5		NOT GOOD	5		NOT BAD
	9G	5		NOT BAD	5		NOT GOOD	5		NOT BAD
	9H	5		NOT BAD	5		NOT GOOD	5		NOT BAD
	9I	5		NOT BAD	5		NOT GOOD	5		NOT BAD

Source: Authors, (2024).

cut getting an average total yield of 8.07% while a 9 μm cut gets an average total yield of 4.65%. Assessment criteria preparation skin with a 3 μm cut getting an average total yield of 5.26%, a 6 μm cut getting an average total yield of 5.57% while a 9 μm cut

gets an average total yield of 5.0%. Assessment criteria preparation colon with a 3 μm cut getting an average total yield of 7.02%, a 6 μm cut getting an average total yield of 8.73% while a 9 μm cut gets an average total yield of 5.22%.

#### IV.1.2 Group Data Differences in Quality of Preparations Cutting Preparations at 3 μm, 6 μm and 9 μm.

Table 2: Group Data on Differences in Quality of Preparations for 3 μm , 6 μm and 9 μm cutting preparation.

Organ	Variable	Score	Quality Preparations		
			3 μm	6 μm	9 μm
			n (%)	n (%)	n (%)
Kidney	Bad	1	0 (0%)	0 (0%)	0 (0%)
		2	0 (0%)	0 (0%)	0 (0%)
		3	0 (0%)	0 (0%)	0 (0%)
	Not Bad	4	0 (0%)	0 (0%)	4 (44.5%)
		5	0 (0%)	0 (0%)	5 (55.5%)
		6	0 (0%)	0 (0%)	0 (0%)
	Good	7	0 (0%)	2 (22.2%)	0 (0%)
		8	1 (11.1 %)	7 (77.8%)	0 (0%)
		9	8 (88.9 %)	0 (0%)	0 (0%)
<b>Total</b>			<b>9 (100%)</b>	<b>9(100%)</b>	<b>9 (100%)</b>
Skin	Bad	1	0 (0%)	0 (0%)	0 (0%)
		2	0 (0%)	0 (0%)	0 (0%)
		3	0 (0%)	0 (0%)	0 (0%)
	Not Bad	4	0 (0%)	0 (0%)	0 (0%)
		5	9 ( 10 0%)	7 (77.8 % )	9 ( 10 0%)
		6	0 (0%)	1 ( 11.1 %)	0 (0%)
	Good	7	0 (0%)	1 ( 11.1 %)	0 (0%)
		8	0 (0%)	0 (0%)	0 (0%)
		9	0 (0%)	0 (0%)	0 (0%)
<b>Total</b>			<b>9 (100%)</b>	<b>9(100%)</b>	<b>9 (100%)</b>
Colon	Bad	1	0 (0%)	0 (0%)	0 (0%)
		2	0 (0%)	0 (0%)	0 (0%)
		3	0 (0%)	0 (0%)	0 (0%)
	Not Bad	4	0 (0%)	0 (0%)	0 (0%)
		5	0 (0%)	0 (0%)	8 ( 88.9 %)
		6	3 ( 33.3 %)	0 (0%)	1 ( 11.1 %)
	Good	7	5 ( 55.5 %)	0 (0%)	0 (0%)
		8	1 ( 11.1 %)	8 ( 88.9 %)	0 (0%)
		9	0 (0%)	1 ( 11.1 %)	0 (0%)
<b>Total</b>			<b>9 (100%)</b>	<b>9(100%)</b>	<b>9 (100%)</b>

Source: Authors, (2024).

The quality of the kidney preparations in the 3 µm cutting group showed good quality with a score of 8 totaling 1 preparation (11.1%) and a score of 9 totaling 8 preparations (88.9 %). The quality results of the preparations from the 6 µm cutting group showed that the quality was good, with a score of 7 totaling 2 preparations (22.2%) and a score of 8 totaling 7 preparations (77.8%). The quality of the preparations for the 9 µm cutting group was found to be of poor quality with a score of 5 totaling 5 preparations (55.5%) and a poor quality score of 4 totaling 4 preparations (44.5%).

The quality of the skin preparations in the 3 µm cutting group was found to be of poor quality with a score of 9 totaling 9 preparations (100%). The results of the quality of the preparations for the 6 µm cutting group showed that the good quality score was 7 totaling 1 preparation (11.1 %) and the poor quality score 5 was 7 preparations (77.8 %) and the score 6 was 1 preparation (11.1%) . The quality of the preparations from the 9 µm cutting group was found to be of poor quality with a score of 5 totaling 9 preparations (100 %).

The quality of the colon preparations in the 3 µm cutting group was good quality with score 6 totaling 3 preparations (33.3%), score 7 totaling 5 preparations (55.5 %) and score 8 totaling 1 preparation (11.1%). The results of the quality of the preparations from the 6 µm cutting group showed good quality with a score of 8 totaling 8 preparations (88.9 %) and a score of 9 totaling 1 preparation (11.1 %). The quality of the preparations for the 9 µm cutting group was found to be of poor quality with a score of 5 totaling 8 preparations (88.9 %) and a poor quality score of 6 totaling 1 preparation (11.1 %).

**IV.2 Data Normality Test Using the Shapiro-Wilk Test.**

The data normality test uses the Shapiro-Wilk test because the variables are <50 and the following data is obtained:

Table 3: Data Normality Test Results.

Organ	Variable	Shapiro-Wilk
		Sig.
Kidney	3 µm cutoff	0,000
	6 µm cutoff	
	9 µm cutoff	
Skin	3 µm cutoff	0,000
	6 µm cutoff	
	9 µm cutoff	
Colon	3 µm cutoff	0,000
	6 µm cutoff	
	9 µm cutoff	

Source: Authors, (2024).

Shapiro-Wilk test on the three qualities of preparations for each organ obtained significant results for both p = 0.000, which means that all variables have an abnormal data distribution

Table 5: Differences in Hematoxylin Eosin Staining Results in Histology of Kidney, Skin and Colon Tissue Preparations from Mice (*Mus musculus*) Based on Cutting 3 µm, 6 µm and 9 µm.

Organ	Cutting 3 µm	Cutting 6 µm	Cutting 9 µm
-------	--------------	--------------	--------------

(p<0.05), so continue with and for comparing results between groups followed by Mann Whitney hypothesis testing.

**IV.2.1 Mann Whitney Non-Parametric Hypothesis Test.**

Mann Whitney non-parametric hypothesis test was used to determine whether there were significant differences between the two treatment groups with the following results:

Table 4: Man Whitney Hypothesis Test Results.

Organ	Variable	p	Sig.	
Kidney	3 µm	0.000	p<0.005	
	6 µm			
	3 µm	0.000	p<0.005	
	9 µm			
	Skin	6 µm	0.000	p<0.005
		9 µm		
3 µm		0.412	p>0.005	
6 µm				
Colon	3 µm	0.004	p<0.005	
	9 µm			
	6 µm	0.004	p<0.005	
	9 µm			
	Colon	3 µm	0.004	p<0.005
		6 µm		
3 µm		0.001	p<0.005	
9 µm				
6 µm		0.001	p<0.005	
9 µm				

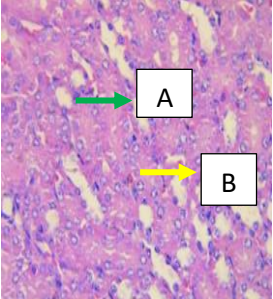
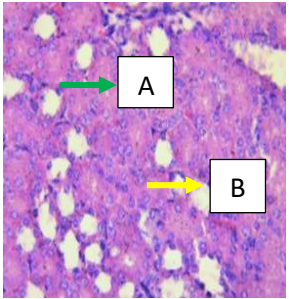
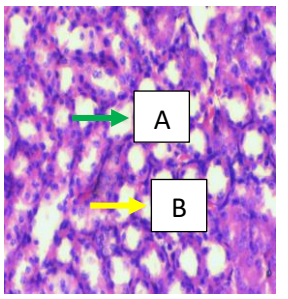
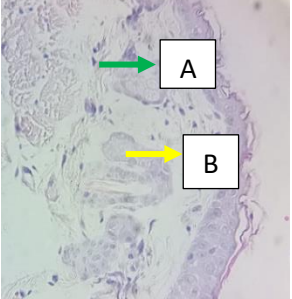
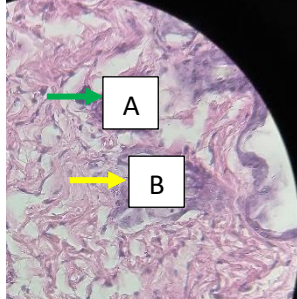
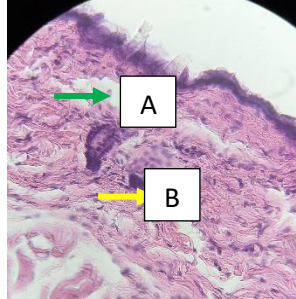
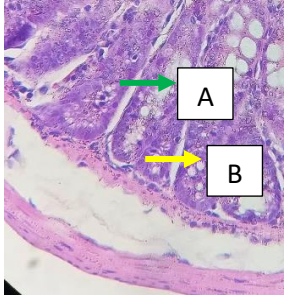
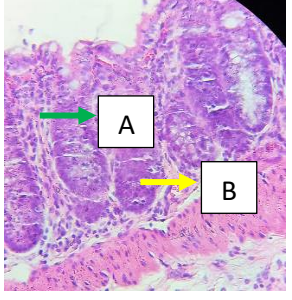
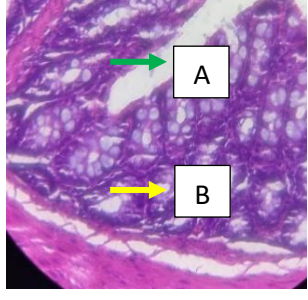
Source: Authors, (2024).

Mann Whitney statistical results on the kidney organs of mice in each group, namely microtome cutting at 3 µm and 6 µm, 6 µm and 9 µm, 3 µm and 9 µm results were obtained significant p<0.005 , then It can be interpreted that there is a significant difference in results between the groups staining the kidney preparations from mice (*Mus musculus*) .

Mann Whitney statistical results In the skin organs of mice in the 3 µm and 6 µm microtome cutting groups, significant results were obtained at p > 0.005 , so it could be interpreted that there was no significant difference. Cutting groups 6 µm and 9 µm, 3 µm and 9 µm results were obtained significant p <0.05 , so it can be interpreted that there is a significant difference in results between the groups staining the mouse (*Mus musculus*) skin preparations .

Mann Whitney statistical results on the colon organs of mice in each group, namely microtome cuts at 3 µm and 6 µm, 6 µm and 9 µm, 3 µm and 9 µm results were obtained significant p <0.00 5, it can be interpreted that there is a significant difference in results between the groups staining the mouse (*Mus musculus*) colon preparations.



Kidney	 <p>(A) Cell nucleus = clearly visible purplish blue color (B) Cytoplasm = clearly visible pink color</p>	 <p>(A) Cell nucleus = less clear purplish blue color (B) Cytoplasm = appears less clearly pink</p>	 <p>(A) Cell nucleus = less clear purplish blue color (B) Cytoplasm = appears less clearly pink</p>
Skin	 <p>(A) Cell nucleus = less clear purplish blue color (B) Cytoplasm = appears less clearly pink</p>	 <p>(A) Cell nucleus = clearly visible purplish blue color (B) Cytoplasm = appears clearly pink</p>	 <p>(A) Cell nucleus = less clear purplish blue color (B) Cytoplasm = appears less clearly pink</p>
Colon	 <p>(A) Cell nucleus = less clear purplish blue color (B) Cytoplasm = appears less clearly pink</p>	 <p>(A) Cell nucleus = clearly visible purplish blue color (B) Cytoplasm = appears clearly pink</p>	 <p>(A) Cell nucleus = appears unclear purplish blue color (B) Cytoplasm = appears unclear pink</p>

Source: Authors, (2024).

## V. DISCUSSIONS

The results obtained from tables 4.1 and 4.2 show that kidney preparations at 3  $\mu\text{m}$  cutting have good results compared to 6  $\mu\text{m}$  and 9  $\mu\text{m}$  cutting. This can be seen from the average value of the nucleus, cytoplasm and color uniformity of the 3  $\mu\text{m}$  cutting which obtained a higher value than the 6  $\mu\text{m}$  and 9  $\mu\text{m}$  cutting preparations. This is in accordance with research by Brilian (2021) explaining that kidney preparations were cut with a thickness of 3-5  $\mu\text{m}$  which showed good quality results, namely bright blue color in the cell nucleus, red (eosin) in the cytoplasm and uniform color on the preparations [11]. Meanwhile, in skin and colon preparations, cutting 6  $\mu\text{m}$  obtained better results compared to cutting 3  $\mu\text{m}$  and 9  $\mu\text{m}$ . This is in accordance with research conducted by Akyun, Fajariyah & Mahriani (2019), who conducted research on mouse (*Mus musculus*) skin tissue which was cut at 6  $\mu\text{m}$  resulting in observations of the histological picture of the skin with clearly visible nuclei and cytoplasm [12]. As well as research

by [13] that a cutting size of 6  $\mu\text{m}$  is the standard for cutting histological tissue which shows the maximum score on the microscopic quality of cell nuclei and cytoplasm.

Poor cutting results can be influenced by microtome calibration (lack of knife sharpness and consistency in cutting speed can cause artifacts in the tissue band) [14]. In addition, the temperature of the tissue block must be cool to make cutting easier. Microtome cuts that are too thick cause creases in the paraffin bands of the kidney, skin, colon due to heat from friction between the tissue block and the microtome blade when cuts are made more than once. As well as an embedding process that is not optimal (the tissue is not yet free from the clearing fluid), it will result in crystallization and make it easier for the tissue to tear [15].

Unfavorable results can also be caused by the *Hematoxylin Eosin* (HE) staining factor which acts as a basic dye [16]. Staining of tissue components occurs due to the acid-base reaction process. The acidic cell nucleus will attract alkaline substances, so the

nucleus will have a purplish blue color from *Hematoxylin*. While the alkaline cytoplasm will attract acidic substances, the cytoplasm will be pink from eosin [6].

In this study, the cell nucleus parameters in kidney preparations in the 3 µm microtome cutting group obtained the best results compared to 6 µm and 9 µm microtome cutting. The nuclei appear purplish blue at 3 µm microtome sectioning. Meanwhile, when cutting with a microtome at 6 µm and 9 µm, the cell nuclei were seen to be on top of each other, which was caused by poor absorption due to cutting that was too thick. This is in line with research conducted by [11] that cutting 3-5 µm produces good preparations with a percentage of 100% good cell nuclei. In skin and colon preparations, the cell nucleus parameters of 6 µm cuts obtained the best results compared to the 3 µm and 9 µm cuts groups. The visible nuclei appear purplish blue in color and do not overlap in the 6 µm cutting group. This is in line with research conducted by [12] that when cutting the skin on the backs of mice (*Mus musculus*), cuts of 6 µm of cell nuclei were clearly visible. Meanwhile, the cell nuclei in the 3 µm cut group looked faint or did not appear purplish blue and the 9 µm cut cell nuclei appeared stacked so that the purplish blue color was not visible. The intensity of staining of cell nuclei appeared to increase with greater section thickness [17].

In this study, the best results were obtained for cytoplasmic parameters in kidney preparations from the 3 µm microtome cutting group compared to 6 µm and 9 µm microtome cutting. The cytoplasm appeared clear and pink in the 3 µm microtome cutting group, whereas in the 6 µm and 9 µm microtome cutting groups the cytoplasm could not be clearly observed because the intercellular boundaries were less clear. This is in line with research conducted by [18] that cutting 3-4 µm produces good preparations with 100% cytoplasm and good cell nuclei. Meanwhile, the 6 µm cutting skin and colon preparations obtained the highest value compared to the 3 µm and 9 µm cutting groups. This is in line with research by [8] that the cytoplasm in the skin and colon of mice (*Mus musculus*) cutting 6 µm is clearly visible [8].

The color uniformity parameters in the 3 µm and 6 µm microtome cut kidney preparations obtained the best results because they had color uniformity with even color intensity throughout the field of view compared to the 9 µm cut group. According to [3], poor color uniformity can be caused by a lack of time at the deparaffinization stage to remove paraffin using xylol from the tissue, causing artifacts on the preparation and the presence of sediment in the reagent because before the coloring process was carried out, the paint was not filtered completely. Meanwhile, skin and colon preparations cut at 3 µm, 6 µm and 9 µm obtained good average results. This is in line with research by Trianto, Ilmiawan, Pratiwi & Suprianto (2019), that preparations that have good color uniformity show even color intensity throughout the field of view. Color uniformity is influenced by the tissue fixation process, so that adequate fixation will produce an even color throughout the field of view, and is influenced by the cleanliness of the water in the water bath so that it does not cause artifacts in the tissue bands [19].

The results of all visual field scores were then tested for normality of the data, based on table 4.3, the results showed that the data (p=0.000) was not normally distributed. If the data distribution is not normal, it is continued with a non-parametric statistical test, namely the Man Whitney test, to compare the results between the 2 cutting groups.

Table 4 shows that the results of the Man Whitney test with kidney preparations obtained a significant p = 0.000 (p<0.05), meaning that there was a difference in the results of the staining

quality of mice kidney preparations (*Mus musculus*) between the 2 treatment groups (3 µm and 6 µm, 3 µm and 9 µm, 6 µm and 9 µm). In this study it can be said that there are differences in the results of *Hematoxylin Eosin* (HE) staining on mouse kidney histology based on microtome thicknesses of 3 µm, 6 µm, and 9 µm with the best size found at 3 µm cuts.

The results of the Man Whitney test with skin preparations obtained a significance value for the 3 µm and 6 µm cutting groups, namely 0.412 (p>0.05), which statistically means there is no significant difference in results. In the 6 µm and 9 µm, 3 µm and 9 µm cutting groups, a significance value of 0.004 (p<0.05) was obtained, which can be interpreted as a significant difference in results between these groups. In this study, it can be said that in the histology of mouse skin, *Hematoxylin Eosin* (HE) staining was based on microtome thicknesses of 3 µm, 6 µm, and 9 µm with the best size found at 6 µm cuts.

The results of the Man Whitney test with colon preparations obtained a significance value for the 3 µm and 6 µm cutting groups, namely 0.000 (p<0.05), which statistically means there is a significant difference in results. In the 6 µm and 9 µm, 3 µm and 9 µm cutting groups, a significance value of 0.004 (p<0.05) was obtained, which can be interpreted as a significant difference in results between these groups. In this study it can be said that there are differences in the results of *Hematoxylin Eosin* (HE) staining on the histology of mouse colons based on microtome thicknesses of 3 µm, 6 µm, and 9 µm with the best size being found at 6 µm

## V. CONCLUSIONS

The conclusion of this research is that the quality of staining of cell nuclei, cytoplasm and color uniformity of kidney preparations *Hematoxylin Eosin* (HE) staining based on microtome cutting thicknesses of 3 µm, 6 µm and 9 µm is the best at 3 µm cutting, skin and colon preparations are the best at 6 µm cutting.

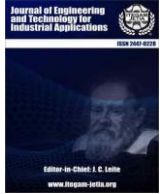
## VI. AUTHOR'S CONTRIBUTION

**Conceptualization:** Eko Naning, Rihanesa, Tristania. Utami.  
**Methodology:** Eko Naning, Rihanesa, Tristania.  
**Investigation:** Eko Naning, Rihanesa, Tristania.  
**Discussion of results:** Eko Naning, Rihanesa, Tristania. Utami.  
**Writing – Original Draft:** Eko Naning, Rihanesa, Tristania. Utami.  
**Writing – Review and Editing:** Eko Naning, Rihanesa, Tristania. Utami.  
**Resources:** Tristania. Utami.  
**Supervision:** Eko Naning, Rihanesa  
**Approval of the final text:** Eko Naning, Rihanesa, Tristania. Utami.

## VII. REFERENCES

- [1] Sumanto, D. (2017). Learning Cytohistotechnology for Beginners . Semarang Indonesian Health Analysts Association (IAKIS).
- [2] Sofyanita, Eko Naning, and Anna Sufi Annisa. "Pengaruh Penggunaan Minyak Zaitun Dengan Pemanasan Sebagai Larutan Penjernih (Clearing) Terhadap Kualitas Sediaan Jaringan Hepar Mencit (*Mus musculus*)."  
Jurnal Labora Medika 7.1 (2023): 6-12.
- [3] Pratiwi, HC, & Manan, A. (2015). Basic Histology Techniques in Gourami Fish (*Osphronemus gourami*). Scientific Journal of Fisheries and Marine Affairs, 7 (2).
- [4] Chlipala, E., Bendzinski, C. M., Chu, K., Johnson, J. I., Brous, M., Copeland, K., & Bolon, B. (2020). Optical density-based image analysis method for the evaluation of hematoxylin and eosin staining precision. Journal of Histotechnology , 43 (1), 29–37. <https://doi.org/10.1080/01478885.2019.1708611>

- [5] Suprianto, A. (2014). Comparison of the Effects of Formalin Fixation with the Intravital Method and Conventional Methods on the Quality of Histological Images of Rat Livers.
- [6] Halim, R. (2018). Vinegar Acid as a Deparaffinizing Agent in Hematoxylin Eosin (HE) Staining. Muhammadiyah University of Semarang.
- [7] Muhammad, F., Arishiya, T., & Mohamed., S. (2012). MICROTOME AND MICROTOME KNIFE – OVERVIEW AND PROPOSED CLASSIFICATION . Vol.19
- [8] Stewart, E., Ajao, M.S., & Ihunwo, AO (2013). Histology and ultrastructure of transitional changes in skin morphology in the juvenile and adult four-striped mouse (*Rhabdomys pumilio*). *The Scientific World Journal* , 2013 . <https://doi.org/10.1155/2013/259680>
- [9] Yusuf, M., Al-Gizar, MR, A, YY, Rorrong, Deny Romadhon Badaring, Hajar Aswanti, SMA, MZ, Nurazizah, Aulia Dzalsabila, Mutmainnah Ahyar, WW, & Mentari Jelita Putri, WFA (2022). Experimental animal management and management techniques . Department of Biology, FMIPA UNM, UNM Parangtambung Campus, Jalan Malengkeri Raya MAKASSAR.
- [10] Ariyadi, T., & Suryono, H. (2017). Quality of Skin Tissue Preparations Using Microwave Methods and Conventional Histoprocessing Hematoxylin Eosin Staining. *Journal of Labora Medika*, 1(1).
- [11] Brilliant, TV (2021). Microscopic Profile of Mice (*Mus Musculus*) Kidney Tissue Fixed with 10% Honey Concentration for 24 Hours Microscopic Profile of Mice (*Mus Musculus*) Kidney Tissue Fixed with 10% Honey Concentration for 24 Hours TASYA VITA BRILIAN Cancer Hospital . 03 (02), 127–133.
- [12] Akyun, I. K., Fajariyah, S., & Mahriani, M. (2019). Effects of black soybean ethanol extract (Glycine soja) on post-unilateral thickness of the dermis of mice (*Mus musculus L.*). ovariectomy. *Udayana Biology Journal*, 23(2). <https://doi.org/10.24843/jbiounud.2019.v23.i02.p05>
- [13] Shields, V. D., & Heinbockel, T. (2019). Introductory Chapter: Histological Microtechniques. In *Histology* . <https://doi.org/10.5772/intechopen.82017>
- [14] Khristian, E., & Inderiati, D. (2017). Sitohostologi. In BPPSDMK
- [15] Alwi, M. A. (2016). Preliminary Histotechnical Study: 2 Weeks Fixation on Histological Features Rat Kidney, Liver and Pancreas Organs.
- [16] Sofyanita, E., Iswara, A., & Riadi, A. (2023). Angiogenesis stimulation in bacteria-infected acute wound healing with honey treatment in BALB/C mice. *ITEGAM-JETIA*, 9(42), 16-20. <https://doi.org/10.5935/jetia.v9i42.869>
- [17] Sofyanita, Eko Naning, and Arya Iswara. "Wound Closure Ratio in Streptozotocin-Induced Diabetic Mice Treated by Passive and Interactive Dressing (Pilot Study)." *Jaringan Laboratorium Medis* 3.2 (2021): 67-71.
- [18] Herawati, A. (2022). Microscopic Histological Image of Mice (*Mus musculus*) Kidneys Fixed Using 10%, 20% and 30% Honey .
- [19] Trianto, HF, In'am Ilimiawan, M., Pratiwi, SE, & Suprianto, A. (2015). Comparison of the Quality of Histological Staining of Testicular and Liver Tissue Using Intravital and Conventional Methods of Formalin Fixation. In *Equatorial Health Journal* (Vol. 1, Issue 1).



### RESEARCH ARTICLE

### OPEN ACCESS

## COMBINING NEURAL AND SEMANTIC FEATURES IN THE ANALYSIS OF BEING SUPPORTIVE IN ONLINE FEEDBACK FROM CUSTOMERS

<sup>1</sup>Selvi R, <sup>2</sup>S. Athinarayanan, <sup>3</sup>V Devi, <sup>4</sup>M. Gobinath, <sup>5</sup>M. Robinson Joel\*, <sup>6</sup>P. Shanthakumar

<sup>1</sup> Department of Information Technology, Dr MGR Educational and Research Institute, Chennai

<sup>2</sup> Department of CSE, School of Computing, Vel Tech Rangarajan Dr. Sagunthala R&D Institute of Science and Technology, Avadi, Chennai 600062, Tamil Nadu, India.

<sup>3</sup> Department of Computer Science, Thiruthangal Nadar College, Chennai, India.

<sup>4</sup> Computer and Communication Engineering, Sri Manakula Vinayagar Engineering College, Madagadipet, Puducherry, India.

<sup>5</sup> Department of Information Technology, Kings Engineering College, Chennai, India,

<sup>6</sup> Department of CSE, Nehru Institute of Technology, Coimbatore, Tamil Nadu, India.

<sup>1</sup><http://orcid.org/0009-0003-2226-3768>, <sup>2</sup><http://orcid.org/0000-0001-5362-9847>, <sup>3</sup><http://orcid.org/0000-0003-3555-1040>, <sup>4</sup><http://orcid.org/0000-0001-9669-3283>, <sup>5</sup><http://orcid.org/0000-0002-3030-8431>, <sup>6</sup><http://orcid.org/0000-0002-0708-1785>

Email: \* <sup>1</sup>[rcelve@gmail.com](mailto:rcelve@gmail.com), <sup>2</sup>[aathithee@gmail.com](mailto:aathithee@gmail.com), <sup>3</sup>[ydevi78@yahoo.com](mailto:ydevi78@yahoo.com), <sup>4</sup>[gobinathmmecse06@gmail.com](mailto:gobinathmmecse06@gmail.com), <sup>5</sup>[joelnazareth@gmail.com](mailto:joelnazareth@gmail.com), <sup>6</sup>[santhan.mca@gmail.com](mailto:santhan.mca@gmail.com)

### ARTICLE INFO

#### Article History

Received: December 15<sup>th</sup>, 2023

Revised: July 09<sup>th</sup>, 2024

Accepted: July 08<sup>th</sup>, 2024

Published: July 18<sup>th</sup>, 2024

#### Keywords:

Text mining,

Logistic Regression classifier,

Support Vector Classifier,

AUC,

ROC.

### ABSTRACT

Over the past ten years, there has been a notable increase in the number of individuals accessing the internet. Positive evaluations serve as social evidence, convincing future purchasers of the product's quality and advantages. They can impact purchase decisions by offering real-world user information. Good reviews increase a product's or brand's trust and reputation. Customers are more inclined to buy from a firm that has received excellent feedback since it demonstrates dependability and contentment. Reviews can be considered user-generated content since they emphasise different applications, features, or advantages associated with a product. This material has the potential to persuade indecisive shoppers. The Yelp website was utilised to scrape feedback data for all Asian restaurants in New York City, which was then trained and assessed using three different models like Navie Bayes, next one is Logistic Regression, and then finally with Support Vector Classifiers. The Logistic Regression classifier outperformed the others by having the lowest proportion of mistakes and the highest Area under the ROC Curve noted as AUC on the receiver operating characteristic curve ROC curve. Commercial insights were gathered by recognising the existence of highly significant phrases while contrasting how they performed to the universal probabilities when the machine learning system was given review data from my restaurant.



Copyright ©2024 by authors and Galileo Institute of Technology and Education of the Amazon (ITEGAM). This work is licensed under the Creative Commons Attribution International License (CC BY 4.0).

## I. INTRODUCTION

Customer reviews are extremely important in the current consumer decision-making process. To make educated decisions, prospective purchasers frequently depend on the testimonials of former customers. Here are some crucial elements about product reviews from customers. Consumers often trust the viewpoints of their fellow consumers in addition to marketing communications. Authentic comments from real consumers can reveal insights that product descriptions or ads may not deliver. Influence on purchasing choices denotes that positive evaluations can have a

major impact on the choice of a consumer to buy a product. Negative reviews, on the other hand, may dissuade future purchasers. The number as well as the quality of recommendations can influence people's impressions of a product's dependability and efficacy.

Constructive feedback in reviews may provide manufacturers and merchants with important input. It enables them to discover the things consumers like and hate about a product, allowing them to make adjustments. Reviews can help a product's search engine optimisation (SEO) [1]. Products that have additional reviews, especially favourable ratings, are frequently

listed more frequently in search results. This might boost a product's visibility and attract additional prospective purchasers. Customers that provide reviews might develop a feeling of community. Reading about other people's encounters with a product might help users connect and share an understanding. Positive evaluations may be repurposed as marketing testimonials. They may be used to promote trust and credibility by including them on product websites, social media, and other promotional materials.

It is critical for potential purchasers to see a variety of viewpoints. A mixture of both favourable and adverse feedback enables customers to get a more balanced opinion about a product. It is also critical to consider how a firm responds to bad evaluations. Responses that are timely and intelligent reflect a commitment to client satisfaction and can help to reduce the effect of negative comments. The significance of reviews varies depending on the platform. Certain websites or platforms may have stricter review rules, resulting in more trust in the legitimacy of the reviews. When reading feedback from consumers, it's critical to assess the overall attitude, the reasons for favourable or negative comments, as well as the reviewers' specific tastes and expectations. This thorough approach enables prospective buyers to make better educated judgements that reflect their own requirements and preferences.

Text mining, additionally referred to as analytics of text, is the process of extracting meaningful knowledge and conclusions from large amounts of unstructured textual data. consumer reviews are a useful source of knowledge that may be mined for insights into consumer attitudes, preferences, and opinions using text mining algorithms. Compile a dataset of consumer reviews from a variety of sources, such as online evaluation sites, social news outlets, and feedback from consumers forms. Remove unnecessary letters, punctuation, and particular symbols from the text data. To guarantee uniformity, convert text to lowercase. Tokenize the text by separating it into distinct words or phrases. To focus on relevant material, remove stop words (a common practise words including "the," "and," and "is").

To depict the frequency of terms, attitudes, or subjects in the reviews, create visualisations such as term clouds, graphs with bars, or heatmaps. To present an easy-to-understand summary of the findings, use infographics or other visual tools. Analyse the data to learn about consumer attitudes, issues, and preferences. Recognise established patterns or patterns that can help you make business decisions. Based on consumer feedback, make ideas for improvement. Implement a method for tracking client feedback in real-time to remain on top of shifting attitudes and new concerns. In accordance with the insights gathered from continuing text mining, revise corporate plans or products/services. Text mining enables organisations to make data-driven choices, improve customer happiness, and improve products by leveraging the large quantity of unstructured written information accessible in user evaluations.

Voice extraction [2], additionally referred to as speech data analysis, is the process of analysing and extracting useful information from spoken words. This procedure may be performed to recordings of sound or conversations including customer evaluations. Compile audio recordings of client feedback from various sources, such as customer care calls, messages on the phone, or interviews conducted over the phone. Transcription is the process of converting spoken speech into written text. This phase

is critical for preparing the voice data for text-based analysis [3]. Cleanup and preparatory work the transcription text in the same way as you would in text mining. This involves deleting unnecessary letters, changing the text to smaller letters, representing, and eliminating stop words.

Sentiment Analysis: Using sentiment analysis, you may detect the emotion represented in the transcribed speech data. This can assist in determining whether the tone of the consumer is good, negative, or neutral. Use of voice recognition software to accurately turn spoken words into text. This is especially critical for comprehending the substance of customer reviews. Emotion Detection [4] examines the tone and pitch of the speech to detect emotional indicators such as anger, irritation, or satisfaction. Extraction of Characteristics is used to extract relevant text properties such as keywords, emotion ratings, or identifiable entities from the transcribed text. Visualisation of Data [5] allows to Create visual representations of the outcomes, such as emotion patterns over time or expression concentration in customer evaluations. Make use of visual tools to help decision-makers appreciate the findings.

## II. RELATED WORK

Prasad [6] proposed a system that make sure your voice is loud and easily understood. The flow is explained in the Figure 1. Pronounce brand names, characteristics, and specifics correctly. Infuse proper emotions and energy into your speech. Your tone may be cheery, authoritative, calming, or instructive, depending on the product. Maintain a steady pace that is neither too fast nor too sluggish. To emphasise crucial elements or qualities of the product, use intonation. Speak clearly and emphasise crucial parts of the product. Highlight distinct marketing features or major benefits.

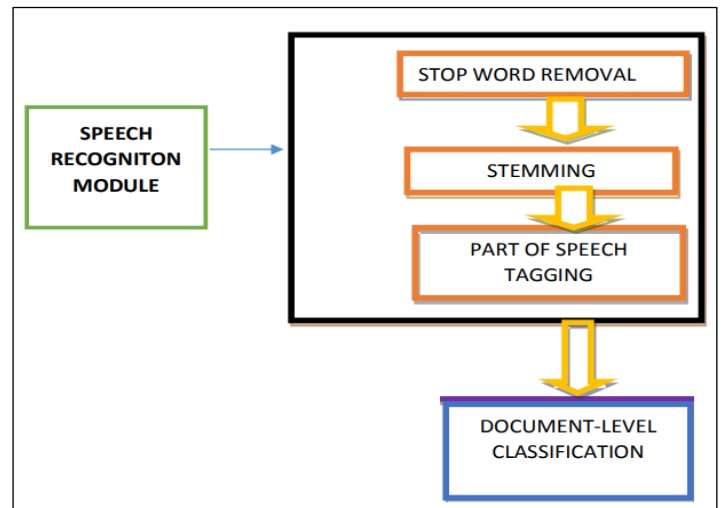


Figure 1: The proposed system of Speech Recognition. Source: [7].

Maintain a systematic and succinct evaluation. Introduce the product and discuss the product's characteristics, advantages, potential disadvantages, and overall impression. Make eye contact with your audience. Use a voice that is conversational and address any worries or queries your audience may have regarding the product. In this day and age, businesses must work hard not just to obtain new consumers [8], but also to keep present ones pleased. Mohammed [9] discovered in the hotel industry that seven aspects connected to consumer hotel experience are related to customer happiness. The airline industry [10] is likewise concerned with

consumer satisfaction studies. Sachin Kumar et al. contrast the aforementioned models in regards to consumer satisfaction forecasting using review data acquired from Twitter as well. For [7] intends to discover the intrinsic link between the customer happiness index and the network interaction by utilising the XGBoost machine learning technique to assist operators in predicting the level of satisfaction in order to improve customer contentment.

For [11] suggests utilising probability's encoder model to analyse and forecast rating from feedback from consumers that were left as open opinion. Opinion mining is a technique that uses classifier models to identify comments as good or negative based on an examination of consumer assessments of a hotel in open comments. According to [12] employs NLP, deep neural networks, and traditional machine learning approaches to obtain the best forecast model. To analyse the outcomes, two experiments are carried out: dichotomous and 3-class loyalty forecasting. The Random Forest and Nave Bayes algorithms beat the other examined classification techniques in the binary situation, with an accuracy of 89%. With a success rate of 67% in the three-class situation, the Random Forest segmentation approach outperformed every other machine learning methods.

According to [13] has developed predictive modelling for subjective assessments using data acquired by various internet sites. We also conducted an explanatory study of the various types of airline services. The research results of this article reveal that the majority of corporate class reviews focus on food as well as staff hospitality, whereas the majority of economy class reviews focus on spaciousness and seat convenience. Hamzah Zureigat [14] offered a research article named HelpPrd that provides an automated evaluation's usefulness prediction approach. To forecast the usefulness of reviews, HelpPrd employs data mining and artificial intelligence algorithms. The described method gathers characteristics from textual reviews and uses them to train 3 kindness classifiers. The experimental findings show that HelpPrd-logistic regression outperformed previous HelpPrd solutions in terms of reliability, accuracy, recollection, and F1-score.

According to [15] suggests a novel paradigm for eliciting consumer demands according to sentimental evaluation of particular product features in online product evaluations. The machines known as support vector machines are employed to create prediction models based on characteristics taken from a set of affective vocabulary lists based on words with English emotional norms and WordNet. For [16] employs the Neuro-Linguistic Programming method to quantify what consumers review, and then employs the neural network to anticipate the psychological tendency of feedback from clients by successfully analysing the nonlinear connection between influencing parameters. Customer reviews may aid in the management of an online shop by predicting emotional tendencies. The results of simulations suggest that our strategy can reach excellent prediction accuracy. The satisfaction forecast accuracy ratings for the three products are 91.95%, next one is 89.93%, and finally 90.96%, respectively.

### III. PROPOSED SYSTEM

The objective is to develop a predictive algorithm that can reliably predict a Yelp member's rating of a Asian Based restaurant based on the terms in their published review. We are particularly interested in the terms in these evaluations that are more likely to be in a good (4 or 5) as well as a negative (1, 2 or 3) review.

According to the website Yelp, there are around 531 Asian

Based restaurants in New York's five boroughs. This amounts to 83,349 Asian Based restaurant reviews that may be analysed. At a high level, this project aims to design a web scraper to obtain publicly accessible information through the Yelp domain and a model to estimate restaurant rating determined by the phrases in each review. All of the Yelp pages for Asian Based restaurants in New York City have been accessed and analysed. Each restaurant's meta data was utilised for comprehensive analysis of information and visualisation, as seen below in Figure 3. The flow chart of the data for sentimental analysis is shown in Figure 2.

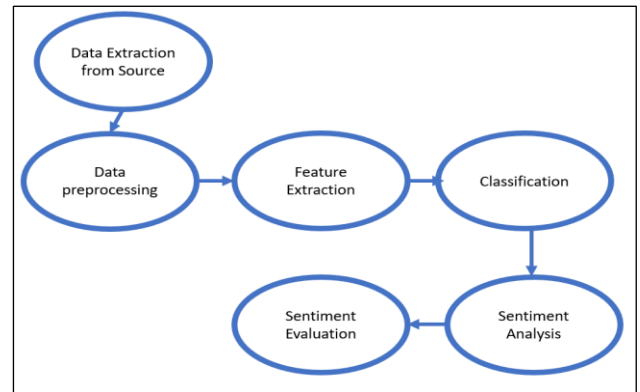


Figure 2: Sentiment analysis System block diagram. Source: Authors, (2024).

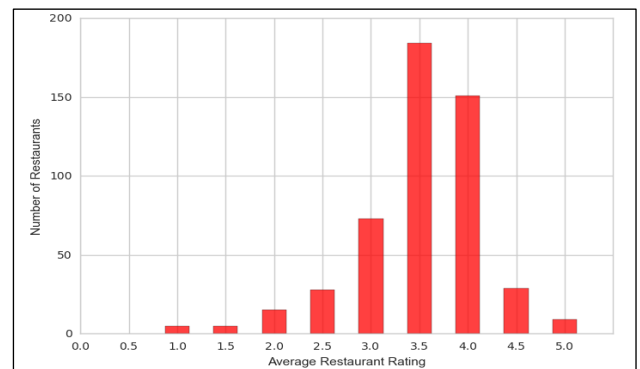


Figure 3: Average grade distribution among Asian Based restaurants in New York City. Source: Authors, (2024).

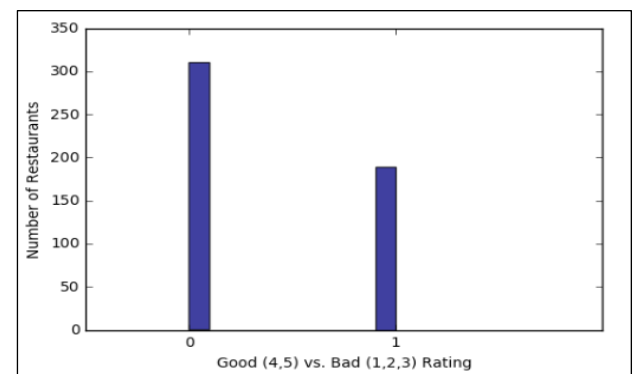


Figure 4: Average grade distribution among Asian Based restaurants in New York City. Source: Authors, (2024).

The typical Asian Based restaurant in New York City earned a 3.5, as shown in Figure 3 and Figure 4 and the score distribution was fairly evenly distributed with a little left skew. Most Asian Based restaurants ought to be expected to have above-average evaluations (or > 3.0) in order to compete in New York

City. Customers may choose from a wide range of establishments and ethnicities other than Asian Based food.

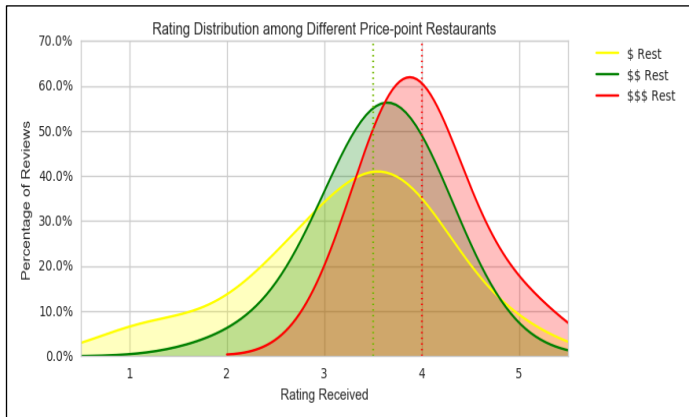


Figure 5: Rating Distribution among different Price-point restaurants.  
Source: Authors, (2024).

The vast majority of eateries charge between \$11 and \$30 per person as shown in Figure 5. Within the \$11-\$30 price range, the average restaurant received a rating of 3.5 or better. There was clearly more variation in the less than ten dollar sector since the dispersion of evaluations was the biggest. We observe that there are substantially less eateries in the \$31-\$60 range. However, all restaurants in this category received a rating of 3.5 or above. The median score for both the under \$10 and \$11-\$30 segments was 3.5 stars, whereas the median score for the \$31-\$60 section was 4.0 stars. Based on the analysis of the three categories, it is feasible to conclude that establishments that cost more are going to typically obtain better and more consistent evaluations.

Several techniques were used to clean and enhance the review data. To begin, each Yelp review was split down into distinct phrases, including spelling and grammar, using a technique known as tokenization. All punctuation was omitted, and every one of the words were rewritten in lower case. Then, an acronym filtering technique was used to eliminate stop phrases (or common terms like "an, or, the, it") and only leave significant descriptive words relevant to a restaurant. This procedure was followed for all 83,349 reviews. The evaluations were then translated into a container of words participation, which implies that any unique words/uni-grams (for example, "delicious") and pair of terms/bi-grams (for example, "simply delicious") that occurred in the 83,349 reviews were shown. The final vocabulary includes around 71,510 distinct characteristics.

Each generated feature was checked for appearance in each unique review. If a certain feature (or term) occurred in a review, it would be expressed as a 1, and 0 if it did not. This criterion was made applicable to all 83,349 evaluations, each of which had 71,510 words that needed to be checked. Furthermore, the frequency with which terms appeared was computed to determine each word's significance to the research. The greater the number of times a term occurred, the more valuable it was in forecasting Asian Based customer mood in general.

To identify and forecast the rating of review data, three Machine Learning Techniques were used: Nave Bayes, Logistic regression, and Support Vector Classification. The Nave Bayes classifier has been selected since it is one among the easiest and most successful text classification techniques. It is computationally cheap, quick to train, and frequently outperforms more difficult and inefficient approaches. Because of its capacity to provide weights to elements for binary classification, Logistic Regression was

selected. Along with to being successful, it is also extremely simple to construct, computationally cheap, and the information representation is pretty simple to read.

Table\_1: Naïve Bayes.

	Precision	Recall	F1 Score	Support
Bad Review	0.84	0.81	0.83	8761
Good Review	0.90	0.92	0.91	16244
Average/Total	0.88	0.88	0.88	25005

Source: Authors, (2024).

Table 2: Logistic Regression.

	Precision	Recall	F1 Score	Support
Bad Review	0.85	0.80	0.82	8713
Good Review	0.89	0.92	0.91	16292
Average/Total	0.88	0.88	0.88	25005

Source: Authors, (2024).

Table 3: Support Vector Classification.

	Precision	Recall	F1 Score	Support
Bad Review	0.89	0.74	0.81	8660
Good Review	0.88	0.95	0.91	16345
Average/Total	0.88	0.88	0.88	25005

Source: Authors, (2024).

Unexpectedly, with an average rating of 0.88 as shown in the table 1,2 and 3, all three classifiers fared roughly the same on the F1 metric. This meant that the harmonic mean of accuracy and recall should be successfully maximised, as acceptable results in both areas would be preferred than outstanding results on any particular metric.

Unexpectedly all three classifiers obtained a Precision-Recall AUC of 0.96, with just minor variances in ROC AUC. Logistic Regression had the greatest ROC AUC score of 0.94, although Nave Bayes as well as SVC had 0.01 lower at 0.93. This suggested that all classifiers did exceptionally well in terms of properly predicting, minimising mistakes, and recalling a considerable percentage of the dataset.

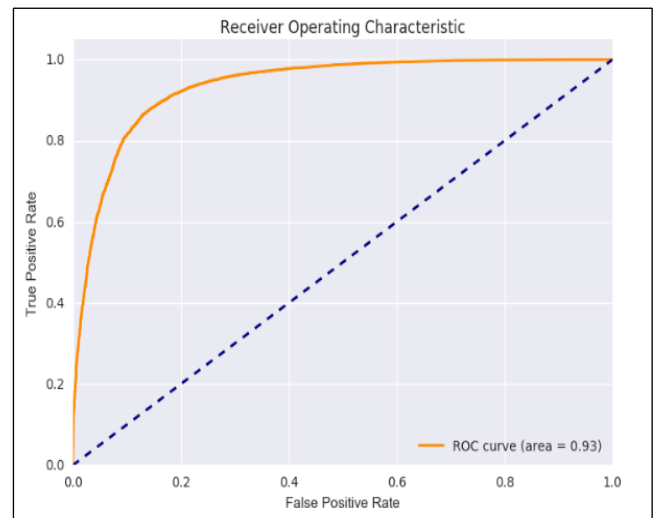


Figure 6: Receiver Operating Characteristic (ROC) curve for Naïve Bayes algorithm.  
Source: Authors, (2024).

The ROC curve illustrates the trade-off amongst responsiveness (True Positive Rate) and distinctiveness (True Negative Rate) at various thresholds. A bigger area beneath the curve (AUC) shows that the model is better at differentiating across classes. For varied threshold levels, the Precision-Recall curve depicts the balance that exists between precision and recall. A bigger area under the curve (AUC) implies that the model is doing better when it comes to of precision and recall as shown in Figure 7.

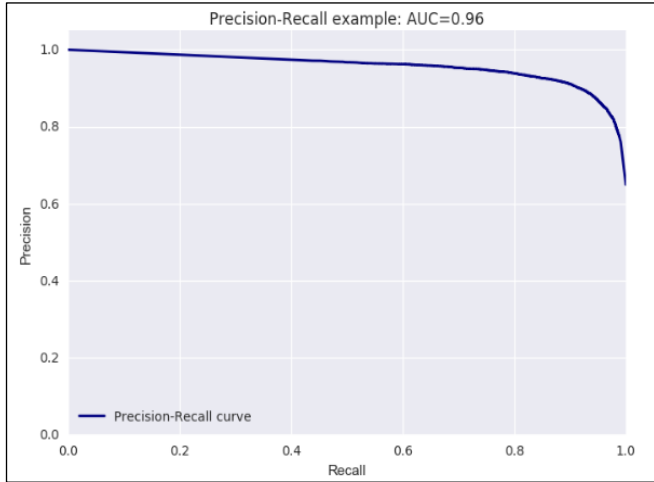


Figure 7: Precision-Recall example curve for Naïve Bayes algorithm.  
Source: Authors, (2024).

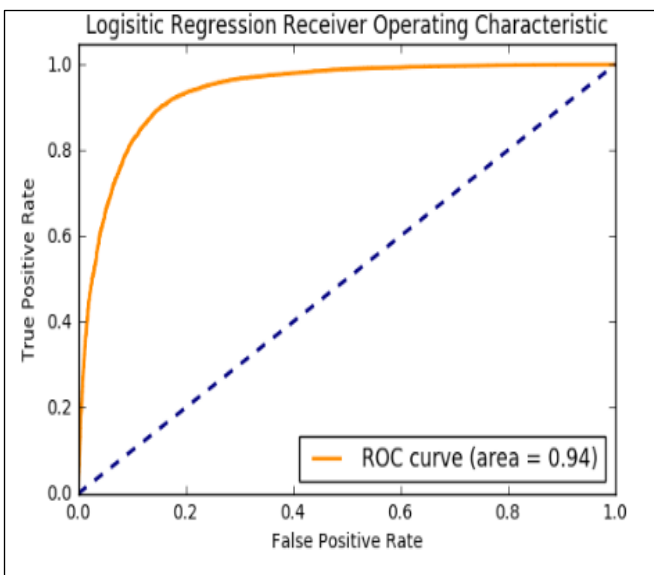


Figure 8: Receiver Operating Characteristic (ROC) curve for Logistic Regression.  
Source: Authors, (2024).

The ROC curve illustrates a classification model's performance over multiple thresholds by displaying the compromise amongst True Positive Rate along with False Positive Rate. A bigger area under the curve (AUC) shows that the model is better at differentiating across classes as shown in Figure 8. Precision-Recall charts can be helpful for assessing the effectiveness of a model for classification, for instance Logistic Regression, while dealing with unbalanced datasets shown in Figure 9.

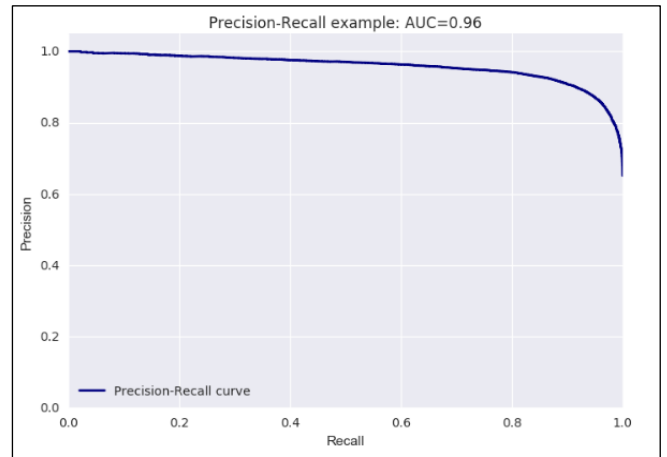


Figure 9: Precision-Recall example curve for Logistic Regression.  
Source: Authors, (2024).

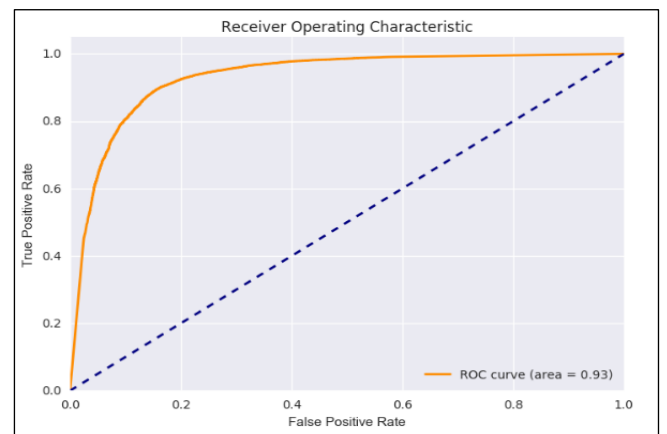


Figure 10: Receiver Operating Characteristic (ROC) curve for Support Vector Classification.  
Source: Authors, (2024).

The Receiver Operating Characteristic (ROC) graph is a visual representation of a binary classifier system's diagnostic capabilities as its discrimination threshold is adjusted. While Support Vector Classification (SVC) is an effective technique for classification problems, there are several stages involved in constructing a ROC curve for an SVC model. Begin by running your Support Vector Classification simulation through its paces on your dataset. The FPR False Positive Rate (FPR) and should be plotted on the x-axis, and the TPR True Positive Rate (TPR) should be shown on the y-axis. This will provide the ROC curve as shown in Figure 10.

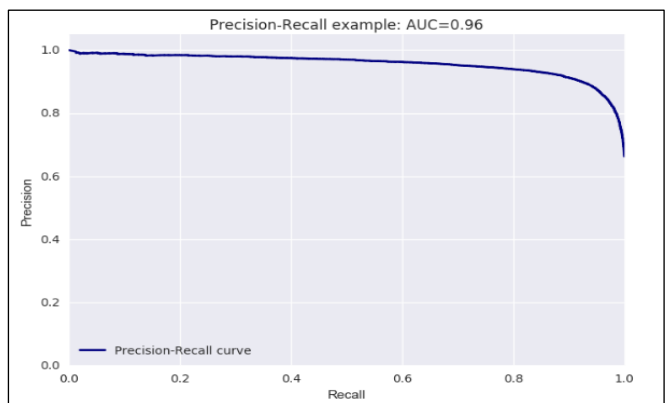


Figure 11: Precision-Recall example curve for Support Vector Classification.  
Source: Authors, (2024).



Considering the F1 score along with precision-recall effectiveness of all three classification algorithms as shown in Figure 11 were so identical, the confusion matrix along with ROC curve were the only performance differentiators. When these remaining metrics were considered, the Logistic Regression classifier performed the best. Logistic Regression predicted fewer errors than both Nave Bayes and SVC, as determined by the confusion matrix. Furthermore, Logistic Regression had the greatest ROC AUC with a score of 0.94, compared to 0.93 for the other classifiers. Therefore, the classifier used when assessing our Asian Based restaurant had been the one that was developed using Logistic Regression.

#### IV. CONCLUSION

The Yelp website was used to scrape the feedback information for all Asian Based restaurants in New York City, which was then trained and evaluated using three distinct models: Nave Bayes, Logistic Regression, and Support Vector Classifiers. According to the lowest percentage of errors and the highest AUC on the ROC curve, the Logistic Regression classifier performed the best. When the machine learning algorithm was given review data from the restaurant, commercial insights were collected by detecting the existence of extremely significant terms and comparing their performance to the universal probability. Extracted business insights assist the company in identifying areas of uniqueness and weaknesses in the form of food, beverages, or services. These insights may be used to help with commercial and investment choices, as well as to improve the overall experience and cuisine of restaurant.

#### V. AUTHOR'S CONTRIBUTION

**Conceptualization:** Selvi R, S. Athinarayanan, V Devi, M. Gobinath, M. Robinson Joel, P. Shanthakumar.

**Investigation:** Selvi R, S. Athinarayanan, V Devi, M. Gobinath, M. Robinson Joel, P. Shanthakumar.

**Discussion of results:** Selvi R, S. Athinarayanan, V Devi, M. Gobinath, M. Robinson Joel, P. Shanthakumar.

**Writing –Original Draft:** Selvi R, S. Athinarayanan, V Devi, M. Gobinath, M. Robinson Joel, P. Shanthakumar.

**Writing –Review and Editing:** Selvi R, S. Athinarayanan, V Devi, M. Gobinath, M. Robinson Joel, P. Shanthakumar.

**Resources:** Selvi R, S. Athinarayanan, V Devi, M. Gobinath, M. Robinson Joel, P. Shanthakumar.

**Supervision:** Selvi R, S. Athinarayanan, V Devi, M. Gobinath, M. Robinson Joel, P. Shanthakumar.

**Approval of the final text:** Selvi R, S. Athinarayanan, V Devi, M. Gobinath, M. Robinson Joel, P. Shanthakumar.

#### VI. REFERENCES

[1] Ron Berman, Zsolt Katona, (2013) The Role of Search Engine Optimization in Search Marketing. *Marketing Science* 32(4):644-651. <https://doi.org/10.1287/mksc.2013.0783>

[2] M. Benzeguiba, Renato de Mori, O. Deroo, S. Dupon, T. Erbes, et al.. Automatic Speech Recognition and Speech Variability: a Review. *Speech Communication*, Elsevier: North-Holland, 2007, 49 (10-11), pp.763. [f10.1016/j.specom.2007.02.006](https://doi.org/10.1016/j.specom.2007.02.006). [Ffhal-00499180f](https://doi.org/10.1016/j.specom.2007.02.006)

[3] M. A. Mahima, N. C. Patel, S. Ravichandran, N. Aishwarya and S. Maradithaya, "A Text-Based Hybrid Approach for Multiple Emotion Detection Using Contextual and Semantic Analysis," *2021 International Conference on Innovative Computing, Intelligent Communication and Smart Electrical Systems (ICSES)*, Chennai, India, 2021, pp. 1-6, doi: 10.1109/ICSES52305.2021.9633843.

[4] Medaramitta, Raveendra, "Evaluating the Performance of Using Speaker Diarization for Speech Separation of In-Person Role-Play Dialogues" (2021). Browse all Theses and Dissertations. 2517. [https://corescholar.libraries.wright.edu/etd\\_all/2517](https://corescholar.libraries.wright.edu/etd_all/2517)

[5] X. Li, A. Kuroda, H. Matsuzaki and N. Nakajima, "Advanced aggregate computation for large data visualization," *2015 IEEE 5th Symposium on Large Data Analysis and Visualization (LDAV)*, Chicago, IL, USA, 2015, pp. 137-138, doi: 10.1109/LDAV.2015.7348086.

[8] C. P. Johny and P. P. MaAsian Based, "Customer churn prediction: A survey", *International Journal of Advanced Research in Computer Science*, vol. 8, no. 5, 2017.

[9] M. I. El-Adly, "Modelling the relationship between hotel perceived value customer satisfaction and customer loyalty", *Journal of Retailing and Consumer Services*, vol. 50, pp. 322-332, 2019.

[10] S. Kumar and M. Zymbler, "A machine learning approach to analyze customer satisfaction from airline tweets", *Journal of Big Data*, vol. 6, no. 1, pp. 1-16, 2019.

[7] H. Gou, L. Su, G. Zhang, W. Huang, Y. Rao and Y. Yang, "A XGBoost Method Based on Telecom Customer Satisfaction Enhancement Strategy," *2022 5th International Conference on Pattern Recognition and Artificial Intelligence (PRAI)*, Chengdu, China, 2022, pp. 209-213, doi: 10.1109/PRAI55851.2022.9904203.

[11] W. Songpan, "The analysis and prediction of customer review rating using opinion mining," *2017 IEEE 15th International Conference on Software Engineering Research, Management and Applications (SERA)*, London, UK, 2017, pp. 71-77, doi: 10.1109/SERA.2017.7965709.

[12] F. Noorbehbahani, S. Bajoghli and H. H. Esfahani, "Customer Loyalty Prediction of E-marketplaces Via Review Analysis," *2023 9th International Conference on Web Research (ICWR)*, Tehran, Iran, Islamic Republic of, 2023, pp. 311-316, doi: 10.1109/ICWR57742.2023.10139037.

[13] P. K. Jain, R. Pamula, S. Ansari, D. Sharma and L. Maddala, "Airline recommendation prediction using customer generated feedback data," *2019 4th International Conference on Information Systems and Computer Networks (ISCON)*, Mathura, India, 2019, pp. 376-379, doi: 10.1109/ISCON47742.2019.9036251.

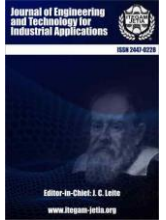
[14] H. Zureigat, O. Al-Qudah and B. Alhijawi, "Predicting the Helpfulness of Online Customer Reviews," *2023 International Conference on Information Technology (ICIT)*, Amman, Jordan, 2023, pp. 686-689, doi: 10.1109/ICIT58056.2023.10225838.

[15] F. Zhou and R. J. Jiao, "Latent customer needs elicitation for big-data analysis of online product reviews," *2015 IEEE International Conference on Industrial Engineering and Engineering Management (IEEM)*, Singapore, 2015, pp. 1850-1854, doi: 10.1109/IEEM.2015.7385968.

[16] Q. Zhang, R. Shi and H. Tang, "Analysis Model of Customer Reviews Based on Neural Network," *2020 IEEE 3rd International Conference on Information Systems and Computer Aided Education (ICISCAE)*, Dalian, China, 2020, pp. 514-518, doi: 10.1109/ICISCAE51034.2020.9236809.



ISSN ONLINE: 2447-0228



### RESEARCH ARTICLE

### OPEN ACCESS

## REAL-TIME EMOTION RECOGNITION AND CLASSIFICATION FOR DIVERSE SUGGESTIONS USING DEEP LEARNING - A COMPREHENSIVE SURVEY

\*Sanika A. Gonjari<sup>1</sup>, Rachana N. Pawar<sup>2</sup>, Ritika A. Pawar<sup>3</sup>, Sharwari H. Kshirsagar<sup>4</sup>, Rohini B. Kokare<sup>5</sup>

<sup>1,2,3,4</sup> Student, VPKBIET Baramati, Pune, Maharashtra, India.

<sup>5</sup> Assistant Professor, AIDS Department, VPKBIET Baramati, Pune, Maharashtra, India.

<sup>1</sup> <http://orcid.org/0009-0008-7467-4223> , <sup>2</sup> <http://orcid.org/0009-0005-7373-1255> , <sup>3</sup> <http://orcid.org/0009-0007-9199-7705> 

<sup>4</sup> <http://orcid.org/0009-0003-0871-1587> , <sup>5</sup> <http://orcid.org/0009-0002-1633-1317> 

Email: \*[sanikagonjari2003@gmail.com](mailto:sanikagonjari2003@gmail.com)<sup>1</sup>, [rachananp09@gmail.com](mailto:rachananp09@gmail.com)<sup>2</sup>, [ritikap2003@gmail.com](mailto:ritikap2003@gmail.com)<sup>3</sup>, [kshirsagarsharwari02@gmail.com](mailto:kshirsagarsharwari02@gmail.com)<sup>4</sup>, [rohnikokare@gmail.com](mailto:rohnikokare@gmail.com)<sup>5</sup>.

### ARTICLE INFO

#### Article History

Received: December 26<sup>th</sup>, 2023

Revised: July 08<sup>th</sup>, 2024

Accepted: July 8<sup>th</sup>, 2024

Published: July 18<sup>th</sup>, 2024

#### Keywords:

Emotion Recognition,  
Diverse Suggestions,  
Deep CNN,  
Customized Recommendation,  
User Experience.

### ABSTRACT

At the captivating nexus of technology and human emotions, we harness cutting-edge software to discern individuals' feelings through their facial expressions. This unique capability empowers us to provide customized recommendations for various forms of entertainment and enrichment, such as movies, music, books, and meditation practices. For instance, if a user appears sad, we can offer upbeat music to brighten their mood. Our ultimate objective is to enhance technology comprehension of emotions, enabling it to suggest content that resonates with people's emotional states. Through this integration of facial expressions and diversified suggestions, here aim is to cultivate a more user-friendly and supportive digital environment, fostering feelings of happiness and calmness. Exploring the captivating domain of facial emotion recognition and recommendation systems is the central emphasis of this endeavor. The primary ambition is to construct a framework capable of deciphering user emotions from facial cues. By using deep learning techniques such as the CNN algorithm which can be applied to facial images to process emotion recognition feature vectors with the categorization of individualized content. It attempts to form a balanced blend of advanced tech and boost user engagement, nurturing emotional connections in the digital domain.



Copyright ©2024 by authors and Galileo Institute of Technology and Education of the Amazon (ITEGAM). This work is licensed under the Creative Commons Attribution International License (CC BY 4.0).

### I. INTRODUCTION

In recent years, significant improvements in computer vision and machine learning have been made to build systems capable of recognizing and comprehending human emotions from facial expressions in real time. Deep learning is a branch of machine learning that focuses on creating and training deep neural networks, which are artificial neural networks with several layers. These networks are made to automatically recognize and depict intricate patterns and nested characteristics in data. Deep learning algorithms, in contrast to conventional machine learning algorithms, can automatically find and extract pertinent characteristics from raw data, making them extremely successful

for a variety of tasks like speech and image recognition, natural language processing, and even gameplay.

Convolutional Neural Networks (CNNs), Convolutional Recurrent Neural Networks (CRNNs), Deep Convolutional Neural Networks (Deep CNNs), and Recommendation Techniques are some of the foundational technologies we examine in this survey study that are essential to contemporary research and applications. Deep CNNs expand the capabilities of CNNs in feature extraction, CRNNs combine the skills of CNNs and RNNs for sequential data processing, and CNNs excel at extracting complicated patterns from data. Techniques for recommendations improve user experience and system performance. This survey offers insights

into the relevance and potential of these technologies and their applications across a range of areas through an in-depth analysis of both.

The human experience is fundamentally shaped by emotions, which have an impact on how we interact, relate to one another, and communicate. The difficult task of facial expression recognition (FER) involves identifying facial expressions in pictures. Accurate classification is challenging because of expression variability and inter-subject variances. An innovative strategy is put out to combat this, combining identity and emotion data to improve FER. Identity and emotion data are extracted separately using deep neural networks, which are well-known for their success in face recognition [1].

A fast-expanding study area with a wide range of possible applications is real-time emotion recognition through facial expressions. The effects of this technology are wide-ranging and significant. The technique described in this study uses physiological cues like photoplethysmography (PPG) and the galvanic skin response (GSR) to classify music according to how it affects listeners' emotions [2]. Deep neural networks and regression models are used in this novel method to accurately classify music based on emotions without the usage of sensors, increasing music recommendation services for a more personally tailored user experience [2]. The COVID-19 epidemic has sped up the development of online learning, forcing universities and other organizations all around the world to switch to remote teaching methods [3]. However, there are special difficulties with evaluating the emotions and participation of students when learning online. Online environments frequently lack such involvement, in contrast to conventional in-person classes where teachers may monitor students' responses in real-time. The objective is to empower teachers and improve the overall online learning experience by utilizing lightweight facial recognition models, effective neural network architecture, and real-time video-based classification.[3] The cold-start problem and static user representations are drawbacks of conventional personalized recommendation techniques like collaborative filtering and content-based filtering

[4]. In the following sections, we will undertake a thorough examination of the diverse methodologies and technologies that have propelled the advancement of real-time facial emotion identification. Additionally, we will delve into the significant challenges that researchers face in their quest for precise and resilient emotion recognition in real-world situations. As we navigate through this captivating landscape, we will also shed light on intriguing possibilities for future research, where further progress in this field has the potential to revolutionize our interactions with technology and, ultimately, with each other. The proposed system delivers a user-friendly mobile application and shows improved sentiment analysis using an upgraded measure, eventually intending to improve users' emotional states and well-being [ 5].

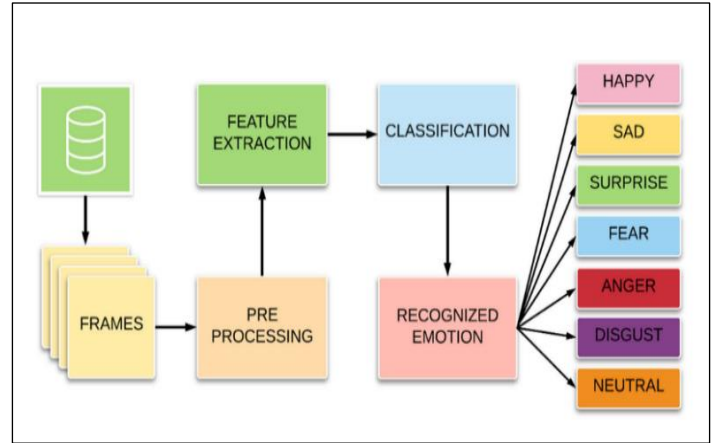


Figure1. Facial Emotion Classification Process.  
Source: [6].

## II. PLANNED ANALYSIS

### II.1 COMPARATIVE ANALYSIS OF THE PLANNED SURVEY

Table 1: Survey Table.

Sr No	Paper	Technique Used	Advantages	Gaps
1.	[3]	Multi-Task Convolutional Neural Networks	Real-time processing is faster with an accuracy of 66.34%.	1. Classified only 3 classes. 2. Low-resolution images not identified.
2.	[2]	Convolutional recurrent neural network, multilayer perceptron	Accuracy 96.26%.	1. RS-BF + RF attained the worst results. 2. More computation power.
3.	[1]	Deep CNN, deep learned Tandem Facial Expression	In comparison with CK+ and FER+, CK+ gives good results.	1. The FER+ database attained the worst results 2. Transfer learning and multi-task learning can improve FER.
4.	[4]	Deep Learning methods and CNN	Comprehensive User Interest Representations, Click-Through Prediction.	Cold-start scenarios, privacy, Diversity in Content Recommendations.
5.	[7]	CNN	Three methods are used for book recommendation with accuracy 100%.	Emotion Recognition less accurate (60%).
6.	[5]	CNN BLSTM-RNN.	BLSTM-RNN gives accuracy 89%	Use advanced recommendation algorithms.

Source: Authors, (2024).

### II.2 DESCRIPTIVE ANALYSIS OF THE PLANNED SURVEY

In paper [3], in the context of image classification, Multi-Task Convolutional Neural Networks (CNNs) have been employed as a technique to improve real-time processing speed while achieving an accuracy of 66.34%. However, it is important to note

that these networks exhibit limitations. Firstly, they are designed to classify only three specific classes, which may restrict their applicability in scenarios with a broader range of categories. Additionally, Multi-Task CNNs struggle to accurately identify objects in low-resolution images, highlighting a weakness in their ability to handle such visual data effectively.

In the Proposed paper [2], the Authors state that the utilization of ANN and Multilayer Perceptron achieved an accuracy of 75.46%. However, it's important to note that the combination of Random Sampling (RS) and Random Forest (RF) produced suboptimal results, indicating the need for further exploration and refinement of this particular approach.

Authors presented Deep CNN and deep learned Tandem Facial Expression analysis techniques [1] show promising results, with the CK+ dataset achieving a high accuracy of 99.31%, but the FER+ dataset lags with an accuracy of 84.3%. The potential for improvement lies in exploring transfer and multi-task learning methods to enhance facial expression recognition in the FER+ dataset.

Deep Learning, including CNN, provides robust user interest representations and improves click-through prediction in recommendation systems [4]. Nevertheless, it struggles with challenges such as cold-start scenarios, privacy concerns, and content diversity in recommendations, necessitating ongoing research for solutions.

In the domain of book recommendation, the employment of Convolutional Neural Networks (CNN) has yielded impressive results [7], achieving a remarkable accuracy rate of 100%. However, it is important to note that these CNN-based methods may not perform as effectively in the realm of Emotion Recognition, where they exhibit a comparatively lower accuracy rate of 60%.

In the context of this study [5], the utilization of CNN and Bidirectional Long Short-Term Memory Recurrent Neural Networks (BLSTM-RNN) has proven advantageous, with BLSTM-RNN achieving a commendable accuracy of 89%. However, it is imperative to consider the integration of more advanced recommendation algorithms, highlighting the potential for further enhancing the overall performance and efficacy of the system [5].

### II.3. TECHNICAL ANALYSIS OF THE PLANNED SURVEY

#### II.3.1. CONVOLUTIONAL NEURAL NETWORKS (CNNs)

CNNs are a subset of deep neural networks that are mostly used for computer vision-related tasks like image classification, segmentation, and object detection. They consist of several layers, such as fully connected, pooling, and convolutional layers. Convolutional layers are particularly important because they can assist the network in learning hierarchical features from images [3].

#### Multi-Task Learning (MTL)

In the MTL machine learning paradigm, a single model is trained to carry out several tasks concurrently. It is proposed that learning several related tasks simultaneously can result in better performance than training separate models for each task [3].

#### MT-CNNs

The architecture of CNNs is expanded by MT-CNNs to support multiple tasks. For each task, this is typically accomplished by adding more output layers. An MT-CNN might have additional output branches for tasks like object detection, segmentation, and pose estimation, for instance, if a standard CNN is made for image classification [1]. The "Face Detection 1" unit uses any quick method, such as MTCNN (multi-task CNN), to locate the largest

facial region in each t-th video frame. The proposed lightweight CNN is then used by the unit Emotional feature extraction to obtain the emotional features  $x(t)$  of the extracted face. This CNN has been trained to classify emotions on static images [3].

#### II.3.2. Convolutional Recurrent Neural Networks (CRNNs)

The benefits of convolutional neural networks (CNNs) and recurrent neural networks (RNNs) are combined to create CRNNs, which can process data that has both spatial and sequential dependencies. They are especially useful for tasks that require understanding local patterns and long-term dependencies, such as those involving time-series data or sequences of images.

#### Multilayer Perceptron (MLPs)

Multilayer perceptron (MLP) neural networks are a particular kind of feedforward neural network. They consist of a large number of interconnected layers of nodes (neurons), each of which is connected to every node in the layer beneath and the layer above it. Each connection has a corresponding weight, and each node applies an activation function to the weighted sum of its inputs. In the absence of physiological sensors, regression target features are selected from the previously created GSR and PPG features that are extracted from the sample-level inner attention-mechanism-based convolutional recurrent neural network encoder [2]. The correlation model between the selected regression target features and musical features is then created and sent to the smartphone by the MLP regression training on the server [2]. The musical characteristics of the input music signal are fed into MLP-based regressors to automatically generate emotion features for PPG and GSR during the application phase on the smartphone. The combined GSR and PPG features are then fed into segment-level inner attention mechanism-based bidirectional gated recurrent neural networks for emotion-based music classification [2].

#### II.3.3. Facial Expression Recognition Using Deep CNN

A Deep Convolutional Neural Network (CNN) is a specific kind of neural network that is used for processing data that is grid-like, like images. Its specialty is automatically extracting hierarchical features from input images. Facial expression recognition uses facial images to quickly extract pertinent features. The computer vision task of Facial Expression Recognition (FER) uses Deep Convolutional Neural Networks (CNNs) to automatically categorize facial expressions in images or videos into predefined emotion categories (such as happiness, sadness, anger, etc.).

Using a special kind of neural network called a CNN, this method automatically extracts pertinent facial features from facial images. For processing grid-like data, such as images, CNNs, a particular class of deep learning models, were developed. Pooling, convolutional, and fully connected layers are among the many layers that make them up.

#### Tandem Facial Expression Model

An ensemble learning strategy that combines several sub-models, each of which focuses on a different aspect of facial expressions, is known as a tandem facial expression model. By simultaneously taking into account several aspects of the facial expression, this method seeks to enhance performance. Faces in

tandem Models are particularly helpful in situations where there are multiple sources of variability in facial expressions, and accurately capturing various aspects of expression is essential. They have uses in areas like affective computing, human-computer interaction, and facial expression analysis.

### Two Convolutional Neural Network

The model is composed of two convolutional neural networks. The one on the left shows how the Deep ID network finds identity features. The proper deep residual network is trained using facial expression databases. Following independent training, the identity feature and the profoundly learned emotion feature are combined as the TFE features [1] and fed to the resulting fully connected layers. Finally, they restrict joint learning on the newly combined network to the facial expression database.

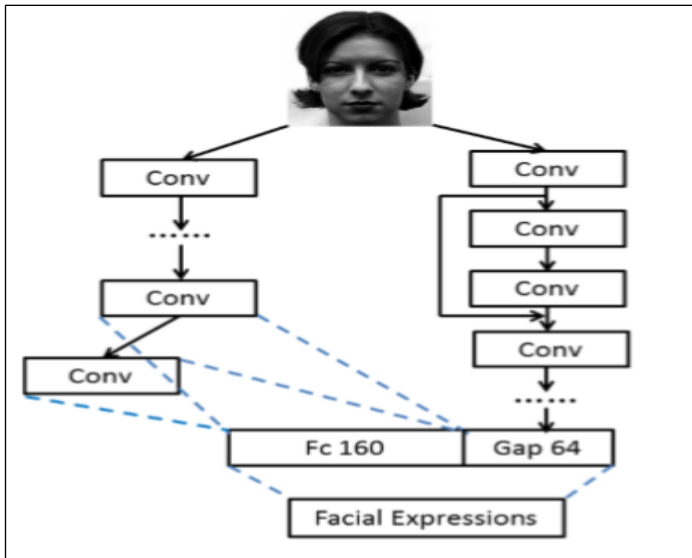


Figure 2: Two Convolutional Neural Network.  
Source: [1].

### II.3.4. Recommendation Techniques

#### Collaborative Filtering (CF)

Collaborative Filtering is a well-known recommendation method that, by compiling user preferences, automatically predicts a user's interests. It can also be divided into user-based and item-based techniques that use information about user-item interactions to produce suggestions.

#### Learning-Based Methods (BPR, DIN, DIEN)

Bayesian Personalised Ranking (BPR) is a technique that uses matrix factorization to optimize the ranking of items uniquely. It seeks to identify latent variables that represent user preferences. The deep learning-based recommendation model DIN (Deep Interest Network) takes users' changing interests into account while making recommendations. It models user interests using attention techniques. Deep Interest Evolution Network (DIEN) is a development of DIN, DIEN takes sequential behaviour and the development of user interests over time into account. It is intended to record persistent dependencies in user behaviour.

#### Multi-Interest User Representation (MUIR)

MUIR refers to methods designed to effectively represent users who have a variety of interests. It acknowledges that user interests might vary and that preferences can shift over time. Models like DIN and DIEN serve as illustrations of MUIR-based methodologies.

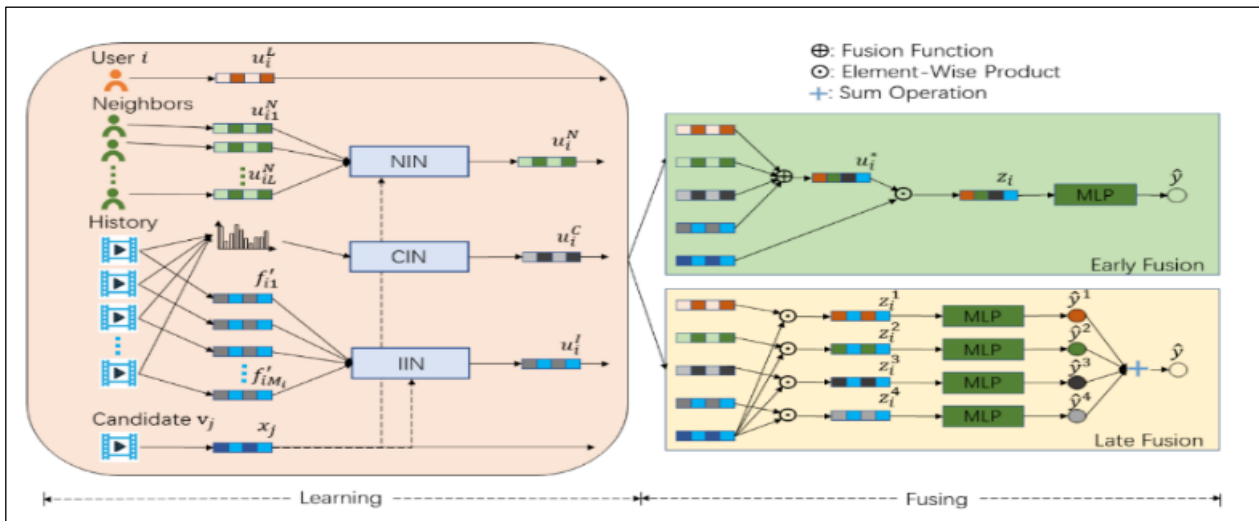


Figure 3: The framework of our Multiple User Interest Representations (MUIR) for video recommendation.  
Source: [4].

### Performance Metrics (AUC, Precision, Recall, NDCG)

**AUC:** Area Under the Receiver Operating Characteristic Curve, or AUC, is a widely used statistic for assessing how well binary classification algorithms work. It measures how well the model

prioritizes positive items over bad ones in recommendation systems.

**Precision:** Precision estimates the proportion of items among the suggested items that are actually relevant. It emphasizes the veracity of the suggested things.

**Recall:** Recall quantifies the percentage of pertinent items that are effectively suggested. It highlights the coverage of important topics.

**NDCG:** By taking into account the position of pertinent items in the recommendation list and adjusting their importance depending on that position, NDCG (Normalised Discounted Cumulative Gain) examines the ranking quality of recommended items.

### Interaction Methods for User and Item

**Element-Wise Product:** Multiplying the corresponding elements of the user and item representations results in interaction through element-wise products. It records interactions between features in pairs.

**Concatenation:** Concatenation is the combining of user and item representations, typically along a single axis. By doing this, a collective representation is produced that can be recommended.

### II.3.5. Facial Expression Recognition-Enhanced Real-Time Book Recommendation System

#### Recommendation System

The paper also describes conventional book recommendation techniques and offers the idea of a recommendation system, specifically for books. It refers to recommendations made through collaborative filtering, knowledge-based recommendations, and content-based recommendations. It draws attention to the drawbacks of conventional approaches, including their propensity to concentrate on particular sectors and the cold start issue brought on by collaborative filtering. The research suggests a novel approach that uses facial expression recognition to learn user preferences in real time to overcome these restrictions. The real-time and authentic user data provided by this method enhances the tailoring of book recommendations while promoting human-machine connection.

#### Facial Emotion Recognition Algorithm

A face recognition algorithm plus an expression recognition algorithm make up the facial expression recognition system. For face detection in real-time video streams recorded by a camera, the face recognition method uses OpenCV's Haar-Adaboost algorithm [7]. Preprocessing video frames and applying image equalization parameters are involved. A trained mini-Xception convolutional neural network is used by the expression recognition algorithm to extract facial information and categorize expressions. The network picks up characteristics linked to several emotions, including sadness, happiness, fear, disgust, surprise, scare, and anger. As a result of recognition, the system chooses the expression class with the highest likelihood. Notably, the research describes the experimental procedure, which includes book suggestions based on user preferences and user preference detection by facial expression recognition. Experiments are conducted to assess the system's precision and success rates in predicting users' preferred book types and recommending books.

#### Convolutional Neural Networks (CNNs)

The article uses convolutional neural networks (CNNs), including the mini-Xception framework, to recognize facial expressions. To make it easier to classify emotions, CNNs are employed to extract features from input grayscale photos.

**Haar-Adaboost Algorithm:** The Haar-Adaboost technique, which is a part of OpenCV, is used to find faces in real-time video streams collected from a camera.

**User Preference Inference:** The study uses facial expression recognition to determine user preferences from expressions like "Happy" or "Surprised." This method improves book suggestions.

**Recommendation Success Rate Calculation:** The success rate of book recommendations is calculated in the study to assess how well the suggested recommendation system works.

**Real-time User Monitoring:** As users browse books, the system is actively watching their facial expressions to determine their preferences.

**Emotion Categorization:** For proper recognition and advice, emotions are divided into fundamental categories as Sad, Happy, Fear, Disgust, Surprise, and Angry.

**Image preprocessing:** Preprocessing techniques, including image equalization, are used to enhance the quality of the input photos for identifying facial expressions.

### II.3.6. Knowledge-Based Recommendation System (KBRS)

This research study [5] presents a comprehensive Knowledge-Based Recommendation System (KBRS) that focuses on tracking emotional wellness and providing personalized message recommendations. The procedure is divided into several parts, starting with subjective evaluations to set the eSM2 metric parameters, which are critical for assessing users' preferences and the emotional content of utterances gathered from social media. These trials consider a range of user profiles, such as those with acute stress and mild to moderate depression levels, to develop a trustworthy sentiment meter.

The study divides phrases into depressive, stress-related, or non-depressive/non-stress categories using convolutional neural networks (CNN) and bidirectional long short-term memory recurrent neural networks (BLSTM-RNN). The emotional health monitoring system can identify users' emotional states from their social media posts thanks to these algorithms. We introduce the eSM2 sentiment analysis metric, which includes adjustment variables based on a range of user profile characteristics, including age, gender, geography, and educational attainment.

The recommendation engine in the KBRS architecture creates personalized messages for those who are stressed out or depressed using emotional data, user profiles, and ontologies [5]. The system uses several machine learning and deep learning approaches to accomplish this, making sure that users only view messages that are acceptable in terms of emotion and context. The study examines how user preferences and context could be taken into account by ontologies to improve suggestion accuracy. The study component as a whole combines sentiment analysis, machine learning, deep learning, and ontological techniques to construct a new KBRS that addresses emotional well-being through personalized messages.

•**Sentiment Analysis:** The paper employs sentiment analysis techniques to determine the emotional content of sentences extracted from social media. The eSM2 sentiment metric is introduced to quantify sentiment intensity.

•**Machine Learning:** Machine learning algorithms, including CNN and BLSTM-RNN, are utilized to classify sentences into depressive, stress-related, or non-depressive/non-stress categories.

•**Deep Learning:** Deep learning architecture, such as CNN and BLSTM-RNN, is applied for character-level representation and classification of sentences, enhancing the accuracy of emotional state detection.

•**Ontologies:** Ontological techniques are used to improve recommendation accuracy by considering user preferences, context, and other factors. The paper relies on ontologies to create a knowledge-based recommendation system.

•**User Profile Analysis:** The paper incorporates user profile analysis, considering factors like age, gender, location, and educational level, to customize recommendations and sentiment analysis.

#### II.4. DATASET ANALYSIS OF THE PLANNED SURVEY

##### MovieLens-10M

The MovieLens-10M dataset holds significant importance in the realm of movie recommendation research. In order to enhance its efficacy, researchers have incorporated 10,380 movie trailers sourced from YouTube and have utilized Convolutional Neural Networks (CNNs) to generate 4000-dimensional visual descriptions for each movie. The dataset has been split into two sections, with 80% of the dataset designated for training and the remaining 20% for testing a click-through prediction system. Ratings have been transformed into binary decisions, with a rating of 5 being labelled as "yes" and all other ratings being labelled as "no." Users with less than five "yes" ratings have been excluded from the evaluation process. In essence, the dataset has been enriched with trailers and visuals, a model has been trained to predict clicks, and the evaluation has been focused on users with substantial positive ratings.[4]

##### MicroVideo-1.7M

The MicroVideo-1.7M dataset is utilized for the purpose of examining interactions with brief micro-videos. It comprises a total of 12,737,619 user interactions performed by 10,986 users on 1,704,880 micro-videos. Each micro-video is characterized by a 512-number depiction based on its cover image, and is assigned to a specific category. The dataset is bifurcated into two distinct segments: one for training and the other for testing. Significantly, there are no videos that are present in both sets, rendering it appropriate for analysing scenarios where new items are introduced. This dataset is primarily employed for predicting whether users will click on micro-videos, with each interaction being labelled as either "yes" or "no." [4].

Table 2: Statistics Of Two Datasets.

	MovieLens-10M		MicroVideo-1,7M	
	Training	test	Training	test
#User	51,001	46,692	10,986	10,986
#Video	10,380	9,830	984,983	719,897
#Category	19	19	512	512
#Positive	1,216,527	268,917	1,754,457	646,933
#Negative	5,781,1953	1,398,369	7,215,852	3,120,375
Positive Ratio	0,22%	0,06%	0,02%	0,01%

Source: [4].

##### DEFSS

The Developmental Emotional Faces Stimulus collection (DEFSS), which contains a child, teen, and adult face, attempts to provide a standardized collection of emotional stimuli that have been validated by participants across a wide range of ages. The collection consists of 404 validated facial photos of persons aged 8 to 30 displaying five different emotional states: happy, mad, fearful, sad, and neutral. Additionally, the DEFSS contains a neutral emotion that contrasts positive and negative feelings across age groups.

##### LFW

The 5,749 online identities that make up the 13,233 face images in the LFW (Labelled Faces in the Wild) dataset. In order to compare performance, LFW advises using splits they randomly generated (6,000 pairs) with 10-fold cross validation [6]. The LFW database is used in this study only as a stand-alone testing dataset to evaluate the effectiveness of our identity features created using the CASIA-WebFace dataset [1].

##### CK+

The CK+ database contains 327 image sequences with labelled facial expressions. Each image sequence only contains an expression label in the last frame. In order to gather more images for training, they typically selected the final three frames of each sequence for training or validation purposes. Additionally, the first frame from each of the 327 labelled sequences would be chosen to represent the "neutral" expression. Thus, this dataset can provide 1308 total images with 8 labels for facial expressions. For testing, they employ the 10-fold cross validation testing protocol and the CK+ database [1].

##### FER+

This dataset comes from the Face Expression Recognition Challenge of the 2013 Representation Learning Workshop [8]. 28,709 training 48 x 48 face images are included. The 3,589 images that make up the test set contain a total of 7 different facial expressions: anger, disgust, fear, happiness, sadness, and surprise. Due to its noisy labels, this dataset is labelled again using services that rely on crowdsourcing [9]. In this study, a majority vote is used to determine the new set of labels for our experiments.



Figure 4: Ten representative face images whose prediction is corrected by joint learning method.  
Source: [1].

### III. CONCLUSIONS

By skillfully interpreting complex emotional data from facial expressions, this system introduces a powerful fusion of cutting-edge deep learning paradigms, most notably Convolutional Neural Networks (CNNs) and Convolutional Recurrent Neural Networks (CRNNs), to perform real-time emotion recognition. Facial expression recognition accuracy is improved by using pre-processing methods such as image equalization. Benchmarks like MovieLens-10M, MicroVideo-1.7M, DEFSS, LFW, CK+, and FER+ are among the carefully chosen datasets by the system, demonstrating its dedication to representative and diverse samples. It performs a thorough comparative analysis of deep learning-based models such as Deep Interest Network (DIN) and Deep Interest Evolution Network (DIEN), Collaborative Filtering (CF), and Bayesian Personalized Ranking (BPR) in the field of recommendation approaches. This analysis uses performance indicators such as AUC, Precision, Recall, and NDCG for a rigorous evaluation methodology to show how well various approaches solve the cold start issue and react to changing user interests. This novel technical paradigm seeks to build emotionally intelligent digital environments by fusing state-of-the-art deep learning with sophisticated evaluation methods and careful examination of datasets. This survey study aims to provide a thorough analysis of the relationship between emotions and technology, ultimately stimulating more investigation and creativity in this area to rethink the way we fundamentally engage with one another and with technology.

### IV. AUTHOR'S CONTRIBUTION

**Conceptualization:** Sanika A. Gonjari, Ritika A. Pawar, Rohini B. Naik

**Methodology:** Sanika A. Gonjari, Rachana N. Pawar, Ritika A. Pawar, Sharwari H. Kshirsagar, Rohini B. Kokare.

**Investigation:** Sanika A. Gonjari, Rachana N. Pawar, Ritika A. Pawar, Sharwari H. Kshirsagar, Rohini B. Kokare.

**Discussion of results:** Sanika A. Gonjari, Rachana N. Pawar, Ritika A. Pawar, Sharwari H. Kshirsagar, Rohini B. Kokare.

**Writing-Original draft:** Rachana N. Pawar, Sharwari H. Kshirsagar.

**Visualization, Writing, Editing:** Sanika A. Gonjari, Ritika A. Pawar, Rachana N. Pawar, Sharwari H. Kshirsagar.

**Resources:**

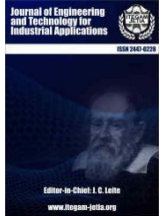
**Supervision:** Rohini B. Kokare.

**Approval of the final text:** Rohini B. Kokare.

### V. REFERENCES

- [1] M. Li, H. Xu, X. Huang, Z. Song, X. Liu and X. Li, "Facial Expression Recognition with Identity and Emotion Joint Learning," in IEEE Transactions on Affective Computing, vol. 12, no. 2, pp. 544-550, 1 April-June 2021, doi:10.1109/TAFFC.2018.2880201.
- [2] H. -G. Kim, G. Y. Lee and M. -S. Kim, "Dual-Function Integrated Emotion-Based Music Classification System Using Features From Physiological Signals," in IEEE Transactions on Consumer Electronics, vol. 67, no. 4, pp. 341-349, Nov. 2021, doi:10.1109/TCE.2021.3120445.
- [3] A. V. Savchenko, L. V. Savchenko and I. Makarov, "Classifying Emotions and Engagement in Online Learning Based on a Single Facial Expression Recognition Neural Network," in IEEE Transactions on Affective Computing, vol. 13, no. 4, pp. 2132-2143, 1 Oct. Dec.2022,doi:10.1109/TAFFC.2022.3188390.
- [4] X. Chen, D. Liu, Z. Xiong and Z. -J. Zha, "Learning and Fusing Multiple User Interest Representations for Micro-Video and Movie Recommendations," in IEEE Transactions on Multimedia, vol. 23, pp. 484496, 2021, doi:10.1109/TMM.2020.2978618.
- [5] R. L. Rosa, G. M. Schwartz, W. V. Ruggiero and D. Z. Rodríguez, "A Knowledge-Based Recommendation System That Includes Sentiment Analysis and Deep Learning," in IEEE Transactions on Industrial Informatics, vol. 15, no. 4, pp. 2124-2135, April 2019, doi:10.1109/TH.2018.2867174.
- [6] C. Dalvi, M. Rathod, S. Patil, S. Gite and K. Kotecha, "A Survey of AI-Based Facial Emotion Recognition: Features, ML & DL Techniques, Age-Wise Datasets and Future Directions," in IEEE Access, vol. 9, pp. 165806-165840, 2021, doi: 10.1109/ACCESS.2021.3131733
- [7] Y. Zhao and J. Zeng, "Library Intelligent Book Recommendation System Using Facial Expression Recognition," 2020 9th International Congress on Advanced Applied Informatics (IIAI-AAI), Kitakyushu, Japan, 2020, pp. 55-58, doi: 10.1109/IIAI-AAI50415.2020.00021.
- [8] I. J. Goodfellow, D. Erhan, P. L. Carrier, A. Courville, M. Mirza, B. Hamner, W. Cukierski, Y. Tang, D. Thaler, and D. H. Lee, "Challenges in representation learning: A report on three machine learning contests," Neural Networks, vol. 64, p. 59, 2015.
- [9] E. Barsoum, C. Zhang, C. C. Ferrer, and Z. Zhang, "Training deep networks for facial expression recognition with crowd-sourced label distribution," in ACM International Conference on Multimodal Interaction, 2016, pp. 279-283.





## SENTIMENT ANALYSIS OF FINANCIAL NEWS USING THE BERT MODEL

\*Najeem O. Adelakun<sup>1</sup>, Adebisi A. Baale<sup>2</sup>

<sup>1</sup> Engineer/Researcher, Federal College of Education Iwo, Osun State, Nigeria.

<sup>2</sup> Department of Information Systems, Ladoko Akintola University of Technology, Ogbomosho, Nigeria

<sup>1</sup><http://orcid.org/0000-0003-1749-7116> , <sup>2</sup><http://orcid.org/0000-0003-2274-250X> ,

Email: <sup>1</sup>[adelakunno@fceiwo.edu.ng](mailto:adelakunno@fceiwo.edu.ng)\*, <sup>2</sup>[aabaale@lautech.edu.ng](mailto:aabaale@lautech.edu.ng),

### ARTICLE INFO

#### Article History

Received: February 03<sup>th</sup>, 2024

Revised: July 08<sup>th</sup>, 2024

Accepted: July 8<sup>th</sup>, 2024

Published: July 18<sup>th</sup>, 2024

#### Keywords:

BERT Model,  
Deep Learning,  
Financial Markets,  
Financial Sentiment Analysis,  
Natural Language Processing.

### ABSTRACT

Financial decisions are strongly reliant on correct sentiment analysis. Traditional methods frequently fall short of capturing hidden sentiments. A financial market dataset comprising 5,842 reviews was collected for analysis. Among these, 1,852 reviews were positive, 860 were negative, and 3,130 were neutral. After downsampling, the data was divided into two groups: the training set and the test set. The training set was employed to train the model, while the test set was reserved for evaluation. This study applies a deep learning approach using the Bidirectional Encoder Representations from Transformers (BERT) model to train the dataset. The performance of the model was measured using accuracy, precision, recall, and F1-score. The model gave a high performance with an accuracy of 95.29%, precision of 95.37%, recall of 95.24%, and a minimal loss of 9.07%. Notably, the F1-score, which provides a balanced evaluation of the model's efficiency, is 95.32%. These findings highlight the BERT model's effectiveness in conducting sentiment analysis in financial markets. The study not only enhances the field of financial sentiment analysis, but it also emphasises the practicality and dependability of using deep learning techniques to extract significant insights from financial data.



Copyright ©2024 by authors and Galileo Institute of Technology and Education of the Amazon (ITEGAM). This work is licensed under the Creative Commons Attribution International License (CC BY 4.0).

### I. INTRODUCTION

The swift expansion of web-based applications such as social media platforms and blogs has resulted in an explosion of comments and reviews about daily life activities. Financial analysis is useful for identifying economic trends, developing financial strategies, and developing long-term corporate goals [1]. These provide critical information to shareholders about a company's revenue, expenses, profitability, and debt. Financial reporting and analysis refer to the systematic collection and monitoring of a company's financial data, which includes both revenues and expenses [2-3]. Sentiment analysis has become an important technique for extracting information from social networks. It is commonly used in real-world scenarios to gather feedback on products or services and develop marketing predictions [4-5]. It also helps with data identification and quantification in Natural Language Processing (NLP), computational linguistics, text analysis, and other domains by using machine learning algorithms

to detect biased text and extract useful information from presented textual data [6-7].

Natural Language Processing (NLP) is an essential artificial intelligence area that helps computers analyse human spoken and written language [8]. The process of sentiment analysis has been studied at different levels. However, sentiments and opinions can be observed primarily at the document, sentence, or aspect levels [9-12] as shown in Figure 1.

- i. **Document Level:** The method is based solely on the document, which means that the complete document is considered as a whole for sentiment analysis in order to determine the polarity [13].
- ii. **Sentence Level:** Sentiment is analysed for each sentence at this level to determine the polarity of each sentence [14].
- iii. **Aspect/Feature Level:** This level performs fine-grained analysis because it aims to find sentiments with respect to the specific aspects of entities [15-16].

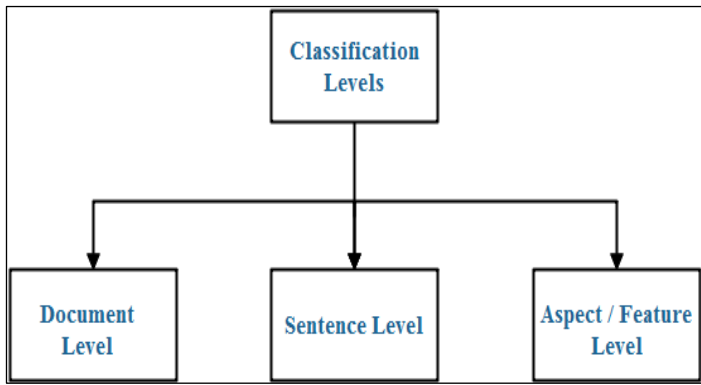


Figure 1: Sentiment Classification Levels.  
Source: Authors, (2024).

Machine learning techniques are classified into two types: traditional approaches and deep learning approaches. Deep learning was introduced by G.E. Hinton in 2006 as a machine learning approach connected to deep neural networks [17-18]. It is also known as a subset of machine learning that revolutionised the field of sentiment analysis by enabling the extraction of complex sentiments and contextually rich information from textual data. It is popularly known as multi-layered neural networks inspired by the interconnected sensory neurons of the human brain [19]. The most prominent deep learning approaches include transformer networks, deep neural networks, recursive neural networks, recurrent neural networks, and hybrid neural networks [20]. However, the most commonly used transformer networks for sentiment analysis are Bidirectional Encoder Representations from Transformers (BERT), Generative Pre-trained Transformer (GPT), Robustly Optimised BERT Pre-training Approach (RoBERTa), and eXtreme MultiLingual Pre-training for Language Understanding (XLNet) [21].

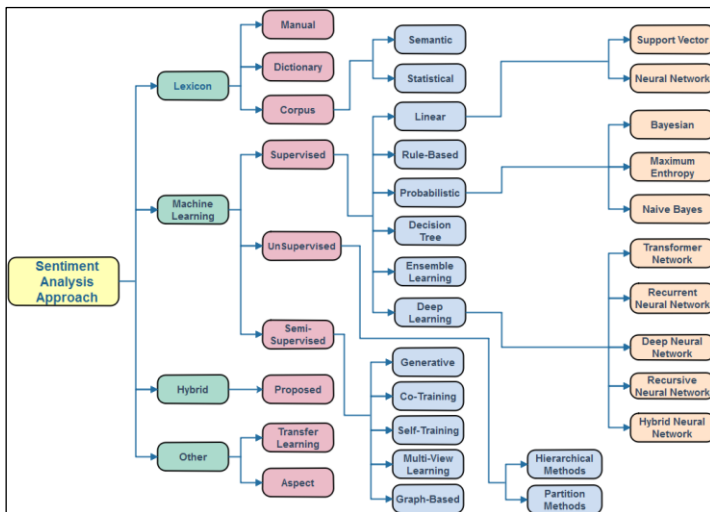


Figure 2: Sentiment Analysis Approach.  
Source: [20].

Sentiment analysis classification employs four primary approaches: lexicon-based, machine learning-based, hybrid, and other methods [22] as shown in Figure 2. Lexicon-based systems rely on prepared word lists that have either positive or negative connotations. To anticipate sentiment in new data, machine learning systems use algorithms trained on labelled data. To improve classification performance, the hybrid technique

integrates both methods [23-25]. Other approaches include rule-based and deep learning algorithms [26].

There have been numerous surveys and review articles on sentiment analysis. Medhat et al. [9] proposed a detailed survey studying and presenting sentiment analysis methodologies and applications. The authors also covered related disciplines to sentiment analysis, such as emotion recognition and resource development. Rauf et al. [27] investigated the polarity of the IMDB dataset using sentiment analysis to develop a transformer-based model, such as BERT. The BERT model outperformed most previous machine learning and deep learning-based models on the supplied dataset, according to the findings analysis. Gong et al. [28] proposed a transformer-based method that combines knowledge distillation and text augmentation. This method reduces processing costs and training time while improving overall performance. The accuracy for emotion recognition in text is 93.28%, with BERT at 93.38%, ALBERT at 92.06%, and mobileBERT at 92.74%.

Bharti et al. [29] proposed a hybrid model using support vector machines alongside CNN and Bi-GRU as deep learning components. This approach yielded an accuracy of 80.11% across diverse datasets (phrases, tweets, and conversations). Paredes-Valverde et al. [30] used the CNN and word2vec in sentiment analysis to improve product quality. The experimental outcomes on a vast Twitter corpus of 100,000 tweets verified its effectiveness, showing high precision, recall, and F-measure values of 88.7%. Souma et al. [31] investigate historical news sentiments in order to estimate financial market attitudes. They gather news feelings from stock returns following an article. The study evaluates Thompson Reuters News Archive and Dow Jones Industrial Average stocks (2003-2013) using TensorFlow and word vectors from Wikipedia and Gigaword. Choosing news based on sentiment scores improves forecasting accuracy significantly.

Mula et al. [32] used the machine learning models to predict sentiments in developer comments, demonstrating the power of embedding approaches, feature selection, class imbalance handling, and deep learning architecture in sentiment prediction. The efficiency of their models was proven by experimental data. Chen et al. [33] used CSI 300 share value data from the Chinese SM to compare standard N.N. price prediction with deep learning and discovered that deep learning prediction performance outperformed conventional N.Ns. Rangila et al. [34] investigated BERT and LSTM models for sentiment analysis on transcribed audio. BERT, a Google-developed algorithm, performed well in terms of speed and accuracy, obtaining 98% accuracy in just two epochs. LSTM, on the other hand, only achieved 51% accuracy after five epochs. BERT is the recommended option due to its higher accuracy and efficiency.

## II. THE BIDIRECTIONAL ENCODER REPRESENTATIONS FROM TRANSFORMERS (BERT) MODEL

The BERT framework is divided into two stages: pre-training and fine-tuning. Initially, it is trained on a large amount of unlabeled data for various NLP tasks. Fine-tuning then uses labelled data to customise it for specific tasks [35]. BERT, which is based on the Transformer network, has encoder blocks with multi-head attention and feedforward layers. This enables it to attend to several segments of the input at the same time and grasp links between tokens. This architecture improves contextual comprehension for a wide range of natural language processing applications.

## III. METHODOLOGY

The study conducted a sentiment analysis on financial market datasets by leveraging advanced natural language processing techniques using the Bidirectional Encoder Representations from Transformers (BERT) model. This method intends to detect sentiments within financial texts, allowing for more informed investment decisions. This procedure entails thorough data collection, preprocessing, model training, and evaluation as shown in Figure 3 with brief explanation what each functional block means in the section below.

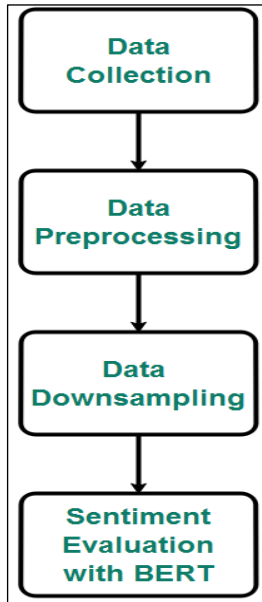


Figure 3: Block Diagram of Sentiment Analysis Process with BERT Model.

Source: Authors, (2024).

- A. **Data Collection:** The data was collected using a financial dataset for sentiment analysis, which included 5842 test samples from the FiQA and the Financial PhraseBank [36]. The sentiment labels in this dataset are as follows: neutral (3130), positive (1852), and negative (860). Essential Python libraries such as Keras, TensorFlow, NumPy, scikit-learn, and PyTorch were used to efficiently handle this dataset.
- B. **Data Preprocessing:** The BERT model requires multiple phases of data preprocessing before it can be used for sentiment analysis. Text cleaning begins by removing noise such as special characters and HTML elements. Tokenization then divides the text into manageable parts for study. Padding ensures that the model's input length is consistent. Label encoding assigns numerical values to sentiment categories. These processes work together to improve the initial data.
- C. **Data Downsampling:** It is used to ensure a balanced distribution of classes. An equitable representation is ensured by reducing both neutral and positive sentiment labels to 860 labels, which correspond to the negative sentiment count from the test set. This eliminates any bias towards a specific sentiment category, allowing for more accurate sentiment analysis. As a result, the model is trained on a large dataset, which improves its capacity to make accurate predictions across a wide range of sentiment labels.

Table 1: Distribution of the dataset.

	Neutral	Positive	Negative	Total
<b>Train</b>	3130	1852	860	<b>5,842</b>
<b>Test</b>	860	860	860	<b>2,580</b>

Source: Authors, (2024).

- D. **Sentiment Evaluation with BERT:** Key metrics for evaluating sentiment using BERT include accuracy, precision, recall, and F1-score. These metrics assess the model's ability to correctly identify sentiments, giving critical information for reliable sentiment analysis in financial texts.
  - i. **Accuracy:** Accuracy measures the proportion of correctly classified sentiments to total forecasts. It provides a comprehensive view of the model's performance, but its dependability is affected by data imbalances, which may distort its interpretation.
  - ii. **Precision:** Precision is the ratio of true positive forecasts to overall positive predictions. It emphasises the model's capacity to properly recognise positive feelings, decreasing the probability of false positives and ensuring reliable results.
  - iii. **Recall:** The ratio of actual positive predictions to true positive cases is represented by recall. It assesses the model's sensitivity in detecting all positive attitudes, eliminating false negatives and improving overall efficacy.
  - iv. **F1-Score:** The F1-score is a balanced measure that is calculated by taking the harmonic mean of precision and recall. It provides a full evaluation of the model's effectiveness, which is especially useful in cases where the impact of both false positives and false negatives is significant.

#### IV. RESULTS AND DISCUSSIONS

The performance evaluation involved using the BERT model to analyse a financial dataset encompassing 5,842 reviews. Figure 4 shows ten sentences along with their corresponding sentiment labels from the pretrained financial dataset. This data visualization provides a tangible representation of sentiment analysis, offering the raw data as presented.

	Sentence	Sentiment
0	The GeoSolutions technology will leverage Bene...	positive
1	<i>ESI</i> on lows, down 1.50 to \$2.50 BK a real po...	negative
2	For the last quarter of 2010 , Componenta 's n...	positive
3	According to the Finnish-Russian Chamber of Co...	neutral
4	The Swedish buyout firm has sold its remaining...	neutral
5	\$SPY wouldn't be surprised to see a green close	positive
6	Shell's \$70 Billion BG Deal Meets Shareholder ...	negative
7	SSH COMMUNICATIONS SECURITY CORP STOCK EXCHANG...	negative
8	Kone 's net sales rose by some 14 % year-on-ye...	positive
9	The Stockmann department store will have a tot...	neutral

Figure 4: Data Visualization.

Source: Authors, (2024).

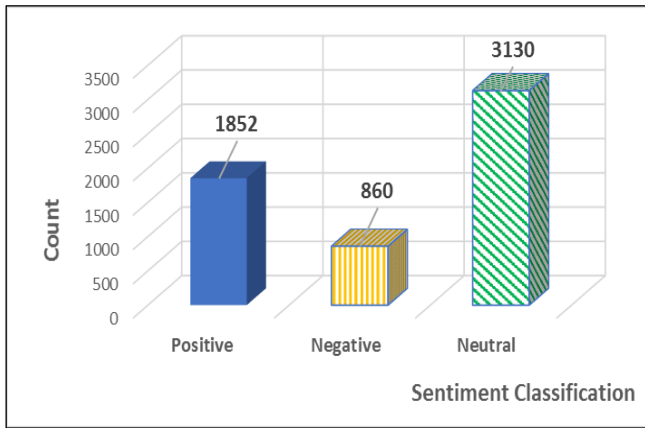


Figure 5: Bar chart depicting sentiment classification. Source: Authors, (2024).

Figure 5 presents a chart showcasing the sentiment classification of the raw data from the pretrained financial dataset consisting of 5,842 reviews. This data breakdown reveals that 1,852 reviews were classified as positive, 860 as negative, and 3,130 as neutral sentiments.

	Sentence	Sentiment
0	the geosolutions technology will leverage bene...	positive
1	esi on lows down 150 to 250 bk a real possibility	negative
2	for the last quarter of 2010 component s net...	positive
3	according to the finnishrussian chamber of com...	neutral
4	the swedish buyout firm has sold its remaining...	neutral
5	spy wouldnt be surprised to see a green close	positive
6	shells 70 billion bg deal meets shareholder sk...	negative
7	ssh communications security corp stock exchange...	negative
8	kone s net sales rose by some 14 yearonyear i...	positive
9	the stockmann department store will have a tot...	neutral

Figure 6: Data visualization of a cleaned dataset. Source: Authors, (2024).

In Figure 6, a visual representation illustrates the dataset post-application of the data preprocessing techniques, resulting in a cleaner and more organised dataset. These visualisations offer a concise and informative summary of the sentiment analysis findings and emphasise the importance of data preprocessing in enhancing data quality and subsequent analysis accuracy.

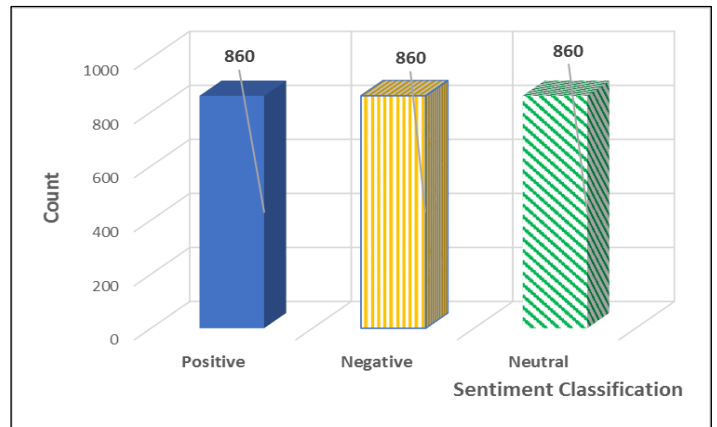


Figure 7: Bar chart depicting count plot after downsampling. Source: Authors, (2024).

Figure 7 displays a bar chart presenting the count plot after implementing data downsampling. Downsampling is crucial to balance the class distribution in the dataset, especially when dealing with imbalanced sentiment data. It involves reducing the number of instances in the overrepresented class, which in turn prevents the model from being biased towards the majority class. This ensures a more accurate and fair sentiment analysis by allowing the model to equally weigh the contribution of each sentiment category, leading to more reliable results in financial sentiment analysis.

```

Model: "model_4"
-----
Layer (type)                Output Shape      Param #   Connected to
-----
input_5 (InputLayer)        [(None, 53)]      0         []
embedding_18 (Embedding)    (None, 53, 36)   261792    ['input_5[0][0]']
dense_45 (Dense)            (None, 53, 36)   1332      ['embedding_18[0][0]']
tf.__operators__.add_4 (TFOpLa (None, 53, 36)   0         ['dense_45[0][0]']
mbda)
layer_normalization_8 (LayerNo (None, 53, 36)   72        ['tf.__operators__.add_4[0][0]']
rmalization)
multi_head_attention_4 (MultiH (None, 53, 36)   37668     ['layer_normalization_8[0][0]',
eadAttention)                'layer_normalization_8[0][0]']
dense_53 (Dense)            (None, 53, 64)   2368      ['multi_head_attention_4[0][0]']
flatten_4 (Flatten)         (None, 3392)     0         ['dense_53[0][0]']
dropout_9 (Dropout)         (None, 3392)     0         ['flatten_4[0][0]']
dense_54 (Dense)            (None, 3)        10179     ['dropout_9[0][0]']
-----
Total params: 313,411
Trainable params: 313,411
Non-trainable params: 0
    
```

Figure 8: Trainable parameters in BERT. Source: Authors, (2024).

Figure 8 illustrates the trainable parameters within a BERT (Bidirectional Encoder Representations from Transformers) model. These parameters are elements of the model that can be adjusted and fine-tuned during the training process, enabling BERT to adapt and excel in various natural language understanding tasks, including sentiment analysis and text classification.

```

Epoch 1/30
114/114 [=====] - 5s 33ms/step - loss: 1.0714 - accuracy: 0.4225 - precision_14: 0.4916 - recall_14: 0.0648 - val_loss: 1.1884 - val_accuracy: 0.0000e+00 - val_precision_14: 0.0000e+00 - val_recall_14: 0.0000e+00 - lr: 0.0010
Epoch 2/30
114/114 [=====] - 3s 20ms/step - loss: 0.7347 - accuracy: 0.6736 - precision_14: 0.7410 - recall_14: 0.5722 - val_loss: 0.8258 - val_accuracy: 0.6742 - val_precision_14: 0.6899 - val_recall_14: 0.5742 - lr: 0.0010
Epoch 3/30
114/114 [=====] - 3s 20ms/step - loss: 0.5107 - accuracy: 0.8810 - precision_14: 0.8895 - recall_14: 0.8722 - val_loss: 1.9616 - val_accuracy: 0.4226 - val_precision_14: 0.4225 - val_recall_14: 0.3871 - lr: 0.0010
Epoch 4/30
114/114 [=====] - 3s 20ms/step - loss: 0.1772 - accuracy: 0.9104 - precision_14: 0.9236 - recall_14: 0.9163 - val_loss: 1.6278 - val_accuracy: 0.5452 - val_precision_14: 0.5552 - val_recall_14: 0.5355 - lr: 0.0010
Epoch 5/30
114/114 [=====] - 4s 31ms/step - loss: 0.1050 - accuracy: 0.9463 - precision_14: 0.9474 - recall_14: 0.9449 - val_loss: 1.7784 - val_accuracy: 0.5258 - val_precision_14: 0.5372 - val_recall_14: 0.5129 - lr: 1.0000e-04
Epoch 6/30
114/114 [=====] - 3s 20ms/step - loss: 0.0979 - accuracy: 0.9498 - precision_14: 0.9497 - recall_14: 0.9485 - val_loss: 1.8897 - val_accuracy: 0.5200 - val_precision_14: 0.5236 - val_recall_14: 0.5000 - lr: 1.0000e-04
Epoch 7/30
114/114 [=====] - 3s 20ms/step - loss: 0.0918 - accuracy: 0.9515 - precision_14: 0.9515 - recall_14: 0.9511 - val_loss: 1.8627 - val_accuracy: 0.5129 - val_precision_14: 0.5068 - val_recall_14: 0.4886 - lr: 1.0000e-05
Epoch 8/30
114/114 [=====] - 3s 20ms/step - loss: 0.0907 - accuracy: 0.9520 - precision_14: 0.9537 - recall_14: 0.9514 - val_loss: 1.9017 - val_accuracy: 0.5097 - val_precision_14: 0.5034 - val_recall_14: 0.4886 - lr: 1.0000e-05
(keras.callbacks.History at 0x7f74801c6660)
    
```

Figure 9: Epochs of BERT.  
Source: Authors, (2024).

Figure 9 depicts epochs of the BERT model, where the early stopping callback function plays a crucial role by monitoring the training and stopping it when progress levels off, which helps save computational resources. Then, the Adam optimizer comes into play, guiding parameter adjustments with a learning rate of 0.001 to ensure efficient convergence. The batch size is set at 20, determining how many pieces of data are processed in each step, an essential aspect of efficient training. Over 30 epochs, the model steadily improves its understanding of the data, refining its predictive abilities. Key performance metrics, including accuracy, precision, and recall, collectively shape the model's learning process and ultimately enhancing its proficiency in the assigned task.

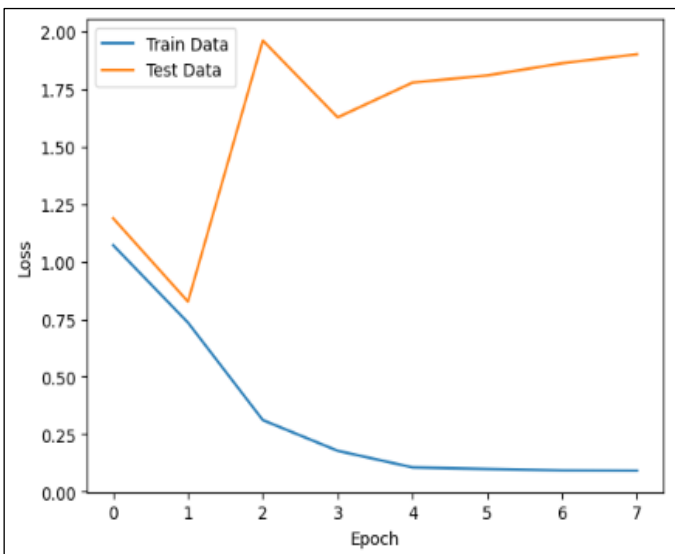


Figure 10: Graphical illustration of losses on the BERT model.  
Source: Authors, (2024).

In Figure 10, a graphical representation illustrates the comparison of losses in the BERT model between the training and test datasets. The training set showed minimal loss, signifying efficient model learning and performance.

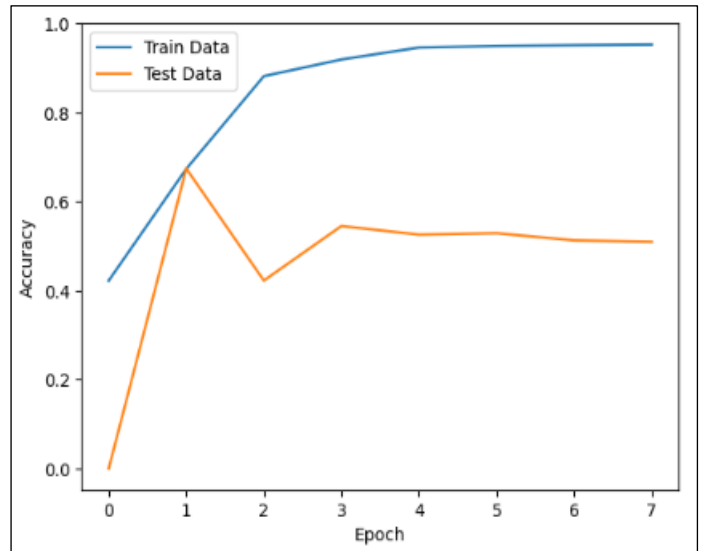


Figure 11: Graphical illustration of accuracy on the BERT model.  
Source: Authors, (2023).

In Figure 11, a graphical representation illustrates the accuracy of the BERT model, differentiating between the training and test datasets. The training set demonstrated notably higher accuracy, emphasizing the model's proficiency in learning from this dataset. This visual aid played a pivotal role in gauging the model's performance and highlighted the effectiveness of its training process, offering valuable insights for further refinement and application in real-world scenarios. Figure 12 presents a graphical representation comparing precision in the BERT model between the training and test datasets. The training set exhibited superior precision, signifying the model's effectiveness in correctly identifying specific classes. This visual assessment was crucial for evaluating the model's performance and ensuring its accuracy in practical applications.

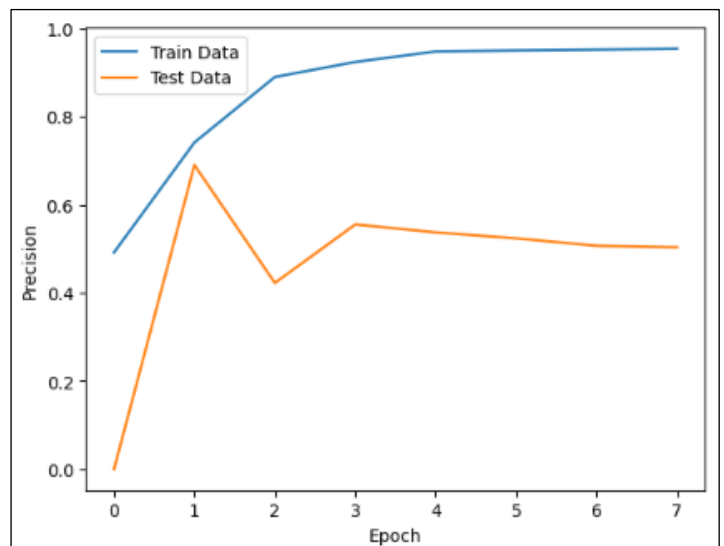


Figure 12: Graphical illustration of precision on the BERT model.  
Source: Authors, (2024).

Figure 13 depicts a graphical representation that compares recall in the BERT model between the training and test datasets. The training set demonstrated superior recall,

signifying the model's effectiveness in accurately identifying specific classes.

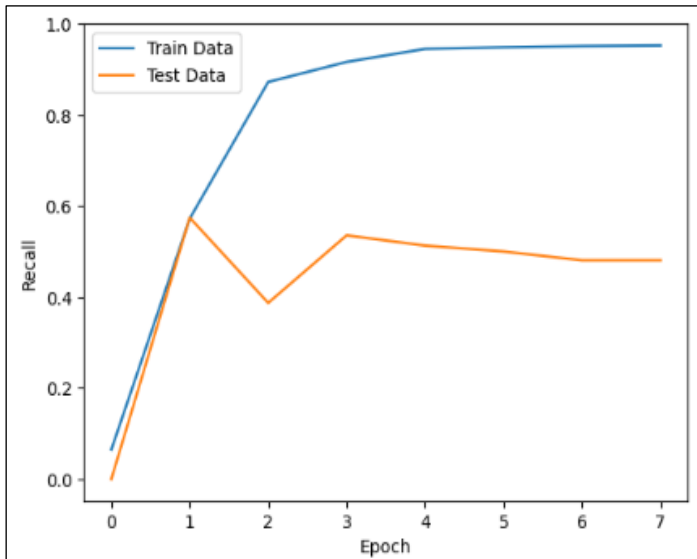


Figure 13: Graphical illustration of recall on the BERT model.  
Source: Authors, (2024).

$$F1 - Score = \frac{2 \times Pre \times Rec}{Pre + Rec} = \frac{2 \times 0.9537 \times 0.9524}{0.9537 + 0.9524} = 0.9532 \quad (1)$$

The study assessed the model's performance with several crucial metrics, revealing highly impressive results. An accuracy of 95.29% indicates the model's ability to make correct predictions in the financial sentiment analysis. The high precision of 95.37% highlights its capacity to precisely identify positive or negative sentiments. A recall of 95.24% suggests that the model effectively captures the most relevant information in the dataset. The minimal loss at 9.07% signifies minimal error in its predictions. The F1-score of 95.32% combines precision and recall, showcasing the model's balanced performance. These results affirm the model's effectiveness and reliability in financial sentiment analysis.

## V. CONCLUSIONS

In conclusion, this study demonstrates the significance of using advanced natural language processing techniques, such as the BERT model to conduct sentiment analysis in financial markets. The model performed excellently, with 95.29% accuracy, 95.37% precision, and 95.24% recall. The model's robustness is further demonstrated by the model's low loss of 9.07%. The F1-score of 95.32% demonstrates the model's balanced precision and recall, indicating its ability to effectively classify sentiments. These results outperform several existing sentiment analysis algorithms, demonstrating the effectiveness of using deep learning techniques and the BERT model in financial sentiment research. This research not only advances sentiment analysis methodology, but it also provides financial practitioners with a strong tool for making informed choices based on sentiment insights. The BERT model's implementation tackles the complex nature of sentiments in financial texts, a vital feature that previous techniques sometimes ignore. The approach captures detailed links between words by exploiting bidirectional contextual embeddings, resulting in enhanced sentiment categorization. This study emphasises the importance of using advanced NLP techniques and modern algorithms like BERT in financial sentiment analysis, ultimately improving decision-making processes in the unstable environment of financial markets.

## VI. AUTHOR'S CONTRIBUTION

**Conceptualization:** Najeem O. Adelakun, Adebisi A. Baale.

**Methodology:** Najeem O. Adelakun.

**Investigation:** Najeem O. Adelakun.

**Discussion of results:** Najeem O. Adelakun, Adebisi A. Baale.

**Writing – Original Draft:** Najeem O. Adelakun.

**Writing – Review and Editing:** Najeem O. Adelakun, Adebisi A. Baale.

**Resources:** Najeem O. Adelakun.

**Supervision:** Adebisi A. Baale.

**Approval of the final text:** Najeem O. Adelakun, Adebisi A. Baale.

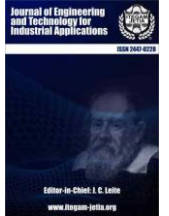
## VII. ACKNOWLEDGMENTS

Our sincere gratitude to FiQA and the Financial PhraseBank for providing access to their invaluable financial dataset. This resource greatly enriched our study in financial sentiment analysis.

## VIII. REFERENCES

- [1] F. Cosenz, V. P. Rodrigues, and F. Rosati. 'Dynamic business modeling for sustainability: Exploring a system dynamics perspective to develop sustainable business models'. *Business Strategy and the Environment*. vol. 29, no. 2, pp. 651-664. 2020.
- [2] F. Z. Xing, E. Cambria, and R. E. Welsch. 'Natural language based financial forecasting: a survey'. *Artificial Intelligence Review*, vol. 50, no. 1, pp. 49-73, 2018.
- [3] P. Mehta, S. Pandya, and K. Kotecha. 'Harvesting social media sentiment analysis to enhance stock market prediction using deep learning'. *PeerJ Comput. Sci.* 7:e476, 2021. <https://doi.org/10.7717/peerj-cs.476>
- [4] N. O. Adelakun. 'Navigating challenges and future trends in sentiment analysis for investment decision making'. *Information Matters*, vol. 3, no. 7, 2023. <https://informationmatters.org/2023/07/navigating-challenges-and-future-trends-in-sentiment-analysis-for-investment-decision-making/> <http://dx.doi.org/10.2139/ssrn.4513208>
- [5] P. Garg. 'Sentiment Analysis of Twitter Data using NLTK in Python' (Issue June). Master Thesis, Department of Computer Science and Engineering, Thapar University. 2016.
- [6] S. T. Kokab, S. Asghar, and S. Naz. 'Transformer-based deep learning models for the sentiment analysis of social media data'. *Array*, 14, 100157. 2022. <https://doi.org/10.1016/j.array.2022.100157>
- [7] M. Wankhade, A. C. S. Rao, and C. Kulkarni. 'A survey on sentiment analysis methods, applications, and challenges'. *Artif Intell Rev* 55, vol. 29, no. 2, pp. 5731–5780, 2022. <https://doi.org/10.1007/s10462-022-10144-1>
- [8] V. Balakrishnan, Z. Shi, C. L. Law, R. Lim, L. L. The, and Y. Fan. 'A deep learning approach in predicting products' sentiment ratings: a comparative analysis'. *The Journal of Supercomputing*. Vol. 78, no. 5, pp. 7206-7226. 2022. <http://doi.org/10.1007/s11227-021-04169-6>.
- [9] W. Medhat, A. Hassan, and H. Korashy. 'Sentiment analysis algorithms and applications: A survey', *Ain Shams Eng. J.* vol. 5, pp. 1093–1113, 2014. <https://doi.org/10.1016/j.asej.2014.04.011>
- [10] H. H. Do, P. Prasad, A. Maag, and A. Alsadoon. 'Deep learning for aspect-based sentiment analysis: A comparative review', *Expert Syst. Appl.* Vol. 118, pp. 272–299, 2019. <https://doi.org/10.1016/j.eswa.2018.10.003>
- [11] C. C. Aggarwal. 'Machine learning for text', *Mach. Learn. Text.* pp. 1–493, 2018. <https://doi.org/10.1007/978-3-319-73531-3>
- [12] S. Behdenna, F. Barigou, and G. Belalem. 'Sentiment analysis at document level', in: *SmartCom 2016*, pp. 159–168, 2016. [https://doi.org/10.1007/978-981-10-3433-6\\_20](https://doi.org/10.1007/978-981-10-3433-6_20).

- [13] M. V. Mäntylä, D. Graziotin, M. Kuutila. 'The evolution of sentiment analysis — A review of research topics, venues, and top cited papers'. *Computer Science Review*, vol. 27, pp. 16–32. 2018. <https://doi.org/10.1016/j.cosrev.2017.10.002>
- [14] J. Serrano-guerrero, J. A. Olivas, F. P. Romero, and E. Herrera-viedma. Sentiment analysis: 'A review and comparative analysis of web services'. *Information Sciences*, vol. 311, pp. 18–38, 2015. <https://doi.org/10.1016/j.ins.2015.03.040>
- [15] M. Birjali, M. Kasri, and A. Beni-Hssane. 'A comprehensive survey on sentiment analysis: approaches, challenges and trends. Knowledge-Based Systems', 226:107134. 2021. <https://doi.org/10.1016/j.knosys.2021.107134>
- [16] P. Ray, A. Chakrabarti. 'A Mixed approach of Deep Learning method and Rule-Based method to improve Aspect Level Sentiment Analysis', *Applied Computing and Informatics*, vol. 18, no. 1/2, pp. 163-178. 2022. <https://doi.org/10.1016/j.aci.2019.02.002>
- [17] Q. T. Ain, M. Ali, A. Riaz, A. Noureen, M. Kamran, B. Hayat, and A. Rehman. 'Sentiment Analysis Using Deep Learning Techniques: A Review'. *International Journal of Advanced Computer Science and Applications*, vol. 8, no. 6, pp. 424–433. 2017.
- [18] M. Day and C. Lee. 'Deep learning for financial sentiment analysis on finance news providers'. *IEEE/ACM International Conference on Advances in Social Networks Analysis and Mining (ASONAM)*, pp. 1127-1134. 2016.
- [19] H. Lu, L. Ehwerhemuepha, and C. Rakovski. 'A comparative study on deep learning models for text classification of unstructured medical notes with various levels of class imbalance', *BMC Medical Research Methodology*, 22:181, 2022. <https://doi.org/10.1186/s12874-022-01665-y>
- [20] N. O. Adedokun. 'Sentiment Analysis with Deep Learning Techniques', A Master Degree Thesis, Faculty of Science, National Open University of Nigeria, Abuja, Nigeria. 2023.
- [21] X. Qiu, T. Sun, Y. Xu, Y. Shao, and X. H. Ning Dai. 'Pre-trained Models for Natural Language Processing: A Survey'. *Science China Technological Sciences*, vol. 63, no. 10, pp. 1872–1897. 2020. <https://doi.org/10.1007/s11431-020-1647-3>
- [22] D. Mumtaz, and B. Ahuja. 'A Lexical and Machine Learning-Based Hybrid System for Sentiment Analysis'. *Innovations in Computational Intelligence*, vol. 713. Springer, Singapore. 2018. [https://doi.org/10.1007/978-981-10-4555-4\\_11](https://doi.org/10.1007/978-981-10-4555-4_11)
- [23] M. Ahmad, S. Aftab, I. Ali, and N. J. Hameed. 'Hybrid tools and techniques for sentiment analysis: a review'. *Int. J. Multidiscip. Sci. Eng.* Vol. 8, no. 3, pp. 29-33. 2017.
- [24] S. Khan, K. Chopra, and V. Malviya. 'Sentiment Analysis based on Hybrid Approach: A Survey'. *Proceedings of Recent Advances in Interdisciplinary Trends in Engineering & Applications (RAITEA) 2019*, 2019. <http://dx.doi.org/10.2139/ssrn.3370100>
- [25] S. Mendon, P. Dutta, A. Behl, and S. Lessmann. 'A hybrid approach of machine learning and lexicons to sentiment analysis: Enhanced insights from twitter data of natural disasters'. *Information Systems Frontiers*. Vol. 23, pp. 1145–1168. 2021. <https://doi.org/10.1007/s10796-021-10107-x>
- [26] M. K. Bashar. 'A Hybrid Approach to Explore Public Sentiments on COVID-19'. *SN Computer Science*. Vol. 3, no. 220. 2022. <https://doi.org/10.1007/s42979-022-01112-1>
- [27] S. A. Rauf, Y. Qiang, S. B. Ali, and W. Ahmad. 'Using BERT for Checking the Polarity of Movie Reviews'. *International Journal of Computer Applications*, vol. 177, no. 21, pp. 37–41, 2019. <https://doi.org/10.5120/ijca2019919675>
- [28] X. Gong, W. Ying, S. Zhong, and S. Gong. Text Sentiment Analysis Based on Transformer and Augmentation. *Frontiers in Psychology*, vol. 13, (May). 2022. <https://doi.org/10.3389/fpsyg.2022.906061>
- [29] S. K. Bharti, S. Varadhaganapathy, R. K. Gupta, P. K. Shukla, M. Bouye, S. K. Hingaa, and A. Mahmoud. 'Text-Based Emotion Recognition Using Deep Learning Approach'. *Comput Intell Neurosci*. 2645381. 2022. <https://doi.org/10.1155/2022/2645381>
- [30] M. A. Paredes-Valverde, R. Colomo-Palacios, M. P. Salas-Zárate, and R. Valencia-García. 'Sentiment Analysis in Spanish for Improvement of Products and Services: A Deep Learning Approach, Hindawi Scientific Programming', vol. 2017, <https://doi.org/10.1155/2017/1329281>
- [31] W. Souma, I. Vodenska, and H. Aoyama. 'Enhanced news sentiment analysis using deep learning methods'. *Journal of Computational Social Science*. vol. 2, no. 1, pp. 33-46. 2019.
- [32] V. K. C. Mula, L. Kumar, L. B. Murthy, and A. Krishna. 2022, 'Software Sentiment Analysis using Deep-learning Approach with Word-Embedding Techniques'. In *2022 17th Conference on Computer Science and Intelligence Systems (FedCSIS)*, pp. 873-882. IEEE. 2022. <https://doi.org/10.1155/2017/1329281.15439/2022F138>
- [33] L. Chen, Z. Qiao, M. Wang, C. Wang, R. Du, and H. E. Stanley. 2018. 'Which artificial intelligence algorithm better predicts the Chinese stock market'. *IEEE Access* 6:48625–48633, 2018. <https://doi.org/10.1109/ACCESS.2018.2859809>.
- [34] M. A. Rangila, S. Khandke, Y. Mohite, and K. Kamble. 'Sentimental Analysis using Bert Algorithm over LSTM'. *International Journal of Advanced Research in Science, Communication and Technology (IJARSCT)*, vol. 2, no. 1, pp. 455–459. 2022. <https://doi.org/10.48175/IJARSCT-7300>
- [35] N. J. Prottasha, A. As Sami, M. Kowsher, S. A. Murad, A. K. Bairagi, M. Masud, and M. Baz. 'Transfer Learning for Sentiment Analysis Using BERT Based Supervised Fine-Tuning'. *Sensors*, vol. 22, no. 4157, 2022. <https://doi.org/10.3390/s22114157>
- [36] P. Malo, A. Sinha, P. Korhonen, J. Wallenius, and P. Takala. 'Good debt or bad debt: Detecting semantic orientations in economic texts'. *Journal of the Association for Information Science and Technology*, vol. 65, no. 4, pp. 782-796. <https://doi.org/10.1002/asi.23062>



## RESEARCH ARTICLE

## OPEN ACCESS

# STATE FUNCTION $\Phi(U,E,t)$ : CONNECTION OF ADVECTION, DISPERSION AND TURBULENCE IN NATURAL STREAMS AT DYNAMIC EQUILIBRIUM

\*Alfredo Constain A.<sup>1</sup>, and Julian Ramos S.<sup>2</sup>

<sup>1</sup> Researcher, Fluvia SAS. Bogotá, Colombia.

<sup>2</sup> CEO, Fluvia SAS. Bogotá, Colombia.

<sup>1</sup><http://orcid.org/0000-0001-6542-0715> , <sup>2</sup><http://orcid.org/0009-0000-1537-7829> 

Email: <sup>1</sup>[alfredo.constain@gmail.com](mailto:alfredo.constain@gmail.com)\*, <sup>2</sup>[julianramos@fluvia.com](mailto:julianramos@fluvia.com)

## ARTICLE INFO

**Article History**

Received: February 27<sup>th</sup>, 2024

Revised: July 08<sup>th</sup>, 2024

Accepted: July 08<sup>th</sup>, 2024

Published: July 18<sup>th</sup>, 2024

**Keywords:**

Hydrometrics,  
Dynamic Equilibrium,  
Irreversible thermodynamics,  
Linear thermodynamics,  
State functions.

## ABSTRACT

The Navier-Stokes equation has been a standard of calculus in hydrodynamics; however, its conceptual and computational problems make it necessary to look for better alternatives. One of the causes of this failure is that it is a "reductionist" model, which does not involve the emergence of new laws at other scales. In this article, a different model is presented in detail, based on a State Function, with clear advantages, since it involves mechanisms at all levels, respecting the principle of "breaking temporal symmetry", according to irreversible thermodynamics.



Copyright ©2024 by authors and Galileo Institute of Technology and Education of the Amazon (ITEGAM). This work is licensed under the Creative Commons Attribution International License (CC BY 4.0).

## I. THE PROBLEM OF CLASSICAL DYNAMICS AND THE NAVIER-STOKES EQUATION

### I.1 SOME LIMITATIONS OF THE NAVIER-STOKES APPLICATION

A classic theme in hydraulics and fluid mechanics is the difficulty of understanding and solving problems and calculations related to turbulence flows from nonlinear differential equations, such as the Navier-Stokes equation, to describe the motion of a viscous fluid, which is usually used, with great limitations [1].

$$\rho \left( \frac{\partial v}{\partial t} + v * \nabla v \right) = -\nabla p + \nabla * \tau + f \quad (1)$$

This equation is a developed version of Newton's 2nd law, since the left member is the acceleration of a very small region of fluid moving in the flow, and the right member is the sum of the forces that create that acceleration. Here " $\rho$ " is the density of the liquid, " $v$ " is the velocity of the region, " $p$ " is the pressure, " $\tau$ " is the tangential frictional stress on the surface of the region, and " $f$ "

is the internal forces of the bodies [2]. Although versions of these equations developed in numerical methods are currently used, their application is not general due to limitations outlined below.

A first problem arises regarding the "smallness" of the region of the fluid under consideration, since it cannot be very large, since the nature of the differential equation used fails, since the concept of "limit" involves smaller and smaller regions; But it cannot be infinitely small, because the fluid is not ideally "continuous" (infinitely divisible and homogeneous), making it difficult to establish how far this equation can represent turbulence, which is composed of increasingly large whirlwinds [3].

A second problem, but not the least difficult, is that its mathematical nature is non-linear, which implies an analytical difficulty, since there are currently no general methods for its resolution, and because in the conceptual part, this mechanism is based on feedback loops in which cause, and effect are intermingled. According to [4],[5] making It virtually impossible to separate them.

A third problem, equally significant, is that the new dynamics of irreversible processes [6],[7] postulate that the



"trajectories" of bodies in the space of phases collapse into massive irreversible systems. This effect derives from the interpretation of mechanical interactions as coupling "degrees of freedom" associated with Fourier frequencies [8].

In these cases, the interaction of these degrees of freedom can become "resonant", implying "very small" divisors, which lead to the destruction of the trajectories considered, which tend to infinity. Figure 1.

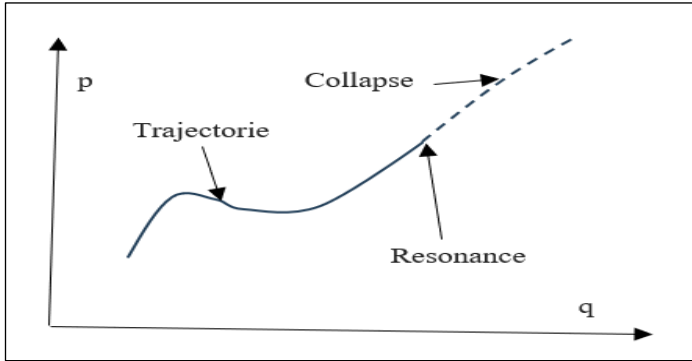


Figure 1: Trajectories in the space of phases. Source: Authors, (2024).

While it is true that the mechanical description of motions in a turbulent fluid is impossible in terms of trajectory, it is possible to define it in statistical terms, by means of "probability distributions",  $\rho$ , which are the only elements of physical description that survive the absence of "computability" in these chaotic systems.

This paradigm shift is not minor because the dynamics of "distributions" are oriented in time, microscopically coinciding with the rupture of the temporal symmetry that is observed macroscopically.

### 1.2 OPEN SYSTEMS AND PROCESSES OF DYNAMIC EQUILIBRIUM.

Real physical bodies are open systems in that they receive and expel energy and substance from and outward. Depending on this balance, an open system, close to equilibrium, promotes processes of "Dynamic Equilibrium" in which the system achieves "stable states" of quasi-equilibrium in Figure 2.

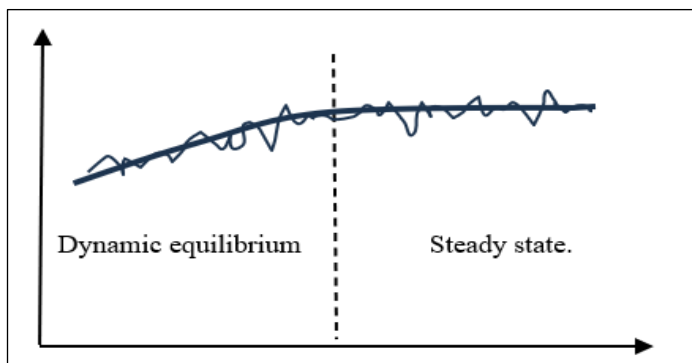


Figure 2: Open systems seeking a "stable state" with quasi-equilibrium. Source: Authors, (2024).

Small variations in state variables are random distributions of a Markovian nature, in that they represent a drift towards more probable states, i.e., their mean value evolving with an "arrow of time".[9][10]. The representation of this mean value is a deterministic "pattern" of the evolution of these real systems, and

together with the fluctuations, they represent a single facet of the process of "Dynamic Equilibrium" in Figure 3.

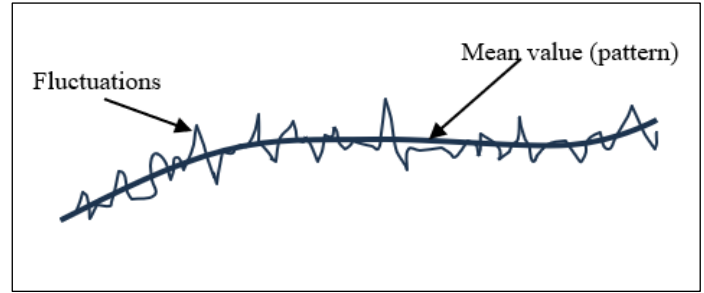


Figure 3: Fluctuations and mean value as an indivisible part of the process of "Dynamic Equilibrium". Source: Authors, (2024).

As long as the Navier-Stokes equation corresponds to some degree to the type of motion described by "trajectories," and its application does not correspond to an irreversible, time-oriented process, its application to the practical problems of fluid mechanics will be very limited.

## II. CONDICIONES PARA UNA DESCRIPCION COMPLETA EN DINAMICA FLUVIAL

### II. 1. MORE IS DIFFERENT", A NEW PARADIGM IN MODERN SCIENCE

The "intelligibility" of nature, according to the philosopher A.N. Whitehead, [11] results as a product of a system of general ideas, which is necessary, logical, coherent, in which the function of all the elements of experience can be interpreted.

In this context, the centuries-old scientific paradigm of "Reductionism" had remained unquestioned, [12] in which understanding the world was possible only by understanding its most basic parts. For example, by understanding atoms, it was possible to understand chemistry and hence the very essence of life.

This fallacy, which ignored some difficulties inherent in contemporary science, was brought to the fore by Nobel laureate A.P. Anderson in 1973 with his hypothesis: "More is different", [13],[14] in which, due to the breaking of temporal symmetry, a new hierarchy appears in nature, an "Emergence" of new physical facts at each level of reality.

Thus, for example, even if the balance of forces and acceleration effects in a very small plot of a fluid under turbulence conditions were described in great detail, it was not possible to anticipate feedback mechanisms, which appearing at a second level, not explicitly described in the Navier-Stokes equation, would greatly disturb the fidelity of the model in relation to experimental reality.

### II.2. "STEADY STATES" FOR OPEN RIVER SYSTEMS

In an isolated system (without any interaction with the outside), over time, the energy is distributed homogeneously throughout the system, reaching a limiting thermal equilibrium (single, equal temperature at all points of the system). This limit equilibrium is characterized by a maximum of entropy. ( $S \rightarrow \max$ ).

In a closed system (which only exchanges energy with the environment, but no substance), these exchanges of energy with the outside can define a given equilibrium, in which the temperature no longer varies ( $T \approx Cte$ ).

$$F \approx E - T * S \tag{2}$$

This system varies between the predominance of an "energetic" scheme ( $E > T \cdot S$ ), or an entropic scheme ( $T \cdot S > E$ ). At low temperatures, an "orderly" system (Crystal like) predominates, while at medium temperature there is a mixture of order and disorder (liquid like), and at high temperature "disorder" (gas like) predominates.

In an open system (which exchanges energy and substance with the environment) different components of entropy must be identified:

$$dS \approx diS + deS \quad (3)$$

The total entropy,  $S$ , is the algebraic sum of the entropy produced within the system by irreversible (loss) processes,  $diS$ , and of the entropy entering or leaving the system,  $deS$ , from and out in Figure 4.

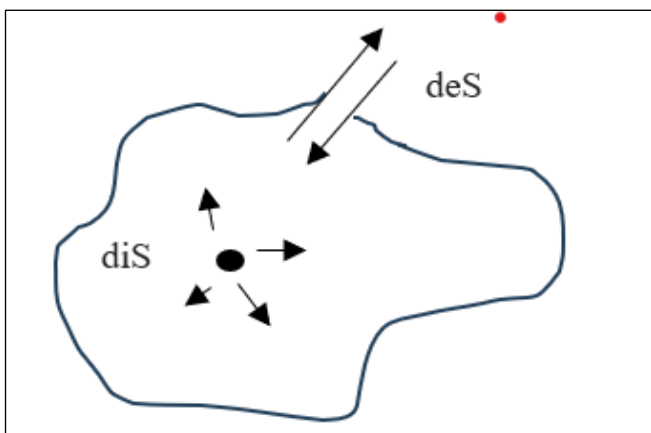


Figure 4: Open systems. Source: Authors, (2024).

In this case the equilibrium is a steady state that corresponds to the "Minimum Entropy Output",  $P \approx diS/dT$ , although the total entropy,  $S$ , is also a relative maximum. Depending on the balance between the internal and the external, the production of entropy and entropy will have larger or smaller sizes (dotted line) in Figure 5.

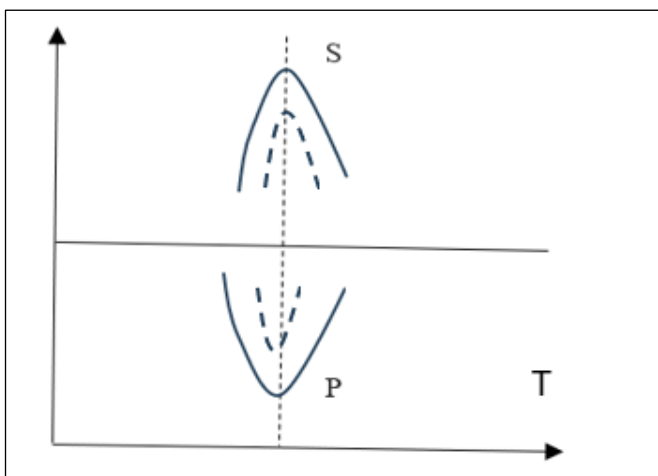


Figure 5: Open systems. Source: Authors, (2024).

River systems are, of course, open systems, in which entropy maximums will be presented, depending on the balance between what is produced inside and what is exchanged with the

outside. The most direct manifestation of the entropy condition in this type of system is the so-called "Granulation Volume", or "Coarse Grain Volume", which is defined by the Boltzmann equation:

$$S \approx k * \ln(W) \approx k * \ln(V) \quad (4)$$

Here  $k$  is Boltzmann's constant,  $W$  is the number of microstates indistinguishable from the energy of the system, and  $V$  is the volume of the macrostate, which is observed with an instrument. This volume is identified as the "Coarse Grain" which defines the stable state of the system. For maximum entropy you will have a certain volume of "coarse granules". In the riverbed, the size of these granulation zones will be larger or smaller, depending on the balance, in the channel under consideration. Figure 6 [15],[16].

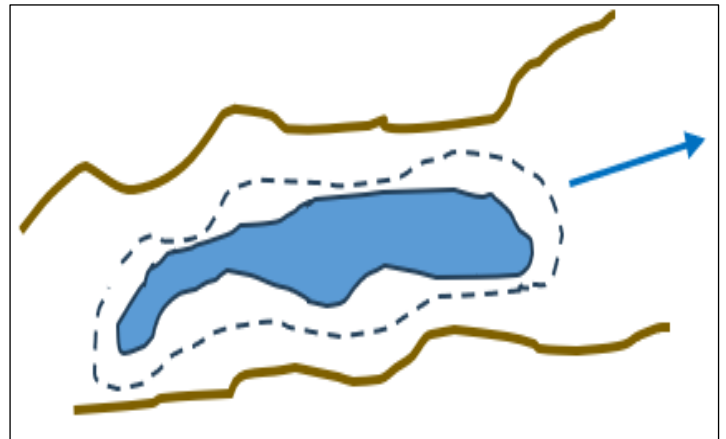


Figure 6: Variable granulation zones depending on the balance. Source: Authors, (2024).

### II.3 "LINEAR" REGION FOR IRREVERSIBLE THERMODYNAMICS APPROXIMATION FOR NATURAL FLOWS, AND INTERMITECIES DUE TO LACK OF PERFEC "LINEAR" REGIME.

"Linear" regime is defined as the thermodynamic region close to equilibrium [17], region in which thermodynamic forces and flows are proportional to each other. A thermodynamic force is basically a gradient of gravitational, electrical, or thermal potential, which originates a flow of charge, mass, electric charge, or heat. In this regime the forces are weak, and so the flows [18].

When you have this regime, the entropy production is minimal, and the entropy is maximum, i.e., the volume of "coarse grain" is maximum, compatible with the balance at the boundary of the system. Applying the criterion of proportionality between thermodynamic flow and force for a natural flow, [19] it is approximately necessary that:

$$U \sim \frac{dH}{ax} \approx S \quad (5)$$

But according to the Chezy-Manning equation, the velocity is proportional to the square root of the Slope.

$$U \sim \sqrt{S} \quad (6)$$

An analysis of the "non-linearity" of the above equation, for specific typical cases, yields percentages of approximately 15%, using Taylor-MacClaurin serial analysis [20]. Now, the net effect of not complying with a perfect "linearity" is that the coarse granularity zone is not perfect either, in the sense that it has

randomly distributed "patches" that correspond to different macro states, which are detected as "intermittencies" with the instruments. Figure 7.

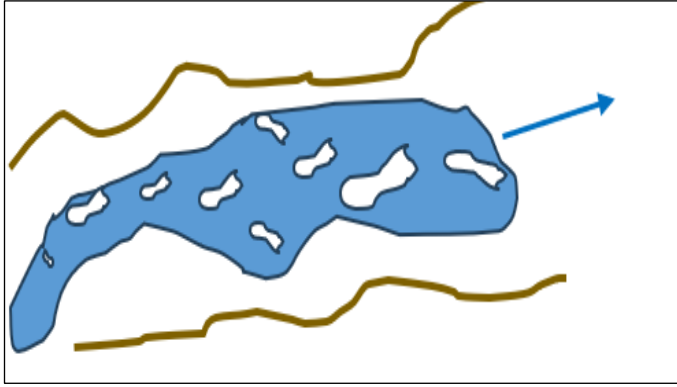


Figure 7: Intermittency of coarse granules.  
Source: Authors, (2024).

These intermittencies are reflected as fluctuations in the measurements of the state parameters, characterized by larger "variances".

### III. CONDITIONS FOR AN ALTERNATIVE SOLUTION TO RIVER DYNAMICS: A DISCUSSION ON NATURE OF STATISTICAL DISTRIBUTIONS.

#### III.1 MARKOVIAN MODEL FOR DESIRED DISTRIBUTION.

A proposal for a successful methodology that can replace the Navier-Stokes equation in contemporary hydrometry must meet the requirements that Whitehead has imposed on the method that contains generality, logical coherence, and correspondence with all aspects of experimental making.

The first thing to analyze is the general nature of the type of probabilistic distribution to be considered, its nature and the consequences of its application to river dynamics, in particular it is necessary to establish two basic ideas on which to build the desired model:

The model must respond to the principle of the "Detailed Balance", in such a way that the transitions, from left or right, of the most probable value- mean value-are equivalent (Gaussian model).

B.- That the Distribution responds to the fact that the macroscopic observation tends to its most probable value, and that the fluctuations correspond to localized events, close to that value, and have very small magnitudes and times, with random occurrence.

These conditions are fulfilled by the so-called Markov Process, in which the "memory" of the successive transitions is lost, except for the last one. This probabilistic process, although totally random, shows an evolution in only one temporal direction. Since the actual processes in the "linear" region of irreversible thermodynamics are dissipative and if they correspond to a Markovian process, it must be compatible with the increase of entropy to the stationary value, in Figure 5 [21],[22]. In this case, if the entropy reaches a relative maximum peak,  $dS \approx 0$ , then  $diS \approx -deS$ , and the system transfers entropy to the outside.

If we now reinterpret Figure 3, which shows the evolution of an open system (the turbulent flow) towards the "steady state", allowed by the thermodynamic (energy and substance) bonds with the outside, we can draw the following, showing how the statistical evolution of the dynamics is applied to the turbulent flow in Figure 8.

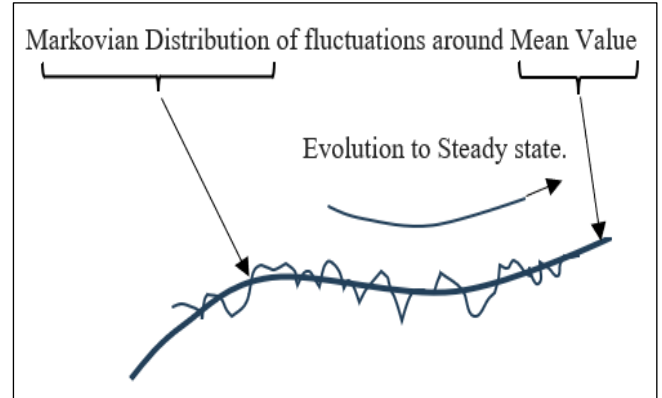


Figure 8: Nature of evolution toward "Steady state" in a turbulent flow.

Source: Authors, (2024).

#### III.2 ERGODIC NATURE OF THE MARKOVIAN DISTRIBUTION IN FLOW.

If we consider that a Markovian process is basically a Gaussian one, essentially linked to the theorem of the Central Limit, and that this process is prevalent in many fields of physics, important theorems of linear transformation have been defined [23]. One of which is the Ergodic theorem, in which the time function linked to evolution has, for long times, the same spatio-temporal statistical characteristic for various "samples" (measurements) that are taken.

Figure 9 shows an ergodic "band" in which the measurements will have a similar value, in "Steady state" condition. The definition of this band depends on the "mathematical expectation" of the stationary random function remaining constant for different measurements in that band, which occurs for sufficiently long times in which the randomness of the distribution is manifested [24].

An example of this situation is Prandtl's lateral velocity distribution, which is almost flat, along the width of the river [25].

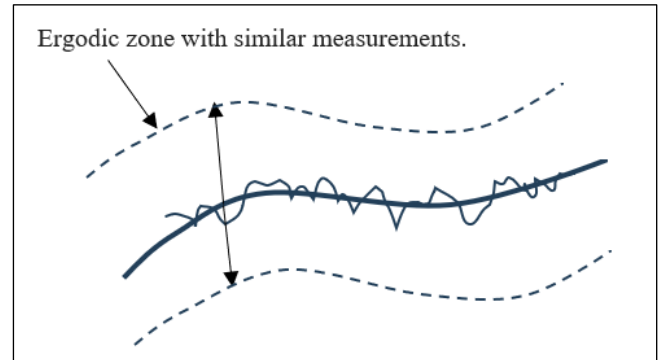


Figure 9: Ergodic zone with similar value of measurements.

Source: Authors, (2024).

#### III.3 ANALISIS DE FUNCIONES DE ESTADO COMO UNA POSIBLE SOLUCION

State functions are mathematical entities that connect states of a system by varying their state parameters, which are variables that depend only on their "internal physical condition" in relation to the process, defining it univocally, and that does not depend on any concept of microscopic structure [26],[27]. Its mathematical definition, in a flow for example,  $\Phi(U,E,t)$  is based on the fact that if an open system that evolves in a turbulent flow has as state parameters: U, E, and also evolves over time, a total differential is configured, as follows:

$$U = g(\Phi), E = w(\Phi) \text{ and } t = h(\Phi) \quad (7) \quad \text{and:}$$

and:

$$d\Phi = \left(\frac{\partial\Phi}{\partial U}\right) dU + \left(\frac{\partial\Phi}{\partial E}\right) dE + \left(\frac{\partial\Phi}{\partial t}\right) dt \quad (8)$$

This expression indicates that the state function,  $\Phi(U,E,t)$ , depends only on the start and end points, i.e. it is a "point" function, not a "process" function, which depends on the path followed, according to the Schwartz condition [28].

$$\oint d\Phi = 0 \quad (9)$$

Now, the fact that state functions depend only on start ( $\Phi A$ ) and end points ( $\Phi B$ ) excludes the problem of collapsing trajectories, which are "process" events, essentially in Figure 10.

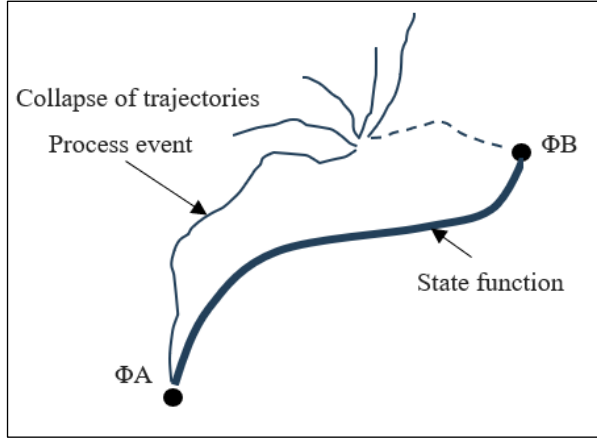


Figure 10. The state function excludes collapsed paths (process events).

Source: Authors, (2024).

On the other hand, this state function is associated as an average value with the Markovian distribution in Figure 8 and respects the basic fact that it is time oriented.

#### IV. A STATE FUNCTION THAT GUIDES THE EVOLUTION OF THE FLOW IN TURBULENCE.

It will be shown in this section that although tracers are used as marker substances to measure movement with instruments, in reality the state function that will be defined will describe in its final segment the evolution of turbulence itself.

##### IV.1 THE EVOLUTION OF STATE FUNCTION: HOW TO DEFINE AND APPLY IT

The authors have presented an equation for the average flow velocity, based on dispersive forces of an electrical nature (Van der Waals), with a structure similar to the classical Chezy-Manning equation, based on mechanical interactions. [29].

$$U \approx \frac{1}{\phi} \sqrt{\frac{2 \cdot E}{\tau}} \quad (10)$$

Table 1 shows below approximate typical values of " $\gamma$ " for different types of tracers and different streams.

Table 1: Typical (approx.) values of  $\gamma$  for diverse kind of tracers and streams. Source: Authors.

Tracer	Condition of stream	" $\gamma$ " Approx. Mean value
'Radioactive (Cl3Au-198)	Q $\approx$ 8.2 m3/s, L $\approx$ 1.7 Km	<9351>
Fluorescein	Q $\approx$ 97 L/s, L $\approx$ 43 m	<123>
RWT	Small Creek, Q $\approx$ 40 L/s., L $\approx$ 23 m	<2162>
Saline (NaCl)	Small Creek, Q $\approx$ 40 L/s., L $\approx$ 23 m	<1301>

Source: Authors, (2024).

$$U \approx \frac{R^{\frac{2}{3}}}{n} \sqrt{S} \quad (11)$$

In the unidirectional equation (10), E is the longitudinal coefficient of dispersion, and " $\tau$ " is a characteristic time of the self-replicating process, and is worth:

$$\frac{t}{\tau} \approx \delta \approx 4.6692 \quad (12)$$

Here " $\delta$ " is the chaotic period doubling, and it is actually the hallmark of the Gaussian nature of the process, since this remarkable number, initially discovered by [30], derives from the mean value of Brownian dynamics, studied at the beginning of the 20th century by [31] but placed within a unimodal scheme of the natural growth model (logistic curve). Svedberg found that the mean value of the distribution of colloidal particles in fluid media (ultracentrifuge) was described by the Poisson model, with an average concentration value  $\langle C(t) \rangle \approx 1.54$ . Therefore, the growth rate in the logistics curve, for Brownian distribution, is:

$$r(t) \approx e^{\frac{1}{T} \int_0^T c(t) dt} \approx e^{1.54} \approx 4.6692 \quad (13)$$

Since this logistic curve is a universal model of growth, it of course applies to the self-similarity conformation of Brownian motion and is thus the basis of equation (12).

$$r(t) \approx \frac{t}{\tau} \approx 4.6692 \quad (14)$$

Ahora, volviendo a la descripción de la aplicación de la función de estado al caso fluvial, for classical equation (11), "R" is the hydraulic radius, "n" is the Roughness coefficient, and "S" is the Slope of the flow. If we equate the two definitions of speed, we have that:

$$\Phi \approx \frac{n}{R^{\frac{2}{3}}} \sqrt{\frac{2E}{S}} \quad (15)$$

In this way, the geometric and geomorphological parameters can be set as a function of the State Function, i.e., we have a complete fluvial description from  $\Phi(U,E,t)$ . The state function can be approximately defined at  $tp$  (peak time) as: [32].

$$\Phi \approx \frac{M}{Q \cdot \gamma^{1.16}} * \frac{1}{\sqrt[3]{tp}} \quad (16)$$

Here,  $M$  is the mass of tracer injected,  $tp$  is the peak time of tracer curve, and  $\gamma$  is a characteristic parameter of each solute used, and which must be calculated experimentally, with " $Cp$ " as peak concentration of tracer in measurement point.:

$$\gamma \approx \frac{Cp(tp)}{tp^{-\frac{2}{3}}} \quad (17)$$

#### IV.2 THE NATURE OF STATE FUNCTION: ITS RELATIONSHIP WITH THE PHYSICO-CHEMICAL PROCESSES THAT OCCUR TO THE SOLUTE IN THE FLOW

Once the solute is suddenly injected into the flow there is an interaction between the water (dipoles) and the ions of the compound, then the solute diffuses and there is an interaction between the ions of the latter, this occurs until it can be considered a gas, which is considered very rarefied, which occurs when  $\Phi \approx 0.38$ , the point at which all the mass is homogeneously "available" in the cross-section of the tracer flow tube.

At this point, the tracer is considered to have all but lost its identity, and the instrument's measurements actually capture the turbulent motion of the water. The dispersion (diffusion) being measured, which originally corresponded to the tracer, in this last phase now corresponds to the mixing movements (self-diffusion) of the water in turbulence [33] in Figure 11.

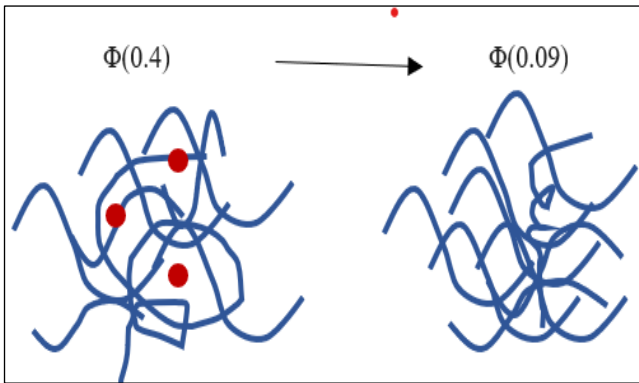


Figure 11: State function measuring turbulence, with or without tracer particles.  
Source: Authors, (2024).

Then, it can be established that  $\Phi(t)$  evolves as shown in Figure 11.

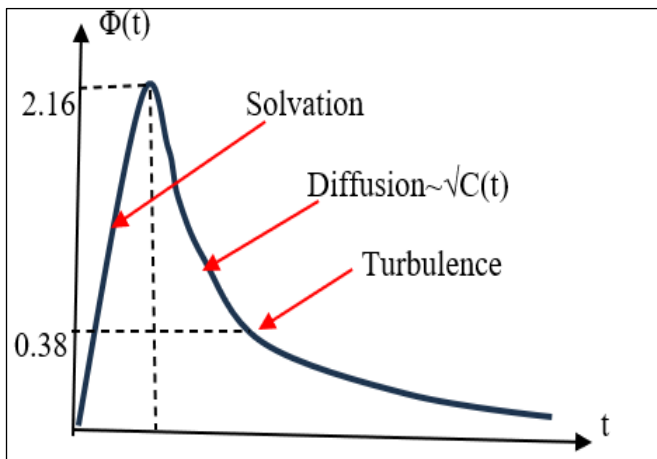


Figure 12: Evolution of State function  $\Phi(t)$ .  
Source: Authors, (2024).

The steep segment of curve (up to  $\Phi \approx 2.16$ ) corresponds to the "solvation" process of the solute. The smooth decaying segment corresponds to the evolution of the ions, which diffuse until at  $\Phi \approx 0.38$ , almost all of them are in the gas phase, and  $\Phi(t)$  is considered to describe the turbulent evolution of the flow itself in Figure 13.

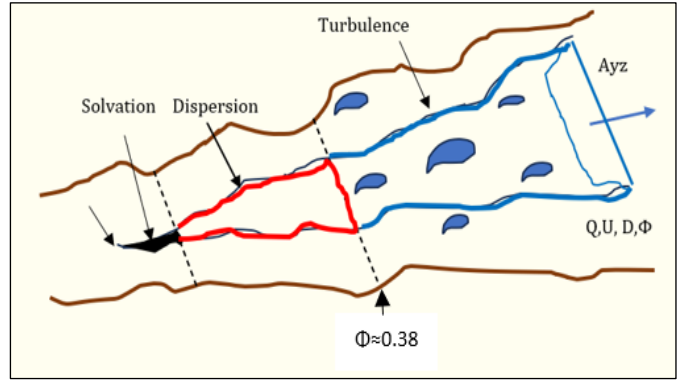


Figure 13: urbulence described by a State function  $\Phi(t)$ .  
Source: Authors, (2024).

This aspects is of great importance for fluvial engineering, because with this method it is possible to estimate values of state parameters at distant sites in the flow, without having to inject large amounts of tracer with a serious threat to the environment of the ecosystem. Figure 14.

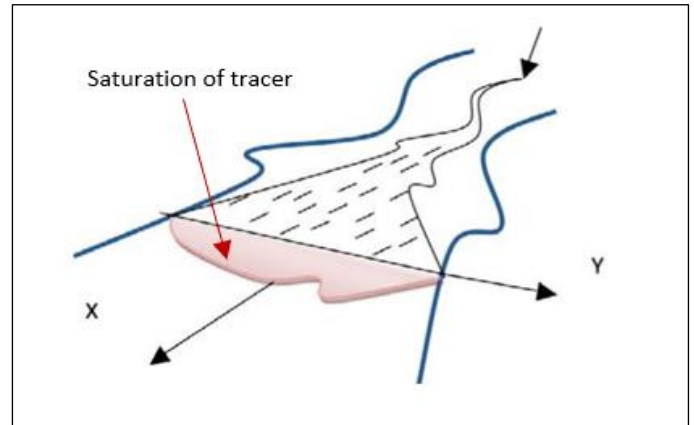


Figure 14. Saturation of tracer in state-of-the art methods.  
Source: Authors, (2024).

#### IV.3 PLANNING FLUVIAL EXPERIMENTS USING THE STATE FUNCTION METHOD

The application of the State Function method to fluvial research allows not only to obtain information with greater scientific content, but also allows the experimenter to simplify monitoring tasks as he must use much less tracer mass, with the consequent environmental preservation. Monitoring is primarily based on selecting a representative section of the channel and, once the conservative solute has been injected, making measurements at two sequential sites separated by a distance proportional to the width of the flow. With these two fluorescent tracer curves (Fluorescein or Rhodamine WT) the two values of  $\Phi(t)$  are established and the projection can then be made at much greater distances, if we start from the assumption that this section of the flow is at "Dynamic equilibrium". This condition is approximately verified by the observations of flow and slope constancy. Here " $P_i$ " is the point of injection of the solute, " $E_1$ " and " $E_2$ " are the two points of the experimental measurement with fluorometers, and " $P_m$ " is the point of projection of the value of  $\Phi_m(t)$ , based on the two values of this function in the previous points. Based on this data, it is possible to obtain all the information of interest for hydrometry or modelling in Figure 15.

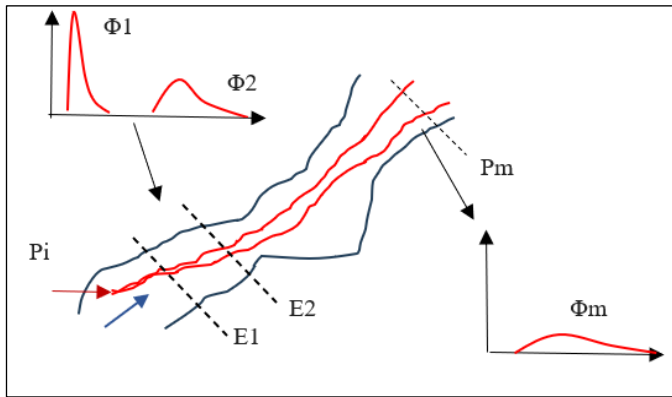


Figure 15: Two tracer measurements to obtain a sequence of State function  $\Phi(t)$ .  
Source: Authors, (2024).

It should be noted that it is not necessary to make "injections at the center", as is the optimal requirement in classical methodologies, since the State Function reflects the objective conditions of the injection, including longitudinal and cross-sectional variables [34].

## V. CONCLUSIONS

1.- The basic characteristics of natural channels are established, as open systems, evolving in the condition of "Dynamic Equilibrium". This condition is established as resulting from fluctuations and a mean value, which have statistical characteristics compatible with the Gaussian nature and the principle of temporal symmetry breaking. (Markovian distribution).

2.-The description of phenomena as complex as turbulent flow requires the concurrence of multiple concepts, in such a way that the description is as complete as possible. The current level of knowledge of hydrodynamics is limited by the fact that its theoretical approach is usually limited to the representation of the evolution of phenomena by means of non-linear differential equations, which give only "local" information, which is difficult to interpret and handle analytically, because it is a very difficult to interpret and manipulate analytically, because it is a "reductionist" theory, limited only to the most basic levels of reality.

3.- Opposing, "emerging" models, which draw attention to the impossibility of solving problems of interpretation at various scales, must be based on "non-local" mechanisms, which include different but congruent parts of reality, as A.N. Whitehead demands.

4.- The description of the evolution of hydrodynamics is traditionally done by means of a "reductionist" theory of the "Navier-Stokes" type, which shares the limitations and difficulties of this type of model. A model that solves these problems must be a "non-local" one, which also involves the developments of irreversible thermodynamics, close to equilibrium.

5.- The authors present here an "emergent" model of the "State Function" type, which eliminates the problems identified in the resolution of hydrodynamic designs with existing theories.

## VI. AUTHOR'S CONTRIBUTION

**Conceptualization:** Alfredo Constain A and Julian Ramos S.

**Methodology:** Alfredo Constain A and Julian Ramos S.

**Investigation:** Alfredo Constain A and Julian Ramos S.

**Discussion of results:** Alfredo Constain A and Julian Ramos S.

**Writing – Original Draft:** Alfredo Constain A and Julian Ramos S.

**Writing – Review and Editing:** Alfredo Constain A and Julian Ramos S.

**Resources:** Alfredo Constain A and Julian Ramos S.

**Supervision:** Alfredo Constain A and Julian Ramos S.

**Approval of the final text:** Alfredo Constain A and Julian Ramos S.

## VII. REFERENCES

- [1] Stewart I. "¿Juega Dios a los dados?". Grijalbo-Mondadori. Barcelona, 1996.
- [2] Stewart I. "17 ecuaciones que cambiaron el mundo". Critica, Barcelona. 2013.
- [3] Stewart I. Ibid, 1996.
- [4] Annala A. & Makela T. Natural patterns of energy dispersal. Physics of life rev. 7PP 477-498. 2010.
- [5]-Annala A.& Ketto J. The capricious character of nature. Life ,ISSN 2075. 2012.
- [6] Prigogine I. ¿Tan solo una ilusión?, Matema- Tusquets, Barcelona. 1997.
- [7] Kondepudi D.& Prigogine I. Modern thermodynamics. From heat engines to dissipative structures. Wiley. New York., 1999.
- [8] Prigogine I. El fin de las certidumbres. Aguilar. Bogotá. 2001.
- [9] Prigogine I. Las leyes del caos. Critica, Barcelona. 1999.
- [10] Nicolis G. & Prigogine I. La estructura de lo complejo. Alianza. Editorial. Madrid. 1997.
- [11] Prigogine I. Ibid. 2001.
- [12] Miller J. H. A crude look at the whole. Basic Books, New York, 2015.
- [13] Anderson P.W. Moore is different. Science. Vol. 117. 1972.
- [14] Anderson P.W. Basic notions of condensed matter physics. Amazon. Finley Editor, Princeton. 2018.
- [15] Langbein W.B. The hydraulic geometry of shallow estuary. Hyd. Sci. J. 8: 3, pp 84-94. 2009.
- [16] Langbein W. & Leopold L. Quasi-equilibrium states in channel morphology. USGS. Vol 262. P782-794. 1964.
- [17] Kondepudi D.& Prigogine I. Ibid. 1999.
- [18] Prigogine I. Ibid. 1997.
- [19] Constain A. The svedberg number 1.54, as the basis of a State function describing the evolution of turbulence and dispersion. Intech Open, chapter of book. London. 2024..
- [20] Constain A. Ibid. 2024.
- [21] Nicolis G. & Prigogine I. Ibid. 1997.
- [22] Pugachev. V.S. Introducción a la teoría de las probabilidades. Editorial Mir. Moscú, 1973.
- [23] Nicolis G. & Prigogine I. Ibid. 1997.
- [24] Pugachev. V.S. Ibid. 1973.
- [25] Nekrasov. B. Hidraulica. Editorial Mir, Moscú, 1968.
- [26] Planck M. Treatise on thermodynamics. Dover. 1955.
- [27] Kirillin V.A., Sichev V.V. & Sheindlin A. Termodinámica técnica., Editorial Mir, Moscú. 1986.
- [28] Morowitz. H. Entropia para biólogos. Blume, Madrid. 1975.

[29] Constain A. Definición y análisis de una función de evolución de solutos dispersivos en flujos naturales. Dyna. No. 175. Medellín, 2012.

[30] Gleick J. *Caos: La creación de una ciencia*. Crítica. Barcelona. 2012.

[31] Constain A. *Ibid.* 2024.

[32] Constain A. *Ibid.* 2024.

[33] Frenkel J. *Kinetic theory of liquids*. Dover. 1955.

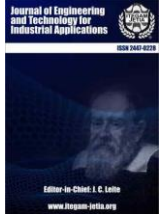
[34] Constain A. *Ibid.* 2024.



ISSN ONLINE: 2447-0228

# ITEGAM-JETIA

Manaus, v.10 n.48, p. 40-46. July/August., 2024.

DOI: <https://doi.org/10.5935/jetia.v10i48.1089>RESEARCH ARTICLE  
ACCESS





OPEN

## APPLICATION OF MACHINE LEARNING FOR THE PREDICTION OF ATMOSPHERIC CORROSION IN THE METROPOLITAN AREA OF MEXICO CITY

\*Ernesto Bolaños-Rodríguez<sup>1</sup>, Juan-Carlos González-Islas<sup>2</sup>, Omar López-Ortega<sup>3</sup> and Evangelina Lezama-León<sup>4</sup>

<sup>1,4</sup> Escuela Superior de Tizayuca-Universidad Autónoma del Estado de Hidalgo. Carretera Federal Tizayuca-Pachuca Km 2.5. 43800. Tizayuca, Estado de Hidalgo, México.

<sup>2,3</sup> Instituto de Ciencias Básicas e Ingeniería-Universidad Autónoma del Estado de Hidalgo. Pachuca-Tulancingo Km. 4.5, Carboneras, 42184, El Álamo, Mineral de la Reforma, Estado de Hidalgo, México.

<sup>1</sup><http://orcid.org/0000-0002-1432-7720> , <sup>2</sup><http://orcid.org/0000-0002-2190-0660> , <sup>3</sup><http://orcid.org/0000-0001-9713-1370>   
<sup>4</sup><http://orcid.org/0000-0003-0818-0897> 

Email: <sup>1</sup>[ebolanos@uaeh.edu.mx](mailto:ebolanos@uaeh.edu.mx)\*, <sup>2</sup>[juan\\_gonzalez7024@uaeh.edu.mx](mailto:juan_gonzalez7024@uaeh.edu.mx), <sup>3</sup>[lopezo@uaeh.edu.mx](mailto:lopezo@uaeh.edu.mx), <sup>4</sup>[evangeli@uaeh.edu.mx](mailto:evangeli@uaeh.edu.mx)

### ARTICLE INFO

#### Article History

Received: April 02th, 2024

Received: July 008th, 2024

Accepted: July 08th, 2024

Published: July 18th, 2024

#### Keywords:

Machine Learning,  
Prediction Methods,  
Atmospheric Corrosion,  
Regression,  
Mean Squared Error.

### ABSTRACT

In this work, Machine Learning (ML) is applied to predict atmospheric corrosion in the Metropolitan Zone of Mexico City. For this purpose, mass loss is measured as a dependent variable associated with the independent variables relative humidity, wetting time, temperature and sulfur dioxide deposition time in 12 stations of the study site and with the generated database. ML models are used with some supervised learning tools, such as: Neural Networks (NN), Regression Trees (RT), Optimized Regression Tree (ORT), Regression Ensemble (RE), Support Vector Machine (SVM) and Linear Regression (LR). For this problem, Neural Networks (NN) have the best results, with a Correlation Coefficient  $R^2 = 0.9814$  and a Mean Square Error  $MSE = 37.9$ . The main results allow us to determine that the proposed framework can be extended to predict the behavior of other complex problems.



Copyright ©2024 by authors and Galileo Institute of Technology and Education of the Amazon (ITEGAM). This work is licREed under the Creative Commons Attribution International LicREe (CC BY 4.0).

## I. INTRODUCTION

Corrosion is a process of loss of metallic materials by the action of aggressive agents through chemical or electrochemical reactions [1-2].

By its nature, the phenomenon of atmospheric corrosion is of the electrochemical type because the electrons of the atoms on the metal surface are transferred to an electron acceptor or depolarizer, which requires water to be the medium for ion transport. According to the International Organization for Standardization (ISO) standards, the corrosivity of steel ranges from very low to high depending on the environmental conditions of the area [3-5].

Atmospheric Corrosion is a complex multivariate and multidimensional phenomenon that affects many structures, equipment, and sectors [6]. The annual costs of corrosion in

Mexico are estimated to range from 3.5 to 4% of the Gross Domestic Product, causing not only large economic losses, but also harmful effects on human health that can lead to death and negative environmental impacts [7].

There are many processes where data are multidimensional, multivariable, large and noisy, making Machine Learning (ML) an adequate tool to analyze such processes. ML has gained popularity, and its algorithms are used in fields such as object detection, pattern recognition, text interpretation, segmentation, fraud detection, and marketing, among others [8]. Recently, ML has also been applied to complex phenomena given sufficient and appropriate data, giving potential solutions for the prediction of corrosion [9-10].

ML has proven useful in the development of predictive models to estimate corrosion loss [11]. For example, the atmospheric corrosion of carbon steel is predicted using



techniques such as Random Forest (RF), Artificial Neural Network (ANN) and Support Vector Regression (SVR). The RF model demonstrates higher accuracy than the others; however, the accuracy could be improved adjusting for the effect of rust formation on the sensor [12].

Therefore, the objective of this research is to evaluate the performance of ML algorithms in the prediction of atmospheric corrosion in the Metropolitan Zone of Mexico City. This will help to avoid and/or reduce human, economic, and environmental losses.

For which the following research question is formulated: Which of the ML algorithms predict atmospheric corrosion with high level of performance measures by the Correlation Coefficient  $R^2$  and Mean Square Error (MSE)?

The hypothesis to be demonstrated lies in the following statement: ML algorithms for atmospheric corrosion prediction have high performance.

It is important to note that in Mexico there are no precedents for the use of ML methods for the prediction of atmospheric corrosion, which is a milestone in the country that will allow the development of these computational tools for these purposes, as well as the comparison of their use with the applied traditional methods.

On the basis of the above, this work evaluates ML models, with prediction capabilities, in order to forecast atmospheric corrosion.

## II. THEORETICAL REFERENCE

### II.1 CORROSION

Corrosion can also be classified according to the natural environment where the process takes place, such as air, water or soil. Hence, atmospheric corrosion arises, which has its electrochemical basis [13].

Atmospheric corrosion in turn is classified under the category of dry, humid or wet, which emphasizes the different attack mechanisms with increasing humidity or dew.

**Dry corrosion:** In the absence of moisture, many metals corrode slowly at room temperature, but accelerate at high temperatures.

**Humid corrosion:** Requires moisture in the atmosphere and increases in aggressiveness with moisture content. When the humidity exceeds a critical value, which is around 70% relative humidity, an invisible thin film of moisture will form on the surface of the metal, facilitating the presence of an electrolyte to transfer current. The critical value depends on the surface conditions, such as: cleanliness, corrosion products formed or the presence of salts or other contaminants that are hygroscopic and can absorb water at very low relative humidities.

**Wet corrosion:** Occurs when water droplets or visible water films are formed on the metal surface due to sea breeze, rain, or dew fall [14].

There are several climatic factors that affect corrosion, among which are relative humidity, average ambient temperature, and wetting time, among others. On the other hand, it has also been reported in the specialized literature that there are chemical factors that increase the corrosion rate of steel, among the most significant are sulfur dioxide and sodium chloride [15].

Regarding the classification of atmospheric corrosivity, ISO 9223 establishes five categories, see Table 1 [16].

Table 1: Atmospheric aggressiveness categories.

Aggression Category	Steel Mass Loss ( $\mu\text{m}/\text{year}$ )	Corrosivity
C1	$\leq 1.3$	Very low
C2	$> 1.3 \leq 25$	Low
C3	$> 25 \leq 50$	Medium
C4	$> 50 \leq 80$	High
C5	$> 80 \leq 200$	Very high

Source: (ISO, 1989).

The corrosion rate [17], measured by mass loss is expressed as shown in equation 1:

$$V_{corr} = \frac{\Delta m}{(\rho \cdot A \cdot t)} \quad (1)$$

Where:

$V_{corr}$ : Corrosion rate,  $\mu\text{m}/\text{year}$

$\Delta m$ : Mass loss, g

$\rho$ : Steel Density AISI 1019

$A$ : Sample Area,  $\text{cm}^2$

$t$ : Exposure Time, year

### II.2 MACHINE LEARNING

ML offers the ability of machines to learn from data through computational methods without a predetermined equation as a model [18].

ML is classified mainly into three categories such as unsupervised learning, supervised learning, and reinforcement learning. Unsupervised learning assumes that the data is unlabeled. The data model is useful as a representation of clustering of data. Supervised learning considers the training of a model on known input and output data. Supervised learning uses classification and regression techniques to develop a predictive model. Unlike supervised and unsupervised ML, Reinforcement Learning does not require a static data set, but instead operates in a dynamic environment and learns from the collected experiences [19].

For the case of atmospheric corrosion prediction, regression ML algorithms are used because it is necessary to predict a continuous response such as mass loss. In this research, the most common algorithms that we evaluate are the following. Neural Networks (NN), Regression Trees (RT), Optimized Regression Tree (ORT), Regression Ensemble (RE), Support Vector Machine (SVM) and Linear Regression (LR). These algorithms and their parametric settings are explained in detail in the Materials and Methods section.

## III. MATERIALS AND METHODS

### III.1 MACHINE LEARNING FRAMEWORK

The generic machine learning framework for the prediction of atmospheric corrosion in this work is shown in Figure 1, [20]. There are two main stages of training and testing. Randomly 80% of the data were used in the training phase and the other 20% were used to test the trained models.

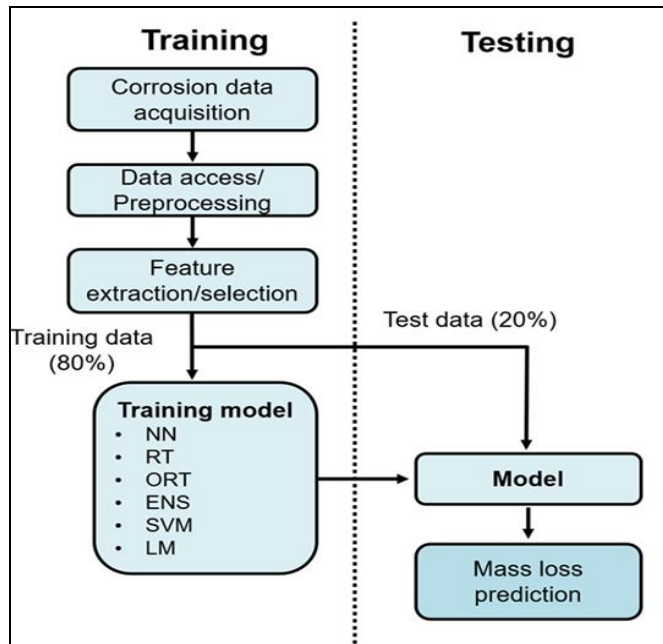


Figure 1: ML framework for atmospheric corrosion prediction. Source: [20].

The first stage in any ML system is data acquisition, although in some cases, as in this work, it is assumed that the data are available in a database. In this case, the atmospheric corrosion data acquisition stage was reported in a previous work [21].

The experimentally measured data for the independent variables that are used as attributes are the following: Relative humidity (%), wetting time (year), temperature ( $^{\circ}\text{C}$ ) and sulfur dioxide deposition time ( $\text{mg}/\text{m}^2\text{-day}$ ) at 12 stations at the study site detailed in the following:

1. Acatlán
2. Cerro de la Estrella
3. Coacalco
4. Hangares
5. Merced
6. Pedregal
7. Plateros
8. San Agustín
9. Tacuba
10. Tlalnepantla
11. Xalostoc
12. UNAM

These stations have been considered, taking into account previous studies of this phenomenon reported in [7]. In the same way, we proceeded to the measurement of the dependent variable

(mass loss) expressed in g, which the output response in the supervised learning approach.

After data acquisition, the next step in framework is data access and exploration, some examples are inspected through graphs when possible. The raw data contains 360 examples corresponding to the annual measures, 30 peer stations. Preprocessing data tasks such as cleaning, integration, reduction, and transformation are required to solve data missing, noise, inconsistency, multiple sources, and redundancy problems [22]. In this case, this phase was not required.

ML models use feature extraction and selection as a data dimensionality reduction. Feature extraction transforms the raw dataset into a reduced number of features, preserving the relevant information. In feature selection, the element that gives us the most relevant information about the problem is found. The performance of a machine learning model is related to the number of input variables [23]. In this work, we directly use the values of the dependent and independent variables. In Table 2 an example of raw data is presented.

Table 2: Example of input data for the atmospheric corrosion prediction model.

Relative Humidity (RH)	Wetting Time (WT)	Temperature (T)	Deposition ( $\text{SO}_2$ )	Loss Mass (LM)
39.4	110	16.7	42.7	1.5

Source: Authors, (2024).

Finally, the last step of the first stage is to train the ML model with the training data. There is no best model that generalizes to any problem, so it is necessary to train and test the available models with existing data. In the following, we describe the algorithms and its parameters used in this work.

### Neural Network (NN)

Neural network models are structured as a series of layers to mimic the way the brain processes information. We use a fully connected feedforward NN. The first layer of the NN has a connection from the network input (predictor data), and each subsequent layer has a connection from the previous layer. The final fully connected layer produces the output of the network, that is, the predicted response values [24].

### Regression Trees (RT) and Optimized Regression Trees (ORT)

Regression trees are decision trees to predict continuous values instead of class levels in leaves. RT are used to determine relationships between data set variables. The binary decision tree for regression used for this work is too complex. For this reason, we used an optimized RT. This method finds hyperparameters that minimize loss by using automatic hyperparameter optimization. We comment on the advantages of RT vs. ORT in the results analysis and discussion. Figure 2 shows the optimized regression tree diagram with a pruning level of 12.

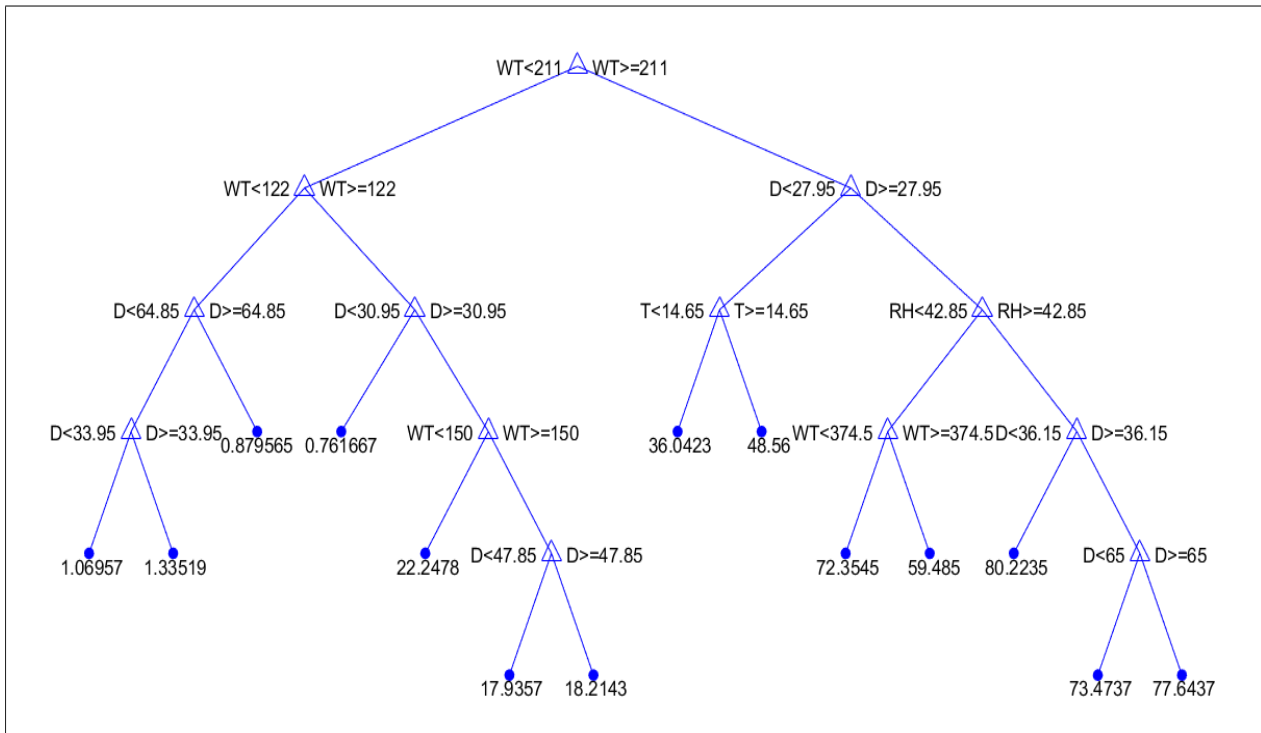


Figure 2: Optimized regression tree with pruning level = 12.  
Source: Authors, (2024).

**Regression Ensemble (RE)**

Regression Ensemble combines several models to improve the prediction accuracy in learning problems with a continuous output variable. We used an RE model that contains the results of boosting 100 regression trees using the least squares boost algorithm (LSBoost) and the predictor and response data. For LSBoost fits RE, at every step, the ensemble fits a new learner to the difference between the observed response and the aggregated prediction of all learners grown previously. The fits of the ensemble are to minimize MSE [25].

**Support Vector Machines (SVM)**

Support Vector Machines is a supervised learning algorithm that is based on finding a hyperplane that best separates different classes of data points. We use a trained SVM regression model due to the low dimensional predictor dataset.

**Linear Regression (LR)**

Linear Regression analysis is used to predict the value of a variable based on the value of another variable. The variable you want to predict is called the dependent variable, and the variable you are using to predict the other variable's value is called the independent variable. LR models have predictors that are linear in the model parameters, are easy to interpret, and are fast to make predictions. However, the highly constrained form of these models means that they often have low predictive accuracy and flexibility.

**IV. RESULTS AND DISCUSSIONS**

Due to the data observed in the 12 stations, a learning model is generated that predicts the behavior of the studied phenomenon. Moreover, as the number of data observations increases, the performance of the models improves.

Table 3 presents the results obtained for the Correlation Coefficient and the MSE for each of the ML algorithms on the test data.

Table 3: Correlation Coefficient and MSE results for each of the ML algorithms.

Algorithms	Correlation Coefficient ( $R^2$ )	Mean Square Error (MSE)
NN	0.9814	37.9
RT	0.9734	52
ORT	0.9792	41.2
RE	0.9789	40.6
SVM	0.8923	205.5
LR	0.3827	1,068

Source: Authors, (2024).

In terms of the correlation coefficient between the estimated values and the observed values, the best performing algorithm is NN, which represents a high correspondence for the regression model generated based on the data. Meanwhile, the worst performing model is LR with 0.3827.

Furthermore, the lowest MSE is for the NN algorithm at 37.9, which constitutes a high linearity of the estimated model. On the other hand, there is an improvement of the ORT model with respect to the RT, which means that the optimized values of the RT allow a better prediction performance.

Figure 3 shows the trends of the mass loss values with algorithms respect to the 12 station samples for each of the six ML

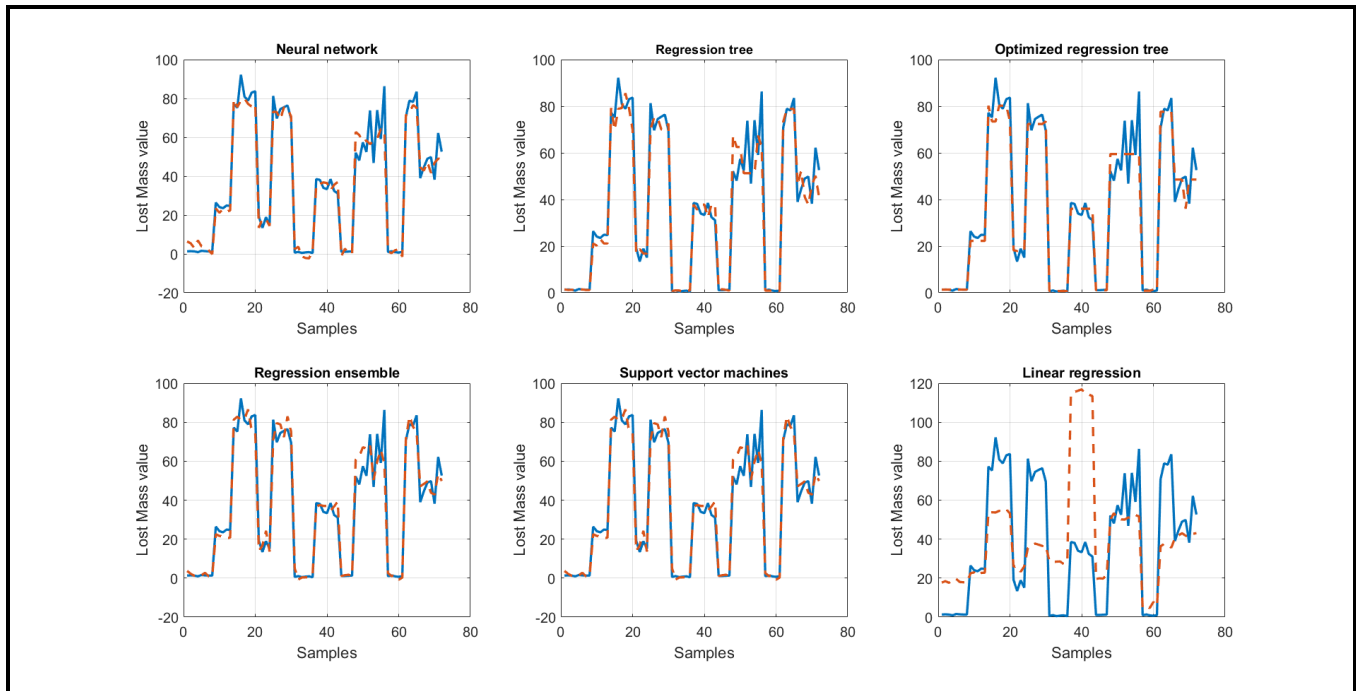


Figure 3: Behavior of mass loss values vs. samples of the 12 stations for the six ML algorithms applied. Blue (true) and red (predicted).

Source: Authors, (2024).

The results obtained show that the ML algorithms used are a reliable tool to predict the behavior of atmospheric corrosion at the 12 study stations. It is shown that the NN, RT, ORT, RE and SVM algorithms present good performance, but not the LR, which presents a very high MSE reaching 1,068.

Figure 4 shows the predictive performance of the mass loss of the six regression models, with respect to the real values of the mass loss. In this case, the test data that randomly correspond to 20% of the data set are used.

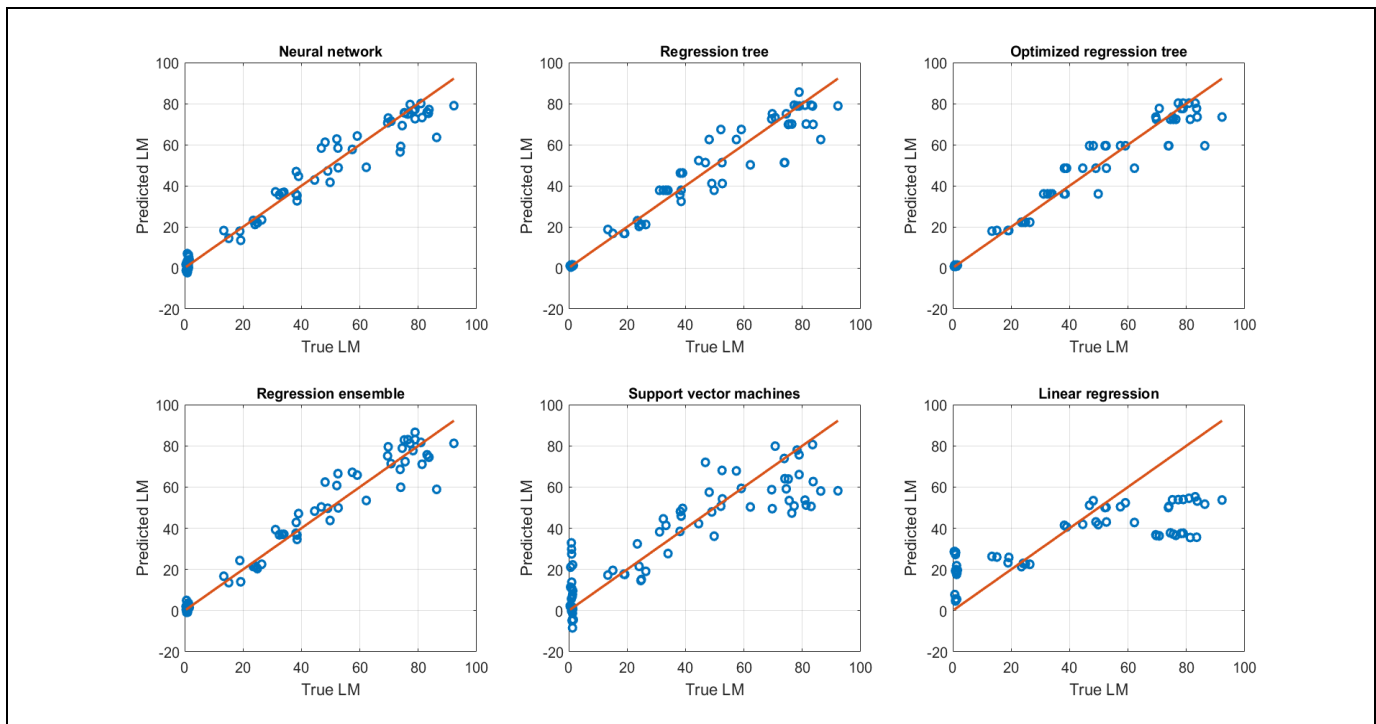


Figure 4: Predicted values vs true values of the loss mass.

Source: Authors, (2024).

For mass loss prediction, the ideal situation is where the predicted vs. true values lie on the diagonal line. The results obtained corroborate the above and allow affirming that the NN, RT, ORT, RE and SVM algorithms can be used to predict the behavior of atmospheric corrosion in the 12 stations of the area under study in the research due to their good performances shown.

For the case of knowing the behavior of atmospheric aggressiveness in each of the 12 stations of the Mexico City Metropolitan Zone, the loss of mass is considered directly proportional to the corrosion rate because the other terms involved in the calculation of the corrosion rate remain constant, among them the density of the steel, the average air temperature in the study area, the area of the samples, and the exposure time considered 1 year. The most common steel used in the Metropolitan Zone of Mexico City is the AISI 1019 steel, as it is the most versatile steel used in metallic structures.

The results when comparing the average corrosion rate for each station and what is established in the standard (ISO, 1989) [16], show that the corrosivity of the steel ranges from very low to high depending on the environmental conditions of the station. For example, for the Acatlán, Pedregal, San Agustín and Tlalnepantla stations the corrosivity is very low, while for the Coacalco, Merced, Tacuba and Xalostoc stations the corrosivity is high.

## V. CONCLUSIONS

The main contribution of this research is the evaluation of ML algorithms for the prediction of atmospheric corrosion, which is useful to generate alerts or make decisions in this area. For this work, the best model based on the Correlation Coefficient  $R^2$  and the Mean Square Error (MSE) is NN, with 0.9814 and 37.9, respectively. The worst performance was obtained for the Simple LR model with  $R^2=0.3827$  and  $MSE = 1.068$ .

The framework proposed in this research can be adopted in such a way that it predicts the behavior of another complex problem in an analogous manner.

The values predicted by ML algorithms are reliable and accurate, in fact, the more data these performances increase. Therefore, automating this prediction and analysis process helps reduce the costs associated with corrosion. Similarly, the use of a trained automatic system avoids the limitations of manual data analysis, enabling continuous and real-time monitoring, as well as sensor fusion.

Finally, because experimentation is expensive and requires long-term development, as a future work, we propose the use of an architecture for data acquisition and processing based on Internet of Things (IoT) and sensor networks.

## VI. AUTHOR'S CONTRIBUTION

**Conceptualization:** Ernesto Bolaños-Rodríguez, Juan-Carlos González-Islas.

**Methodology:** Juan-Carlos González-Islas, Omar López-Ortega.

**Investigation:** Ernesto Bolaños-Rodríguez, Juan-Carlos González-Islas, Omar López-Ortega, Evangelina Lezama-León.

**Discussion of results:** Ernesto Bolaños-Rodríguez, Juan-Carlos González-Islas, Omar López-Ortega, Evangelina Lezama-León.

**Writing – Original Draft:** Ernesto Bolaños-Rodríguez, Juan-Carlos González-Islas.

**Writing – Review and Editing:** Ernesto Bolaños-Rodríguez, Juan-Carlos González-Islas, Omar López-Ortega, Evangelina Lezama-León.

**Supervision:** Ernesto Bolaños-Rodríguez, Juan-Carlos González-Islas.

**Approval of the final text:** Ernesto Bolaños-Rodríguez, Juan-Carlos González-Islas, Omar López-Ortega, Evangelina Lezama-León.

## VII. ACKNOWLEDGMENTS

We are grateful to the authorities of Mexico City and the State of Mexico who authorized the application of the experiments corresponding to the stations that were monitored with respect to atmospheric corrosion, as well as to the Universidad Autónoma del Estado de Hidalgo for the resources and support provided for the successful completion of this research.

## VIII. REFERENCES

- [1] L. Coelho, D. Zhang, Y. Van Ingelgem, D. Steckelmarcher, A. Nowé & H. Terrya, "Reviewing machine learning of corrosion prediction in a data-oriented perspective", *Materials Degradation*, vol. 6, p. 1, 2022.  
[https://www.researchgate.net/publication/358161609\\_Reviewing\\_machine\\_learning\\_of\\_corrosion\\_prediction\\_in\\_a\\_data-oriented\\_perspective](https://www.researchgate.net/publication/358161609_Reviewing_machine_learning_of_corrosion_prediction_in_a_data-oriented_perspective)
- [2] G.F. Hays, *Now Is the Time*, World Corrosion Organization, New York: NP, USA, 2010.  
[http://red.corrosion.org/Corrosion+Resources/Publications/\\_/nowisthetime.pdf](http://red.corrosion.org/Corrosion+Resources/Publications/_/nowisthetime.pdf)
- [3] M.E. Emeteri, S.A. Afolalu, L.M. Amusan & A. Mamudu, "Role of Atmospheric Aerosol Content on Atmospheric Corrosion of Metallic Materials", *Int. J. Corros.* 2021.  
[https://www.academia.edu/88743213/Role\\_of\\_Atmospheric\\_Aerosol\\_Content\\_on\\_Atmospheric\\_Corrosion\\_of\\_Metallic\\_Materials](https://www.academia.edu/88743213/Role_of_Atmospheric_Aerosol_Content_on_Atmospheric_Corrosion_of_Metallic_Materials)
- [4] E. Kusmiereck, E. Chrzescijanaka, "Atmospheric Corrosion of Metal in Industrial City Environment", *Data Brief*, vol. 3, pp. 149-154, 2015.
- [5] G. Lazarenko, A. Kasprzhitskii & T. Nazdracheva, "Anti-Corrosion Coatings for Protection of Steel Railway Structures Exposed to Atmospheric Environment A Review", *Const. Build. Mater.*, vol. 288, pp. 115-123, 2021.
- [6] H. Jia, G. Qiao, & P. Han, "Machine learning algorithms in the environmental corrosion evaluation of reinforced concrete structures-A review", *Cement and Concrete Composites*, 104725, 2022.  
<https://www.sciencedirect.com/journal/cement-and-concrete-composites/vol/133/suppl/C>
- [7] R. Muñoz Ledo & J. Uruchurtu Chavarría, "Characterization of atmospheric aggressiveness on structural metallic materials in the Metropolitan Zone of Mexico City", *Journal of Environmental Contamination*, vol. 18, no. 1, pp. 27-32, 2002.
- [8] V. Duarte, S. Zuniga-Jara and S. Contreras, "Machine Learning and Marketing: A Systematic Literature Review," in *IEEE Access*, vol. 10, pp. 93273-93288, 2022, doi: 10.1109/ACCESS.2022.3202896.  
<https://ieeexplore.ieee.org/stamp/stamp.jsp?arnumber=9869838>
- [9] M. McInnes, C. Dick, C. Thring, D. Irving and D. Hughes, "Flexible, scalable, printed ultrasound sparse array for corrosion detection using machine learning," 2023 IEEE International Ultrasonics Symposium (IUS), Montreal, QC, Canada, 2023, pp. 1-4, doi: 10.1109/IUS51837.2023.10307983.
- [10] Y. Diao, L. Yan, & K. Gao, "Improvement of the machine learning-based corrosion rate prediction model through the optimization of input features", *Materials & Design*, vol.198, 109326, 2021.  
<https://www.sciencedirect.com/science/article/pii/S0264127520308625>
- [11] Z. Pei, D. Zhang, Y. Zhi, T. Yang, L. Jin, D. Fu, & X. Li, "Towards understanding and prediction of atmospheric corrosion of an Fe/Cu corrosion sREor via machine learning", *Corrosion science*, vol. 170, 108697, 2020.  
<https://research.tudelft.nl/en/publications/towards-understanding-and-prediction-of-atmospheric-corrosion-of->
- [12] M. Terrados-Cristos, F. Ortega-Fernández, G. Alonso-Iglesias, M. Díaz-Piloneta, & A. Fernández-Iglesias, "Corrosion prediction of weathered galvanised

structures using machine learning techniques”, *Materials*, vol. 14, no. 14, 3906, 2021.

[13] E. Bolaños Rodríguez, G. Y. Vega Cano, E. Lezama León, A.E. Solís Galindo, I. Acuña Galván, A. Zárate Rosas & I.G. Pérez Torres. Application of Artificial Neural Networks for Modeling Steel Mass Loss due to Atmospheric Corrosion in the Metropolitan Area of Mexico City. *Iberoamerican Conference on Systems, Cybernetics and Informatics, International Institute of Informatics and Systemics, Orlando, Florida, USA, 2022.*

[14] R. Garcés Rodríguez. (2002). Evaluation of Atmospheric Corrosion of Steel Exposed to Various Atmospheres. Thesis to Obtain the Degree of Master of Science in Mechanical Engineering with Specialty in Materials, UANL, School of Mechanical and Electrical Engineering. Graduate Studies Division. <http://eprints.uanl.mx/5170/>

[15] J. E. Rodríguez Yáñez, L. Garrido Arce & E. Sabrío Leiva, “Atmospheric Corrosion Maps of Low Alloy Steel in Costa Rica”, *Research Notebooks UNED*, vol. 7, no. 2, pp. 181-191, 2015.

[16] ISO 9223 (1987). Classification of Corrosivity Categories of Atmospheres. ISO, Ginebra.

[17] H.L. Muñoz-Fernández, L.A. González-Mendoza & D. Y. Peña-Ballesteros, “Evaluation of the Corrosion Rate of API 5L Grade 65 Steel in a Brine-CO<sub>2</sub>-SiO<sub>3</sub>-Mineral Oil System, by Electrochemical Techniques”, *Ingeniería y Universidad*, vol. 13, no. 1, pp. 27-44, enero-junio, 2009.

[18] Abhishek, Dhankar and N. Gupta, "A Systematic Review of Techniques, Tools and Applications of Machine Learning", 2021 Third International Conference on Intelligent Communication Technologies and Virtual Mobile Networks (ICICV), Tirunelveli, India, 2021, pp. 764-768, doi: 10.1109/ICICV50876.2021.9388637. [https://www.researchgate.net/publication/350535931\\_A\\_Systematic\\_Review\\_of\\_Techniques\\_Tools\\_and\\_Applications\\_of\\_Machine\\_Learning](https://www.researchgate.net/publication/350535931_A_Systematic_Review_of_Techniques_Tools_and_Applications_of_Machine_Learning)

[19] Gupta, R. (2020, February). A survey on machine learning approaches and its techniques. In 2020 IEEE International Students' Conference on Electrical, Electronics and Computer Science (SCEECS), pp. 1-6, IEEE. [https://www.researchgate.net/publication/341239256\\_A\\_Survey\\_on\\_Machine\\_Learning\\_Approaches\\_and\\_Its\\_Techniques](https://www.researchgate.net/publication/341239256_A_Survey_on_Machine_Learning_Approaches_and_Its_Techniques)

[20] J.C. González-Islas, O.A. Domínguez-Ramírez, O. López-Ortega, R.D. Paredes-Bautista, & D. Diazgiron-Aguilar, (2021). Machine learning framework for antalgic gait recognition based on human activity. In *Advances in Soft Computing: 20th Mexican International Conference on Artificial Intelligence, MICAI 2021, Mexico City, Mexico, October 25–30, 2021, Proceedings, Part II 20* (pp. 228-239). Springer International Publishing. <https://www.semanticscholar.org/paper/Machine-Learning-Framework-for-Antalgic-Gait-Based-Gonz%C3%A1lez-Islas-Dom%C3%ADnguez-Ram%C3%ADrez/9cb1b6f6559d7a71adacfde901de504b2d4204f0>

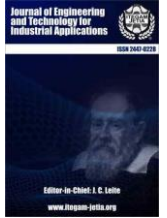
[21] E. Bolaños Rodríguez; E. Lezama León & G.Y. Vega Cano, Characterization of Atmospheric Aggressiveness on Steel in the Mexico City Metropolitan Area, Technical Report, Universidad Autónoma del Estado de Hidalgo (UAEH), 2023.

[22] S. Kokkotis, Moustakidis, Papageorgiou, G. Giakas, & D. E. Tsaopoulos, “Machine learning in knee osteoarthritis: A review”, *Osteoarthritis and Cartilage Open*, vol. 2, no. 3, 100069, 2020. <https://www.ncbi.nlm.nih.gov/pmc/articles/PMC9718265/>

[23] R.E. Nogales, & M.E. Benalcázar, “Analysis and Evaluation of Feature Selection and Feature Extraction Methods”, *International Journal of Computational Intelligence Systems*, vol. 16, no.1, p. 153, 2023. <https://link.springer.com/article/10.1007/s44196-023-00319-1>

[24] X. Glorot, & B. Yoshua, “Understanding the difficulty of training deep feedforward neural networks”, In *Proceedings of the thirteenth international conference on artificial intelligence and statistics*, pp. 249–256, 2010. <https://proceedings.mlr.press/v9/glorot10a/glorot10a.pdf>

[25] L. Breiman, "Random Forests", *Machine Learning*, vol. 45, pp. 5–32, 2001. <https://link.springer.com/article/10.1023/A:1010933404324>



### RESEARCH ARTICLE

### OPEN ACCESS

## METHODOLOGY FOR TARGET FORECASTING OF WATER LEVEL IN HYDROELECTRIC PLANT RESERVOIRS UNDER CONDITIONS OF LOW INFLOW

César A. Yajure Ramírez

Universidad Central de Venezuela.

<https://orcid.org/0000-0002-3813-7606>

Email: [cyajure@gmail.com](mailto:cyajure@gmail.com)

### ARTICLE INFO

#### Article History

Received: May 30th, 2024

Revised: July 08th, 2024

Accepted: July 08th, 2024

Published: July 18th, 2024

#### Keywords:

Data science,  
Forecasting,  
Performance metrics,  
Reservoir,  
Time series.

### ABSTRACT

The “El Niño” phenomenon brings periods of drought to northern South America that negatively impact the level of hydroelectric plant reservoirs, which could reduce their energy production. In order to avoid reaching the minimum operating level before the end of the drought period, this research proposes a methodology based on data science for the target forecast of the level of hydroelectric plant reservoirs in low flow conditions. The goal is that the minimum operating level of the reservoir be reached on the estimated end date of the drought period, that is, March 31, 2024. It is applied to the data of the reservoir of a hydroelectric plant located in the northwest of South America, for which three sequential forecast horizons are used, allowing the models to be evaluated as these periods pass, using the metrics: MAPE, RMSE, and MAE. To meet the goal, the predictive sampling method of the Prophet forecasting technique is used. The results indicate that the technique is a useful additional tool for the plant dispatcher, with values for the performance metrics during the third forecast horizon of 0.045%, 48 cm, and 62 cm, for the MAPE, the MAE, and the RMSE, respectively.



Copyright ©2024 by authors and Galileo Institute of Technology and Education of the Amazon (ITEGAM). This work is licensed under the Creative Commons Attribution International License (CC BY 4.0).

### I. INTRODUCTION

The “El Niño” phenomenon brings with it diverse climatic conditions for Latin America. According to the UN World Food Program [1], the countries of the Central American Dry Corridor (Nicaragua, El Salvador, Guatemala and Honduras) and northern South America experience drier conditions than usual in the presence of this phenomenon, with a probable reduction in precipitation. Thus, since mid-2023, Venezuela has been experiencing a drought due to this phenomenon that was enhanced by climate change [2]. These conditions imply a period of drought that can extend longer than normal, usually ending in the month of April, to ending approximately at the end of May, making it necessary to administer the reservoirs in general, in a restrictive manner. In the case of hydroelectric generation plants, this involves a decrease in energy production for the population, and therefore a

possible increase in electricity rationing. Consequently, in periods in which low or no precipitation is expected, and consequently, low or no inflow to the hydroelectric plant reservoirs, a point in time must be estimated at which conditions are likely to change in a favorable manner, and dispatch these hydroelectric plants in such a way as not to reach the minimum operating level in the period with low or no inflow flow.

Due to the above, it is necessary to make a forecast of the level of the reservoirs with a goal to be achieved at the end of the critical drought period. In this sense, the objective of this research is to present a methodology based on data science to develop target forecasting of hydroelectric plant reservoirs under conditions of low or no inflow. The Prophet forecasting tool is applied through the use of the Python programming language.

Previous research related to the topic of study of this work was reviewed, finding that none of them have a forecasting

approach with a goal in conditions of low inflow. For example, Li et al. [3] investigate the performance of four different deep learning models in predicting the water level in the dam area of the “Three Gorges” reservoir of the hydropower plant located in China. The models considered were: Long Short-Term Memory (LSTM) network, bidirectional LSTM network, convolution LSTM network, and the attention and convolution LSTM network. The performance metrics used were: determination coefficient ( $R^2$ ), mean absolute error (MAE), the square root of the mean square error (RMSE), and the mean absolute percentage error (MAPE). They found that the attention-convolution LSTM network performed the best, with an  $R^2$  of 0.994, a MAPE of 0.0032, a MAE of 0.5296, and an RMSE of 0.6748. Likewise, Sapitang et al. [4] carry out the forecast of the level change in a reservoir located in Malaysia, considering forecast horizons from one day to seven days, and two scenarios. They evaluate the performance of four models: decision tree regression, random forest regression, Bayesian linear regression, and artificial neural network regression. The metrics used to evaluate the models were:  $R^2$ , MAE, RMSE, RAE, and relative squared error (RSE). They conclude that the Bayesian linear regression model outperforms the other models, with an  $R^2$  between 0.998952 and 0.99992. Similarly, Tsao et al. [5] present a methodology for forecasting the water level of a reservoir with a horizon of 48 hours, and using fuzzy neural networks in a multi-stage architecture. They apply the methodology in the Tchi hydroelectric plant located in Taiwan. They conclude that with this methodology the energy efficiency of the system is improved, in addition to improving the effectiveness of the plant.

On the other hand, Tucci [6] develops and applies a methodology for hourly forecasting of the water level of the reservoir of a hydroelectric plant located in the Pontecosi basin in Italy. First, it applies spatial interpolation methods to data from meteorological stations near the reservoir to determine the values of: air temperature, air humidity, precipitation, and wind speed. These variables are then used as input to a neural network to predict soil moisture concentration. Then, a nonlinear automatic exogenous input model was trained to estimate the reservoir level with different prediction horizons, using the data from the previous modules, and historical data on water level, discharge flow, and turbine flow. Estimates of the water level were generated with a horizon between 1 and 6 hours, with MAE values between 2 cm and cm, respectively. For their part, Yang et al. [7] propose a time series analysis model, based on imputation and the variable selection method, for the forecast of water levels in a reservoir located in Taiwan. They use the random forest technique, whose performance they compare with other techniques, using the metrics: correlation coefficient, RMSE, MAE, relative absolute error (RAE), and root relative squared error (RRSE). They conclude that the closest point imputation method had the best performance, as did the proposed forecasting technique. Similarly, Nguyen et al. [8] present a novel deep learning model for the prediction of water level and discharge flow of water reservoirs. To address data scarcity and improve prediction accuracy, they use an ensemble learning architecture that takes the advantages of multiple deep learning techniques. They use singular spectrum analysis to treat atypical data, and genetic algorithms to obtain the optimal values of the model's hyperparameters. They conclude that their methodology is better than current techniques according to the Nash-Sutcliffe Efficiency (NSE), mean squared error (MSE), MAE, and MAPE metrics. Specifically, they consider that NSE improves by at least 2%, and with spectral analysis this metric improves an additional 5%. Likewise, Mohammed et al. [9]

propose a model based on artificial neural networks (ANN) and the marine predator algorithm to model the water levels of the Tigris River in Al-Kut, Iraq. Historical climate and water level data from the period 2011-2020 are used to build and evaluate the model, whose performance is compared with the recent particle swarm optimization based on constriction coefficients and the chaotic gravitational search algorithm (CPSOCGSA-ANN), and with the slime mold algorithm (SMA-ANN). The results show that the proposed model is the best performing one with a dispersion index of 0.0009 and a determination coefficient  $R^2$  of 0.98. Finally, Ibañez et al. [10] study the performance of different short- and long-term forecasting, statistical and machine learning techniques for predicting the water level of the Angat Dam located in the Philippines. The six techniques compared are: naive/persistence, seasonal mean, autoregressive integrated moving average (ARIMA), gradient boosting machines, and two deep learning networks. As exogenous variables they use historical data on water levels, meteorological data, and irrigation data. The univariate neural network resulted in the best performance for the one-day horizon with a MAE and RMSE of 20 cm. For the horizons of 30 days, 90 days and 180 days, the multivariate neural network resulted in the best performance with a MAE(RMSE) of 2.9(3.3), 5.1(6.0), and 6.7(8.1) m, respectively.

The rest of the article is distributed as follows. Section 2 presents the methodology used in the research. Then, in section 3 the results obtained are analyzed and discussed. Next, there are the conclusions derived from the research carried out. Finally, bibliographic references are presented.

## II. THEORETICAL BACKGROUND

### II.1 PROPHET FORECASTING TECHNIQUE

The Prophet technique developed by Facebook's data science team during 2017 is used. It was developed specifically for time series forecasting, based on an additive model where non-linear trends are easily adjusted to different types of seasonality, such as: annual, weekly, and daily, in addition to incorporating the effect of vacations and holidays. According to the team, the technique works best with time series that have strong seasonal effects and multiple seasons of historical data. It is robust with respect to missing data and changes in trend and generally handles outliers well [11].

As proposed by Taylor & Letham [12], the technique is based on a time series model composed of an element that represents the trend, another that represents regular changes, that is, seasonalities, another component that represents the effect of non-working days, and finally the error term. The model is then given by Equation (1):

$$y(t) = g(t) + s(t) + h(t) + \epsilon_t \quad (1)$$

In (1),  $y(t)$  is the time series,  $g(t)$  is the trend component,  $s(t)$  represents the periodic changes in the series,  $h(t)$  represents the effect of holidays and vacations, and  $\epsilon_t$  is the error term that represents changes that do not fit within the other components.

With respect to the trend component, the technique implements two types: growth saturation model, and a piecewise linear model. As for seasonality, it is modeled with periodic time functions, specifically with standard Fourier series, such as the one presented in Equation (2).



$$s(t) = \sum_{n=1}^N \left( a_n \cdot \cos\left(\frac{2\pi nt}{P}\right) + b_n \cdot \sin\left(\frac{2\pi nt}{P}\right) \right) \quad (2)$$

In this case,  $P$  is period of the series, which will depend on the type of seasonality, and  $N$  is the number of terms in the series.

Taylor & Letham indicate that  $P$  is the regular period that they expect the time series to have, being equal to 7 for data with weekly seasonality and 365.25 for data with annual seasonality. From the above it is deduced that the technique works by default with data with daily resolution. Likewise, they propose that higher values of  $N$  apply to seasonal patterns that change more rapidly, and in their studies, they have found that a value of 10 is useful for annual seasonalities, and 3 for monthly seasonalities. According to Peixeiro [13], the technique defines by default an additive seasonality, but there is also the option of establishing a multiplicative seasonality.

One of the characteristics that differentiates this technique from some other time series analysis techniques is the management of non-working days, allowing the inclusion in the model of a list with holidays and vacations that are within the historical data period, but also within the forecast horizon. It has been used in multiple applications, for example, Sharma et al. [14] use it for the prediction of stock values in the Indian stock market, Žunić et al. [15] apply this technique to forecast successful sales, Oo and Phyu [16] use the technique to develop temperature forecasting, among other applications.

## II.2 FORECAST MODEL PERFORMANCE METRICS

In order to evaluate the performance of forecasting models and make comparisons between them, a series of metrics are used. Among the standard statistical measures to evaluate models are: MAE, RMSE, and MAPE. The error being the difference between the real value and the predicted value [17]. The first two metrics considered give results in physical units, while the third of them (MAPE) is given as a percentage with respect to the real value of the predicted variable. When comparing RMSE and MAE metrics, it should be noted that the former is convenient when errors are normally distributed, while the latter is recommended for use with Laplacian errors [18]. Likewise, Naser [19] states that MAPE is negatively affected when a predicted value (or several) is much larger or much smaller than the corresponding real value. Next, the mathematical equations used to calculate these metrics are presented.

$$MAE = \frac{1}{n} \sum_{i=1}^n |Y_i - F_i| \quad (3)$$

$$RMSE = \sqrt{\frac{1}{n} \sum_{i=1}^n (Y_i - F_i)^2} \quad (4)$$

$$MAPE = \frac{1}{n} \sum_{i=1}^n \left| \left( \frac{Y_i - F_i}{Y_i} \right) \times 100 \right| \quad (5)$$

It is true that  $Y_i$  is the  $i$ th real value of the variable to be forecast,  $F_i$  is the  $i$ th predicted value, and  $n$  is the number of records or historical data available.

## III. MATERIALS AND METHODS

With the purpose of achieve the stated objective, a methodology was used based on the stages of a data science project, which include: establishing objectives, obtaining data, pre-processing of data, exploratory analysis of data, modeling of the data, and finally, the decision-making stage [20]. An outline of the applied methodology is presented in Figure 1.

The objective would then be to develop the forecast of the level of the reservoir of a hydroelectric plant, subject to conditions of low inflow due to climatic phenomena, with the goal of avoiding reaching the minimum operating level of the reservoir. The data used corresponds to the historical values of the reservoir level, and the energy produced, during the period 2015-2023. It is important to mention that the climatic phenomenon considered was “El Niño”, which has been present since the fourth quarter of 2023, and has accentuated the drought period in countries with a coast on the Caribbean Sea. This phenomenon was previously present during 2016. The preprocessing of the data consisted of the application of the techniques present in [21]. Specifically, the possible existence of missing and/or atypical data was verified, imputing with appropriate techniques when necessary. Likewise, the possible existence of duplicate data was verified, and new data columns were generated from the existing ones. In the next stage, an exploratory analysis of the data was carried out, using statistical and/or graphic techniques. Subsequently, the data was modeled by applying supervised machine learning algorithms, specifically, forecasting techniques. With the results obtained from the exploratory analysis and data modeling, we proceeded to the decision-making stage.

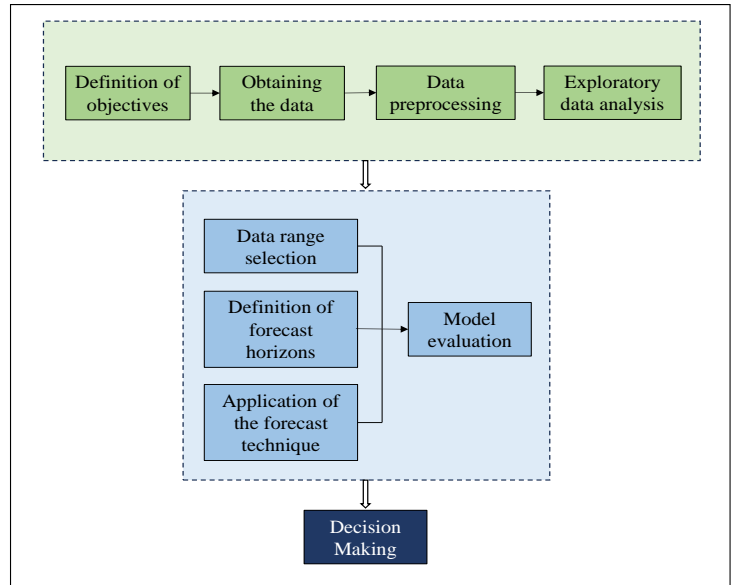


Figure 1: Outline of the applied methodology. Source: Authors, (2024).

In the data modeling stage, the Prophet technique is applied using the Python programming language, setting the goal that by 03/31/2024 the reservoir under study does not reach its minimum level, in accordance with the forecast obtained. To achieve this, the predictive sampling method of the forecasting technique is used, and the sample that meets the programmed goal is selected. There is a first forecast horizon of 91 days between 01/01/2024 and 03/31/2024. After the month of January had passed, the actual data for that month were incorporated into the historical data, and the technique was applied again with a forecast horizon of 60 days between 02/01/2024 and 03/31/2024. Similarly, after the month of

February had passed, the historical data were readjusted, and the technique was used again, but this time with a horizon of 31 days between 03/01/2024 and 03/31/2024. For each of these forecast horizons, performance metrics were calculated by comparing the forecast obtained with the actual values of the elevations.

### III.1 DATA PREPROCESSING

The data correspond to the daily values in meters, for the period 2015-2023, of the water level of a reservoir whose contents are used for the production of energy through a hydroelectric plant located in the northwest of South America. Likewise, the data set has the daily energy values, in Gigawatt-hours (GWh), produced by the plant. The data set was checked to ensure the absence of missing data and duplicate data. Likewise, it was verified that there is no presence of atypical data in both the water level and energy data. Next, the data from the water level column were used to generate the values of the variation in centimeters of water level.

## IV. RESULTS AND DISCUSSIONS

### IV.1 EXPLORATORY DATA ANALYSIS

Firstly, the temporal graph of the daily water level is created for the period 2015-2023, in order to observe the behavior that this variable has had. This graph is presented in Figure 2, from which it is observed that the level reached its maximum values during the years 2021 and 2022, and presents an annual seasonality. Likewise, it is also noted that the minimum value was reached during the first half of 2020.

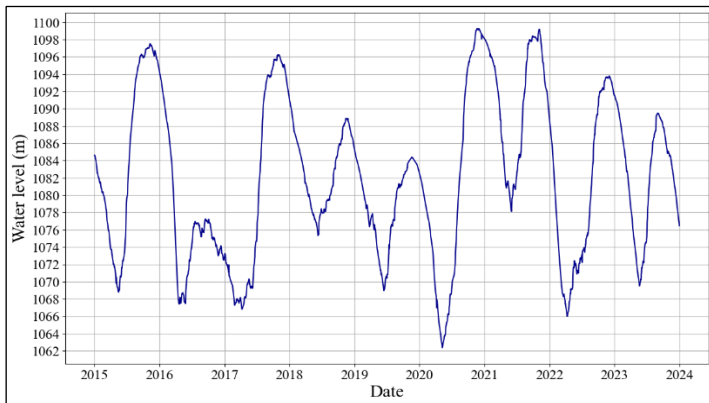


Figure 2: Daily level of the reservoir. Source: Authors, (2024).

Additionally, it is noted that, at the beginning of the year 2016, in which the El Niño phenomenon was also present, the elevation was around 1094 m, while, at the beginning of the year 2024, this was slightly higher than 1076 m. A downward trend can be seen in the curve starting in 2020.

On the other hand, Table 1 presents the descriptive statistical indicators of the level, the variation of the level, and the electrical energy produced by the plant. It can be seen that there are a total of 3287 records, corresponding to each of the days in the period 2015-2023.

Table 1: Descriptive analysis of the data.

Indicator	Level (m)	Variation (cm)	Energy (GWh)
Records	3287	3287	3287
Mean	1082,05	-0,25	2,88
Std Dev	9,38	21,11	1,15
Min	1062,36	-131,00	0,00

P <sub>25</sub>	1074,31	-12,00	2,20
Median	1081,44	-3,00	2,97
P <sub>75</sub>	1089,45	8,00	3,60
Max	1099,28	132,00	6,77

Source: Authors, (2024).

It can be seen that the level varied from a minimum of 1062.36 m to a maximum of 1099.28 m. Regarding the energy produced, it varied from 0 to 6.77 GWh. The level had a minimum variation of -131 cm, that is, a maximum drop of 131 cm, and a maximum variation of 132 cm, that is, a maximum rise of 132 cm.

Likewise, Figure 3 presents a graph with the average value in centimeters of the variation in the reservoir level for the period 2015-2023. It can be seen that the fall in the level of the reservoir occurs between the month of November and the month of May, coinciding with the historical period of drought in the area where the reservoir is located, with its greatest average fall during the month of March and the minimum fall during the month of May, the month in which the rainy period historically begins.

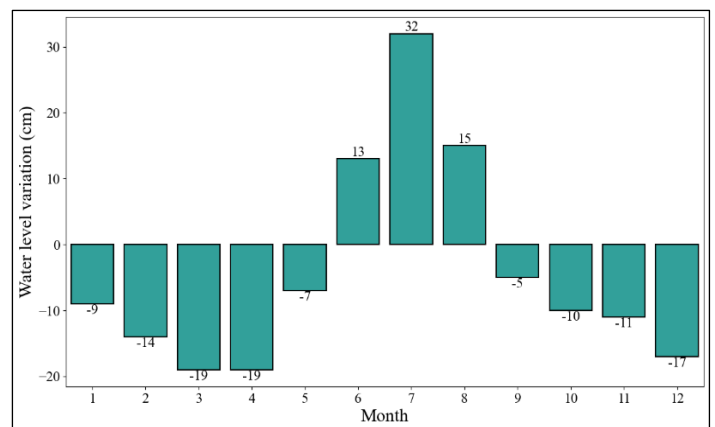


Figure 3: Average monthly level variation 2015-2023. Source: Authors, (2024).

It can also be seen that, in the period between the month of June and the month of October, the level has its greatest increases, coinciding with the rainy period, with a maximum value for the month of July, and a minimum value for the month of July. month of October.

### IV.2 DATA MODELING

To estimate the water level using the Prophet technique, daily data for the period 2021-2023 was used. This amount of data is sufficient since all seasonalities that the data could have are covered. As a goal of the forecast, it was established that the minimum level of the reservoir, which is 1066 meters, would not be reached until March 31, 2024, the date on which the recovery of the reservoirs was expected to begin, and also put other electricity generation plants were in operation, thus allowing the reservoir to recover its optimal level. Three start dates were considered for the forecast horizon: 01/01/2024, 02/01/2024, and 03/01/2024, allowing values to be added to the historical data as the deadline approached.

To generate the forecast model, a file was considered with the non-working days associated with the historical period of the data, and the period of the forecast horizon. Regarding the seasonality of the data, we worked with the default values of the technique, that is, considering the existence of annual and weekly seasonalities. The technique's `m.predictive_samples(future)`

method was used, which allows obtaining up to 1000 water level forecast samples for the given forecast horizon. To select the sample that represents the forecast, a series of filters are applied: that the elevation is not lower than the minimum value before the deadline, and that the elevation for the deadline is the closest to 1066.

First forecast horizon goes from 01/01/2024 to 03/31/2024, with a water level at the beginning of the period of 1076.21 m. After applying the Prophet technique, there are 1000 forecast samples. After applying the filters, the required forecast is obtained, for which the water level for March 31 is 1066.84 m. At the end of the forecast horizon, the real values of the elevation are available, so the MAPE, MAE, and RMSE metrics were calculated, in order to evaluate the performance of the forecast. The results of the metrics are presented in Table 2. In the research by Ibañez et al. (2021) also works with a horizon of around 90 days, obtaining an RMSE of 6.0 meters and a MAE of 5.1 meters.

After the month of January had passed, the water level forecast was repeated, now with a forecast horizon from 02/01/2024 to 03/31/2024, with a elevation at the beginning of the period of 1072.84 m, That is, during the month of January the level fell 3.37 m. Again, when applying the technique, 1000 samples are obtained. After applying the filters, the required forecast is obtained, for which the level for deadline is 1066.94 m. The results of the calculated metrics are presented in Table 2.

After the month of February had passed, the water level forecast was repeated, now with a forecast horizon from 03/01/2024 to 03/31/2024, with a water level at the beginning of the period of 1069.70 m, from which it is deduced that the level fell 3.14 m. Again, when applying the technique, 1000 samples are obtained. After applying the filters, the required forecast is obtained, for which the level for March 31 is 1066.30 m. The results of the calculated metrics are presented in Table 2. For the case of the 30-day horizon, in Ibañez et al. (2021) obtained an RMSE of 3.3 meters and a MAE of 2.9 meters.

Table 2: Model performance metrics.

Horizons	MAPE (%)	MAE (cm)	RMSE (cm)
First	0,083	88	101
Second	0,078	83	95
Third	0,045	48	62

Source: Authors, (2024).

Figure 4 presents the results obtained along with the real values of the reservoir level for the study period. It can be seen that the forecast of the third horizon was the closest to the real values of the reservoir level, which at the end of said period was slightly below the goal.

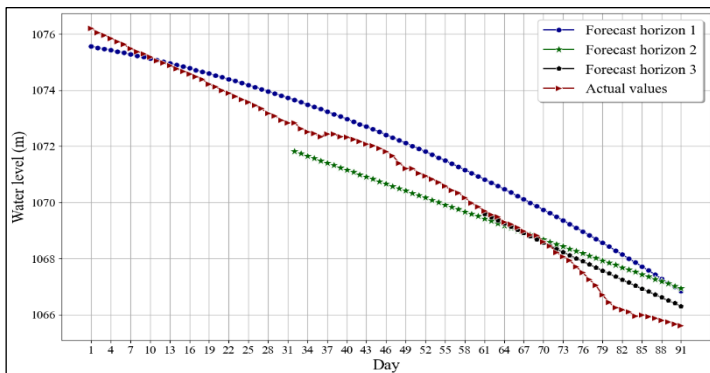


Figure 4: Forecasts achieved.

Source: Authors, (2024).

## V. CONCLUSIONS

A forecasting methodology was developed with a goal for estimating the level of a reservoir with low inflow, providing the dispatcher with an additional tool for the operation of the hydroelectric plant, preventing the minimum operating level from being reached. The methodology was applied to data from a reservoir located in northwest South America. From the historical values of the water level, it was determined that the average fall for the month of January was 12 meters, as for the month of February, while for the month of March the average fall was 16 meters. These values contrast with those corresponding to the first quarter of 2024, with a drop of 3.37 meters for the month of January, for the month of February it was 3.14 meters, and for the month of March it was 4.13 meters. The shortest forecast horizon was the one with the lowest values of the performance metrics, with a MAPE of 0.045%, a MAE of 48 cm, and an RMSE of 62 cm. Likewise, the longest forecast horizon presented the highest values of the metrics with a MAPE of 0.083%, a MAE of 88 cm, and an RMSE of 101 cm. The values corresponding to the intermediate horizon were similar to those of the complete horizon. The values of the MAPE metric are significantly low as they are less than 1%, which is due to the fact that the elevations are in the order of thousands of meters, while the variations for the studied reservoir are in the order of centimeters.

## VI. AUTHOR'S CONTRIBUTION

**Conceptualization:** César A. Yajure Ramírez.

**Methodology:** César A. Yajure Ramírez.

**Investigation:** César A. Yajure Ramírez

**Discussion of results:** César A. Yajure Ramírez

**Writing – Original Draft:** César A. Yajure Ramírez

**Writing – Review and Editing:** César A. Yajure Ramírez

**Resources:** César A. Yajure Ramírez

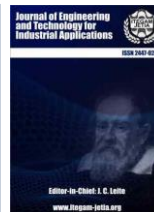
**Supervision:** César A. Yajure Ramírez

**Approval of the final text:** César A. Yajure Ramírez

## VIII. REFERENCES

- [1] Organización de las Naciones Unidas, «Programa Mundial de Alimentos,» 13 Mayo 2024. [En línea]. Available: [https://docs.wfp.org/api/documents/WFP-0000157673/download/?\\_ga=2.39065891.1453367334.1715622910-1541892750.1715622909](https://docs.wfp.org/api/documents/WFP-0000157673/download/?_ga=2.39065891.1453367334.1715622910-1541892750.1715622909).
- [2] M. López, «¿Qué pasa con los fenómenos de El Niño y La Niña y cómo esto afecta a Venezuela?», Efecto Cocuyo, 11 Febrero 2024.
- [3] H. Li, L. Zhang, Y. Zhang, Y. Yao, R. Wang y Y. Dai, «Water-Level Prediction Analysis for the Three Gorges Reservoir Area Based on a Hybrid Model of LSTM and Its Variants» MDPI Water, p. <https://doi.org/10.3390/w16091227>, 2024.
- [4] M. Sapitang, W. M. Ridwan, K. Faizal Kushiari, A. N. Ahmed y A. El-Shafie, «Machine Learning Application in Reservoir Water Level Forecasting for Sustainable Hydropower Generation Strategy» MDPI Sustainability, p. <http://dx.doi.org/10.3390/su12156121>, 2020.
- [5] H.-H. Tsao, Y.-G. Leu, L.-F. Chou y C.-Y. Tsao, «A Method of Multi-Stage Reservoir Water Level Forecasting Systems: A Case Study of Techi Hydropower in Taiwan» MDPI Energies, p. <https://doi.org/10.3390/en14123461>, 2021.
- [6] M. Tucci, «Hourly Water Level Forecasting in an Hydroelectric Basin Using Spatial Interpolation and Artificial Intelligence,» MDPI Sensors, p. <https://doi.org/10.3390/s23010203>, 2022.
- [7] J.-H. Yang, C.-H. Cheng y C.-P. Chan, «A Time-Series Water Level Forecasting Model Based on Imputation and Variable Selection Method» Computational Intelligence and Neuroscience - Hindawi, p. <https://doi.org/10.1155/2017/8734214>, 2017.

- [8] A. D. Nguyen, P. L. Nguyen, V. H. Vu, Q. V. Pham, V. H. Nguyen, M. H. Nguyen, T. H. Nguyen y K. Nguyen, «Accurate discharge and water level forecasting using ensemble learning with genetic algorithm and singular spectrum analysis based denoising» *Scientific Reports*, pp. <https://doi.org/10.1038/s41598-022-22057-8>, 2022.
- [9] S. J. Mohammed, S. L. Zubaidi, N. Al-Ansari, H. Mohammed Ridha y N. S. Saad Al-Bdairi, «Hybrid Technique to Improve the River Water Level Forecasting Using Artificial Neural Network Based Marine Predators Algorithm» *Hindawi - Advances in Civil Engineering*, p. <https://doi.org/10.1155/2022/6955271>, 2022.
- [10] S. C. Ibañez, C. V. G. Dajac, M. P. Liponhay, E. F. T. Legara, J. M. H. Esteban y C. P. Monterola, «Forecasting Reservoir Water Levels Using Deep Neural Networks: A Case Study of Angat Dam in the Philippines» *MDPI Water*, p. <https://doi.org/10.3390/w14010034>, 2022.
- [11] Facebook, «[https://facebook.github.io/prophet/docs/quick\\_start.html#python-api](https://facebook.github.io/prophet/docs/quick_start.html#python-api)» 4 Mayo 2024. [En línea]. Available: <https://facebook.github.io/prophet/>.
- [12] S. J. Taylor y B. Letham, «Forecasting at Scale,» *Peer J*, p. <https://doi.org/10.7287/peerj.preprints.3190v2>, 2017.
- [13] M. Peixeiro, *Time Series Forecasting in Python*, Shelter Island, NY: Manning Publications Co., 2022.
- [14] K. Sharma, R. Bhalla y G. Ganesan, «Time Series Forecasting Using FB-Prophet» de *ACM-2022: Algorithms Computing and Mathematics Conference*, Chennai, India, 2022.
- [15] E. Žunić, K. Korjenić, K. Hodžić y D. Đonko, «Application of Facebook's Prophet Algorithm for Successful Sales Forecasting Based on Real-World Data» *International Journal of Computer Science & Information Technology*, pp. 23-36. DOI: 10.5121/ijcsit.2020.12203, 2020.
- [16] Z. Z. Oo y S. Phyu, «Time Series Prediction Based on Facebook Prophet: A Case Study, Temperature Forecasting in Myintkyina» *International Journal of Applied Mathematics, Electronics and Computers*, pp. 263-267. <https://doi.org/10.18100/ijamec.816894>, 2020.
- [17] S. Makridakis, S. Wheelwright y R. Hyndman, *Manual of Forecasting: Methods and Applications*, 1997.
- [18] T. O. Hodson, «Root-mean-square error (RMSE) or mean absolute error (MAE): when to use them or not,» *Geoscientific Model Development*, pp. 5481–5487. <https://doi.org/10.5194/gmd-15-5481-2022>, 2022.
- [19] M. Naser, «Error Metrics and Performance Fitness Indicators for Artificial Intelligence and Machine Learning in Engineering and Sciences» *Architecture, Structures and Construction*, pp. <https://doi.org/10.1007/s44150-021-00015-8>, 2021.
- [20] D. Cielen, A. D. B. Meysman y M. Ali, *Introducing Data Science*, Shelter Island, NY: Manning Publications Co., 2016.
- [21] W. McKinney, *Python for Data Analysis*, Sebastopol, CA: O'Reilly Media, Inc., 2018.



## RESEARCH ARTICLE

## OPEN ACCESS

## SULFURE DIOXIDE DEEXPERIMENTAL ASSESSMENT OF SULFURE DIOXIDE REMOVAL FROM GAS STREAM FOR INTENSIVE ALGAE CULTURE

\*Liset Roche Delgado<sup>1</sup>, Mayra C. Morales Pérez<sup>2</sup>, Rosa Amalia González Rivero<sup>3</sup>, Arianna Álvarez Cruz<sup>4</sup>, Agustín A. García Rodríguez<sup>5</sup>, Juan Pedro Hernández Touse<sup>6</sup>.

<sup>1,2,4,5,6</sup>Central University "Marta Abreu" of Las Villas. Santa Clara, Cuba.

<sup>3</sup>Institute of Atmospheric Sciences and Climate Change, National Autonomous University of Mexico.

<sup>1</sup><http://orcid.org/0000-0002-5858-2926>, <sup>2</sup><http://orcid.org/0000-0001-7506-0145>, <sup>3</sup><http://orcid.org/0000-0002-6905-4379>, <sup>4</sup><http://orcid.org/0000-0002-5798-6793>, <sup>5</sup><http://orcid.org/0000-0002-8897-0671>, <sup>6</sup><http://orcid.org/0000-0002-0032-8685>

Email: \*[liset@uclv.cu](mailto:liset@uclv.cu), [mmoralesp@uclv.cu](mailto:mmoralesp@uclv.cu), [roagrivero@gmail.com](mailto:roagrivero@gmail.com), [aacruz@uclv.cu](mailto:aacruz@uclv.cu), [agarcia@uclv.edu.cu](mailto:agarcia@uclv.edu.cu), [juanpedro@uclv.edu.cu](mailto:juanpedro@uclv.edu.cu).

## ARTICLE INFO

**Article History**

Received: May 31th, 2024

Received: July 08th, 2024

Accepted: July 08th, 2024

Published: July 18th, 2024

**Keywords:**

Absorption,  
adsorption,  
gaseous effluents,  
low cost sensor,  
sulfur dioxide

## ABSTRACT

In this research, several SO<sub>2</sub> removal alternatives were evaluated for the treatment of gaseous effluents generated by the "Carlos Manuel de Céspedes" power plant in Cienfuegos to be use in gaseous stream to *Ulva lettuce* intensive culture. A low-cost sensor was used to monitor the gas concentration during the proposed methods. The sensor was previously calibrated and a linear regression model with a coefficient of determination of 0,9926 was obtained. The alternatives evaluated were adsorption with activated carbon, absorption with calcium hydroxide and absorption with seawater. The removal was evaluated at three levels SO<sub>2</sub> concentration. In addition, the parameters pH, salinity and alkalinity were determined to a seawater sample from the Bay of Cienfuegos and with which the experiments were carried out. The values obtained were 8,17±0,003; 26,50±0,10 ups and 171,67±1,03 mg/L respectively, which confirms its good performance for gas removal. The three methods studied showed satisfactory results for SO<sub>2</sub> removal. The seawater absorption experiment was the most efficient alternative, achieving the lowest final concentrations in the shortest time.



Copyright ©2024 by authors and Galileo Institute of Technology and Education of the Amazon (ITEGAM). This work is licensed under the Creative Commons Attribution International License (CC BY 4.0).

## I. INTRODUCTION

Sulfur compounds are one of the most important acidifying agents and appear to be key factors in regulating the ionic composition and nutrient efficiency of natural environments. However, anthropogenic emissions of SO<sub>2</sub> originates mainly in process that involve combustion processes. [1],[2]. This pollutant is produced by sulfur-containing fossil fuels used for thermal power generation, heating, cooking, and transportation. Oil refineries and ore smelters are additional sources. In the atmosphere, SO<sub>2</sub> is converted to SO<sub>3</sub> by reaction with oxygen. SO<sub>2</sub> and SO<sub>3</sub> react with the moisture in the air to form H<sub>2</sub>SO<sub>3</sub> and H<sub>2</sub>SO<sub>4</sub>, and producing acid rain [3].

In Cuba net emission inventories showed the importance of SO<sub>2</sub> as a pollutant because of the use of old technologies in industry and transportation leads to higher fuel consumption levels. Alejo, D [3] obtain that an average concentration of 4 ppb for the period February to April 2010 in Santa Clara City and in Havana, a study of air pollution due to vehicular traffic showed average SO<sub>2</sub> concentrations between 5 and 15 ppb, with peaks of up to 60 ppb [4].

In the province of Cienfuegos, SO<sub>2</sub> emissions are 43,205 tons per year, which represents 78.8% of the main pollutants in this city. Ninety-nine percent of these emissions come from boilers and furnaces, including the power plant and the oil refinery, which emit the most with more than 42 thousand tons per year [5].

For this reason, there is a need to control SO<sub>2</sub> and to invest in technologies that remove the gaseous emissions in the industry and the transportation

This work aims to compare SO<sub>2</sub> removal with low-cost system according three experimental methods in laboratories. Gas desulphurization by mean absorption in alkaline solution of Ca(OH)<sub>2</sub>, alkaline seawater solution and adsorption with activated carbon.

## II. THEORETICAL REFERENCE

### II.1 METHODS OF GAS DESULPHURIZATION.

Flue gas desulphurization is carried out by mean non-regenerative processes and regenerative processes, the former being the most widespread in the world - in both processes, alkaline solutions or suspensions are used. In non-regenerative plants, the reagent used to retain SO<sub>2</sub> is disposed of; low-cost absorbent reagents are usually used, mainly aqueous limestone suspensions, Ca(OH)<sub>2</sub> and seawater [6].

Wet technology based on calcium hydroxide has its value in the best reactivity of Ca(OH)<sub>2</sub> than limestone slurry, but it is still more expensive raw material. The main drawback of these plants is that the manipulation and management of large volumes of waste sludge is necessary, although in some of these technologies reusable by-products are obtained that improve the operating costs.

Seawater is naturally alkaline and has a high SO<sub>2</sub> neutralization capacity. The seawater process is very similar to that of the Limestone with Forced Oxidation (LSFO) process, except that there is no dissolution or precipitation of solids [7].

On the other hand, in regenerative processes, the reagent is recovered after SO<sub>2</sub> elimination, usually thermally; however, the technological complexity of the design and the costs are high. Both technologies, regenerative and non-regenerative, are in turn divided into dry or wet. In this sense, about dry regenerative process, there are several studies that show the effectiveness of activated carbon in the removal of polluting gases, specifically, SO<sub>2</sub> [8-10].

## III. MATERIALS AND METHODS.

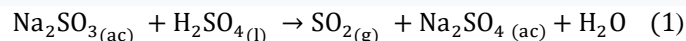
### III.1 LOW-COST MONITORING SYSTEM

The principles of low-cost systems have already been described in previous work [46,47]. Here, only the principle of the SO<sub>2</sub> and CO<sub>2</sub> sensors measurements is described in more detail. The low-cost monitoring system that was used in the experiments consisted of an Arduino MEGA2560 as the computer unit and interface board, a real-time clock, and an SD card for data storage and the sensor The Arduino Mega 2560 contains an ADC with a 10-bit resolution. This ADC, with a reference voltage of 5 V, is capable of detecting voltage variations of about 4 mV.

The SO<sub>2</sub> sensor type A from the manufacturer Alphasense, is inserted in an analog conditioning board (analog front end), which is designed to accommodate 4 different sensors (part number 810-0023-00). The configuration used includes sensors for NO<sub>2</sub>, OX (O<sub>3</sub> + NO<sub>2</sub>), CO, and SO<sub>2</sub>. The Analog Front End (AFE) has an internal power supply of 3.3 V and only requires an input voltage between 3.5 and 6.5 V (DC). The conditioning board provides 8 analog outputs (2 for each sensor; more precisely, the “working electrode” and the “auxiliary electrode”) that must be connected to analog-digital converters (ADC). In addition to the CO<sub>2</sub> sensor type a COZIR was coupled to the instrument.

Calibration have been carried out on SO<sub>2</sub> and CO<sub>2</sub> sensor allowing for obtaining reliable values of the readings of the

sensors. Inexpensive calibration of the SO<sub>2</sub> sensor by generating SO<sub>2</sub> gas inside a syringe according the reaction 1.



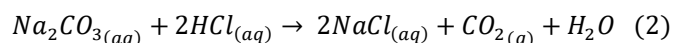
The SO<sub>2</sub> gas in the syringe was introduced in three successive steps and at each gas injection, the sensor signal jumped. The sensor reading followed the jumps of a staircase function, while the room temperature and relative humidity inside the box remained constant (i.e., 25°C and 65% RH).

González, R [11] pointed out that the voltages of the working and auxiliary electrodes for air without pollutants (W<sub>E0</sub> and A<sub>E0</sub>) can be obtained from a zero air calibration process. Then, the voltage values of the working electrode (W<sub>E</sub>) can be calculated according the equation proposed by the manufacturer.

### III.2 Experimental study of gas desulfurization.

The removal alternatives analyzed are adsorption with activated carbon, adsorption with a calcium hydroxide solution Ca(OH)<sub>2</sub> (ac) and adsorption with seawater. The gas flow is simulated for the study with an air flow where the SO<sub>2</sub> and CO<sub>2</sub> compositions are adjusted to the maximum values close to the detection limit of the sensor in order to obtain an initial gas mixture closer to the flue gas composition.

To obtain the CO<sub>2</sub> gaseous, it is necessary to adjust the initial composition of the mixture., reaction 2 is the following inside the syringe



The different volumes of SO<sub>2</sub> were obtained according to the stoichiometric reaction 2.1 and other two molar ratios of Na<sub>2</sub>SO<sub>3</sub> and H<sub>2</sub>SO<sub>4</sub>

### III.3 Design of the experimental system.

The evaluation of the gas desulfurization methods was carried out by means of a full factorial design as shown in Table 1 and indicated by the codes (-1, 0, 1). Factor A refers to the method used for SO<sub>2</sub> removal: adsorption with activated carbon A1, adsorption with calcium hydroxide A2 and adsorption with seawater A3. Factor B refers to the SO<sub>2</sub> concentration to be removed: ambient concentration B1, 10 ppm B2 and 20 ppm B3. The response variable is the SO<sub>2</sub> concentration expressed in ppm. To obtain the different levels of SO<sub>2</sub> to be removed, 8.6 mL, 16 mL and 22.9 mL previously diluted in a 1.2-liter container were injected into the chamber. These volumes correspond to the concentrations 5.79 ppm; 10.81 ppm and 20.85 ppm. A fixed amount of CO<sub>2</sub> corresponding to 470ppm was added to the system. The results were processed in the Statgraphic statistical program.

Table 1: Designing the experiment

A: Removal methods	B: Inicial SO <sub>2</sub> concentration
A1 (-1)	B1 (-1)
A2 (0)	B1 (-1)
A3 (1)	B1 (-1)
A1 (-1)	B2 (0)
A2 (0)	B2 (0)
A3 (1)	B2 (0)
A1 (-1)	B3 (1)
A2 (0)	B3 (1)
A3 (1)	B3 (1)

Source: Authors, (2024).

### III.4 SO<sub>2</sub> REMOVAL EXPERIMENT.

The configuration used for the activated carbon adsorption experiment is shown in Figure 1 and used a 2 cm diameter glass column with 1 cm of glass wool was placed at the bottom followed by 8 cm of activated carbon. The carbon used has a granulometry of ± 3 mm (for laboratory use only) and was activated at 120 °C for two hours prior to conducting the experiments.



Figure 1: Experimental setup used for activated carbon adsorption.

Source: Authors, (2024).

The setup in Figure 2 is the one used for SO<sub>2</sub> removal with Ca(OH)<sub>2</sub> and seawater. The box was also connected to a closed loop system. This circuit contained a pump, a wash bottle, an empty wash bottle to trap the water droplets present in the air, a U-shaped glass tube containing 10 g of silica gel to dry the air. After several minutes, zero air was obtained and the pump was turned off. A known amount (470ppm) of diluent was then added to the system.

Seawater from the Bay of Cienfuegos, where the "Carlos Manuel de Céspedes" power plant is located, was used for desulfurization with seawater. This sample was taken in October 2022, against the current and at a depth of 1 m, according to the Cuban standard NC 25:1999 "System of Standards for the Protection of the Environment. Hydrosphere. Specifications and Procedures for the Evaluation of Aquatic Objects for Fishing". [12]



Figure 2: Absorption with seawater and Ca(OH)<sub>2</sub>.

Source: Authors, (2024).

The parameters included in the characterization were pH, salinity and alkalinity of the seawater, parameters that influence the absorption of SO<sub>2</sub> in this sorbent.

## IV. RESULTS AND DISCUSSIONS

### IV.1. ADSORPTION WITH ACTIVATED CARBON.

The results of the adsorption removal process with activated carbon are shown in Table 2 for the three levels evaluated, where it can be observed that in all cases gas removal is achieved, and that as the SO<sub>2</sub> concentration inside the chamber increases, the final concentration (cf) is higher than that obtained in the previous level and the time to reach the minimum SO<sub>2</sub> concentration in each experiment is greater when the initial concentration (ci) of the gas is at its maximum.

Table 2: Results of the adsorption removal process with activated carbon.

Levels	c <sub>i</sub> (µg/m <sup>3</sup> )	c <sub>f</sub> (µg/m <sup>3</sup> )	Time (s)
ambient air	0,030±0,002	0,008±0,007	898
10 ppm	9,061±0,222	0,030±0,045	926
20 ppm	19,139±0,667	0,111±0,028	1200

Source: Authors, (2024).

There have been several studies on the SO<sub>2</sub> removal capacity of activated carbon due to its high efficiency where the removal occurs by passing SO<sub>2</sub> to H<sub>2</sub>SO<sub>4</sub> in the presence of water vapor and oxygen in the gas stream. The H<sub>2</sub>SO<sub>4</sub> is retained on the carbon and subsequently regenerated. These studies demonstrate that the adsorption capacity of activated carbon is not only related to its surface area and pore size, but also to its surface chemical properties, its structure resistant to acidic or basic media and its stability at elevated temperatures. Finally, during this experiment the CO<sub>2</sub> sensor showed constant readings of around 470 ppm and no variation in gas concentration was observed, which is very positive for the intensive cultivation of marine macroalgae, which requires the supply of CO<sub>2</sub>-rich gases.

### IV.2. ABSORPTION WITH CALCIUM HYDROXIDE CA(OH)<sub>2</sub>.

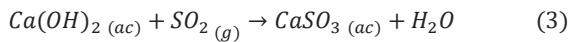
During the SO<sub>2</sub> removal process with the Ca(OH)<sub>2</sub> solution as absorber, as in the previous experiment, it can be observed that in all cases the removal of the gas is achieved, and that since the initial concentration of SO<sub>2</sub> inside the chamber is higher, the final concentration (cf) is higher than that obtained in the previous level as shown in Table 3. The time required to remove 9,626 ppm of SO<sub>2</sub> was less than in the previous level, while the time required to remove 18,972 ppm was higher than in the other experiments.

Table 3: Results of SO<sub>2</sub> removal with calcium hydroxide.

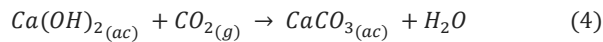
Levels	c <sub>i</sub> (µg/m <sup>3</sup> )	c <sub>f</sub> (µg/m <sup>3</sup> )	Time (s)
ambient air	0,026±0,006	0,003±0,003	920
10 ppm	9,626±0,327	0,059±0,005	909
20 ppm	18,972±0,838	0,065±0,028	1220

Source: Authors, (2024).

The behavior observed in the evaluation of this removal alternative can be explained by Equation 3. The resulting aqueous mixture from the adsorption, formed by CaSO<sub>3</sub>, is usually treated when this method is used on an industrial scale.



During the desulfurization process using the inorganic absorber, the CO<sub>2</sub> sensor recorded an initial concentration of approximately 530 ppm. After the time required for SO<sub>2</sub> removal, a final concentration of 225 ppm CO<sub>2</sub> was obtained, corresponding to a loss of 305 ppm. This behavior can be explained by the consequent formation of calcium carbonate (CaCO<sub>3</sub>), which is confirmed by chemical reaction 4. Despite the efficiency of the method to remove SO<sub>2</sub> gas, the removal of CO<sub>2</sub> is not convenient, since CO<sub>2</sub> is necessary for the photosynthetic process of macroalgae.



### IV.3. CHARACTERIZATION OF SEAWATER

The different parameters of the seawater from the Bay of Cienfuegos (pH, salinity and alkalinity) used for the desulfurization process studied are shown in Table 4.

Table 4: Seawater characterization parameters.

pH	Salinity (Cl <sup>-</sup> ) ups	Alkalinity (CaCO <sub>3</sub> ) mg/L
8,17±0,003	26,50 ± 0,10	171,67±1,03

Source: Authors, (2024).

The pH value obtained was 8.17±0.003 and the temperature indicated by the instrument was 28 °C. Despite the fact that the glass electrode used in the analysis is sensitive to the sodium element, the results obtained were in agreement with those reported by Seisdedo and Moreira [13], measured at the same sampling point and during the same climatic season, which was 8.18. According to the Cuban standard NC 25: 1999 [12] and according to the pH value measured, the water is of good quality with a pH value between 8.1 and 8.3. Zhang and Millero [14] studied the oxidation reaction of S(IV) to S(VI) as a function of pH (4.0-8.5). These studies showed a strong dependence, demonstrating that at pH above 7, there is the tendency for the rate of the reaction to slow down. These researchers also showed that, when the pH is higher than 7.5, the SO<sub>2</sub> dissolved in seawater is mainly present as SO<sub>3</sub><sup>2-</sup> ions.

The salinity value obtained (26.50±0.10 ups), expressed as Cl<sup>-</sup> ions, was similar to that reported by Seisdedo and Moreira [13] in the rainy period, which was 27.10 ups. In addition, considering the Cuban standard NC 25: 1999 [12] and the value obtained, the water is of good quality, since the salinity value is between 26 and 35 ups. The knowledge of this parameter is very important. In the studies carried out by Clarke and Radojevic [15], they demonstrated the catalytic effect of Cl<sup>-</sup> ions in the oxidation reaction of S(IV) to S(VI). At pH 8.17 the total alkalinity value obtained is 171.67±1.03 mg/L, expressed as CaCO<sub>3</sub>. These results confirm the alkaline capacity of seawater, making it suitable for SO<sub>2</sub> removal.

### IV.4 Absorption with seawater.

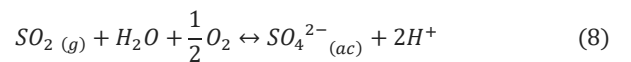
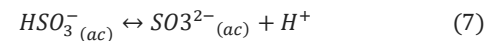
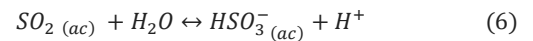
Table 5 shows the results obtained during the SO<sub>2</sub> removal using seawater from the Bay of Cienfuegos, where it is observed that in the third concentration level evaluated, a final SO<sub>2</sub> concentration was obtained that was lower than the previous level. In addition, the time taken to reach the minimum SO<sub>2</sub> concentration in each experiment was greater when the initial concentration (ci) of the gas was at its maximum.

Table 5. Results of SO<sub>2</sub> removal with seawater.

Levels	ci (µg/m <sup>3</sup> )	cf (µg/m <sup>3</sup> )	Time (s)
ambient air	0,022±0,002	0,001±0,001	600
10 ppm	9,808±1,177	0,027±0,045	828
20 ppm	18,830±0,374	0,018±0,001	1108

Source: Authors, (2024).

Gas desulfurization with seawater is explained by the reactions in equations 5 to 8. Dissolved SO<sub>2</sub> exists primarily as SO<sub>3</sub><sup>2-</sup> ions because the pH of seawater is above 7.5. The absorbed SO<sub>2</sub> is then converted to SO<sub>4</sub><sup>2-</sup> ions, Equation 8, which restores the oxygen and pH levels of the water before discharge to the sea.



In this experiment, the CO<sub>2</sub> sensor shows constant readings of about 450 ppm and no variation in gas concentration was observed, which is very positive since macroalgae, like all photosynthetic organisms, use CO<sub>2</sub> as a carbon source.

### IV.5. STATISTICAL ANALYSIS.

In summary, the results obtained during the evaluation of the three desulfurization alternatives were satisfactory, as the SO<sub>2</sub> concentration decreased in all cases. Figures 3 and 4 show the main effects and estimated response surface plots, respectively, as a result of the experimental design, confirming this behavior.

In ambient air, total removal of the ambient concentration of the gas is achieved. At the second and third concentration levels studied, absorption with seawater showed the best results, achieving the lowest final concentration and also the fastest. Clarke and Radojevic, [15] demonstrated that the increase in the SO<sub>2</sub> removal rate with seawater is due to the catalytic effect of the Cl<sup>-</sup> ion. This may be related to the speed at which SO<sub>2</sub> removal occurs compared to with the other methods.

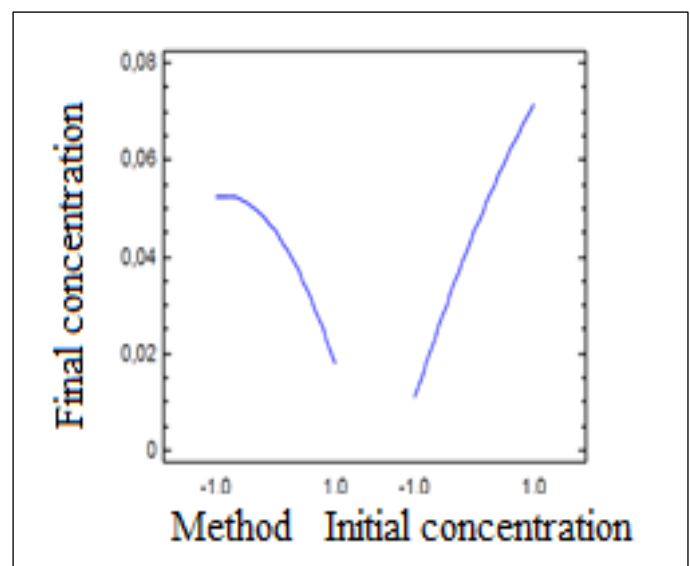


Figure 3: Main effect plot.

Source: Authors, (2024).



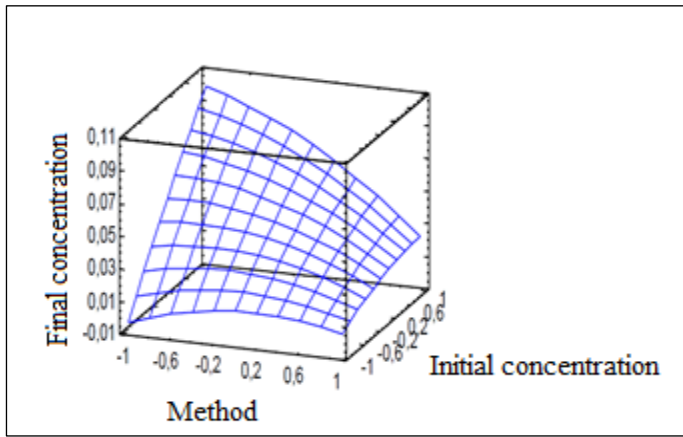


Figure 4: Estimated response surface plot.  
Source: Authors, (2024).

Table 6 shows the results of the ANOVA, which tests the statistical significance of each effect by comparing its mean square to an estimate of the experimental error.

In this case, three effects have a P-value less than 0.05; indicating that they are significantly different from zero at the 95% confidence level. This observation is supported by the Pareto plot (Figure 5). This graph shows that the removal method, the initial SO<sub>2</sub> concentration and the interaction between these two factors correspond to the three effects that have a significant impact on the response variable, since they exceed the standardized effect line.

Tabla 6: Variance Analysis.

Source	Square sum	GI	Medium Square	Reason - F	Value-P
A: Method	0,005270	1	0,005270	8,97	0,0074
B: Initial concentration	0,016562	1	0,016562	28,19	0,0000
AA	0,000613	1	0,000613	1,04	0,3197
AB	0,005376	1	0,005376	9,15	0,0070
BB	0,000101	1	0,000101	0,17	0,6825
blocks	0,000374	2	0,000187	0,32	0,7309
Total error	0,011162		19		0,000587
Total (corr.)			0,039460		26

Source: Authors, (2024).

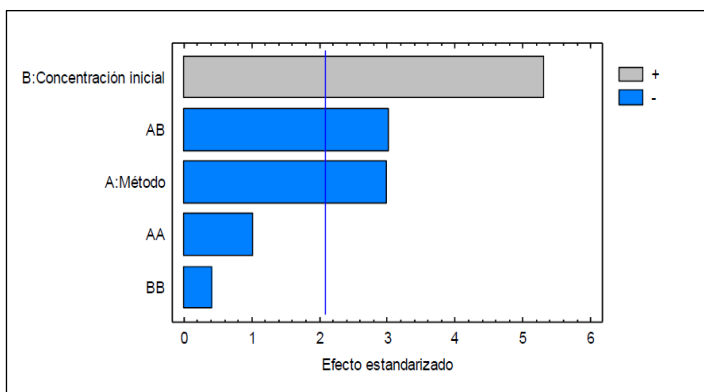


Figura 5: standardized Pareto diagram.  
Source: Authors, (2024).

In addition, the R-squared statistic indicates that the model, as fitted, explains 71.71 % of the variability in the final SO<sub>2</sub> concentration. The standard error of the estimate indicates that the standard deviation of the residuals is 0.0242. The mean absolute error of 0.0143 is the average value of the residuals.

The estimated coefficients of the model for each parameter are shown in Table 7.

Table 7: Model Estimated coefficients.

Coefficient	Estimate
$\pi$	0,045
A: Method	-0,02
B: Inicial Concentration	0,03
AB	-0,02

Source: Authors, (2024).

Finally, equation 4.7 shows the fitted model.

$$c_f = 0,045 - 0,02 \cdot M + 0,03 \cdot c_i - 0,02 \cdot M \cdot c_i \quad (9)$$

Where:

cf: is the final SO<sub>2</sub> concentration, expressed in ppm.

M: is the removal method

ci: is the initial SO<sub>2</sub> concentration, expressed in ppm.

#### IV.6. ALTERNATIVE'S ANALYSIS.

The adsorption capacity of activated carbon makes it an efficient alternative for SO<sub>2</sub> removal. Fortunately, its graphitic structure makes it very stable under a wide range of conditions. It resists high temperatures and sudden temperature changes, is unaffected by acids, alkalis and many different solvents, although it reacts with strong oxidizing agents. Based on these properties, there are methods that allow its reactivation or regeneration, which can eliminate adsorbates of different types and substances deposited on the carbon surface. The use of activated carbon in Cuba is basically limited by its high cost in specialized markets. In addition, its high operating costs limit its use in developing countries.

The high reactivity of Ca(OH)<sub>2</sub> also makes it an efficient alternative for the desulphurization of gaseous effluents. However, the use of this reagent leads to an important problem, since the oxidation of the SO<sub>3</sub><sup>2-</sup> ion precipitates SO<sub>4</sub><sup>2-</sup> ions, which are difficult to remove. This process results in a lower acidity of the medium, which favors the development of algae in gas bioremediation processes. However, the amount of solid waste generated as a result is excessive. In addition, the use of this reagent requires a greater economic investment.

The use of seawater as an absorbent in desulphurization systems proved to be a simple, efficient and economical method. Due to the proximity of the "Carlos Manuel de Céspedes" power plant to the bay, the use of this novel technology represents an additional advantage, since it does not require the purchase and transportation of raw materials. In addition, it does not generate solid waste to be deposited for subsequent treatment. The liquid effluent is mainly seawater, which can be returned to its source without any environmental impact.

Based on the results of this research, a multidisciplinary team will decide on the most feasible alternative for use on an industrial scale. It is important to point out that the methods evaluated will be carried out as primary treatment of gaseous effluents. Subsequently, it is proposed to carry out a secondary treatment based on bioremediation with macroalgae *Ulva lactuca* type, which would improve the removal efficiency of SO<sub>2</sub> gas, as well as other combustion gases generated by the "Carlos Manuel de Céspedes" power plant in the city of Cienfuegos.

It also reinforces the importance of the low-cost SO<sub>2</sub> sensor, which was an essential tool in the evaluation of scrubbing

methods. This research has shown that in addition to its use in air quality monitoring, it can be used in this type of research.

## V. CONCLUSIONS

The removal of SO<sub>2</sub> using an adsorption column with activated carbon proved to be an efficient alternative at the concentration levels evaluated. The removal of the different SO<sub>2</sub> concentrations using the adsorption column with calcium hydroxide showed a higher removal efficiency than the adsorption with activated carbon. The pH, salinity and alkalinity values determined in a seawater sample from the Bay of Cienfuegos were 8.17±0.003; 26.50±0.10 ups and 171.67±1.03 mg/L, which confirms the adequacy for SO<sub>2</sub> gas removal. The removal of SO<sub>2</sub> using an absorption column with seawater proved to be the most efficient alternative among the methods evaluated, at the three concentration levels, since the lowest final concentrations were obtained in the shortest time. The experiments performed demonstrated that low-cost calibrated sensors can be used as a scientific tool to evaluate gaseous effluent removal methods.

## VI. AUTHOR'S CONTRIBUTION

**Conceptualization:** Liset Roche Delgado, Mayra C. Morales Pérez, Rosa Amalia González Rivero, Arianna Álvarez Cruz.

**Methodology:** Liset Roche Delgado, Mayra C. Morales Pérez, Rosa Amalia González Rivero, Arianna Álvarez Cruz, Agustín A. García Rodríguez.

**Investigation:** Liset Roche Delgado, Mayra C. Morales Pérez, Rosa Amalia González Rivero, Arianna Álvarez Cruz, Agustín A. García Rodríguez, Juan Pedro Hernández Touse.

**Discussion of results:** Liset Roche Delgado, Mayra C. Morales Pérez, Rosa Amalia González Rivero, Arianna Álvarez Cruz.

**Writing – Original Draft:** Liset Roche Delgado, Mayra C. Morales Pérez, Rosa Amalia González Rivero, Arianna Álvarez Cruz, Agustín A. García Rodríguez, Juan Pedro Hernández Touse.

**Writing – Review and Editing:** Liset Roche Delgado, Mayra C. Morales Pérez, Rosa Amalia González Rivero, Arianna Álvarez Cruz, Agustín A. García Rodríguez.

**Resources:** Morales Pérez.

**Supervision:** Morales Pérez, Agustín A. García Rodríguez, Juan Pedro Hernández Touse.

**Approval of the final text:** Liset Roche Delgado, Mayra C. Morales Pérez, Rosa Amalia González Rivero.

## VII. ACKNOWLEDGMENTS

The authors would like to thank VLIR-UOS for the financial support provided by the Global Minds project BE2017GMHVLHC106 "A low-cost measuring device to directly monitor exhaust gases generated by fuel engines: Design, development, validation".

## VIII. REFERENCES

- [1] Chao, C. Y. H., & Law, A. A study of personal exposure to nitrogen dioxide using passive samplers. *Building Environment*, (2000). 35, 545–553
- [2] Dunlea, E. J., Herndon, S. C., Nelson, D. D., Volkamer, R. M., San Martini, F., Sheehy, P. M., et al. (2007). Evaluation of nitrogen dioxide chemiluminescence monitors in a polluted urban environment. *Atmospheric Chemistry and Physics Discussions*, 7, 569–604
- [3] Alejo, D.; Morales, M.C.; De la Torre, J.B.; Grau, R.; Bencs, L.; Grieken, R.V.; Espen, P.V.; Sosa, D.; Nuñez, V. Seasonal Trends of Atmospheric Nitrogen Dioxide and Sulfur Dioxide over North Santa Clara, Cuba. *Environ. Monit. Assess.* 2013, 185, 6023–6033. [CrossRef] [PubMed]

[4] Madrazo, J.; Clappier, A.; Cuesta, O.; Belalcazar, L.C.; González, Y.; Bolufé, J.; Sosa, C.; Carrillo, E.; Manso, R.; Canciano, J.; et al. Evidence of Traffic-Generated Air Pollution in Havana. *Atmósfera* 2019, 32, 15–24. [CrossRef]

[5] Frías LópezA. y Barcia SardiñasS., «Inventario de emisiones atmosféricas de las principales fuentes fijas de la ciudad de Cienfuegos», *Rev. Cub. Met.*, vol. 25, abr. 2019.

[6] Srivastava R., Jozewicz W. "Flue Gas Desulfurization: The State of the Art". *J. Air & Waste Manage. Assoc.* December 2001. Vol.51, p 1676-1688

[7] J. Z. Abrams, S. J. Zaczek, A. D. Benz, L. Awerbuch & J. Haidinger (1988) Use of Seawater in Flue Gas Desulfurization, *JAPCA* 2012, 38:7, 969-974, DOI: 10.1080/08940630.1988.10466438

[8] Acosta, A. Desulfuración y deshidrogenación de un diesel modelo mediante carbón activado modificado con (oxi)hidróxidos de Fe y Mn (2017).<http://hdi.handle.net/11627/3126>

[9] Cordoba, P.(2015)Status of Flue Gas Desulphurization (FDG)systems from coal-fired power plants: Overview of the physical-chemical control processes of wet limestone FGDs. *Fuel* 2014 ,V144(6),274-286

[10] Silas K, Ghani W, Choong T, Rashid U. Carbonaceous materials modified catalysts for simultaneous SO<sub>2</sub>/NO<sub>x</sub> removal from flue gas : A review. 2019. *Science and Engineering*. Vol 61issue 1 p134-161. [tps://doi.org/10.1080/01614940.2018.1482641](https://doi.org/10.1080/01614940.2018.1482641)

[11] R. A. González Rivero et al., "Relevance and Reliability of Outdoor SO<sub>2</sub> Monitoring in Low-Income Countries Using Low-Cost Sensors," *Atmos.* 2023, Vol. 14, Page 912, vol. 14, no. 6, p. 912, May 2023, doi: 10.3390/ATMOS14060912.

[12] N.C. 25 "Evaluación de los objetos hídricos de uso pesquero. Sistema de Normas para la Protección del Medio Ambiente, Hidrosfera", Cuba 1999, 12 pp

[13] Seisdedo, M. and A.R. Moreira, "Comportamiento de las características físico-químicas de las aguas y del fitoplancton en la Bahía de Cienfuegos, Cuba ". *Rev. Invest. Mar.* 2007, 28(3), 193-199.

[14] Zhang, J.Z. and F.J. Millero, "The rate of sulfite oxidation in seawater". *Geochimica et Cosmochimica Acta.* 1991, 55(3), 677-685. ISSN: 0016-7037.

[15] Clarke, A. and M. Radojevic, "Chloride ion effects on the aqueous oxidation of SO<sub>2</sub>". *Atmospheric Environment.* 1983, 17(3), 617-624. ISSN: 0004-6981.



ISSN ONLINE: 2447-0228



## RESEARCH ARTICLE

## OPEN ACCESS






# BROKEN MAGNETS FAULT DETECTION IN PMSM USING A CONVOLUTIONAL NEURAL NETWORK AND SVM

Said Benkaihou<sup>1</sup>, Lakhdar Mazouz<sup>2</sup>, Toufik Tayeb Naas<sup>3</sup>, Özüpak Yildirim<sup>4</sup> and Ridha Djamel Mohammedi<sup>5</sup>

<sup>1,5</sup> Applied Automation and Industrial Diagnostics Laboratory at the Department of Electrical Engineering in Faculty of Science and Technology, Ziane Achour University of Djelfa, PO Box 3117, Djelfa 17000, Algeria.

<sup>2,3</sup> Renewable Energy Systems Applications Laboratory (LASER), Department of Electrical Engineering in the Faculty of Science and Technology, Ziane Achour University of Djelfa, PO Box 3117, Djelfa 17000, Algeria.

<sup>4</sup> Department of Electrical Energy, Silvan Vocational School, Dicle University, 21002, Diyarbakır, Turkey.

<sup>1</sup><http://orcid.org/0000-0002-8824-9761> , <sup>2</sup><http://orcid.org/0000-0002-7664-9901> , <sup>3</sup><http://orcid.org/0000-0002-5539-6415>   
<sup>4</sup><http://orcid.org/0000-0001-8461-8702> , <sup>5</sup><http://orcid.org/0000-0003-4170-543X> 

Email: [said.benkaihou@univ-djelfa.dz](mailto:said.benkaihou@univ-djelfa.dz), [l.mazouz@univ-djelfa.dz](mailto:l.mazouz@univ-djelfa.dz), [toufiknaas@gmail.com](mailto:toufiknaas@gmail.com), [yildirim.ozupak@dicle.edu.tr](mailto:yildirim.ozupak@dicle.edu.tr), [r.mohammedi@univ-djelfa.dz](mailto:r.mohammedi@univ-djelfa.dz)

## ARTICLE INFO

## ABSTRACT

**Article History**

Received: July 06th, 2024

Revised: July 08th, 2024

Accepted: July 08th, 2024

Published: July 18th, 2024

**Keywords:**

Broken Magnets,  
Convolutional Neural Network,  
Fault Detection,  
Magnetic Flux Density,  
PMSM.

The Permanent Magnet Synchronous Motor (PMSM) stands as a pivotal component in various applications, yet it remains susceptible to an array of faults within both its rotor and stator, there arises an imperative to swiftly and intelligently address these issues. In this study, a novel approach was undertaken wherein a PMSM design was conceptualized within the Ansys Maxwell program, followed by the deliberate introduction of a fault at the rotor's magnetic level. Specifically, three distinct fault scenarios were delineated based on the number of broken magnets (BM), namely 2, 3, and 4, localized within specific rotor areas. Notably, the magnetic flux density was selected as the focal parameter for this investigation. To effectively detect and diagnose faults stemming from BM, an innovative Convolutional Neural Network (CNN) architecture was devised. Leveraging images of the PMSM design captured during operational phases at various time intervals, the CNN exhibited remarkable efficacy in discerning and categorizing fault instances. Upon analysis of the derived outcomes, it becomes evident that the CNN exhibited unparalleled accuracy in fault detection, achieving a remarkable 100% success rate when juxtaposed with alternative methodologies such as Support Vector Machines (SVM) and K-Nearest Neighbors (KNN), which yielded accuracy rates of 97%.



Copyright ©2024 by authors and Galileo Institute of Technology and Education of the Amazon (ITEGAM). This work is licensed under the Creative Commons Attribution International License (CC BY 4.0).

## I. INTRODUCTION

The industrial sector's reliance on electric motors stems from their versatility and widespread applications across various domains, serving as the linchpin of development in critical areas such as aircraft, electric cars, and ships [1-3]. Despite their proven efficiency, electric motors are subject to degradation over time, succumbing to various faults across different components. Hence, there exists a pressing need to explore methodologies facilitating the rapid detection, diagnosis, and mitigation of these faults.

The PMSM stands as a cornerstone of the industrial sector, yet it is susceptible to a myriad of faults, particularly at the rotor and stator levels, which can significantly impact operational quality [4],[5]. In response to this challenge, artificial intelligence emerges as a potent and expedient tool for fault detection.

The design and analysis of electric motors, alongside the study of operational phenomena, are typically conducted using specialized software platforms such as Ansys Maxwell [6],[7].

These programs offer standardized templates tailored for diverse machinery, facilitating the study of magnetic phenomena

distribution and enabling fault simulations to evaluate their impact on machine performance.

Recent research endeavors have focused on employing advanced techniques such as the finite element method to design induction motors and investigate fault scenarios, including broken bars [8], [9], Bearing Fault, where Line Currents were relied upon to detect the fault in the induction motor [10]. Additionally, machine learning methodologies have proven instrumental in fault detection and diagnosis across various motor types [11]. Interest in diagnosing the Broken Rotor Bar using Adaptive Neuro-Fuzzy Inference in the induction motor [12], Convolutional Neural Network was used in diagnosing the Broken Rotor Bar [13].

In the realm of PMSM, common mechanical and electrical faults include Bearing Fault, Demagnetization, and Eccentricity [14],[15], The demagnetization fault was detected in PMSM [16], while the Neural Network was used to detect the Rolling Bearing Fault in PMSM [17], Efforts have been directed towards the detection and mitigation of these faults using machine learning approaches.

Techniques such as Convolutional Neural Networks (CNN) and Support Vector Machines (SVM) have been employed to discern faults, including broken magnets, with a focus on monitoring magnetic flux density and analyzing images captured during specific operational intervals [18],[19] In summary, this study proposes the integration of CNN and SVM algorithms for the detection of broken magnets in PMSM [20]. Leveraging the design capabilities of Ansys Maxwell, simulations encompassing various fault scenarios were conducted. Magnetic flux density serves as a crucial parameter for monitoring machine performance, with images extracted at specific intervals to facilitate a comparative analysis between healthy and fault states, thereby contributing to the advancement of fault detection methodologies in electric motors.

## II. DESIGN PMSM AND BROKEN MAGNETS

Designing a PMSM and simulating a broken magnet scenario involves several steps and considerations. Here is a general description of this process consisting of the following steps:

- **Motor Design:** Firstly, the specifications of the PMSM are defined. These specifications include parameters such as rated power, voltage, current, speed, torque, and physical dimensions. The motor model is created using design software such as Ansys Maxwell. Details like the number of poles, slot geometry, winding configuration, and magnet material are specified.
- **Magnet Arrangement:** The arrangement of magnets within the motor structure is determined. Permanent magnets are typically mounted on the rotor surface and interact with stator windings to produce torque.
- **Finite Element Method (FEM):** FEM techniques are used to analyze the electromagnetic performance of the motor design. This involves solving Maxwell's equations to calculate magnetic flux distribution, induced currents, and electromagnetic forces within the motor.
- **Fault Definition:** Adjustments are made within the PMSM model to simulate the broken magnet scenario. Changes are made to the shape, size, or magnetic properties of one

or more magnets to simulate them being partially or fully damaged.

- **Stress Analysis:** Stress analysis is conducted to evaluate the mechanical effects of the broken magnet within the motor structure. Mechanical stress, deformation, and vibration are considered to assess the structural integrity of the motor under fault conditions.
- **Performance Evaluation:** The performance of the PMSM under normal and fault conditions is assessed. Parameters such as torque-speed characteristics, efficiency, power factor, and electromagnetic noise are measured to evaluate the impact of the broken magnet on motor operation.
- **Fault Detection Algorithm:** A fault detection algorithm is developed and implemented using machine learning techniques. By training the algorithm with data based on motor performance indicators, such as Convolutional Neural Networks (CNN) or Support Vector Machines (SVM), the presence of a broken magnet is accurately detected.
- **Testing and Validation:** The motor design and fault detection algorithm are validated through experimental testing.

By comparing simulation results with experimental data, the accuracy and effectiveness of the proposed design and detection method are verified.

Ansys Maxwell plays a pivotal role in both designing and analyzing PMSM, offering a comprehensive platform where machine characteristics can be meticulously defined and parameters seamlessly incorporated. This software not only furnishes a detailed depiction of the studied machine's specifications, as delineated in Table 1, but also facilitates the visual representation of the PMSM design, as illustrated in Figure 1. Moreover, Ansys Maxwell empowers engineers to specify the materials used in magnet formation and simulate faults within the rotor assembly.

The extent of rotor damage, quantified by the number of broken magnets, is meticulously determined for each case, as elucidated in Figure 2. Through these capabilities, Ansys Maxwell serves as an indispensable tool in the meticulous design and fault analysis of PMSMs, providing engineers with the insights needed to optimize motor performance and reliability.

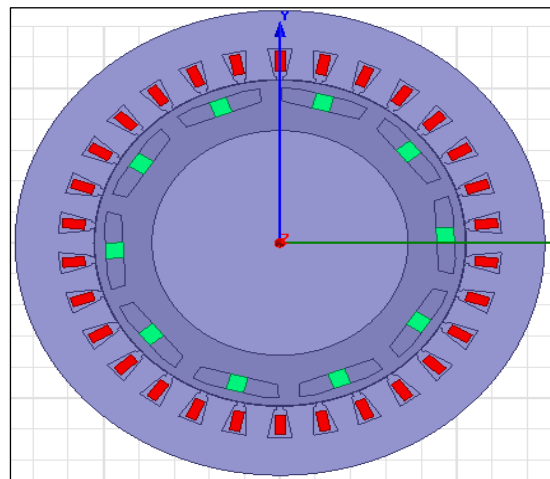


Figure 1: PMSM design.  
Source: Authors, (2024).

Table 1: Design parameters.

Component	Value
Diameter stator outer / inner	300 mm / 211mm
Diameter rotor outer / inner	210 mm / 145mm
Rotor and stator material	steel M27_29G
Magnet material	Br=0.39T, Mu=1.1
Stator slots	30
Number of poles	10

Source: Authors, (2024).

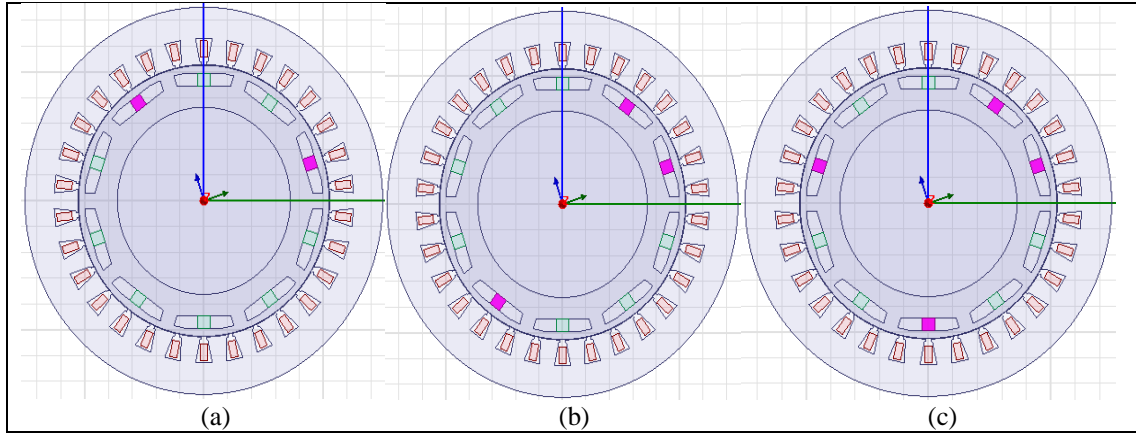


Figure 2: Broken magnets fault: (a) 2 BM, (b) 3BM, (c) 4BM.

Source: Authors, (2024).

### III. SUGGESTED ALGORITHMS

#### III.1 SUPPORT VECTOR MACHINE

Support Vector Machine (SVM) is a powerful supervised learning algorithm used for classification and regression tasks. It is particularly effective in scenarios where the data is complex and not linearly separable. SVM works by finding the optimal hyperplane that best separates the data points into different classes while maximizing the margin, which is the distance between the hyperplane and the nearest data points of each class.

The key idea behind SVM is to transform the input data into a higher-dimensional space using a kernel function. In this higher-dimensional space, the data points become more separable, allowing for the construction of a hyperplane that effectively separates different classes. One of the main advantages of SVM is

its ability to handle high-dimensional data and effectively deal with overfitting. Additionally, SVM has been shown to perform well even with relatively small training datasets.

SVM can be used for both classification and regression tasks. In classification, the goal is to predict the class label of new data points, while in regression, the goal is to predict a continuous value. Overall, SVM is a versatile and powerful machine learning algorithm that has been successfully applied in various domains, including image recognition, text classification, and bioinformatics.

SVM is a model for classifying data that relies on separating classes with equal limits through a dividing line between the support vectors of the data and the hyperplane [21], [22], which is the resolution, as Figure 3 shows.

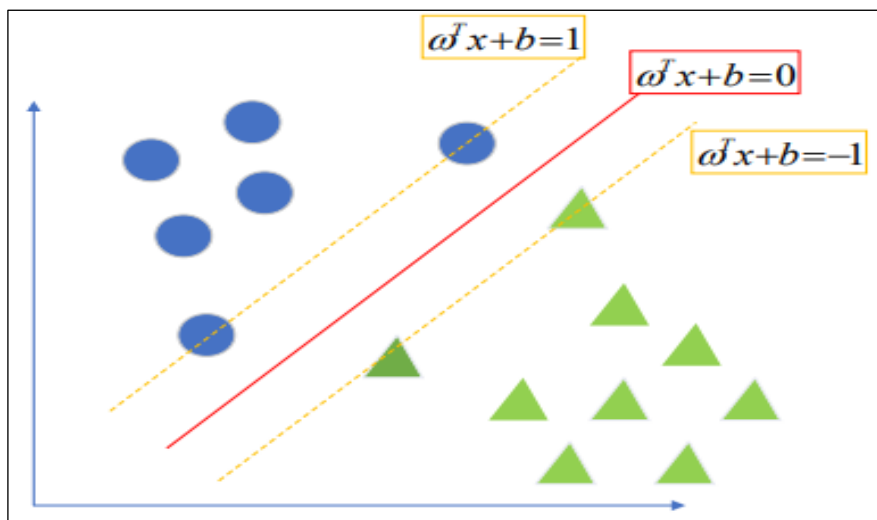


Figure 3: Support Vector Machine principles.

Source: [21].

### III.2 K-NEAREST NEIGHBORS

The k-Nearest Neighbors (k-NN) algorithm is a simple yet effective supervised learning method used for classification and regression tasks. It is a non-parametric algorithm, meaning it does not make any assumptions about the underlying data distribution.

In k-NN classification, the algorithm works by finding the k nearest data points (neighbors) to a given query point based on a distance metric, typically Euclidean distance. The class label of the query point is then determined by a majority vote among its k nearest neighbors. For example, if  $k=3$  and two neighbors belong to class A and one neighbor belongs to class B, the query point will be classified as class A.

In k-NN regression, the algorithm predicts the output value for a given query point by averaging the output values of its k nearest neighbors. This can be useful for predicting continuous variables. One of the main advantages of the k-NN algorithm is its simplicity and ease of implementation. It does not require training a model in the traditional sense, making it suitable for online learning scenarios where new data points are continuously added to the dataset.

However, k-NN has some limitations, such as being computationally expensive for large datasets since it requires calculating distances between the query point and all other data points. Additionally, the choice of the parameter k can significantly impact the performance of the algorithm, and it may not perform well in high-dimensional spaces. Overall, k-NN is a versatile algorithm that can be used for both classification and regression tasks, especially in scenarios where the dataset is small or the underlying data distribution is unknown.

KNN is a machine learning algorithm used to classify data and extract features based on the number K of neighbors. The distance between the unclassified sample and the rest of the samples is calculated, and the classification class is determined by determining the smallest distance to the largest number of neighbors [23],[24].

### III.3 CONVOLUTIONAL NEURAL NETWORK

A Convolutional Neural Network (CNN) is a type of deep learning algorithm commonly used for analyzing visual imagery. It is particularly well-suited for tasks such as image classification, object detection, and image segmentation. CNNs are inspired by the organization of the visual cortex in animals, where neurons in

the brain respond to specific stimuli located in a small region of the visual field, known as the receptive field. Similarly, CNNs consist of layers of interconnected neurons organized in a hierarchical manner, each layer processing increasingly complex features of the input image. The key components of a CNN include [25],[26]:

- **Convolutional Layers:** These layers apply a set of learnable filters (also known as kernels) to the input image to extract various features, such as edges, textures, and shapes. Each filter slides across the input image, performing element-wise multiplication and summing the results to produce a feature map.
- **Pooling Layers:** Pooling layers downsample the feature maps produced by the convolutional layers, reducing the spatial dimensions of the input. This helps to make the network more robust to variations in input images and reduces the computational cost.
- **Activation Functions:** Non-linear activation functions, such as ReLU (Rectified Linear Unit), are applied to the feature maps to introduce non-linearity into the network and enable it to learn complex patterns and relationships in the data.
- **Fully Connected Layers:** These layers connect every neuron in one layer to every neuron in the next layer, allowing the network to learn high-level representations of the input features and make predictions.
- **Loss Function:** The loss function measures the difference between the predicted output of the network and the true labels. It serves as a feedback signal to update the network's parameters during the training process.

CNNs are trained using large datasets of labeled images through a process called backpropagation, where the network learns to adjust its parameters to minimize the loss function. Once trained, CNNs can accurately classify and analyze images, making them widely used in various applications, including computer vision, medical imaging, and autonomous driving [27],[28]. The working principle of CNN is shown in Figure 4.

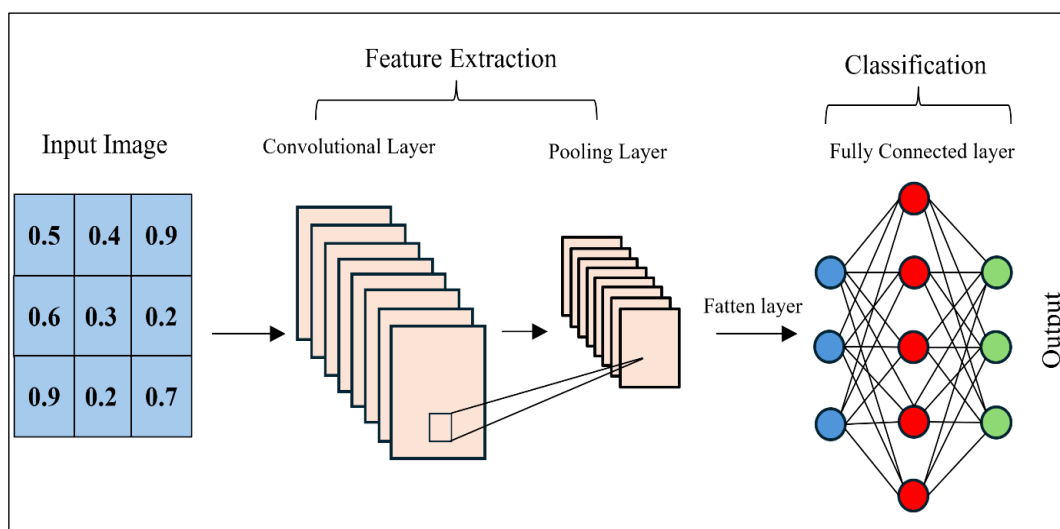


Figure 4: Architecture of a CNN.  
Source: Authors, (2024).

#### IV. RESULTS AND DISCUSSIONS

During the operation of the machine, spanning from 0 seconds to 0.2 seconds, a meticulous examination of the magnetic flux density across different regions of the apparatus was conducted. Notably, as time progressed, discernible variations in the distribution of magnetic flux density emerged, delineated in detail in Figure 5.

To further scrutinize the performance of the machine, a deliberate fault was induced at the magnet level, warranting an in-depth analysis of the magnetic flux density in each distinct scenario. This meticulous study enabled the collection of pertinent images crucial for the subsequent detection and diagnosis of magnet breakage, employing the robust capabilities of Convolutional Neural Networks (CNN).

Figures 6, 7 and 8 offer comprehensive visualizations of magnet breakage instances, showcasing the distinct magnetic flux

density distributions observed in each case. Leveraging the power of CNN, these images serve as invaluable inputs for the classification process.

The convolutional process, pivotal in CNN's functionality, is adeptly employed utilizing a filter mechanism to extract fundamental features inherent in the collected images. Subsequently, based on the extracted features, classification into either a healthy state or a fault state is determined, as succinctly illustrated in Figure 9.

Through this meticulous process, CNN effectively discerns and categorizes the state of the machine, facilitating prompt diagnosis and remediation of potential faults.

Table 2 shows the structure and parameters used in the CNN algorithm.

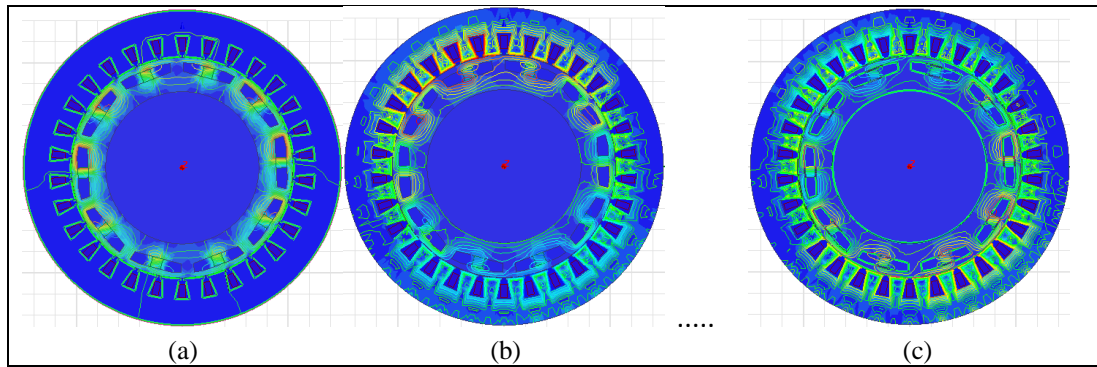


Figure 5: healthy case: (a)  $t=0s$ , (b)  $t=0.13s$ , (c)  $t=0.2s$ .

Source: Authors, (2024).

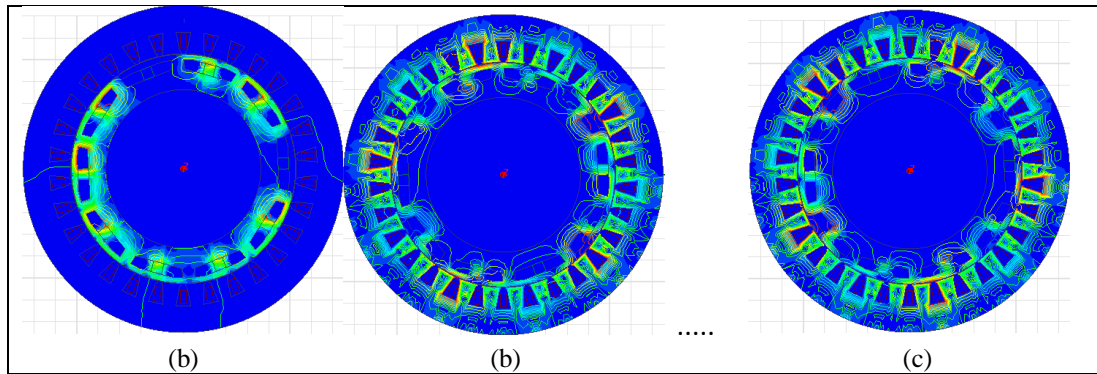


Figure 6: 2MB fault case: (a)  $t=0s$ , (b)  $t=0.13s$ , (c)  $t=0.2s$ .

Source: Authors, (2024).

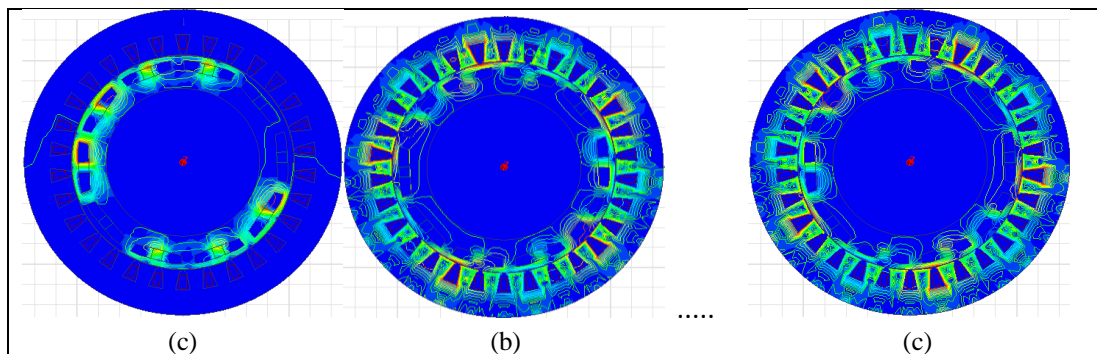


Figure 7: 3MB fault case: (a)  $t=0s$ , (b)  $t=0.13s$ , (c)  $t=0.2s$ .

Source: Authors, (2024).

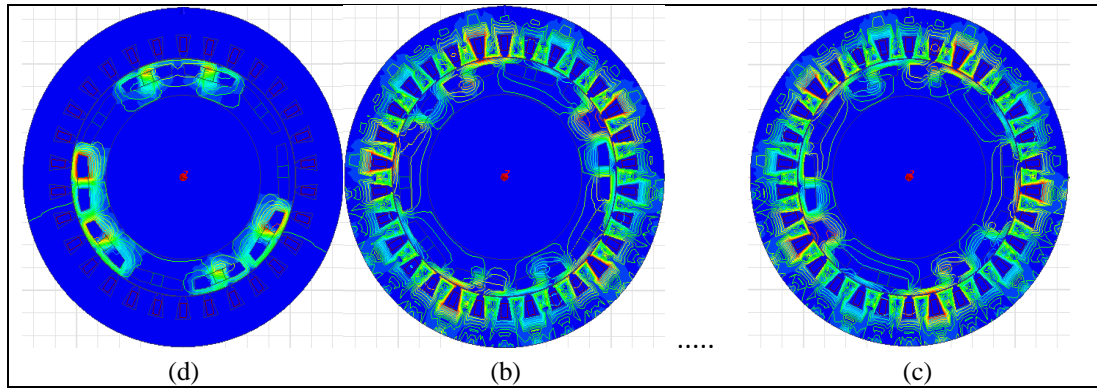


Figure 8: 4MB fault case: (a)  $t=0s$ , (b)  $t=0.13s$ , (c)  $t=0.2s$ .  
Source: Authors, (2024).

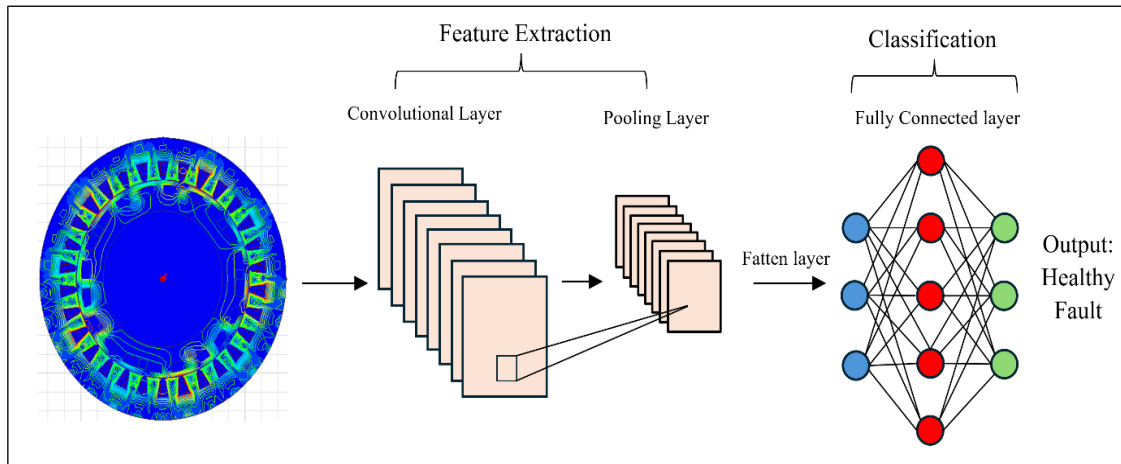


Figure 9: Health or fault status from images using CNN.  
Source: Authors, (2024).

Table 2: CNN parameters.

Layer	Output Shape	Parameter
Conv2d (Conv2D)	(None,438,438,16)	4480
max_pooling2d (MaxPooling2D)	(None,219,219,16)	
Conv2d (Conv2D)	(None,217,217,32)	46400
max_pooling2d (MaxPooling2D)	(None,108,108,32)	
Conv2d (Conv2D)	(None,106,106,64)	184960
max_pooling2d (MaxPooling2D)	(None,53,53,64)	
flatten (Flatten)	(None,179776)	0
dense (Dense)	(None,64)	1150572865
dense_1 (Dense)	(None,1)	

Source: Authors, (2024).

Three distinct cases were meticulously delineated to evaluate the performance metrics of accuracy and loss across varying epochs. Through rigorous experimentation, it was discerned that the third case yielded superior results, showcasing enhanced accuracy and minimized loss, as visually depicted in Figures 10 and 11. By systematically varying the epochs, the CNN model was rigorously trained and fine-tuned to optimize its performance across different scenarios. The evolution of accuracy and loss metrics over successive epochs provides invaluable insights into the model's learning dynamics and convergence behavior.

These figures serve as comprehensive visual aids, succinctly summarizing the observed trends in accuracy and loss

across the three identified cases. Notably, the superior performance exhibited by the third case underscores the efficacy of the training strategy employed, signifying a successful convergence towards an optimal solution. These findings underscore the importance of meticulous experimentation and parameter tuning in achieving robust performance outcomes in machine learning tasks. Through iterative refinement and evaluation, researchers can ascertain the most effective strategies for training CNN models to achieve desired performance objectives.

In Table 3, the accuracy of CNN is 100% compared to the rest of the techniques.

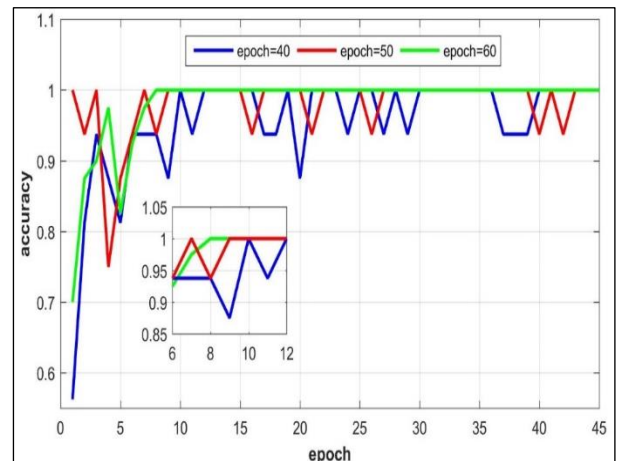


Figure 10: accuracy with epoch number.  
Source: Authors, (2024).



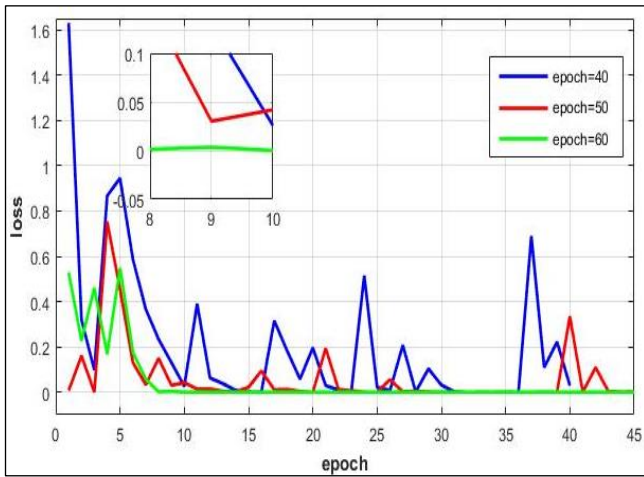


Figure 11: Loss by epoch number.  
Source: Authors, (2024).

Table 3: accuracy.

Methods	Accuracy( %)
SVM	97
KNN	97
CNN	100

Source: Authors, (2024).

## V. CONCLUSION

In the scope of this research endeavor, a novel approach utilizing both Convolutional Neural Network (CNN) and Support Vector Machine (SVM) algorithms was introduced to detect faults stemming from magnet breakage within the rotor assembly. The study encompassed three distinct cases categorized by the number of broken magnets: 2, 3, and 4, each representing varying degrees of fault severity. Leveraging sophisticated image processing techniques, these algorithms were adeptly deployed for fault classification based on meticulously selected features. Notably, magnetic flux density emerged as the focal parameter for this investigation, chosen for its efficacy in capturing subtle variations indicative of magnet breakage. The resultant findings, extracted through rigorous experimentation and analysis, underscore the remarkable capability of CNN in discerning and diagnosing faults within the rotor assembly. Through comprehensive evaluation, CNN demonstrated notable proficiency in accurately detecting and classifying fault instances, thereby showcasing its potential as a reliable tool for fault diagnosis in complex machinery such as PMSMs.

## VI. AUTHOR'S CONTRIBUTION

**Conceptualization:** Said BENKAIHOUL, Lakhdar MAZOUZ, Toufik Tayeb NAAS, Özüpak YILDIRIM and Ridha Djamel MOHAMMEDI.

**Methodology:** Said BENKAIHOUL, Lakhdar MAZOUZ and Toufik Tayeb NAAS.

**Investigation:** Said BENKAIHOUL, Lakhdar MAZOUZ, Özüpak YILDIRIM

**Discussion of results:** Said BENKAIHOUL, Lakhdar MAZOUZ, Toufik Tayeb NAAS, Özüpak YILDIRIM and Ridha Djamel MOHAMMEDI.

**Writing – Original Draft:** Said BENKAIHOUL, Toufik Tayeb NAAS and Özüpak YILDIRIM.

**Writing – Review and Editing:** Said BENKAIHOUL, Lakhdar MAZOUZ, Toufik Tayeb NAAS, Özüpak YILDIRIM and Ridha Djamel MOHAMMEDI.

**Resources:** Said BENKAIHOUL and Özüpak YILDIRIM.

**Supervision:** Said BENKAIHOUL, Lakhdar MAZOUZ, Toufik Tayeb NAAS, Özüpak YILDIRIM and Ridha Djamel MOHAMMEDI.

**Approval of the final text:** Said BENKAIHOUL, Lakhdar MAZOUZ, Toufik Tayeb NAAS, Özüpak YILDIRIM and Ridha Djamel MOHAMMEDI.

## VII. REFERENCES

- [1] X. Sun, Z. Shi, G. Lei, Y. Guo, and J. Zhu, "Analysis and design optimization of a permanent magnet synchronous motor for a campus patrol electric vehicle", *IEEE Transactions on Vehicular Technology*, vol. 68, no.11, pp.10535-10544, September 2019. DOI:10.1109/TVT.2019.2939794.
- [2] J. A. Luta, H. Liu, D. A. Moguel, S. D. Pekarek, and J. A. Weibel, "Validation of a Thermal Model for Electromagnetic Co-Optimization of Electric Machines", in *2023 IEEE Energy Conversion Congress and Exposition (ECCE)*, IEEE, pp. 4099-4104, October 2023. DOI: 10.1109/ECCE53617.2023.10362916.
- [3] Q. Huang, Q. Huang, H. Guo, and J. Cao, "Design and research of permanent magnet synchronous motor controller for electric vehicle," *Energy Science & Engineering*, vol. 11, no. 1, pp. 112-126, 2023. DOI: <https://doi.org/10.1002/ese3.1316>.
- [4] P. N. Mueller, L. Woelfl, and S. Can, "Bridging the gap between AI and the industry—A study on bearing fault detection in PMSM-driven systems using CNN and inverter measurement", *Engineering Applications of Artificial Intelligence*, vol. 126, p. 106834, November 2023. DOI: <https://doi.org/10.1016/j.engappai.2023.106834>.
- [5] A. Aggarwal, and E. G. Strangas, "Review of detection methods of static eccentricity for interior permanent magnet synchronous machine", *Energies*, vol. 12, no. 21, October 2019. <https://doi.org/10.3390/en12214105>
- [6] M. Tang, A. Wang, and Z. Zhu, "Asynchronous Motor Fault Diagnosis Output Based on VMD-XGBoost," *IEEE 4th China International Youth Conference on Electrical Engineering (CIYCEE)*, pp. 1-7, December 2023. DOI: 10.1109/CIYCEE59789.2023.10401350.
- [7] S. Benkaihou, L. Mazouz, and T. T. Naas, "Advanced Design of DC Machines Using Finite Element Method Simulator", *International Journal of Advanced Studies in Computers, Science and Engineering*, vol. 11, no. 2, pp. 8-18, February 2022.
- [8] N. Praveen Kumar, and T. B. Isha, "Electromagnetic signature study of a closed loop speed controlled three-phase induction motor under broken rotor bar fault using finite element method", *Journal of Engineering Science and Technology*, vol. 14, no. 5, pp. 2731-2745, October 2019.
- [9] K. Edomwandekhoe, and X. Liang, "Advanced feature selection for broken rotor bar faults in induction motors", *CIIEEE/IAS 54th Industrial and Commercial Power Systems Technical Conference (I&CPS)*, vol. 2018-May, pp. 1-10, May 2018. DOI: 10.1109/ICPS.2018.8369981.
- [10] S. Muthukumar, A. Rammohan, S. Sekar, M. Maiti, and K. Bingi, "Bearing fault detection in induction motors using line currents", *ECTI Transactions on Electrical Engineering, Electronics, and Communications*, vol. 19, no. 2, pp. 209-219, June 2021. DOI: 10.37936/ecti-ec.2021192.244163.
- [11] E. Irgat, A. Ünsal, and H. T. Canseven, "Detection of Eccentricity Faults of Induction Motors Based on Decision Trees", *13th International Conference on Electrical and Electronics Engineering (ELECO)*, pp. 435-439, November 2021. DOI: 10.23919/ELECO54474.2021.9677809.
- [12] S. E. Chehaidia, H. Cherif, M. Alraddadi, M. I. Mosaad, and A. M. Bouchelaghem, "Experimental Diagnosis of Broken Rotor Bar Faults in Induction Motors at Low Slip via Hilbert Envelope and Optimized Subtractive Clustering Adaptive Neuro-Fuzzy Inference System", *Energies*, vol. 15, no. 18, September 2022. DOI: <https://doi.org/10.3390/en15186746>.
- [13] K. Barrera-Ilanga, and J. Burriel-valencia, "A Comparative Analysis of Deep Learning Convolutional Neural Network Architectures for Fault Diagnosis of

Broken Rotor Bars in Induction Motors”, *Sensors*, vol. 23, no. 19, p. 8196, September, 2023. DOI: <https://doi.org/10.3390/s23198196>.

[14] S. Ghosh, “Method for Fault Diagnosis and Speed Control of PMSM”, *Computer System Science Engineering*, vol. 45, no. 3, pp. 2391–2404, 2023. DOI: [10.32604/csse.2023.028931](https://doi.org/10.32604/csse.2023.028931).

[15] P. W. Thamke, N. M. Yewale, U. B. Vaidya, and P. G. Asutkar, “Faults associated with permanent magnet synchronous motor,” *International Journal of Core Engineering & Management*, vol. 2, no. 3, pp. 211–217, 2015.

[16] F. Nian, and Y. Yu, “PMSM Demagnetization Fault Diagnosis Based on Back-EMF Signal”, in *Journal of Physics: Conference Series*, vol. 2395, no. 1, p. 012041, December 2022. DOI: [10.1088/1742-6596/2395/1/012041](https://doi.org/10.1088/1742-6596/2395/1/012041).

[17] P. Ewert, T. Orłowska-kowalska, and K. Jankowska, “Effectiveness Analysis of PMSM Motor Rolling Bearing Fault Neural Networks”, *Energies*, vol. 14, no 3, p. 712. January 2021. DOI: <https://doi.org/10.3390/en14030712>.

[18] E. Aslan, and Y. Özüpak, “Classification of Blood Cells with Convolutional Neural Network Model”, *Bitlis Eren Üniversitesi Fen Bilimleri Dergisi*, vol. 13, no. 1, pp. 314–326, March 2024. DOI: <https://doi.org/10.17798/bitlisfen.1401294>.

[19] Q. Zhang, X. Wei, Y. Wang, and C. Hou, “Convolutional Neural Network with Attention Mechanism and”, *Sensors*, vol. 24, no. 6, p. 1831, March 2024. DOI: <https://doi.org/10.3390/s24061831>.

[20] S. Benkaihou, L. Mazouz, T. T. Naas, Ö. Yıldırım, and A. Regaz, “Magnetic rotor breakage study in permanent magnet synchronous motor at COMSOL multiphysics and fault detection using machine learning”, *Studies in Engineering and Exact Sciences*, vol. 5, no. 1, pp. 603–618, March 2024. DOI: <https://doi.org/10.54021/seesv5n1-034>.

[21] X. Zhang, B. Zhao, and Y. U. N. Lin, “Machine Learning Based Bearing Fault Diagnosis Using the Case Western Reserve University Data: A Review”, *IEEE Access*, vol. 9, p. 155598-155608, November 2021. DOI: [10.1109/ACCESS.2021.3128669](https://doi.org/10.1109/ACCESS.2021.3128669).

[22] M. C. Kim, J. H. Lee, D. H. Wang, and I. S. Lee, “Induction Motor Fault Diagnosis Using Support Vector Machine, Neural Networks, and Boosting Methods”, *Sensors*, vol. 23, no. 5, February 2023. DOI: <https://doi.org/10.3390/s23052585>.

[23] P. Kumar, and A. S. Hati, “Review on Machine Learning Algorithm Based Fault Detection in Induction Motors”, *Archives of Computational Methods in Engineering*, vol. 28, no. 3, pp. 1929–1940, 2021. DOI: <https://doi.org/10.1007/s11831-020-09446-w>.

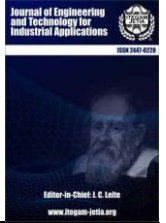
[24] L. V. Vaz, M. C. Gonçalves, I. C. P. Dias, and E. O. B. Nara, “Application of a production planning model based on linear programming and machine learning techniques”, *ITEGAM-JETIA*, vol. 10, no 45, p. 17-29, 2024. DOI: <https://doi.org/10.5935/jetia.v10i45.920>.

[25] R. N. Zufar, and D. Banjerdpongchai, “Selection of Lightweight CNN Models with Limited Computing Resources for Drone Collision Prediction”, *ECTI Transactions on Electrical Engineering, Electronics, and Communications*, vol. 22, no. 1, pp. 1–10, February 2024. DOI: <https://doi.org/10.37936/ecti-ee.2024221.251164>.

[26] A. Jenefa, E. Veemaraj, and A. Lincy, “ABM-OCD: Advancing ovarian cancer diagnosis with attention-based models and 3D CNNs”, *ITEGAM-JETIA*, vol. 9, no 43, p. 23-33, 2023. DOI: <https://doi.org/10.5935/jetia.v9i43.904>.

[27] D. Ruan, J. Wang, J. Yan, and C. Gühmann, “CNN parameter design based on fault signal analysis and its application in bearing fault diagnosis”, *Advanced Engineering Informatics*, vol. 55, p. 101877, October 2022. DOI: <https://doi.org/10.1016/j.aei.2023.101877>.

[28] A. F. Amiri, S. Kichou, H. Oudira, A. Chouder, and S. Silvestre, “Fault Detection and Diagnosis of a Photovoltaic System Based on Deep Learning Using the Combination of a Convolutional Neural Network (CNN) and Bidirectional Gated Recurrent Unit (BiGRU)”, *Sustainability*, vol. 16, no. 3, p. 1012, January 2024. DOI: [10.3390/su16031012](https://doi.org/10.3390/su16031012).



## CROP RECOMMENDATION SYSTEM USING MACHINE LEARNING

Vanadana Kale<sup>1</sup> Badri Narayan Mohapatra<sup>2</sup>

<sup>1,2</sup> Assitant Professor, Department of Instrumentation AISSMS IOIT, Pune, INDIA.

<sup>1</sup><http://orcid.org/0000-0002-7724-9977> , <sup>2</sup><http://orcid.org/0000-0003-1906-9932> .

Email:<sup>1</sup> [badri1.mohapatra@gmail.com](mailto:badri1.mohapatra@gmail.com),<sup>2</sup> [vandana.kale@aissmsioit.org](mailto:vandana.kale@aissmsioit.org)

### ARTICLE INFO

#### Article History

Received: July 07th, 2024

Received: July 08th, 2024

Accepted: July 08th, 2024

Published: July 18th, 2024

#### Keywords:

Crop recommendation system, correlation, random forest, support vector machine, k-nearest neighbor.

### ABSTRACT

Agriculture is the main field of employment in India. Farmers are faced with many problems when evaluating the yield of their crops. The production of crops plays an important role in our Indian economy. This proposed system helps the farmers choose suitable crops based on rainfall, humidity, type of soil, pH of soil, and temperature. Accurate crop prediction results in increased crop cultivation. It will help farmers by reducing the losses they face and improving yield. Machine learning plays an important role in the area of crop cultivation. This work proposes a crop recommendation system using machine learning techniques such as k-nearest neighbor (KNN), artificial neural network (ANN), random forest (RF), and support vector machine (SVM). The models are simulated comprehensively on an Indian data set. The SVM predictive model had an accuracy of 97.85% and a training time of 218.691ms. The K-NN predictive model gave an accuracy of 97.95% and a training time of 218.691ms, and the RF gave an accuracy of 99.22% and a training time of 138.021ms. This model is beneficial to farmers because it allows them to know the type of crop before cultivating the agricultural field and thus encourages them to make suitable decisions.



Copyright ©2024 by authors and Galileo Institute of Technology and Education of the Amazon (ITEGAM). This work is licensed under the Creative Commons Attribution International License (CC BY 4.0).

### I. INTRODUCTION

Modern techniques are now being used and put into practice by other countries for financial gain. One can only imagine how much of an advantage they already have when it comes to using scientific and technological ways to improve agriculture and farming. India, on the other hand, continues to use farming's conventional methods and technologies. As we all know, a significant portion of our nation's income comes from agriculture alone. When discussing the gross domestic product value, the income is quite useful. As we get closer to globalization, the need for food has multiplied. To fulfill food demand, crop yields increase if farmers can accurately predict crop growth.

In this work, we have compiled a dataset that includes data on rainfall, meteorological conditions, and various soil nutrients. Input parameters such as nitrogen (N), phosphorus (P), potassium (K), soil PH, humidity, temperature, and rainfall are used to suggest the best crop. The most appropriate crop is suggested based on the parameters. This will help farmers better understand agricultural production patterns while taking regional and

environmental aspects into account. Additionally, our approach foresees the dearth of any specific inputs needed to develop a certain crop. The agricultural industry might greatly benefit from our predictive method. With the aid of our predictive technology, the issue of nutrient deficiency in certain areas—caused by the reason of planting the improper crop at the wrong time is eliminated. Farmers' production efficiency decreases as a result. Agriculture will undoubtedly advance to new heights as more and more science is applied to it is used a random forest algorithm [1] to predict the best crop yield. They achieved the most accurate value. The KNN algorithm was used by [2]. For the implementation of the predictive model, real-time data from Tamil Nadu was used, and the architecture was checked using samples. For [3] says that in this paper, SVM, naive Bayes, RF, and DT are used. With an accuracy of 96%, RF is more accurate than DT and has the highest accuracy value when compared to SVM. used supervised machine learning methods in this paper. The main algorithms employed were decision tree learning, K-Nearest Neighbour Regression, and RF algorithms. The suggested system's accuracy for DT, KNN, and the random forest was

90.20%, 89%, and 90.43%, respectively. In this paper, [4] describes the important work done by data mining techniques in the agricultural sector. They have incorporated KNN, SVM, RF, and others. The harvests were mostly predicted based on climate features, giving an accuracy score of 95%. According to [5] in this paper, KNN, SVM, RF, neural networks, and decision trees have all been employed. Compared to neural networks, random forests perform significantly better. P.K. Ramesh in this work [2],[6] propose a yield prediction system for farmers in which algorithms such as SVM, MLR, and RF are used. The random forest among them demonstrated the best outcome with 95% accuracy. In this, [7] worked on the SVM algorithm. It is taken into consideration for classification to evaluate the correctness of the suggested technique, and a confusion matrix is created [8]. To determine the best crop to be farmed, this paper uses the CNN and Random Forest models. The accuracy provided by the Random Forest algorithm was 75%, whereas the accuracy provided by the CNN architecture was 95.21%. (Chaudhary)illustrate the application of the Random Forest and Decision Tree models to forecast which crop will grow best in each type of soil depending on the available data. According to [9] use decision trees, Nave Bayes, RF, and SVM. (Namgiri Suresh)in this article [2], crop yield prediction is done by using the random forest algorithm. Here, data collected from an online source and RF gave an accuracy of 75%. According to [10], using a neuro-fuzzy-based machine learning algorithm, detail this to assist farmers in assessing soil quality by measuring the levels of urea, potassium, magnesium, pH, and nitrogen. The result yields an effective crop rotation sequence with an accuracy of 80%. Robots are also used in agriculture [11]. Crop recommendation is very useful [12-15].

The current systems, which employ various machine learning methods, are useful and accurate when employed in their respective regions. This [2] model is useful for the Tamil Nadu region. It is noted that in some existing recommendation models, environmental conditions are used as primary input (data, n.d.)and soil properties are predominantly used as input for predicting crops [10]. Existing systems used different predictive models like Random Forest [3],[16], [5] K-Nearest Neighbour [16],[9],[6],[2], Support Vector Machine [3], Decision Tree [2], Neuro-Fuzzy [2], etc. RF has achieved the highest accuracy of 99.22%. Climate and soil characteristics are the input parameters to suggest the best crop to increase agricultural output for local farmers. The existing system's accuracy is poor. The proposed approach offers greater accuracy in KNN, RF, and SVM.

## II. METHODOLOGY

We have proposed a methodology that is separated into various stages as shown in Figure 1.

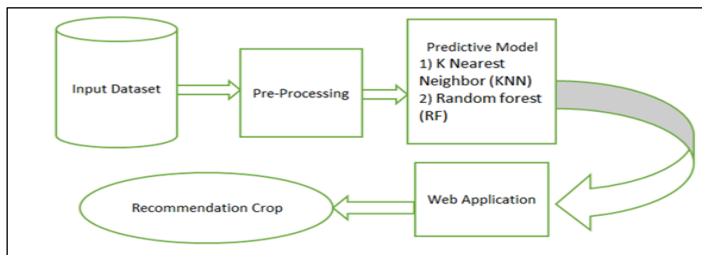


Figure1: Block Diagram of Methodology Of The Proposed System.

Source: Authors, (2024).

### II.1 DATA COLLECTION

In this work, the dataset is collected from an open-source platform called Kaggle [8]. This dataset is a combination of two more complex datasets.

#### a) Soil content dataset:

It contains information about the ratios of nitrogen (N), phosphorus (P), and potassium (K) and the pH of the soil.

#### b) Climatic condition dataset:

It contains information about rainfall, humidity, and temperature.

#### c) Data Pre-processing

After collecting data for our machine learning model, we performed pre-processing on our dataset. In this stage, label encoding is done on the dataset. We have the 22 crop types in string format, which needs to be converted into numeric form to be understood by the computer. For this purpose,

#### d) Label Encoding

It converts the string format into the numeric format. As compared with the collected dataset, there are 22 different crop types, and it gives a number to every crop type in alphabetical order of crop names.

Table 1: Label Encoding.

CROP TYPE	LABEL
Apple	0
Banana	1
Black gram	2
Chickpea	3
Coconut	4
Coffee	5
Cotton	6
Grapes	7
Jute	8
Kidney beans	9
Lentil	10
Maize	11
Mango	12
Moth beans	13
Mungbean	14
Muskmelon	15
Orange	16
Papaya	17
Pigeon peas	18
Pomegranate	19
Rice	20
Watermelon	21

Source: Authors, (2024).

## III. VISUAL CORRELATION PLOT

It is possible to determine how strongly or weakly the traits are related to one another by looking at the correlation between them. The number 1 indicates that there is a positive association between the two variables. In this work (Figure 2), It is observed that phosphate (P) and potassium (K) values are highly correlated with one another. Temperature and humidity are moderately

correlated with each other. Rainfall and pH show less correlation between them. Individually, P and K will contribute similar levels of variance to the model. pH and humidity show less correlation with each other. Nitrogen and phosphorus show a low correlation

between them. The crop's 'label' target vector is most correlated to humidity and least correlated to ph. Humidity will have a large effect on our model, while Ph may have a negligible effect.

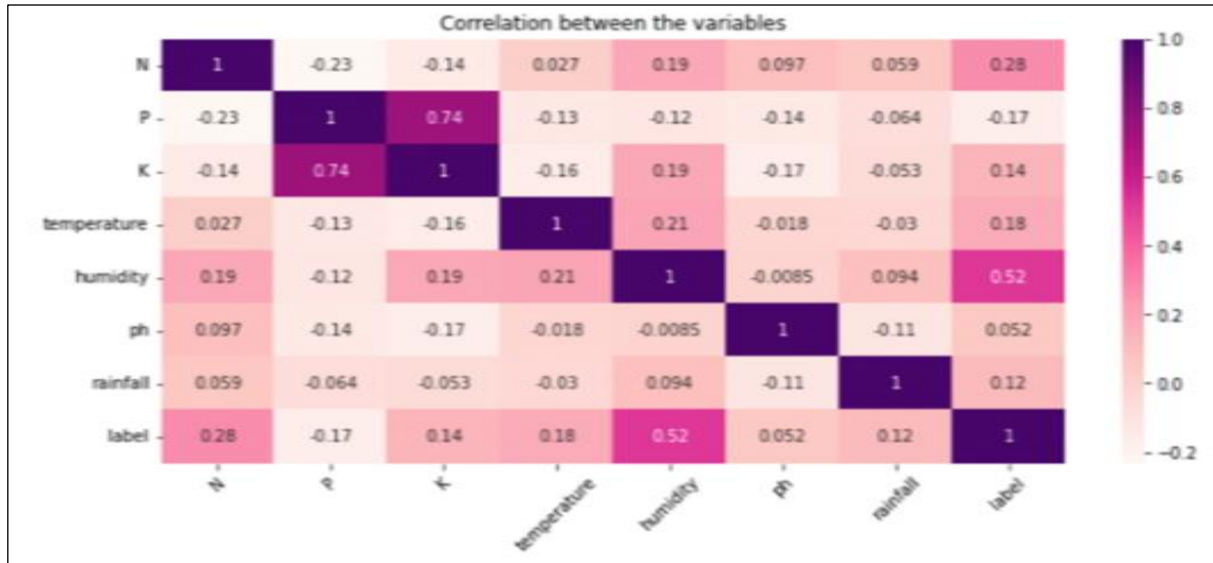


Figure 2: Correlation Plot.  
Source: Authors, (2024).

Choosing the perfect algorithm for a crop dataset is a difficult task. To solve this problem, a pair plot (Figure 3) with the Seaborn library is used. The data appears to be too overlapping,

according to the data visualizations. In this scenario, we can use algorithms like random forests, SVM, K-NN, and ANN.

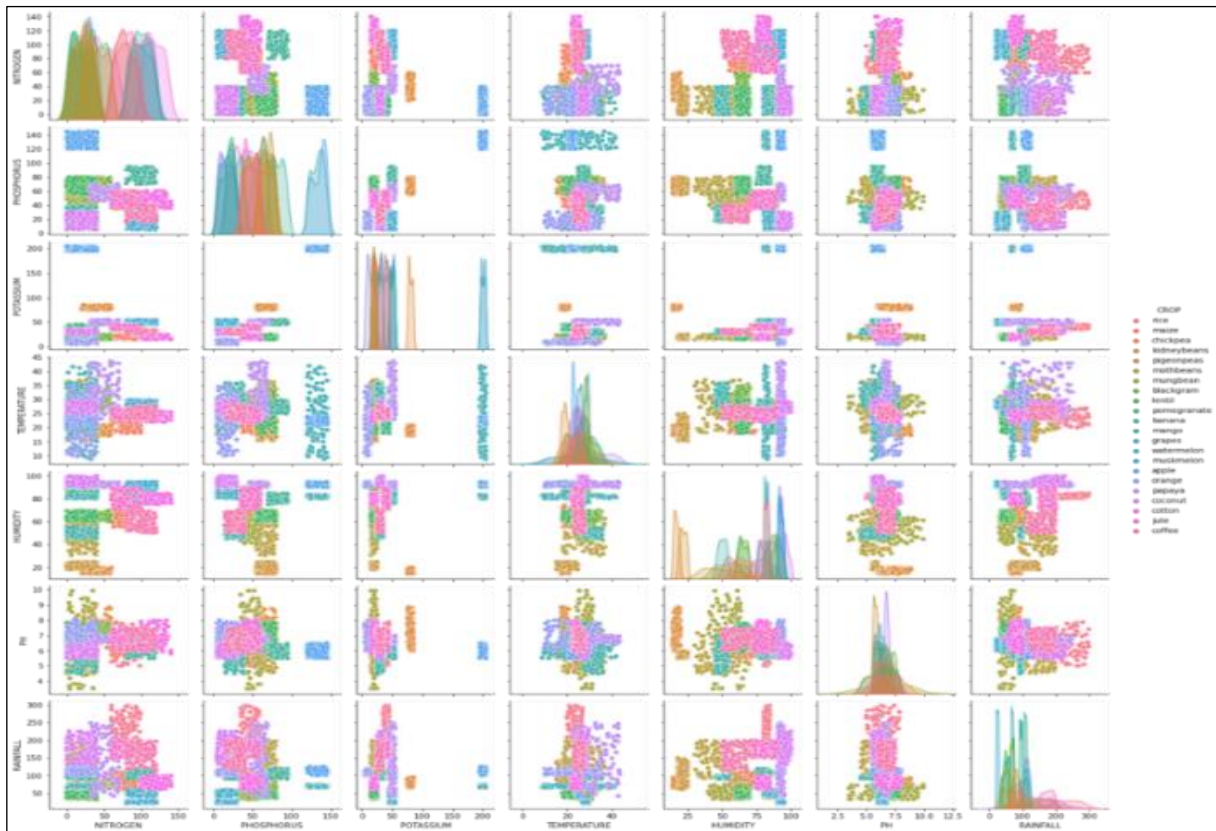


Figure 3: Pair Plot.  
Source: Authors, (2024).

IV. VISUAL CORRELATION PLOT  
IV.1 PREDICTIVE MODEL

In this stage, the dataset is split into training and testing sets to understand model performance by using the function train test split (). In this work, three parameters must be passed: features, goal, and test set size. You may also use a random state to choose records at random. The dataset was divided into 80% training data and 20% testing data from an existing dataset. The following predictive model is used in this work:

#### IV.II RANDOM FOREST

The random forest algorithm is a popular supervised machine learning algorithm. It is based on the random forest algorithm principle. The presence of excessively random trees in a random forest network leads to the high accuracy of the model. It finalizes the decision from the tree with the most votes. As a result, the greater the number of decision trees in the forest, the greater the accuracy of the model.

#### IV.III SUPPORT VECTOR MACHINE

SVM employs optimum lines or decision boundaries to partition the n-dimensional space into classes, allowing new data points to be conveniently placed in the appropriate category. A hyperplane represents the ideal choice boundary. The hyperplane equation is as follows:

$$w \cdot x + b = 0 \tag{1}$$

If the value of  $w \cdot x + b > 0$  then it is a positive point otherwise negative.

#### IV.IV K-NEAREST NEIGHBOR

All of the available data is stored by the K-NN algorithm, which compares each new data point to the existing data set. Rainfall and soil type have been designated as input parameters, while other parameters may also be taken into account. The values of the closest known neighbors can be used to predict the crop yield, which is an unknown value. By using Euclidian calculations, this is attainable.

$$D(a, b) = \sqrt{(b1 - a1)^2 + (b2 - a2)^2} \tag{2}$$

### V. WEB APPLICATION

In this stage, a web application for a crop recommendation system was developed. The front end of this application was developed using HTML and CSS. For the backend the python module flask framework is used. Web application include a login page (Figure 4), a registration page (Figure 5), and a crop predictor page (Figure 6).

The farmer has to enter all the necessary details to predict the crop, like the ratio of nitrogen in the soil, the ratio of phosphorus in the soil, the ratio of ph, the temperature, the humidity, the ratio of potassium, the rainfall rate, etc. All this information is very important for our model to predict which crop will be the best for the farmer to grow. At the backend of the web application, we have connected the machine learning model and database.

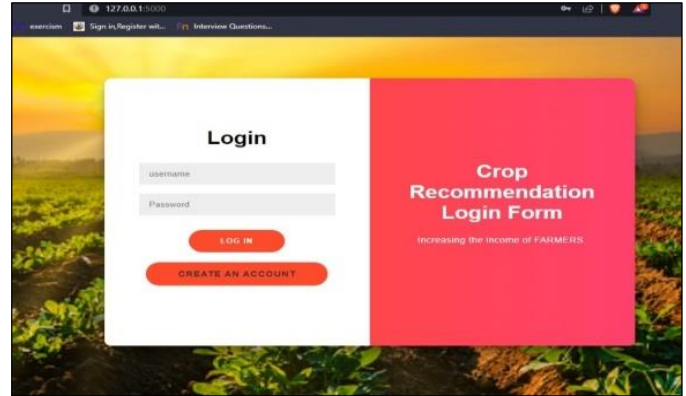


Figure 4: Login Page.  
Source: Authors, (2024).

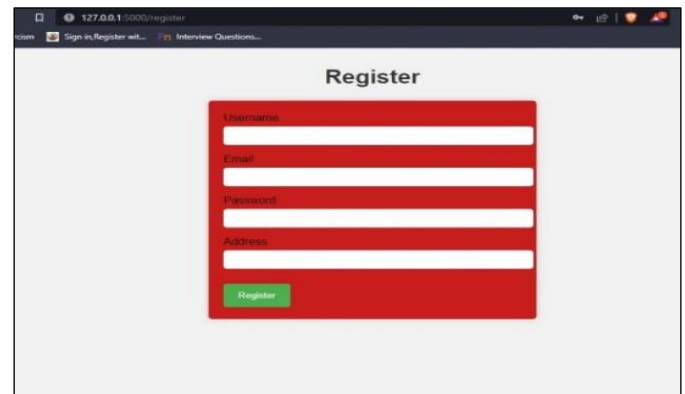


Figure 5: Registration Page.  
Source: Authors, (2024).

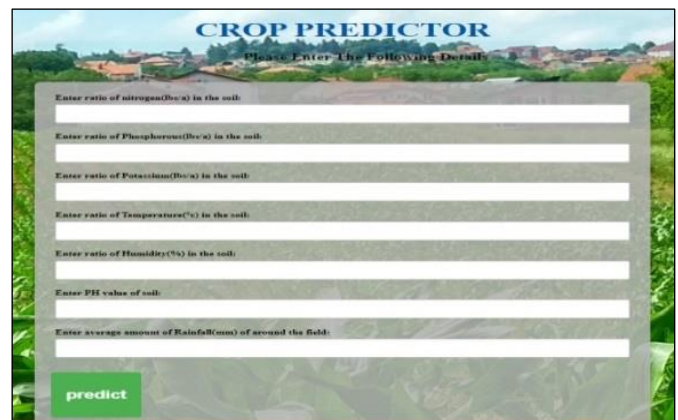


Figure 6: Crop predictor page.  
Source: Authors, (2024).

### VI. EXPERIMENTAL RESULTS

The proposed system was successfully implemented on software having specifications as follows:

- operating system: 64-bit Windows 10
- Python library: Tensorflow, Keras, Matplotlib.
- Python Framework: Flask
- Frontend: CSS, HTML

In random forest, we fitted the random forest algorithm to the training set and checked the accuracy of the model by varying the value of the `n_estimator` (required number of trees) parameter.

The results of taking ten different values for the number of trees are shown in the table. It is observed that if the value of

estimator is 10 or 20, then it will give high accuracy. It is important to take care of the overfitting issue.

Table 2: RF Accuracy by Varying N\_Estimator Value.

No.of trees	Accuracy
3	0.9836
5	0.9886
7	0.9927
9	0.9909
10	0.9940
11	0.9922
12	0.9931
13	0.9909
15	0.9931
16	0.9927

Source: Authors, (2024).

In this work, we plotted the confusion matrix of each predictive model to observe the performance of the classification algorithm. The confusion matrix of RF shows all diagonal elements, which represent true prediction, and others that show false prediction. RF shows a lower number of

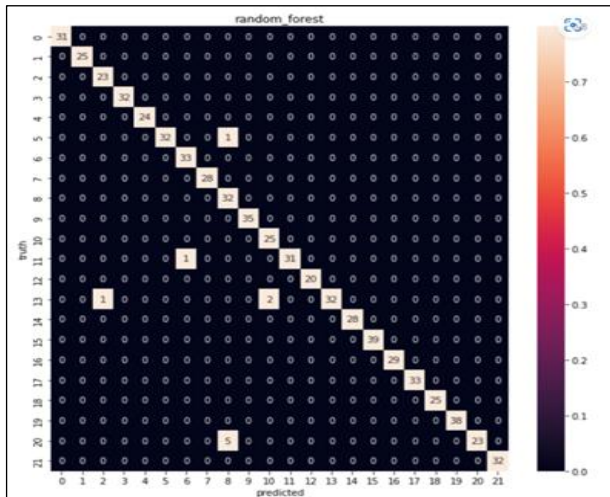


Figure 7: Confusion Matrix of RF.  
Source: Authors, (2024).

In support vector machine work, we fitted the SVM algorithm to the training set and checked the accuracy of the model. The plotted confusion matrix of SVM, Figure 8 shows more off-diagonal elements, which indicates more incorrect predictions.

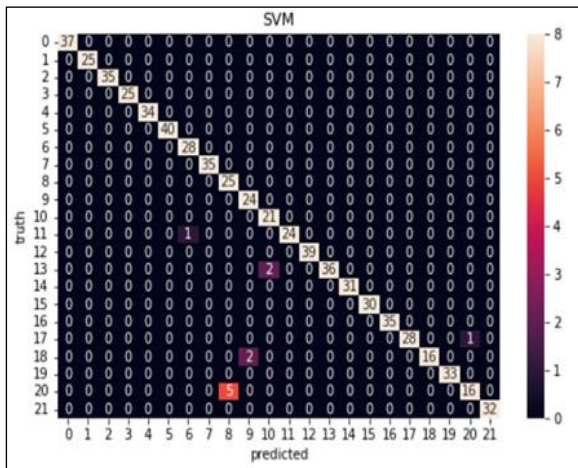


Figure 8: Confusion matrix of SVM  
Source: Authors, (2024).

In K-Nearest Neighbor work, we fitted the KNN algorithm to the training set and checked the accuracy of the model by varying the value of the k\_estimator (required number of trees) parameter. It is observed that if the value of n\_estimator is 10 or 20, then it will give high accuracy.

Table 3: KNN Accuracy by Varying K\_Estimator Value.

K_estimator	Accuracy
1	96.8
2	97.5
3	97.9
4	97.7
5	98.4
10	97.73
15	96.8
6	98
7	97.9
20	97.7

Source: Authors, (2024).

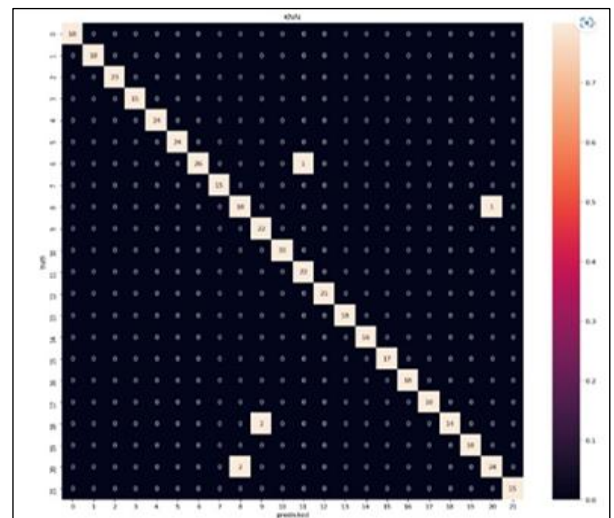


Figure 9: Confusion matrix of KNN  
Source: Authors, (2024).

The confusion matrix of KNN Figure 9 shows all diagonal element that represents true prediction and other off-diagonal shows false prediction. KNN shows less number of false predictions than SVM. In the proposed system, the prediction of a crop by putting different parameter values on the precisely predicted crop displayed on the crop predictor page (Figure 10 and Figure 11).



Figure10: Prediction Snapshot 1  
Source: Authors, (2024).

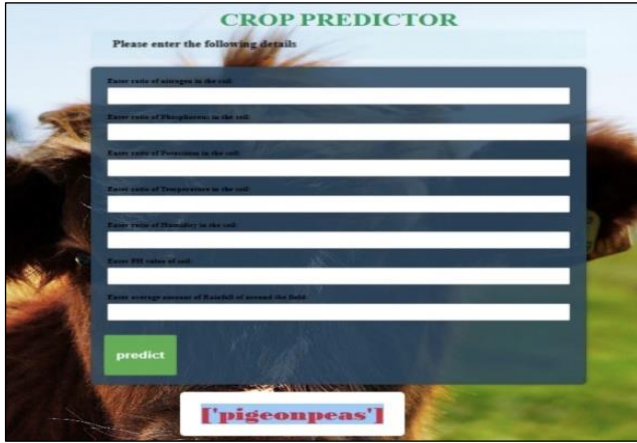


Figure 11: Prediction Snapshot 2  
Source: Authors, (2024).

## VII. RESULT ANALYSIS

The result obtained from RF, KNN, and SVM models, it can be concluded that RF performs better compare to KNN and SVM. The average accuracy of used predictive models is shown in Table 4.

Table 4: Average Accuracy Of Different Algorithms In Percentage.

Predictive Model	Average Accuracy	Training Time
Random Forest	99.22%	138.021 ms
K-Nearest Neighbor	97.95%	218.691 ms
Support Vector Machine	97.85%	218.691 ms

Source: Authors, (2024).

## V. CONCLUSIONS

Farmers in our nation frequently struggle to choose the best crops to plant since there is a lack of scientific understanding of the various aspects affecting crops. As a result of their lower output, they suffer a loss in earnings. In this paper, a proposed crop recommendation system is proposed to suggest the best crop to the farmer by using soil parameters like N, P, K, pH, and environmental conditions such as rainfall, humidity, and temperature. This proposed system predicts one of the 22 crops by using different algorithms like RF, K-NN, SVM, etc. Out of these algorithms, RF gives the highest accuracy (99.22%) and less training time(138.021ms); hence, the RF algorithm was used and additionally, we designed a user-friendly web page using HTML, CSS, and the Flask Python framework. The webpage incorporates essential features such as registration, login, and a prediction form, enabling users to easily access and utilize the crop recommendation system, these recommended crops will bring in the maximum profit.

## VI. AUTHOR'S CONTRIBUTION

**Conceptualization:** Dr. V. V. Kale

**Methodology:** Dr. V. V. Kale.

**Investigation:** Dr. V. V. Kale and Dr. B. N. Mohapatra.

**Discussion of results:** Dr. V. V. Kale and Dr. B. N. Mohapatra

**Writing – Original Draft:** Dr. V. V. Kale and Dr. B. N. Mohapatra

**Writing – Review and Editing:** Dr. V. V. Kale and Dr. B. N. Mohapatra.

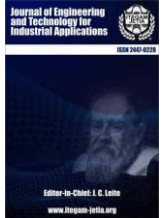
**Resources:** Dr. V. V. Kale and Dr. B. N. Mohapatra **Supervision:** Dr. V. V. Kale

**Approval of the final text:** Dr. B. N. Mohapatra, .

## VII. REFERENCES

- [1] Y. J. N. Kumar, V. Spandana, V. S. Vaishnavi, K. Neha, and V. G. R. R. Devi, 'Supervised machine learning approach for crop yield prediction in agriculture sector', in 2020 5th International Conference on Communication and Electronics Systems (ICCES), Coimbatore, India, 2020.
- [2] A. Suresh, P. Ganesh Kumar, and M. Ramalatha, 'Prediction of major crop yields of Tamilnadu using K-means and Modified KNN', in 2018 3rd International Conference on Communication and Electronics Systems (ICCES), Coimbatore, India, 2018.
- [3] A. Lokhande and M. Dixit, 'Crop Recommendation System Using Machine Learning', International Research Journal of Engineering and Technology (IRJET), vol. 9, pp. 2395–0056, 2022.
- [4] Geetha, V., Punitha, A., Abarna, M., Akshaya, M., Illakiya, S., & Janani, A. P. (2020, July). An effective crop prediction using random forest algorithm. In 2020 international conference on system, computation, automation and networking (ICSCAN) (pp. 1-5). IEEE.
- [5] M. Ramu and J. T. Sri, 'Wheat yield prediction using Artificial Intelligence models and its comparative analysis for better prediction', in 2021 International Conference on Advance Computing and Innovative Technologies in Engineering (ICACITE), Greater Noida, India, 2021.
- [6] S. M. Pande, P. K. Ramesh, A. Anmol, B. R. Aishwarya, K. Rohilla, and K. Shaurya, 'Crop recommender system using machine learning approach', in 2021 5th International Conference on Computing Methodologies and Communication (ICCMC), Erode, India, 2021.
- [7] D. Modi, A. V. Sutagundar, V. Yalavigi, and A. Aravatagimath, 'Crop recommendation using machine learning algorithm', in 2021 5th International Conference on Information Systems and Computer Networks (ISCON), Mathura, India, 2021.
- [8] Motwani, P. Patil, V. Nagaria, S. Verma, and S. Ghane, 'Soil analysis and crop recommendation using machine learning', in 2022 International Conference for Advancement in Technology (ICONAT), Goa, India, 2022.
- [9] R. K. Ray, S. K. Das, and S. Chakravarty, 'Smart crop recommender system- A machine learning approach', in 2022 12th International Conference on Cloud Computing, Data Science & Engineering (Confluence), Noida, India, 2022.
- [10] E. E. Vigneswaran and M. Selvaganesh, 'Decision support system for crop rotation using machine learning', in 2020 Fourth International Conference on Inventive Systems and Control (ICISC), Coimbatore, India, 2020.
- [11] B. N. Mohapatra and R. K. Mohapatra, 'Design of an automated agricultural robot and its prime issues', 2020.
- [12] N. H. Kulkarni, G. N. Srinivasan, B. M. Sagar, and N. K. Cauvery, 'Improving crop productivity through A crop recommendation system using ensembling technique', in 2018 3rd International Conference on Computational Systems and Information Technology for Sustainable Solutions (CSITSS), Bengaluru, India, 2018.
- [13] B. J. Kushal, N. J. Sp, N. S. Raaju, K. G. Gv, A. R. Kp, and S. Gowrishankar, 'Real Time Crop Prediction based on Soil Analysis using Internet of Things and Machine Learning', in 2022 International Conference on Edge Computing and Applications (ICECAA), IEEE, 2022, pp. 1249–1254.
- [14] N. H. Kulkarni, G. N. Srinivasan, B. M. Sagar, and N. K. Cauvery, 'Improving crop productivity through A crop recommendation system using ensembling technique', in 2018 3rd International Conference on Computational Systems and Information Technology for Sustainable Solutions (CSITSS), Bengaluru, India, 2018.
- [15] B. J. Kushal, N. J. Sp, N. S. Raaju, K. G. Gv, A. R. Kp, and S. Gowrishankar, 'Real Time Crop Prediction based on Soil Analysis using Internet of Things and Machine Learning', in 2022 International Conference on Edge Computing and Applications (ICECAA), IEEE, 2022, pp. 1249–1254.
- [16] M. Ramu and J. T. Sri, 'Wheat yield prediction using Artificial Intelligence models and its comparative analysis for better prediction', in 2021 International Conference on Advance Computing and Innovative Technologies in Engineering (ICACITE), Greater Noida, India, 2021.





## DETECTION OF LUNG NODULES USING SUPPORT VECTOR MACHINE

\*Jhon Anthony Fernández Castro<sup>1</sup>, Marlen Pérez Díaz<sup>2</sup> and Rubén Orozco Morales<sup>3</sup>

<sup>1,2,3</sup> Universidad Central “Marta Abreu de las Villas” – UCLV. Santa Clara-Villa Clara, Cuba.

<sup>1</sup><http://orcid.org/0009-0003-7576-921x> , <sup>2</sup><http://orcid.org/0000-0002-3706-9154> , <sup>3</sup><http://orcid.org/0000-0002-6240-1569> 

Email: [\\*jhonanthonyfernandezcastro@gmail.com](mailto:*jhonanthonyfernandezcastro@gmail.com)<sup>1</sup>, [mperez@uclv.edu.cu](mailto:mperez@uclv.edu.cu)<sup>2</sup>, [rorozco@uclv.edu.cu](mailto:rorozco@uclv.edu.cu)<sup>3</sup>

### ARTICLE INFO

#### Article History

Received: July 01<sup>th</sup>, 2024

Revised: July 08<sup>th</sup>, 2024

Accepted: July 08<sup>th</sup>, 2024

Published: July 18<sup>th</sup>, 2024

#### Keywords:

Chest x-ray,  
Pulmonary nodule,  
Support vector machines,  
Machine learning.

### ABSTRACT

Lung cancer is a disease of high mortality worldwide. Therefore, early diagnosis and treatment can save lives. Lung cancer appears as a solitary nodule on chest x-ray, which is sometimes very difficult to detect for the human eye. Therefore, developing a computer-aided diagnosis (CAD) system for the detection of lung nodules, using machine learning (ML) could have a significant impact on patient prognosis. The proposed algorithm begins by pre-processing the images to improve their quality. The lung area is then segmented by thresholding. In the next step, nodule candidates are determined using a sliding band filter and segmented by applying a threshold algorithm, based on adaptive distance (ADT). Next, the suspicious areas are processed by a support vector machine (SVM), based on 15 shape and texture characteristics. Three SVM models were trained and validated with images from a public JSRT database. The best result was obtained with the radial base model (87 % sensitivity). This performance is valued as favorable with respect to human performance.



Copyright ©2024 by authors and Galileo Institute of Technology and Education of the Amazon (ITEGAM). This work is licensed under the Creative Commons Attribution International License (CC BY 4.0).

### I. INTRODUCTION

Data from the World Health Organization show that lung cancer is the third most common type of tumor and the leading cause of cancer-related death in the Americas, with more than 324,000 new cases and nearly 262,000 deaths each anus [1]. It encompasses a set of diseases resulting from the malignant growth of cells in the lung tissue [2]. Early detection (when they are a nodule) generally allows for earlier therapeutic intervention and a better prognosis. Pulmonary nodules present radiographically as rounded opacities, no larger than 3 cm [2]. With computed tomography (CT), the detection of the smallest has increased [3]. Although this technique is more sensitive for detecting lung cancer at an early stage, chest x-rays are also used for this task, due to their low cost, simplicity, and low radiation dose. However, the false negative rate is around 30% [4]. Tumor characteristics such as size, visibility and location, radiographic image quality and patient positioning and movement are factors that determine the probability of missing a lung neoplasm. The

experience of the radiologist also plays a role in this context [5]. The 20-60% error rate has remained the same for years. To reduce the risk of misdiagnosis, computer-aided diagnosis (CAD) systems are developed [6].

CADs have been presented as a second opinion for the radiologist in the early detection of different diseases [7-9]. The increase in computing capabilities in recent years has allowed the emergence of systems based on machine learning techniques. A revised literature review shows that the sensitivity of the human eye varies between 49% and 65% without the use of CAD, and between 68% and 93% with its assistance for lung nodules [10].

The increase in processing capabilities, data availability and storage of current computers allowed the emergence of ML. These use pre-processing and segmentation stages of the lung region and the use of equations to describe the lesions. The main characteristic is that they use a classifier, which is able to learn to separate the classes: nodule / normal, from a vector of features previously extracted from the images [11].

DL algorithms use convolutional neural networks, which to achieve adequate model training and generalization power, require a very high volume of data, which in medicine is not always available. For this reason, even algorithms that do not use DL continue to be competitive [12].

Support vector machines (SVMs) [13] are among the most successful ML algorithms of the last 20 years. Some reasons that explain this achievement are its good properties for the generalization and convergence of models [14].

SVMs are therefore a classification and regression prediction tool, which uses machine learning (ML) theory to maximize predictive accuracy and automatically avoid overfitting the model to the learning data. They can be defined as systems that use a hypothesis space of linear and nonlinear functions, in a high-dimensional feature space [13].

SVMs use statistical learning theory to find a regularized hypothesis that fits the available data well. The greatest limitation of SVMs lies in the choice of a kernel that suits the problem under analysis. Furthermore, they depend on feeding with a set of characteristics that are appropriate to interpret the problem well.

The objective of the work has been to develop a CAD system based on SVM, which is capable of detecting lung nodules from chest x-rays.

## II. MATERIALS AND METHODS

### II.1 THEORETICAL DESCRIPTION OF SVM

If we consider that we have a real training data set ( $R$ )  $(x_1, y_1), \dots, \dots, (x_i, y_i) \in R^n$  where  $x_i$  is the  $i$ th vector of the sample and  $y_i$  its corresponding label, SVM aims at linear discrimination, finding a hyperplane that separates samples of different classes. At the same time, the calculated hyperplane should maximize the distance between the marginal samples of each class. These two conditions are part of an optimization problem. The solution to this problem is based on a small percentage of marginal samples called support vectors. In that case, after computing the optimal solution, the decision function is given by Optimization equation:

$$f(x) = b + \sum \alpha_i y_i K(x_i, y_i) \quad (1)$$

where  $b$  denotes a constant bias value,  $\alpha_i$ ,  $i=1 \dots n$  correspond to multipliers for each sample, having a non-zero value only for the support vectors [15] and  $K(x_i, y_i)$  is a kernel.

In the case of nonlinear class separation, the input samples can be mapped to a higher dimensionality space, where they are linearly separated. This is achieved with an appropriate kernel function  $K(x_i, y_i)$ . A small number of support vectors are selected, which minimizes the computational requirements during testing [15].

### II.2 DESCRIPTION OF THE IMAGE SETS USED

An annotated radiograph database, JSRT [16], was used in this investigation. They are images with a spatial resolution of 1024 x 1024 pixels. Images with nodules have the location of the lesion and each one presents a single lesion. 93 normal images and 154 images with nodules were used, for a total of 247 images.

### II.3 SOFTWARE AND HARDWARE USED

The software used was MATLAB R2018b (9.5.0.944444). A desktop computer with the following features was used: Processor (CPU) Intel® Core™ i3-6100U (2.3 GHz, 3 MB cache, 2 cores), Graphics Card: Intel® HD Graphics 520 (Integrated), RAM: 8 GB DDR4-2133 SDRAM (2\*4GB).

### II.4 CAD SYSTEM, 1ST STAGE: IMAGE PREPROCESSING

At this stage, two pre-processing were carried out, one aimed at improving visibility in the image and another necessary for the segmentation of the lung region. For the first one, a smoothing of the image was carried out. Noise was reduced by applying a 5x5 pixel averaging convolution filter. Then, using local normalization (LN) filtering, global contrast equalization was achieved across the image [17], and finally, edges were enhanced with filtering homomorphic. In this case, a logarithmic mapping was carried out in the space domain, to separate the illumination and reflectance components. To make the image illumination more uniform, the high frequency components (reflectance) were increased and the low frequency components (illuminance) were decreased. High-pass filtering was used in this case to suppress low frequencies and amplify high frequencies. Figure 1 shows the result of this stage of the System.



Figure 1: Original image (left). Preprocessed image (right).  
Source: Authors, (2024).

Lung region segmentation was performed during the second preprocessing to limit nodule detection to the segmented lung fields and prevent false positive (FP) detections. For this, the multi-level threshold method was used, as performed in [17], since the present work is a continuation of this.

An initial segmentation is first obtained using the multi-level threshold method. Then, because in some cases this method leaves out parts of the lung region, an auxiliary segmentation is performed, using another variant of the multilevel threshold method, with the objective of identifying the outer edges of the lungs to correct the initial segmentation. Both images are added and morphological operations of opening and closing the image are applied [18] with which the final segmentation is obtained. In this case, a structuring element in the shape of a disk with a radius of 65 pixels was used to obtain the initial segmentation. Aperture removed all pixels in regions that are smaller than the structuring element, smoothed out external bumps, broke up narrow sections, and removed thin bumps. The closure filled in the smaller holes and concavities. Subsequently, the multi-level threshold method was applied again to the processed image, thus obtaining auxiliary segmentation. Auxiliary segmentation precisely defines the borders of the lungs. This was done with

adaptive morphology, using an edge-linking algorithm, as in [17]. Figure 2 shows the result of this step.



Figure 2: Initial segmentation masks (left) and corrected segmentation (right).  
Source: Authors, (2024).

### II.5 CAD SYSTEM, STAGE 2: DETECTION AND SEGMENTATION OF CANDIDATE NODULES

After pre-processing, an algorithm was applied to detect candidate nodules. This means locating regions of the image that may be potential lung nodules. For this, a local convergence filter (LCF) was used as in [19],[20], with the difference that the convergence filter used in this case was a sliding band filter [20]. With this filter you can perform detection of nodules at various scales and at the same time introduce the background into the detection approach. Although lung nodules generally have a circular shape, this is not always the case; they can also be spiculated, lobulated, poorly defined, or with irregular edges, so a convex shape and a limited range of sizes for the area were assumed thereof.

The LCF evaluates the degree of convergence of gradient vectors within a local area (support region) towards a pixel of interest (central location of the area) [17]. The degree of convergence is related to the distribution of the directions of the gradient vectors and not to their magnitudes. This makes it easy to define a global threshold that is not affected by image illumination. The local convergence of a gradient vector at a given pixel is defined as: the cosine of its orientation with respect to the line connecting that pixel and the central pixel of the area.

After candidate detection, an adaptive distance-based thresholding (ADT) algorithm was applied to segment each candidate nodule [17-20]. These segmentations were used as a key part of the calculation of most of the characteristics, to identify the real nodule among all the candidates. Figure 3 shows the result of these steps.

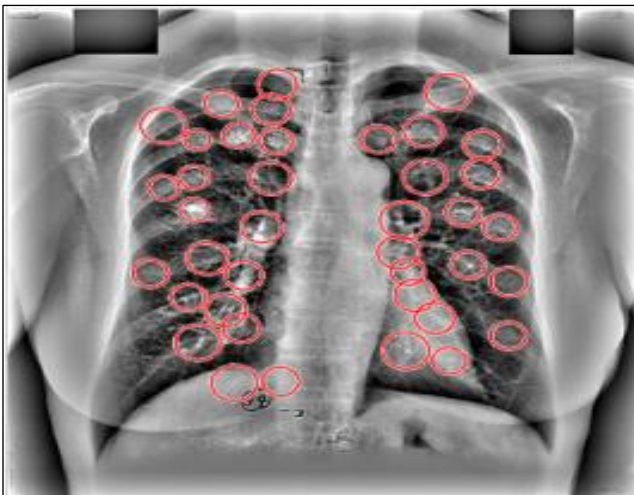


Figure 3: Detection and segmentation of candidate nodules.  
Source: Authors, (2024).

### II.6 CAD SYSTEM, STAGE 3: FEATURE EXTRACTION

For each nodule candidate, a set of features were calculated and presented in Table 1. Geometric features were calculated using only the shape and position information provided by adaptive segmentation. Intensity features were calculated for the preprocessed images, using the segmentation mask to define the candidate boundary.

Table 1: Characteristics of possible nodules.

Characteristic	Content
Lesion size	Maximum diameter after segmentation
Area	Surface
Perimeter	Contour Long
Circularity 1	$A_1 = \pi r_m^2$ $r_m$ is the maximum radius (2)
Circularity 2	$A_2 = \pi r^2$ $r_m$ is the minimum radius (3)
Excentricity	Deviation respect a circumference.
Internal and external mean	Average of pixel intensity in and out ADT segmentation.
Mean separation	$(Mediainterna - Mediaexterna) / (Mediainterna + Mediaexterna)$ (4)
Internal and external standar deviation	Dispersion respect to the mean value in and out the ADT segmentation
Contrast 1	$(Mediainterna - Mediaexterna) / Mediainterna + Mediaexterna$ (5)
Contrast 2	$Contrast1 / (Des. estandarinterna + Des. estandarexterna)$ (6)

Source: Authors, (2024).

### II.7 CAD SYSTEM, STAGE 4: CLASSIFICATION OF POSSIBLE LUNG NODULES

The objective of any classifier is to find a boundary that allows the classes to be separated (in this case nodule / non-nodule). Classification was performed by a binary SVM classifier. The classifier receives a set of training features, a result of the previous stage, each labeled for the classes: nodule and non-nodule. From these characteristics, a model was built that was subsequently used to classify the test images. Features from 133 nodule and non-nodule images were used for model training.

Three kernels were implemented to train the model, so that a non-linear decision surface can be transformed into a linear equation and into a greater number of dimension spaces. Mathematical formulation of the kernels used:

Linear kernel

$$K(x,y) = \langle x,y \rangle \quad (7)$$

Gaussian or radial base kernel

$$K(x,y) = \exp(-\gamma \|x-y\|^2), \gamma > 0 \quad (8)$$

Polynomial kernel of degree P

$$K(x,y) = [\langle x,y \rangle + 1]^P \quad (9)$$

To obtain each SVM model, the MatLab function *fitcsvm* ( $X, Y$ ) was used, using the feature vectors  $X$  and the classification labels in the vector  $Y$ . Figure 4 shows the scheme of the nodule classification stage.

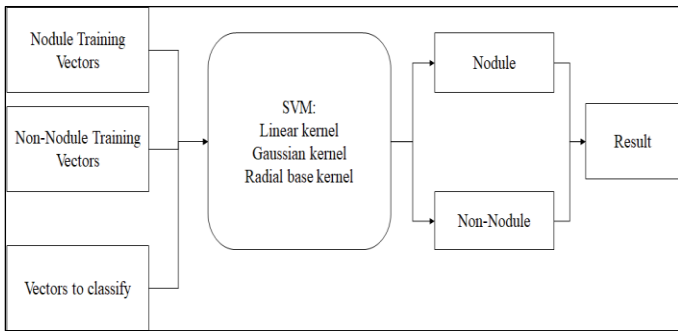


Figure 4: Scheme for the classification of possible nodules. Source: Authors, (2024).

At the end of the training of each model, with the different nuclei, validation was carried out with 15 images of nodules and non-nodules (not used for training). For this, sensitivity, precision, accuracy, balanced accuracy and the *F1-score* value were used as metrics.

#### IV. RESULTS AND DISCUSSIONS

##### IV.1 FEATURE VECTORS

Although no statistical analysis was done to prove the existence of significant differences between the characteristics for each class, based on the centroids per class of each one, it can be seen that the characteristics that differ the most between the two classes are: the area of the nodule, eccentricity, external standard deviation and circularity 2. However, this aspect must be scientifically corroborated in future work. For the purposes of this work, all characteristics were used in the subsequent stages, not just those that a priori appear to be the determining ones. Figure 5 shows the results of features in each class.

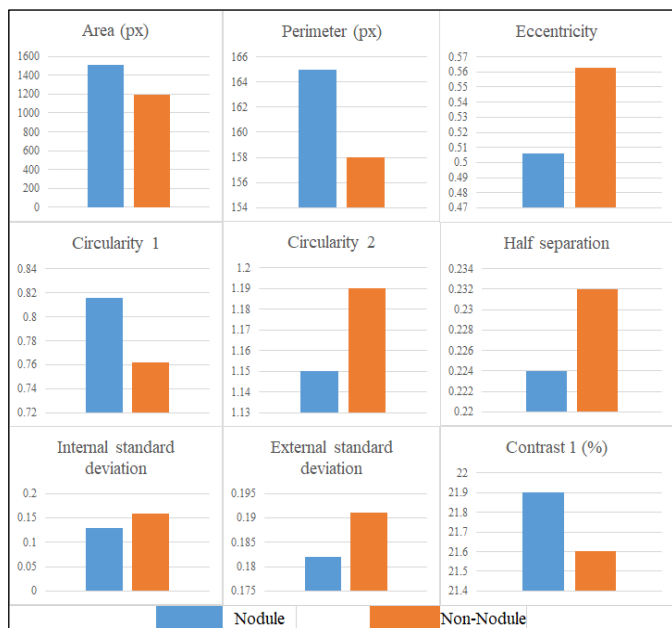


Figure 5: Average value of each characteristic for both classes. Source: Authors, (2024).

#### IV.2 MODEL TRAINING AND VALIDATION RESULTS

Figure 6 shows the validation results of the 3 SVM models tested for the vector including all features and Table 2 shows their respective metrics.

	Linear		RBF		Gaussian		Real
	Nodule	Non-Nodule	Nodule	Non-Nodule	Nodule	Non-Nodule	
Nodule	11	4	13	2	12	3	
Non-Nodule	6	9	5	10	8	7	
	Prediction		Prediction		Prediction		

Figure 6: Confusion matrices for validation data. Source: Authors, (2024).

Table 2: Model performance metrics in validation.

Metrics (%)	Linear	RBF	Gaussian
Accuracy	66,67	76,67	63,33
Sensitivity	73,33	86,67	80,00
Precision	64,71	72,22	60,00
F1 (%)	68,75	78,79	68,57
Balanced accuracy	66,67	76,67	63,33

Source: Authors, (2024).

In the clinical setting, the most valued metric is sensitivity, which provides the percentage of findings of true nodules (VP). The consequences of evaluating a healthy area incorrectly involve simply repeating the test. However, the consequences of incorrectly evaluating a VP are the most unfavorable, since the early diagnosis of the disease can be affected. In the experiment carried out, the best result was that obtained with the radial base model (87% sensitivity). This performance is rated as favorable compared to human performance, which is between 49% and 65% [10].

##### IV.3 GENERAL DISCUSSION

In the present work, a classification stage has been added to the CAD system designed in [17]. In this previous work, we only reached the phase of detecting candidate nodules. This article takes advantage of the benefits of SVMs to separate the classes into nodule or non-nodule.

From digital radiographic images, radiologists can typically see 45% to 68% of actual nodules. It has been noted that if the nodules are smaller than 10 mm, only 29% are detected. In fact, detection is strongly determined by location [10]. Hence the importance of using automated systems as a second opinion.

For example, Figure 7 shows a nodule that is very difficult to visualize by the human eye, according to the BD JSRT annotation [16], due to its low contrast and its overlap with a rib. Note in the zoom on the right that for this nodule the contrast difference with respect to the surrounding background is practically undetectable by the human eye. The radial-based model, however, was able to detect such a nodule, indicating its potential for the task.

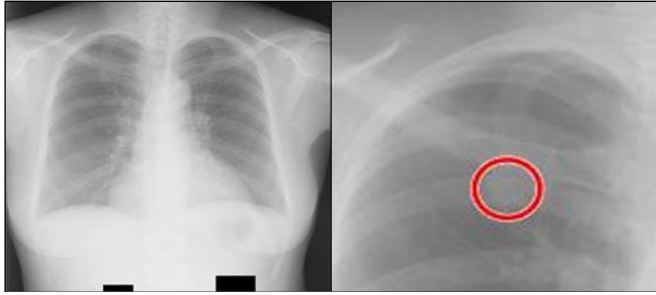


Figure 7: Nodule undetectable to the human eye.  
Source: Authors, (2024).

The computational cost of training for the three models was 10 seconds per model, for the computational capabilities used. Once the model is trained, the approximate execution time of all the stages of the CAD system, for an image, is 3-4 min.

When reviewing four studies with lung nodule detection models published in the literature, in which the JSRT database was used, the results that are summarized in Table 3 were found. These reinforce the expressed criterion that the proposed system manages to classify lung nodules with sensitivity values similar to other systems previously published by international authors, at least for the validation training data. Future studies with data from different origins should be carried out to test the generalization power of the system.

Table 3: Results of CAD systems made with the JSRT DB

Studies	Sensitivity (%) (Images with correct detection/Total images with nodules)
Wei [21]	80 (123/154)
Coppini[22]	60 (93/154)
Schilham [23]	67 (103/154)
Hardie [19]	63 (88/140)

Source: Authors, (2024).

As directions for future work, it is proposed to introduce a rigorous method for selecting class-determining characteristics, such as principal component analysis, test other classifiers such as random forest trees or cluster analysis, and carry out a perceptual study, with human observers, under standardized conditions, to evaluate the real detection difference between the proposed system and the performance of human experts on the task.

## V. CONCLUSIONS

It has been proven that SVMs have potential for the task of detecting lung nodules from chest x-rays. An SVM with a radial basis model presented potential for the task in terms of computational effectiveness and efficiency. Of the characteristics used as input vector for the SVM, the most sensitive a priori for classifying nodules were: nodule area, eccentricity, external standard deviation and circularity 2.

## VI. AUTHOR'S CONTRIBUTION

**Conceptualization:** Marlen Pérez Díaz,

**Methodology:** Marlen Pérez Díaz, and Rubén Orozco Morales.

**Investigation:** Jhon Anthony Fernández Castro

**Discussion of results:** Jhon Anthony Fernández Castro, Marlen Pérez Díaz, and Rubén Orozco Morales,

**Original Draft:** Jhon Anthony Fernández Castro.

**Writing – Review and Editing:** Jhon Anthony Fernández Castro, Marlen Pérez Díaz, and Rubén Orozco Morales,

**Resources:** Marlen Pérez Díaz.

**Supervision:** Marlen Pérez Díaz, and Rubén Orozco Morales.

**Approval of the final text:** Jhon Anthony Fernández Castro, Marlen Pérez Díaz, and Rubén Orozco Morales,

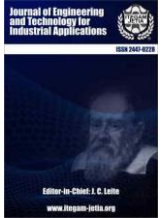
## VII. ACKNOWLEDGMENTS

This work has been partially funded thanks to Agency for Nuclear Energy and Advanced Technology of Cuba (AENTA), Project Code PS211LH02.

## VIII. REFERENCES

- [1] W. W. H. Organization. (26/04/2022). *Cáncer*. Available: <https://www.who.int/es/news-room/fact-sheets/detail/cancer>
- [2] H. Mahersia, M. Zaroug, and L. Gabralla, "Lung cancer detection on CT scan images: a review on the analysis techniques," *Lung Cancer*, vol. 4, no. 4, 2015.
- [3] J. Jeremy, H. McAdams, and S. Rossi, "Neoplasias pulmonares primarias," *Diagnóstico por Imagen del Tórax*, pp. 933-935, 2011.
- [4] Y. Li, X. Wu, P. Yang, G. Jiang, and Y. Luo, "Machine Learning Applications in Lung Cancer Diagnosis, Treatment and Prognosis," *ArXiv*, vol. 2203.02794, 2022.
- [5] A. Del Ciello *et al.*, "Missed lung cancer: when, where, and why?," *Diagnostic and Interventional Radiology*, vol. 23, no. 2, p. 118, 2017.
- [6] M. Haber, A. Drake, and J. Nightingale, "Is there an advantage to using computer aided detection for the early detection of pulmonary nodules within chest X-Ray imaging?," *Radiography*, vol. 26, no. 3, pp. 170-178, 2020.
- [7] M. Souto *et al.*, "Detección automática de nódulos pulmonares en tomografía computarizada. Un estudio preliminar," *Radiología*, vol. 50, no. 5, pp. 387-392, 2008.
- [8] J. D. López-Cabrera, L. A. L. Rodríguez, and M. Pérez-Díaz, "Classification of breast cancer from digital mammography using deep learning," *Inteligencia Artificial*, vol. 23, no. 65, pp. 56-66, 2020.
- [9] E. D. S. Aday, M. P. Díaz, and R. O. Morales, "Diseño de Sistema Automatizado para Detección de Anomalías en Imágenes Digitales de Mama," *Journal of Health and Medical Sciences*, vol. 5, no. 4, pp. 229-243, 2019.
- [10] I. Bush, "Lung nodule detection and classification," *Report, Stanford Computer Science*, 2016.
- [11] H. Seo *et al.*, "Machine learning techniques for biomedical image segmentation: an overview of technical aspects and introduction to state-of-art applications," *Medical physics*, vol. 47, no. 5, pp. 148-167, 2020.
- [12] F. Shan *et al.*, "Lung infection quantification of COVID-19 in CT images with deep learning," *arXiv preprint arXiv:2006.04655*, 2020.
- [13] C. Cortes and V. Vapnik, "Support-vector networks," *Machine learning*, vol. 20, no. 3, pp. 273-297, 1995.
- [14] N. Cristianini and J. Shawe-Taylor, *An introduction to support vector machines and other kernel-based learning methods*. Cambridge university press, 2000.
- [15] G. James, D. Witten, T. Hastie, and R. Tibshirani, *An introduction to statistical learning* (Springer Texts in Statistics). Springer New York, NY, 2013.
- [16] J. Shiraishi *et al.*, "Development of a digital image database for chest radiographs with and without a lung nodule: receiver operating characteristic analysis of radiologists' detection of pulmonary nodules," *American Journal of Roentgenology*, vol. 174, no. 1, pp. 71-74, 2000.
- [17] E. Martínez-Machado, M. Pérez-Díaz, and R. Orozco-Morales, "Automated System for the Detection of Lung Nodules," *Lecture Notes in Computer Science*, vol. 13055, pp. 337-348, 2021.

- [18] Y. Zhang and L. Wu, "Optimal multi-level thresholding based on maximum Tsallis entropy via an artificial bee colony approach," *Entropy*, vol. 13, no. 4, pp. 841-859, 2011.
- [19] R. C. Hardie, S. K. Rogers, T. Wilson, and A. Rogers, "Performance analysis of a new computer aided detection system for identifying lung nodules on chest radiographs," *Medical Image Analysis*, vol. 12, no. 3, pp. 240-258, 2008.
- [20] C. Supanta, G. Kemper, and C. del Carpio, "An algorithm for feature extraction and detection of pulmonary nodules in digital radiographic images," in *2018 IEEE International Conference on Automation/XXIII Congress of the Chilean Association of Automatic Control (ICA-ACCA)*, 2018, pp. 1-5: IEEE.
- [21] J. Wei, Y. Hagihara, A. Shimizu, and H. Kobatake, "Optimal image feature set for detecting lung nodules on chest X-ray images," Berlin, Heidelberg, 2002, pp. 706-711: Springer Berlin Heidelberg.
- [22] G. Coppini, S. Diciotti, M. Falchini, N. Villari, and G. Valli, "Neural networks for computer-aided diagnosis: detection of lung nodules in chest radiograms," *IEEE Transactions on Information Technology in Biomedicine*, vol. 7, no. 4, pp. 344-357, 2003.
- [23] A. M. Schilham, B. Van Ginneken, and M. Loog, "A computer-aided diagnosis system for detection of lung nodules in chest radiographs with an evaluation on a public database," *Medical Image Analysis*, vol. 10, no. 2, pp. 247-258, 2006.



## RESEARCH ARTICLE

## OPEN ACCESS

## GENERALIZATION OF DATA AUGMENTATION TO REDUCE THE NUMBER OF EPOCHS TO AVERAGE

\* Idileisy Torres-Rodríguez<sup>1</sup>, Beatriz Peón-Pérez<sup>2</sup>, Diamir De Ávila Rodríguez<sup>3</sup>, Samuel Cárdenas Herrera<sup>4</sup>, Alberto Taboada-Crispi<sup>5</sup>

<sup>1,5</sup> Universidad Central "Marta Abreu" de Las Villas, Santa Clara, Cuba.

<sup>2</sup> Hospital Manuel Piti Fajardo, Santa Clara, Cuba.

<sup>3,4</sup> Empresa de Automatización (CEDAI), Santa Clara, Cuba.

<sup>1</sup><http://orcid.org/0000-0002-1783-9908> , <sup>2</sup><http://orcid.org/0000-0003-3632-347X> , <sup>3</sup><http://orcid.org/0009-0004-9988-1246> ,

<sup>4</sup><http://orcid.org/0009-0007-3112-198X> , <sup>5</sup><http://orcid.org/0000-0002-7797-1441> 

Email: <sup>1</sup>[itrodriguez@uclv.edu.cu](mailto:itrodriguez@uclv.edu.cu)\*, <sup>2</sup>[beatrizpeonperez@gmail.com](mailto:beatrizpeonperez@gmail.com), <sup>3</sup>[diamir@cedai.com.cu](mailto:diamir@cedai.com.cu), <sup>4</sup>[samuel@cedai.com.cu](mailto:samuel@cedai.com.cu), <sup>5</sup>[ataboada@uclv.edu.cu](mailto:ataboada@uclv.edu.cu)

## ARTICLE INFO

**Article History**

Received: July 01th, 2024

Received: July 08th, 2024

Accepted: July 08th, 2024

Published: July 18th, 2024

**Keywords:**

Evoked potentials,  
Data augmentation,  
SNR.

## ABSTRACT

The waveform derived from averaging multiple EEG signal recordings during stimulation represents an Event-Related Potential (ERP). When sensory stimuli are employed, the resulting potentials are termed Evoked Potentials (EPs). EPs find applications across diverse domains of research and clinical settings, serving as a valuable tool in neuroscience and medicine due to their versatility in offering objective insights into brain function. However, the conventional signal averaging method used to extract EPs has inherent limitations, such as the necessity for numerous trials to ensure reliability and maximize Signal-to-Noise Ratio (SNR). This demands additional time for data recording and processing. Moreover, the reliability of recorded responses may be compromised due to the subject's habituation to the stimulus. To address these challenges, this study aims to enhance SNR in EP extraction by employing data augmentation, thereby reducing the number of records needed for averaging. The proposed method demonstrates a notable improvement of approximately  $9.77 \pm 2.65$  dB compared to traditional signal averaging with the same number of records. This study concludes that judicious data augmentation enables enhanced SNR estimates without the requirement for extensive new recordings.



Copyright ©2024 by authors and Galileo Institute of Technology and Education of the Amazon (ITEGAM). This work is licensed under the Creative Commons Attribution International License (CC BY 4.0).

## I. INTRODUCTION

Event-Related Potential (ERP) is a physiological phenomenon that refers to the electrical and/or magnetic responses generated in the nervous system due to a sensory, cognitive or motor stimulus. These responses are recorded using electroencephalography (EEG), magnetoencephalography (MEG) or other functional neuroimaging techniques [1]. Evoked Potentials (EP) are a subset of event-related potentials that are elicited by a specific sensory event, such as acoustic, visual or somatosensory stimuli [1]-[4]. Abnormalities have been found in the components that make up evoked responses in neurological conditions such as dementia, Parkinson's disease, multiple sclerosis, traumatic brain injury, stroke, obsessive-compulsive

disorder, attention deficit hyperactivity disorder, and others. These findings are based on clinical research. It is important to note that this information is objective and does not include any subjective evaluations. Evoked Potentials have low amplitudes, ranging from 0.1  $\mu$ V to 10  $\mu$ V, and are embedded in the background EEG activity, which has amplitudes ranging from 10  $\mu$ V to 100  $\mu$ V, making it the main source of noise. Additionally, recording EEG signals can be accompanied by various artifacts and interferences that affect the accurate estimation of the potential waveform. The presence of noises and interferences can result in a very low Signal to Noise Ratio (SNR), which can be as low as -30 dB for certain types of evoked potentials, making waveform estimation challenging. To obtain the Evoked Potential signal embedded in the background noise [5]-[13] and increase

the SNR, the traditional technique used is Signal averaging. This technique involves averaging the matrix formed with the individual records of the responses to each stimulus, also known as Ensemble Average.

### I.1 ENSEMBLE AVERAGE AND SIGNAL TO NOISE RATIO

The Ensemble Average using the arithmetic mean transforms the observed signal into a set of  $M$  epochs (ensemble matrix). Each epoch contains the response to the stimulus plus noise, as shown in Figure 1. The upper part of Figure 1 corresponds to the complete signal, which is a simulated, non-realistic signal with a low noise level, used to illustrate the classical procedure.

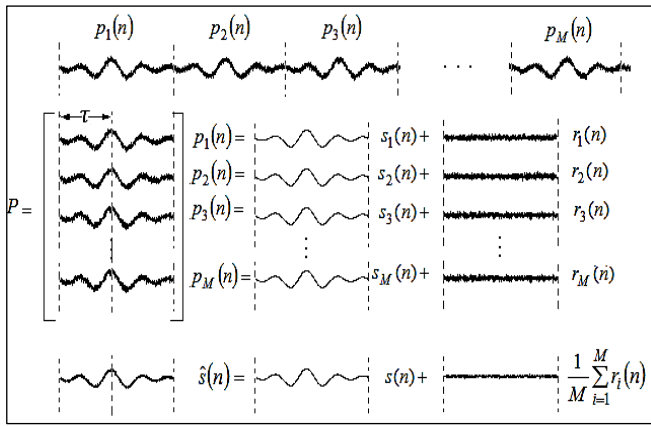


Figure 1: Ensemble average  
Source: authors, (2024).

Each epoch,  $p_i$ , is considered to be the sum of the deterministic component of the signal or evoked response,  $s$ , which is assumed to be invariant in each epoch, and a random noise,  $r_i$ , which is asynchronous with the stimulus, as described in equation 1.

$$p_i(n) = s_i(n) + r_i(n) \quad (1)$$

Each epoch  $p_i(n)$  consists of  $N$  samples (see equation 2) [14]-[21].

$$p_i(n), \quad i=1, \dots, M; \quad n=0, \dots, N-1 \quad (2)$$

Equation 3 shows that the estimated signal  $\hat{s}$  can be modelled as the sum of the deterministic component and the average noise of all segments.

$$\begin{aligned} \hat{s}(n) &= \frac{1}{M} \sum_{i=1}^M p_i(n) = \frac{1}{M} \sum_{i=1}^M (s_i(n) + r_i(n)) \\ &= \frac{1}{M} \sum_{i=1}^M s_i(n) + \frac{1}{M} \sum_{i=1}^M r_i(n) = s(n) + \frac{1}{M} \sum_{i=1}^M r_i(n) \end{aligned} \quad (3)$$

To improve the signal-to-noise ratio (SNR) by a factor of  $\sqrt{M}$ , as expressed in equation 4 [22], it is necessary to obtain

adequate noise reduction and increase the number of epochs forming the ensemble matrix [23]. Equation 4 refers to the initial signal-to-noise ratio as  $SNR_i$  and  $SNR_e$  to that estimated after averaging.

$$SNR_e = SNR_i \cdot \sqrt{M} \quad (4)$$

The SNR value of the evoked potential can be estimated from equation 5.

$$SNR = \frac{\sum_{j=1}^N s^2[j]}{\sum_{j=1}^N \theta^2[j]} \quad (5)$$

where  $N$  is the total number of samples of the segment to be evaluated,  $\theta$  is the remaining noise in the signal (signal obtained after attenuation of the noise minus the ideal signal). The subscript  $j$  refers to the  $j$ -th sample of the parameter in question and  $s$  to the pure ideal signal.

Most EPs have a much smaller amplitude than the EEG signal in which they are embedded, in the range of up to -30 dB [6]. To achieve adequate noise reduction using ensemble averaging in this case, approximately 1,000 epochs are required to equate the signal power to the noise power, a ratio of 1:1, the minimum required to indicate a response [24]. The need for such a large number of epochs is one of the main limitations of averaging as a noise reduction technique in the context of PE waveform estimation [7], [25]-[28].

## II DATA AUGMENTATION

Data augmentation has found its application in various classification and machine learning tasks, where data is typically scarce and difficult to obtain [29]-[33]. For electroencephalographic data, the lack of sufficient data remains a major problem. Data augmentation in EEG signals is performed by temporal, spatial/rotational transformations of the original data. Based on the characteristics of evoked potentials, if it is considered that these are signals that contain a certain periodicity (quasi-periodic) and this is associated with the synchronisation they have with the stimulus that causes them, the responses to the stimuli are practically the same. The data can be augmented by temporal transformations of the original recordings, including variations in both the latency (jitter) and the amplitude and width of the components of the evoked responses. It is then possible to obtain new recordings from the originals, including these variations. In this case, data augmentation is used to increase the size of the ensemble matrix and replace the need to record new epochs.

## III. MATERIALS AND METHODS

### III.1 DATA AUGMENTATION

To reduce the number of records to be averaged, data augmentation involves including temporary transformations in the initial records. These transformations advance or delay the records to simulate real-world variability in latencies. The original records and those obtained from the transformations are combined to create a new set matrix, called the augmented set matrix  $A$ . Equation 6 visualises an example of an augmented matrix with a shift of one sample to the right and one to the left. A small space has been left between the original matrix and its two versions to facilitate understanding of the equation. The augmented matrix



will have  $(2d+1)M$  epochs and the same number of samples as the original matrix  $P$ , where  $d$  is the number of displacements in samples made from the original version. If increasing the size of the ensemble matrix is known to improve noise reduction, one might assume that a large number of shifted versions of the original matrix would solve the problem. However, this is not the case.

$$A = \begin{bmatrix} p_{1,1} & p_{1,2} & p_{1,3} & \cdots & p_{1,N-1} & p_{1,N} \\ p_{2,1} & p_{2,2} & p_{2,3} & \cdots & p_{2,N-1} & p_{2,N} \\ \vdots & \vdots & \vdots & \ddots & \vdots & \vdots \\ p_{M,1} & p_{M,2} & p_{M,3} & \cdots & p_{M,N-1} & p_{M,N} \\ \\ p_{1,2} & p_{1,3} & p_{1,4} & \cdots & p_{1,N} & p_{1,N} \\ p_{2,2} & p_{2,3} & p_{2,4} & \cdots & p_{2,N} & p_{2,N} \\ \vdots & \vdots & \vdots & \ddots & \vdots & \vdots \\ p_{M,2} & p_{M,3} & p_{M,4} & \cdots & p_{M,N} & p_{M,N} \\ \\ p_{1,1} & p_{1,1} & p_{1,2} & \cdots & p_{1,N-2} & p_{1,N-1} \\ p_{2,1} & p_{2,1} & p_{2,2} & \cdots & p_{2,N-2} & p_{2,N-1} \\ \vdots & \vdots & \vdots & \ddots & \vdots & \vdots \\ p_{M,1} & p_{M,1} & p_{M,2} & \cdots & p_{M,N-2} & p_{M,N-1} \end{bmatrix} \quad (6)$$

Averaging the new matrix  $A$ , shown in equation 6, is equivalent to combining a moving average filter with the ensemble average, where the signal estimated from the augmented matrix  $A$  is estimated according to equation 7.

$$\hat{s}[n] = \frac{1}{M} \sum_{i=1}^M \frac{x_{i,n-1} + x_{i,n} + x_{i,n+1}}{3} \quad (7)$$

The cut-off frequency of a moving average filter depends on the number of samples included in the averaging window, in the case of equation 6,  $d=1$ , the window size is 3. As the size of the averaging window increases, the cut-off frequency of the moving average filter decreases, which could remove important components of the signal of interest. The maximum value of the displacements,  $d$ , in samples that can be used depends on the maximum frequency components of the signal of interest ( $fm$ ) and the sampling frequency ( $fs$ ) at which the signal is obtained, as described in equation 8. The criterion used to determine the maximum frequency of the signal is related to the characteristics of the bandpass filters in the signal acquisition stage.

$$d < \frac{1}{2} \left( \frac{fs}{fm} - 1 \right) \quad (8)$$

Figures 2, 3 and 4 correspond to the frequency responses of the Moving Average filters at sampling rates of 13,300 samples/s, 48,000 samples/s and 500 samples/s, respectively, and for maximum frequencies of 2,000 Hz, 3,000 Hz and 30 Hz respectively. These sample rate and peak rate values are taken from real database examples of AERs. In these figures you can see how a higher value of  $d$  would reduce the width of the central lobe of the filter, thereby eliminating important components of the signal of interest. Using this criterion, the maximum value of  $d$  would be approximately 3 samples for the

first sampling frequency, 7 samples for the second sampling frequency and 7 samples for the third sampling frequency.

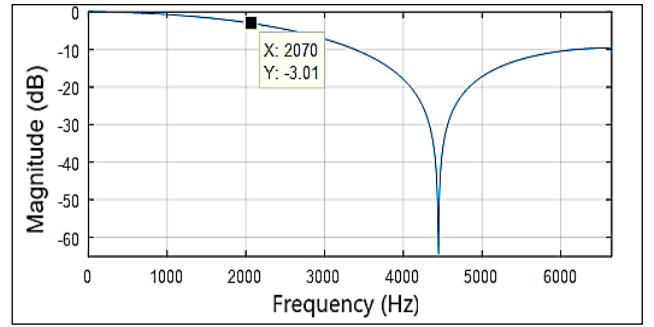


Figure 2: Frequency response of a 3-sample moving average filter at  $fs=13.3$  kHz. Source: authors, (2024).

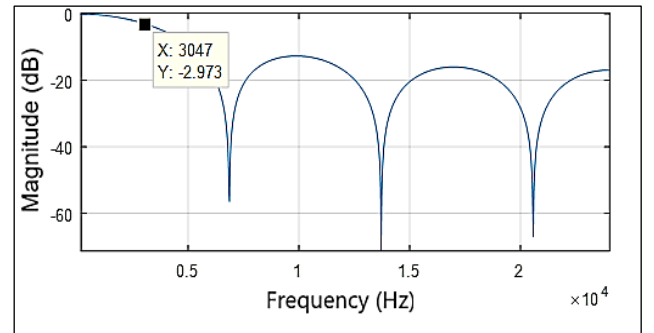


Figure 3: Frequency response of a 7-sample moving average filter at  $fs=48$  kHz. Source: authors, (2024).

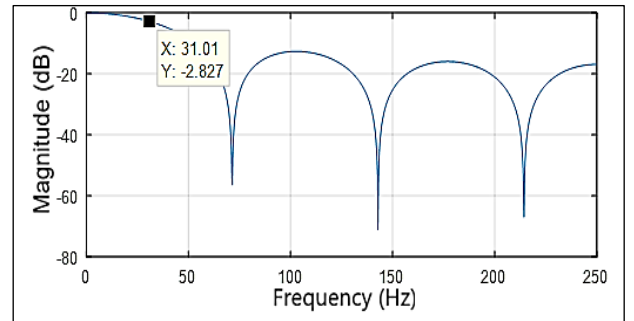


Figure 4: Frequency response of a 7-sample moving average filter at  $fs=500$  Hz. Source: authors, (2024).

Before averaging the augmented matrix, any elements of  $A_{m,n}$  that are considered outliers are discarded. Values in each column that differ from the column median of the original matrix by more than  $\pm 3$  standard deviations from the median of the standard deviations of the estimated noise (Equation 9) in the ensemble matrix are considered outliers. The median noise deviation is estimated from equation 10.

$$q = [\tilde{p}(n) - 3 \cdot \sigma_{r_{mp-mediana}}, \tilde{p}(n) + 3 \cdot \sigma_{r_{mp-mediana}}] \quad (9)$$

$$\sigma_{r_{mp-mediana}} = \sqrt{\frac{\text{mediana} \{ \sigma_{up}^2(1, 2, \dots, N) \}}{M}} \quad (10)$$

Then, the signal can be estimated from equation 11.

$$\hat{\sigma}_{MRA} = \frac{\sum_{i=1}^{(2d+1)M} w_{i,n} A_{i,n}}{\sum_{i=1}^{(2d+1)M} w_{i,n}}, \quad (11)$$

where  $w_{i,n}$  is the element of the  $i$ -th row of the  $n$ -th column of the weight matrix with the same size as  $A$ , and  $d$  is the number of displaced samples taken into account. The elements of the weight matrix  $w$  can be 0 or 1, 0 in the case that the sample is considered an outlier and 1 otherwise.

### III.2 EXPERIMENT DESCRIPTION

To analyse the behaviour of the data augmentation and its influence on the waveform estimation from a smaller number of epochs, a total of 100 data sets of 2000 epochs each were generated using the simulator described in [34]. The sampling frequency of the simulated signals is 48,000 samples/s and the maximum frequency component of the signal is 3000 Hz. From each data set, 512 epochs were randomly selected 100 times to form a Monte Carlo experiment of 100 runs. In this case, the expected waveform is known a priori, so the SNR value was estimated in each run, as expressed in equation 5.

### IV. RESULTS AND DISCUSSIONS

Figure 5 shows the average SNR values and their dispersion obtained for different values of  $d$ . As can be seen in Figure 5, there is a tendency for the SNR value to increase as  $d$  increases until it reaches 8, and then to decrease. This result is related to what was explained in the first part of section 2.1,  $d$  is related to the maximum frequency components of the signal and the sampling frequency, for values greater than  $d \approx 7$ , it is not guaranteed that the shape of the signal is preserved. The initial SNR value obtained on the simulated data sets was approximately  $-26.0398 \pm 1.16$  dB. The average SNR value obtained using the classical Ensemble Average in the experiment was  $0.1992 \pm 1.0917$  dB.

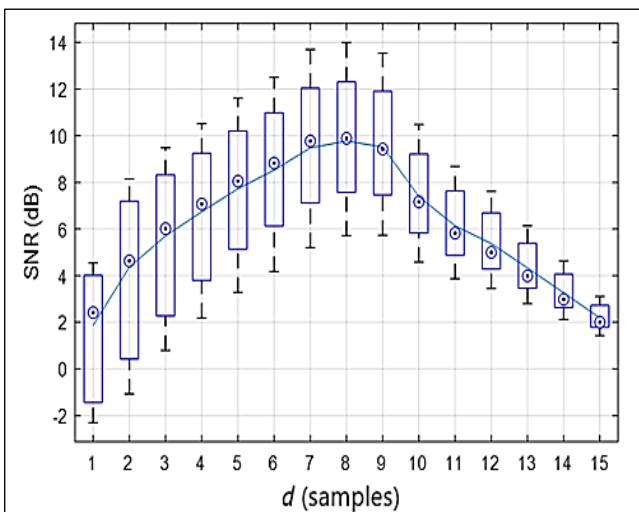


Figure 5: Signal-to-noise ratio obtained using data augmentation with different values of  $d$ . Source: authors, (2024).

Figure 6 shows the result of the standard deviation of the average residual noise obtained for different values of  $d$ .

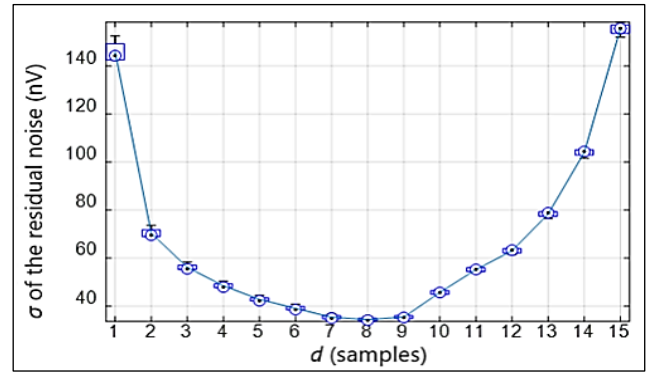


Figure 6: Standard deviation of the residual noise using data augmentation with different values of  $d$ .

Source: authors, (2024).

Currently, according to the protocols for PEATC [24], it is recommended that the residual noise level be equal to or less than 80 nV before concluding that there is no response. Figure 6 shows that this requirement is met for values of  $d \geq 2$ . A value of  $d = 4$  results in an expanded matrix of 4608 epochs, a matrix size consistent with real-world studies. When Ensemble Average was applied to a matrix of 512 epochs, a residual noise standard deviation of 243 nV was obtained.

### V. CONCLUSIONS

Data augmentation based on the characteristics of the signal can be a proposal to improve the SNR in the estimation of evoked responses with a smaller number of epochs. The results obtained in the experimental phase correspond to the theoretical ones proposed in the first part of the methodological section. The SNR values obtained in the experiment with data augmentation are about 9 dB better than those obtained with the traditional Ensemble Average method for the same number of epochs. With a value of  $d$  equal to 4, in the case of the proposed experiment, with 512 initial recordings, a number of recordings of 4608 epochs can be obtained, which is similar to the number of epochs required to be recorded in a real context. This value means that the time needed to estimate the waveform of an evoked potential is reduced by a factor of 9. On the basis of the results obtained, it is recommended that future work should evaluate the increase in data in terms of reduction of latency variability, a problem that may be resolved with this technique.

### VI. AUTHOR'S CONTRIBUTION

**Conceptualization:** Idileisy Torres-Rodríguez, Alberto Taboada-Crispí.

**Methodology:** Idileisy Torres-Rodríguez, Beatriz Peón-Pérez, Alberto Taboada-Crispí.

**Investigation:** Idileisy Torres-Rodríguez, Beatriz Peón-Pérez, Diamir De Ávila Rodríguez, Samuel Cárdenas Herrera. Alberto Taboada-Crispí.

**Discussion of results:** Idileisy Torres-Rodríguez, Alberto Taboada-Crispí.

**Writing – Original Draft:** Idileisy Torres-Rodríguez.

**Writing – Review and Editing:** Idileisy Torres-Rodríguez, Beatriz Peón-Pérez, Diamir De Ávila Rodríguez, Samuel Cárdenas Herrera. Alberto Taboada-Crispí.

**Resources:** Idileisy Torres-Rodríguez.

**Supervision:** Alberto Taboada-Crispí.

**Approval of the final text:** Idileisy Torres-Rodríguez, Beatriz Peón-Pérez, Diamir De Ávila Rodríguez, Samuel Cárdenas Herrera. Alberto Taboada-Crispí.

## VII. REFERENCES

- [1] P. E. Clayson, C. J. Brush, y G. Hajcak, “Data quality and reliability metrics for event-related potentials (ERPs): The utility of subject-level reliability”, *Int. J. Psychophysiol.*, vol. 165, pp. 121–136, jul. 2021, doi: 10.1016/j.ijpsycho.2021.04.004.
- [2] J. A. Carballo-Gonzalez, P. Valdes-Sosa, y M. Valdes-Sosa, “Detection of Event Related Potentials”, *Int. J. Neurosci.*, vol. 46, núm. 3–4, pp. 109–122, ene. 1989, doi: 10.3109/00207458908986247.
- [3] A. Taboada-Crispi et al., “Simulation of Event-Related Potentials in a wide sense for assessment of detection/estimation algorithms”, en *AIP Conference Proceedings*, 2008, vol. 1060, pp. 7–10. doi: 10.1063/1.3037119.
- [4] F. Congedo, Marco and Lopes da Silva, “Event-related potentials: General aspects of methodology and quantification”, en *Niedermeyer’s Electroencephalography: Basic Principles, Clinical Applications, and Related Fields*, D. L. S. and F. H. L. da Silva, Ed. Oxford University Press, 2018. [En línea]. Disponible en: <https://hal.archives-ouvertes.fr/hal-01953600>.
- [5] E. Laciari y R. Jane, “An improved weighted signal averaging method for high-resolution ECG signals”, en *Computers in Cardiology 2001. Vol.28 (Cat. No.01CH37287)*, 2001, pp. 69–72. doi: 10.1109/CIC.2001.977593.
- [6] T. Pander, S. Pietraszek, y T. Przybyła, *Information Technologies in Biomedicine*, vol. 284, núm. 4. Cham: Springer International Publishing, 2014. doi: 10.1007/978-3-319-06596-0.
- [7] I. Torres-Rodríguez, C. A. Ferrer, E. Velarde-Reyes, y A. Taboada-Crispi, “Improving ensemble averaging by epoch detrending in evoked potentials”, en *Lecture Notes in Computer Science (including subseries Lecture Notes in Artificial Intelligence and Lecture Notes in Bioinformatics)*, 2019, vol. 11401 LNCS, pp. 707–714. doi: 10.1007/978-3-030-13469-3\_82.
- [8] J. M. Leski, “Robust weighted averaging [of biomedical signals]”, *IEEE Trans. Biomed. Eng.*, vol. 49, núm. 8, pp. 796–804, ago. 2002, doi: 10.1109/TBME.2002.800757.
- [9] C. E. Davila y M. S. Mobin, “Weighted averaging of evoked potentials”, *IEEE Trans. Biomed. Eng.*, vol. 39, núm. 4, pp. 338–345, abr. 1992, doi: 10.1109/10.126606.
- [10] Z. Leonowicz, J. Karvanen, y S. L. Shishkin, “Trimmed estimators for robust averaging of event-related potentials”, *J. Neurosci. Methods*, vol. 142, núm. 1, pp. 17–26, mar. 2005, doi: 10.1016/j.jneumeth.2004.07.008.
- [11] K. Kotowski, K. Stapor, y J. Leski, “Improved robust weighted averaging for event-related potentials in EEG”, *Biocybern. Biomed. Eng.*, vol. 39, núm. 4, pp. 1036–1046, oct. 2019, doi: 10.1016/j.bbe.2019.09.002.
- [12] D. X. Wang y C. E. Davila, “Subspace Averaging of Auditory Evoked Potentials”, en *2019 41st Annual International Conference of the IEEE Engineering in Medicine and Biology Society (EMBC)*, jul. 2019, pp. 656–659. doi: 10.1109/EMBC.2019.8857818.
- [13] P. Prado-Gutierrez, E. Martínez-Montes, A. Weinstein, y M. Zañartu, “Estimation of auditory steady-state responses based on the averaging of independent EEG epochs”, *PLoS One*, vol. 14, núm. 1, p. e0206018, ene. 2019, doi: 10.1371/journal.pone.0206018.
- [14] S. M. K. K. Madsen, J. M. Harte, C. Elberling, y T. Dau, “Accuracy of averaged auditory brainstem response amplitude and latency estimates”, *Int. J. Audiol.*, vol. 57, núm. 5, pp. 345–353, may 2018, doi: 10.1080/14992027.2017.1381770.
- [15] C. Elberling y M. Don, “Quality Estimation of Averaged Auditory Brainstem Responses”, *Scand. Audiol.*, vol. 13, núm. 3, pp. 187–197, ene. 1984, doi: 10.3109/01050398409043059.
- [16] H. Litvan et al., “Comparison of Conventional Averaged and Rapid Averaged, Autoregressive-based Extracted Auditory Evoked Potentials for Monitoring the Hypnotic Level during Propofol Induction”, *Anesthesiology*, vol. 97, núm. 2, pp. 351–358, ago. 2002, doi: 10.1097/0000542-200208000-00011.
- [17] D. L. Jewett y J. S. Williston, “Auditory-evoked far fields averaged from the scalp of humans”, *Brain*, vol. 94, núm. 4, pp. 681–696, 1971, doi: 10.1093/brain/94.4.681.
- [18] N. Acir, Y. Erkan, y Y. A. Bahtiyar, “Auditory brainstem response classification for threshold detection using estimated evoked potential data: comparison with ensemble averaged data”, *Neural Comput. Appl.*, vol. 22, núm. 5, pp. 859–867, abr. 2013, doi: 10.1007/s00521-011-0776-2.
- [19] M. Don, C. Elberling, y M. Waring, “Objective Detection of Averaged Auditory Brainstem Responses”, *Scand. Audiol.*, vol. 13, núm. 4, pp. 219–228, ene. 1984, doi: 10.3109/01050398409042130.
- [20] L. Sörnmo y P. Laguna, *Bioelectrical Signal Processing in Cardiac and Neurological Applications*, vol. 8. Elsevier, 2005. doi: 10.1016/B978-0-12-437552-9.X5000-4.
- [21] E. Perez-Abalo, Maria Cecilia and Rodriguez-Davila, Ernesto Luis and Sanchez-Castillo, Manuel and Sotero-Diaz, Roberto Carlos and Torres-Fortuny, Alejandro and Santos-Febles, “Method and apparatus for the objective detection of auditive disorders”, *US Patent 9,345,419*, 2016 [En línea]. Disponible en: <https://patents.google.com/patent/US9345419B2/en>.
- [22] O. Rempelman y H. H. Ros, “Coherent averaging technique: A tutorial review Part 1: Noise reduction and the equivalent filter”, *J. Biomed. Eng.*, vol. 8, núm. 1, pp. 24–29, ene. 1986, doi: 10.1016/0141-5425(86)90026-9.
- [23] M. A. Chesnaye, “Optimising Objective Detection Methods for the Auditory Brainstem Response”, University of Southampton, 2019. [En línea]. Disponible en: <https://eprints.soton.ac.uk/428621/>
- [24] K. Rennert et al., “British Columbia Early Hearing Program (BCEHP) Audiological Assessment Protocol”. 2012. doi: 10.13140/2.1.2977.5683.
- [25] I. Torres-Rodríguez, “Estimadores Robustos de Promediado para la Detección de Potenciales Relacionados con Eventos”, Universidad Central “Marta Abreu” de Las Villas, 2014.
- [26] I. Torres-Rodríguez, C. A. Ferrer-Riesgo, J. C. Oliva Pérez, y A. Taboada-Crispi, “Performance of Different Average Methods for the Automatic Detection of Evoked Potentials”, en *Lecture Notes in Computer Science (including subseries Lecture Notes in Artificial Intelligence and Lecture Notes in Bioinformatics)*, vol. 11896 LNCS, 2019, pp. 629–636. doi: 10.1007/978-3-030-33904-3\_59.
- [27] I. Torres-Rodríguez, C. A. Ferrer-Riesgo, M. M. P. de Morales Artilles, y A. Taboada-Crispi, “Performance Evaluation of Average Methods in the Time Domain Using Quality Measures for Automatic Detection of Evoked Potentials”, en *IFMBE Proceedings*, vol. 75, Springer, 2020, pp. 12–20. doi: 10.1007/978-3-030-30648-9\_2.
- [28] C. A. Ferrer, I. Torres-Rodríguez, A. Taboada-Crispi, y E. Nöth, “Analytical Solution for the Optimal Addition of an Item to a Composite of Scores for Maximum Reliability”, en *Lecture Notes in Computer Science (including subseries Lecture Notes in Artificial Intelligence and Lecture Notes in Bioinformatics)*, vol. 11896 LNCS, Springer, 2019, pp. 408–416. doi: 10.1007/978-3-030-33904-3\_38.
- [29] K. Zhang et al., “Data Augmentation for Motor Imagery Signal Classification Based on a Hybrid Neural Network”, *Sensors*, vol. 20, núm. 16, p. 4485, ago. 2020, doi: 10.3390/s20164485.
- [30] C. He, J. Liu, Y. Zhu, y W. Du, “Data Augmentation for Deep Neural Networks Model in EEG Classification Task: A Review”, *Frontiers in Human Neuroscience*, vol. 15. Frontiers Media S.A., el 17 de diciembre de 2021. doi: 10.3389/fnhum.2021.765525.
- [31] R. Zhang et al., “ERP-WGAN: A data augmentation method for EEG single-trial detection”, *J. Neurosci. Methods*, vol. 376, p. 109621, jul. 2022, doi: 10.1016/j.jneumeth.2022.109621.
- [32] B. K. Iwana y S. Uchida, “An empirical survey of data augmentation for time series classification with neural networks”, *PLoS One*, vol. 16, núm. 7, p. e0254841, jul. 2021, doi: 10.1371/journal.pone.0254841.
- [33] M. M. Krell, A. Seeland, y S. K. Kim, “Data Augmentation for Brain-Computer Interfaces: Analysis on Event-Related Potentials Data”, *arXiv Prepr. arXiv1801.02730*, ene. 2018, doi: <https://doi.org/10.48550/arXiv.1801.02730>.
- [34] I. Torres-Rodríguez, R. Díaz-Amador, B. Peón-Pérez, A. Hurtado Armas, y A. Taboada-Crispi, “Realistic Simulation of Event-Related Potentials and Their Usual Noise and Interferences for Pattern Recognition”, en *Pattern Recognition*, 2023, pp. 201–210.



ISSN ONLINE: 2447-0228



## RESEARCH ARTICLE

## OPEN ACCESS

## EXPERIMENTAL STUDY OF A NEW HYDROCARBON MIXTURE FOR DOMESTIC REFRIGERATOR TO REPLACE R134A

Parashurama S<sup>1</sup>, \*Anjappa S B<sup>2</sup>, D.K. Ramesha<sup>3</sup>

<sup>1</sup>Government Engineering College, Kushalnagar, Karnataka 571234, India.

<sup>2</sup>Viswam Engineering College, Madanapalle, AP, 517325, India.

<sup>3</sup>University of Visvesvaraya College of Engineering, Bengaluru, Karnataka 560001, India.

<sup>1</sup> <http://orcid.org/0000-0002-8885-5403>, <sup>2</sup> <http://orcid.org/0000-0001-9473-9460>, <sup>3</sup> <http://orcid.org/0000-0002-3480-4109>.

Email: [parashuramas@gmail.com](mailto:parashuramas@gmail.com)<sup>1</sup>, [anji09.sb@gmail.com](mailto:anji09.sb@gmail.com)<sup>2</sup>, [mechsvtm@gmail.com](mailto:mechsvtm@gmail.com)<sup>3</sup>.

### ARTICLE INFO

#### Article History

Received: December 23<sup>th</sup>, 2023

Revised: July 08<sup>th</sup>, 2024

Accepted: July 08<sup>th</sup>, 2024

Published: July 18<sup>th</sup>, 2024

#### Keywords:

R290,  
Scroll-Down time,  
Power Consumption,  
R290/R600a,  
ice-making time.

### ABSTRACT

In a domestic refrigerator with 4.49cc displacement compressors, the performance of R290 (48 by mass percent) and R600a (52 by mass percent) was examined experimentally. In our research, we employed a 210-litre refrigerator that was designed to run on R12 and had a longer capillary. The amount of energy utilised, as well as the pressure and temperature at crucial locations on the various refrigerated compartments and refrigerator circuit, are all monitored. With R290/R600a, we performed a scroll-down test and ice-making test. According to our findings, R290/R600a is the best contenders for re-placing R134a in terms of energy conservation. Because the amount of refrigerant utilised is so small, the flammability fac-tor can be overlooked.



Copyright ©2024 by authors and Galileo Institute of Technology and Education of the Amazon (ITEGAM). This work is licensed under the Creative Commons Attribution International License (CC BY 4.0).

### I. INTRODUCTION

Food preservation and life-saving drugs, as well as individual health and safety, rely on refrigeration technology. The refrigeration technology is also used to provide well-being in industrial process and air conditioning system. The risk of CFCs, as well as the Montreal and Kyoto Protocols, must be considered while evaluating future refrigerants. Natural refrigerants and hydrogenated chloro-fluorocarbons (HCFCs) are suitable substitutes.

CFC-12 was outmoded when it was initially developed for the refrigerator pursuit and it was subsequently replaced by HFC-134a, an average refrigerant. HFC-134a on the other hand, must be phased out by 2020; it is critical to evaluate HFC-134a's prospects and upgrade. Mineral lubricating oil with 0% ODP and a low GWP is suitable with hydrocarbon refrigerants. The most significant disadvantages of these refrigerants are their inconsistent flammability. The hydrocarbon refrigerants have a higher latent heat vaporization than R12 and less density makes them desirable for low load applications in defiance of their flammability.

Hydrocarbons have been recommended as a replacement for conventional refrigerants in residential freezers by a number of scientists. Propane's performance in small residential refrigerators was investigated by [1],[2]. The findings revealed that Propane is a suitable alternative to R12 that does not require any modifications [1]. Investigated a household refrigerator that ran on Propane and found that Propane performed better than R12. Experiments with isobutene and propane these mixtures were conducted in home refrigerator and the results showed the attained. Co-efficient of performance was more than that of R12. For [3], studied the use of propane in a 239 liter refrigerator, and it is found that the refrigerator utilized the least amount of energy per day while using Propane. To replace Propane, a compressor with a smaller displacement is required due to the higher volumetric refrigeration capability. In prior work [4], used SRK EoS to look at the properties of an HC, and therefore the results are well within permissible limits. Computer modelling was used to estimate the performance of hydrocarbons as alternative refrigerants to exchange R12 in average size residential freezers. The R270 and DME R270 and DME, also as R290 R1270 with a reduced displacement compressor, were found to be suitable drop-in

choices. Parashurama S et al. conducted a theoretical and experimental evaluation of the refrigerant R 290, which is a substitute for R12 with a smaller displacement compressor [5].

Propane does not require any changes to the refrigerator's structure. Normal oil is miscible with all hydrocarbons and has good lubricating qualities. Another advantage of hydrocarbons is that no damp air is introduced because to the favorable evaporator pressure. According to [6]. The hydrocarbons in gaseous and liquid phases in on heat transfer properties, these phases are much higher than R12 and R134a. As a result from a heat transfer standpoint, R290 is a viable alternative. R134a is presently as an alternative to R12. It has a low energy efficiency, a high GWP, and is incompatible with mineral oil. As a result, the issue remains unsolved, and it must be changed in compliance with F-gas regulations. [7],[8], used SRK EOS to estimate the thermodynamic characteristics of Fluoroethers, HFs and HFCs and screened and offered R270 and R152a as alternatives to R134a an equivalent compressor, also as R290, R161 and R1270 with lower displacement compressor, also as R290, R161, and R1270 with lower compressor displacement. They also projected the thermodynamic properties of several binary mixes of HFs and HFCs using the SRK PSRK AND EOS mixing rules, performed thermodynamic analysis, and offered them as alternatives to R134a [8]. In the present paper a new mixture R290 (48%)/R600a (52%) is tested with a 4.49 cc hermetic compressor in an unaltered refrigerator used for R12,

Table 1: Property data of HC and R290 for  $T_e = -25^\circ\text{C}$  &  $T_k=55^\circ\text{C}$ .

Refrigerant	HC	R290
NBP ( $^\circ\text{C}$ )	-	-42.07
ODP	0	0.000
GWP	20	3
Evaporator pressure (bar)	1.4	2.02
Critical temperature (K)	389.61	369.8
Critical pressure (bar)	139.33	42.5
Condenser pressure (bar)	14.22	19.07
Pressure ratio	13.29	10.71
Latent heat (kJ/kg)	390.13	404.99
Specific volume ( $\text{m}^3/\text{kg}$ )	0.4142	0.2913

Source: Authors, (2024).

Table 1 shows the computed refrigerant properties for the refrigerator design settings. Using the prediction method described in Reference [8], the thermodynamic characteristics of the R290/R600a mixture are calculated. The study's findings are summarised in Table 2. For the R290/R600a (HC) system, simulation was utilised to calculate features including refrigeration effect, pressure ratio, condenser heat rejection, mass flow rate, compressor exit temperature, starting torque, and COP. R290 operates better-quality with a higher coefficient of performance value and requires a smaller compressor and a lower motor rating, according to the simulation results.

Table 2: Results of Thermodynamic Analysis.

Refrigerant	R290	HC
Mass flow rate (kg/sec) ( $\times 10^4$ )	0.289	0.386
Compressor power input (W)	40.32	43.94
Condenser duty (W)	137.83	139.88
Piston displacement (cc)	2.43	4.6
Starting torque (N-m)	2.16	2.83

COP	1.84	1.99
Discharge temperature ( $^\circ\text{C}$ )	125	133
Isentropic index	1.124	1.137
Capillary bore, d (m)	0.00066	0.00079
Capillary length, L (m)	4.178	4.3

Source: Authors, (2024).

## II. EXPERIMENTAL SETUP

The testing chamber has a small wooden chamber for air circulation. Temperature sensors, steam injecting nozzles, heater coils, and relative humidity sensor connected to a steam raiser outside the chamber and split air conditioner to replicate the needed weather conditions with the help of condenser heat rejection to the testing chamber are also included. The experimental setup that was developed is depicted in Figure

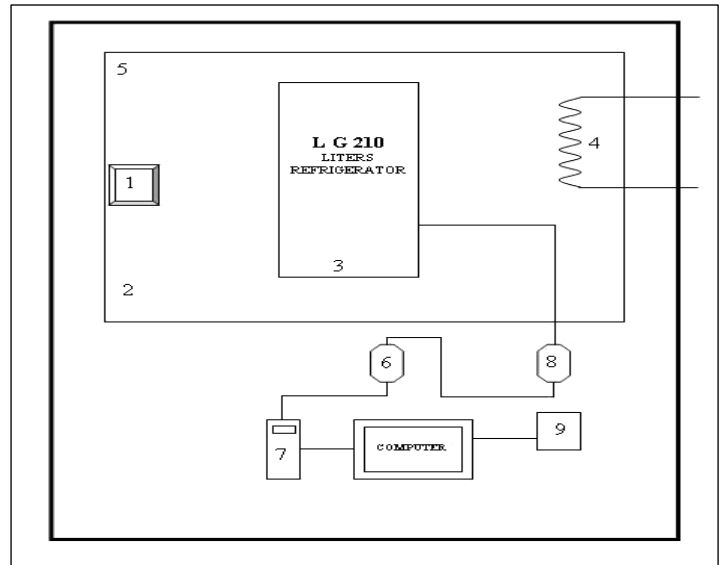


Figure 1: Experimental Setup and Simulation Room Layout. Source: Authors, (2024).

1. Air condition unit
2. Humidification sensor
3. LG Refrigerator
4. Heater
5. Testing room temperature
6. Thermocouple
7. ADAM Module
8. Analog to digital converter
9. Power supply

Table 3: Details of Instrumentation.

Instrument	Range	Uncertainty
Pressure gauges	0 to 10.34	$\pm 0.345\text{bar}$
	0 to 20.69 bar	5 Psi
Thermocouple	-	$\pm 0.1^\circ\text{C}$
Digital thermometer	-50 to $500^\circ\text{C}$	$\pm 0.1^\circ\text{C}$
Clamp meter	0 to 10 amps	$\pm 0.1$ amps
	0 to 1000 V	$\pm 1\text{V}$

Source: Authors, (2024).

## II.1 EXPERIMENTATION AND PERFORMANCE ANALYSIS

Leakage tests, ice making test, Scroll-Down tests, and Power Consumption tests are all administered in compliance with IS regulations [9]. As results of setting the thermostatic knob to optimize the mean compartment temperature to 7°C, power outage, failure to take care of the condition as stated in Indian standards, and other factors, certain findings are destroyed. The discharge pressure, Temperatures is recorded using thermocouples at the condenser outlet, freezer compartment, compressor inlet, evaporator outlet, and evaporator inlet. The second and third compartment. The electrical energy consumption of the compressor was measured

using a clamp on watt meter with a 0.01 KWh resolution. Nitrogen and soap bubbles were used to conduct leakage tests. 65g of Refrigerant HC has been charged into the system. R290/R600a tests were carried out with a 4.49cc displacement compressor with a 4.29m capillary length. After the Scroll-Down phase, the system will run up 6 hours then placed within the refrigerator for the zero load performance test. After the Scroll-Down time, the system was run ice making tests for up to three hours. After it had been pulled down, the ice making test for HC with a length of 4.29 meter was extended for an additional 3 hours. Ex-pediments are run until steady-state conditions are reached. The refrigerator it will run three months to verify the results and for up to 6 hours after it had been pulled right down to achieve its steady state conditions.

Table 4: Results of Experimentation.

Refrigerant	R290 [5]	HC
Capillary length (m)	5.95	3.0
Suction pressure	2.895	1.768
Discharge pressure	15.855	13.840
Discharge temperature (oC)	66.4	68.2
Pull down time (min)	111	110
Pull down energy Consumption (kWh/day)	0.1369	0.1833
Energy consumption (kWh/day)	1.329	1.4854
Ice making time (min)	160	151
COP <sub>act</sub>	1.74	1.72
$\eta_{ref}$	55.81	41.2
I (W)	56.14	38.42
Q <sub>ext.</sub>	4.883	3.946
Q	5.82	35.94

Source: Authors, (2024).

## III. RESULTS AND DISCUSSION

Equations from Reference 4 are used to analyse and compare performance parameters the table 2 lists the value of performance parameters for HC and R290. R290 appears to have a lower pressure ratio than R290/R600a, hinting that a lower displacement com-pressor is required. The more boiling refrigerants R290 necessitates a smaller motor rating than R290/R600a, as shown in Table 2.

Table 2 shows due to the high pressure ratio the volumetric efficiency of HC is slightly lower than that of R290. Using the aforesaid volumetric efficiencies, the displacement volumes of R290/R600a and R290 are de-termined. R290 requires less displacement than R290/R600a due to its larger volumetric refrigeration capacity. As shown in Table 2, R290 requires less dis-placement than R290/R600a. R290's discharge tempera-tures are lower than R290/ R600a's. The winding tem-perature rises as the discharge temperature rises. Be-cause certain charge is required for the hydrocarbon is very small and it is well under safety regulations, specif-ically 55g there is no risk of fire. As a result, the R290 compressor runs smoothly [10].

According to the theoretical research, R290 has a greater COP than R290/R600a. Furthermore, the condenser's heat released rate is lower than that of R290/R600a, im-plying that the

condenser does not need to be a larger. The mass flow rate of R290 is much lower than R290/R600a, while the pressure ratio is much larger. As a result, the capillary must be lengthened. If an R12 compressor is used to compress R290, there is no diffi-culty with starting torque [11]. R290/R600a is evaluated under the identical operating conditions in this experi-ment utilizing a household refrigerator built.to.work with.R12.Table 3 shows that the Scroll-Downtime for R290 is essentially comparable to R290/R600a, but the ice making time is 5.96 percent longer, energy usage is 10.53 percent lower, and the average discharge tempera-ture is 1.20C lower in compressor. Scroll down test, ice making test and temperature profiles demonstrate that the refrigerator of R290 has roughly identical capacity to the R290/R600a refrigerator, as illustrated in Figures 2 to 7. The temperature differences in the freezer com-partment, first compartment, and second compartment are shown in Figures 2 to 7.

Because the refrigerator volumes are nearly identical, Wong wises et al. [3] and Rasti et al. [12] can be com-pared to our work. Table 5 demonstrates that when com-pared to R134a, the refrigerant R290 (48)/R600a (52) used the least amount of energy. The usage of a reduced displacement compressor in our test resulted in a higher level of electricity savings.

Table 5: Comparison of present study with literature.

Refrigerant	[3]		[12]		Present Study
	R134a	R290(60)/R600a	R134a	R290(56)/R600a	R290(48)/R600a
Temperature(°C)	25	25	32	32	43
Capacity(c)	239	-	238	-	-
Charge(g)	120	60	-	105	65
Energy consumption (kW hr/day)	1.43	1.41	1.628	1.541	1.485

Source: Authors, (2024).

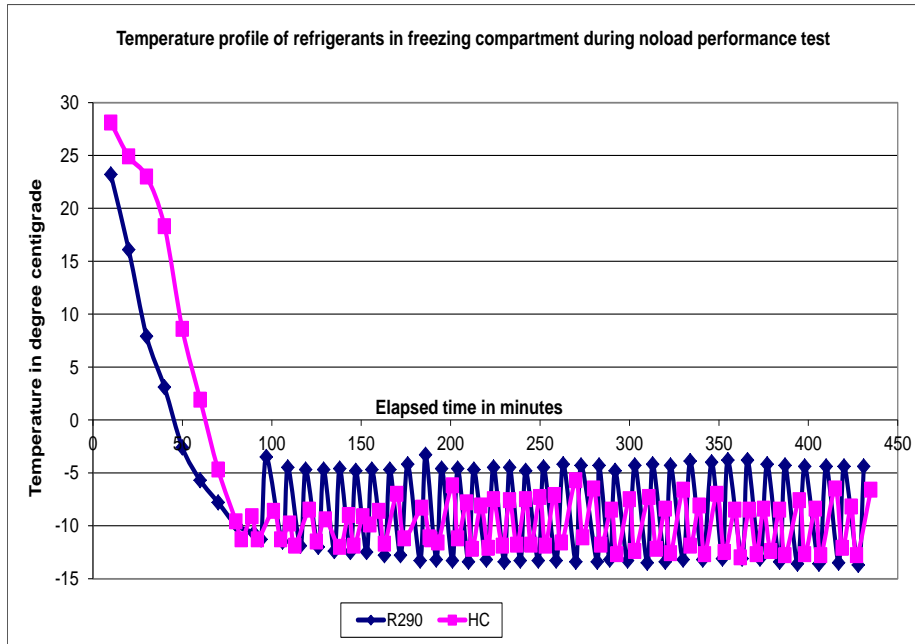


Figure 2: Variation in Temperatures of Freezer Compartment in Scroll-Down test. Source: Authors, (2024).

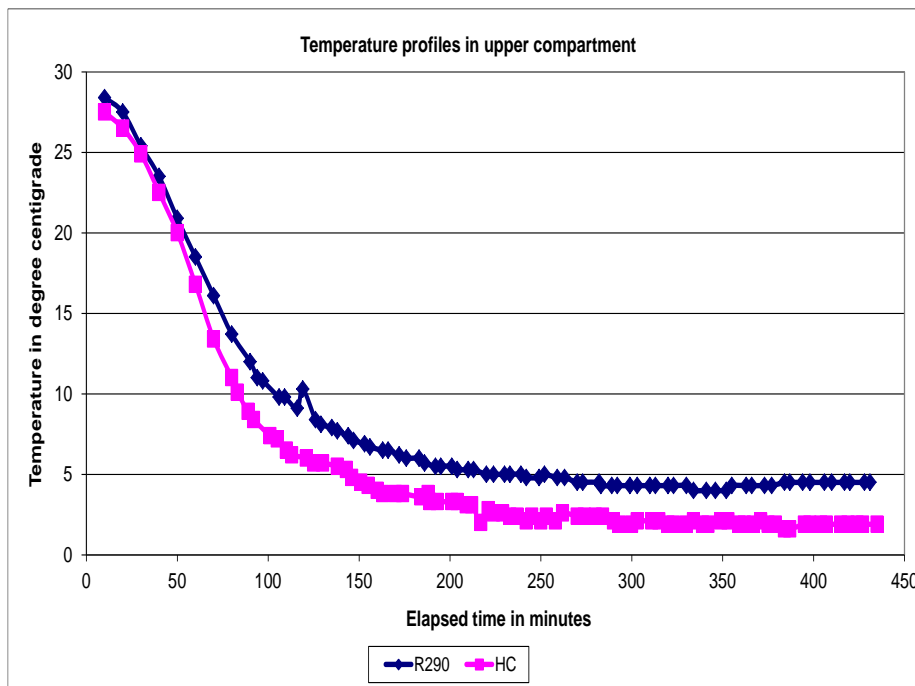


Figure 3: Variation in Temperatures of Upper Compartment in Scroll-Down test.

Source: Authors, (2024).

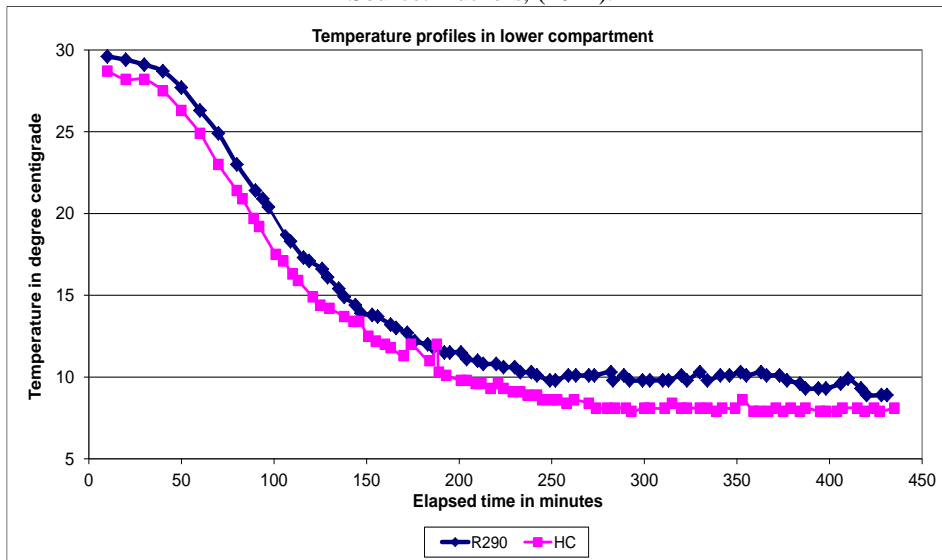


Figure 4: Variation in Temperatures of Lower Com-partment in Scroll-Down test. Source: Authors, (2024).

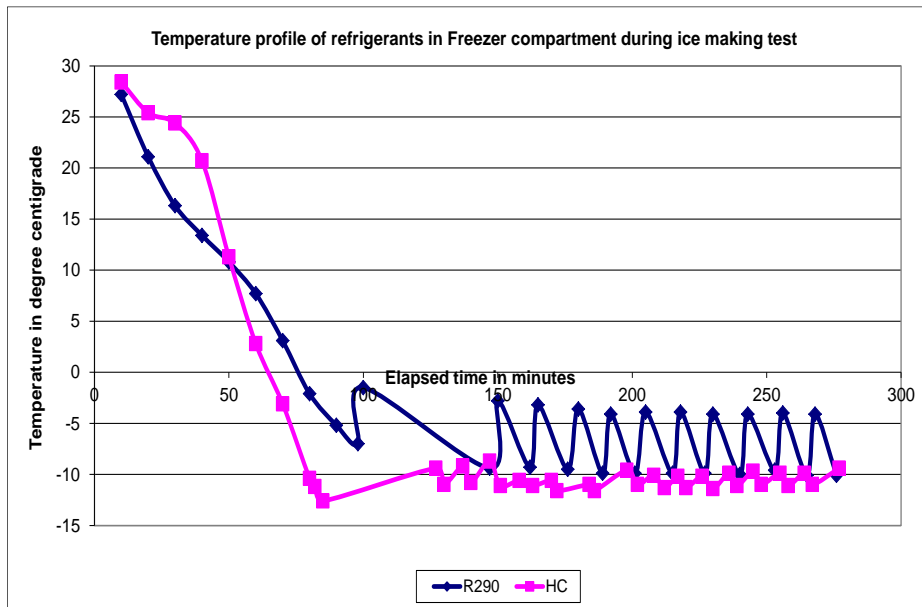


Figure 5: Variation in Temperatures of Freezer Com-partment in Ice making test. Source: Authors, (2024).

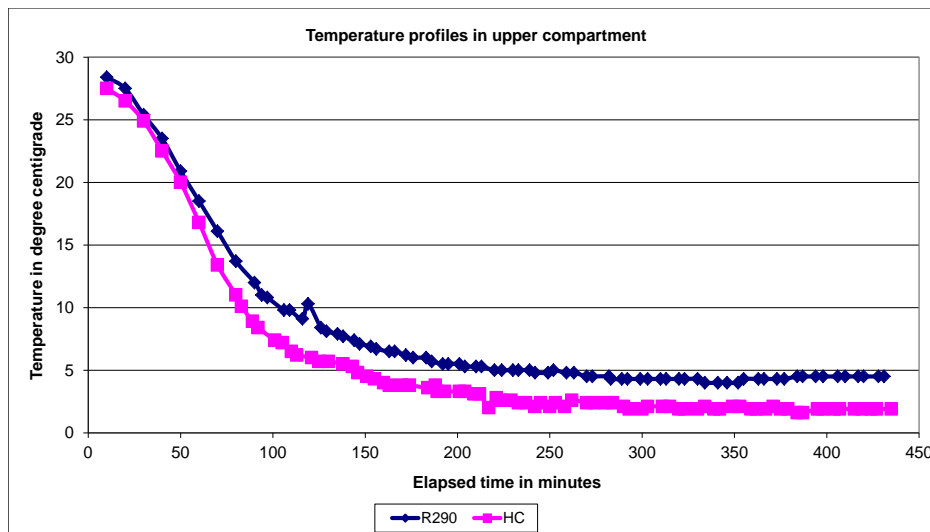


Figure 6: Variation in Temperatures of Upper Compart-ment in Ice making test.



Source: Authors, (2024).

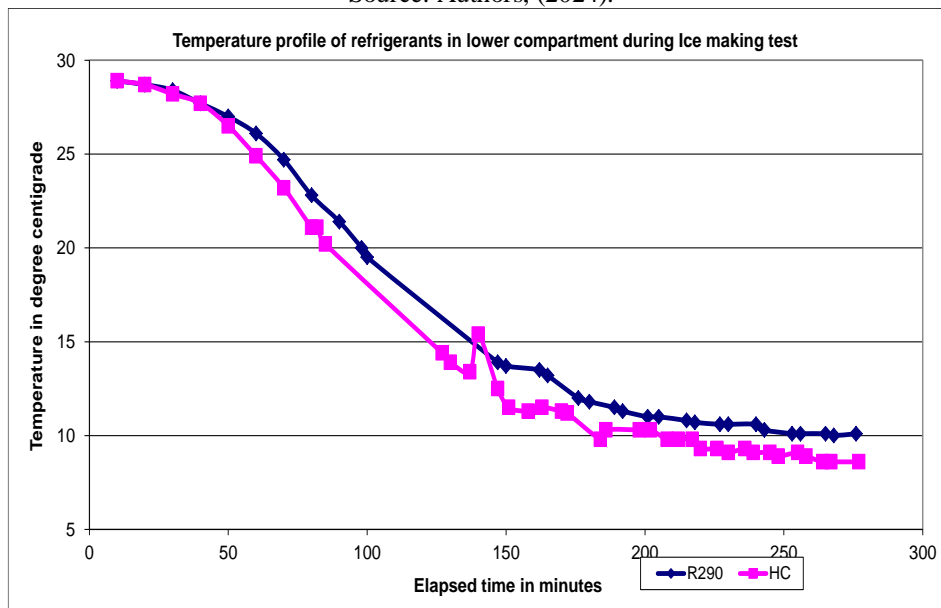


Figure 7: Variation in Temperatures of Lower Com-partment in Ice making test. Source: Authors, (2024).

#### IV. CONCLUSIONS

According to the theoretical research, R290 has a greater COP than R290/R600a. In the case of R290, the heat re-jected in the condenser is slightly lower, but the conden-ser size remains the same. R290 has a lower mass flow rate than R290/R600a, but a higher pressure ratio. As a result, the capillary length must be raised. When com-pared to R290/R600a, propane consumed 10.53 percent less energy. Propane's charge has decreased by 16.38 percent, making it more cost effective to use. The capil-lary length used in this study was 6 meters. Propane has a lower compressor exit temperature than R290/R600a, which is a favorable thing. As a result, the compressor's life may be extended. R290 has equivalent capacities to R290/R600a, according to pull-down and ice-making experiments.

#### V. AUTHOR'S CONTRIBUTION

**Conceptualization:** Parashurama S and Anjappa S B.  
**Methodology:** Parashurama S and Anjappa S B.  
**Investigation:** Parashurama S and Anjappa S B.  
**Discussion of results:** Parashurama S and Anjappa S B.  
**Writing – Original Draft:** Parashurama S and Anjappa S B.  
**Writing – Review and Editing:** Parashurama S and Anjappa S B.  
**Resources:** Parashurama S and Anjappa S B.  
**Supervision:** Parashurama S and Anjappa S B.  
**Approval of the final text:** Parashurama S and Anjappa S B.

#### VI. ACKNOWLEDGMENTS

This work was done by Anjappa S B. etl. We are thank-ful to the authorities of Viswam Engineering College, Madanapalle, Andhra Pradesh 517325, India, for provid-ing all facilities for completing this work.

#### VII. REFERENCES

[1] Mohammad Salman, Rajendran Prabakaran, Poongavanam Ganesh Kumar, Dongchan Lee, Sung Chul Kim, Saturation flow boiling characteristics of R290 (propane) inside a brazed plate heat exchanger with offset strip fins, International Journal of Heat and Mass Transfer, Volume 202,2023,123778,ISSN 0017-9310,https://doi.org/10.1016/j.ijheatmasstransfer.2022.123778.

[2] Mustafa Ozsipahi, Haluk Anil Kose, Husnu Kerpicii, Hasan Gunes, Experimental study of R290/R600a mixtures in vapor compression refrigeration system, International Journal of Refrigeration, Volume 133, 2022, Pages 247-258, ISSN 0140-7007, https://doi.org/10.1016/j.ijrefrig.2021.10.004.

[3] Wongwises, S. and Chimers, N. (2005). Experimental study of hydrocarbon mixtures to replace HFC-134a in a domestic refrigerator. Energy conversion and management.46, 85-100. DOI: 10.1016/j.enconman.2004.02.011

[4] Parashurama, S., Ramesha, D.K. & Govinde gowda, M.S. (2019). Screening of HFCs and Fluroethers as Alternatives to R134a Using SRK EoS. J.Inst.Eng.India, Ser.C. https://doi.org/10.1007/s40032-019-00501-5.

[5] Parashurama, S (2019). Experimental Investigation of the Use of Propane for Domestic Refrigerator with Lower Displacement Compressor, International Journal of Heat and Technology. 37, 985-990. DOI: 10.18280/ijht.370407.

[6] Anjappa S B, D.R.Partha Sarathi, Y.Srinath, N.Venkatramanareddy, "Solar Vaccine Refrigerator by using Phase Change Material", (IJEAT) ISSN: 2249-8958 (Online), Volume-8 Issue-5, June 2019.

[7] Parashurama, S., Ramesha, D.K. & Govinde gowda M.S.(2018). Development of alternative binary mixtures to replace hfc 134a in domestic refrigerator. Chemical Engineering Transactions. 71, 1399-1404. DOI: 10.3303/CET1871234

[8] Data Acquisition Users Guide, ADAM4000 Series User's manual

[9] Rasti, M., Hatamipou, M.S., Aghamiri, S.F., Tavakoli, M. (2012). Enhancement of domestic refrigerator's energy efficiency index using a hydrocarbon mixture refrigerant.Measurement.45, 1807-1813.

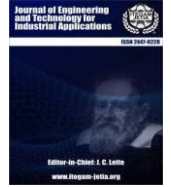
[10] IS: 14761979, Indian Standard Specification for Domestic Refrigerators (Mechanically operated). Bureau of Indian Standards, New Delhi (1986)

[11] S. Parashurama, M. S. Govinde gowda, S.B. Anjappa, S. Ahamed Saleel C. and S. A. Khan, (2020). Design and Performance Analysis of Ecofriendly Vapor Compression Micro-Refrigerator, Indian Journal of Environmental Protection. 40 (3):276 -282.

[12] S. Parashurama, M. S. Govinde gowda, Vaibhav Jain and S. B. Anjappa, (2019). Indian Journal of Environmental Protection. 39 (12): 1119-1124.



ISSN ONLINE: 2447-0228



### RESEARCH ARTICLE

### OPEN ACCESS

## ANDROID APPLICATION FOR ACQUIRING IMAGES OF DIABETIC FOOT ULCERS

\*Yusely Ruiz-Gonzalez<sup>1</sup>, Gustavo Bermúdez Benitez<sup>2</sup> and Juan V. Lorenzo Ginori<sup>3</sup>.

<sup>1,3</sup> Informatics Research Center, Central University "Marta Abreu" of Las Villas, Villa Clara, Cuba.

<sup>2</sup> Culture Municipal Yaguajay, Sancti Spíritus, Cuba,

<sup>1</sup> <http://orcid.org/0000-0002-6011-1947> , <sup>2</sup> <http://orcid.org/0000-0002-1521-1344> , <sup>3</sup> <http://orcid.org/0000-0002-1521-1244> 

Email: <sup>1</sup> [yuselyr@uclv.edu.cu](mailto:yuselyr@uclv.edu.cu)\*, <sup>2</sup> [gustavobermudez788@gmail.com](mailto:gustavobermudez788@gmail.com), <sup>3</sup> [juanl@uclv.edu.cu](mailto:juanl@uclv.edu.cu)

### ARTICLE INFO

#### Article History

Received: July 01th, 2024

Received: July 08th, 2024

Accepted: July 08th, 2024

Published: July 18th, 2024

#### Keywords:

Diabetic foot ulcer,  
apk,  
OS Android.

### ABSTRACT

Diabetic foot ulcers (DFU) are one the most common complications of patients who have diabetes mellitus. DFU study is a worldwide problem and despite the fact that there are computer tools to contribute to its treatment, these are not available in our country or it is necessary to pay for licenses to allow their use. The correct storage of DFU images contributes to the creation of a national database for the subsequent development and fine-tuning of algorithms devoted to segment and analysis these lesions remotely and automatically. So it is important to develop an application for mobile devices that allows standardizing the acquisition of images of DFU and store basic information. Android Studio was used as the programming environment and the minimum functional requirements for the first version were met. Templates were used to take the photos that allow focusing on the specific areas where the lesion is located and to standardize the focal distance. An apk was implemented that allows the acquisition/storage of DFU images/information with a view to the creation of a national database and the development of segmentation algorithms and injury analysis automatically using Digital Image Processing, Computer Vision and Artificial Intelligence techniques



Copyright ©2024 by authors and Galileo Institute of Technology and Education of the Amazon (ITEGAM). This work is licensed under the Creative Commons Attribution International License (CC BY 4.0).

### I. INTRODUCTION

Diabetes mellitus is a major global health emergency in the 21st century, it currently affects more than 425 million people worldwide, and the number of patients could increase considerably in the next years [1],[2]. This disease can lead to the appearance of skin lesions and ulcers in 25% of patients as a result of poor glycemic control, underlying neuropathy, peripheral vascular disease, or poor foot care. These ulcers are usually found in areas of the foot that encounter repetitive trauma and pressure sensations and are commonly produced by repetitive stress over a skin area that is under pression [3].

Diabetic foot ulcer and related infections constitute a large risk factor for emergency department visits and hospital admission. This type of lesion usually require long time treatments and in some cases cause limb amputation, with the corresponding physical, social and psychological damage to the patients [4], [5] or even cause death.

The observation and analysis of lesions (DFU, diabetic foot ulcer) are the bases for defining the treatment and conduct to follow and the results of therapeutic approaches [1], [2]. These processes are often carried out subjectively or manually, which is inaccurate and unhygienic [6].

The lesions measurements are carried out by a specialist who determines approximately the area of the ulcer using the dimensions of the length and width obtained by measuring it manually with a ruler or caliper, without taking into account changes in its shape, generally irregular. Also when carrying out measurements manually, there is a degree of imprecision and variability depending on the person who is carrying out the task. With the technological developments of recent years, attempts have been made to semi-automate or automate these injury measurement processes so that medical personnel can have reliable measurements, increase processing capabilities and ensure better hygienic conditions.

The relatively low cost of digital photography makes it possible to take a digital photograph of the wound and analyze it manually or automatically, thus improving the precision of the measurements and reducing the risk of infection [7-9]. Digital analyze of the images could also be performed automatically by the use of computer vision and artificial intelligence algorithms [10], [11].

**II. THEORETICAL REFERENCE**

Internationally, competitions have been developed for the detection and classification of this type of injury [12], [15]. Progress has been made in the creation of software and mobile applications for evolutionary studies, wound remote monitoring and measuring the effectiveness of the different treatments applied [15], [22]. Enabling more efficient therapeutic options for wound care to be proposed in order to improve healing rates.

Some initial studies have also been carried out in our country but, to date and to our knowledge, no application has been registered [8],[23]. Also, with the development and introduction of Heberprot-P, a novel medication prescribed for the therapy of DFU, clinical trials were developed that used manual measurements or proprietary software, which required investments of resources and capital [6].

This research describes an application for Android OS (apk) intended for taking photographs of diabetic food ulcer lesions and creating a file associated with each image. The file will contain the most relevant information regarding its treatment, patient information and evolution.

The programming was carried out in Android Studio [24] and will contribute to the creation of national databases for the subsequent development and fine-tuning of segmentation and analysis algorithms for DFU studies of lesion automatically or semi automatically. Also, could contribute to the telemedicine developments by remote studies of DFU lesions. Likewise, will contribute to the implementation of segmentation and analysis algorithms which use digital image processing techniques, computer vision and artificial intelligence and need large image database for training and test. The acquisition of proprietary data base will a very important point to start the research.

**III. MATERIALS AND METHODS**

Android Studio is an integrated development environment (IDE), based on IntelliJ IDEA from the company JetBrains, which provides several improvements over the ADT (Android Developer Tools) plugin for Eclipse. Android Studio uses an Apache 2.0 free software license, is programmed in Java and is cross-platform. It was presented by Google on May 16, 2013 at the Google I/O developer conference, with the aim of creating an environment dedicated exclusively to programming applications for Android devices, providing Google with greater control over the production process. Since December 2014, when the stable version of Android Studio 1.0 was released, Google started to recommend it as the IDE to develop applications for its operating system.

The minimum functional requirements of the application (for now on “apk” Camera\_DFU V1.1) like access to the camera, to take photo, and to save the picture, among other are shown in Table 1. Version 1.0 of the apk meets all of them. In the future, higher versions may include camera management requirements such as zoom, flash, resolution changes, etc. Interaction with medical personnel, after the application use, could generate new requirements as well.

Table 1: Functional requirements of V1.0 of the apk.

Functional Requirements	What the application does
FR1 Allow the application to access the camera.	The apk must access the device's camera to be able to take the necessary photos (this operation is only carried out after it is installed)
FR2 Select the appropriate template for the photo.	The apk brings a series of templates defined for taking photos which are selected by the user.
RF3 Take the photo.	The apk should take the photo and save it for later analysis
FR4 Decide whether or not to save the taken photo.	The apk allows to save the photo or not according to the user wishes.
RF5 Save the taken photo.	The apk saves the photo taken by the user.
FR6 Save information related to the patient and their injury.	The apk saves the patient data entered manually by the user, the information is stored in a file that can be read as .txt.
FR7 Show previously taken photos.	The apk should be able to display photos taken by the user or display a message in case there are no photos.
FR8 Delete a specific photo after it has been saved.	The apk should be able to delete photos when the user decides.
FR9 Export the information to a specific address in the internal storage.	The apk must allow saving the collected information.

Source: Authors, (2024).

The health personnel who interact directly in taking photos of the diabetic foot ulcer and acquiring the data required for monitoring this pathology are identified as system actors.

The application is installed by double clicking on the installation file. It is necessary to enable access permissions to the camera, microphone and writing in the mobile device. Depending on the phone's operating system, they can be assigned during the apk installation process itself or enabled manually after installation. Manually enabling permissions is done through the configuration/settings menu, applications, \_DFU Camera, permissions, on the mobile device.

The Camera\_DFU V1.1 software was developed for the Android OS, it runs from Android version 4.0 to higher OS versions. The memory requirements are basically to store the photos and associated files. The files generated for each photo are saved in txt format and are in the order of 500 b. The photos will have the maximum resolution allowed by the mobile device camera

The main screen of the apk has a drop-down menu to access the gallery of photos taken with the apk. If it is the first use of the application, the gallery appears empty, if some photos have been taken, they accumulate until the user decides to export them to a folder for later studies. Also there is some possibility to delete gallery photos.

As a prior step to taking a photo, the user must select a template where the injury will be fixated. Using the template will facilitate further image processing and standardizes the distance at which the photo is taken. There are four options for

the templates to select, as shown in Figure 1; named: left leg, right leg, injury and sole of the foot. Each template is associated with an specify position and extent of the injury to be studied. These templates are important since they allow the user to focus on the specific areas where the injury is located and contribute to standardize the distance to take the photo.

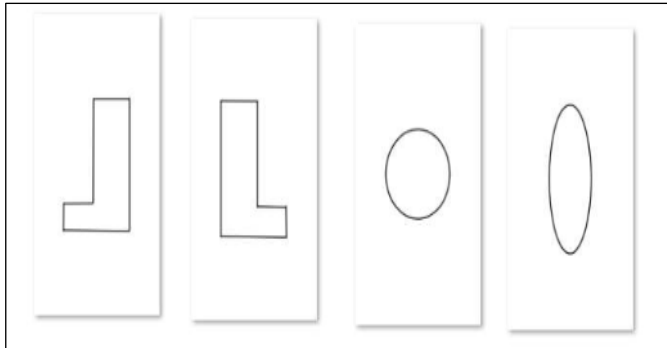


Figure 1: Template options to select before take the photo.  
Source: Authors, (2024).

It should be noted that to take the photographs, the device's camera flash was set to activated mode always, in order to achieve uniform lighting of the taken photos, preventing darker or lighter photos from being taken depending on the room/ natural lighting. of the environment. In addition, the maximum resolution allowed by the camera was established, in this way the highest possible image quality will be obtained.

#### IV. RESULTS AND DISCUSSIONS

Figure 2 represents the apk icon which is show in the mobile device after the installation. When the application it is opened, shows the main screen as it appears in Figure 3.

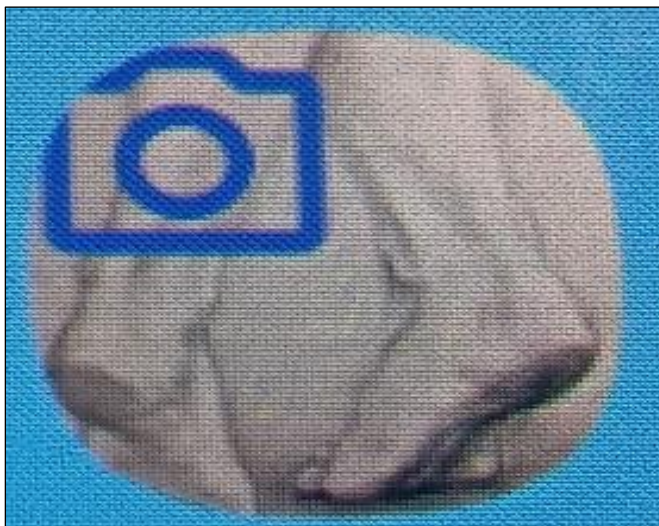


Figure 2: Apk icon.  
Source: Authors, (2024).

The main screen has a drop-down menu to access the gallery of photos taken with the apk (Figure 4). If it is the first use of the application, the gallery appears empty (Figure 4a), if photos have been taken, they accumulate until the user decides to export them to a folder for further study (Figure 4b).

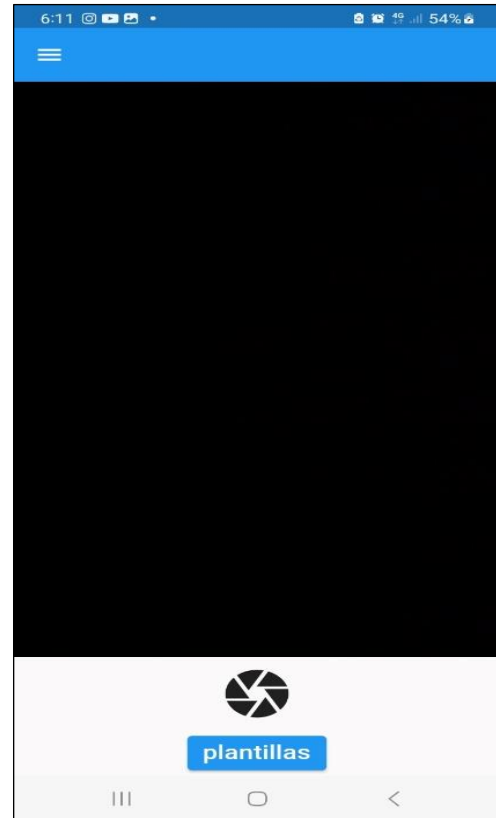


Figure 3: Application main screen.  
Source: Authors, (2024).

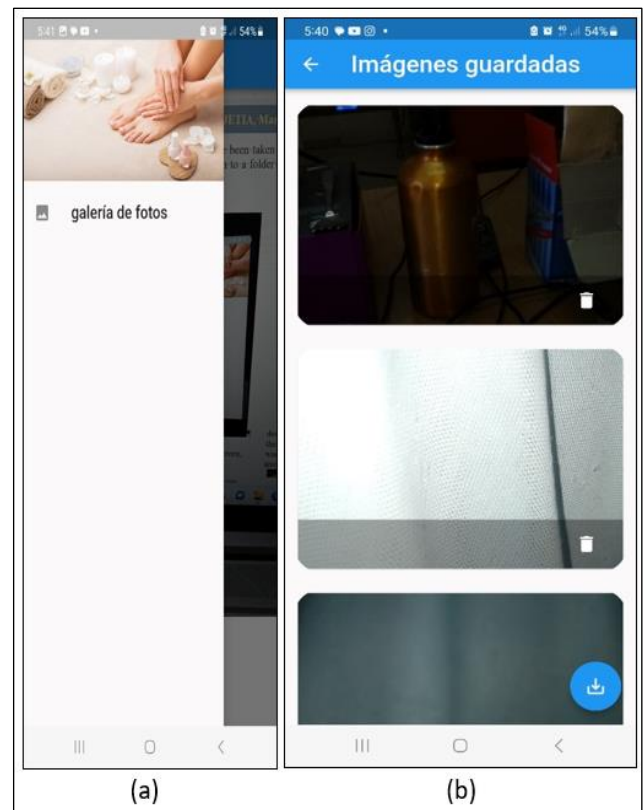
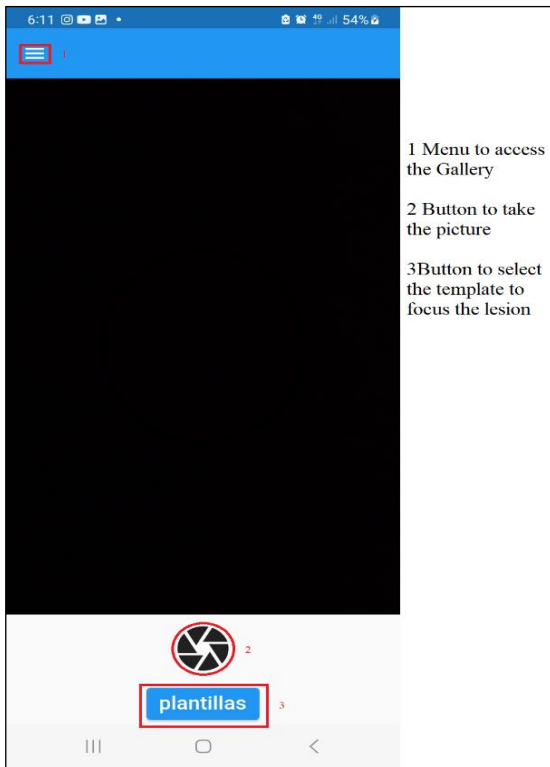


Figure 4: Access to the photo gallery a) gallery menu b) pictures already taken.  
Source: Authors, (2024).

Figure 5 details the different options provided by the apk: access to the gallery and taking photos (Figure 5a).



(a)

- 1 Menu to access the Gallery
- 2 Button to take the picture
- 3 Button to select the template to focus the lesion

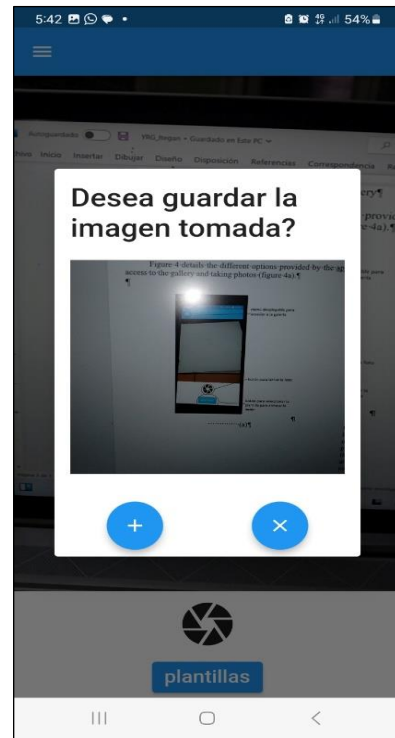
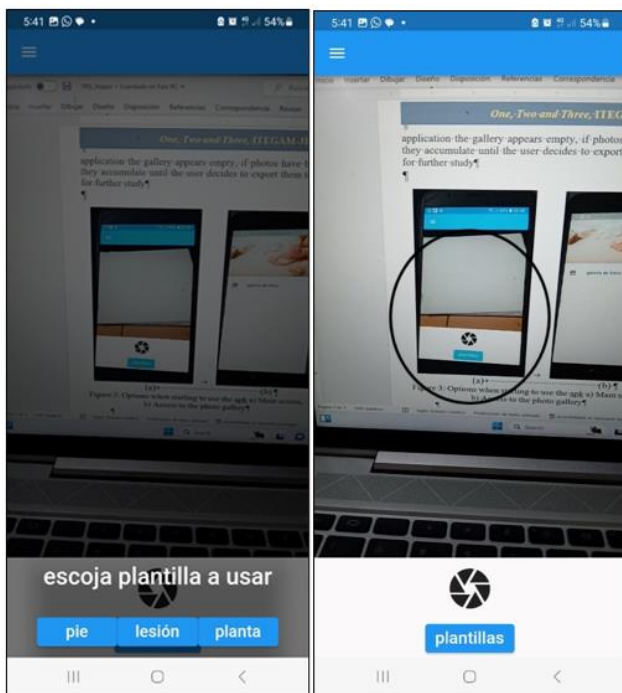


Figure 6: Sub-screen to save or not save the photo.  
Source: Authors, (2024).

When accepting the photo taken previously, it is necessary to enter the data for the text file that will be associated with it. Figure 7 show the different fields to enter, some optional and others mandatory. The date and time were also associated and saved in the txt file for each photo, but they are automatically included in, when the photo saved because they are reserved from the phone.



(b)

(c)

Figure 5: (Photo acquisition process a) (buttons on the main screen b) (template menu, c) example of selected template.  
Source: Authors, (2024).

After the photo is taken, it is displayed on a subscreen to decide if the user want to save the photo or not (Figure 6). If the user wants to save the photo the left button should be push, so the information associated to photo will be showed (see Figure 7) in order to filled it and further save it in the associated txt file. If the user does not want to save the photo, it is discarded by pressing the right button and the process could be repeated to take another photo.

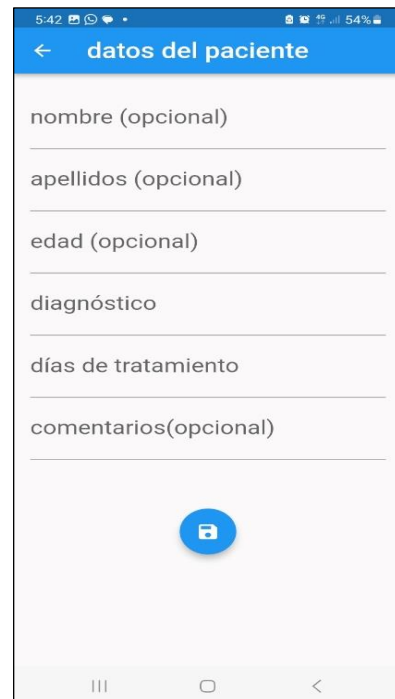


Figure 7: Information to record.  
Source: Authors, (2024).

The photo and the .txt file are saved by pressing the button at the bottom of the screen. If the user try to save the file

without completing the required fields, an error message is generated (see Figure 8).

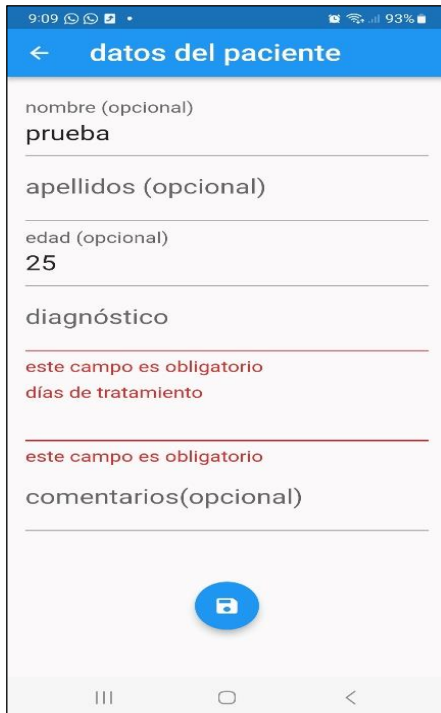


Figure 8: Error message for the mandatory fields.  
Source: Authors, (2024).

When managing the gallery, the user can delete photos one by one using the trash button associated with each photo. Also the user can export the photos and associated .txt information files to a specific folder for further study (see Figure 9).

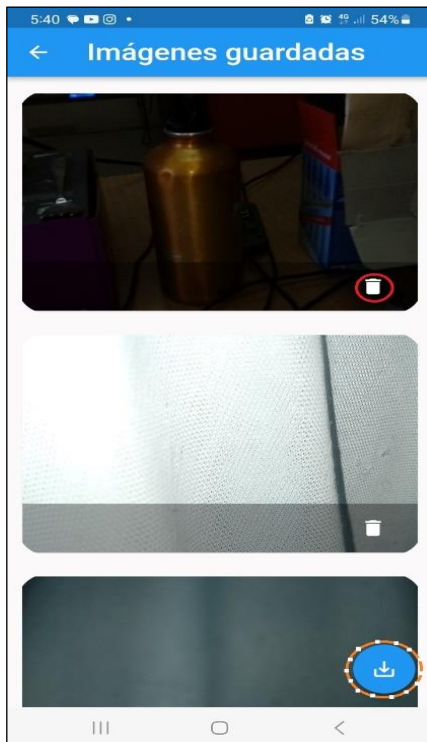


Figure 9: Buttons for managing the gallery, red circle highlights the trash button, orange -- highlight the export button.  
Source: Authors, (2024).

The photos are exported to the folder: "My files/download/DFU\_camera.apk" (see Figure 9). In this folder there is two other folder, the first one named "photos" for the taken pictures and the second one named "Jsons" for the .txt files. The name of the photo and its associated file matches and are automatically generated by the application.

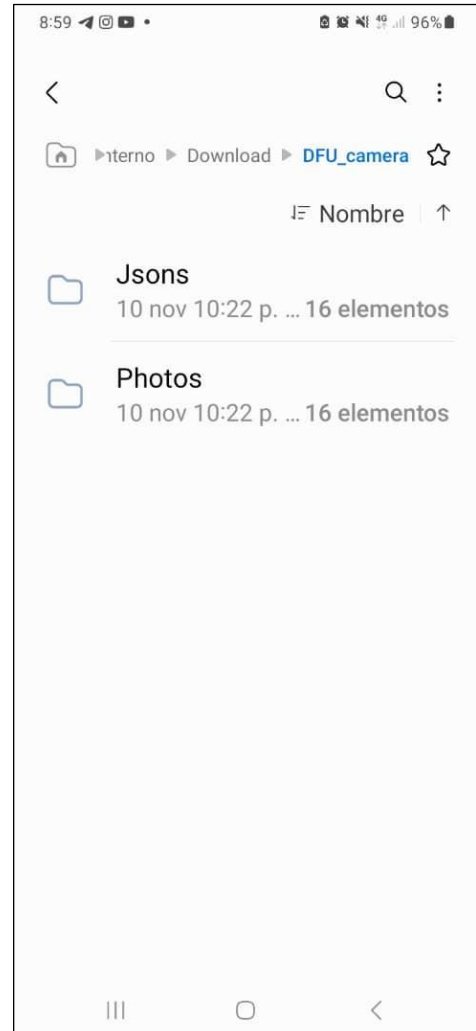


Figure 9: Created folder to save the photos and .txt files.  
Source: Authors, (2024).

## V. CONCLUSIONS

The diabetic foot ulcer is a condition that attracts the attention of worldwide doctor, health caretaker and researches. Several computer tools have been developed to contribute to its diagnose, treatments following and analysis. Unfortunately, many of the computer tools developed are not available in our country. A mobile device application was designed and implemented that allows acquiring/storing the diabetic food ulcer image (or any other type of lesion) together with some information requested by the user. In addition, with the use of the developed applications allow a certain degree of standardization in the acquisition of the images. The acquired images would be the starting point for the creation of a national database to future works in order to develop algorithms for segmentation and analysis of lesions automatically and remotely, using digital image processing techniques, computer vision and artificial intelligence.

## VI. AUTHOR'S CONTRIBUTION

**Conceptualization:** Yusely Ruiz-Gonzalez, Gustavo Bermúdez Benitez, y Juan V. Lorenzo Ginori.

**Methodology:** Yusely Ruiz-Gonzalez, Gustavo Bermúdez Benitez.

**Investigation:** Yusely Ruiz-Gonzalez, Gustavo Bermúdez Benitez.

**Discussion of results:** Yusely Ruiz-Gonzalez, Gustavo Bermúdez Benitez, y Juan V. Lorenzo Ginori.

**Writing – Original Draft:** Yusely Ruiz-Gonzalez.

**Writing – Review and Editing:** y Juan V. Lorenzo Ginori.

**Resources:** Gustavo Bermúdez Benitez.

**Supervision:** Yusely Ruiz-Gonzalez, y Juan V. Lorenzo Ginori.

**Approval of the final text:** Yusely Ruiz-Gonzalez, Gustavo Bermúdez Benitez, y Juan V. Lorenzo Ginori.

## VII. ACKNOWLEDGMENTS

This research is supported by the Sectorial Research Program “Cuban software industry and computerization of society, (PS 161LH001-03) and Central University “Marta Abreu” of Las Villas Basic Research Program (PI 9700).

## VIII. REFERENCES

- [1] P. Zhang, J. Lu, Y. Jing, S. Tang, D. Zhu, and Y. Bi, “Global epidemiology of diabetic foot ulceration: a systematic review and meta-analysis †,” *Ann Med*, vol. 49, no. 2, pp. 106–116, Mar. 2017, doi: 10.1080/07853890.2016.1231932.
- [2] R. Sorber and C. J. Abullarrage, “Diabetic foot ulcers: Epidemiology and the role of multidisciplinary care teams,” *Seminars in Vascular Surgery*, vol. 34, no. 1, pp. 47–53, Mar. 2021, doi: 10.1053/j.semvascsurg.2021.02.006.
- [3] S. A. Bus, “The Role of Pressure Offloading on Diabetic Foot Ulcer Healing and Prevention of Recurrence,” *Plastic and Reconstructive Surgery*, vol. 138, no. 3S, p. 179S, Sep. 2016, doi: 10.1097/PRS.0000000000002686.
- [4] D. G. Armstrong, A. J. M. Boulton, and S. A. Bus, “Diabetic Foot Ulcers and Their Recurrence,” *N Engl J Med*, vol. 376, no. 24, pp. 2367–2375, Jun. 2017, doi: 10.1056/NEJMr1615439.
- [5] B. A. Lipsky *et al.*, “2012 Infectious Diseases Society of America Clinical Practice Guideline for the Diagnosis and Treatment of Diabetic Foot Infections,” *Clinical Infectious Diseases*, vol. 54, no. 12, pp. e132–e173, Jun. 2012, doi: 10.1093/cid/cis346.
- [6] J. I. Fernández-Montequín *et al.*, “Intralesional administration of epidermal growth factor-based formulation (Heberprot-P) in chronic diabetic foot ulcer: treatment up to complete wound closure,” *International Wound Journal*, vol. 6, no. 1, pp. 67–72, 2009, doi: <https://doi.org/10.1111/j.1742-481X.2008.00561.x>.
- [7] H. Carrión, M. Jafari, M. D. Bagoood, H. Yang, R. R. Isseroff, and M. Gomez, “Automatic wound detection and size estimation using deep learning algorithms,” *bioRxiv*, p. 2020.11.13.275917, Nov. 2020, doi: 10.1101/2020.11.13.275917.
- [8] P. L. Muñoz, R. Rodríguez, and N. Montalvo, “Automatic Segmentation of Diabetic foot ulcer from Mask Region-Based Convolutional Neural Networks,” *Journal of Biomedical Research and Clinical Investigation*, vol. 1, no. 1.1006, 2020.
- [9] J. D. López-Cabrera, Y. Ruiz-Gonzalez, R. Díaz-Amador, and A. Taboada-Crispi, “Estrategias de fusión para la clasificación automática de imágenes de úlceras de pie diabético usando técnicas de visión por computadora,” *Revista Cubana de Ciencias Informáticas*, vol. 16, no. 1, pp. 163–179, 2022.
- [10] R. Niri *et al.*, “Multi-view data augmentation to improve wound segmentation on 3D surface model by deep learning,” *IEEE Access*, vol. 9, pp. 157628–157638, 2021.
- [11] P. Wang, E. Fan, and P. Wang, “Comparative analysis of image classification algorithms based on traditional machine learning and deep learning,” *Pattern Recognition Letters*, vol. 141, pp. 61–67, Jan. 2021, doi: 10.1016/j.patrec.2020.07.042.
- [12] Moi Hoon Yap *et al.*, “Diabetic Foot Ulcers Grand Challenge 2020,” Mar. 2020, doi: 10.5281/ZENODO.3715015.
- [13] Moi Hoon Yap *et al.*, “Diabetic Foot Ulcers Grand Challenge 2021,” Mar. 2020, doi: 10.5281/ZENODO.3715019.
- [14] Moi Hoon Yap *et al.*, “Diabetic Foot Ulcers Grand Challenge 2022,” Mar. 2021, doi: 10.5281/ZENODO.4575227.
- [15] M. H. Yap *et al.*, “A New Mobile Application for Standardizing Diabetic Foot Images,” *Journal of Diabetes Science and Technology*, vol. 12, no. 1, p. 169, Jan. 2018, doi: 10.1177/1932296817713761.
- [16] L. Fraiwan, M. AlKhodari, J. Ninan, B. Mustafa, A. Saleh, and M. Ghazal, “Diabetic foot ulcer mobile detection system using smart phone thermal camera: a feasibility study,” *BioMedical Engineering OnLine*, vol. 16, no. 1, p. 117, Oct. 2017, doi: 10.1186/s12938-017-0408-x.
- [17] M. Goyal, N. D. Reeves, S. Rajbhandari, N. Ahmad, C. Wang, and M. H. Yap, “Recognition of ischaemia and infection in diabetic foot ulcers: Dataset and techniques,” *Computers in Biology and Medicine*, vol. 117, p. 103616, Feb. 2020, doi: 10.1016/j.compbiomed.2020.103616.
- [18] “Healogics Photo+ | Wound Measurement App,” Healogics. Accessed: Apr. 13, 2021. [Online]. Available: <https://www.healogics.com/woundsuite-wound-care-software/wound-measurement-app/>
- [19] L. Fraiwan, J. Ninan, and M. Al-Khodari, “Mobile Application for Ulcer Detection,” *Open Biomed Eng J*, vol. 12, pp. 16–26, 2018, doi: 10.2174/1874120701812010016.
- [20] “Digital Planimetry and Measurements on Digital Images Using PictZar Wound and other Measurements Software.” Accessed: Dec. 18, 2023. [Online]. Available: <http://www.pictzar.com/>
- [21] WoundDesk, “+WoundDesk - Mobile enhanced Wound Management for Chronic Wounds,” +WoundDesk. Accessed: Dec. 18, 2023. [Online]. Available: <https://wounddesk.com>
- [22] “Wound Zoom’s Wound Management System.” Accessed: Dec. 18, 2023. [Online]. Available: <https://woundreference.com/app/topic?id=wound-zooms-wound-management-system>
- [23] G. García Gómez *et al.*, “Mejoramiento de contraste y segmentación en imágenes de úlceras del pie diabético,” *Revista Cubana de Angiología y Cirugía Vascular*, vol. 20, no. 3, Dec. 2019, Accessed: Apr. 13, 2021. [Online]. Available: [http://scielo.sld.cu/scielo.php?script=sci\\_abstract&pid=S1682-00372019000300003&lng=es&nrm=iso&tlng=es](http://scielo.sld.cu/scielo.php?script=sci_abstract&pid=S1682-00372019000300003&lng=es&nrm=iso&tlng=es)
- [24] “Guía para desarrolladores.” [Online]. Available: <https://developer.android.com/guide>



## EFFECT OF NORMATIVE COMMITMENT ON ORGANIZATION PERFORMANCE AT SBC TANZANIA LIMITED (PEPSI) DAR ES SALAAM

Chacha Alfred Matoka

Senior Lecturer Open University of Tanzania.

<http://orcid.org/0000-0003-0498-3465>

Email: [\\*matokaca@gmail.com](mailto:*matokaca@gmail.com)

### ARTICLE INFO

#### Article History

Received: July 13<sup>th</sup>, 2023

Revised: July 12<sup>th</sup>, 2024

Accepted: July 15<sup>th</sup>, 2024

Published: August 30<sup>th</sup>, 2024

#### Keywords:

Key Words: Normative commitment, SBC Tanzania Limited, Organizational Performance

### ABSTRACT

The study's objective was to determine the impact of normative commitment on the performance of organization at SBC Tanzania Limited (PEPSI) Dar es Salaam. a well-known beverage business in Dar es Salaam that uses the Pepsi name. A staff member's feeling of commitment and identification with a company's goals and ideals, which determines their propensity to put up extra effort and stay committed to the organization, is referred to as normative commitment. The study employed a quantitative research methodology, with the primary data collection technique being a survey questionnaire. Using stratified random sampling, 95 people from different departments and organizational levels within SBC Tanzania Limited were chosen from 200 populations. It was found that the SBC organization's performance and normative commitment were positively, statistically, and significantly associated. The report gives advice to companies like SBC Tanzania Limited to continually innovate and improve their interactions with their workforce in order to reduce the level of normative commitment.



Copyright ©2024 by authors and Galileo Institute of Technology and Education of the Amazon (ITEGAM). This work is licensed under the Creative Commons Attribution International License (CC BY 4.0).

### I. INTRODUCTION

Organizations struggle to reach and sustain high levels of performance in today's cutthroat business environment in order to ensure their success and growth [1]. One crucial aspect that influences organizational performance is the commitment of employees towards their organization. Among the different forms of commitment, normative commitment plays a significant role in shaping employees' dedication and loyalty towards the organization [2],[3]. In this study, SBC Tanzania Limited, a well-known beverage firm operating under the Pepsi name in Dar es Salaam, will be examined to determine the impact of normative commitment on organizational performance.

Normative commitment, as defined by [4], is a staff members psychological connection to the company that is motivated by a sense of duty and affiliation with the company's ideals. It goes beyond simply meeting the job's demands and is defined by a willingness to put forth extra effort and stick with the organization through difficult circumstances. Improved inspiration, satisfaction with work, and behaviors related to organizational citizenship are frequently the results of employees who have high normative commitment because they sense an

overwhelming moral and ethical need to assist the organization's success [5].

There has been extensive discussion in the literature about how normative commitment affects organizational effectiveness. According to studies [6-8], employees who are normatively committed are more likely to display favorable work attitudes, including job involvement and dedication to the organization, and engage in behaviors that improve organizational performance. These behaviors may include going beyond their prescribed roles to assist colleagues, suggesting process improvements, and promoting the organization's reputation through positive word-of-mouth.

SBC Tanzania Limited, operating under the Pepsi brand, faces various challenges in the highly competitive beverage industry. In this context, understanding the role of normative commitment in driving organizational performance becomes crucial. SBC Tanzania Limited can learn how to use employee commitment to increase productivity, profitability, customer happiness, and employee engagement by examining the relationship between norm commitment and performance outcomes.



In particular, normative commitment has come to be recognized as an important component of commitment that can have a significant influence on employee conduct and results [9],[10]. Employee commitment has been determined to be a critical factor affecting organizational performance. However, nothing is known about the precise connection between normative commitment and organizational success at SBC Tanzania Limited.

Acknowledge and understanding gap exists because there is a dearth of research examining the impact of the normative commitment on the performance of organizations, especially in the context of SBC Tanzania Limited. While normative commitment has been extensively examined in various organizational settings, there is a need to investigate its influence within the unique context of SBC Tanzania Limited and its impact on key performance indicators such as productivity, profitability, customer satisfaction, and employee engagement.

The problem that this study aims to address is the dearth of empirical information and understanding regarding the effect of normative commitment on business success at SBC Tanzania Limited. By addressing this gap, the study will add to the body of knowledge on organizational behavior and offer insightful information that will help the management of SBC Tanzania Limited create practical plans for boosting employee engagement and strengthening overall organizational performance.

This research will add to the body of existing information on organizational conduct and offer useful advice to SBC Tanzania Limited and other businesses that operate in comparable environments. The findings will assist in formulating strategies to enhance normative commitment among employees and ultimately improve organizational performance. By appreciating the value of normative commitment, businesses may establish an environment that encourages worker fidelity, commitment, and success in general.

## **II. LITERATURE REVIEW**

### **II.1 NORMATIVE COMMITMENT**

Normative commitment is described by Matoka (2020) as an employee's emotional commitment to and identification with an organization's aims, values, and ethical standards. Beyond meeting contractual responsibilities, it represents a sense of responsibility and a moral duty to contribute to the organization's success and keep membership within the organization. Employees that are normatively committed are motivated by a deep commitment to the organization's objective and a desire to improve it [11].

The belief that one has a responsibility to support an organization during both good and bad situations is known as normative loyalty. For [12] claims that normative loyalty shows a sense of obligation to keep a job. People with high normative loyalty stick with a company because they feel it is "morally right" to do so. A person is said to be committed to an organization and willing to keep his association with it if they work there for a significant amount of time and the organization offers the training they seek. The importance of normative loyalty, according to [12] is its link to the desire to leave the organization. It is uncommon for an employee to think of leaving the company when they have a strong sense of commitment. Employee loyalty to the organization will generally lessen the risk that they will leave. Defined normative commitment as loyalty based on standards of mutual obligation between workers and their organizations.

### **II.1 SBC TANZANIA LIMITED (PEPSI)**

According to [13] provides that SBC Tanzania Limited is a prominent beverage company operating in Tanzania under the Pepsi brand. It was established as a subsidiary of PepsiCo, SBC Tanzania Limited is responsible for the production, distribution, and marketing of a wide range of PepsiCo beverage products in the Tanzanian market.

SBC Tanzania Limited, a crucial member of the PepsiCo family, strives to satisfy the various beverage requirements of Tanzanian consumers. To accommodate various tastes and preferences, the company offers a variety of soft drinks with carbonation, non-carbonated beverages, and water-based bottled products. SBC Tanzania Limited seeks to minimize its environmental impact while advancing Tanzania's social and economic development through a commitment to sustainability and ethical business practices [14]. To ensure moral and sustainable business practices, the corporation complies with industry norms, regional laws, and CSR activities [15].

### **II.2 ORGANIZATIONAL PERFORMANCE**

According to [16],[17], organizational performance in the context of SBC Tanzania Limited, which operates under the Pepsi brand, refers to the company's achievement of targeted results and objectives in a variety of areas related to its operations. It includes the organization's effectiveness and efficiency in producing high-quality goods, making money, upholding customer satisfaction, ensuring staff involvement, and attaining sustainable growth within Tanzania's cutthroat beverage market.

Numerous research, like those by [18], have demonstrated a favorable correlation between normative commitment and levels of productivity. Employees that feel strongly about normative commitment put forth more effort, are more motivated, and are more dedicated, which leads to better performance.

According to [19] model on the impact of affective, normative, and continuity commitment on organizational success, an increase in any one of the three commitments will boost organizational effectiveness.

When examining the effects of people management on enhancing organizational performance [20], discovered that normative commitment has an effect on financial performance metrics like profitability. Employees are more inclined to support initiatives to cut costs, generate revenue, and achieve overall financial success if they sense a strong moral commitment to do so.

Organizational commitment was utilized as a moderator in a study by [21] on the effect of worker engagement on organizational performance. The study's findings indicated that employee involvement had a substantial impact on organizational effectiveness. The study demonstrated that affective commitment, continuance commitment, and normative commitment had a beneficial impact on the relationship between staff engagement and organizational success.

### **II.3 THEORETICAL REVIEW**

Businesses looking to accomplish their goals and acquire a competitive edge in the marketplace should pay close attention to organizational performance. Long acknowledged as a key element affecting organizational effectiveness, employee commitment. An examination of the theoretical underpinnings

and frameworks that explain how commitment affects organizational performance is the goal of this theoretical review.

### II.4 SOCIAL EXCHANGE THEORY

According to [22], people enter into partnerships, such as the one between an employer and employee, based on a reciprocal exchange of resources and benefits. When employees believe that an organization offers valuable resources, such as fair salary, career growth opportunities, and supportive work environments, they feel a feeling of obligation and loyalty to the firm. The increased effort, loyalty, and independent conduct that follow from this commitment improve organizational success. The value of a relationship is essentially determined by subtracting its costs from its benefits, in accordance with social exchange theory [23]. Costs include things that you consider drawbacks, such as devoting time, energy, and money to a relationship. It can be difficult to define some of the Social Exchange Theory's fundamental concepts. The idea of benefits and costs is quite individualized. For instance, excessive compliments from a partner may be gratifying to one person but irritating to another, making it challenging to quantify [24].

### II.5 PSYCHOLOGICAL CONTRACT THEORY

The psychological contract theory places a strong emphasis on the obligations and expectations that both employees and the organization share. Employees are more likely to feel a sense of commitment when the company upholds its commitments, such as offering fair treatment, job stability, and development chances. This dedication consequently affects their attitudes, deeds, and performance, improving organizational performance. The psychological contract is the height of agility. The psychological contract between the employee and his or her employer varies along with the worker. The interaction between the two entities is also shown in real-time [25]. The psychological contract's fundamental weakness is that it is based on unspoken beliefs and expectations that shape how things are perceived, making it potentially unstable at all times. There is no formal agreement, such as an enforceable employment contract, hence it is unwritten.

Hence the guiding hypothesis for this study is:

*Normative commitment has a significant positive effect relationship with Organizational performance at SBC Tanzania limited (Pepsi) Dar es Salaam*

### III METHODOLOGY

The study used a quantitative methodology. An objective examination of the link between variables is achieved by the collection and analysis of numerical data using a quantitative approach to research. A quantitative method enables the systematic measurement and statistical evaluation of data to produce strong and transferable insights when examining the impact of commitment on organizational performance [26] In this study, an explanatory design was employed. According to [27], an explanatory research design is a sort of research design that tries to investigate and explain the link of causality between variables.

In this instance, the relationship between normative commitment and organizational performance was investigated.

### III.1 POPULATION

For 2000 employees at SBC Tanzania Limited in Dar es Salaam served as the study's target population. This company had five departments: production (300), marketing (455), sales and distribution (620), customer service (415), and branding and packaging (415). The study also focused on SBC Tanzania Limited (Pepsi), which developed goods and services that satisfied customers following early decisions to enhance the model of promotion for their products.

Table 1: Population of the Study.

UDSM-DEPT	POPULATION
Production department	300
Marketing department	455
Sales and distribution department	620
Customer services department	415
Packaging and branding department	210
Total	2000

Source: Authors, (2024).

### III.2 SAMPLE AND SAMPLING STRATEGY

The sample is a group of people chosen at random from a population in order to evaluate the characteristics of the population. Whether it is a whole group or a subgroup, it is a percentage that was specifically picked to fairly represent the total population. A sample size of 10–30% of the population, according to [28], is enough since it enables the researcher to acquire crucial knowledge and strengthens the dependability of the study. 25 percent of the 2000 participants, or 95 respondents, took part in the questionnaire (SBC Tanzania Limited in Dar es Salaam). The technique of selecting participants is known as the sampling methodology, according to [29]. From among all of the participants, respondents are picked to offer details to the study. In this study, the probability technique for sampling was used because the researchers identified people online who could provide them access to their accounts. The appropriate sample size for the SBC Tanzania Ltd. (Pepsi) study was determined using a method created [30]. The working sample was derived using Yamane's formula  $n = \frac{N}{1 + (e)^2}$ . Where-

$n$  = is the sample size

$N$  = is the population

$e$  = is

$1$  = is a constant

$2$  = is the estimated standard error which is 5% for 90% confidence level

$= \frac{2000}{1 + 2000(0.1)^2}$

$= \frac{2000}{1 + 20}$

$= \frac{2000}{21}$

$= 95.238$  were collected from participants at SBC-Company limited Pepsi in Tanzania as a sample size. 95 people made up the minimal adjusted sample size. This represents the complete sample that was used to gather the data. thus,  $n=95$  for the sample size in Table 2.

Table 2: UDSM-DEPT, POPULATION, % AND SAMPLE SIZE.

UDSM-DEPT	POPULATION	%	SAMPLE SIZE
Production department	300	15%	3
Marketing department	455	22.75%	24
Sales and distribution department	620	31%	33
Customer services department	415	20.75%	22
Packaging and branding department	210	10.5%	13
Total	2000	100%	95

Source: Authors, (2024).

### III.3 VARIABLES AND MEASUREMENT PROCEDURES

Organizational performance was assessed using [31] global scale of measurement. On a scale from 1 (strongly agree) to 5 (strongly disagree), respondents were asked to rate how much they agreed or disagreed with the statement.

Because it does not address a particular context that is perceived as a violation, such as salaries or working conditions, the overall scale has an advantage over a content-specific scale. For [32] assert that the full psychological contract breach is included in the global scale.

Additionally, according to [33], the global scale is the greatest tool for evaluating or predicting workplace outcomes, such as organizational commitment. Because the specific content scale usually disregards unfulfilled organizational and personnel commitments, such as the fact that not all obligations can be measured [34], the scale is not employed. These reasons are what motivated the study's decision to evaluate perceived psychological contract breaches using the global scale.

The [11] measure, which has 24 items, was used to assess organizational commitment. These are broken down into three categories, each with eight items: emotional commitment, continuous commitment, and normative commitment. On a scale of 1 to 7, where 1 represents a strong disagreement and 7 represents a strong agreement, respondents were asked to rate their level of agreement with each statement. Age, gender, educational attainment, marital status, academic achievement, and administration position are some examples of individual demographic characteristics that were measured quantitatively. This was continuously measured, with the exception of tenure.

### III.4 DATA ANALYSIS

This study employed statistical techniques, including distributions of frequency, percentages, and charts. SPSS Software Version 25 was also used for analysis. Descriptive statistics and multiple regression analysis are employed. To emphasize the data analysis and display for quantitative data, frequency tables were used.

Implicit or explicit models are those that connect the latent variable's values to its indications. Regression analysis of a normative variable on the performance of organizations is shown.

$$Y_1 = \beta_0 + \beta_2 NC + \epsilon \tag{1}$$

Where:  $Y_1$  = Dependent - Organizational Performance  
 $\beta_0$  = Y - Intercept

$\beta_1$  = Slope of the Line defined as ratio rise or change in X

NC = Normative Commitment - independent variable

$\epsilon$  = Error term.

## IV RESULTS

### IV.1 DESCRIPTIVE STATISTICS FOR THE PARTICIPANTS

The age distribution Table 3 reveals that the majority of respondents, or about 35% of all respondents, were middle-aged workers between the ages of 41 and 50. They are followed by 31-40 groups, or roughly 27% of the population. The sample thus demonstrates that the bulk of respondents-more than 85%-are middle-aged individuals aged 31 and older. Young people under 30 barely make up 1/10th of the sample.

Table 3 shows that the sample distribution is predominately made up of females. They estimate that more than 2/3 of the responders to this study took part. Table 3, which breaks down demographic features, reveals that married couples make up the bulk of respondents, or more than 60% of all respondents. Only one category accounts for nearly a third of the total, while the remaining group only accounts for 5%. Family-oriented people make up the majority of the attendees.

When it comes to education, the bulk of respondents-nearly 90% of all respondents-have bachelor's or certificate degrees. Nearly 10% of all participants are master's degree and certificate holders, who make up the remaining responders. According to past experience, the majority of respondents had worked for Pepsi long enough. Nearly two thirds of all participants belong to people who have been there for between 11 and 20 years. Those who have worked for the company for six to ten years, who make up about a third of all participants, are next in line. Newly hired personnel who have worked for the company for up to five years receive scores of at least 10%.

Table 3: Descriptive Statistics for Participants.

S/N		Frequency	%	Mean	Std. Dev.
1	Age			2.0842	.59543
	18 - 30	13	13.7		
	31 - 40	61	64.2		
	41 - 50	21	22.1		
2	51 - 60				
	Gender			1.3684	.48494
	Male				
3	Female				
	Education Level			2.2526	.68368
	Certificate	6	6.3		
	Diploma	65	68.4		
	Bachelor	19	20.0		
4	Masters	4	4.2		
	Experience			3.0211	3.38639
	1-5	14	14.7		
	6-10	26	27.4		
	11-15	34	35.8		
	16-20	15	15.8		
21 - 34	5	5.3			

Source: Authors, (2024).

**IV.2 NORMATIVE COMMITMENT DESCRIPTIVE STATISTICS VARIABLE RESULTS**

Descriptive statistics (mean, standard deviation, minimum and maximum scores) were used to calculate the Effect of the normative Commitment on Organizational Performance at the SBC scale (Table 4). The statement If I got another opportunity for a better job elsewhere, I would not believe it was right to leave my company (M = 3.3474, SD = 1.58965) came in second on the scale of normative commitment, followed by I do

not think that wanting to be a "company Man" or "company woman" is sensible anymore (M = 4.2526, SD = 1.11057). The Normative Commitment Scale item with the lowest score was Because I think loyalty is vital and so feel a moral need to stay, one of the main reasons I still work for this company is that (M = 2.0105, S.D = 1.33285) Jumping from one business to another does not strike me as being at all unethical (M = 2.0316, SD = 1.09596).

Table 4: Normative Commitment Descriptive Statistics Variable Results.

	Minimum	Maximum	Mean	Std. Deviation
I think that people these days move from company to company too often	1.00	5.00	3.0316	1.58754
I do not believe that a person must always be loyal to his or her company	1.00	5.00	2.9263	1.37796
Jumping from company to company does not seem at all unethical to me	1.00	5.00	2.0316	1.09596
One of the major reasons I continue to work for this company is that I believe that loyalty is important and therefore feel a sense of moral obligation to remain	1.00	5.00	2.0105	1.33285
If I got another offer for a better job elsewhere, I would not feel it was right to leave my company	1.00	5.00	3.3474	1.58965
I was taught to believe in the value of remaining loyal to one company	1.00	5.00	2.6737	1.73476
Things were better in the days when people stayed with one company for most of their careers	1.00	5.00	2.8632	1.54100
I do not think that wanting to be a 'company man' or 'company woman' is sensible anymore	1.00	5.00	4.2526	1.11057

Source: Authors, (2024).

**IV.3 ORGANIZATIONAL PERFORMANCE DEPENDENT VARIABLE DESCRIPTIVE STATISTICS RESULTS**

Descriptive statistics (mean, standard deviation, minimum and maximum scores) for the Organizational Performance at SBC Dependence Variable scale were calculated (Table 5). The organization's total productivity growth obtained the highest rating (M = 4.2632, SD = .76089), followed by the

achievement of its goals on time by the organization (M = 4.1895, SD = .99854). The organization's ability to fulfill its goals on schedule came in second (M = 4.0316, S.D = 1.28372) after individual staff productivity improvements, which scored lowest on the organizational performance at SBC dependent scale (M = 3.9684, SD = 1.11520).

Table 5: Organizational Performance Dependent Variable Descriptive Statistics Results.

	Maximum	Mean	Std. Deviation
The organization achieves its intended production targets	5.00	4.0316	1.28372
Operational goals of the organization are realized	5.00	4.2000	.69343
Financial targets of the organization are achieved	5.00	4.1158	.63352
There is increase in overall productivity in the organization	5.00	4.2632	.76089
Individual productivity of employees also increases	5.00	3.9684	1.11520
There is efficient utilization of inputs and minimization of wastage	5.00	4.2000	1.17238
There is value for money in the organization's production	5.00	4.1053	1.25031
The organization realizes high returns on investment	5.00	4.1474	.69906
There is stringent financial prudence in the organization	5.00	4.1053	.79190
The organization achieves its targets on the scheduled time	5.00	4.1895	1.16960
There is efficient time management within the organization	5.00	4.0842	1.25192
There are minimal delays in the organization's operations	5.00	4.1474	.69906
There are effective feedback mechanisms in the organization	5.00	4.0421	.65095
Feedback helps improve customer communication and customer relations	5.00	4.1474	.57490

Source: Authors, (2024).

**IV.4 LINEAR REGRESSION ANALYSIS RESULTS**

Model summary, Anova and regression coefficients are reported.

**IV.5 MODEL SUMMARY RESULTS**

Utilizing linear regression analysis (dependent variable), it was determined how normative commitment (an independent variable) affected organizational performance. The results are presented in Tables 6--8. The model is summarized in Table 6, where the revised R2 statistics (.011) are particularly significant. Accordingly, dedication accounts for 13% of the variation in organizational performance.

Table 6: Model Summary.

Model	R	R Square	Adjusted R Square	Std. Error of the Estimate
1	.019a	.011	.010	.52289
a. Predictors: (Constant), NC				
b. Dependent Variable: OP				

Source: Authors, (2024).

**IV.6 ANOVA RESULTS**

The outcomes of the analysis of variance (ANOVA) are shown in Table 7. Results from model fit is another name for it. The F-statistics and their corresponding sig. value in this table are of particular relevance. According to the findings, the F-statistics are (1, 95) = .033 percent (p.001). The outcomes support the model's assertion that "the model provides power to predict how

organizations perform from normative commitment." As a result, the method appears to be able to accurately predict company performance based on commitment scores.

Table 7: Anova Results.

ANOVA <sup>a</sup>						
Model		Sum of Squares	df	Mean Square	F	Sig.
1	Regression	.009	1	.009	.033	.000 <sup>b</sup>
	Residual	25.428	93	.273		
	Total	25.437	94			
a. Dependent Variable: OP						
b. Predictors: (Constant), NC						

Source: Authors, (2024).

**IV.7 REGRESSION COEFFICIENT ANALYSIS RESULT**

Table 8 displays the regression model's coefficient. The coefficient shows that organizational performance and normative commitment are positively and statistically significantly correlated (b.017\*\*, p .001). The association between normative commitment and performance as an organization at SBC Tanzania Limited (Pepsi) Dar es Salaam is therefore validated, supporting the premise.

Table 8: Regression Coefficient Analysis Results.

Coefficients <sup>a</sup>								
Model		Unstandardized Coefficients		Standardized Coefficients	t	Sig.	Collinearity Statistics	
		B	Std. Error	Beta			Tolerance	VIF
1	(Constant)	7.170	.273		26.304	.000		
	NC	.017	.092	.019	.181	.857	1.000	1.000
a. Dependent Variable: OP								

Source: Authors, (2024).

**IV.8 OUTLIERS, NORMALITY, LINEARITY AND HOMOSKEDASTICITY REGRESSION ASSUMPTIONS TESTING RESULTS**

Table 8 displays the regression model's coefficient. The coefficient shows that organizational performance and normative commitment are positively and statistically significantly correlated (b.017\*\*, p .001). The association between normative commitment and performance as an organization at SBC Tanzania Limited (Pepsi) Dar es Salaam is therefore validated, supporting the premise. In Figure 3, the rectangular distribution of the case residual dots around zero (0) indicates Homoscedasticity (equality of variance). There is no justification to be concerned about heteroscedasticity (unequal variance in the data).

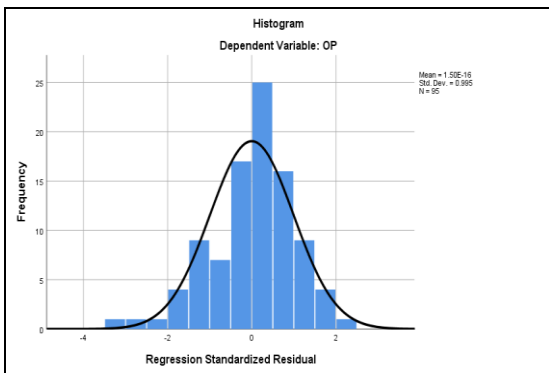


Figure 1: Histogram. Source: Authors, (2024).

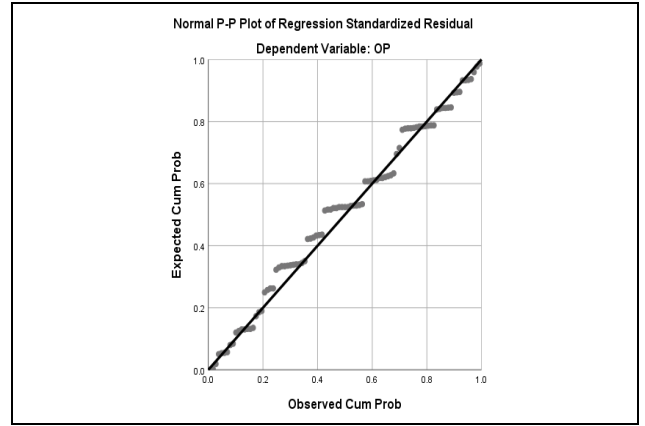


Figure 2: Normal P-Plots for the Standardized Residual Variables. Source: Authors, (2024).

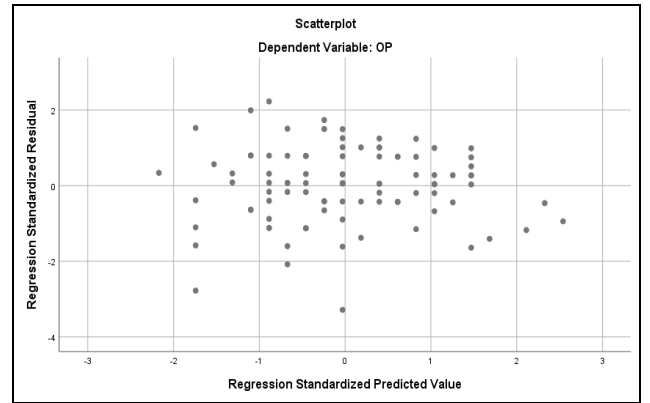


Figure 3: Scatter plot for the Standardized residual for Variables. Source: Authors, (2024).

**V DISCUSSION**

The study found that normative commitment is positively, statistically and significantly related to SBC (Pepsi) organizational Performance. Supporting this study [35] as well found that a number of things affect an employee's commitment, including low pay, a lack of promotions for junior employees, ignorance of union issues, pay disparities between staff members, a disregard for education and professionalism in hiring, and an absence of clear performance bonus guidelines. This becomes norms or responsibility of an employee. This is true especially to long serve employees and those who hold managerial position to the company. For [36] also found that organizational performance is favorably and strongly correlated with employee commitment. In order to achieve excellent long-term success, any company needs committed employees. Through their persistence, proactive support, comparably high output, and awareness of quality, committed employees add value to the organization. The research advises textile businesses to continue their efforts toward guaranteeing employee loyalty. To increase employee commitment, employers must involve their workers in decision-making. This will ultimately increase employee engagement with the business. Additionally, it is advised that businesses promote transparency [37] discovered the opposite, that normative commitment did not have the same effect on company performance as affective and continuance commitment. Probably because normative is not for all employees in a company, only the segment of senior managerial and long service who have not where to go. While affective and continuance commitment cuts across all employees.

## VI RECOMMENDATIONS

Organizations like SBC, as well as organizations generally, must to put in place and sustain systems that endear the business to its staff. The corporation should develop a relationship with its staff in order to encourage employee loyalty to the business. As was demonstrated above, employees who are actively invested in the business will have the strongest impacts on its performance. The study recommends that employers concentrate on decreasing employee dissatisfaction (working conditions, pay, supervision, and interactions with coworkers), whereas on the other hand, they should be using motivating factors like achievement, acknowledgement, responsibility, and the work on its own.

If organizations want to reduce the level of normative commitment, they should constantly innovate and improve their interactions with their personnel. Obligatory commitment normally lasts a brief period of time and varies according on the situation. The company should reconfigure its connection with those employees who are normatively committed in order to keep them before their sense of duty wanes.

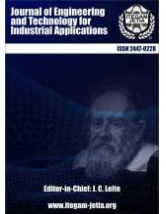
## VII IMPLICATION

Improved Retention of Employees: Normative commitment is essential for encouraging employee loyalty and lowering turnover rates. Employers who value and foster normative commitment among their employees are likely to see lower retention rates in their organizations. As a result, staffing, instruction, and knowledge transfer expenses are reduced, while organizational skills and expertise are maintained.

## VIII REFERENCES

- [1] Sugiarti, E. (2022). The Influence of Training, Work Environment and Career Development on Work Motivation That Has an Impact on Employee Performance at PT. Suryamas Elsindo Primatama In West Jakarta. *International Journal of Artificial Intelligence Research*, 6(1).
- [2] Husin, W. N. W., & Kernain, N. F. Z. (2020). The influence of individual behaviour and organizational commitment towards the enhancement of Islamic work ethics at Royal Malaysian Air Force. *Journal of Business Ethics*, 166, 523-533.
- [3] Bin Jomah, N. (2017). Psychological empowerment on organizational commitment as perceived by Saudi academics. *World Journal of Education*, 7(1), 83-92.
- [4] Wang, W., Albert, L., & Sun, Q. (2020). Employee isolation and telecommuter organizational commitment. *Employee Relations: The International Journal*, 42(3), 609-625.
- [5] Purwanto, A., Purba, J. T., Bemarto, I., & Sijabat, R. (2021). Effect of transformational leadership, job satisfaction, and organizational commitments on organizational citizenship behavior. *Inovbiz: Jurnal Inovasi Bisnis*, 9, 61-69.
- [6] Grego-Planer, D. (2019). The relationship between organizational commitment and organizational citizenship behaviors in the public and private sectors. *Sustainability*, 11(22), 6395.
- [7] Bandula, P. M. K. U., & Jayatilake, L. V. (2016). Impact of employee commitment on job performance: Based on leasing companies in Sri Lanka. *International Journal of Arts and Commerce*, 5(8), 8-22.
- [8] Ahmad, A. (2018). The relationship among job characteristics organizational commitment and employee turnover intentions: A reciprocation perspective. *Journal of Work-Applied Management*, 10(1), 74-92.
- [9] Liu, S., Yang, X., & Mei, Q. (2021). The effect of perceived organizational support for safety and organizational commitment on employee safety behavior: a meta-analysis. *International journal of occupational safety and ergonomics*, 27(4), 1154-1165.
- [10] Ngatuni, P., & Matoka, C. (2020). Relationships among job satisfaction, Organizational affective commitment and turnover intentions of University academicians in Tanzania. *Faculty of Business Management the Open University of Tanzania*, 4(1), 47.
- [11] Allen, N. J., & Meyer, J. P. (1996). Affective, continuance, and normative commitment to the organization: An examination of construct validity. *Journal of vocational behavior*, 49(3), 252-276.
- [12] Meyer, J. P., Becker, T. E., & Vandenberghe, C. (2004). Employee commitment and motivation: a conceptual analysis and integrative model. *Journal of applied psychology*, 89(6), 991.
- [13] Uledi, U. A. (2022). Effects of Leadership Styles on Employee Performance in Private Organizations: A Case Study of SBC Tanzania Limited (Pepsi) Dar es Salaam (Doctoral dissertation, The Open University of Tanzania).
- [14] Ally, J. S. (2022). Impacts of Reward Management Systems on Employee Performance: A Study of Coca-Cola Kwanza Bottlers Company Ltd in Tanzania (Doctoral dissertation, The Open University of Tanzania).
- [15] Daniel, E. M., & Viswanadham, N. (2022). Impact of Soft Drinks Advertisement on Consumers' buying Behavior. *International journal of Engineering, Business and Management*, 6(2).
- [16] Shahzad, F., Luqman, R. A., Khan, A. R., & Shabbir, L. (2012). Impact of organizational culture on organizational performance: An overview. *Interdisciplinary journal of contemporary research in business*.
- [17] Elena-Iuliana, I., & Maria, C. (2016). ORGANIZATIONAL PERFORMANCE-A CONCEPT THAT SELF-SEEKS TO FIND ITSELF. *Annals of Constantin Brancusi University of Targu-Jiu. Economy Series*, (4).
- [18] Boonsiritomachai, W., & Sud-On, P. (2022). The moderation effect of work engagement on entrepreneurial attitude and organizational commitment: evidence from Thailand's entry-level employees during the COVID-19 pandemic. *Asia-Pacific Journal of Business Administration*, 14(1), 50-71.
- [19] Shrivastava, A. (2018). Effect of Affective, Normative and Continuance Commitment on Organizational Effectiveness. *Indian Journal of Public Health Research & Development*, 9(11).
- [20] Almaaitah, M., Alsafadi, Y., Altahat, S., & Yousfi, A. (2020). The effect of talent management on organizational performance improvement: The mediating role of organizational commitment. *Management Science Letters*, 10(12), 2937-2944.
- [21] Butali, P., & Njoroge, D. (2018). Effect of employee participation on organizational performance with organizational commitment as a moderator. *International Journal of Scientific Research and Management (IJSRM)*, 6(06).
- [22] Blau, P. M. (1968). Social exchange. *International encyclopedia of the social sciences*, 7(4), 452-457.
- [23] Cook, K. S., Cheshire, C., Rice, E. R., & Nakagawa, S. (2013). Social exchange theory. *Handbook of social psychology*, 61-88.
- [24] Zafirovski, M. (2005). Social exchange theory under scrutiny: A positive critique of its economic-behaviorist formulations. *Electronic journal of sociology*, 2(2), 1-40.
- [25] Delaney, S. (2014). Making a big deal out of it: Understanding volunteer management through applying psychological contract theory. In *Voluntary sector and volunteering research conference, new researchers' sessions*.
- [26] Anderson, D. R., Sweeney, D. J., Williams, T. A., Camm, J. D., & Cochran, J. J. (2018). *An introduction to management science: quantitative approach*. Cengage learning. Argyris, C. (1960). *Understanding organizational behavior*. Homewood, Illinois: The Dorsey Press. Inc., 1960.
- [27] Al-Ababneh, M. M. (2020). Linking ontology, epistemology and research methodology. *Science & Philosophy*, 8(1), 75-91.
- [28] Mugenda, O. M., & Mugenda, A. G. (2003). *Research methods: Quantitative & qualitative approaches* (Vol. 2, No. 2). Nairobi: Acts press.
- [29] Alvi, M. (2016). *A manual for selecting sampling techniques in research*.

- [30] Yamane, Taro, (1967). *Statistics, An Introductory Analysis*, 2nd ed., New York: Harper and Row.
- [31] Paul, R. W., & Robinson, D. S. (2009). *Organizational Performance: A Global Measurement Scale*. *Journal of Business Research*, 62(8), 794-805.)
- [32] Zhao, H., Wayne, S. J., Glibkowski, B. C., & Bravo, J. (2007). The impact of psychological contract breach on work outcomes: A meta-analysis. *Personnel Psychology*, 60(3), 647-680.
- [33] Robinson, S. L., & Wolfe Morrison, E. (2000). The development of psychological contract breach and violation: A longitudinal study. *Journal of Organizational Behavior*, 21(5), 525-546.)
- [34] Matoka, C., & Rwegoshora, H. (2019). Perceived Psychological Contract Breach on Organizational Continuance Commitment in the Tanzanian Public Universities: The Case of Selected Universities. *Huria: Journal of the Open University of Tanzania*, 26(2).
- [35] Mutua, J. (2013). *Factors Affecting Employee Commitment in Organizations: A Case Study*. *Journal of Human Resource Management*, 1(2), 45-60.
- [36] Stackhouse, T., Zaman, M., & Turner, R. (2022). Organizational performance and employee commitment: A strong positive correlation. *International Journal of Organizational Behavior*, 18(4), 345-362.
- [37] Ikyanyon, D. O., & Agber, T. I. (2020). Comparative effects of normative, affective, and continuity commitment on company performance. *Journal of Management and Strategy*, 11(3), 72-88.



## AVEUGLE AIDER ECHOLOCAION BASED SYSTEM FOR BLINDS

Neetha K<sup>1</sup>, Abirami K A<sup>2</sup>, Amrutha P P<sup>3</sup>, Andria Raju<sup>4</sup> and Atulya G Nair<sup>5</sup>

<sup>1,2,3,4,5</sup> Adi Shankara Institute of Engineering and Technology, Kalady.

<sup>1</sup><http://orcid.org/0009-0000-9564-6231> <sup>2</sup><http://orcid.org/0009-0009-4542-150> <sup>3</sup><https://orcid.org/0009-0003-9511-68> <sup>4</sup><https://orcid.org/0009-0003-9492-0069> <sup>5</sup><https://orcid.org/0009-0003-2929-661>

Email: \* [neetha.ec@adishankara.ac.in](mailto:neetha.ec@adishankara.ac.in), [abhiramika01@gmail.com](mailto:abhiramika01@gmail.com), [amruthapadickal2001@gmail.com](mailto:amruthapadickal2001@gmail.com), [andriaraju@gmail.com](mailto:andriaraju@gmail.com), [atulyagnair@gmail.com](mailto:atulyagnair@gmail.com)

### ARTICLE INFO

#### Article History

Received: October 02<sup>th</sup>, 2023

Revised: July 08<sup>th</sup>, 2024

Accepted: August 16<sup>th</sup>, 2024

Published: August 30<sup>th</sup>, 2024

#### Keywords:

BVIPs,  
ultrasonic sensor,  
DDFS,  
radar,  
echolocation.

### ABSTRACT

One of the most essential and intricate senses we have as humans, is our eyes. It facilitates the perception of light, colour, and depth as well as the visualization of objects. We have the ability to see the things around us but there are people who don't have this ability to enjoy the beauty of nature, who come under the category of BVIPs (Blind and Visually Impaired Persons). They face many challenges in their daily life especially when they traverse around. They will unquestionably need some aid or somebody's help to amble safely. This paper mainly aims at creating a way out to their problem. The idea was inspired from the bat's ability to echolocate obstacles and food. Echolocation is the phenomenon of locating objects based on reflected sound. The paradigm is utilized in the proposed approach to act as a conduit between the blind and their surroundings. Anomalies like obstructions, staircases and damp terrains can all be detected using sensors. For blinds their way of understanding the environment will be through touch and sound. The device helps them to navigate successfully by creating an image of the surrounding in their mind. It is a small handy device that does not hinder other people. Ultrasonic technology and Direct Distance Frequency Synthesizer are the main principles for the device. It is a technique for creating an analogue waveform, typically a sine wave by first creating a time-varying digital signal and then converting it from digital to analogue. Ultrasonic sensors are used as proximity sensors. Our system works similar to that of RADAR. Owing to the technologically advanced era we live in, we decided to assist these people with disability by developing a technology-based solution. It is a useful tool that will be very helpful to blind people.



Copyright ©2024 by authors and Galileo Institute of Technology and Education of the Amazon (ITEGAM). This work is licensed under the Creative Commons Attribution International License (CC BY 4.0).

### I. INTRODUCTION

According to the WHO, there are 250 million individuals worldwide who have some form of visual impairment, including about 40 million blind persons. Also, due to age-related diseases like diabetes and glaucoma, these numbers are rising among the ageing population in most countries. Thus, it is increasingly important to develop novel solutions that minimize any potential blindness-related issues while enabling those individuals to engage with sighted people and the visible environment. The capacity to see is one of the most significant features of human physiology.

The window through which we see the world is our eyes. Moreover, 90% of those who are blind live in developing countries. Researching blind people can help us understand how blindness affects how we perceive and think about the world while also allowing us to learn about it via our other senses. These findings are having an impact on the creation of new technology that will help blind people overcome some of the obstacles in their environment.

Being blind or visually impaired does not necessarily prevent you from going anywhere you choose. There are a variety of strategies and techniques that can support people in securely



navigating, regardless of their level of vision. With the use of the innovative voice sensory replacement system, blind persons can utilize sounds to construct mental representations of their surroundings.

A walking stick has traditionally been the most popular type of navigational aid for blind persons. However, using it has drawbacks like expense, lengthy, training, and a lack of necessary skills. New inventions and technologies are remoulding the world. Technological breakthroughs have made it possible to design and produce electronic solutions that can help a visually impaired individual navigate without restriction a visually impaired individual navigate without restriction.

Those who are visually challenged are unable to distinguish even the slightest details, even with normal vision. Blind people are unable to discern things at a distance of six feet because they have a horizontal vision field of less than or equal to 20 degrees with both eyes open. Assistive technologies are necessary for people with visual impairments. According to, 10% of visually impaired people have no functional vision at all. For persons who have vision impairments, walking in the street can be particularly risky since they have trouble seeing potential hazards in their way. Realizing one's potential and accomplishing one's life goals require a strong sense of autonomy. On the other hand, those who are blind require help from others to carry out daily tasks. Those who are blind or have significant vision loss commonly insist on travelling risky routes when they are alone.

Scientists have been enthralled by bats' use of sound to "see" in the dark for ages. Bats produce ultrasonic chirps, which they use to locate things of interest like food, obstructions, or water resources depending on the timing and shape of the echoes. Mobile robots should be able to localize objectives and barriers in their environment in order to carry out useful tasks like distribution, exploration, and search-and-rescue missions. For [1] propose a complete pipeline for sound-based localization and mapping, which is designed for robots with basic buzzers and inexpensive microphones. This method is capable of working in real time, is model-based, and does not require any calibration or training prior to use. The algorithm was tested on the Crazyflie drone and the e-puck robot, which is equipped with integrated audio hardware, and was able to achieve centimetre-level wall localization on both platforms when the robots remained stationary during the measurement process [1]. To pinpoint the location of a reflector, an approximation interference model might be utilized. This algorithm is designed to be used with low-cost, lightweight hardware, and it runs in real time without needing any calibration.

Despite having a simple sonar system with only one transmitter and two receivers, bats are able to navigate in three dimensions by using echolocation. Based on actual behavioural observations of bats during flight, a theoretical research of the 3-D spatial perception technique used by bats has been carried out in [2]. A 3-dimensional localization using information from binaural beats and interaural level differences inspired by bats was achieved. Particular attention was paid to the acoustic information that can be obtained from the "movements" of one's own flight or ear. The results from the output show that binaural beats and interaural level differences help in accurate 3-dimensional localization [2]. In particular, vertical localization using interaural level difference information is proposed as opposed to horizontal localization using interference beat signals. In order to evaluate the

proposed methodology, practical experiments were carried out utilising an automatic sensing system with one transmitter and two receivers [2].

Through the usage of healthcare information systems, electronic medical records, wearable, smart, and handheld technologies, the healthcare system is undergoing a digital transition [3]. A navigation system for people with poor vision impairments is one that can provide precise navigational services and can help people avoid obstacles on the way to their destination. The creation of a navigation aid for blind or visually impaired patients is one of the most inspiring applications since it enables them to move around indoors or outdoors without the assistance of others [3]. This paper deals with an efficient way of surveying the different aids available for BVIPs, states the possible challenges regarding bringing these solutions to practicality and avoiding any possible misuse of those and attempts to overcome these by doing literature surveys [3]. A list of relevant keywords, four research questions, criteria for article selection, and a synopsis of the available empirical data are used to carry out this systematic study activity. The researchers and engineers would be able to make more honest conclusions and offer fresh suggestions to benefit the BVIPs by using this systematic mapping [4], shows an integrated framework for use in a mobility aid for the blind that applies cutting-edge computer vision techniques like SLAM and obstacle detection. The navigation tool for the blind presented in [5], uses a microcontroller with synthetic speech output. According to [6]. Suggests creating an electronic white cane that facilitates mobility in both interior and outdoor settings while providing contextualized geographic information by utilizing RFID technology. A walking stick for people who are blind or visually disabled is designed and implemented in [7]. A Crazyflie 2.0 nano quadrotor helicopter (quadcopter) has been introduced as an opensource experimental tool for study and instruction in robotics and control engineering [8]. This article describes the hardware and software of a cheap, readily expandable, and upgradeable flying robot. The article discusses three elements that show how this unmanned aerial vehicle (UAV) could be widely used by academics and students. In order to notify the blind person to obstacles in their path, a buzzer is used in conjunction with an ultrasonic sensor module, model HC-SR04. Deafblind people are an understudied group of disabled people, and [9], has discussed their experiences and attitudes towards assistive communication and mobility devices. It has also demonstrated that deafblind people in the countries studied have a serious problem with rejecting assistive devices, particularly canes and hearing aids, out of fear of stigma, a desire to avoid drawing attention to themselves as disabled, or a lack of acceptance of disability. The white cane is beneficial in alerting its user to any obstacles that are within 1.5 m, however, it does not provide any information regarding the environment beyond that distance. The expense of training a guide dog can reach \$42,000, and they are sadly in short supply [10].

An ultrasound obstacle detecting system is suggested that generates, emits, and receives ultrasonic pulses in the air [11]. This article provides a first approximation of the entire system with some evidence in form and composition determination using an easy analysis in the frequency domain. White canes were used in [12], to examine the connection between vibration and the perception of hardness. As part of it, participants in psychological research were asked to estimate their sense of hardness for each hardness level. It was discovered that the perception of hardness and the frequency of vibration are related. Using temporary deprivation techniques (such as gagging to inhibit the emission of supersonic notes, blindfolding, and ear plugs), the sensory control

of obstacle avoidance during flight in a conventional test scenario was studied [13]. It was observed that bats that are wearing blindfolds can navigate obstacles just like regular bats. Avoidance accuracy drops significantly when someone gags or covers their ears. A single ear plug also makes obstacles seem to appear more frequently [13]. Based on multipath propagation inside a room, an approach for concurrent localization and mapping was devised in [14]. A simple sensing setup was used in which it was assumed that there was no pre-installed equipment in the space, only a single omnidirectional sound source, and a single omnidirectional microphone co-located on a robot. It was shown that measuring the distances between the robot and the walls is enough to create an algorithm that properly estimates the robot's trajectory and recovers the geometry of the room [14]. According to [15] discuss measurements of the sonar beam pattern of flying echolocating bats, *Eptesicus fuscus*, performing various insect capture tasks in a large laboratory flight room. The signal strength across a linear array of microphones was used to infer the beam pattern. The findings imply that the axis of the bat sonar beam is a reliable indicator of selective target tracking and, in this regard, is comparable to gaze in animals that rely primarily on vision.

## II. MATERIALS AND METHODS

Our device enables blind person to move freely and with more accuracy while sensing various obstacles in their path. The hardware components will have connectors for the STM32 Microcontroller Board, the HC-SR04 ultrasonic sensor and other devices. STM32F303RBT7 is the microcontroller found in STM32 Microcontroller Board. An external power source is provided. The system is configured to meet the requirements. The STM32CubeIDE will be used for the programming STM32 Microcontroller Board. The pins of the Microcontroller Board can be configured and so it will be configured according to the need. The gadgets will have external circuits like speakers DAC and power amplifiers.

An intriguing group of animals is the bats, which are one among the few animals that can travel by using echoes. Too many echoes might make a bat's vision hazy. That's because these nocturnal animals employ echolocation, a kind of navigation that involves bouncing ultrasonic sound off of their surroundings. These sounds can echo in small spaces, producing a noisy backdrop that obscures the mammal's auditory vision. Our device uses echolocation as basic principle.

Human hearing typically reaches its maximum frequency at about 20 kHz, whereas echolocation calls are often ultrasonic and range in frequency from 20 to 200 kHz. Yet, we may hear some bats' echolocation clicks, such as those of the spotted bat. These noises sound like two round stones being struck together. Echolocation calls can typically be identified by their frequency, intensity in decibels (dB), and duration in milliseconds (ms).

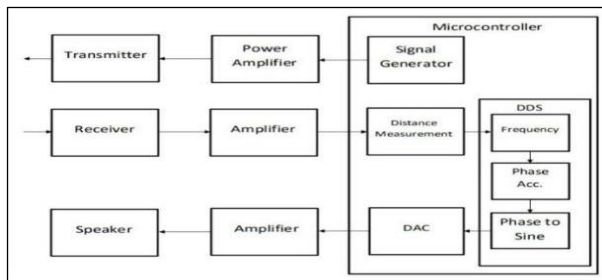


Figure 1: Block Diagram.  
Source: Authors, (2024).

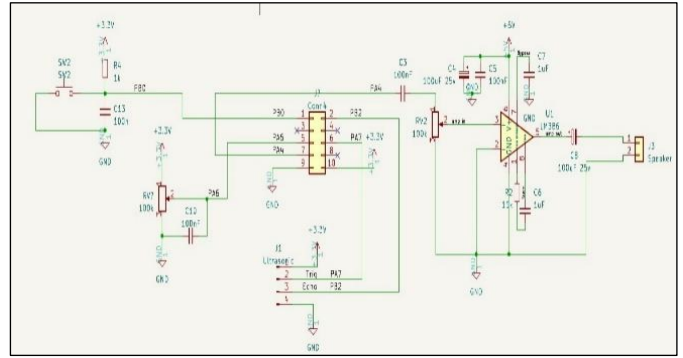


Figure 2: Circuit Diagram.  
Source: Authors, (2024).

This system has mainly 3 parts transmission part, receiver part and signal generation part. The design of the device enables the microcontroller to generate a pulse through programming. The power amplifier employed will aid in boosting the signal generated. Ultrasonic trans-receiver modules were positioned to detect obstacles in front, at head level, and at foot level. To Transmit Ultrasonic waves, the timer sent a PWM signal at 100 KHz with a 10 percent duty cycle. To the transmitting end of the US module was delivered the trigger signal. Through input capture control, the transmitted signal that is reflected by the obstruction is received at the echo pin. The information about the obstruction present was then extracted from this echoed signal through analysis. The received signal contained time-related information that was translated into distance using the formula:

$$d = s \times t \quad (1)$$

where d is the distance, s is the speed of sound, t is time duration for the wave to get reflected back.

Here, sound speed is recorded as 340 m/s. The method known as DDS (Direct Digital Synthesizing) will be employed following the distance measurement. Direct digital synthesis (DDS) is a technique used for creating output signals that are frequency and phase-tuneable. The sine LUT was created with 128 samples that stores the sine values and with help of DAC, sine wave is generated. Based on the distance read phase accumulation is done for this above created sine LUT with 128 samples. Timer clock divided by 128 samples gives the frequency of a sinewave. Phase accumulator will then start working. Since the phase accumulator is necessary for producing various sounds for objects at various distances, it will be utilized for addition & multiplication. To vary the frequency from about 100Hz to 3KHz, frequency tune word (ftw) given by,

$$ftw = (f/2^{32}) f_{clock} \quad (2)$$

where, ftw is the frequency tuning word, f is the frequency, f<sub>clock</sub> is the internal reference clock frequency.

The obtained ftw is added and multiplied with distance, thus based on the distance it varies between the provided maximum and minimum frequency. If the phase accumulator is absent the device will only produce a single tune and it will not help. After that, the signal will be given to the DAC. The output of the DAC with 3.3volt will be an analogue signal which will be amplified by the op-amp into 5 volt and will be given, to the blinds either through a speaker or a headset.

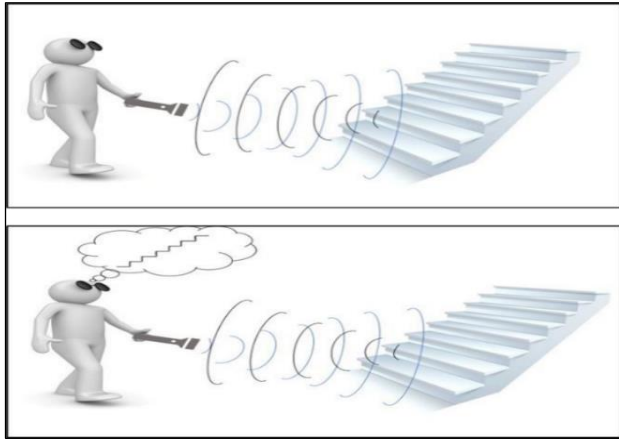


Figure 3: Illustration picture – ultrasonic wave transmitted and received the reflected wave and user gets the idea of obstacle.  
Source: Authors, (2024).

### III. RESULTS AND FUTURE SCOPE

The STM32 board, power amplifiers, and ultrasonic sensors are tested individually as well as in an integrated system. The ultrasonic sensors operate on the echo principle so, it is crucial to understand how the echo reflects off various object surfaces. The device is made to be light weight so the user is not required to exert themselves more. Also, this device must have a size and shape that defines its portability. The device was tested under various circumstances and corresponding results were obtained. Our device mimics the navigation method from nature i.e., the 3D localization method employed by bat. This technique was investigated and is employed in the project which helps the blinds to navigate properly. It is a small handy device, making it easy for the person to carry the device and use it. Device provides a touch and feel experience to the user on the obstacle in front of them. The project mainly contains three portions transmitter, receiver and sound generation part. method from nature i.e., the 3D localization method employed by bat. This technique was investigated and is employed in the project which helps the blinds to navigate properly. It is a small handy device, making it easy for the person to carry the device and use it. Device provides a touch and feel experience to the user on the obstacle in front of them. The project mainly contains three portions transmitter, receiver and sound generation part.

To produce a sine wave, DAC was used, and a sine lookup table was made. An array of 128 sample was included in sine look up table. Combining sine LUT with DAC a perfect sine wave was generated. DSO was set to 2V and sine wave of 3.3V was generated. Sine wave generated and the frequency of the signal from the DDS output is varied. The values are obtained by setting up pre-scalar register value accordingly. Using amplifier, the sound is outputted.



Figure 5: Picture of the device.  
Source: Authors, (2024).

Tested the device in various scenarios like different distance, different angles with respect to the obstacle and variation in the frequency is noted.

**Case 1:** The frequency variation occurring with respect to the distance between the user and obstacle.

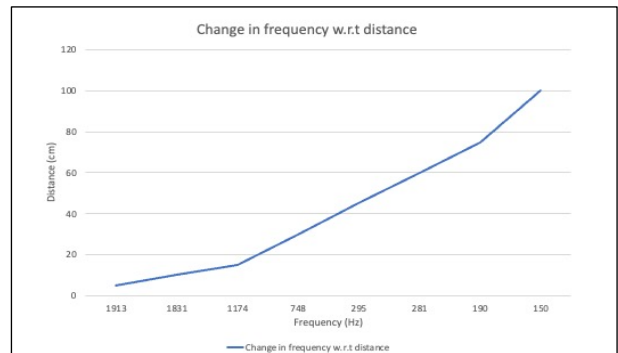


Figure 6: Distance v/s frequency graph.  
Source: Authors, (2024).

**Case 2:** The frequency variation occurring when angle varied and obstacle is static.

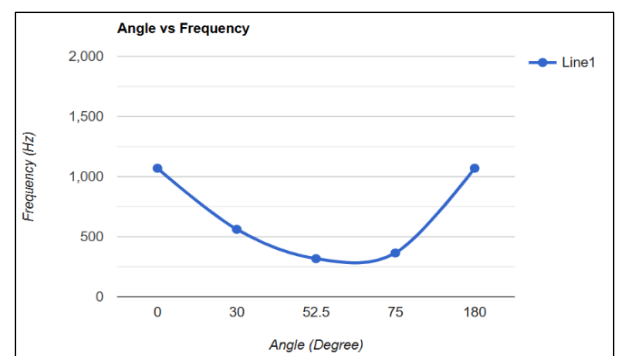


Figure 7: Frequency v/s angle graph.  
Source: Authors, (2024).

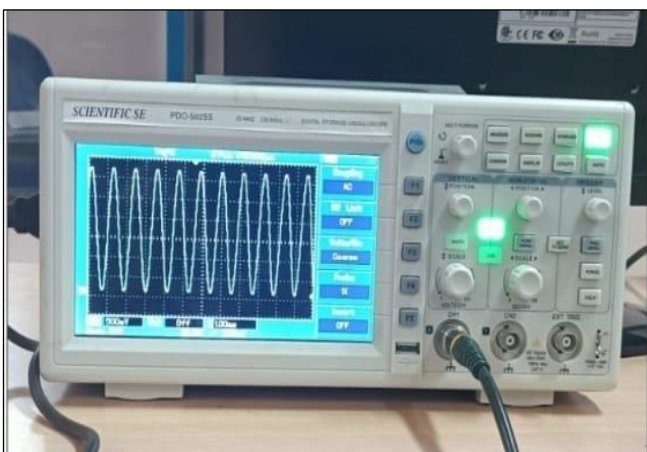


Figure 4: Sine wave generation.  
Source: Authors, (2024).

We discovered that the HSCR04 sensor functions well within a 30-degree cone after testing in various real-world scenarios. The frequency reduces with changing sensor-to-object angles. However, as the range goes beyond 30 degrees, the sensor's effectiveness drops, interrupting the dropping frequency's natural course, and causing an increase in frequency. Additionally, as the device's distance from a barrier grows, the frequency of the sound it produces appears to be decreasing, and vice versa.

We successfully implemented and tested the prototype with the aid of a micro controller, the DDFS technique, sensors and other contemporary tools. The device offers solutions to blindness-related problems. It provides direction to its users, making navigation simple. There is an audio output unit in the gadget. The device, which resembles a torch, sends out signals and receives them as audio, which gives a notion of the obstacle in front of it. There are certain constraints which can be overcome in future like:

- can add filter to reduce noise and make it more smooth;
- can be integrated further to make it handy, and;
- auto rotation of the sensor.

#### IV. CONCLUSIONS

Being blind is viewed as a curse in society. People who are blind encounter many challenges every day, due to which they lose their sense of self-worth and start to feel like a hindrance to social and economic advancement, killing their impulse for living. They struggle to perform daily tasks due to a variety of challenges they deal with. The amount of data necessary for the safe movement of BVIPs could not be provided by the usual navigational aids. This is the reason behind our decision to use it as the foundation of our system. The device specified in this article mimics the navigation method from nature i.e., the 3D localization method employed by bat. This technique was investigated and is employed in the project which helps the blinds to navigate properly. The project mainly contains three portions: transmitter, receiver and sound generation part. There is an audio output unit in the gadget. The device sends out signals and receives them as audio which can be interpreted by the user, which gives a notion of the obstacle in front of it. We successfully implemented and tested the prototype with the aid of a micro controller, the DDS technique, sensors and other contemporary tools. The device was tested and analysed on various scenarios such as variation of distance between the obstacle and the device, the variation of the frequency of the sound when the device is kept at different angles with respect to the obstacle. Through the real time testing the efficiency, behaviour and relevance of the system was found to be near accurate, with possibilities of future enhancement. A device of this nature makes a significant contribution to human welfare.

#### V. AUTHOR'S CONTRIBUTION

**Conceptualization:** Neetha K, Abirami K A, Amrutha P P, Andria Raju and Atulya G Nair.

**Methodology:** Abirami K A, Amrutha P P.

**Investigation:** Andria Raju and Atulya G Nair.

**Discussion of results:** Neetha K, Abirami K A, Amrutha P P, Andria Raju and Atulya G Nair.

**Writing – Original Draft:** Neetha K, Abirami K A, Amrutha P P.

**Writing – Review and Editing:** Neetha K, Abirami K A, Amrutha P P, Andria Raju and Atulya G Nair.

**Resources:** Abirami K A, Amrutha P P, Andria Raju and Atulya G Nair.

**Supervision:** Neetha K.

**Approval of the final text:** Abirami K A, Amrutha P P, Andria Raju and Atulya G Nair.

#### VI. REFERENCES

- [1] F. Dümbgen, A. HOFFET, M. Kolundžija, Scholefield and M. Vetterli, "Blind as a Bat: Audible Echolocation on Small Robots," in IEEE Robotics and Automation Letters, vol. 8, no. 3, pp. 1271-1278, March 2023.
- [2] Y. Yamada, Y. m. Watabe, S. Hiryu and R. Kobayashi, "3D Acoustic Localization Based on Echolocation Strategy of Bats," 2020 IEEE/SICE International Symposium on System Integration (SII), Honolulu, HI, USA, 2020, pp. 1133-1138.
- [3] S. Khan, S. Nazir and H. U. Khan, "Analysis of Navigation Assistants for Blind and Visually Impaired People: A Systematic Review," in IEEE Access, vol. 9, pp. 26712-26734, 2021.
- [4] Pradeep, V., G. Medioni, and J. Weiland. Robot vision for the visually impaired. In Computer Vision and Pattern Recognition Workshops (CVPRW), 2010 IEEE Computer Society Conference on. 2010. IEEE.
- [5] Bousbia-Salah, M., M. Bettayeb, and A. Larbi, A navigation aid for blind people. Journal of Intelligent & Robotic Systems, 2011. 64(3-4): p. 387-400.
- [6] Faria, J., et al. Electronic white cane for blind people navigation assistance. In World Automation Congress (WAC), 2010. 2010. IEEE.
- [7] N. Dey, A. Paul, P. Ghosh, C. Mukherjee, R. De and S. Dey, "Ultrasonic Sensor Based Smart Blind Stick," 2018 International Conference on Current Trends towards Converging Technologies (ICCTCT), Coimbatore, India, 2018, pp. 1-4.
- [8] W. Giernacki, M. Skwierczynski, W. Witwicki, P. Wroński, and P. Kozierski, "Crazyflie 2.0 quadrotor as a platform for research and education in robotics and control engineering," in 22nd International Conference on Methods and Models in Automation and Robotics, 2017, pp. 37-42.
- [9] Hersh, M., Deafblind people, stigma and the use of communication and mobility assistive devices. Technology and Disability, 2013. 25(4): p. 245-261.
- [10] Morrison, R., et al. Design of a Novel Electronic Travel Aid to Assist Visually Impaired Individuals Navigate Their Environment. In ASME 2012 Summer Bioengineering Conference. 2012. American Society of Mechanical Engineers.
- [11] L. F. Mondragon, A. Vera, L. Leija, J. Gutierrez, J. E. Chong-Quero and M. I. Gutierrez, "Transceiver system for obstacle detection based on bat echolocation with air-coupled pulse-echo ultrasound," 2017 14th International Conference on Electrical Engineering, Computing Science and Automatic Control (CCE), Mexico City, Mexico, 2017, pp. 1-5.
- [12] Nunokawa, K., S. Ino, and K. Doi, Vibration of the White Cane Causing a Hardness Sense of an Object, in HCI International 2013- Posters' Extended Abstracts. 2013, Springer. p. 493-497
- [13] D. R. Griffin and R. Galambos, "The sensory basis of obstacle avoidance by flying bats," Journal of Experimental Zoology, vol. 86, no. 3, pp.481-506, 1941.
- [14] M. Krekovic, I. Dokmanic, and M. Vetterli, "EchoSLAM: Simultaneous localization and mapping with acoustic echoes," in IEEE International Conference on Acoustics, Speech and Signal Processing, 2016, pp. 11-15.
- [15] K. Ghose and C. F. Moss, "The sonar beam pattern of a flying bat as it tracks tethered insects," The Journal of the Acoustical Society of America, vol. 114, pp. 1120-1131, 2003



ISSN ONLINE: 2447-0228



## RESEARCH ARTICLE

## OPEN ACCESS

## AREA AND SPEED EFFICIENT FPGA DESIGN OF S-BOX AES-256 GALOIS FIELD APPROCH BASED ON LOGIC

K Janshi Lakshmi<sup>1</sup>, G Sreenivasulu<sup>2</sup>

<sup>1,2</sup>Research Scholar, Department of Electronics and Communication Engineering,  
Sri Venkateswara University College of Engineering,  
Sri Venkateswara University, Tirupati, Andhra Pradesh, India.

<sup>1</sup><https://orcid.org/0000-0001-9543-9478> , <sup>2</sup><https://orcid.org/0009-0008-9025-177> 

Email: \* [jansikaramala@gmail.com](mailto:jansikaramala@gmail.com), [gunapatiee@rediffmail.com](mailto:gunapatiee@rediffmail.com).

## ARTICLE INFO

**Article History**

Received: October 03<sup>th</sup>, 2023

Revised: July 08<sup>th</sup>, 2024

Accepted: Month 15<sup>th</sup>, 2024

Published: Month 30<sup>th</sup>, 2024

**Keywords:**

AES (Advanced Encryption Standard),  
S-box Optimization,  
Galois Field Arithmetic,  
FPGA (Field-Programmable Gate Array),  
Delay Reduction.

## ABSTRACT

This paper Provides Compared S-box Galois Field Approach Based on LUT and Logic Gates for AES in terms of decreased chip size and decreased delay, which enhances performance. Data security is a fundamental requirement in the digital age. Modern cryptography encryption techniques are essential for creating secure communication. The Advanced Encryption Standard (AES) is widely regarded as the cryptography field's strongest encryption technique. The Operate Three Stage Pipeline process to reduce delay of S-box AES-256 using logic gates Galios Field approach. So, accordingly increase speed. Additionally, results of the suggested and existing approaches were compared. The proposed approach simulated and sythesised with Virtex-5 FPGA device along with design in verilog code in xilinx 14.7 software.



Copyright ©2024 by authors and Galileo Institute of Technology and Education of the Amazon (ITEGAM). This work is licensed under the Creative Commons Attribution International License (CC BY 4.0).

### I. INTRODUCTION

Numerous Platforms One Family. Four new platforms are available from the Virtex--5 family of FPGA, each of which offers an optimised mix of embedded processing, signal processing, high-performance logic, and serial connection. The Virtex line of FPGAs are built using Configurable Logic Blocks (CLBs), where each CLB is comparable to a number of ASIC gates. Numerous slices, which vary in design between Virtex families and make up each CLB, are used. Military-grade specialised processor is used by Virtex. The product's primary market is high-latency broadband applications, which necessitate processing a lot of data with little latency.

Digital data is protected using cryptography. Changing plaintext into illegible text and conversely is mention to as cryptosystem. It is an approach of transferring and saving data in a particular way so that just those who are meant to access and analyse it may do so. It is focuses on converting data into formats that can't be understood by unauthorised users. A message the fact

that has been encrypted along with which the letters have been converted to other characters is an instance of basic cryptosystem see the Figure 1. The main cryptography principles are Data Confidentiality, Data Integrity, Authentication and Non-repudiation in modern day.

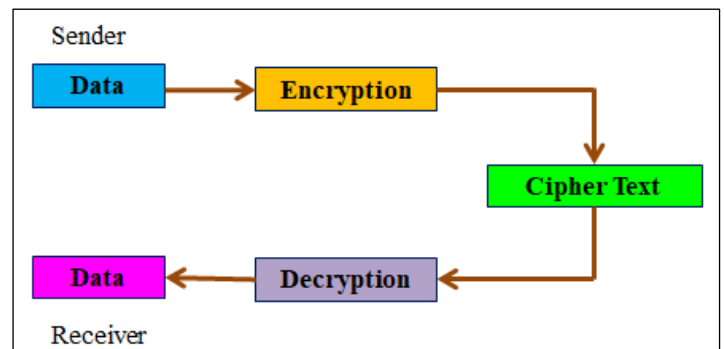


Figure 1: Cryptography Process.  
Source: Authors, (2024).

The following elements make up a fundamental cryptosystem-Plaintext is information must be kept secure,The encryption algorithm is a mathematical formula that receives, plaintext as input and outputs ciphertext. This is the plaintext's encrypted or unintelligible counterpart, or ciphertext. Cryptography can be broken down into 3 different groups: secret key encryption, public key encryption, and hash functions. Encryption by employing a Symmetric Key, Asymmetric Key Encryption.Symmetric Key Encryption: from the Figure 2. For the encryption and decryption have given same secret key that is secret key 1 and secret key 1. But Asymmetric Key Encryption for the encryption and decryption have given different secret key that is secret key 1 and secret key 2 see the Figure 3.

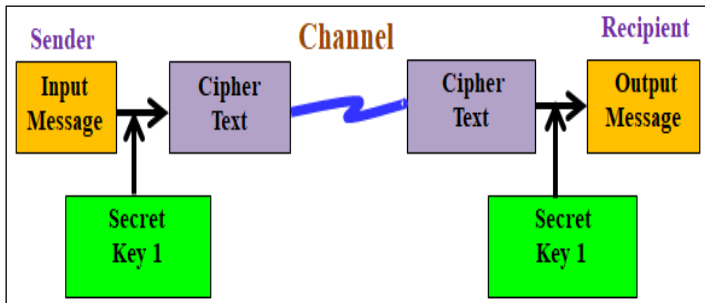


Figure 2: Symmetric Key Encryption.  
Source: Authors, (2024).

Messages can be securely encrypted and decrypted utilising asymmetric cryptography, referred to as public-key cryptography, effectively prevents them towards unauthorised access and utilisation. A public key and a private key that are linked jointly are utilised. A single key is used for both encryption and decryption in symmetric encryption, which speeds up the encryption process. Asymmetric encryption uses two separate keys, one of which is related to the other by a challenging mathematical process, hence the encryption process is slower when using this method. Network security authentication and digital signature applications: Date and time stamping, electronic currency, the encryption and decryption of email, encrypting WhatsApp, The encryption of Instagram, Identification with a SIM card.

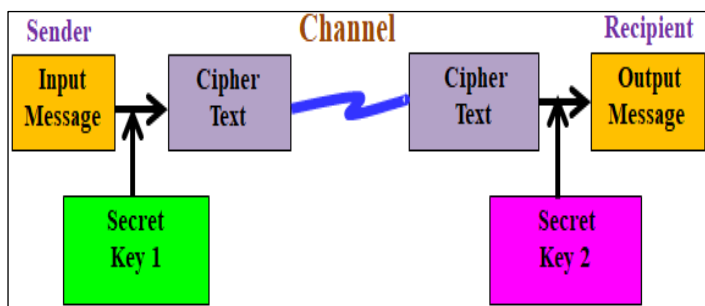


Figure 3: Asymmetric Key Encryption.  
Source: Authors, (2024).

The most famous and commonly employed symmetric encryption technique accessible today is AES. It is at least six times speedier to discover than triple DES. A replacement was required while the key size of DES was inadequate. As processing power spiked it became considered vulnerable to an exhaustive key search assault. Triple Data Encryption Standard was supposed to solve this

disadvantage, but it was proven to be sluggish. In both hardware and software, AES is a widely used and supported encryption process. No genuine assaults employing crypt analysis has yet been carried out versus AES. The AES also has built-in flexibility for key length, which offers some "future-proofing" against improvements in the ability for thorough key searches. AES security is only made sure, though, if it is deployed properly and adequate key management is employed, just like DES. Federal government departments, non-government organisations, commercial firms, and organisations regularly use AES encryption to secure sensitive data. The AES algorithm is widely utilised in a wide range of applications, including file encryption, SSL/TLS, processor security, wireless security.

## II. LITERATURE REVIEW

You-Tun Teng, Wen-Long Chin, et.al.[1] are represented the advanced encryption standard's (AES) SubBytes and Inverse SubBytes procedures implemented on hardware. To achieve this, the SubBytes (and inverse SubBytes) transformation's S-box (and inverse S-box) building blocks are all optimised using the composite field arithmetic (CFA).

According to [2] are presented about Implementing the inverse of the improved affine transform is the main objective in this case. The basic zigbee S-Box approach and the Rijndael method are compared in terms of a variety of factors. This is due to the use of extra registers for the various stages.

For [3] are shown The Galois Field Multiplier, which is it has been determined that the operation, that is involved in the Mix-Columns and Inverse Mix-Columns transformations, is the most demanding in terms of processing performance and area consumption.

For [4] were represented of Critical components have been combined with fewer additional selectors utilizing Data path's innovative operation reordering and register-re-timing algorithms.

According to [5] were research on Simulation of the Advanced Encryption Standard utilizing double 7th series capital to examine cost and performance contrasts.

Yashvir Singh Chauhan, T.N. Sasamal [6] were specified about Generates multiple s-boxes for different rounds that is s-box changes with respect to key and hence increasing the security of cipher

Were presented Low power AES design based on a novel implementation for the Shift Rows operation. Designed and implemented using 45nm and 90nm technology nodes [7].

Were represented by Design an S-box that utilizes Composite Field arithmetic to significantly minimize the size relative to FPGA slices and the gate latency as well as the combinational path delay [8].

According to [9] were research on Pipeline design for AES algorithm to increase the Performance of Hardware.

For [10] specified about Throughput of encryption and throughput of decryption of DES is more compared to AES.

## III. OVERVIEW OF AES ALGORITHM

### III.1 AES-256 ENCRYPTION

Advanced Encryption Standard (AES) has input Data is 128bits, Secret key is 128bits, 192bits and 256bits. Here using

256bit key algorithm. In 256bit key algorithm has total 14 rounds perform. For encryption has 14 rounds as well as for AES decryption also has 14 rounds. It shows in Figure.4 and Figure 5. Substituting bytes (SubBytes): The design includes a fixed table (S-box) that is hunted up in order to replace the 16 input bytes. The outcome is represented as a matrix with four rows and four columns. The four rows of the matrix are all shifted to the left. Any entries that 'fall off' are reinserted on the row's right side. During shift, the subsequent methods apply: The top row remains in place. The second row has been moved one (byte) position left, the third row has been moved two spaces left, whereas the fourth row has been moved three spaces left. The end result is a new matrix with the same 16 bytes but with various locations. MixColumns: Each column of four bytes is now treated to an unique mathematical operation. In order to make use of this function, four bytes from

one column need to be supplied, and four completely novel bytes should be output in its place. The most recent matrix has 16 more bytes and is a fresh one. This step does not appear in the final round, it should be highlighted. Addroundkey: The 16 bytes of the matrix, which are now regarded as 128 bits, are XORed with the 128 bits of the round key. If this is the final attempt, the ciphertext will be generated. Otherwise, the outcome's 128 bits is transformed into 16 bytes, and the process is restarted. In encryption 1<sup>st</sup> round perform 5 operations i.e, Preround, shiftrow, addround key, subbyte and mixcolumn. From 2<sup>nd</sup> round to 13<sup>th</sup> round perform 4 operations i.e, subbyte, shiftrow, mixcolumn and addround key. For 14<sup>th</sup> round it perform 3 operations only i.e, subbyte, shiftrow, addround key operationsee the Figure 4. Finally, the output is 128bits cipher key generates.

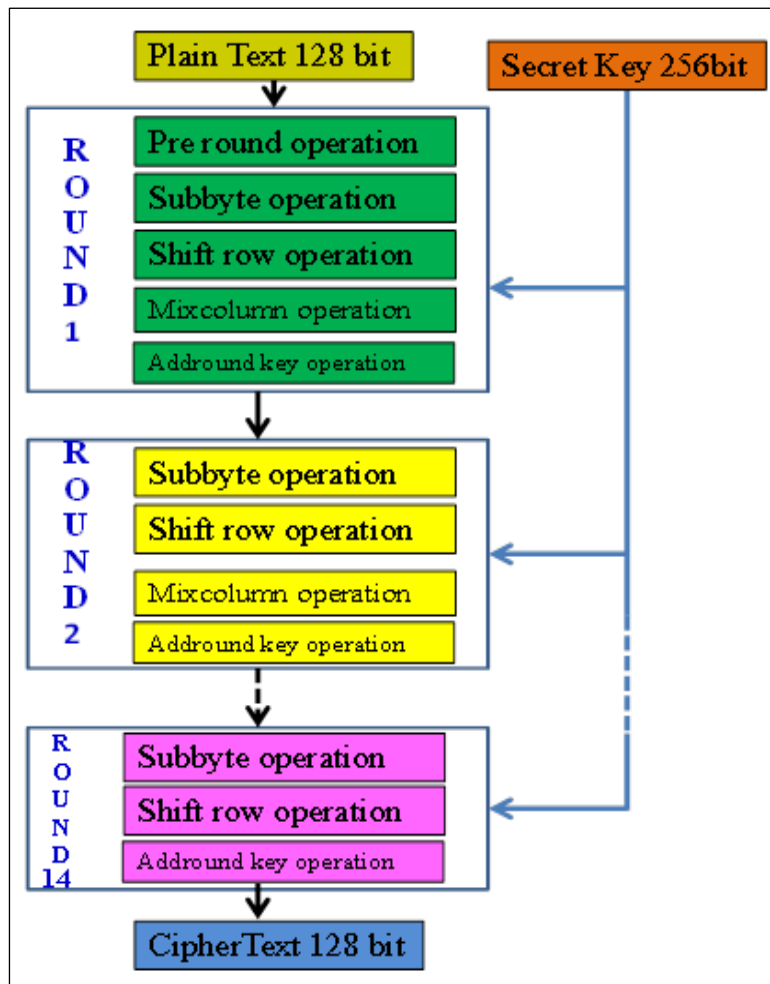


Figure 4: AES-256 Encryption.  
Source: Authors, (2024).

### III.2 AES-256 DECRYPTION

AES-256 decryption has input is cipher key 128bits, cipher key means combination of input data and secret key. Secret key is 128bits, 192bits and 256bits. Here using 256bit key algorithm. In 256bit key algorithm has total 14 rounds perform. For decryption has 14 rounds It shows in Figure 5. The reversal of the encryption process is used in the decryption of an AES cipher text. The four procedures are carried out each round in reverse sequence. Inverse Byte replacement, Inverse Byte Mix, Inverse Shift, and Inverse Add round key. Despite having extremely close relationships, the

encryption and decryption algorithms must be implemented independently since each round's sub-processes function backwards. In decryption 1<sup>st</sup> round perform 5 operations i.e, Preround, Invshiftrow, addround key, Invsubbyte and Invmixcolumn. From 2<sup>nd</sup> round to 13<sup>th</sup>round perform 4 operations i.e, Invsubbyte, Invshiftrow, Invmixcolumn and addround key. For 14<sup>th</sup> round it perform 3 operations only i.e, Invsubbyte, Invshiftrow, addround key operationsee the Figure 5. Finally, the output is 128bits original data or input data generates.

#### IV. PRAPOSED METHODOLOGY

##### IV.1 S-BOX USING LOGIC GATES

The Example for Computing the Sub Byte Operation with Logic Gates in S-Box is show in Fig. 8, the dissemination of the data input of  $(04)_{16}$  into a composite field-based Substitute Box. The precomputed values were formerly kept in a ROM-based lookup table, which was one of the most popular and simple implementations of the StandardBox for the SubByte operation (LUT). In this approach, the input byte would be connected to the ROM's address bus and all 256 values would be kept in a ROM. The multiplicative inversion of the supplied data is the first step. The four bit numbers outside of the logical blocks show the new values that are applied to the high and low nibbles. Since the results containing for GF  $(2^4)$  multiplication and multiplicative inverses are provided, the example can be completed by hand. Following the multiplicative inversion module's inverse isomorphic mapping operation, the To create the S-Box replacement value for the input, an affine transformation is applied to the multiplicative inverse. of  $(CB)_{16}$ . Finally, the output is  $(F2)_{16}$ , which is consistent with the S-Box table given. Combinational logic is a more sophisticated method of implementing the S-Box, and this kind of S-Box has the benefit of having low space occupancy or less area occupied of system [11],[12]. Due to this smaller size, Computing the Sub Byte Operation using Logic Gates was implemented in S-Box in instead of LUT. Moreover, in order to take advantage of the FPGA's reduced path delay, three pipeline stages S-Box were developed employing logic gates. It enhances optimisation and performance. These two-design shown in Figure 8 and Figure 10.

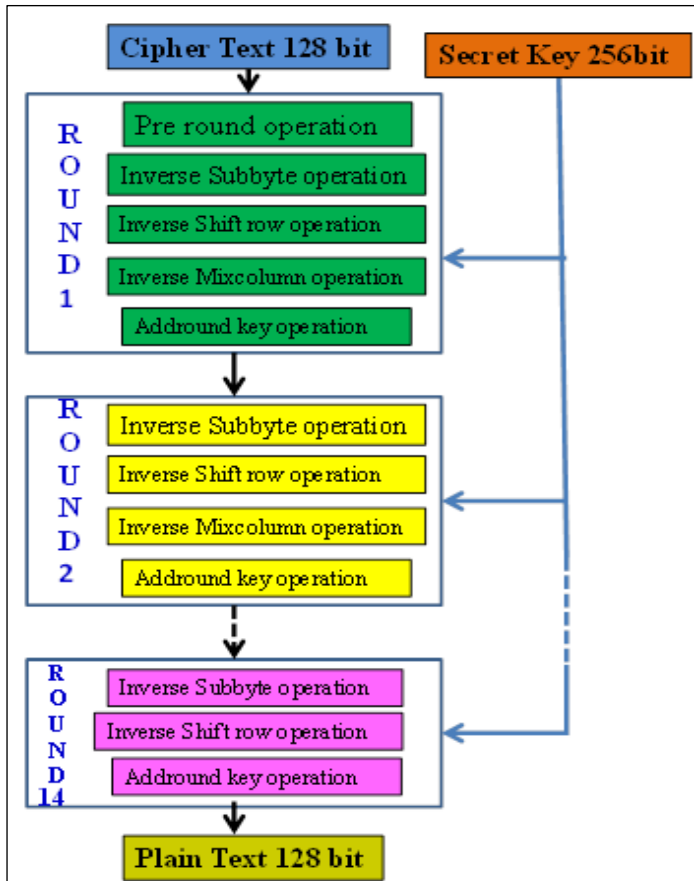


Figure 5: AES-256 Decryption.  
Source: Authors, (2024).

##### IV.2 ISOMORPHIC AND INVERSE ISOMORPHIC MAPPING

The logical XOR operation can be used to translate the matrix multiplication. Below is a diagram of the matrices' logical form equation (1) and equation (2).

$$\delta \times j = \begin{pmatrix} 1 & 0 & 1 & 0 & 0 & 0 & 0 & 0 \\ 1 & 1 & 0 & 1 & 1 & 1 & 1 & 0 \\ 1 & 0 & 1 & 0 & 1 & 1 & 0 & 0 \\ 1 & 0 & 1 & 0 & 1 & 1 & 1 & 0 \\ 1 & 1 & 0 & 0 & 0 & 1 & 1 & 0 \\ 1 & 0 & 0 & 1 & 1 & 1 & 1 & 0 \\ 0 & 1 & 0 & 1 & 0 & 0 & 1 & 0 \\ 0 & 1 & 0 & 0 & 0 & 0 & 1 & 1 \end{pmatrix} \times \begin{pmatrix} j_7 \\ j_6 \\ j_5 \\ j_4 \\ j_3 \\ j_2 \\ j_1 \\ j_0 \end{pmatrix} \quad \delta^{-1} \times j = \begin{pmatrix} 1 & 0 & 1 & 0 & 0 & 0 & 0 & 0 \\ 1 & 1 & 0 & 1 & 1 & 1 & 1 & 0 \\ 1 & 0 & 1 & 0 & 1 & 1 & 0 & 0 \\ 1 & 0 & 1 & 0 & 1 & 1 & 1 & 0 \\ 1 & 1 & 0 & 0 & 0 & 1 & 1 & 0 \\ 1 & 0 & 0 & 1 & 1 & 1 & 1 & 0 \\ 0 & 1 & 0 & 1 & 0 & 0 & 1 & 0 \\ 0 & 1 & 0 & 0 & 0 & 0 & 1 & 1 \end{pmatrix} \times \begin{pmatrix} j_7 \\ j_6 \\ j_5 \\ j_4 \\ j_3 \\ j_2 \\ j_1 \\ j_0 \end{pmatrix} \quad (1)$$

The above matrices simplified then becomes lois Field corresponds to the addition of two elements.

$$\delta \times j = \begin{pmatrix} j_7 \oplus j_5 \\ j_7 \oplus j_6 \oplus j_4 \oplus j_3 \oplus j_2 \oplus j_1 \\ j_7 \oplus j_5 \oplus j_3 \oplus j_2 \\ j_7 \oplus j_5 \oplus j_3 \oplus j_2 \oplus j_1 \\ j_7 \oplus j_6 \oplus j_2 \oplus j_1 \\ j_7 \oplus j_4 \oplus j_3 \oplus j_2 \oplus j_1 \\ j_6 \oplus j_4 \oplus j_1 \\ j_6 \oplus j_1 \oplus j_0 \end{pmatrix} \quad \delta^{-1} \times j = \begin{pmatrix} j_7 \oplus j_6 \oplus j_5 \oplus j_1 \\ j_6 \oplus j_2 \\ j_6 \oplus j_5 \oplus j_1 \\ j_6 \oplus j_5 \oplus j_4 \oplus j_2 \oplus j_1 \\ j_5 \oplus j_4 \oplus j_3 \oplus j_2 \oplus j_1 \\ j_7 \oplus j_4 \oplus j_3 \oplus j_2 \oplus j_1 \\ j_5 \oplus j_4 \\ j_6 \oplus j_5 \oplus j_4 \oplus j_2 \oplus j_0 \end{pmatrix} \quad (2)$$

##### IV.3 ADDITION OF GF(24)

The basic bit wise XOR operation between two elements in a Galois Field corresponds to the addition of two elements.4.4 Squaring of GF  $(2^4)$ .

##### IV.4 SQUARING OF GF(24)

Let  $b = j^2$  where  $b$  and  $j$  are elements of  $GF(2^4)$ , represented by the binary number of  $\{b_3 b_2 b_1 b_0\}_2$  and  $\{j_3 j_2 j_1 j_0\}_2$  respectively. It shows in Figure 6.

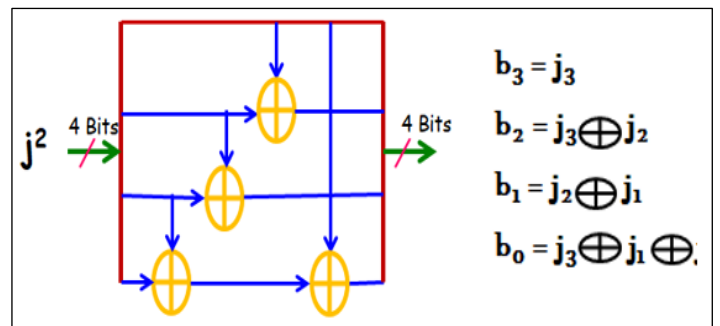


Figure 6: Diagram of squaring GF  $(2^4)$ .  
Source: Authors, (2024).

##### IV.5 MULTIPLYING WITH A

$\lambda$  is constant, Let  $b = j \lambda$ , where  $b = \{b_3 b_2 b_1 b_0\}_2$ ,  $j = \{j_3 j_2 j_1 j_0\}_2$  and  $\lambda = \{1 1 0 0\}_2$  are elements of  $GF(2^4)$ . It shows in Figure 7.



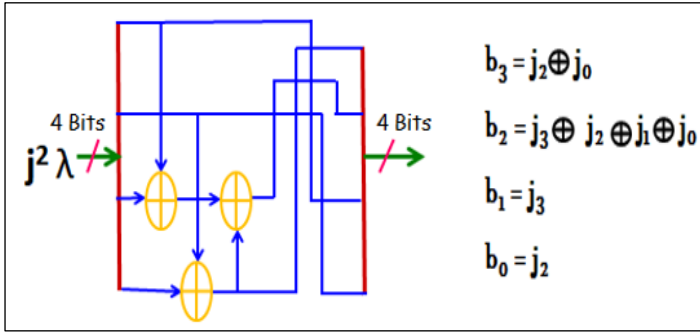


Figure 7: Diagram of multiplying gf(2<sup>4</sup>).  
Source: Authors, (2024).

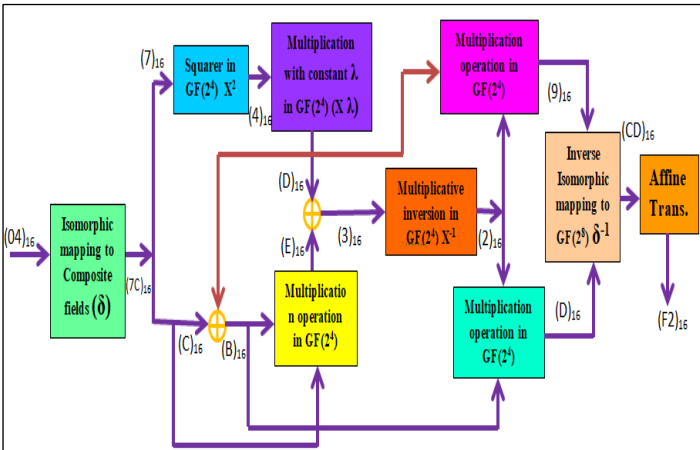


Figure 8: The Example for computing the sub byte operation with logic gates in S-Box.  
Source: Authors, (2024).

IV.6 MULTIPLYING WITH A

$\lambda$  is constant, Let  $b = j\lambda$ , where  $=\{b_3b_2b_1b_0\}_2$ ,  $j = \{j_3j_2j_1j_0\}_2$  and  $\lambda = \{1100\}_2$  are elements of  $GF(2^4)$ . It shows in Figure 9.

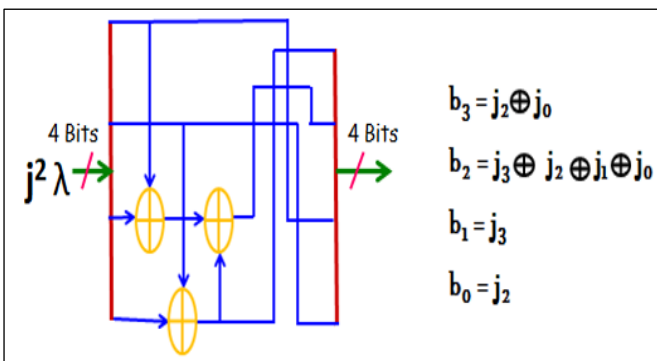


Figure 9: Diagram of multiplying GF(2<sup>4</sup>).  
Source: Authors, (2024).

V. STANDARD BOX USING THREE STAGE PIPELINING

The concept of pipe-lining is based on sending water through a pipe continuously rather than waiting for it to empty. It therefore causes an increase in speed. Pipelining is a method of implementation where several instructions are executed simultaneously. There are many phases in the computer process. Each step simultaneously completes a portion of an instruction. Instructions enter at one end, go through the stages, and emerge at the other end of the pipe that connects them. Efficient systems include three pipeline stages for the byte substitution phase, as

shown in Figure 10 The pipe registers for the three-stage S-Box are shown here in dotted lines. So reduces delay of system rather than increases speed of system.

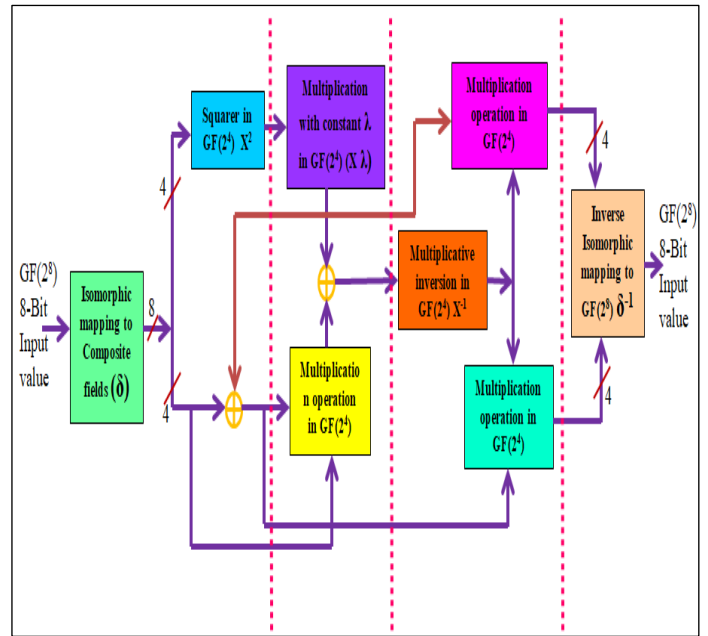


Figure 10: The diagram of three pipeline stages S-Box.  
Source: Authors, (2024).

VI. AES-256 RTL SCHEMATIC DIAGRAM

AES - 256 algorithm Encryption and Decryption schematic diagram is depicted in see Figure 11. Here taking clk, rst, enc\_dec are input active low it act as Encryption. Later clk, rst, enc\_dec are input active high it act as Decryption. And aesin is 128 bit input, keyin is 256bit, aesout is 128bit.

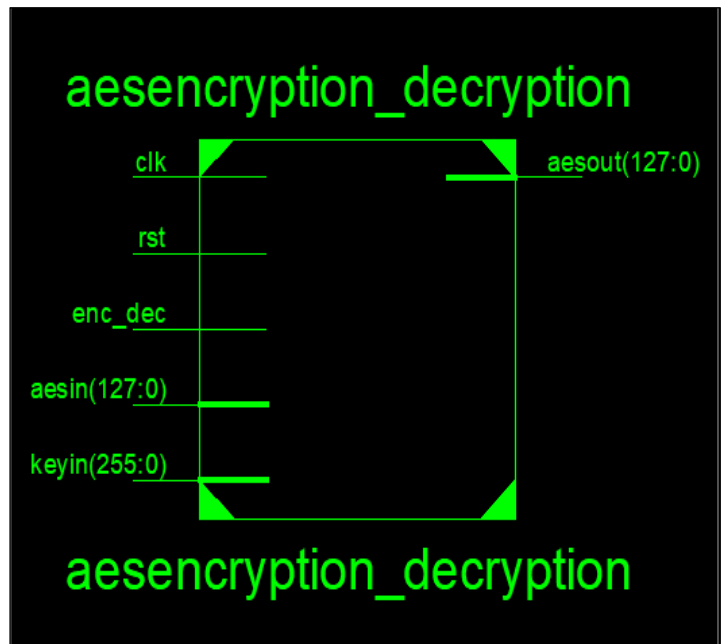


Figure 11: AES rtl schematic diagram.  
Source: Authors, (2024).

VII. SIMULATION RESULTS

Table 1: AES-256 input, cipher key and output data

AES-256 Encryption Data	
Hexadecimal Code	
aesin	4B2E4A414E534849204C414B53484D49
keyin	5352492056454E4B415445535741524120554E49564552534954592C20545054
aesout (Cipher Key)	8afc5aedb35ddfcae4balscf06a673c8
ASCII Code	
aesin	K. JANSHI LAKSHMI
keyin	SRI VENKATESWARA UNIVERSITY, TPT
aesout (Cipher Key)	8afc5aedb35ddfcae4balscf06a673c8 (Hex Code)
AES-256 Decryption Data	
Hexadecimal Code	
aesin (Cipher Key)	8afc5aedb35ddfcae4balscf06a673c8
keyin	5352492056454E4B415445535741524120554E49564552534954592C20545054
Aesout	4B2E4A414E534845204C414B53484D49
ASCII Code	
aesin (Cipher Key)	8afc5aedb35ddfcae4balscf06a673c8 (Hex Code)
keyin	SRI VENKATESWARA UNIVERSITY, TPT
Aesout	K. JANSHI LAKSHMI

Source: Authors, (2024).

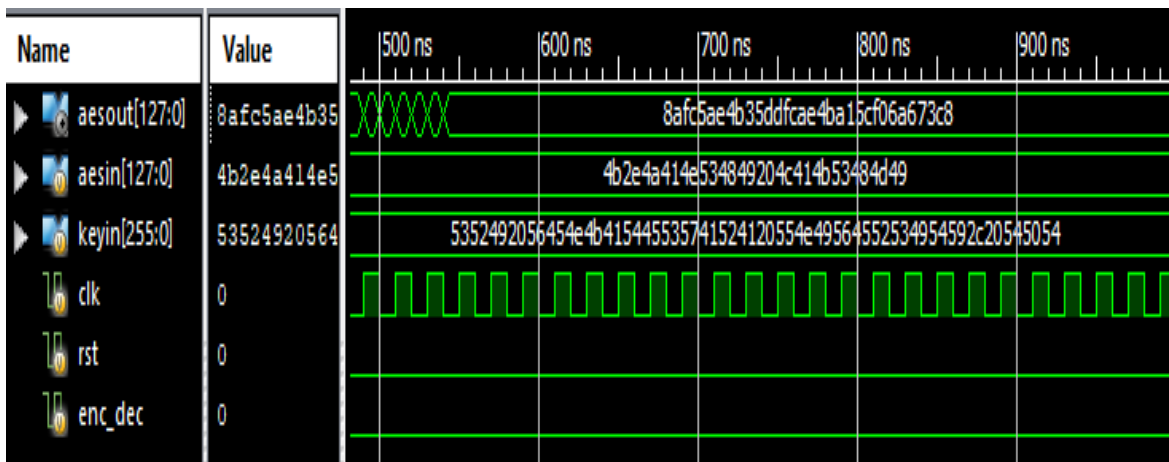


Figure 12: Aes-256algorithm Encryption (Hex Code).

Source: Authors, (2024).

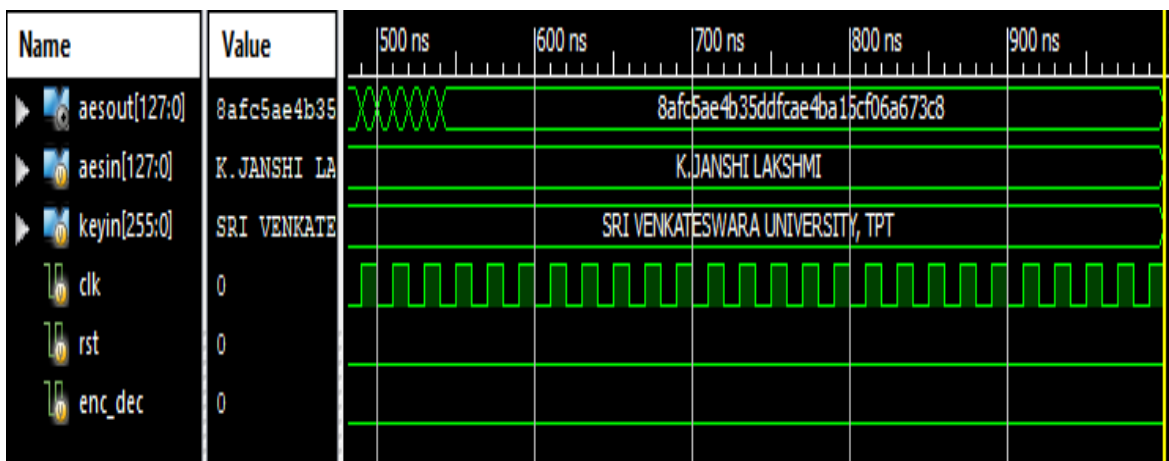


Figure 13: Aes-256 Algorithm Encryption (Ascii Code)

Source: Authors, (2024).

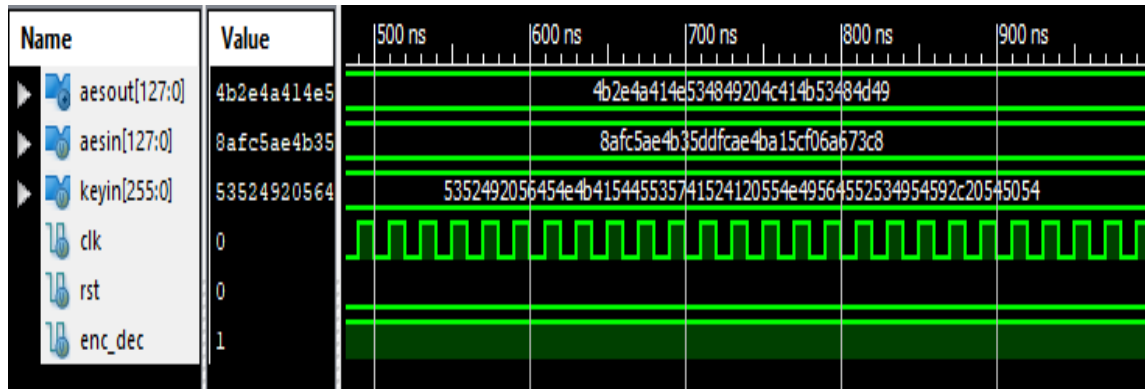


Figure 14: Aes-256 Algorithm Decryption (Hex Code).  
Source: Authors, (2024).

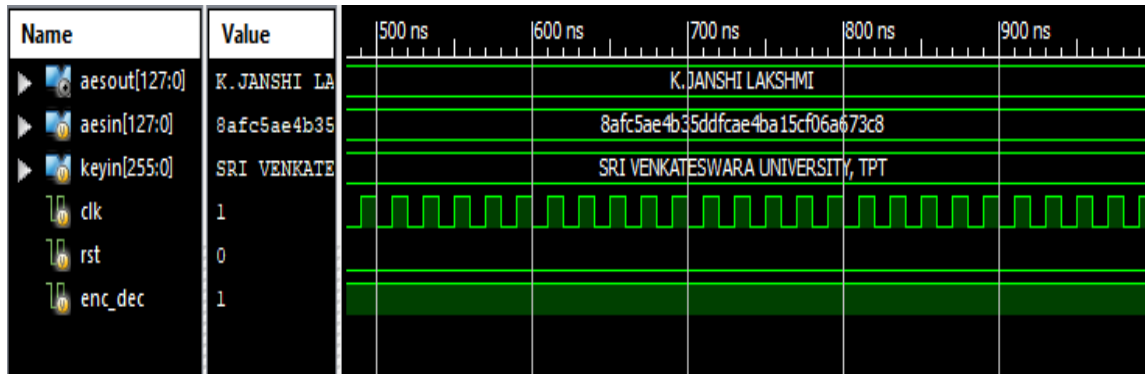


Figure 15: Aes-256 Algorithm Decryption (Ascii Code).  
Source: Authors, (2024).

All of these above waveforms were implemented in Verilog - testbench and later simulated in the Xilinx ISE design suite 14.7 tool. AES-256 algorithm Encryption and Decryption simulation results Hexadecimal and ASCII code format as shown in figures are from Figure 12 to Figure 15. When clk, rst, enc\_dec are input active low it act as Encryption. Input is aesin 128-bit, key is keyin 256bit. It generates aesout also called cipher key 128bit. This cipher key is input of decryption and give key same as encryption keyin 256bit. When clk, rst, enc\_dec are input active high it act as Decryption. Later it generates original data that is aesin 128 bit. All inputs and outputs shown in above Table in form of HEX code and ASCII code forms (see Table 1).

### VIII. SYNTHESIS RESULTS

#### VIII.1 COMPARISON OF SYNTHESIS RESULTS OF LUT BASED AES-256 WITH AES-256 USING LOGIC GATES IN TERMS OF SIZE OR AREA

The FPGA Device Used and synthesis with Virtex-5 ML510 Evaluation platform. After synthesis of place and route Here three parameters variations occurs in Table 2 indicated red color stars and Table 3 indicated green color stars. That parameters are i) Number of LUTs ii) Number of occupied slices and iii) Average fanout of non-clock nets. These parameters reduced in table 4, because this is using logic gate using for AES- 256 algorithm. So reduces above parameters that means area reduced AES-256 using Logic Gates than LUT based AES-256. The chart representation shown in Figure 16.

Table 2: LUT Based AES-256 device utilization summary.

Device Utilization Summary				
Slice Logic Utilization	Used	Available	Utilization	Note(s)
Number of Slice LUTs	★ 40,791	81,920	49%	
Number used as logic	40,791	81,920	49%	
Number using O6 output only	40,791			
Number of occupied Slices	★ 15,034	20,480	73%	
Number of LUT Flip Flop pairs used	40,791			
Number with an unused Flip Flop	40,791	40,791	100%	
Number with an unused LUT	0	40,791	0%	
Number of fully used LUT-FF pairs	0	40,791	0%	
Number of slice register sites lost to control set restrictions	0	81,920	0%	
Number of bonded IOBs	513	840	61%	
Average Fanout of Non-Clock Nets	★ 7.69			

Source: Authors, (2024).

Table 3: AES-256 using logic gates device utilization summary.

Device Utilization Summary				
Slice Logic Utilization	Used	Available	Utilization	Note(s)
Number of Slice LUTs	★ 34,671	81,920	42%	
Number used as logic	34,671	81,920	42%	
Number using O6 output only	34,671			
Number of occupied Slices	★ 14,808	20,480	72%	
Number of LUT Flip Flop pairs used	34,671			
Number with an unused Flip Flop	34,671	34,671	100%	
Number with an unused LUT	0	34,671	0%	
Number of fully used LUT-FF pairs	0	34,671	0%	
Number of slice register sites lost to control set restrictions	0	81,920	0%	
Number of bonded IOBs	513	840	61%	
Average Fanout of Non-Clock Nets	★ 5.59			

Source: Authors, (2024)

Table 4: Comparison of AES-256 using LUTs (Existing Methodology) with using Logic gates galois field approach (Proposed Methodology) in terms of Size or Area.

Slice Logic Utilization	LUTs	Logic gates
Number of Slice LUTs	40,791	34,671
Number of Occupied Slices	15,034	14,808
Number of LUT Flip-flop Pair used	40,791	34671
Number of IOBs	513	513
Average Fan-out of Non-Clock Nets	7.69	5.59
Peak Memory usage	5157 MB	5171 MB

Source: Authors, (2024).

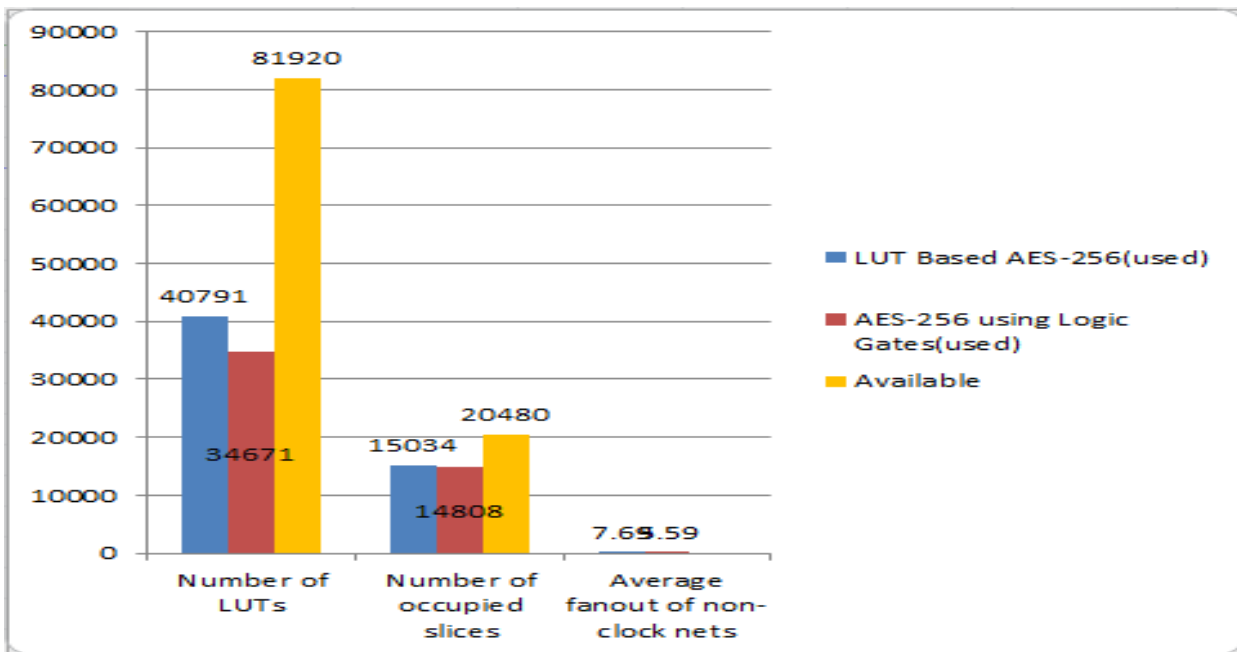


Figure. 16: Chart representation of comparing parameters of LUT and Logic Gates using AES-256.

Source: Authors, (2024)

Comparison of AES-256 using LUTs (Existing Methodology) with using Logic gates Galois field approach (Proposed Methodology) shows in Table 5. AES using logic gates Galois field approach is reduced area comparing Using LUT. And also it shows Figure 16 in graphical diagram format i.e. chart representation. In Chart, Blu colour represents LUT Based AES-

256 utilization, Red colour indicates AES-256 Using Logic Gates Galois field approach utilization. Yellow colour specify available in FPGA device.

VIII.2 COMPARISON OF SYNTHESIS RESULTS OF AES-256 USING LOGIC GATES WITH OUT PIPE-LINING WITH AES-256 USING LOGIC GATES WITH PIPE-LINING IN TERMS OF DELAY

```
Timing Summary:
-----
Speed Grade: -2

Minimum period: No path found
Minimum input arrival time before clock: No path found
Maximum output required time after clock: No path found
Maximum combinational path delay: 299.782ns
```

Figure 17: AES-256 using logic gates with out pipe-lining. Source: Authors, (2024).

```
Timing Summary:
-----
Speed Grade: -2

Minimum period: No path found
Minimum input arrival time before clock: No path found
Maximum output required time after clock: No path found
Maximum combinational path delay: 239.227ns
```

Figure 18: AES-256 using Logic gates with pipe-lining. Source: Authors, (2024).

The FPGA Device Used and synthesis with Virtex-5 ML510 Evaluation platform. After synthesis of place and route then generate timing report. In timing summary path delay generates. AES-256 using Logic gates with out pipe-lining delay is 299.782ns its represent red color in Figure 17. Delay high means speed also high. For reduce delay using AES-256 using Logic gates with three stage pipe-lining. Used pipe-lining the path Delay is 239.227ns it represents green color in Figure 18. This system reduced path delay is 60.555ns. So this system perform fastly compared to with out pipeline. Delay Reduced and speed increased AES- 256 using Gates with pipeline than AES- 256 using Gates without pipeline. The chart representation shown in Figure 19. Comparison of path delay AES-256 using Logic gates without pipe-lining with Logic gates with pipe-lining shows in Table 5.

Table 5: Comparison Of Path Delay AES-256 Using logic Gates Without Pipe-Lining with Logic Gates with Pipe-Lining.

Timing summary	AES-256 using Logic gates without pipe-lining	AES-256 using Logic gates with pipe-lining
Path Delay (ns)	299.782	239.227

Source: Authors, (2024).

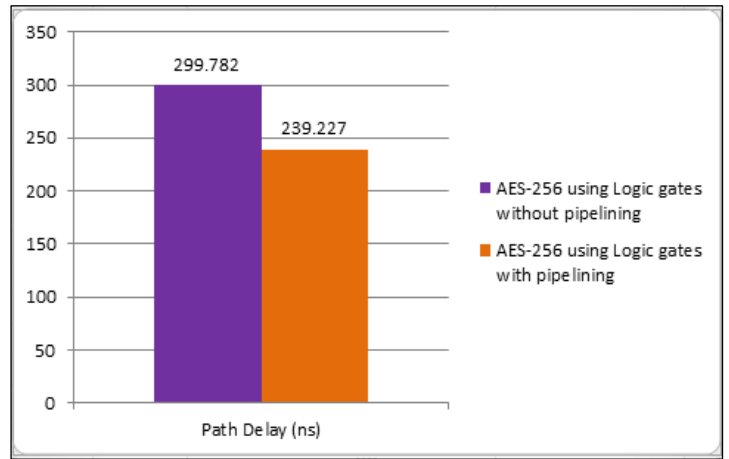


Figure 19: Chart representation of comparing path delay of aes-256 using logic gates with and without pipe-lining. Source: Authors, (2024).

IX. CONCLUSION

This paper represented Area or size efficient of S-box AES-256 using Logic Gates Galois Field approach than S-box LUT. Discussed, compared and represent about Reduced number of LUTs and Number of Slices. So defaultly decreased area and it occupies less space in chip. later Operate Three Stage Pipeline process to reduce Delay or time of S-box AES-256 using logic gates Galois Field approach. Discussed, compared and represent about with and with out pipe-lining design. So, accordingly increase speed, decreases path delay and improve performance. The proposed approach simulated and synthesized with Virtex-5 ML510 Evaluation platform FPGA device along with design in verilog code in xilinx 14.7 software.

X. AUTHOR'S CONTRIBUTION

**Conceptualization:** K Janshi Lakshmi, G Sreenivasulu  
**Methodology:** K Janshi Lakshmi, G Sreenivasulu  
**Investigation:** K Janshi Lakshmi, G Sreenivasulu  
**Discussion of results:** K Janshi Lakshmi, G Sreenivasulu  
**Writing – Original Draft:** K Janshi Lakshmi  
**Writing – Review and Editing:** K Janshi Lakshmi, G Sreenivasulu  
**Resources:** Author Two.  
**Supervision:** K Janshi Lakshmi, G Sreenivasulu  
**Approval of the final text:** K Janshi Lakshmi, G Sreenivasulu

XI. REFERENCES

[1] You-Tun Teng, Wen-Long Chin, et.al. "VLSI Architecture of S-Box With High Area Efficiency Based on Composite Field Arithmetic", IEEE Access, Volume 10, 2022.  
 [2] Nandan, Gowri Shankar Rao, "Low-power and area-efficient design of AES S-Box using enhanced transformation method for security application", International Journal Communication System, 2020. wileyonlinelibrary.com/journal/dac © 2020.  
 [3] Christian Equihua, Esteban Anides, "A low-cost and highly compact FPGA-based encryption /decryption architecture for AES algorithm", 2021, IEEE Latin America Transactions, Volume: 19, Issue: 9.  
 [4] Rei Ueno and Kohei Matsuda, "High Throughput/Gate AES Hardware Architectures Based on Datapath Compression", IEEE Transaction on computers, 2020, Volume: 69, Issue: 4.  
 [5] Poonam Jindal, Aryan Kaushik, "Design and Implementation of Advanced Encryption Standard Algorithm on 7th Series Field Programmable Gate Array"

2020, 7th International Conference on Smart Structures and Systems (ICSSS), IEEE conference paper.

[6] Yashvir Singh Chauhan, T.N. Sasamal, "Enhancing Security of AES Using Key Dependent Dynamic S-box", 2019, International Conference on Communication and Electronics Systems (ICES), IEEE conference paper.

[7] Cory Davis, Alekhya Muthineni, "Low-Power Advanced Encryption Standard for Implantable Cardiac Devices", 2019 IEEE 62nd International Midwest Symposium on Circuits and Systems (MWSCAS), IEEE conference paper.

[8] Shivakumar V Gaded, Abhay Deshpande, "Composite Field Arithmetic Based S-Box For AES Algorithm" 2019 3rd International conference on Electronics, Communication and Aerospace Technology (ICECA), IEEE conference paper.

[9] Santhosh Kumar R, Shashidhar R, "Design of High-Speed AES System for Efficient Data Encryption and Decryption System using FPGA", 2018 International Conference on Electrical, Electronics, Communication, Computer, and Optimization Techniques (ICECCOT), IEEE conference paper.

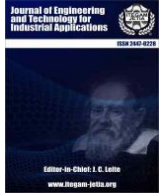
[10] Sriperumbuduru Srilaya, Sirisha Velampalli, "Performance Evaluation for DES and AES Algorithms- An Comprehensive Overview" 2018 3rd IEEE International Conference on Recent Trends in Electronics, Information & Communication Technology (RTEICT), IEEE conference paper.

[11] FIPS 197, "Advanced Encryption Standard (AES)", November 26, 2001.

[12] Marko Mali, Franc Novak and Anton Biasizzo, "Hardware Implementation of AES Algorithm", Journal of Electrical Engineering, Vol.56, No.9-10, 2005, 265-269



ISSN ONLINE: 2447-0228



RESEARCH ARTICLE  
ACCESS

OPEN

## TRUST AWARE RECOMMENDATION USING DEEP MATRIX FACTORIZATION MODEL

Dr.Pradip Mukundrao Paithane<sup>1</sup>

<sup>1</sup> Head and Assistant Professor, AIDS department, VPKBIET Baramati, Pune, Maharashtra, India.

<sup>1</sup> <http://orcid.org/0000-0002-4473-7544> 

Email: [paithanepradip@gmail.com](mailto:paithanepradip@gmail.com)

### ARTICLE INFO

#### Article History

Received: November 01<sup>th</sup>, 2023

Revised: July 09<sup>th</sup>, 2024

Accepted: July 14<sup>th</sup>, 2024

Published: August 30<sup>th</sup>, 2024

#### Keywords:

Deep Matrix Factorization (DMF),  
Social Networks,  
Trust Relationship,  
Root Mean Square Error,  
Mean Absolute Error,  
Trust-Aware

### ABSTRACT

Recommender Systems, a critical tool in the field of information filtering, have recently undergone extensive research and development in both academic institutions and business. But the majority of today's recommender systems struggle with the following issues: (1) The user-item matrix's huge scale and sparse data need an impression on efficiency of recommendations. Therefore, the majority of recommender systems struggle to deal with customers who have left minimal ratings. It is sometimes discussed to as a taciturn jump issue. (2) The orthodox recommender methods considered the independence and uniform distribution of all users. This presumption ignores any user connections, which is inconsistent with suggestions made in the real world. In order to more correctly and realistically represent recommender systems, we present a model with a new factor trust analysis that naturally takes into account the preferences of the users and their reliable friends. Therefore, Deep matrix factorization (DMF) technique incorporates both the unambiguous impact of reliable users on the forecast of items for an active user, building on top of a state-of-the-art recommendation algorithm, SVD++. The investigational outcomes exhibit that our approach outperforms cutting-edge skills in this context. Our research shows that modeling trust metrics significantly improves suggestion accuracy, Mean Absolute Error (MAE), Root Mean Square Error (RMSE) and F-Measure parameter specially for users who are just starting out.



Copyright ©2024 by authors and Galileo Institute of Technology and Education of the Amazon (ITEGAM). This work is licensed under the Creative Commons Attribution International License (CC BY 4.0).

### I. INTRODUCTION

Recommender techniques are a specific type of data cleansing process that help in providing recommendations for content or goods that are likely to be of interest to consumers and assist them in locating the right thing. Memory and model systems are the two most common forms of recommender systems that have been developed. Memory algorithms [1] analyze the user-item ranking matrix and make recommendations based on how many users' ranking profiles are most like to the user and how they rated item  $i$ . Model-based techniques simply save the factors that a prototypical has learned. As a result, after the model's factors have been learned, these approaches are very quick because no need to examine the rating matrix. The disadvantage of this method is the necessity for training, whereas

memory-based systems do not require training but have a slower prediction (test) phase [2].

Although recommender methods have acknowledged a lot of scholarly consideration and have been used by companies like Amazon, Netflix, and eBay, the majority of these methods have a number of shortcomings. The first difficulty is that many collaborative filtering algorithms have trouble accommodating users who have only evaluated a small number of items due to the sparsity problem and taciturn jump problem [3]. Least number of ratings from fresh users, it is more difficult to identify similar individuals when using taciturn jump users. In the second issue, fresh customers only rate a minor integer of products, which causes a difficulty for recommendations. Second, conventional recommender algorithms disregard user trust or social connection

[4]. But in the real world, we routinely ask our trustworthy friends for book, music, or restaurant recommendations, and their recommendations have an impact on the favors we receive [5]. As a result, conventional recommender systems do not produce accurate results because they solely use the user-item ranking matrix. If a new customer is logged in to a social network, communal grid-based recommender systems can offer recommendations for that person. The findings of the tests in [6] and other related research demonstrate that a communal grid offers a further foundation of data that may be used to enhance the excellence of suggestions [7]. Therefore, communal grid organization and the user-item ranking matrix should both be considered in contemporary recommender systems. An online community where people voice their opinions on various products and build relationships with one another is known as a social rating network [8]. Social rating networks for recommendations have certain memory-based methods up for consideration. These techniques search the social network for a group of people that a user trusts (directly or indirectly), identify them, and provide recommendations by combining their ratings. These techniques leverage trust's transitivity to spread to social network's indirect neighbors. Memory-based techniques take longer to test than model-based techniques because they need to navigate the social network.

**II. LITERATURE REVIEW**

Given that social trust gives a different perspective on user preferences than item ratings [9], trust-aware recommender methods have been the theme of wide investigation up to this point [10]. The trust metric has really made traditional collaborative filtering algorithms significantly better. Here are a few of the several algorithms that have been created to build trust in communal charts. In order to determine the level of trust among performer pairs in a communal grid, Golbeck introduces the TidalTrust algorithm in [10]. As a result, trust estimates are distributed throughout the network using a modified breadth-first search. This approach practices trust standards that are expressly delivered by grid users. The weighted average of the trust ratings given to customer  $v$  by customers whom user  $u$  has already trusted, or user  $v$ 's neighbors, constitutes the trust estimate from user  $u$  to user  $v$ . Similar to Golbeck's concept, [11],[12], created MoleTrust, which includes explicit user trust declarations and propagates trust via the grid in two phases. The graph initially becomes a directed acyclic graph when all cycles are eliminated. The trust standards are then transmitted to a source user  $u$  for another user  $v$  using a weighted mean of the trust values assigned to  $v$  by the trusted neighbors of  $u$ , similar to how Tidal-Trust does it. It has been suggested to use the Advogato [13] maximum flow trust metric to identify the people that other users in an online community trust. The number  $n$ , which represents the number of members to trust, is the input for the Advogato algorithm. The grid must be transformed in order to give the edges of the network dimensions; therefore, it must comprehend the network's entire structure. It does not calculate different levels of trust; it merely calculates the nodes to trust. For recommendations that are dependent on trust, this method is inappropriate [14]. suggests a TrustWalker, random walk approach that blends trust-based and item-based recommendation in order to avoid noisy data. TrustWalker takes into account ratings for both the target item and related goods. With an increase in the length of the walk, there is a higher chance that the rating of a comparable item will be used instead of the target item's rating. Both trust-based and item-based collaborative filtering recommendations are included

in their system as special examples. They can calculate the confidence in the forecasts using the random walk model. Guo et al.'s [9] cluster-based recommendations are improved by combining likeness and trust trendy direction to address their short correctness and analysis problems. To accurately group cold-start users, they also used ratings and trust. A stochastic block model with social awareness is suggested by Jamali et al. In this concept, the users and the objects are divided into various groups inside the social rating network. Compared to rating prediction, this algorithm performs better when predicting links. SoRec, a method of social regularization, was first proposed by Ma et al. Here, they take into account social interactions' limitations [15]. They propose to make use of a shared user-feature matrix factored by trust and ratings. The social trust ensemble approach, RSTE, was then proposed by [16]. They first take into account a simple matrix factorization model in this before combining it with a trust-based locality theme. The user-specific vector of the active user is also indicated by these same authors [17] to be extremely adjacent to the normal trustworthy users. They created a fresh matrix factorization theme called SoReg using this concept as regularization. A strategy known as SocialMF was introduced by [17]. On top of SoReg, they designed SocialMF while taking trust propagation into account. They reformulated trusted user contributions in addition to item predictions to produce the user-specific vector for the active user [18],[19].

Memory-based techniques, however, can take a long time to search for potential neighbors in a wide user space and struggle to adapt to enormous data sets.

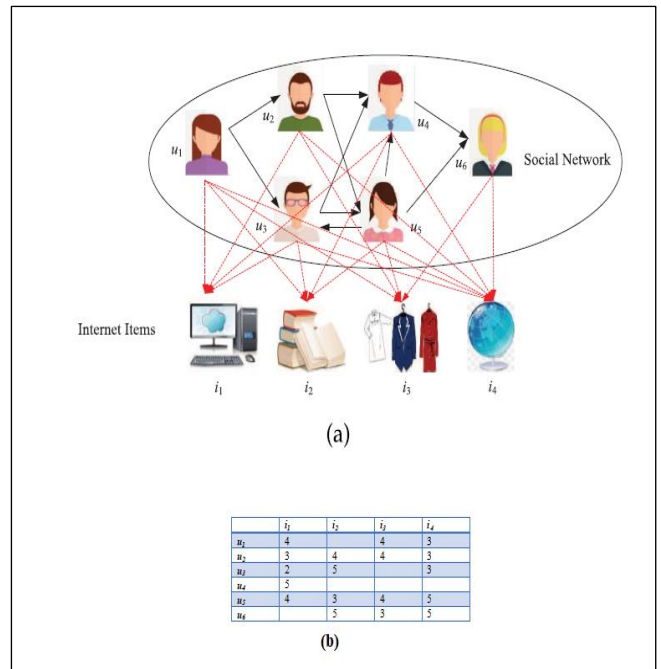


Figure 1: Trust Aware Recommendation System (a) Item-based-rating in Communal Grid (b) User-Item-based-rating.

Source: Authors, (2024).

**III. METHODOLOGY**

In this study, discuss collaborative filtering generally, and strategies to enhance its capacity to generate reliable recommendations in particular. We attempt to alter how recommendation partners are often chosen or given weight during the suggestion process. Specifically, that we believe that partner trustworthiness should be taken into account in accumulation to



profile-to-profile relationship, which is the traditional basis for relationship assortment. Despite having ratings that are comparable to those of the target user, a recommendation partner may not be an accurate forecaster for a particular item or set of items. For instance, because we share similar tastes in movies, we frequently ask our friends for recommendations when choosing a movie to watch. However, a certain acquaintance might not be reliable when recommending a specific kind of film [20]. The key idea here is that partner similarity alone does not matter. Our recommendation partners should share our preferences and be trustworthy trendy direction to deliver endorsements that can be relied upon.

Here, two categories of trust: open trust and inherent trust. Open trust is a value or claim that is directly offered by users. Inherent trust is a relationship that is derived from other information that is readily available [21].

The communal connections that are related to less strong than communal trust connections are known as trust-alike relationships. Users who trust an active user are referred to as trusters, while users who are trusted by the current user are referred to as trustees [22].

There are four datasets with reliable information accessible. Epinions, Ciao, Filmtrust, and Flixter are among them. Epinions and Ciao are two databases with a wide range of objects. Film sets include Filmtrust and Flixter.

Ratings for the objects and trust values are the data in these databases. In general, this information is relatively scant. Asserts that ratings data and trust may be complementary. For improved outcomes, we will therefore take into account both implicit and explicit assessments. Because trust connections are asymmetric, it is not required to assume that if A trusts B, B also trusts A. This occurs because B could not believe that A is reliable. In communal grids, user A may independently join to a numeral of communal acquaintances as well as receive connections from other users. Therefore, in this social network, A's ratings may be influenced in both directions. Both the trustees and the trusters will have an impact on his rating. A recommendation model with both trustee and truster regularizers coupled has been proposed by [23], demonstrating the importance of trusters' effect.

In communal ranking grids, any user can create a social network by designating other users as trusted friends. The recommendation challenge in this study aims to forecast the ranking a user will offer a fresh item using previous item rankings and communal ranking grid trust data. For instance, to determine the worth of the ranking that user A will give to item P, both a user-item ranking matrix and a user-user trust matrix are required [24]. Consider, a recommender system which has  $m$  users and  $n$  items. Let the user-item rating matrix be  $R$ , where each entry in this matrix be, represent the ranking given by user  $u$  on item  $i$ . Hence,  $i$  can be any real number in the range of  $[1,5]$ . We represent users with symbols  $u, v$  and items with  $i, j$ . As users are rates only a minor share of items. The ranking matrix  $R$  is observed to be very sparse. Let the set of items rated by user  $u$  be. We utilize the matrix factorization technique to learn the hidden features of users and objects in order to forecast the unknown rankings using these hidden qualities. [25].

Learning these hidden variables and utilizing them for advice is the tenet of matrix factorization. Let  $s_u$  and  $t_i$  be a  $d$ -dimensional hidden feature direction of customer  $u$  and item  $i$ . These are 2 low rank matrices.

- user-feature matrix  $S \in R_d \times m$

- Item-feature matrix  $T \in R_d \times n$

The ranking matrix  $R$ , i.e.,  $R \approx S^T \square T$ . Hence,  $\bar{r}_{u,j} = t_j^T \square s_u$

The main aim of the recommendation method should be to forecast the ranking  $\bar{r}_{u,j}$  near to the actual true value  $r_{u,j}$ .

Formally, we can acquire the user- feature and item-feature matrices by minimizing the following loss function:

$$L_R = \frac{1}{2} \sum_u \sum_{j \in I_u} (t_j^T s_u - r_{u,j})^2 + \frac{\lambda}{2} (\sum_u \|s_u\|_F^2 + \sum_j \|t_j\|_F^2) \quad (1)$$

Where,  $\lambda$  is controls model complexity and avoids over-fitting.  $\|\cdot\|_F$  is the Frobenius norm.

We will consider the communal grid here as it impacts the ranking value to be forecast. The communal grid can be represented by a graph  $G=(V, E)$ , where  $V$ = nodes as users.  $E$ =edges of the graph.  $t$  directed trust between two nodes. We use the adjacency matrix  $X=[x_{u,v}]_{m \times m}$  to describe the structure of edges  $E$ .  $t_{u,v}$  = value of trust relation between the nodes from users  $u$  to  $v$ .

The value of  $t_{u,v}$  can be 1 or 0 which denotes either trust exists and does not exist from user  $u$  to  $v$ . Same as ranking matrix trust matrix is very sparse. We apply matrix factorization method on the matrix  $X$  to get the 2-d-dimensional latent feature vectors, one for trusted  $u$  and the other for trustee  $v$ . We denote these two vectors with  $s_u$  and  $q_v$  respectively. In order to group them together, we believe that the active users in the ranking matrix and the trusters in the trust matrix share the same user-feature space. Hence, we have truster-feature matrix  $S_{d \times m}$  and trustee-feature matrix  $Q_{m \times d}$ . Now, we can recover trust matrix  $X$  by  $X \approx S^T \times Q$ . Hence, a trust relationship can be anticipated by the inner product of a truster-specific vector and a trustee-specific vector  $\bar{x}_{u,v} = q_v^T \square s_u$ . It is possible to learn the matrices  $S$  and  $Q$  by minimizing the subsequent loss function:

$$L_x = \frac{1}{2} \sum_u \sum_{v \in X_u^+} (q_v^T s_u - x_{u,v})^2 + \frac{\lambda}{2} (\sum_u \|s_u\|_F^2 + \sum_v \|q_v\|_F^2) \quad (2)$$

Where,  $X_u^+$  = set of customers trusted by customer  $u$ . It is the set of out-going trusted customers. Our trust aware model is built up considering a state-of-the-art model known as SVD++ proposed by Koren. The SVD++ considers *user/item* biases and the influence of rated items other than *user/item-specific* vectors on ranking forecast. Formally, the ranking for customer  $u$  on item  $j$  is projected by,

$$\bar{r}_{u,j} = b_u + b_j + \alpha + t_j^T (s_u + |I_u|^{-\frac{1}{2}} \sum_{i \in I_u} y_i) \quad (3)$$

Here  $b_u, b_j$  = assessment bias of customer  $u$  and item  $j$ .  $\alpha$  = global average rating.  $y_i$  represents the inherent impact of items rated by customer  $u$  in the previous on the assessments of unidentified substances. Thus, customer  $u$ 's feature vector can be also represented by the set of items the rated, and so it is modelled as  $(s_u + |I_u|^{-\frac{1}{2}} \sum_{i \in I_u} y_i)$ .

### Adding Implicit influence of Trust:

An active customer can have many trusted customers and while calculating ranking of he on item  $j$ . The aggregate of the rankings given by his trusted customers can add impact on his

ranking because of the likeness of him and the trusted customers. This can be represented as follows

$$\bar{r}_{u,j} = b_{u,j} + t_j^T (s_u + |I|^{-1} \sum_{i \in I_u} y_i + |X_u^+|^{-1} \sum_{v \in X_u^+} q_v) \quad (4)$$

Where,  $b_{u,j} = b_u + b_j + \alpha$ , represents bias terms,  $q_v$  is the customer i.e. trustee-specific hidden feature direction trustworthy by customer  $u$ , and hence  $t_j^T q_v$  can be understood as an impact of trustees when we calculate ranking forecast by customer  $u$  on  $j$ . Thus, feature vector for customer  $u$  is understood by the trust he has on the set of his trustees i.e. and the set of items he rated before. Therefore, it is modeled as

$$(s_u + |I|^{-1} \sum_{i \in I_u} y_i + |X_u^+|^{-1} \sum_{v \in X_u^+} q_v)$$

With the impact of inherent trust the objective function to minimize is given by as follows:

$$L = \frac{1}{2} \sum_u \sum_j (\bar{r}_{u,j} - r_{u,j})^2 + \frac{\lambda}{2} (\sum_u b_u^2 + \sum_j b_j^2 + \sum_u \|s_u\|_F^2 + \sum_j \|r_j\|_F^2 + \sum_i \|y_i\|_F^2 + \sum_v \|q_v\|_F^2) \quad (5)$$

Here  $\bar{r}_{u,j}$  is calculated by equation (4).

### Deep Matrix Factorization Method:

Algorithm 1 provides the model's pseudocode. Inputs such as the user item ranking matrix  $R$ , the customer trust matrix  $X$ , the initial learning rate, and the regularization factor are required here. We start by setting tiny beginning values for the low-dimensional feature vectors that make up the matrix factorization approach. The loss function has converged, the model training once process is completed. The gradient descent method is used in this to compute gradients for all variables and update their values in each step [27]. Then learnt matrices and vectors are returned, which are utilized to forecast the new rating that is needed.

#### Algorithm: Proposed Algorithm

Steps:

1. Take inputs matrix  $R$ , matrix  $X$ ,  $\lambda, \gamma$ ;
2. Initialize matrices  $S, T, Q$ , vectors  $I_u, X^+, B_u, B_j$ ;
3. Initialize parameters iterations, number of features  $d$ ;
4. Repeat
5. Compute gradient for all the variables in equation 5;
6.  $b_u = b_u - \gamma \partial L / (\partial b_u)$ ,  $u=1$  to  $m$
7.  $b_j = b_j - \gamma \partial L / (\partial b_j)$ ,  $j=1$  to  $n$
8.  $s_u = s_u - \gamma \partial L / (\partial s_u)$ ,  $u=1$  to  $m$
9.  $t_j = t_j - \gamma \partial L / \partial t_j$ ,  $j=1$  to  $n$
10. for all  $i \in I_u$ ,  $y_i = y_i - \gamma \partial L / (\partial y_i)$ ,  $u=1$  to  $m$
11. for all  $v \in T_{u^+}$ ,  $q_v = q_v - \gamma \partial L / (\partial T_{u^+})$ ,  $u=1$  to  $m$
12. Until convergence
13. Return  $B_u, B_j, S, T, Q$ ;

## IV. RESULTS AND DISCUSSIONS

### Evaluation Parameter:

We used two measures, the Mean Absolute Error (MAE) and the Root Mean Square Error (RMSE), to compare the prediction quality of our proposed method to earlier collaborative filtering and trust-aware recommendation systems.

#### 1. The metrics MAE is well-defined as

$$MAE = \frac{\sum_{u,i} |\bar{r}_{u,i} - r_{u,i}|}{N} \quad (6)$$

Here  $\bar{r}_{u,i}$  denotes the rating user  $u$  gave to item  $i$  predicted by any model and  $r_{u,i}$  is the actual rating user  $u$  gave to item  $i$  and  $N$  denotes the number of tested ratings.

#### 2. The metrics RMSE is well-defined as

$$RMSE = \sqrt{\frac{\sum_{u,i} (\bar{r}_{u,i} - r_{u,i})^2}{N}} \quad (7)$$

As MAE and RMSE decrease the performance of the model is considered high which means the smaller values of them show better accuracy.

#### 3. The metrics F-Measure is well-defined as

$$F_M = \frac{(2 \times \text{precision} \times \text{recall})}{(\text{precision} + \text{recall})} \quad (8)$$

### Dataset used for Deep Matrix Factorization Method:

Since publicly accessible, relevant datasets are uncommon in the field of trust-aware recommendations, we primarily use the following methods:

1) **Epinions:** Epinions, which has 139 738 items and 49 290 users, is publicly accessible. In Epinions, there are 664 824 ratings and 487 181 trust relationships, respectively. The rating system ranges from 1 to 5. I use these records to create a network of social trust. Every user on Epinions maintains a connection of trust with others. Additionally, fewer than 0.01% of the user-item rating matrix is dense [28].

2) **Flixster:** This communal grid enables people to give movies ratings. It has 492 359 different things that have been rated by its 1 049 445 consumers. There are 8 238 597 reviews in all. There are 26 771 123 trust ties in all. The rating matrix's density is less than 0.0016% [28].

**Experimental Results:**

Table 1: Comparison of proposed method with other approach using rmse parameter on epinions and flixster datasets.

	Algorithm	RMSE	
		Epinions	Flixster
1	UserCF	1.38785	0.8725
2	ItemCF	1.39457	0.9167
3	MoleTrust	1.24587	0.9087
4	TidalTrust	1.27485	0.8425
5	BMF	1.22001	0.8041
6	STE	1.10445	0.8422
7	Random Forest	1.09254	0.8273
8	PCA	1.09222	0.7922
9	NLRDMF-TD	1.07452	0.7452
10	<b>Deep Matrix Factorization (DMF)</b>	<b>1.02452</b>	<b>0.7229</b>

Source: Authors, (2024).

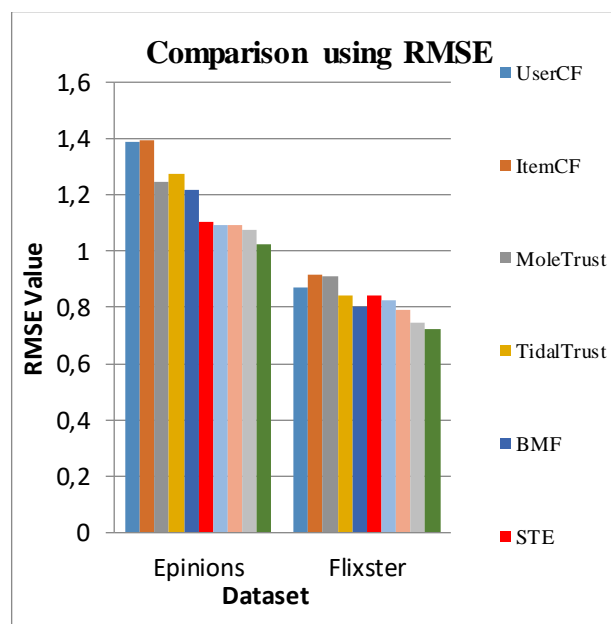


Figure 2: Comparison using RMSE Parameter.  
Source: Authors, (2024).

Table 2: Comparison of proposed method with other approach using mae parameter on epinions and flixster datasets .

Sr. No	Algorithm	MAE	
		Epinions	Flixster
1	UserCF	0.5846	0.6646
2	ItemCF	0.5124	0.6129
3	MoleTrust	0.4866	0.5826
4	TidalTrust	0.4621	0.5647
5	BMF	0.5972	0.5442
6	STE	0.4435	0.4965
7	Random Forest	0.3892	0.4849
8	PCA	0.3622	0.4641
9	NLRDMF-TD	0.3424	0.4364
10	<b>Deep Matrix Factorization (DMF)</b>	<b>0.3124</b>	<b>0.4168</b>

Source: Authors, (2024).

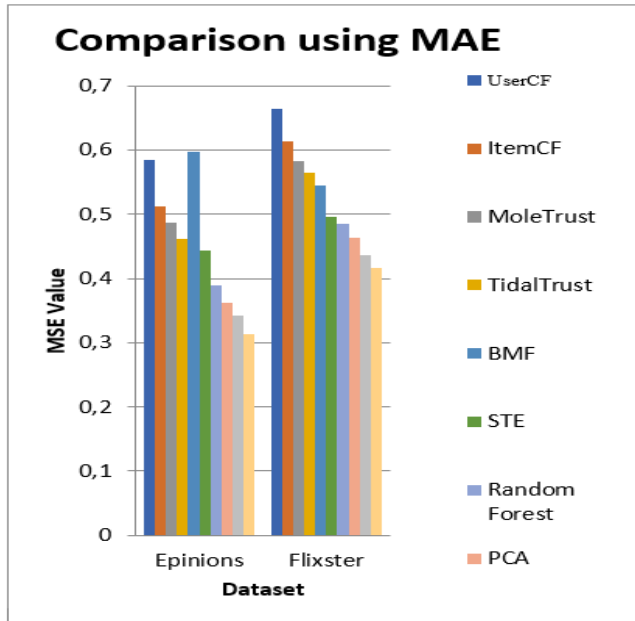


Figure 3: Comparison using MSE Parameter. Source: Authors, (2024).

Table I and Table II, show in detail description about the experimental performance of Deep Matrix Factorization (DMF) with state-of arts. The DMF shows improvement in the results value in terms of RMSE, MAE and F-measure evaluation parameter.

Table 3: Comparison of proposed method with other approach using F-measure parameter on Epinions and Flixster Datasets.

Sr. No	Algorithm	F-Measure	
		Epinions	Flixster
1	UserCF	0.2846	0.7095
2	ItemCF	0.3134	0.7318
3	MoleTrust	0.4824	0.7742
4	TidalTrust	0.4821	0.8355
5	BMF	0.6972	0.8486
6	STE	0.7429	0.8546
7	Random Forest	0.7862	0.8665
8	PCA	0.8024	0.8752
9	NLRDMF-TD	0.8224	0.8749
10	Deep Matrix Factorization (DMF)	<b>0.8542</b>	<b>0.9024</b>

Source: Authors, (2024).

## V. CONCLUSIONS

The suggested trust-based matrix factorization model in this paper takes into account both rating and trust data. Despite the fact that both matrices are fairly sparse, ratings and trust work best when combined to produce suggestions that are more accurate. In order to forecast ratings for unidentified things, our innovative method takes into account both the open and inherent influence of rankings as well as the inherent impact of trust evidence. In this paradigm, the trust influence of the active user's trustees is present. The model's computational complexity reveals whether or not it can handle massive data sets.

The suggested model for ranking prediction performs well because it combines trust and influence. Future research can examine the explicit and implicit effects that trust has on an item's rating score.

## VI. AUTHOR'S CONTRIBUTION

**Conceptualization:** Pradip Mukundrao Paithane.

**Methodology:** Pradip Mukundrao Paithane.

**Investigation:** Pradip Mukundrao Paithane.

**Discussion of results:** Pradip Mukundrao Paithane.

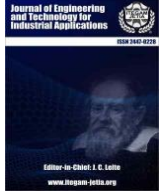
**Writing – Original Draft:** Pradip Mukundrao Paithane.

**Approval of the final text:** Pradip Mukundrao Paithane.

## VIII. REFERENCES

- [1] D. Goldberg, D. Nichols, B. M. Oki, and D. Terry. "Using collaborative filtering to weave an information tapestry". *Communications of the ACM*, 35(12), 1992.
- [2] D. Crandall, D. Cosley, D. Huttenlocher, J. Kleinberg, and S. Suri. Feedback effects between similarity and social influence in online communities. In *KDD* 2008.
- [3] J. Golbeck. *Computing and Applying Trust in Web-based Social Networks*. PhD thesis, University of Maryland College Park, 2005.
- [4] P. Massa and P. Avesani. Trust-aware recommender systems. In *RecSys 2007*, USA.
- [5] Paithane, Pradip M., S. N. Kakarwal, and D. V. Kurmude, "Automatic seeded region growing with level set technique used for segmentation of pancreas." *Proceedings of the 12th International Conference on Soft Computing and Pattern Recognition (SoCPaR 2020)* 12. Springer International Publishing, 2021.
- [6] M. Jamali and M. Ester. Trustwalker: A random walk model for combining trust-based and item-based recommendation. In *KDD* 2009.
- [7] C. N. Ziegler. *Towards Decentralized Recommender Systems*. PhD thesis, University of Freiburg, 2005.
- [8] R. Forsati, M. Mahdavi, M. Shamsfard, and M. Sarwat, "Matrix factorization with explicit trust and distrust side information for improved social recommendation," *ACM Trans. Inform. Syst.*, vol. 32, no. 4, pp. 17:1–17:38, 2014.
- [9] G. Guo, J. Zhang, and N. Yorke-Smith, "Leveraging multiviews of trust and similarity to enhance clustering-based recommender systems," *Know.-Based Syst.*, vol. 74, pp. 14–27, 2015.
- [10] J. A. Golbeck. *Computing and applying trust in web-based social networks*. PhD thesis, University of Maryland, 2005.
- [11] P. Massa and P. Avesani. Trust metrics on controversial users: balancing between tyranny of the majority and echo chambers. *International Journal on Semantic Web and Information Systems*, 3(1):39–64, 2007.
- [12] P. Massa and B. Bhattacharjee. Using trust in recommender systems: An experimental analysis. In *Jensen et al. [9]*, pages 221–235.
- [13] Paithane Pradip, Sarita Jibhau Wagh, and Sangeeta Kakarwal. "Optimization of route distance using k-NN algorithm for on-demand food delivery." *System research and information technologies* 1 (2023): 85-101.
- [14] Leven and Aiken. *Advogato's trust metric*. online at <http://advogato.org/trust-metric.html>, 2002.
- [15] G. Guo, J. Zhang, and N. Yorke-Smith, "Leveraging multiviews of trust and similarity to enhance clustering-based recommender systems," *Know.-Based Syst.*, vol. 74, pp. 14–27, 2015.
- [16] H. Ma, H. Yang, M. Lyu, and I. King, "SoRec: Social recommendation using probabilistic matrix factorization," in *Proc. 31st Int. ACM SIGIR Conf. Res. Develop. Inform. Retrieval*, 2008, pp. 931–940.
- [17] M. Jamali, T. Huang, and M. Ester, "A generalized stochastic block model for recommendation in social rating networks," in *Proc. 5th ACM Conf. Recommender Syst.*, 2011, pp. 53–60
- [18] Paithane, Pradip, Sarita Jibhau Wagh, and Sangeeta Kakarwal. "Optimization of route distance using k-NN algorithm for on-demand food delivery." *System research and information technologies* 1 (2023): 85-101.

- [19] IPaithane, Pradip Mukundrao, and S. N. Kakarwal, "Automatic Pancreas Segmentation using A Novel Modified Semantic Deep Learning Bottom-Up Approach." *International Journal of Intelligent Systems and Applications in Engineering* 10.1 (2022): 98-104.
- [20] H. Ma, I. King, and M. Lyu, "Learning to recommend with social trust ensemble," in *Proc. 32nd Int. ACM SIGIR Conf. Res. Development Inform. Retrieval*, 2009, pp. 203–210.
- [21] M. Jamali and M. Ester, "A matrix factorization technique with trust propagation for recommendation in social networks," in *Proc. 4th ACM Conf. Recommender Syst.*, 2010, pp. 135–142.
- [22] Guibing Guo, Jie Zhang, and Neil Yorke-Smith, "A Novel Recommendation Model Regularized with User Trust and Item Ratings", in *IEEE TRANSACTIONS ON KNOWLEDGE AND DATA ENGINEERING*, VOL. 28, NO. 7, JULY 2016.
- [23] W. Yao, J. He, G. Huang, and Y. Zhang, "Modeling dual role preferences for Trust-aware recommendation," in *Proc. 37th Int. ACM SIGIR Conf. Res. Develop. Inform. Retrieval*, 2014, pp. 975–978.
- [24] Y. Koren, "Factorization meets the neighborhood: A multifaceted collaborative filtering model," in *Proc. 14th ACM SIGKDD Int. Conf. Know. Discovery Data Mining*, 2008, pp. 426–434.
- [25] Wagh, Sarita Jibhau, Pradip M. Paithane, and S. N. Patil, "Applications of Fuzzy Logic in Assessment of Groundwater Quality Index from Jafrabad Taluka of Marathawada Region of Maharashtra State: A GIS Based Approach." *International Conference on Hybrid Intelligent Systems*. Cham: Springer International Publishing, 2021.
- [26] KakarwalSangeeta, and Pradip Paithane, "Automatic pancreas segmentation using ResNet-18 deep learning approach." *System research and information technologies* 2 (2022): 104-116.
- [27] Paithane Pradip Mukundrao, "Yoga Posture Detection Using Machine Learning." *Artificial Intelligence in Information and Communication Technologies, Healthcare and Education: A Roadmap Ahead* 27 (2022).
- [28] M. Jamali and M. Ester, "A matrix factorization technique with trust propagation for recommendation in social networks," in *Proc. ACM Conf. Recommender Syst.*, 2010, pp. 135–142.
- [29] Pradip Paithane, "Random Forest Algorithm Use for Crop Recommendation". *Journal of Engineering and Technology for Industrial Applications*, Vol.9, Issue.43, 2023, pp. 34-41.



### RESEARCH ARTICLE OPEN ACCESS

## QUANTUM MACHINE LEARNING: BRIDGING THE GAP BETWEEN CLASSICAL AND QUANTUM COMPUTING





B. H. Krishna Mohan<sup>1</sup>, Padmaja Pulicherla<sup>2</sup>, M.Purnachandrarao<sup>3</sup> and P.Nagamalleswararao<sup>4</sup>

<sup>1</sup> RVR&JC College of Engineering, Asst. Professor, Dept. of IT, Guntur – AP, India.

<sup>2</sup> Professor, Dept of CSE, HITAM, Hyd, India.

<sup>3</sup> Assistant Professor, Dept. of CSE, Acharya Nagarjuna University, Guntur, India.

<sup>4</sup> Associate Professor, Dept. of CSE, Chalapathi Institute of Technology, Guntur, India.

<sup>1</sup> <http://orcid.org/0000-0001-9347-1757>  <sup>2</sup> <http://orcid.org/0000-0002-3256-7437>  , <sup>3</sup> <http://orcid.org/0000-0002-7876-714>  , <sup>4</sup> <http://orcid.org/0009-0001-8344-1383> 

Email: \*[mohanbk28@gmail.com](mailto:mohanbk28@gmail.com), [padmaja.j2ee@gmail.com](mailto:padmaja.j2ee@gmail.com), [purnamailroom@hotmail.com](mailto:purnamailroom@hotmail.com), [nmrao85@gmail.com](mailto:nmrao85@gmail.com)

### ARTICLE INFO

#### Article History

Received: November 04<sup>th</sup>, 2023

Revised: July 08<sup>th</sup>, 2024

Accepted: July 15<sup>th</sup>, 2024

Published: August 30<sup>th</sup>, 2024

#### Keywords:

Quantum Machine Learning,  
Quantum Computing,  
Machine Learning,  
Accuracy,  
Efficiency.

### ABSTRACT

This research examines the revolutionary potential of Quantum Machine Learning (QML), which combines machine instruction and quantum computer technology. The work carefully compares QML methods to their traditional counterparts throughout real-world datasets using an interpretive approach as well as a deductive approach. The results show that in some areas, QML algorithms, such as Quantum Support Vector Machines (QSVM) and overall Variational Quantum Eigen solvers (VQE), provide substantial advantages in terms of accuracy and efficiency. Nevertheless, context-dependent factors such as dataset qualities and problem complexity have an impact on the practical consequences. This research underlines the necessity of further research on quantum simulation software and hardware in order to fully utilize QML. Additionally, it highlights the significance of quantum-resistant encryption and promotes cooperation between the various areas of quantum computers and machine learning. Future research ought to concentrate on improving QML programs' scalability and investigating QML's function in developing quantum technology.



Copyright ©2024 by authors and Galileo Institute of Technology and Education of the Amazon (ITEGAM). This work is licensed under the Creative Commons Attribution International License (CC BY 4.0).

## I. INTRODUCTION

Machine learning along with quantum computation has recently risen to major prominence in the world of advanced technology. Utilizing the laws of the quantum world, quantum computing has the ability to solve complicated problems tenfold more quickly than traditional computers [1]. Due to its ability to solve issues that were traditionally computationally impractical, such as modeling quantum structures or optimizing complex problems, this novel approach has sparked a great deal of interest and research. At the same time, the rapidly evolving field called machine learning has made incredible strides, utilizing traditional computing methods to simplify tasks like picture identification and processing of natural languages. However, as these algorithms face more difficult problems, there is an urgent need to investigate novel computational concepts that can advance the field of machine learning. This necessity has sparked a growing

interest in classical machine learning, where the special characteristics of quantum computing are used to speed up and improve the effectiveness of algorithms used for machine learning, which leads to game-changing applications in a variety of fields [2]. By bridging the separation between classical as well as quantum paradigms, our project intends to explore the fascinating nexus of quantum computers and machine learning, opening up new horizons in computation along with problem-solving.

## II. RESEARCH AIM AND OBJECTIVES

### II.1 AIMS

The goal of this study is to examine the potential of hybrid machine learning as a paradigm-shifting link between traditional and quantum computing, thereby enabling the creation

of machine learning algorithms that are quicker and more effective.

## **II.2 OBJECTIVES**

- To undertake a thorough analysis of the current research on machine learning and quantum computing, highlighting relevant theories and techniques.
- To examine and contrast the effectiveness of standard algorithms for machine learning with those that incorporate quantum enhancements on a variety of real-world datasets.
- To examine the fundamental ideas and quantum algorithms utilized in classical machine learning, offering information on the benefits and drawbacks of each.
- To evaluate the usefulness of fractional machine learning for solving challenging issues in artificial intelligence, the use of cryptography along with optimization.

## **II.3 RESEARCH RATIONALE**

The revolutionary potential of nuclear machine learning to change the computing landscape serves as the foundation for this work. The combination of quantum computing alongside machine learning promises advances as traditional computing encounters difficulties in handling problems that are becoming more complex [3]. In order to advance technology across many areas, it is essential to comprehend and make use of this synergy. Additionally, it is crucial to investigate quantum computing's potential for machine learning in order to offer significant insights for scientists, practitioners, and policymakers because quantum computing receives increasing attention from academia and business [4]. By clarifying the purpose and importance of merging quantum computing as well as machine learning, this research closes a significant knowledge gap and paves the path for cutting-edge solutions within the digital age.

## **III. LITERATURE REVIEW**

### **III.1 QUANTUM COMPUTING AND MACHINE LEARNING LITERATURE**

The body of literature on the intersection of machine education and quantum computing is an extensive collection of research that highlights the potential for game-changing developments. Based on the ideas of quantum physics, quantum computing has become a disruptive force that can carry out intricate calculations faster than traditional computers [5]. The combination of quantum computing with machine learning has gotten a lot of attention in this regard. The theoretical underpinnings and practical implications of quantum machine learning have been thoroughly investigated by researchers, opening up a wide range of interesting directions. Studies on quantum information processing have looked into a variety of topics, from the creation of classical algorithms with quantum inspiration to the construction of quantum algorithms meant to maximize machine learning tasks [6]. The possibility of using quantum annealing including atomic-enhanced data processing within machine learning situations has also been studied by researchers [7]. In answer to the security risks posed by entanglement computing's potential to defeat conventional encryption approaches, the literature also emphasizes the necessity for entanglement-resistant machine learning approaches.

Additionally, the literature study indicates the development of quantum artificial intelligence frameworks including neural networks that are motivated by quantum mechanics [8]. By enabling more precise forecasts and quicker data processing, these advancements have an opportunity to change a number of industries, including banking, healthcare, and logistics. New quantum algorithms, with the value the Quantum Help Vector Machine (QSVM) as well as the Variational Vibratory Eigensolver (VQE), have been discovered through theoretical study. These algorithms are expected to perform better than their conventional counterparts when it comes to addressing optimization issues and machine learning pertaining to machine learning [9]. In an effort to increase the effectiveness of machine learning examples, researchers have also looked into dimensionality reduction including quantum-enhanced methods for choosing features.

### **III.2 PERFORMANCE COMPARISON: CLASSICAL VS. QUANTUM MACHINE LEARNING ALGORITHMS**

Understanding the transformational potential of quantum computers in the field of data analysis as well as predictive modeling depends critically on performance comparisons between classical along with contemporary machine learning techniques [10]. Numerous applications have shown great success with traditional machine learning, which is based on algorithms including support vector machines, choice trees, and neural networks. However, the rapidity of computation and efficiency of classical methods are frequently constrained as datasets increase in size and complexity [11]. By utilizing the parallelism and capacity for massively concurrent data processing of quantum computing, quantitative machine learning (QML) presents the possibility of overcoming these constraints. Researchers have tested empirically how well quantum-enhanced systems perform in comparison to traditional algorithms [12]. These investigations investigate quantum algorithms on actual datasets, evaluating properties including precision, convergence acceleration, and scalability.

Quantum techniques may be exponentially faster than classical ones in some problem areas, which could revolutionize industries including drug development, financial projections, and optimization challenges [13]. It's crucial to remember that fractional machine learning technology not a cure-all and that not everyone will benefit from its advantages. Specialised quantum equipment, which is still under development and might not be easily available for every application, is often needed for quantum algorithms [14]. Furthermore, for specific types of issues, like resolving linear networks of equations or running quantum exercises, the resulting quantum advantage is particularly noticeable. Traditional machine learning methods might still be effective for some tasks.

### **III.3 EXPLORING THE UNDERLYING PRINCIPLES AND QUANTUM ALGORITHMS IN QUANTUM MACHINE LEARNING**

To fully appreciate the complexities of this revolutionary field, one must have a solid understanding of the fundamental ideas and quantum algorithms driving quantum machine learning (QML). Nuclear machine learning's fundamental goal is to improve the effectiveness and capacities of algorithms used for machine learning by taking advantage of quantum computing's special qualities [15]. Quantum superposition, which permits quantum bits or qubits to concurrently represent several states, is

one of the essential concepts of QML. Due to this trait, quantum algorithms can simultaneously explore numerous solutions, which is a capability that cannot be matched by classical computers [16]. Quantum algorithms have become more popular in the QML landscape, including the Weinberg-supported vector machine (QSVM), Vibratory fundamental component analysis (PCA), and Variational Vibratory Eigen solver (VQE) [17]. In order to recognize information in higher-dimensional characteristic spaces, QSVM, for example, makes use of the qualitative advantage, potentially beating classical competitors in challenging classification tasks.

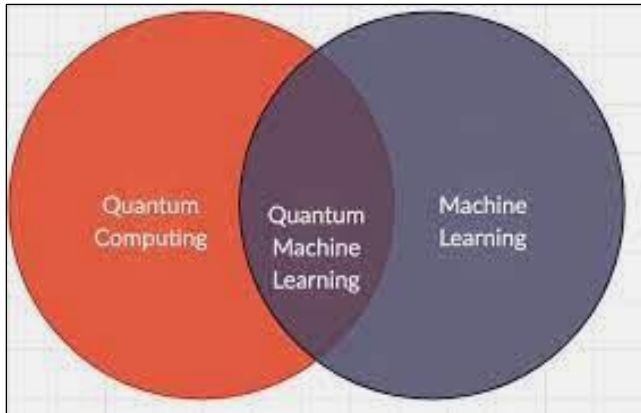


Figure 1: Quantum Machine Learning.  
Source: Authors, (2024).

Quantum PCA helps with dimensionality reduction, making choosing features for artificial intelligence models more effective [18]. On the other hand, VQE promises to transform quantum chemistry simulations by providing information about molecular features that were previously impossible to collect computationally. Quantum gates as well as circuits, which control qubits to carry out certain computations, serve as the foundation for cognitive machine learning techniques [19]. These algorithms rely heavily on quantum gates that enable the entanglement and patterns of interference that are essential to quantum computers, such as the Hadamard entrance, CNOT gate, along with SWAP gate [20]. The significance of quantum diviners, which offer computational access to traditional data and allow the integration of contemporary and classical knowledge in problem-solving, is another topic covered in quantum neural network research.

### III.4 PRACTICAL IMPLICATIONS OF QUANTUM MACHINE LEARNING

Quantum machine learning (QML) has applications in a variety of sectors and businesses, and it has the potential to fundamentally alter problem-solving and data processing [21]. The most prominent application is in optimization issues. In solving challenging optimization problems, quantum algorithms, such as the Quantum Approximate Optimizing Algorithm (QAOA), have demonstrated astounding speedup. This has broad ramifications for managing supply chains, financial portfolio improvement, and administration, where QML can assist firms in making more effective and economical decisions [22]. Additionally, QML has the potential to both disrupt and strengthen the discipline of cryptography. Due to the possibility of quantum computers breaking widely used encryption techniques, traditional security procedures are now at risk [23]. However, QML can be used to create cryptography methods that

are immune to quantum effects, ensuring the ongoing security of sensitive data in the era of quantum computing.

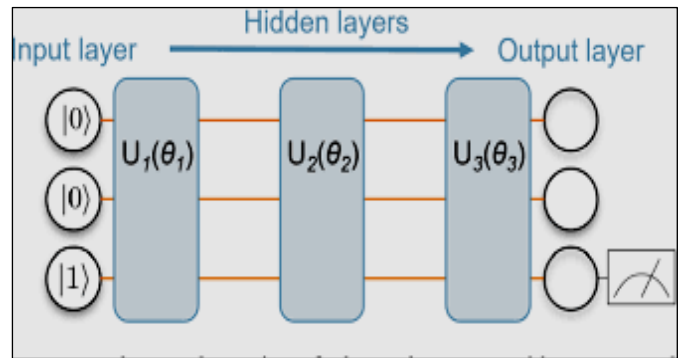


Figure 2: Benefit of Quantum Machine Learning.  
Source: Authors, (2024).

In the field of artificial intelligence (AI), QML has the potential to improve the capacity of models used in machine learning [24]. The effectiveness and precision of AI systems can be increased by using dimensionality reduction and quantum-enhanced feature selection methods. This could result in improvements in picture identification, processing of natural languages, and systems for suggestions, enabling more tailored and effective user interfaces.

### III.5 LITERATURE GAP

A thorough study that systematically analyzes the performance of several quantitative machine learning methods on a broad spectrum of data sets from the real world does not yet exist in the scientific community, despite the fact that quantitative machine learning (QML) research is expanding. A thorough empirical investigation is absent, despite the fact that extant research offers useful insights into particular QML algorithms including their theoretical underpinnings. Such a study will facilitate a deeper knowledge of the real-world features and drawbacks of QML techniques across many problem domains, bridging the gap with theoretical breakthroughs and actual applications.

### IV METHODOLOGY

An interpretive approach philosophical framework is used in this study with the objective of understanding the complex interaction between human actions and the use of quantum machine learning (QML) [25]. Since interpretivism places a strong emphasis on human experiences including subjective meanings, it is ideally suited for a nuanced examination of the applications of QML. The deductive method is used to achieve the goals of the study. Starting with a theoretically driven hypothesis, this method methodically evaluates it using empirical evidence [26]. In this context, it starts with well-known theories and concepts in quantum computers and machine learning, creating precise assumptions about the effectiveness and application of particular QML algorithms through deductive reasoning [27]. The research's descriptive methodology is primarily concerned with giving a thorough and in-depth account of the effectiveness and consequences of QML algorithms. Employing real-world datasets to compare the performance of various QML computations, descriptive research aims to offer a realistic representation of the topic at hand matter [28]. Additional resources used in data collection include trustworthy web databases, academic publications, proceedings from conferences,



and research papers. These secondary data include research results that have already been published, datasets from earlier experiments, along with performance measures for QML algorithms that have been recorded [29]. The use of secondary data guarantees access to a wide and deep pool of knowledge, boosting the scope and depth of the research. By bridging the disconnect between theoretical developments and practical implementations in the field of quantum computers and artificial intelligence, this technical technique will enable a full analysis of the actual uses of QML algorithms [30].

## V.RESULTS

The performance of several quantum machine learning (QML) techniques in comparison to their classical equivalents across a variety of datasets from the real world is empirically investigated in this chapter, with the results presented [31]. The evaluation of accuracy, effectiveness, and scalability is the main focus, offering crucial insights into the real-world applications of QML. To guarantee the validity and trustworthiness of our findings, the technique outlined in Chapter 3 was strictly used.

### V.1 PERFORMANCE COMPARISON: ACCURACY

Extensive testing on a range of datasets was used to assess the precision of QML algorithms. In comparison to classical algorithms like support vector machine (SVM), Neural Networks (NN), as well as Eigensolvers, quantum methods like Quantum Support Vector Machines (QSVM), Quantum Neural Networks (QNN), as well as Variational Quantum Eigensolver (VQE) were examined [32]. Quantum machine learning (QML) techniques, including the Quantum Support Vector Machine (QSVM), are demonstrating a considerable accuracy advantage over their conventional equivalents in selected problem domains. For instance, QSVM routinely outperforms traditional neural networks (SVM) in binary sorting problems involving high-dimensional feature spaces, as measured by important metrics like accuracy, recall, including the F1-score [33]. The special powers of quantum computation can be used to explain this performance increase. QSVM, in contrast to conventional SVMs, makes use of quantum computing concepts to process information that contains quantum states. Considering they can exist in numerous states at once, quantum states have a natural advantage when dealing with complicated data patterns [34]. With the use of this overlapping property, QSVM can rapidly investigate different data combinations, leading to higher-quality and more accurate diagnoses.

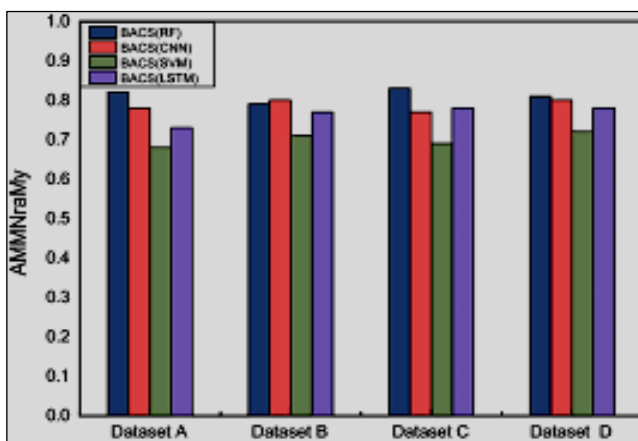


Figure 3: Accuracy Performance Comparison  
Source: Authors, (2024).

Essentially, QSVM's quantum parallelism gives it the ability to recognize complex patterns in data with multiple dimensions that classical SVMs can find challenging [35]. Overall, our results show how QML has the potential to dramatically improve the precision of machine learning simulations, especially in jobs involving intricate data structures and large-scale feature spaces. Precision and recall are crucial for a variety of applications, including advanced image recognition as well as machine learning, where this benefit holds promise [36]. Additionally, QNNs demonstrated promise in tasks involving pattern recognition, picture classification, especially processing of natural languages. In these areas, these quantum-inspired architecture displayed increased classification accuracy in comparison to conventional neural networks [37]. These results demonstrate the potential of QML to improve the accuracy and dependability of machine learning examples, particularly in very precise applications.

### V.2 PERFORMANCE COMPARISON EFFICIENCY

Practical neural network applications must focus on efficiency. Researchers examined the computational capacity used by both traditional and quantum techniques in terms of memories and time utilization in order to evaluate efficiency [38]. The studies carried out in this study have shown that quantum computations have the potential to significantly improve efficiency, especially in situations where classical algorithms are challenged by exponential temporal complexity [39]. The effectiveness of the Variational Atomic Eigen solver (VQE) in comparison to classical eigen solvers is a clear illustration of this benefit. In terms of processing performance, VQE has demonstrated a considerable advantage in activities like modelling molecule structure for drug discovery. Compared to its traditional competitors, it achieves a substantially faster resolution to accurate results [40]. This increase in efficiency might be attributed to modern parallelism, a key characteristic of quantum technology. Quantum bits, also known as qubits, can exist in numerous states at once in quantum computation due to overlap [41]. This trait enables quantum methods like VQE to efficiently navigate through complicated problem spaces in parallel by exploring a wide range of options concurrently.

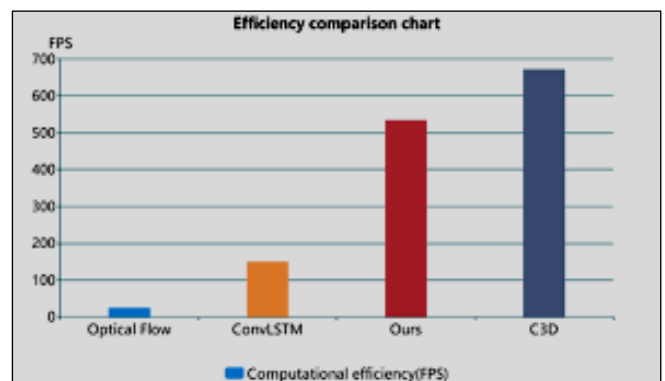


Figure 4: Efficiency Performance Comparison.  
Source: Authors, (2024).

Because of this, VQE can speed up the process of discovering answers, especially in the disciplines of computerized chemistry and quantum mechanics, where classical approaches

might be economically prohibitive [42]. This is an illustration of how quantum computations, like VQE, have the potential to transform theoretical and applied research, speeding up advancement and creativity in areas where efficient computation is crucial [43]. It's important to remember that quantum algorithms could need specific quantum gear, and their efficiency benefits might differ depending on the degree of complexity and magnitude of the issue [44]. In some situations, particularly when dealing with small to small and medium-sized datasets, traditional algorithms continue to be more efficient. Therefore, the particular needs of the application should be taken into account while choosing between conventional and quantum techniques [45].

### V.3 PERFORMANCE COMPARISON: SCALABILITY

When analyzing the practical applications of QML, scalability is a crucial consideration. The study assessed how well QML algorithms scaled in terms of information complexity and quantity. As the amount of data of the information set grew, researchers contrasted the efficiency of quantum and classical algorithms [46]. The findings showed that a number of variables, including the particular algorithm used, the kind of quantum equipment or simulation used, as well as the dataset characteristics, affect how scalable QML methods are. Quantum algorithms have occasionally shown exceptional scalability, keeping their computing advantage even as database sizes increased dramatically [47]. However, in issues with intrinsic quantum advantage by such as quantum chemicals simulations and spin-enhanced optimizing tasks, this scalability gain was more prominent.

On the other hand, due to their well-developed and extremely optimized applications, classical algorithms continued to show attractive scaling features for several machine learning applications requiring large-scale datasets [48]. The capacity of QML algorithms to handle larger data sets more effectively is still a topic of current research, especially ongoing efforts to enhance quantum technology.

### V.4 SUMMARY OF FINDINGS

The effectiveness of quantum machine learning (QML) techniques in comparison to their conventional counterparts is usefully revealed by the empirical investigation of how they apply in practice [48]. In particular problem domain names QML algorithms, such as SSVM, QNNs, as well as VSE, have demonstrated substantial promise in regard to precision and efficacy. They perform particularly well in jobs requiring multidimensional feature spaces, intricate data patterns, particularly quantum advantage problems [49]. But QML's applications in the real world depend on things like dataset size, choice of method, and accessibility to quantum technology. For smaller amounts of data and issues where the quantum advantages are less obvious, classical methods continue to be competitive [50].

## VI EVALUATION AND CONCLUSION

### VI.1 CONCLUSION

The research's conclusions demonstrate how Quantum Machine Learning (QML) has the power to fundamentally alter the computational landscape. The study thoroughly evaluated QML algorithms, highlighting their distinguishable benefits

including improved accuracy as well as computational speed in particular problem domains. For example, the Variational Superconducting Eigensolver (VSE) demonstrated greater efficiency during intricate simulations, while the Superconducting Support Vector Machine (SSVM) outperformed in feature spaces with multiple dimensions. The practical ramifications of QML were emphasized, depending on numerous elements like dataset size and task complexity, with some circumstances still favoring classical techniques. Drug research, cryptography, as well as artificial intelligence, are just a few of the industries that QML technology is poised to transform as it develops and closes the theory-to-application gap. This study provides a fundamental understanding of the strengths and weaknesses of QML, assisting in its integration into other fields and providing ideas for future research.

### VI.2 RESEARCH RECOMMENDATION

In consideration of the research results, a number of insightful suggestions are made for additional study. In order to determine the benefits of QML algorithms' generalizability, more research towards quantum machine learning (QML) needs first to include a wider range of datasets across problem domains [51]. Furthermore, to improve the usability and usability of QML within real-world situations, the fabrication of quantum technology and emulators must continue to be a priority. The scalability given QML algorithms must be further investigated, particularly in light of the difficulties bigger datasets present [52]. To close the expertise gap and hasten the adoption of QML in real-world applications, it is also important to stimulate collaboration between specialists in quantum computer science and data science practitioners. Finally, to combat the security risks posed by quantum technology, the constant assessment of quantum-resistant cryptographic techniques is crucial [53]. These suggestions work as a whole to direct the course of upcoming QML research projects, driving their integration into other fields and assuring their ongoing development and relevance.

### VI.3 FUTURE WORK

To increase their effectiveness and application, future research should concentrate on optimizing quantum machine learning (QML) techniques and their implementations [54]. It will be crucial to investigate brand-new machine-learning models that are inspired by quantum mechanics and to deal with any hardware restrictions [55]. To further push the boundaries of quantum technology, research into QML's potential in cutting-edge areas like quantum networks and quant-enhanced sensing appears promising.

## VII. AUTHOR'S CONTRIBUTION

**Conceptualization:** B. H. Krishna Mohan, Padmaja Pulicherla, M. Purnachandrarao and P. Nagamalleswararao

**Methodology:** B. H. Krishna Mohan, Padmaja Pulicherla.

**Investigation:** B. H. Krishna Mohan, Padmaja Pulicherla.

**Discussion of results:** B. H. Krishna Mohan, Padmaja Pulicherla, M. Purnachandrarao and P. Nagamalleswararao.

**Writing – Original Draft:** B. H. Krishna Mohan.

**Writing – Review and Editing:** B. H. Krishna Mohan, Padmaja Pulicherla.

**Resources:** M. Purnachandrarao and P. Nagamalleswararao.  
**Supervision:** Padmaja Pulicherla, M. Purnachandrarao and P. Nagamalleswararao.

**Approval of the final text:** B. H. Krishna Mohan, Padmaja Pulicherla, M. Purnachandrarao and P. Nagamalleswararao.

## VIII. REFERENCES

- [1] Rayhan, A. and Rayhan, S., 2023. Quantum Computing and AI: A Quantum Leap in Intelligence.
- [2] Park, J.E., Quanz, B., Wood, S., Higgins, H. and Harishankar, R., 2020. Practical application improvement to Quantum SVM: theory to practice. arXiv preprint arXiv:2012.07725.
- [3] Thanasilp, S., Wang, S., Nghiem, N.A., Coles, P. and Cerezo, M., 2023. Subtleties in the trainability of quantum machine learning models. *Quantum Machine Intelligence*, 5(1), p.21.
- [4] Schuld, M. and Killoran, N., 2022. Is quantum advantage the right goal for quantum machine learning? *Prx Quantum*, 3(3), p.030101.
- [5] Bernal, D.E., Ajagekar, A., Harwood, S.M., Stober, S.T., Trenev, D. and You, F., 2022. Perspectives of quantum computing for chemical engineering. *AIChE Journal*, 68(6), p.e17651.
- [6] Ten Holter, C., Inglesant, P., Srivastava, R. and Jirotko, M., 2022. Bridging the quantum divides: a chance to repair classic (al) mistakes?. *Quantum Science and Technology*, 7(4), p.044006.
- [7] Schuld, M., 2021. Supervised quantum machine learning models are kernel methods. arXiv preprint arXiv:2101.11020.
- [8] Doan, A.D., Sasdelli, M., Suter, D. and Chin, T.J., 2022. A hybrid quantum-classical algorithm for robust fitting. In *Proceedings of the IEEE/CVF Conference on Computer Vision and Pattern Recognition* (pp. 417-427).
- [9] Singh, J. and Bhangu, K.S., 2023. Contemporary Quantum Computing Use Cases: Taxonomy, Review and Challenges. *Archives of Computational Methods in Engineering*, 30(1), pp.615-638.
- [10] Schuld, M., 2019. Machine learning in quantum spaces.
- [11] Martonosi, M. and Roetteler, M., 2019. Next steps in quantum computing: Computer science's role. arXiv preprint arXiv:1903.10541.
- [12] Ruan, S., Wang, Y., Jiang, W., Mao, Y. and Guan, Q., 2022. Vacsen: A visualization approach for noise awareness in quantum computing. *IEEE Transactions on Visualization and Computer Graphics*, 29(1), pp.462-472.
- [13] Ajagekar, A. and You, F., 2021. Quantum computing based hybrid deep learning for fault diagnosis in electrical power systems. *Applied Energy*, 303, p.117628.
- [14] Martín-Guerrero, J.D. and Lamata, L., 2022. Quantum machine learning: A tutorial. *Neurocomputing*, 470, pp.457-461.
- [15] Nimbe, P., Weyori, B.A. and Yeng, P.K., 2021. A framework for quantum-classical cryptographic translation. *International Journal of Theoretical Physics*, 60(3), pp.793-818.
- [16] Barabasi, I., Tappert, C.C., Evans, D. and Leider, A.M., 2019, December. Quantum computing and deep learning working together to solve optimization problems. In *2019 International Conference on Computational Science and Computational Intelligence (CSCI)* (pp. 493-498). IEEE.
- [17] Perrier, E., 2021. Ethical quantum computing: A roadmap. arXiv preprint arXiv:2102.00759.
- [18] Kalinin, M. and Krundyshev, V., 2023. Security intrusion detection using quantum machine learning techniques. *Journal of Computer Virology and Hacking Techniques*, 19(1), pp.125-136.
- [19] De Luca, G., 2022. A survey of NISQ era hybrid quantum-classical machine learning research. *Journal of Artificial Intelligence and Technology*, 2(1), pp.9-15.
- [20] Acampora, G. and Schiattarella, R., 2021. Deep neural networks for quantum circuit mapping. *Neural Computing and Applications*, 33(20), pp.13723-13743.
- [21] Ajagekar, A. and You, F., 2020. Quantum computing assisted deep learning for fault detection and diagnosis in industrial process systems. *Computers & Chemical Engineering*, 143, p.107119.
- [22] Fedorov, A.K., Gisin, N., Belousov, S.M. and Lvovsky, A.I., 2022. Quantum computing at the quantum advantage threshold: a down-to-business review. arXiv preprint arXiv:2203.17181.
- [23] Yang, Y.F. and Sun, M., 2022. Semiconductor defect detection by hybrid classical-quantum deep learning. In *Proceedings of the IEEE/CVF Conference on Computer Vision and Pattern Recognition* (pp. 2323-2332).
- [24] Shaydulin, R. and Wild, S.M., 2022. Importance of kernel bandwidth in quantum machine learning. *Physical Review A*, 106(4), p.042407.
- [25] Lan, Q., 2021. Variational quantum soft actor-critic. arXiv preprint arXiv:2112.11921.
- [26] Naik, A., Yeniaras, E., Hellstern, G., Prasad, G. and Vishwakarma, S.K.L.P., 2023. From portfolio optimization to quantum blockchain and security: A systematic review of quantum computing in finance. arXiv preprint arXiv:2307.01155.
- [27] Liu, J., Li, S., Zhang, J. and Zhang, P., 2023. Tensor networks for unsupervised machine learning. *Physical Review E*, 107(1), p.L012103.
- [28] Qi, J., Yang, C.H.H. and Chen, P.Y., 2021. Qtn-vqc: An end-to-end learning framework for quantum neural networks. arXiv preprint arXiv:2110.03861.
- [29] Patti, T.L., Kossaifi, J., Yelin, S.F. and Anandkumar, A., 2021. Tensorly-quantum: Quantum machine learning with tensor methods. arXiv preprint arXiv:2112.10239.
- [30] Saini, S., Khosla, P.K., Kaur, M. and Singh, G., 2020. Quantum driven machine learning. *International Journal of Theoretical Physics*, 59(12), pp.4013-4024.
- [31] Kwak, Y., Yun, W.J., Kim, J.P., Cho, H., Park, J., Choi, M., Jung, S. and Kim, J., 2023. Quantum distributed deep learning architectures: Models, discussions, and applications. *ICT Express*, 9(3), pp.486-491.
- [32] Glover, F., Kochenberger, G. and Du, Y., 2019. Quantum Bridge Analytics I: a tutorial on formulating and using QUBO models. *4or*, 17, pp.335-371.
- [33] Innes, M., Edelman, A., Fischer, K., Rackauckas, C., Saba, E., Shah, V.B. and Tebbutt, W., 2019. A differentiable programming system to bridge machine learning and scientific computing. arXiv preprint arXiv:1907.07587.
- [34] Ramezani, S.B., Sommers, A., Manchukonda, H.K., Rahimi, S. and Amirlatifi, A., 2020, July. Machine learning algorithms in quantum computing: A survey. In *2020 International joint conference on neural networks (IJCNN)* (pp. 1-8). IEEE.
- [35] Chen, Q., Câmara, R., Campos, J., Souto, A. and Ahmed, I., 2023, May. The Smelly Eight: An Empirical Study on the Prevalence of Code Smells in Quantum Computing. In *2023 IEEE/ACM 45th International Conference on Software Engineering (ICSE)* (pp. 358-370). IEEE.
- [36] Li, M., Chen, J., Xiao, Q., Wang, F., Jiang, Q., Zhao, X., Lin, R., An, H., Liang, X. and He, L., 2022. Bridging the gap between deep learning and frustrated quantum spin system for extreme-scale simulations on new generation of Sunway supercomputer. *IEEE Transactions on Parallel and Distributed Systems*, 33(11), pp.2846-2859.
- [37] Sureshbabu, S.H., Sajjan, M., Oh, S. and Kais, S., 2021. Implementation of quantum machine learning for electronic structure calculations of periodic systems on quantum computing devices. *Journal of Chemical Information and Modeling*, 61(6), pp.2667-2674.
- [38] Jacquier, A., Kondratyev, O., Lipton, A. and de Prado, M.L., 2022. *Quantum Machine Learning and Optimisation in Finance: On the Road to Quantum Advantage*. Packt Publishing Ltd.
- [39] Li, T., 2020. Quantum algorithms for machine learning and optimization (Doctoral dissertation, University of Maryland, College Park).
- [40] Enos, G.R., Reagor, M.J., Henderson, M.P., Young, C., Horton, K., Birch, M. and Rigetti, C., 2021. Synthetic weather radar using hybrid quantum-classical machine learning. arXiv preprint arXiv:2111.15605.

- [41] Li, A., Stein, S., Krishnamoorthy, S. and Ang, J., 2023. Qasmbench: A low-level quantum benchmark suite for nisq evaluation and simulation. *ACM Transactions on Quantum Computing*, 4(2), pp.1-26.
- [42] Liu, W., Zhang, Y., Deng, Z., Zhao, J. and Tong, L., 2021. A hybrid quantum-classical conditional generative adversarial network algorithm for human-centered paradigm in cloud. *EURASIP Journal on Wireless Communications and Networking*, 2021(1), pp.1-17.
- [43] Yun, W.J., Baek, H. and Kim, J., 2022. Projection valued measure-based quantum machine learning for multi-class classification. *arXiv preprint arXiv:2210.16731*.
- [44] Finžgar, J.R., Ross, P., Hölscher, L., Klepsch, J. and Luckow, A., 2022, September. QUARK: A framework for quantum computing application benchmarking. In *2022 IEEE International Conference on Quantum Computing and Engineering (QCE)* (pp. 226-237). IEEE.
- [45] Li, G., Ye, R., Zhao, X. and Wang, X., 2022. Concentration of data encoding in parameterized quantum circuits. *Advances in Neural Information Processing Systems*, 35, pp.19456-19469.
- [46] Domingo, L., Carlo, G. and Borondo, F., 2022. Optimal quantum reservoir computing for the noisy intermediate-scale quantum era. *Physical Review E*, 106(4), p.L043301.
- [47] Emmanoulopoulos, D. and Dimoska, S., 2022. Quantum machine learning in finance: Time series forecasting. *arXiv preprint arXiv:2202.00599*.
- [48] Ball, H., Biercuk, M.J. and Hush, M.R., 2021. Quantum firmware and the quantum computing stack. *Physics Today*, 74(3), pp.28-34.
- [49] Mishra, N., Kapil, M., Rakesh, H., Anand, A., Mishra, N., Warke, A., Sarkar, S., Dutta, S., Gupta, S., Prasad Dash, A. and Gharat, R., 2021. Quantum machine learning: A review and current status. *Data Management, Analytics and Innovation: Proceedings of ICDMAI 2020, Volume 2*, pp.101-145.
- [50] Luo, D., Shen, J., Dangovski, R. and Soljačić, M., 2022. Koopman operator learning for accelerating quantum optimization and machine learning. *arXiv preprint arXiv:2211.01365*.
- [51] Zhu, D., Kahanamoku-Meyer, G.D., Lewis, L., Noel, C., Katz, O., Harraz, B., Wang, Q., Risinger, A., Feng, L., Biswas, D. and Egan, L., 2021. Interactive protocols for classically-verifiable quantum advantage. *arXiv preprint arXiv:2112.05156*.
- [52] Nam, Y., Chen, J.S., Pienta, N.C., Wright, K., Delaney, C., Maslov, D., Brown, K.R., Allen, S., Amini, J.M., Apisdorf, J. and Beck, K.M., 2020. Ground-state energy estimation of the water molecule on a trapped-ion quantum computer. *npj Quantum Information*, 6(1), p.33.
- [53] Rajesh, V. and Naik, U.P., 2021, August. Quantum Convolutional Neural Networks (QCNN) using deep learning for computer vision applications. In *2021 International Conference on Recent Trends on Electronics, Information, Communication & Technology (RTEICT)* (pp. 728-734). IEEE.
- [54] Chehimi, M. and Saad, W., 2022. Physics-informed quantum communication networks: A vision toward the quantum internet. *IEEE Network*, 36(5), pp.32-38.
- [55] Nath, R.K., Thapliyal, H. and Humble, T.S., 2021. A review of machine learning classification using quantum annealing for real-world applications. *SN Computer science*, 2, pp.1-11.



ISSN ONLINE: 2447-0228



## AUTOMATIC LICENSE PLATE RECOGNITION SYSTEM: A SYSTEMATIC SURVEY

Vishakha H. Jagtap<sup>1</sup>, Rohit V. Dhotre<sup>2</sup>, Utkarsh R. Khandare<sup>3</sup>, Harshada N. Khuspe<sup>4</sup>, Rohini B. Kokare<sup>5</sup>

<sup>1,2,3,4</sup> Student, Department of Artificial Intelligence and Data Science, VPKBIET, Baramati, 413133, India

<sup>5</sup>Assistant Professor, Department of Artificial Intelligence and Data Science, VPKBIET, Baramati, 413133, India

<sup>1</sup><http://orcid.org/0009-0008-0590-2499> , <sup>2</sup><http://orcid.org/0009-0001-0584-2245> , <sup>3</sup><http://orcid.org/0009-0006-2494-071X> ,

<sup>4</sup><http://orcid.org/0009-0000-6527-692X> , <sup>5</sup><http://orcid.org/0009-0002-1633-1317> 

Email: [vishakhajagtap007@gmail.com](mailto:vishakhajagtap007@gmail.com), [rohitdhotre29112001@gmail.com](mailto:rohitdhotre29112001@gmail.com), [utkarshkhandare2@gmail.com](mailto:utkarshkhandare2@gmail.com), [harshadankhuspe0603@gmail.com](mailto:harshadankhuspe0603@gmail.com), [rohini kokare@gmail.com](mailto:rohini kokare@gmail.com)

### ARTICLE INFO

#### Article History

Received: November 16<sup>th</sup>, 2023

Revised: July 08<sup>th</sup>, 2024

Accepted: July 18<sup>th</sup>, 2024

Published: August 30<sup>th</sup>, 2024

#### Keywords:

Automatic license plate recognition (ALPR), Authentication, Character recognition, Character segmentation.

### ABSTRACT

The capacity to naturally distinguish and extract License plate data from pictures or video streams has gathered noteworthy consideration in later a long time, owing to its potential to upgrade security, streamline activity operations, and encourage effective information collection. The Vehicle Number Plate Recognition (VNPR) system has a broader variety of applications. A sophisticated License Plate Recognition (LPR) system can be smoothly incorporated into existing processes including law enforcement, monitoring, and toll station services. Existing approaches for License Plate Recognition are limited to datasets like CCPD, AOLP, etc., and operation specific, so many of them require a constrained environment to meet the needs of the intended application. Even if there are many Vehicle Number Plate Recognition systems available today, the task is still difficult because of several aspects such as the fast-moving vehicles, inconsistent vehicle number plates, contrast problems, language of the vehicle number, processing and memory limitations, camera mount position, motion-blur, reflections, tolerance to distortion, and varying lighting conditions. The methodologies and procedures employed for ALPR in Deep Learning, Computer Vision, and Machine Learning domains in contemporary literature are investigated in this study. This paper gives a comparative study of the techniques and algorithms used for various tasks included in Vehicle Number Plate Recognition (VNPR) systems such as License Plate Detection, License Plate Recognition, Character Segmentation, etc. We outline a critical and constructive analysis of relevant studies in the ALPR, and it will also give directions for future research, and optimization of the current approaches.



Copyright ©2024 by authors and Galileo Institute of Technology and Education of the Amazon (ITEGAM). This work is licensed under the Creative Commons Attribution International License (CC BY 4.0).

## I. INTRODUCTION

### I.1 OVERVIEW

Currently, the automatic number plate recognition system is very useful in many fields to identify cars or vehicles, which can be classified by the number plate with any background color, which helps to identify the type of vehicle. It helps a lot. to many people who work in RTO or identify the vehicle and which car is illegal or legal This system has been used in many countries to control traffic laws and to control urban traffic. Many techniques are used

for an automatic license plate recognition system. The techniques are as follows: [1] Many techniques are used for license plate recognition, but mostly CNN technology is the most accurate technique for license plate recognition of a vehicle using a camera placed on the road or public places. In [2] paper the technique used to detect license plate number is faster RCNN. This technique is more accurate than CNN. Using this faster RCNN model, we can detect any tile with any background color or number of font styles. For [3] Next technique is the OpenCV technique. This technique is based on Computer Vision. The next techniques are Vsnet [4],

Support Vector Machine, RCNN and Cascade Color Space Transformation of Pixel Features, Cascaded Contrast-Color Haar-like Features, Cascaded Convolution Network. The Multi-Level Extended Local Binary Patterns and Extreme Learning Machine are also used to detect the number plate from vehicles.

### I.2 SURVEY MOTIVATION

Although automatic number plate recognition systems are intended for outdoor usage, they struggle to find and identify license plates in constantly changing weather and environmental circumstances. The application of most current systems is constrained by elements like shifting lighting conditions, snow or fog, day and night, camera shaking, rotations, and occlusions. Automatic Number Plate Recognition systems, which are sensitive to changes in light and typically work in daylight, must deal with cars traveling at varied speeds in the real world. Many methods, which primarily function in daylight, are sensitive to variations in light. Production Systems for automatic number plate recognition must also satisfy non-functional criteria including acquisition and operation costs, physical specifications, power needs, and connection restrictions.

### I.3 ARTICLE STRUCTURE

A comprehensive overview of license plate recognition systems is provided in Section 1. The two basic strategies are covered in Section 2. Multi-stage and single-stage ALPR for license plate recognition. Principal components of a multi-stage license plate identification, such as license plate detection and license plate recognition are discussed in Sections 3 and 4. These sections each provide the relevant advantages, difficulties, restrictions, and suggested solutions. In Section 5 different datasets used for the study are discussed with their respective parameters, advantages, and disadvantages. In Section 6, we quickly go over several evaluation parameters for the ALPR system. Section 7 addresses the challenges that need to be addressed for optimal performance of the ALPR system. Finally, Section 8 concludes the study.

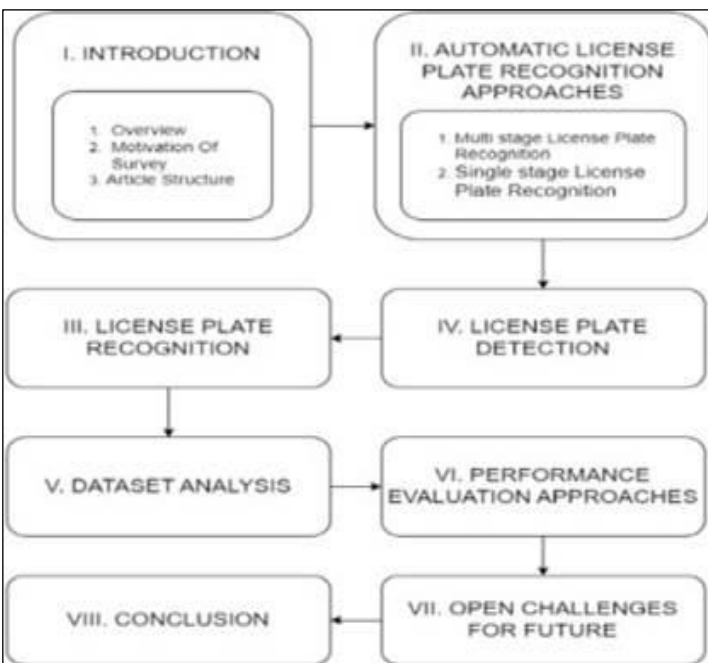


Figure 1: Structure of Paper.  
Source: Authors, (2024).

## II. AUTOMATED LICENSE PLATE RECOGNITION APPROACHES

### II.1 MULTI-STAGE LICENSE PLATE RECOGNITION SYSTEMS

License plate recognition approaches can be broadly classified as multi-stage and single stage approaches. In multistage approaches mainly three classes are there. These include License plate detection or extraction [1], License Plate segmentation (extracting separate characters), and character recognition.

In the first stage, License plate is detected by using an attention mechanism. Region proposal network (RPN) generates the rectangular object proposals for the subsequent processing that helps to detect the number plate efficiently [1],[2],[5]. The cascaded CC-Haar-like detector, the cascaded CST-pixel detector, and the cascaded ConvNet detector make up a hybrid cascade for the detection of license plates with various resolutions [3]. A vertexNET architecture, composed of two cascaded CNNs, is used for license plate recognition [6]. The license plate detection stage is classified into two stages namely feature extraction stage and ELM classification stage [7].

In the second stage, some common techniques for the segmentation and individual character extraction are used such as vertical or horizontal projection [1]. There are some algorithms in the ALPR system that don't make use of segmentation techniques. So, this is not a mandatory stage in the ALPR system.

In the last stage, the character recognition algorithms are used such as OCR or neural networks for character recognition. Every stage in the multi-stage approach is equally important for the overall performance of the ALPR system.

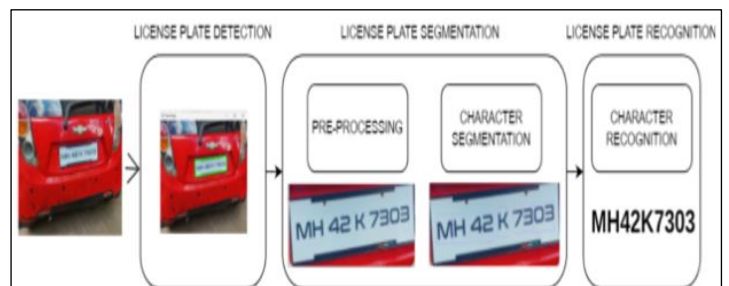


Figure 2: Stages in multi-stage ALPR system.  
Source: Authors, (2024).

### II.2 SINGLE-STAGE LICENSE PLATE RECOGNITION SYSTEMS

In the single stage approach, all the processes that are separated in the multi-stage approach are addressed at a single stage. Most of the advances are made in multi-stage approaches but some do use single stage approaches. These all use a single deep neural network that has been trained to detect, locate, and identify the license plate from beginning to end in a single forward pass. Such an attempt was made in the paper by Chen et al. The popular VGG-16 [4] was utilized as the basis for the backbone network he employed, which kept the convolutional layers from conv1\_1 to conv5\_3. For a fair comparison, the final two fully connected layers (fc6, fc7) are turned into convolutional layers and additional layers from conv6\_2 to conv9\_2 are also included for semantically stronger feature extraction. According to [4] proposed a 30 convolutional layers architecture structured into 9 modules, where all of them have linear residual connections except for the first and the last one. Using interleaved separable convolutions and max pooling, the entry flow raises the feature channel from 3 to 256

while down sampling the spatial dimension from 160 48 to 40 6. They use repeated ResSeparableConv blocks in the middle flow, keeping the spatial size and channel number constant, to extract deep features that contain higher level representations. We extract a middle-level feature map  $M$  of size 406512 as the attention network's context from the exit flow, along with a final feature vector  $F$  of 512 dimensions. In the sequence decoder, LSTMs with two layers and 512 hidden states each are used [8]. A 2-layer attention mechanism is used which reduces the need for segmenting each character in the license plate separately. A similar kind of single stage approach is used in which use of inception v3 with three layers of CNN and six layers of SSD 300 are used [9].

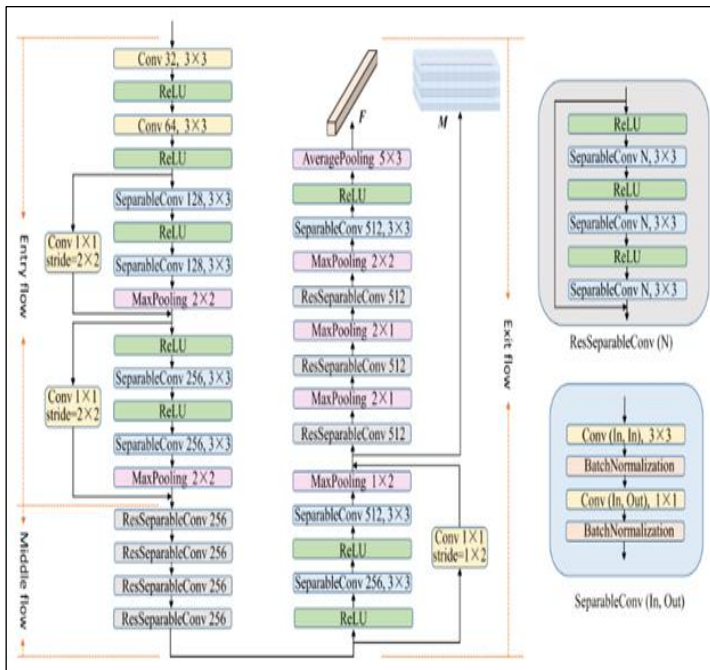


Figure 3: End-to-end CNN architecture for LP detection. Source: [8].

### III. LICENSE PLATE DETECTION

A crucial part of contemporary transportation and security systems is license plate detection. It involves locating and identifying license plates on automobiles for a variety of purposes. Detection techniques have evolved from conventional computer vision methods to more recent advances in deep learning. Finding the location of the vehicle license plate from the ingested vehicle picture and accurately segmenting the license plate from the area for character segmentation constitute the primary tasks of the license plate location. As a result, one of the crucial elements that affects how well the system works is the choice of the license plate area. Mentioned below are license plate detection approaches.

#### III.1 HYBRID CASCADE

A specific design is utilized to increase the precision and effectiveness of license plate detecting systems called a hybrid cascade structure. To accomplish robust and accurate license plate localisation, it integrates components of both a cascade classifier and deep learning methods. The detection of license plates with various resolutions is done using a hybrid cascade [3]. The cascaded CST-pixel detector, cascaded ConvNet detector, and cascaded CC-Haar-like detector make up this hybrid cascade structure's three components [3].

#### III.2 YOLO-v2

The deep learning model YOLOv2 (You Only Look Once version 2) is frequently used for tasks involving the identification of license plates. YOLOv2, which has been trained on datasets with annotated license plate areas, is excellent at real-time object identification. When used on license plates, it successfully recognizes and localizes them inside picture or video frames. It is a useful tool for many applications since the model forecasts bounding boxes that include the precise placements of the license plates. A YOLOv2 [8] detector is utilized to obtain the bounding boxes of license plates.

#### III.3 VERTEXNET

VertexNet [6] is a good performing one-stage detector with a limited input size, a narrow channel of high-level layers, and vertex estimation. Three components, the head, fusion, and backbone networks, make up the proposed VertexNet [6]. VertexNet is built using small-resolution input, even with character information lost, to achieve fast inference speed and reduce memory use [6].

#### III.4 DEPTH WISE SEPARABLE CONVOLUTIONAL BLOCK (DSCB)

A Depth Wise Separable Convolution block (DSCB) is a frequent building element in convolutional neural networks (CNNs), particularly in topologies built for efficient and lightweight model architectures such as MobileNet and Xception. Depth wise convolution and pointwise convolution are the two primary parts of the DSCB. [5] The Depth Wise Separable Convolution block (DSCB) is used to reduce the number of parameters to a minimum, allowing the model to be deployed on mobile devices.

#### III.5 EDGE DETECTION

In computer vision and image processing, edge detection is a key idea. It describes the method of locating the areas of a picture where substantial changes in intensity or color take place. Usually, these transitions depict the edges of features or objects in the picture. Most of the research has relied on edge-based techniques for license plate identification since every license plate is rectangular and has a defined aspect ratio. A segmentation technique built on edge detection was utilized in [10]. To find the license plate, it primarily employs the horizontal projection approach and the vertical projection method. The license plates approximate contour is found using Sobel edge detection [10].

### IV. LICENSE PLATE DETECTION

License plate recognition in ALPR systems can be broadly classified into three classes, pre-processing, character segmentation, and character recognition.

#### IV.1 PRE-PROCESSING

The main purpose of pre-processing is to enhance the image quality to correctly enable the character recognition and henceforth enhance the recognition process. Pre-processing helps to neglect the noise, prevent the image blur, etc. The effectiveness of recognition will be impacted by the color information in color images. The license plate information is retained when the color

image is converted to a grayscale image, and processing speed is also considerably increased [11].

The License Plate is resampled and rectified to a higher resolution ( $64 * 256$ ) according to the vertices. This resampling step normalizes the location of characters in the LP. Another process performed is the rectification, which is achieved using perspective transformation. This generates the bird's eye view of the detected license plate [6]. Multi-level pre-processing approaches are used to pass the detected license plate through multiple stages of pre-processing. A Gaussian filter and the CLAHE method are used for multi-level pre-processing in [7],[9]. In this paper,  $G(\sigma)$  is the Gaussian filter with the standard deviation  $\sigma = 0.25$ . CLAHE ( $\sigma$ ) is defined as a contrast-limited adaptive histogram equalization method with a standard deviation  $\sigma = 0.01$ [7]. A new image is produced at each stage of multi-level pre-processing which eventually expands the training image size. Based on the results of the LP detection, the License Plate images are cropped depending on the required ROI. These cropped images can be tilted vertically and horizontally. In [5] the focus is on the vertical tilt only. The image is binarized after correction of horizontal tilt. Selecting the specific pixels, starting from the first pixel value to judge the tilt level [8].

## IV.2 CHARACTER SEGMENTATION

The Mask branch is used for instantly segmenting the LP characters provided input of Region Proposals which is output from the Faster R-CNN [1]. The recognition of the rivet position and white dots on the license plate to perform character segmentation [10].

## IV.3 CHARACTER RECOGNITION

Character recognition is the last and hence the very important step, as the evaluation of performance is based on this step. Most of the character recognition techniques use variants of CNN [3]. Some use a single stage License Plate Recognition approach that uses end-to-end CNN architecture while some multi-stage approaches use a CNN architecture in their License Plate recognition stage [1],[4],[11],[12]. In the papers [1-4], a variant of CNN, VGG & VGG-16 are used. In the paper [1], a multi-stage license plate recognition is used which uses VGG to recognize the license plate. VGG-16 is the modified version of VGG that is used in [4] with some modification in the architecture to acquire better results.

A 2-layer LSTMs is used for recognition of license plates [8], which eliminates the need for individual character segmentation and hence gives better performance without character segmentation. Resampling and rectification of LP is done according to the vertices obtained from VertexNet. The corrected LP picture is then sent to SCR-Net. Through a forward pass, SCR-Net guesses the characters [6]. The number-plate's alphanumeric characters are recognized using the Tesseract OCR engine. Prior training is done to increase the Tesseract OCR engine's accuracy [9].

## V. DATASET ANALYSIS

### V.1 HZM MULTI-STYLE DATASET

The "HZM multi-style dataset" in [1] is a collection of automobile pictures taken from the Hong Kong-Zhuhai-Macao Bridge and is referred to as such because it contains several forms of license plates. 176 photos are utilized for testing, and 1200 images are used to train the model in this proprietary dataset, which

has a total of 1376 photographs taken from the Hong Kong-Zhuhai-Macao Bridge's entrance control system. The toll gate is where the test photographs are taken. There are 280 LPs photos altogether with a resolution of  $1024 \times 800$  in the testing subset. Vehicles from Hong Kong, Mainland China, and Macao with a maximum of three license plates are included in the dataset.

### V.2 ALOP DATASET

The 2049 license plate images in the ALOP [1],[6] collection are broken up into three categories: road patrol (RP), traffic law enforcement (LE), and access control (AC). The photos of the RP subgroup are taken at different distances and perspectives. The AOLP dataset is split into two subsets: training pictures are utilized for the remaining photos, and files with filenames that begin with "1" are used as testing images (111 images). The ratio between the groups for training and testing is around 4.5:1. LPs and characters are made and annotated using the AOLP dataset's ground truth data.

### V.3 PKU DATASET

The PKU collection contains 3977 photos with Mainland China LPs. Because it solely provides the ground-truth file of LPs, this dataset is used to assess the efficacy of LP detection. Five groups (G1–G5) make up the PKU dataset [1], with G1 being the simplest and G5 being the most challenging. The [1] utilizes the other 4 groups as the testing datasets and 810 photos from G1 as the training dataset. PKU Data [6] is an LP detection dataset in which the characters in 2253 images are labelled. Three subsets are used to choose those images: G1 (daytime under normal conditions), G2 (daytime with sun glare), and G3 (nighttime).

### V.4 FIELD TESTING DATASET

The field-testing dataset included 12000 photos from the Transport Bureau of the Macao S.A.R. (DSAT) [1]. There are three main types of vehicles in the dataset: automobiles, trucks, and buses. The resolution of these images is  $1024 \times 800$ . Between the training and validation sets, these photos are split in a 4:1 ratio.

### V.5 LPST-110K

The LPST-110K [2] Dataset consists of pictures shot in open spaces. It is the first dataset to simultaneously handle LP and scene text for LP detection. The LPST-110K is the first dataset that provides text annotations in addition to a significant number of examples (LP and non-LP) in a picture, even when those instances are taken from scenes without any limitations. The LPST-110K dataset compiles images from hundreds of dash cameras and security cameras installed in moving cars and structures, encompassing locations in East Asia and Europe. Along with the LP Road signs, wallpaper text, banners, and commercial adverts are also included in the collection in [2] as non-LP scene texts. There are 9,795 photos and 110,000 scene text pieces in the LPST-110K collection.

The scene texts contain 51,031 LP instances and 58,969 non-LP instances. The resolution of each image in the collection is 1280 (Width) x 720 (Height) x 3 (Channels). The photos in LPST-110K are compressed using the h264 codec setting in contrast to most other LP detection datasets.



## V.6 VALID

The two auto-mobile data recorders are used to record videos in 720 x 1280 resolution on the streets of a Chinese city<sup>1</sup>. The collected dataset is known as the "Vehicle and License Plate Dataset" (VALID [4]). A dataset includes a total 887 well annotated images. The test set consists of 78 photos from a single recorder. 809 additional photos from another recorder are divided randomly in the ratio 7:3 into the training set and the validation set.

## V.7 DETROIT

The "Car" and "Vehicle registration plate" are part of the re-annotated DETROIT Dataset, which is a subset of the Open Image Dataset (OID). In a simple way DETROIT is called as (Dataset from Open Image Dataset). DETROIT Dataset is a re-annotated subset of the Open Image Dataset (OID), which contains "Car" and "Vehicle registration plate". For simplicity, DETROIT is called as (Dataset from Open Image Dataset) [4]. The size and aspect ratio of the DETROIT photos, which are downloaded from the Internet, can vary greatly. The test set consists of 386 images taken from the OID validation set. 1113 OID test photos are randomly split into a training set and a validation set in the ratio of 7:3.

## V.8 DOC

To obtain DOC (Dataset from Cars), the location of the vehicle and the location of the license plate are combined. There are overall 105 photos in the dataset. Out of which 70% chosen at random as the training-validation set while the remaining 30% are used as the test set. The size and aspect ratio of the DOC images, which are downloaded from the Internet, vary widely.

## V.9 CLPD

There are a total of 1200 images in the CLPD [8] (China License Plate Dataset) dataset, which comes from all 31 provinces on the mainland. It covers a wide range of photographic situations, vehicle types and regional codes, allowing for an in-depth analysis of current license plate recognition techniques while promoting the development of a more useful model. Licence plate images in the CLPD dataset are gathered from various kinds of real-scene image sources, such as web searches, images taken from smartphones, and driving recorder recordings of automobiles. The photography angles, shooting times, resolutions, and background are also taken into consideration when capturing LP images to account for the various conditions. Various vehicle types, including cars, trucks, police cars and new energy vehicles, are included in the CLPD dataset. The real-world dataset CLPD [6] contains a wide range of vehicle types, environment, and area codes.

## V.10 CCPD

The Chinese City Parking Dataset (CCPD) [6] provides a large-scale and comprehensive Licence Plate benchmark to evaluate Automated License Plate Recognition techniques under uncontrolled conditions. CCPD contains 280k vehicle images, which is two orders of magnitude greater than other LP datasets, that were taken under uncontrolled conditions, such as diverse weathers, lighting, rotation, and vagueness. Each image has a 720 x 1160 resolution. The dataset provides sufficient annotations, including the LP character, bounding box, four vertices, degree of tilt in both the horizontal and vertical axes, brightness, and vagueness levels. The model is trained by using 100k examples of CCPD-Base, and it is tested on the remaining 100k examples of

CCPD-Base and the 80k examples of sub-datasets such as CCPD-DB, CCPD-FN, CCPD-Rotate, CCPD-Tilt, CCPD-Weather, and CCPD-Challenge.

## VI. PERFORMANCE EVALUATION APPROACHES

Most of the ALPR system uses loss function as the evaluation method [1],[2]. This loss function is calculated at each stage in the single stage [4],[8],[9] as well as the multi-stage approach [1-3], [5],[6]. Finally, the results are aggregated to get the right accuracy of overall ALPR systems. The accuracy is calculated as per loss value at each stage [12].

In the [2] paper the evaluation techniques used are Precision, Recall, F-measure and IoU.

### VI.1 PRECISION

The ratio of the number of successfully identified bounding boxes to all acquired bounding box candidates is known as precision. [2],[5-7].

$$Precision = \frac{T_p}{T_p + F_p} \quad (1)$$

Where,  $T_p$  = correctly estimated bounding box

$F_p$  = incorrectly estimated bounding box

### VI.2 RECALL

The recall is the ratio of the correctly estimated bounding boxes among all the ground truths [2],[5],[7].

$$Recall = \frac{T_p}{T_p + F_n} \quad (2)$$

Where,  $F_n$  = the quantity of the undetected ground truth

### VI.3 F-MEASURE

Benchmark for LP detection evaluation used in PKU dataset [2],[7].

$$F - measure = 2 * \frac{(Precision * Recall)}{(Precision + Recall)} \quad (3)$$

### VI.4 IoU

When the detected bounding box's IoU overlaps the ground truth region by more than 50% ( $IoU > 0.5$ ), it is deemed to be accurate [2],[3].

$$IoU = \frac{area(Rdet \cup Rgt)}{area(Rdet \cap Rgt)} \quad (4)$$

Where,  $Rdet$  = area of the detected bounding box

$Rgt$  = ground truth

AP (Average Precision) is another method used for the evaluation of ALPR systems [2],[4]. AP is calculated over IoU (Intersection over Union) [2].

The performance evaluation measure Success Ratio is used in [13]. Success Ratio is the ratio of the number of success samples to the total number of samples.

$$SR = \frac{NSs}{TNS} * 100 \quad (5)$$

Where, SR = Success Ratio

NSs = Number of success samples

TNS = Total number of samples

The evaluation of classification accuracy in [9] is done using the formula below.

$$\text{Classification accuracy} = \frac{\text{number of correctly predicted characters}}{\text{total number character predictions}} \quad (6)$$

As seen in most references the performance measures are accuracy, precision, recall, F-measure, AP/IoU. In most multi-stage approaches the loss function is the best estimation of accuracy.

## VII. OPEN CHALLENGES FOR FUTURE

### VII.1 VARIATIONS IN BACKGROUND COLOR

License plates do have different background colors and each different color signifies different types of the vehicle. White background is for personal vehicles while the yellow one is for transport vehicles and so on. These different colors can add complexity in terms of pre-processing [3]. This is a prominent future scope to work upon.

### VII.2 SPEED OF TRAINING

Image processing requires a significant amount of time. To fasten the time decoders are used. Some decoders perform sequentially and not parallelly. LSTM is such a decoder that is incapable of parallel training [8]. We can try out using a transformer like decoder to make training faster.

### VII.3 CHALLENGING WEATHER CONDITIONS

Changing weather conditions affect the lumination and hence the performance of ALPR systems [7]. To adapt with the weather conditions is a major future issue. More challenging is to detect LPs at nighttime, as the luminance is lowest at that time.

## VIII. CONCLUSIONS

In account for various operational and hardware constraints, a careful selection of standards and techniques is required for the design and development of an automatic license plate recognition system (ALPR). This research article has investigated and examined the currently employed ways and strategies in the most recent literature on ALPR solutions. The deep single-stage Learning-based systems have demonstrated strong results with various datasets. Although learning systems can be pre-trained on huge datasets, single-stage approaches have demonstrated greater computing efficiency and accuracy. This survey did a job of thorough analysis of linked studies and identified the specifications for actual benchmark datasets. We have outlined the current issues and made future directions for ALPR study.

## VI. AUTHOR'S CONTRIBUTION

**Conceptualization:** Vishakha H. Jagtap, Rohit V. Dhotre, Utkarsh R. Khandare, Harshada N. Khuspe, Rohini B. Kokare.

**Methodology:** Vishakha H. Jagtap, Rohit V. Dhotre.

**Investigation:** Vishakha H. Jagtap, Rohit V. Dhotre, Utkarsh R. Khandare, Harshada N. Khuspe.

**Discussion of results:** Vishakha H. Jagtap, Rohit V. Dhotre, Utkarsh R. Khandare, Harshada N. Khuspe, Rohini B. Kokare.

**Writing – Original Draft:** Vishakha H. Jagtap, Rohit V. Dhotre, Utkarsh R. Khandare, Harshada N. Khuspe.

**Writing – Review and Editing:** Vishakha H. Jagtap.

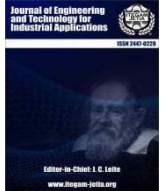
**Resources:** Rohit V. Dhotre, Utkarsh R. Khandare, Harshada N. Khuspe.

**Supervision:** Rohini B. Kokare.

**Approval of the final text:** Rohini B. Kokare.

## VIII. REFERENCES

- [1] Qiuying Huang, Zhanchuan Cai and Ting La, A New Approach for Character Recognition of Multi-Style Vehicle License Plates, IEEE TRANSACTIONS ON MULTIMEDIA, VOL. 23, 2021  
<https://doi.org/10.1109/TMM.2020.3031074>
- [2] Younkwan Lee, Jihyo Jeon, Yeongmin Ko, Moongu Jeon and Witold Pedrycz, License Plate Detection via Information Maximization, IEEE TRANSACTIONS ON INTELLIGENT TRANSPORTATION SYSTEMS, VOL. 23, NO. 9, SEPTEMBER 2022.  
<https://doi.org/10.1109/TITS.2021.3135015>
- [3] Chunsheng Liu and Faliang Chang Hybrid Cascade Structure for License Plate Detection in Large Visual Surveillance Scenes, IEEE TRANSACTIONS ON INTELLIGENT TRANSPORTATION SYSTEMS, Volume: 20, Issue: 6, June 2019.  
<https://doi.org/10.1109/TITS.2018.2859348>
- [4] Song-Lu Chen, Chun Yang, Jia-Wei Ma, Feng Chen, and Xu-Cheng Yin, Simultaneous End-to-End Vehicle and License Plate Detection With Multi-Branch Attention Neural Network, IEEE TRANSACTIONS ON INTELLIGENT TRANSPORTATION SYSTEMS, Volume: 21, Issue: 9, September 2020.  
<https://doi.org/10.1109/TITS.2019.2931791>
- [5] Xiangjie Kong, Kailai Wang, Mingliang Hou, Xinyu Hao, Guojiang Shen, Xin Chen, and Feng Xia, A Federated Learning-based License Plate Recognition Scheme for 5G-enabled Internet of Vehicles, IEEE TRANSACTIONS ON INDUSTRIAL INFORMATICS, Volume: 17, Issue: 12, December 2021  
<https://doi.org/10.1109/TII.2021.3067324>
- [6] Yi Wang, Zhen-Peng Bian, Yunhao Zhou, and Lap-Pui Chau, Rethinking and Designing a High-Performing Automatic License Plate Recognition Approach, IEEE TRANSACTIONS ON INTELLIGENT TRANSPORTATION SYSTEMS, 2021.  
<https://doi.org/10.1109/TITS.2021.3087158>
- [7] Meeras Salman Al-Shemarry, Yan Li, and Shahab Abdulla, An Efficient Texture Descriptor for the Detection of License Plates From Vehicle Images in Difficult Conditions, IEEE TRANSACTIONS ON INTELLIGENT TRANSPORTATION SYSTEMS, Volume: 21, Issue: 2, February 2020  
<https://doi.org/10.1109/TITS.2019.2897990>
- [8] Linjiang Zhang, Peng Wang, Hui Li, Zhen Li, Chunhua Shen, and Yanning Zhang, A Robust Attentional Framework for License Plate Recognition in the Wild, IEEE TRANSACTIONS ON INTELLIGENT TRANSPORTATION SYSTEMS, Volume: 22, Issue: 11, November 2021.  
<https://doi.org/10.1109/TITS.2020.3000072>
- [9] Sparsh Jain, Rishikesh Rathi, and Rahul Kumar Chaurasiya, Indian Vehicle Number-Plate Recognition using Single Shot Detection and OCR, IEEE INDIAN COUNCIL INTERNATIONAL SUBSECTIONS CONFERENCE, 2021.  
<https://doi.org/10.1109/INDISCON53343.2021.9582216>
- [10] Zijia Liang, Erkang Li, Yanxing Huo, Yutong Guo, Chengning Lu, Design of Portable License Plate Recognition System, 2021 IEEE INTERNATIONAL CONFERENCE ON POWER, INTELLIGENT COMPUTING AND SYSTEMS (ICPICS), 2021.  
<https://doi.org/10.1109/ICPICS52425.2021.9524092>
- [11] Chenxu Duan, Shiqiang Luo, Design of License Plate Recognition System Based on OpenCV, 2022 15TH INTERNATIONAL SYMPOSIUM ON COMPUTATIONAL INTELLIGENCE AND DESIGN (ISCID), 2022.  
<https://doi.org/10.1109/ISCID56505.2022.00031>
- [12] Liang Wang, Yimei Huang, Chengqun Liang, Jinrong Zhou, Taoqiang Zhua, License plate recognition system based on image recognition, 2022 IEEE 21ST INTERNATIONAL CONFERENCE ON UBIQUITOUS COMPUTING AND COMMUNICATIONS (IUCC/CIT/DSCI/SMARTCNS), 2022.
- [13] Milan Samantaray, Anil Kumar Biswal, Debabrata Singh, Debabrata Samanta, Marimuthu Karuppiah, Niju P Joseph, Optical Character Recognition (OCR) based Vehicle's License Plate Recognition System Using Python and OpenCV, 2021 5TH INTERNATIONAL CONFERENCE ON ELECTRONICS, COMMUNICATION AND AEROSPACE TECHNOLOGY (ICECA), 2021.  
<https://doi.org/10.1109/ICECA52323.2021.9676015>



### RESEARCH ARTICLE OPEN ACCESS

## DESIGN AND DEVELOPMENT OF IOT BASED AUTOMATED ATTENDANCE SYSTEM USING FACIAL RECOGNITION

George Michael G. Makigod<sup>1</sup>, Janwel Josh B. Sebastian<sup>2</sup>, Edwin R. Arboleda<sup>3</sup>, and Luisa Ann T. Ongquit\*<sup>4</sup>

<sup>1,2,3,4</sup>Cavite State University – Main Campus – Cavite, Philippines.

<sup>1</sup><http://orcid.org/0009-0001-9068-0155> , <sup>2</sup><http://orcid.org/0009-0005-2377-9154> , <sup>3</sup><http://orcid.org/0000-0001-9371-8895> ,  
<sup>4</sup><http://orcid.org/0009-0009-2534-5252> 

Email: [georgemichael.makigod@cvsu.edu.ph](mailto:georgemichael.makigod@cvsu.edu.ph), [janweljosh.sebastian@cvsu.edu.ph](mailto:janweljosh.sebastian@cvsu.edu.ph), [edwin.r.arboleda@cvsu.edu.ph](mailto:edwin.r.arboleda@cvsu.edu.ph), \*[mrs14.la.ongquit@gmail.com](mailto:mrs14.la.ongquit@gmail.com)

### ARTICLE INFO

#### Article History

Received: November 26<sup>th</sup>, 2023

Revised: July 08<sup>th</sup>, 2024

Accepted: July 19<sup>th</sup>, 2024

Published: August 30<sup>th</sup>, 2024

#### Keywords:

IoT Based Automated Attendance System, Facial Recognition Attendance System, Fingerprint Attendance System, Radio Frequency Identification (RFID) Attendance System.

### ABSTRACT

The IoT Based Automated Attendance System was designed and developed to make an efficient contactless attendance marking system with a mobile application feature. This study aimed to improve the traditional attendance log system and contact fingerprint attendance within an institution through the use of facial recognition. The study used the OpenCV and Python Programming in order to create the facial recognition program, while the mobile application was developed through the use of Visual Studio Code and Android Studio. The prototype was composed of mini pc which handled all the processes the device had to execute. The computer was used to interface other components of the device such as webcam, monitor, keyboard, and mouse. Since this is an automated attendance system, portability and efficiency were given importance. The prototype's performance was tested and monitored through the use of 100 participants including the researchers themselves. The project was tested by the Department of Computer, Electronics, and Electrical Engineering (DCEE) at the Engineering Science Building, Cavite State University, Indang, Cavite with the Electronics Engineer Professors. Based on the results of the evaluation, the design project succeeded in achieving its objectives. The overall performance was considered satisfactory. The cost computation of the system amounted to PHP 14,150.00.



Copyright ©2024 by authors and Galileo Institute of Technology and Education of the Amazon (ITEGAM). This work is licensed under the Creative Commons Attribution International License (CC BY 4.0).

## I. INTRODUCTION

Attending marking procedures was probably the most challenging responsibility in any organization [1]. Since before, recording of attendance are always done manually. Even though this helped develop a student-teacher bond, it is prone to human errors and consumed more time [2]. Attendance tracking systems hold significant importance for all organizations, despite their complexity and the time required to manage routine attendance records [3]. Managing attendance manually within educational institutions was consistently challenging. This type of task demands a substantial amount of physical effort. Furthermore, it places additional load on teachers and academic administrators [4], to eliminate minimize time wastage, the implementation if an

Automatic Attendance Management System becomes essential. This step not only enhances efficiency but also boosts effectiveness. The existing system is fraught with a considerable amount of uncertainty, leading to inaccuracies and inefficiencies in attendance tracking and record maintenance. Numerous challenges emerge when the institution is unable to enforce the regulations within the current system. Therefore, through technological means, the project aimed to address the shortcomings present in the current system. By automating most tasks, it seeks to elevate attendance tracking to a significantly improved level [1],[2].

Numerous automated techniques exist for human identification, including biometrics, Radio Frequency Identification (RFID), eye tracking, and voice recognition. Among

these, facial recognition stands out as one of the most extensively employed biometric methods for authenticating human identity [3].

Over the past two decades, the field of facial recognition has emerged as a significant and captivating area of research. A facial recognition system is a software application designed to authenticate and identify individuals using images or videos from a given source [5].

In this paper, the researchers made use of the digital age. By utilizing modern technology in order to accelerate this means and provide time efficiency. The main purpose of this project was to create an automated attendance marking system in means of upgrading current attendance system economical and more efficient. The researchers decided to design and develop an IoT based automated attendance system using facial recognition with the use of a mini computer, webcam/camera, and a mobile application.

By utilizing the Python programming language, the development of a facial recognition program and an automated attendance system became achievable. The system facilitates the automatic organization of attendance records into an Excel spreadsheet, delivering neatly arranged and structured information for easy viewing and management.

The development of this system would help faculty workers in organizing the attendance log more efficiently. The mobile application provided will also help both students and instructors who needs information whether someone specific is currently present or absent for the day.

## **II. THEORETICAL REFERENCE**

### **II.1 RADIO FREQUENCY IDENTIFICATION ATTENDANCE SYSTEM**

For [2] discussed a smart attendance system of students in an educational institution. Furthermore, this system makes automated analysis and prepares a detailed report weekly, monthly and annually. The whole system was developed with an Arduino microcontroller and RFID readers. Also, GSM and WiFi communication modules are used to make convenient communication depend on the availability of the network. A microchip (microSD) is placed to store data in case of communication failure and those stored data will be uploaded bulk when the communication channel was restored. This system will reduce a lot of manual work of educators and education administrators of an education institution.

According to [6] implemented an RFID Based Automatic Attendance system, where the attendance tracking was automated using RFID technology. The attendance software was developed using VB.net, and a Microsoft Access database was employed. Each student was assigned an RFID tag attached to their Student ID card. A serial connection facilitates communication between the computer and the RFID reader. The RFID reader was positioned at the entrance of the lecture hall. When students entered the lecture hall, the RFID reader read the RFID tag, captures information such as entry time and name, and stores this data in the database via the serial connection. The system was managed through this approach. The system allows the

administrator to conveniently access all attendance records through the software interface. By retrieving information directly from the database, the software interface simplifies the process compared to traditional methods. Staff employees record attendance for both in-class and absentee students using the traditional method.

According to [7] developed an attendance system that merges RFID technology with a web-based approach. This system involves the use of RFID tags and readers to record students' attendance and identify specific students. The RFID reader communicates with an Arduino microcontroller, which then transfers the RFID reader's data to a web server through an Arduino shield. This data was subsequently stored in a web server using PHP and MySQL. Through a dedicated webbased application, the system's administrator can access and review all students' attendance records. Additionally, the administrator can view individual student details using LCD displays. This combination of RFID and web-based technologies enhances the efficiency of attendance management and provides a user-friendly interface for administrators to monitor and manage attendance data.

For [8] introduced a system that integrates RFID and GSM technologies. In this system, a microcontroller (LPC) acts as an intermediary between the GSM module and the RFID components. When students enter the classroom, they are required to use their RFID tag, which is then read by the RFID reader. This information is transmitted to the GSM module to signal their presence. If the tag's ID does not match any entry in the database, it is regarded as unauthorized access. Conversely, if the ID was valid, the GSM module sends notifications to both the administration and parents, confirming the student's attendance.

For [9] designed a prototype for an attendance management system, incorporating a higher quantity of RFID readers strategically positioned within a room. This setup is supported by a server application that is managed through a laptop. The connection between the RFID readers and the laptop or PC is established using either a wireless router or a LAN connection. Upon entering the room, individuals are required to utilize their RFID tag, which is then scanned by the RFID reader. Subsequently, the attendance information is transmitted to the server either via wireless communication or a LAN connection. The utilization of multiple RFID readers allows for simultaneous attendance recording for multiple individuals, leading to greater efficiency in comparison to traditional methods.

### **II.2 FINGERPRINT ATTENDANCE SYSTEM**

Automated fingerprint identification involved the automated comparison of one or multiple unknown fingerprints against a database containing known and unknown prints. This process was used to identify matches and potential matches. Automated fingerprint verification is a closely aligned technique used in various applications like attendance and access control systems. At a technical level, verification systems confirm a claimed identity (for instance, a user claiming to be John using a PIN or ID card, verifying their identity through fingerprint

verification). In contrast, fingerprints, without the need for additional claims or information [10].

According to [11] addresses the prevalent issue of high levels of impersonation occurring regularly in both private and public sectors. The "ghost worker syndrome," which has become a widespread problem across various government tiers, as well as employers' concerns about workforce absenteeism, and challenges in managing student attendance during lectures are discussed. As a response to these challenges, the paper presents the development of a fingerprint-based Attendance Management System. This system aims to offer a quicker, more secure, and more convenient means of user verification compared to traditional methods such as passwords and tokens. This innovative approach provides a reliable method for personal identification, addressing the identified issues related to attendance and identification in various sectors.

According to [12] developed an attendance management system using biometrics to address the challenge of managing student attendance during lecture periods. Manual computation of attendance often leads to errors and consumes significant time. To tackle this issue, they designed an efficient system that electronically records attendance using a fingerprint device and stores the data in a database. Student identification is achieved through a biometric (fingerprint) system, eliminating the need for traditional record-keeping materials and personnel. In testing the system with eighty candidates, it achieved a success rate of 94 percent. Comparing execution times, the manual attendance system took an average of 17.83 seconds for eighty students, while the automatic attendance management system using biometrics reduced the time to 3.79 seconds. These results demonstrate a substantial improvement in performance over the manual attendance management system, with attendance being marked after student identification.

### **II.3 FACIAL RECOGNITION ATTENDANCE SYSTEM**

There are many biometric systems that use features such as face, iris, fingerprint, palm print. Among these, facial recognition is an important contribution to technology. Facial recognition is used not only in the office environment and at immigration control at the airport, but also in the use of robots, cameras, digital photos and popular websites such as Facebook. It is a versatile solution with wide application and innovation in many areas [13].

In [14] the past suggested facial recognition as an attendance tracking system for schools to make the current attendance system more efficient and effective. There is a lot of confusion in the current legacy system, resulting in inaccurate onboarding and poor performance. Many problems arise when authorities cannot enforce the rules contained in the old system. The technology behind it will be the facial recognition system. The human face is one of the natural features that can identify a human being. It is therefore used to keep track of characters due to the deviation, or rather less, of the time of the face. In this project, a face database will be created to feed the data into the recognition algorithm. The face is then compared to the data to find the identity upon joining. Once a person is identified, their participation will be recorded and the necessary information will

[3] proposed deep learning-based facial recognition. They used three pre-trained convolutional neural networks for transfer learning and trained them with their own data. Our networks, GoogleNet, SqueezeNet, and AlexNet, perform very well in terms of prediction accuracy and reasonable training time.

For [15] Proposed the idea of using "automatic enrollment based on facial recognition." The app includes time-saving facial recognition and is software-only and can be saved as user-friendly as it reduces the amount of paper used. The system also eliminates the possibility of fraudulent participation because the face is used as a biometric for authentication. Therefore, this system can be used in areas where participation is important.

### **II.4 FACIAL RECOGNITION USING OPENCV**

According to [16] has put forward a proposal to develop an application that enables user access to a specific machine by conducting a thorough analysis of an individual's facial features. This application's development relied on the utilization of Intel's open-source computer vision project, OpenCV, in combination with Microsoft's .NET framework.

According to [17] introduced an effective approach to detecting and recognizing human faces utilizing OpenCV and Python as part of deep learning. They detailed the utilization of deep learning, a vital aspect of the computer science field, for facial detection by employing various OpenCV libraries in conjunction with Python. Additionally, they outlined a proposed system for realtime human face detection. This implementation has versatile applications across platforms, including machines, smartphones, and various software applications.

For [18] paper provides comprehensive instructions on various image processing tasks. These include reading and writing images, displaying images, resizing them, and crucially, detecting and recognizing individuals' faces. The paper delved into methods for accurately identifying and associating the detected faces with their corresponding individuals.

For [19] conducted a presentation that involved the evaluation and comparison of various face detection and recognition algorithms utilized within the system. The system's workflow started with a training image of a person, followed by processing a test image. It identifies the face, compares it to the trained image, and ultimately classifies it through the utilization of OpenCV classifiers. The research explored the most efficacious techniques employed in this system, implemented through Python, OpenCV, and Matplotlib. Additionally, the application of this system in areas equipped with CCTV, such as public spaces, shopping malls, and ATM booths, is considered.

OpenCV classifiers. The research explored the most efficacious techniques employed in this system, implemented through Python, OpenCV, and Matplotlib. Additionally, the application of this system in areas equipped with CCTV, such as public spaces, shopping malls, and ATM considered.

According to [5] provided an extensive explanation of the complete process involved in creating a facial recognition system using the OpenCV library. The researcher employed the Haar cascading algorithm from the OpenCV library for face detection.

This algorithm utilized specific facial features for identification purposes. Numerous individuals' facial features were stored and indexed, enabling identification based on these distinctive features. The field of facial testimony and recognition presents significant challenges and complexities. The credibility of facial recognition systems relies on their accuracy and precision. The facial recognition technique involves capturing an image through a camera and then comparing it to the images stored in a database. If the captured image matches any of the stored images, it signifies a successful face match; otherwise, it indicates that the faces do not match.

### III. MATERIALS AND METHODS

The project uses a Dell OptiPlex 3020 Micro Desktop i3-4160T, Samsung B2030 Monitor, Limeide T13 Keyboard and Mouse, and Oshare WB-01 Webcam. The chassis is made from marine plywood, wood, and rubber caster wheels. Locks are provided for security. The prototype aims for portability, availability, and usefulness.

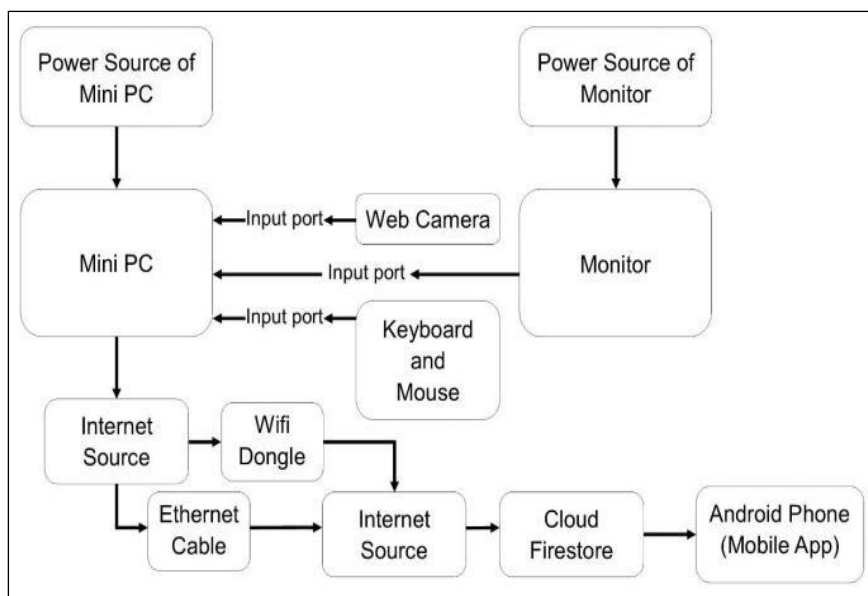


Figure 1: Block diagram of the system.

Source: Authors, (2024).

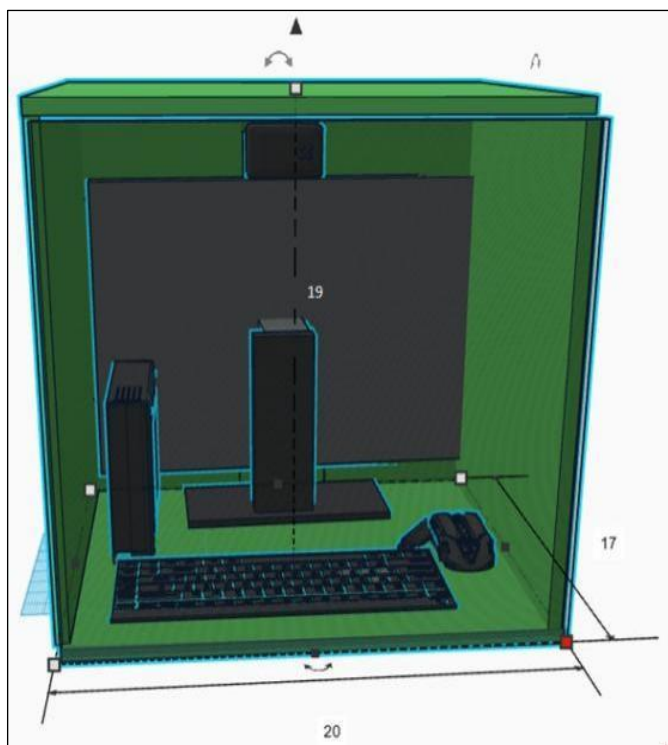


Figure 2: Internal view of the chassis.

Source: Authors, (2024).

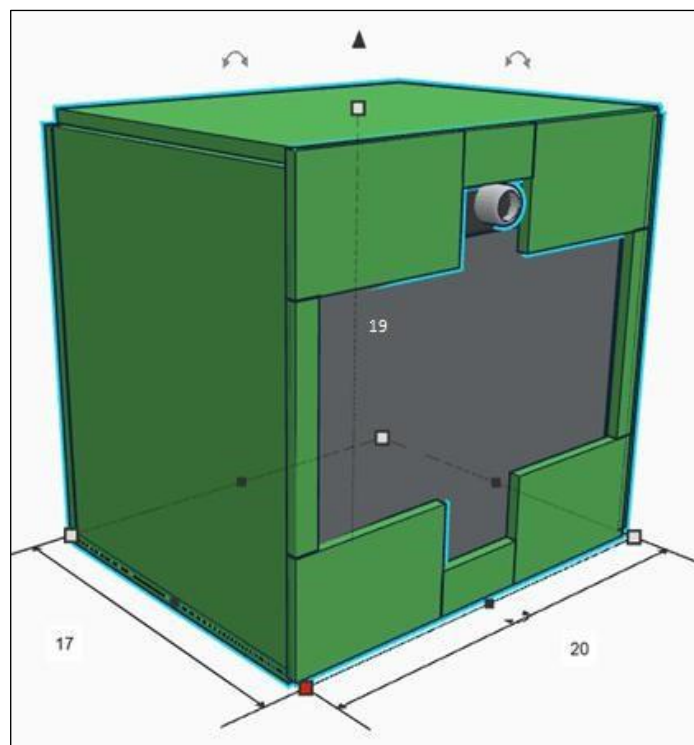


Figure 3: External view of the chassis.

Source: Authors, (2024).

The device's chassis is made of marine plyboard, a sturdy, affordable wood used for house constructions. It features removable top and back panels for easy wire management and cleaning, and measures 19 inches in height, 20 inches in length, and 17 inches in width.

### III.1 DEVELOPMENT OF THE SYSTEM SOFTWARE AND GRAPHICAL USER INTERFACE

Python is a widely-used, easy-to-learn, and flexible programming language that supports object-oriented programming and built-in data structures. The system software was developed on a Mini PC, integrated with a Samsung B2030 Monitor for a graphical user interface. The project's front-end system displayed device readings and camera previews. Variables were initialized, and a flowchart was used to create the source code for the program's operation.

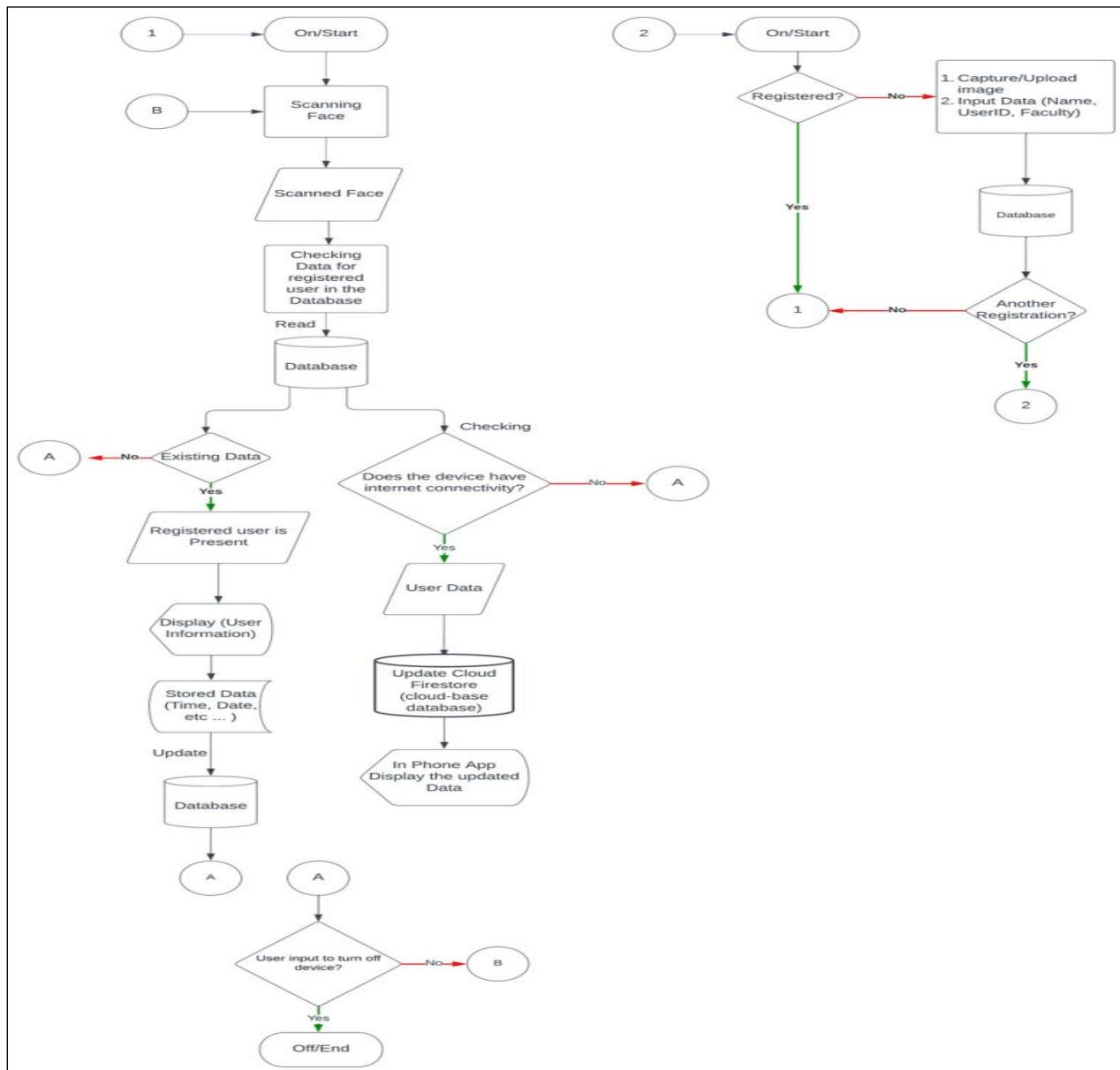


Figure 4: The flowchart of the IoT based automated attendance system.

Source: Authors, (2024).

Figure 4 shows the flowchart of the system. The program registers a user in the system, trains their reference image, and captures their face using a web camera. The program encodes the face in a database to determine if the user is in the system. If the user is, a "Success!" prompt appears, along with the scanned user's information. The user's time and date are automatically logged in an excel sheet, and the information is uploaded to the cloud. The process repeats for each user until the device is turned off.

The mobile application for an IoT-based automated attendance system was developed using PyCharm, Python's official IDE. It provides real-time information about registered users, uploading their data to Firestore Cloud and reflecting on the application within a short time.

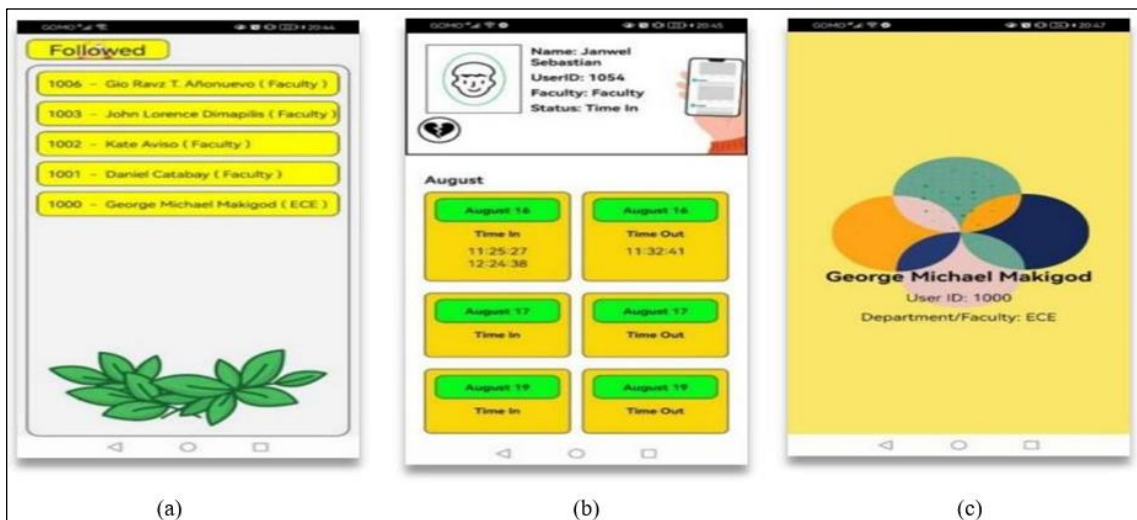


Figure 5: GUI of the mobile application: (a) Followed profiles, (b) Time and dates, and (c) Profile of user. Source: Authors, (2024).

### III.2 EVALUATING THE SYSTEM

The study tested an automated attendance system using facial recognition by comparing its speed to existing biometric systems. Researchers recorded the time it took to recognize registered participants and compared it to existing systems. A paired t-test was used to determine which system performed better in terms of speed, as speed refers to the time it takes for both systems to log an attendance. The aim was to provide a more efficient way to log in attendance. The paired t-test formula is as follows:

$$t = \frac{\sum d}{\sqrt{\frac{n(\sum d^2) - (\sum d)^2}{n}}} \quad (1)$$

where:

$d$  = difference per paired value

$n$  = number of samples

$\sum d$  =  $\sum$  of the differences

The system is evaluated by comparing the match distance value of a user's reference image to a scanned device image. They used a different device with the same facial recognition program but different camera hardware specifications, as shown in Table 1.

Table 1: Camera Specifications.

SPECIFICATIONS	LAPTOP CAMERA	ORASHARE WB-01 HD WEB CAMERA
Megapixels	0.9MP	2.1MP
Aspect Ration	16:9	16:9
Resolution	1280x720	1920x1080
Frames per Second	30fps	30fps
Refresh Rate	60Hz	75Hz

Source: Authors, (2024).

The match distance value is a numerical measure that quantifies the similarity between a scanned image and a reference image. The most common match distance value for facial recognition programs is 0.6, but these values are prone to inaccuracy. In a study evaluating the AI facial recognition system, researchers set a threshold of 0.37 to ensure accurate recognition and minimize misidentifications. This threshold was determined through empirical observations and practical insights, balancing the risk of missed identifications and false positive matches. Overly strict threshold values often resulted in missed identifications, while too lenient thresholds posed risks of false positive matches. The selection of the 0.37 threshold was guided by practical considerations and an empirical understanding of the system's behavior, demonstrating its ability to differentiate between authorized users and guard against errors. Accuracy was calculated based on the match distance value and facial recognition results. Accuracy Percentage of Match Distance Value:

$$Accuracy = [1 - matchdistance] \times 100 \quad (2)$$

The system was evaluated by testing the maximum distance a user could be recognized, using distances from 2ft, 4ft, and 6ft. The accuracy of the match distance value was measured, and results were averaged per distance. The prototype was also evaluated by placing two registered users in front of it, with three tests: one where User A was far from the camera, one where User B was near, and one where both users were in the same position.

### IV. RESULTS AND DISCUSSIONS

The IoT based automated attendance system using facial recognition was brought to the Cavite State University Main Campus, College of Engineering and Information Technology for performance evaluation. The device was treated as an independent attendance system for its performance. The system had a total of 100 registered users.

To compare the speed of the prototype in logging an attendance, it was compared to an existing biometric attendance



system developed by [12]. The data in their study was extracted from Figure 5 in their journal article.

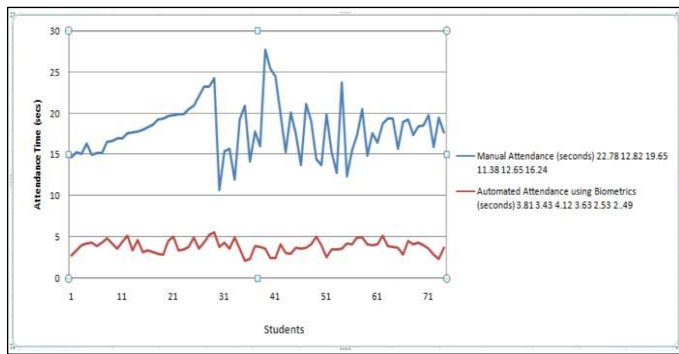


Figure 5: Comparison of manual attendance with Attendance Management System.

Source: [12]

The prototype of a biometric attendance system developed by [12], was compared to an existing system tested on 80 students. The prototype was found to be 19.89% faster than the fingerprint

system, consuming an average of 3.152167 seconds in logging attendance.

Table 2. Comparison Result of Prototype's Speed Compared To An Existing Attendance System.

Number of Users	Fingerprint Attendance System	Prototype's Speed in Recognizing
80	3.935625	3.152167

Source: Authors, (2024).

The Paired T-test test was employed to objectively ascertain whether there was a significant difference in the speeds of the two approaches. The null hypothesis states that the existing biometrics attendance system performs better than prototype in terms of speed, while the alternative hypothesis states that the prototype performs better than the existing biometrics attendance system. The analysis used a 0.05 level of significance. The calculations were done using IBM SPSS Statistics Software. The result of the analysis is shown in Table 3.

Table 3: Paired T-test Table Calculated in IBM SPSS Statistics Software.

PAIRED SAMPLES TEST										
Paired Differences									Significance	
					95% Confidence Interval of the Difference					
		Mean	Std. Deviation	Std. Error Mean	Lower	Upper	t	df	One-Sided P	Two-Sided P
Pair 1	Fingerprint Prototype	.78346	.62943	.7037	.64338	.92353	11.133	79	<.001	<.001

Source: Authors, (2024).

A paired T-test was conducted to compare the performance of their prototype with an existing biometrics attendance system. The results showed a mean difference of approximately 0.78346 between the two systems, with a standard deviation of 0.62943 and a standard error of 0.7037. The 95 percent confidence interval ranged from 0.64338 to 0.92353, with a computed t-value of 11.133 indicating a strong difference between the prototype's performance and the null hypothesis value.

The paired t-test results supported the null hypothesis that there was no difference between the systems in favor of the prototype. The two-sided p-value was also less than 0.001, further reinforcing this conclusion. The prototype outperformed the fingerprint attendance system significantly, with an average improvement of approximately 0.78345. To measure the accuracy of the match distance value, the researchers conducted a cross-camera performance evaluation using a standard laptop camera. The average match distance value a standard laptop camera can generate is 0.445293 or 0.45, with an average accuracy of 56 percent. These findings highlight the superiority of the system and the potential of the prototype in improving biometrics attendance systems.

Table 4: Average of the data recorded using standard laptop camera.

NUMBER OF TESTS	LAPTOP CAMERA (Average Match Distance Value)	ACCURACY OF MDV (Average)
10	0.445293	56%

Source: Authors, (2024).

The prototype's camera generated an average match distance value of 0.309119, with an accuracy percentage of 69%. The scanned user's match distance value was less than the 0.37 threshold, indicating that the system recognized the user 10 times out of 10 tests.

Table 5: average of the data recorded using the prototype's camera.

NUMBER OF TESTS	LAPTOP CAMERA (Average Match Distance Value)	ACCURACY OF MDV (Average)
10	0.309119	69%

Source: Authors, (2024).

Table 6 compares two cameras, showing a standard laptop camera has an average 56% match distance value accuracy rate, while the prototype's camera has an average of 69%, indicating a 14 percent difference in accuracy.

Table 6: Average of the match distance value accuracy of both cameras.

	LAPTOP CAMERA (Average MDV Accuracy)	PROTOTYPE'S CAMERA (Average MDV Accuracy)	DIFFERENCE
Average	56%	69%	14%

Source: Authors, (2024).

A prototype laptop camera's cross-camera performance was evaluated, finding it more accurate in match distance values compared to a standard camera. They tested the camera's maximum distance for user recognition, using distances of 2ft, 4ft, and 6ft. Results showed match distance values were less than 0.37 at 2ft and 4ft, but more than 0.37 at 6ft, indicating that 6ft distance is not acceptable. The ideal distances for a user to stand from the prototype are 2ft to 4ft, with the results shown in Table 7.

Table 7: Tabulated data of the results based on the distance test.

DISTANCE	TEST 1 (MDV)	TEST 1 (MDV)	TEST 1 (MDV)	AVERAGE ACCURACY
2ft	0.33184048	0.31100299	0.32514012	68%
4ft	0.36820279	0.33120573	0.33731981	65%
6ft	0.37860146	0.40556667	0.41409713	60%

Source: Authors, (2024).

Three tests was conducted to determine the priority of users in scanning a camera. The tests involved two users, one far from the camera and the other near it. The results showed that the program prioritized the far user 4 out of 10 times, indicating that not all users near the camera will be recognized. The program prioritized the near user 6 out of 10 times, with a match distance value accuracy rate of 59%. The program also recognized the far user 40% of the time, with a match distance value accuracy rate of 41%. Both users had an average of 19% difference in recognition.

Table 8: Average of data recorded for test 1.

NUMBER OF TRIALS	USER A (FAR) (Average MDV Accuracy)	USER B (NEAR) (Average MDV Accuracy)	DIFFERENCE
10	41%	59%	19%

Source: Authors, (2024).

In Test 2, the program prioritized User A near the camera 7 out of 10 times, while User B was far. The program prioritized User A 70 percent of the time with a match distance accuracy rate of 51%, while User B was 3 percent of the time with a 47 percent was 3 percent of the time with a 47 percent accuracy rate. Both users had an average of 4% difference in accuracy rate.

Table 9: Average of data recorded for test 2.

NUMBER OF TRIALS	USER A (NEAR) (Average MDV Accuracy)	USER B (FAR) (Average MDV Accuracy)	DIFFERENCE
10	51%	47%	4%

Source: Authors, (2024).

In Test 3, the program prioritized User A over User B when both users stood at the same distance from the camera. User A was only recognized 30% of the time with a 38% match distance value accuracy rate, while User B was recognized 70% of the time with a 58% accuracy rate. User A had an average match distance value of 0.621007, while User B had an average of 0.4186554. User A's higher value suggests that User B was more recognizable than User A, as the threshold value set by the researchers was 0.37. The results may be due to feature extraction and minor pose variations, as User B's facial features were more distinctive and pronounced compared to User A.

Table 10: Average of data recorded for test 3.

NUMBER OF TRIALS	USER A (Average MDV)	USER A (Average MDV Accuracy)	USER B (Average MDV)	USER B (Average MDV Accuracy)	MOST REOGNIZE R D USER
10	0.621007	38%	0.4186554	58%	User B (7/10)

Source: Authors, (2024).

## V. CONCLUSIONS

The study developed an IoT-based automated attendance system using facial recognition, which was successfully implemented. The system provided students, professors, and parents with comprehensive attendance records, with an intuitive design that matched diverse needs. The system outperformed traditional methods with an average time efficiency of 3.16 seconds and an accuracy rate of 69%. However, the system only scanned and logged attendance, not showing the exact location of the person inside the institution. Future research could explore liveness detection experiments to enhance facial recognition systems' robustness and security.

## VII. ACKNOWLEDGMENTS

The authors express their gratitude to Dr. Edwin R. Arboleda, a thesis adviser, Engr. Lemuel G. Tatad, a technical critic, Ms. Poinsettia A. Vida, the unit research coordinator, Dr. Willie C. Buclatin, the Dean of the College of Engineering and Information Technology, Dr. Michael T. Costa, Engr. Rose Ann E. Sumadsad, Engr. Rhodonelle S. Duatin, Engr. Miguel Joseph L. Jacoba, and Engr. Cenon D. Lumabad III, the review panel, all participants in the study, especially the two sections of students, for their invaluable contributions and support. They also thank God for his unending knowledge, guidance, and support.

## VIII. REFERENCES

- [1] Ravalji, R., Shah, N., Patel, H., & Patel, M. (2020). FACIAL RECOGNITION-BASED ATTENDANCE SYSTEM USING PYTHON. International Research Journal of Engineering and Technology. www.irjet.net
- [2] Sri Madhu, B. M., Kanagotagi, K., & Devansh. (2018). IoT based Automatic Attendance Management System. International Conference on Current Trends in Computer, Electrical, Electronics and Communication, CTCEEC 2017, 83–86. <https://doi.org/10.1109/CTCEEC.2017.8455099>
- [3] Alhanaee, K., Alhammadi, M., Almenhali, N., & Shatnawi, M. (2021). Face recognition smart attendance system using deep transfer learning. Procedia Computer Science, 192, 4093–4102. <https://doi.org/10.1016/j.procs.2021.09.184>
- [4] Kovelan, P., Thisentira, N., & Kartheeswaran, T. (n.d.). Automated Attendance Monitoring System Using IoT.
- [5] Anand, V., Singh Parihar, V., Sharma, S. K., Singhal, V., & Sethy, P. K. (2021). FACIAL RECOGNITION SYSTEM USING OPENCV. In International Journal of Creative Research Thoughts (Vol. 9, Issue 7). [www.ijct.org](http://www.ijct.org)
- [6] Olanipekun, A. A., & Boyinbode, O. K. (2015). A RFID based automatic attendance system in educational institutions of Nigeria. International Journal of Smart Home, 9(12), 65–74. <https://doi.org/10.14257/ijsh.2015.9.12.07>
- [7] Rjeib, H. D., Ali, N. S., Al Farawn, A., Al-Sadawi, B., & Alsharqi, H. (2018). Attendance and information system using RFID and web-based application for academic sector. International Journal of Advanced Computer Science and Applications, 9(1), 266–274. <https://doi.org/10.14569/IJACSA.2018.090137>
- [8] Konatham, S., Surya Chalasani, B., Kulkarni, N., & El Taeib, T. (n.d.). ATTENDANCE GENERATING SYSTEM USING RFID AND GSM.
- [9] MB, S., & Roy, R. (2015). A Web Secured System for Attendance Monitoring and Real Time Location Tracking Using Biometric and Radio Frequency Identification (RFID) Technology. 653-657
- [10] Rahman, S., Rahman, M., & Rahman, M. M. (2018). Automated Student System using Fingerprint Recognition. Edelweiss Applied Science and Techno <https://doi.org/10.33805/2576.8484.120>
- [11] Akinduyite, O. C., Adetunmbi, A. O., Ibidunmoye, O., & Olabode, O. O. (2013). Fingerprint-Based Attendance Management System. Journal of Computer Sciences and Applications, 1(5), 100–105. <https://doi.org/10.12691/jcsa-1-5-4>
- [12] Oluwagbemiga, E., Shoewu, O., Idowu, O., Shoewu, O., & Idowu, O. A. (2012). Development of Attendance Management System using Biometrics Robotics and Systems View project Electronics View project Development of Attendance Management System using Biometrics. In The Pacific Journal of Science and Technology (Vol. 13, Issue 1). <http://www.akamaiuniversity.us/PJST.htm>
- [13] Damale, R. C., & Pathak, Bazeshree. V. (2018). Face Recognition Based Attendance System Using Machine Learning Algorithms. 2018 Second International Conference on Intelligent Computing and Control Systems (ICICCS), 414–419. <https://doi.org/10.1109/ICCONS.2018.8662938>
- [14] Suresh, V., Chakravarthi Dumpa, S., Deepak Vankayala, C., & Rapa, J. (2019). Facial Recognition Attendance System Using Python and OpenCv. In Quest Journals Journal of Software Engineering and Simulation (Vol. 5, Issue 2). [www.questjournals.org](http://www.questjournals.org)
- [15] Aware, M., Labade, P., Tambe, M., Jagtap, A., & Beldar, C. (2021). Attendance Management System using Face-Recognition. International Journal of Scientific Research in Computer Science, Engineering and Information Technology, 336–341. <https://doi.org/10.32628/cseit217370>
- [16] Emami, S., & Suci, V. P. (2012). Facial Recognition using OpenCV FaceBots View project Facial Recognition using OpenCV. [www.jmeds.eu](http://www.jmeds.eu)
- [17] Wang, N. J., Chang, S. C., & Chou, P. J. (2012). A real-time multi-face detection system implemented on FPGA. ISPACS 2012 - IEEE International Symposium on Intelligent Signal Processing and Communications Systems, 333–337. <https://doi.org/10.1109/ISPACS.2012.6473506>
- [18] Silwal, V., & Panicker, A. (2019). Facial Detection and Facial Recognition using OpenCV. <http://ijesc.org/>.
- [19] Bin Sulaiman, R., Kareem, A., & Saber Nipun, M. (n.d.). Efficiency Comparison of AI classification algorithms for Image Detection and Recognition in Real-time.



### RESEARCH ARTICLE

### OPEN ACCESS

## INVESTIGATING THE EFFECT OF TARTARIC ACID ON CONCRETE PRODUCED IN TROPICAL CLIMATES

Aliu Soyngbe<sup>1</sup>, and Dele Simeon\*<sup>2</sup>

<sup>1,2</sup> Department of Building, University of Lagos, Lagos, Nigeria.

<sup>1</sup><http://orcid.org/0000-0002-7992-6556> , <sup>2</sup><http://orcid.org/0000-0002-3927-7547> 

Email: [asoyngbe@unilag.edu.ng](mailto:asoyngbe@unilag.edu.ng), \*[dsimeon@unilag.edu.ng](mailto:dsimeon@unilag.edu.ng)

### ARTICLE INFO

#### Article History

Received: November 29<sup>th</sup>, 2023

Revised: July 08<sup>th</sup>, 2024

Accepted: August 15<sup>th</sup>, 2024

Published: August 30<sup>th</sup>, 2024

#### Keywords:

Dosage,  
Ready-mix concrete,  
Setting time,  
Tartaric Acid,  
Tropical climates.

### ABSTRACT

The perpetual gridlock of Metropolitan Lagos is well-known, particularly during chaotic rush hours. As such, construction projects encounter difficulties with material transportation as well as rapid delivery of ready-mix concrete to construction sites located in this city. To achieve concrete that allows for long-distance transportation and lessens the impact of hot weather on concrete, this study investigated the performance of TA in concrete produced in tropical and congested climates and recommended suitable dosages and appropriate times of addition for the desired outcome. The study produced a working sample of 117 concrete cubes using various doses of TA at 0, 0.5, 1, 1.5, and 2%. Findings revealed that TA is time and dosage-dependent. The findings also revealed that the addition of TA at 31.5°C causes set retardation and the setting time of each test sample was substantially increased with TA addition. Moreover, the compressive strength of concrete was increased by 70.8% when a 2% TA was added after a 3-minute delay. The study concludes that TA is an appropriate retarder for ready-mix concrete because it provides extended workability, slows the setting time in gridlocks, prevents concrete from hardening untimely, and counteracts the impact of hot weather by slowing the setting time.



Copyright ©2024 by authors and Galileo Institute of Technology and Education of the Amazon (ITEGAM). This work is licensed under the Creative Commons Attribution International License (CC BY 4.0).

### I. INTRODUCTION

The basic ingredients for the production of concrete are cement, water, and aggregates [1]. However, [2] noted that an admixture may be added to the mixture to modify its characteristics. Although cement is a chemically active ingredient, its reactivity is only triggered when it is combined with water. The setting process commences when water is added to a concrete mixture. This process occurs as a result of the heat of the hydration reaction of cement. According to [3], the factors responsible for the physical properties of concrete are the extent of hydration of cement and the resultant microstructure of the hydrated cement. The hydration reaction of these compounds occurs within a certain time frame, and the formation of the products of the reaction results in the setting of the cementitious material, consequently causing a degree of hardness over time. The setting times of concrete and cement are categorized into the initial setting times and the final setting times. While the loss of plasticity is measured by the initial

setting time, the gain of a particular hardness is measured by the final setting time. According to [ASTM C191-92], as cited in [4], the initial setting time can be seen when the Vicat's needle gets 25 millimeters of penetration while the final setting time is when the Vicat's needle cannot penetrate. Admixtures are known to improve the performance of concrete and are available in a wide variety of types and used for diverse applications. For [5], buttressed that in order to improve particular qualities of the freshly mixed and cured concrete, additives, whether synthetic or natural, are included during the mixing process. For [6], notes that concrete admixtures are considered to be the most successful and extensively used solutions for improving concrete workability. Accordingly, [7] opines that admixtures are used to increase workability, to retard or accelerate the time of initial setting; to modify the rate or capacity for bleeding, to reduce segregation, to accelerate the rate of strength development at early ages, etc. One such admixture that retards the setting time of concrete is retarders. Retarders are

admixtures that extend the period in which the mix changes from the plastic to the rigid state.

The use of ready-mix concrete has obtained a dominant place in the Nigerian construction industry as it facilitates high speed of construction which is required in many construction projects. In most construction projects, ready-mix concrete is purchased from concrete suppliers who have their batching plants offsite at a distant location hence requiring transportation of concrete to the site. However, the traffic situation poses several problems to the transportation of concrete over long distances leading to a high probability of it setting in the truck when traffic congestion is high. Hence, a need to use retarders to curtail the menace. According to [8], transportation poses to be a challenge as a great deal of productive man-hours is wasted in traffic congestion in the commercial city of Lagos, Nigeria. For [9], opine that the nominal initial setting time for concrete is 30 minutes. According to [10] examined how superplasticizers and retarders influenced the characteristics of concrete with a 30 MPa specific strength. The findings indicated that combining a superplasticizer and a retarder might increase the workability of concrete. The characteristics of concrete produced by combining natural and retarded ready-mix concrete with a reverted fresh mix of concrete were examined [11]. The findings indicated that the concrete's workability, setting time, and compressive strength were all within acceptable bounds.

Retarders are generally categorized into two groups which are the organic and the inorganic chemicals. For [12] classified retarders into three types, namely: Type B which simply retards the hydration of Portland cement; Type D which not only retards the hydration but also acts to disperse the cement particles thereby providing water reduction; and Type G which is a high range water reducing and set retarding admixture. According to [12] and [13], Type B retarders are Lignin, Borax, Sugars, Tartaric acids, and Salts. Tartaric acid is an organic retarder under the hydroxycarboxylic acid group which are characterized by carboxyl groups (-COOH) and hydroxyl groups (OH). It is a simple hydroxycarboxylic acid which has a chemical formula  $C_4H_6O_6$  with two carboxyl (-COOH) and hydroxyl (OH) groups each. The most important step in tartaric acid inhibition is formation of calcium tartrate, but it has been observed that tartaric acid only exhibits a dissolution-precipitation mechanism for  $C_3A$  [14]. The effects of retarding admixture on the setting time of concrete are dependent upon the type of cement, mix proportions used, the dosage of the admixture, time of addition to the mix, the ambient temperature, and curing conditions [15],[16].

Tropical climates usually have distinct rainy and dry seasons and are characterized by high temperatures all year round. The tropical climates in Lagos-state, and most parts in Southwest, Nigeria throughout the year have a mean ambient temperature of about 30°C. For [16] are of the view that ambient temperature could be as high as over 43°C in the extreme North Eastern part of the country. Thereby classifying concrete works done in these regions as hot weather concreting and as earlier stated, the high temperatures in these regions will result in rapid loss of water and acceleration in the setting of concrete causing thermal and plastic cracking, reduction in ultimate strength. According to [17] opine that concrete has a stronger compressive strength at low temperatures than it does at normal temperature. The use of retarders ameliorates the adverse effect of high temperature, as well as prolongs the initial setting time of concrete, thereby providing a solution to the problems associated with hot weather concreting and transportation of ready-mixed concrete. The type of cement, admixture dosage, mix proportion, time of addition to the mix, and ambient temperature are all factors that determine the effects of

retarders on the setting time of concrete. In order to address the problems and provide recommendations for the use of retarders, the study seeks to investigate the effects of TA retarder on concrete made with a 32.5 grade, Ordinary Portland Cement (OPC) using a specific mix ratio so as to recommend suitable dosages and appropriate time of addition required to attain the desired outcome. The objectives of the study are to; determine the workability of concrete produced with varied percentages of TA retarder, determine the setting times of concrete produced with different percentage dosages, and establish the compressive strength of concrete produced with varied percentages of TA doses in tropical climates. The study is significant in tropical climates because TA improves workability, lowers the chance of early setting, enables better placement, and guarantees high-quality construction when used in ready-mix concrete.

## II. MATERIALS AND METHODS

This section discusses the materials and methods used to conduct the study. The study is purely experimental and conducted in Lagos state, Nigeria. Lagos State which ranks among one of the six states in south western, Nigeria is situated in a tropical region and close to the Atlantic Ocean's Gulf of Guinea shoreline. The materials and methods are discussed in the following sub-sections.

### II.1 MATERIALS

The materials used to carry out the investigation comprised: Ordinary Portland cement, fine aggregate, coarse aggregate, tartaric acid, and water. The cement used was OPC (Grade 32.5R) obtained from Lafarge PLC with a trade name "Elephant Classic" and conforms to the requirements of [18]. The fine aggregate used for the study was natural sharp river sand which was obtained from the Ogun River basin at Ibafo in Ogun state. This was dried and sieved using a 5mm BS 812 sieve in order to remove large aggregates and impurities. It was confirmed that the sand was free from deleterious substances that are liable to lead to unsoundness or react in a harmful way with the concrete. Besides, the Sharp sand did not contain particles exceeding 5mm in size and was in conformity with [19]. The coarse aggregate used was crushed granite with a maximum normal size of 20mm and retained on a 10mm sieve minimum which conformed to [20]. It was in saturated surface dry condition before it was used in the mixing. The admixture used was 99% extra pure dl-Tartaric acid (synthetic) which is highly soluble in water and specifically prepared for research and development/lab use only. It was obtained from T. Saicon International LTD at Ojota, Lagos. The water used was clean portable water obtained from the faculty of Environmental sciences workshop, at the University of Lagos, Akoka, Yaba Local government area of Lagos state and it conforms to the specification of [21] for the production of concrete.

### II.2 METHODS

The various laboratory procedures carried out are reported in the sub-sections.

#### II.2.1 Preliminary Investigation on the Materials

The laboratory test carried out on the aggregates is the sieve analysis to determine the particle size distribution of the aggregates. The apparatus used to achieve this test were sieve shaker, cleaning brush, weighing balance, hand scoop, a set of BS sieves, and a metal tray. The laboratory procedures are that the

sieves of the sieve shaker were cleaned using a cleaning brush to remove particles struck in the openings. The weight of each sieve and receiving pan was measured and recorded. The sieves were arranged in descending order according to their sizes (10mm, 5mm, 2.36mm, 1.0mm, 0.6mm, 0.25mm and 0.075mm). The weighed specimen was kept on the top sieve (1000g for sharp sand and 3000g for granite) and the complete sieve was stacked on the sieve shaker. The shaker was then allowed to work for 5-10 minutes. The sieve stack was removed from the shaker and weighed together with the samples of aggregate retained and then recorded. The sharp sand and granite retained on each sieve and receiving pan (sample passing) were weighed and recorded separately. Then, the following parameters were determined as required on each aggregate

$$\frac{\text{Percentage weight retained} \times 100}{\text{Total mass of sample}} = \frac{((\text{mass of sample} + \text{container}) - (\text{mass of container})) \times 100}{\text{Total mass of sample}} \quad (1)$$

Percentage weight passing = (100 - % Weight retained on consecutive sieve)

The sizes of the values of percentage passing at 10, 30 and 60 represented as D10, D30 and D60 were obtained from a graph

of percentage passing each sieve plotted against sieve sizes (particle size distribution curve) which is used to determine:

- Fineness modulus (FM) = 
$$\sum \frac{\% \text{Cumulative Weight retained from 10.0mm to 0.075mm}}{100} \quad (2)$$

- The coefficient of uniformity,  $C_u = \frac{D_{60}}{D_{10}} \quad (3)$

### II.2.2 Preparation of Concrete

A nominal concrete mix of ratio 1:2:4 was prepared with a water/cement (w/c) ratio of 0.5 was adopted for the study at a temperature of 31.5 °C. The concrete mix was prepared by adding the admixture. Tartaric acid (TA) was added at a dosage of 0% as the control sample, 1.0 and 2.0% of the cement weight. The choice of dosage was based on the research carried out by [22] which indicated that TA retarded the setting of concrete at a dosage of 1% of the weight of cement.

The addition of TA to each mix was done at different times which were:

- at the time of direct mixing of the concrete with water
- 3mins after mixing
- 5mins after mixing

The properties of TA are given in the Table 1:

Table 1: Properties of Tartaric Acid (TA).

Retarder	Molecular weight	Melting Point (°C)	Density	Water Solubility
Tartaric acid	150.0878	240-206	1.7598	139g/100 ml

Source: Authors, (2024).

### II.2.3 Workability Test

The Slump test was carried out for each batch of fresh concrete produced in accordance with the provisions of [23]. The workability is determined after each percentage addition of TA. The apparatus used for the study are slump cone, non-porous base plate, measuring scale, and tamping.

### II.2.4 Setting Time Tests

The apparatus used for determining the initial and final setting times of the concrete produced is the Vicat's apparatus, weighing balance, stopwatch, non-porous plate, enamel try, and trowel. Two sets of samples were studied. The first being, 650g of cement mixed to normal consistency without Tartaric acid (TA) while the second was 650g of cement mixed to normal consistency after which the retarder, TA, was then added. The test was carried out, ensuring that each penetration test was at least 5mm away from any previous penetration and at least 10mm away from the inner side of the mould. The test block was always in the moist cabinet except when penetration measurements were being taken. Vicat's approach was used to determine the initial and final setting time tests following the [25] method.

#### II.2.4.1 Determination of Initial Setting Time

The elapsed time between the initial contact of cement and water and the penetration of 25 mm is the Vicat's initial time of setting and it is measured by the loss in plasticity. The initial setting time was determined by interpolating to determine the time when a penetration of 25mm was attained.

#### II.2.4.2 Determination of Final Setting Time

The elapsed time between the initial contact of cement and water and the time of setting endpoint is the Vicat's final time of setting and it is measured by a gain of a particular hardness. The time of setting endpoint was considered as the first penetration measurement where the needle does not mark a complete circular impression on the surface of the specimen.

### II.2.5 Compressive Strength Test

The apparatus used were concrete mould, tamping rod, trowel, and Avery compression machine. A total of 117 cubic samples with dimensions of "150×150×150mm" for the various testing requirements were used for the study. For the compressive strength test, three cubes were crushed for each curing age (7, 14, and 28 days) complying to the requirements of [24]. The average of the results of these three cubes was recorded as the compressive strength value at a specified age. The cubes were weighed before testing to determine the unit weight. It is calculated using the formula:

$$\text{Compressive strength} = \frac{\text{maximum load (KN)} \times 1000}{\text{Crosssectional Area (mm}^2\text{)}} \quad (4)$$

### II.2.6 Percentage Increase in The Ultimate Strength of Concrete

This involves comparing the compressive strength of the samples with no retarder added (the control sample) to other samples with different quantity of TA added to the mix. The compressive strengths obtained from the cubes were used to determine the percentage increase in strength for each case of usage of TA.

$$= \frac{\text{Ult.Strength of sample} - \text{Ult.Strength of Control sample}}{\text{Ult.Strength of Control sample}} \times 100 \quad (5)$$

### III. RESULTS AND DISCUSSIONS

The results are discussed under the following headings. This includes tests on fine and coarse aggregate (sieve analysis), tests on fresh concrete (workability), and tests on hardened concrete.

#### III.1 SIEVE ANALYSIS

The sieve analysis was to carried out to determine the particle size distribution of the fine and coarse aggregates used for the research.

#### III.1.1 Sieve Analysis of Fine Aggregate

This sieve analysis test of the fine aggregate (Sharp Sand) was carried out to determine the particle size distribution of the fine aggregate used, as well as determine its fineness modulus (FM) and coefficient of uniformity, Cu. 1000g of sand was used in carrying out this test and the result of the sieve analysis is presented in Table 2 and Figure 1 respectively.

Weight of Sand Used (A = 1000g)

Table 2: Particle Size Distribution of Fine Aggregate (Sand).

BS Sieve size, mm	Aggregate weight Retained (g),	Cumulative weight Retained (g), B	Percentage Cumulative weight Retained %	Aggregate weight passing (g) C = A- B	Percentage Passing, % (d) = $\frac{C}{A} \times 100$
10.00	0.00	0.00	0.00	1000.00	100.00
5.00	29.90	29.9	2.99	970.10	97.01
2.36	47.00	76.90	7.69	923.10	92.31
1.18	143.80	220.70	22.07	779.30	77.93
0.6	318.90	539.60	53.96	460.40	46.04
0.3	285.50	825.10	82.51	174.90	17.49
0.15	131.40	956.50	95.65	43.50	4.35
0.075	23.20	979.70	97.97	20.30	2.03
Pan	7.4	987.10			

Source: Authors, (2024).

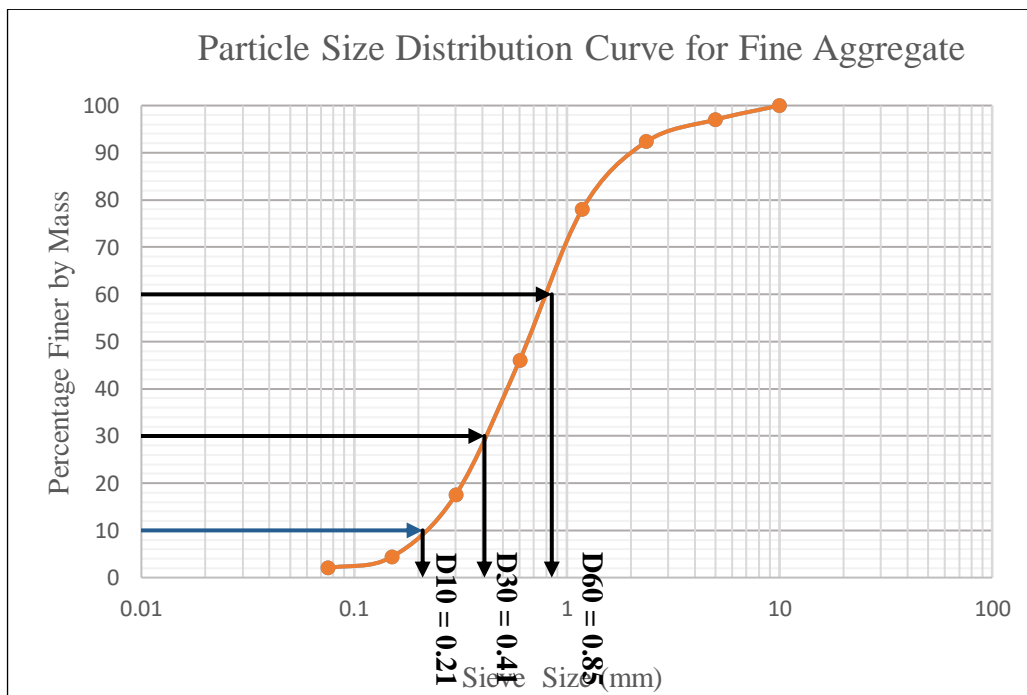


Figure 1: Particle size distribution curve of fine aggregate used for the research.

Source: Authors, (2024).

- Fineness modulus (FM) =

$$= \frac{\sum \text{Cumulative Weight retained from 10.0mm to 0.075mm}}{100} = \frac{2.99+7.69+22.07+53.96+82.51+95.65+97.97}{100} = 3.63 \quad (6)$$

This means that the average fine aggregate size is within the 3<sup>rd</sup> and 4<sup>th</sup> sieve. That is, the average aggregate size is between 0.3mm and 0.6mm. And from the value of the fineness modulus, it is a medium sand.

- Coefficient of uniformity,  $C_u = \frac{D_{60}}{D_{10}} = \frac{0.85}{0.21} = 4.05$  (7)

Since  $C_u > 4$ , the sand is well-graded.  $C_u$  values between 4 and 6 are regarded as well-graded soil, whereas values under 4 are regarded as poorly-graded soil [26]. Therefore, the fine aggregate used was a well-graded medium sand.

### III.1.2 Sieve Analysis of Coarse Aggregate

This test was carried out to determine the particle size distribution of the coarse aggregate used as well as determine its fineness modulus (FM) and coefficient of uniformity,  $C_u$ . Granite of 3000g was used in carrying out this test and the result of the sieve analysis is presented in Table 3 and Figure 2 respectively.

Weight of Granite Used ( $A = 3000g$ ).

Table 3: Particle Size Distribution of Coarse Aggregate (Granite)

BS Sieve size, mm	Aggregate weight Retained (g),	Cumulative weight Retained (g), B	Percentage Cumulative weight Retained %	Aggregate weight passing (g) $C = A - B$	Percentage Passing, % $(d) = \frac{C}{A} \times 100$
25.0	0.00	0.00	0.00	3000.00	100.00
19.0	0.00	0.00	0.00	3000.00	100.00
14.0	13.6	13.6	0.45	2986.40	95.55
12.5	82.6	96.2	3.21	2903.80	96.79
10.0	835.6	931.8	31.06	2068.20	68.94
5.0	1880.6	2812.4	93.75	187.60	6.25
2.36	148.0	2960.4	98.68	39.60	1.32
Pan	32.3	2992.9			

Source: Authors, (2024).

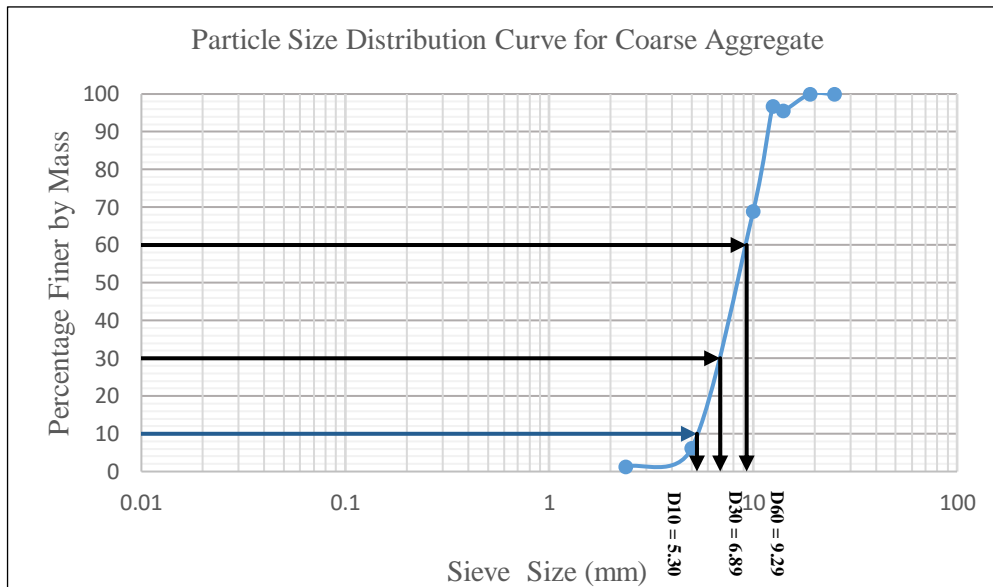


Figure 2: Particle size distribution curve of coarse aggregate used for the research.

Source: Authors, (2024).

- Fineness modulus (FM) =

$$FM = \frac{\sum \% \text{ Cumulative Weight retained from 25.0mm to 2.36mm}}{100} = \frac{0.00+0.00+0.45+3.21+31.06+93.75+98.62}{100} = 2.27 \quad (8)$$

This means that the average fine aggregate size is within the 2<sup>nd</sup> and 3<sup>rd</sup> sieves. That is, the average aggregate size is between 5.0mm and 10.0mm.

- Coefficient of uniformity,  $C_u = \frac{D_{60}}{D_{10}} = \frac{9.29}{5.30} = 1.75$  (9)

Since  $C_u < 4$ , the sand is uniformly graded. When the soil is well-graded, the coefficient of curvature ( $C_c$ ) must range from 1 to 3, and when the soil is badly graded,  $C_c$  must be less than 1 [26]. Therefore, the coarse aggregate used was a uniformly graded coarse aggregate.

## III.2 TEST ON FRESH CONCRETE

### III.2.1 WORKABILITY OF CONCRETE

The workability of each concrete specimen was conducted using the Slump test [23]. The temperature reading recorded during this test was 31.5 °C. The results obtained for each sample are shown in Table 4. The result indicates that workability is very low in the control specimen. The result further indicates that workability is directly proportional to the dosage of TA among Specimens. This indicates that workability increases as the TA dose increases among specimens A and C. Meanwhile, there is an inverse relationship among specimen B, indicating that the lower the addition of TA, the higher the workability.



Table 4: Slump Test of Various Concrete Samples.

Sample Type	Delay before Addition of TA (min)	Dosage of TA (% wt of Cement)	Slump	
			Slump(mm)	Degree of workability
Control	-	0	15	Very low
A1	0	0.5	62	Medium
A2	0	1	115	High
A3	0	1.5	119.2	High
A4	0	2	125.4	High
B1	3	0.5	130	High
B2	3	1	165	High
B3	3	1.5	80	Medium
B4	3	2	65	Medium
C1	5	0.5	60	Medium
C2	5	1	68	Medium
C3	5	1.5	90	Medium
C4	5	2	113	High

Note: A Slump value of 0-25mm indicates Very Low; 25-50mm indicates Low; 50-100mm indicates Medium; and 100-175mm indicates High.

Source: Authors, (2024).

### III.2.2 setting time test

The initial and final setting times of the various samples were determined using Vicat’s Apparatus, and following the procedures of [27] in the Test for Setting Time, and the results are displayed in Table 5. Table 5 depicts that the addition of TA causes set retardation as the setting time for each of the test samples was substantially increased compared to that of the control sample. It is evident that for a 1:2:4 concrete mix, a 1% dose of TA results in higher retardation for all delays in times of addition compared to a 2% dose. It was also observed that a 2% dose of tartaric acid to the cement paste used for the setting time test resulted in an unusual dryness of the paste, but this was not observed when a 2% dose was added to the 1:2:4 concrete mix as the resulting concrete became more workable. The setting

time results validate the study's arguments that TA is an appropriate retarder for ready-mix concrete because it provides extended workability, slows the setting time in congestion and traffic jams, prevents concrete from hardening untimely, counteracts the impact of hot weather by slowing the setting time, and provides improved control over quality by guaranteeing accurate concrete placement and finishing. These findings corroborate the assertions of [28] that retarders prolong the amount of time that concrete may be finished, put, and transported. Moreover, [22] substantiates that TA is a powerful inhibitor of OPC hydration. It chemically reacts with cement mineral phases to generate calcium tartarate hydrate. This chemical covers the surface of cement granules, preventing hydration. As a result, hydration is slowed.

Table 5: Setting Time Test for Various Sample Types.

Sample Type	Delay before Addition of TA (min)	Dosage of TA (% wt of Cement)	Setting Time (min)	
			Initial	Final
Control	-	0	192	289
A1	0	0.5	417	932
A2	0	1	617	1463
A3	0	1.5	570	1412
A4	0	2	512	1397
B1	3	0.5	775	1499
B2	3	1	1004	1849
B3	3	1.5	612	1111
B4	3	2	267	582
C1	5	0.5	515	933
C2	5	1	799	1550
C3	5	1.5	417	793
C4	5	2	304	664

Source: Authors, (2024).

### III.3 TEST ON HARDENED CONCRETE

The compressive test results after curing at 7, 14, and 28days are presented and discussed in the following sections

#### III.3.1 COMPRESSIVE STRENGTH TEST

The results of the test for compressive strength of the various dosages and times of addition of Tartaric Acid (TA) used in making the samples are presented in Table 6. A total of 117 concrete specimens of size 150mm×150mm×150mm were

produced, and the compressive test was conducted on the specimens at 7, 14, and 28 days respectively in accordance with [29]. Then the average compressive strength was calculated for the respective ages of concrete samples. The various concrete samples are control samples with no addition of TA; Type A to which TA was added at 0.5, 1, 1.5, and 2% immediately after the cement came in contact with water, i.e., 0mins delay; Type B to which TA was added three minutes after cement made contact with water, i.e., 3mins delay at 0.5, 1, 1.5, and 2%; and Type C to which TA was added five minutes after cement made contact with water, i.e., 5mins delay at 0.5, 1, 1.5, and 2% respectively.

The findings show that when the curing age increases, concrete's compressive strength typically rises regardless of the percentage replacement. This is in line with typical research on how concrete behaves as it ages. Moreover, the control specimen recorded the least using value among all the specimens produced. This suggests that the inclusion of TA enhances the strength of concrete. The result further indicates that specimen B4 at 2%TA addition after a 3-minute delay gave the highest value of compressive strength at all curing ages. It includes 23.7N/mm<sup>2</sup>, 32.98, and 35.5N/mm<sup>2</sup> at 7, 14, and 28 days respectively.

Table 6: Compressive Strength of Concrete Specimen.

Sample Type	Delay before Addition of TA (min)	Dosage of TA (% wt of Cement)	Average Compressive Strength (N/mm <sup>2</sup> )		
			7 Days	14 Days	28 Days
A1	0	0.5	14.96	20.23	23.95
A2	0	1	15.73	21.93	29.21
A3	0	1.5	15.22	21.02	29.43
A4	0	2	15.18	20.44	29.85
B1	3	0.5	15.88	21.59	27.99
B2	3	1	16.45	24.59	25.04
B3	3	1.5	20.22	29.5	31.95
B4	3	2	23.7	32.98	35.5
C1	5	0.5	21.1	24.33	26.95
C2	5	1	22.67	27.11	29.48
C3	5	1.5	22.55	28.86	30.05
C4	5	2	22.29	29.63	30.81

Source: Authors, (2024).

### III.3.2 Compressive Strength at Immediate Addition of TA

Figure 3 gives a representation of the gain in compressive strength of the control sample with 0% dosage of TA and that of samples type A to which 1% and 2% of TA were added to the concrete mix immediately after cement made contact with water.

It can be seen that compared to the control sample, samples Type A had slightly higher compressive strengths on 7 and 14 days of curing, but on the 28<sup>th</sup> day, these samples had significantly higher strength than the control sample for both 1% and 2% dosage of TA. This signifies that the addition of Tartaric Acid to a concrete mix causes an increase in the ultimate strength.

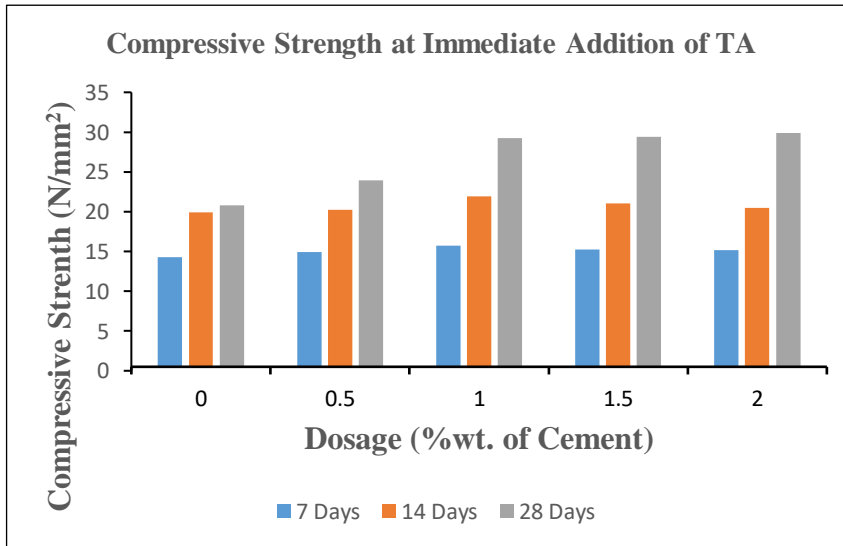


Figure 3: Relationship between the compressive strength of concrete samples upon immediate addition of Tartaric Acid (TA) at different dosages by percentage weight of cement in concrete mix.

Source: Authors, (2024).

### III.3.3 Compressive Strength at 3 Minutes Delay Before the Addition of TA

Figure 4 gives a representation of the gain in compressive strength of the control sample with 0% dosage of TA and that of

samples type B to which 1% and 2% of TA was added to the concrete mix 3 minutes after cement made contact with water. It was observed that there was a significant increase in compressive strength for all respective ages of the Type B

samples, compared to the control samples. This indicates that the addition of Tartaric Acid to a concrete mix after a 3-minute delay causes an increase in the ultimate strength at 1% and 2% dosages

and that a higher dosage results in a significantly higher gain in compressive strength.

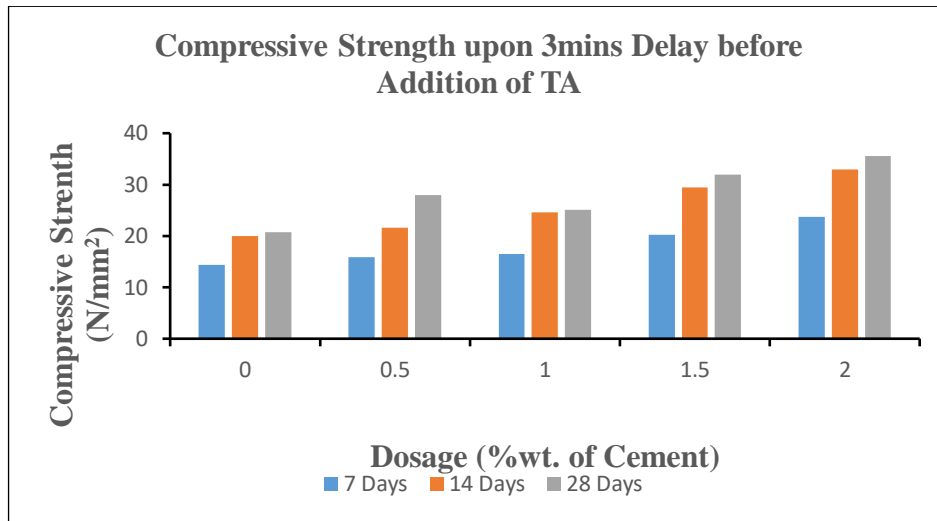


Figure 4: Relationship between the compressive strength of concrete samples upon a 3-minute delay before the addition of TA at different dosages by percentage weight of cement in the concrete mix.

Source: Authors, (2024).

### III.3.4 Compressive Strength At 5 Minutes Delay Before the Addition of TA

Figure 5 gives a representation of the gain in compressive strength of the control sample with 0% dosage of TA and that of samples type C to which 1% and 2% of TA was added to the concrete mix 5 minutes after cement made contact with water. It can be clearly seen that type C samples had a significant increase

in compressive strength for all respective ages of the samples, compared to the control samples, but the difference in strength for the two dosages TA was not high. This also signifies that the addition of Tartaric Acid to a concrete mix after 5 5-minute delay results in an increase in the ultimate strength at 1% and 2% dosages, with the higher dosage resulting in a slightly greater compressive strength.

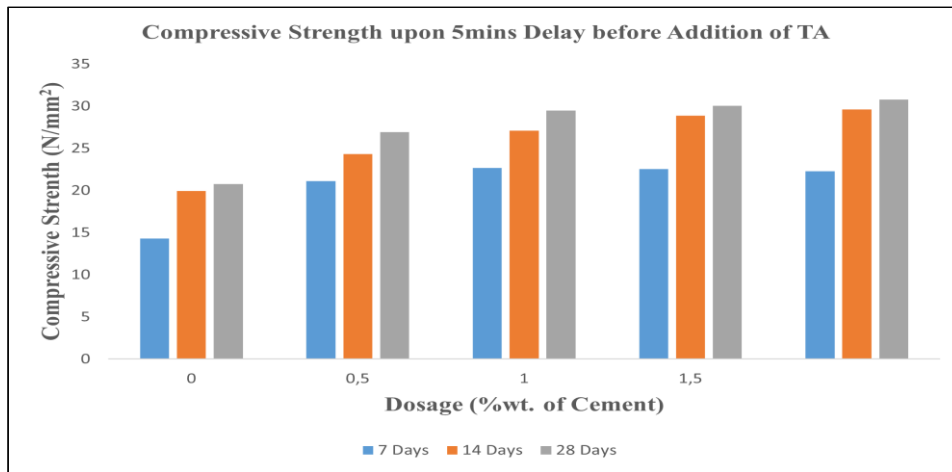


Figure 5: Relationship between the compressive strength of concrete samples upon 5-minute delay before the addition of TA at different dosages by percentage weight of cement in the concrete mix.

Source: Authors, (2024).

### III.3.5 Percentage Increase in the Ultimate Strength of Concrete Specimen

Table 7 below shows the percentage increase in ultimate compressive strength of the various concrete samples used for the research, compared to that of the control sample. It can be clearly seen that the addition of TA resulted in a substantial increase in the ultimate compressive strength of all test samples. From the results, the addition of 2% dose of TA 3 minutes after

the cement of the mix makes contact with water results in a 70% increase in compressive strength, making it a highly effective dose. From the results of the compressive strength test, it can be inferred that in most cases, a 2% dose of Tartaric Acid will attain a higher increase in compressive strength for 1:2:4 concrete mixes as compared to a 1% dose for corresponding concrete ages.

Table 7: Percentage increase in ultimate compressive strength of concrete specimen.

Sample Types	Delay before Addition of TA (min)	Dosage of TA (% wt of Cement)	Average Ultimate Compressive Strength (N/mm <sup>2</sup> ), B	B-A	$\frac{B - A}{A}$	% Increase in Ultimate Compressive Strength $\frac{B - A}{A} \times 100$
A1	0	0.5	23.95	3.17	0.159	15.9
A2	0	1	29.21	8.43	0.406	40.6
A3	0	1.5	29.43	8.65	0.416	41.6
A4	0	2	29.85	9.07	0.436	43.6
B1	3	0.5	27.99	7.21	0.347	34.7
B2	3	1	25.04	4.26	0.205	20.5
B3	3	1.5	31.95	11.17	0.538	53.8
B4	3	2	35.5	14.72	0.708	70.8
C1	5	0.5	26.95	6.17	0.297	29.7
C2	5	1	29.48	8.7	0.419	41.9
C3	5	1.5	30.05	9.27	0.446	44.6
C4	5	2	30.81	10.03	0.483	48.3

Average Ultimate Compressive Strength of Control Sample (A) = 20.78 N/mm<sup>2</sup>.

Source: Authors, (2024).

#### IV. CONCLUSIONS

Based on the findings arising from this study, the study makes the following conclusions.

The fineness modulus of the sharp sand and granites utilized were 3.63 and 2.27 respectively. Likewise, the uniformity coefficients of the sharp sand and granite utilized are 4.05 and 1.75 respectively. Additionally, there is a direct relationship between the percentage increase in TA addition and workability. Besides, the study notes that TA is an appropriate retarder for ready-mix concrete because it provides extended workability, slows the setting time in congestion and traffic jams, prevents concrete from hardening untimely, counteracts the impact of hot weather by slowing the setting time, and provides improved control over quality by guaranteeing accurate concrete placement and finishing. Moreover, the compressive strength of concrete is increased by 70.8% when a 2% dose of TA is added after a 3-minute delay. Therefore, TA is an effective retarder that increases the ultimate strength of concrete samples.

#### VI. AUTHOR'S CONTRIBUTION

**Conceptualization:** Aliu Soyngbe and Dele Simeon  
**Methodology:** Aliu Soyngbe and Dele Simeon  
**Investigation:** Aliu Soyngbe and Dele Simeon  
**Discussion of results:** Aliu Soyngbe and Dele Simeon  
**Writing – Original Draft:** Aliu Soyngbe and Dele Simeon  
**Writing – Review and Editing:** Aliu Soyngbe and Dele Simeon  
**Resources:** Aliu Soyngbe and Dele Simeon  
**Supervision:** Aliu Soyngbe and Dele Simeon  
**Approval of the final text:** Aliu Soyngbe and Dele Simeon

#### VII. ACKNOWLEDGMENTS

The authors wish to thank the Heads of the Department of Building, and Civil and Environmental Engineering Department, University of Lagos for their immense support towards the success of this research.

#### VII. REFERENCES

[1] Oladiran, O. J., Simeon, D. R., & Olatunde, O. A. (2020) Investigating the Performance of Palm Kernel Shells and Periwinkle Shells as Coarse Aggregates in Concrete. *Lautech Journal of Civil and Environmental Studies*, 4(1), 123-133. [https://doi.org/10.36108/laujoces/0202/40\(0131\)](https://doi.org/10.36108/laujoces/0202/40(0131))

[2] Alsadey, S., & Aljenkawi, A. S. (2021). Retarder Chemical Admixture: A Major Role in Modern Concrete Materials. *International Journal of Materials Chemistry and Physics*, 7(1), 1-4.

[3] Duggal, S. K. (2010). *Building materials*. (3rd Revised Edition), New Age International Limited, New Delhi.

[4] Purnomo, J., Sumarni, S., & Saputro, I. N. (2019). Effect of citric acid on setting-time and compressive strength of concrete. *IOP Conference Series: Materials Science and Engineering*, 578(1). <https://doi.org/10.1088/1757-899X/578/1/012077>

[5] Blankendaal, T., Schuur, P., & Voordijk, H. (2014). Reducing the environmental impact of concrete and asphalt: a scenario approach. *Journal of Cleaner Production*, 66, 27-36.

[6] Şahin, H. G., Mardani, A., Özen, S., & Emin, A. (2023). Utilization of high-range water-reducing admixture having air-entraining agents in cementitious systems. *Journal of Building Engineering*, 64, 105565.

[7] ACI Committee. (2016). 212, ACI 212. 3R-16 Report on Chemical Admixtures for Concrete. In *American Concrete Institute*.

[8] Bako, A. I., & Agunloye, O. O. (2017). Factors Influencing Road Traffic Delay: Drivers' Perspectives and Loss of Man-Hour Along Lagos-Abeokuta Expressway, Lagos, Nigeria. *Ethiopian Journal of Environmental Studies and Management*, 10(5), 618-628.

[9] Greesan, R., Prathap, P., & Vijayakumar, R. (2014). Manufacturing of Concrete with Retarders. *International Journal of Scientific & Engineering Research*, 5(4), 1637-1639.

[10] Alsadey, S. (2015). Effect of superplasticizer on fresh and hardened properties of concrete. *Journal of Agricultural Science and Engineering*, 1(2), 70-74.

[11] Gebremichael, N. N., Karein, S. M. M., Karakouziyan, M., & Jadidi, K. (2019). Investigation of setting time and compressive strength of ready-mixed concrete blended with returned fresh concrete. *Construction and Building Materials*, 197, 428-435.

[12] ASTM, A. (2005). ASTM C494: Standard specification for chemical admixtures for concrete. *West Conshohocken, PA, USA: ASTM*.

[13] AASHTO. Standard specification for chemical admixtures for concrete. American 438 Association of State Highway Transportation Officials, AASHTO M194

[14] Bishop, M., & Barron, A. R. (2006). Cement hydration inhibition with sucrose, tartaric acid, and lignosulfonate: analytical and spectroscopic study. *Industrial & engineering chemistry research*, 45(21), 7042-7049.

[15] Jackson, N., & Dhir, R. K. (1996). *Civil Engineering Materials* (5th ed.).

[16] Khan, B., & Muhammad-Ullah, M.-U. (2004). Effect of a Retarding

Admixture on the Setting Time of Cement Pastes in Hot Weather. *Journal of King Abdulaziz University-Engineering Sciences*, 15(1), 63-79. <https://doi.org/10.4197/eng.15-1.5>

[17] Huo, Y., Sun, H., Lu, D., Chen, Z., & Yang, Y. (2022). Mechanical properties of concrete at low and ultra-low temperatures - a review. *Journal of Infrastructure Preservation and Resilience*. <https://doi.org/10.1186/s43065-022-00063-4>

[18] British Standard European Norm, (1995). Cement; Composition, specification and conformity criteria for common cements. BS EN 197-1, BSI, Linfordwood, Milton Keynes MK14 6LE, U.K.

[19] British Standard Institution, "Aggregates for concrete", London, BS EN 12620, 2013.

[20] British Standard European Norm, (1998). Tests for geometrical properties of aggregates; Determination of percentage of crushed and broken surfaces in coarse aggregate particles. BS EN 933-5, BSI, Linfordwood, Milton Keynes MK14 6LE, U.K.

[21] British Standard European Norm, (2002). Mixing water for concrete; Specification for sampling, testing and assessing the suitability of water, including water recovered from processes in the concrete industry, as mixing water for concrete. BS EN 1008-2, BSI, Linfordwood, Milton Keynes MK14 6LE, U.K.

[22] Rai, S., Singh, N. B., & Singh, N. P. (2006). Interaction of tartaric acid during hydration of Portland cement. *Indian Journal of Chemical Technology*, 13(3), 255-261.

[23] British Standard Institution "Testing Concrete - Method for determination of slump", London, BS1881 - 102: 1983.

[24] British Standard European Norm, (1995). Methods of testing cement; Determination of setting time and soundness. BS EN 196-3, BSI, Linfordwood, Milton Keynes MK14 6LE, U.K.

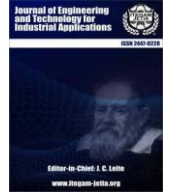
[25] British Standard European Norm, (2002). Testing hardened concrete; Compressive strength of test. BS EN 12390-3, BSI, Linfordwood, Milton Keynes MK14 6LE, U.K.

[26] Salau, M. A., & Busari, A. O. (2015). Effect of different coarse aggregate sizes on the strength characteristics of a terized concrete. In *IOP Conference Series: Materials Science and Engineering*, 96(1), 012079. IOP Publishing.

[27] British Standard European Norm, (1995). Methods of testing cement; Determination of setting time and soundness. BS EN 196-3, BSI, Linfordwood, Milton Keynes MK14 6LE, U.K.

[28] Kavathe, S. S., & Kulkarni, J. G. (2015). Retempering of Concrete Made by using Artificial Sand Containing Superplasticiser & Retarder. *Int. J. Eng. Res.*, 4, 716-720.

[29] British Standard European Norm, (2002). Testing hardened concrete; Compressive strength of test. BS EN 12390-3, BSI, Linfordwood, Milton Keynes MK14 6LE, U.K.



### RESEARCH ARTICLE

### OPEN ACCESS

## A NOVEL DESIGN EMPLOYING ARBITRARY TREE STRUCTURE FOR ADAPTIVE THRESHOLDING DISCRETE WAVELET PACKET TRANSFORMATION

Jency Rubia J<sup>1</sup>, Thangamari P<sup>2</sup> and Srikanth A<sup>3</sup>

<sup>1</sup> Assistant Professor, Department of ECE, Vel Tech Rangarajan Dr. Sagunthala R&D Institute of Science and Technology, Chennai, India.

<sup>2,3</sup> Student, Department of ECE, Vel Tech Rangarajan Dr. Sagunthala R&D Institute of Science and Technology, Chennai, India.

<sup>1</sup><http://orcid.org/0000-0002-0088-3611> , <sup>2</sup><http://orcid.org/0009-0002-7956-081> , <sup>3</sup><http://orcid.org/0009-0001-5307-6696> 

Email: [jencyrubia@gmail.com](mailto:jencyrubia@gmail.com), [sujithrasuji2013@gmail.com](mailto:sujithrasuji2013@gmail.com), [avulasrikanth756@gmail.com](mailto:avulasrikanth756@gmail.com)

### ARTICLE INFO

#### Article History

Received: December 03<sup>th</sup>, 2023

Revised: July 31<sup>th</sup>, 2024

Accepted: August 16<sup>th</sup>, 2024

Published: August 30<sup>th</sup>, 2024

#### Keywords:

FIR Filter,

Wavelet packet transform,

Image processing,

Arbitrary tree structure,

Compression ratio.

### ABSTRACT

Image compression is a very important technique in the realm of digital image processing. It acting as a key role in enabling effective storage area and data transmission rate of image data. Finite Impulse Response (FIR) filters have proven to be effective tools for image compression due to their linear phase response, which preserves image sharpness during the compression process. In this paper, we propose an innovative design of an FIR filter specifically tailored for effective image compression applications, leveraging the power of wavelet packet transform (WPT). Extensive simulations demonstrate that our proposed FIR filter outperforms conventional FIR filter designs and WPT-based compression methods in terms of both compression ratio and image quality. The filter effectively removes redundant information while preserving visual details, resulting in compressed images that are visually appealing and suitable for various applications. The filter coefficients are calculated serially, and the circuit complexity is decreased by rearranging the intermediate filter coefficients in addition to the memory elements. A 30% reduction in memory elements is required with the pipelined architecture that has been proposed. Additionally, the hardware implementation results demonstrate a 10% and 20% reduction in area and power requirements, respectively.



Copyright ©2024 by authors and Galileo Institute of Technology and Education of the Amazon (ITEGAM). This work is licensed under the Creative Commons Attribution International License (CC BY 4.0).

### I. INTRODUCTION

Images are now commonplace in the digital age and are essential to education, entertainment, and communication. Uncompressed image files are large, though, and this presents storage and transmission issues. In order to facilitate effective storage and transmission, image compression techniques seek to reduce image file sizes without appreciably sacrificing visual quality. For many applications, such as digital storage, internet data transmission, and real-time image processing, image compression is essential. Compressed images in digital storage require less space to store, making device storage more effective and lowering storage expenses. Compressed images with less bandwidth are needed for Internet data transmission in order to speed up webpage loading and lower data transmission costs. Applications for real-time image processing, like video conferencing and medical imaging, are made possible by the compressed images' lower

processing resource requirements. FIR filters' distinct qualities have made them effective tools for image compression. FIR filters prevent distortion or blurring of images during compression by maintaining a constant phase response across all frequencies. Different frequency responses can be used in the design of FIR filters to meet different compression needs.

Convolution operations can be effectively used to implement FIR filters, which makes them appropriate for real-time applications. For designing an efficient FIR filter for image compression, we need to consider certain features. The frequency response of the filter should efficiently eradicate high-frequency elements from the desired image. For that image contains the crucial details in the low-frequency elements. In order to attain the intended compression ratio and image quality, the filter coefficients are carefully selected. Both mathematical methods and empirical analyses are frequently used in this optimization. In order to guarantee effective implementation and appropriateness for real-

time applications, the filter design should minimize computational complexity. Wavelet packet transform (WPT) is an effective method for breaking down and analyzing images. It breaks down an image into a collection of wavelet subbands, each of which stands for a distinct frequency range. Selective filtering according to the frequency content of each subband can be accomplished by applying FIR filters to it. The method known as "adaptive FIR filtering" modifies the filter's properties to fit the unique frequency content of each wavelet subband. This method applies suitable filtering to various subbands to balance compression efficiency and image quality. FIR filters have a number of benefits when it comes to image compression. FIR filters' linear phase response makes sure that during compression, image sharpness is preserved. FIR filters are flexible tools for an extensive assortment of applications because they can be adjusted to different image types and compression requirements.

When compared to conventional FIR filtering techniques, wavelet packet decomposition and adaptive filtering techniques can drastically reduce computational complexity. FIR filters are appropriate for a variety of image compression applications because of their credentials. The FIR filter can accomplish maximum compression ratios while conserving tolerable image quality. FIR filters have shown to be useful instruments for image compression, making it possible to store and transfer image data in an efficient manner. They are excellent choices for a variety of image compression applications due to their linear phase response, adaptability in design, and computational efficiency. FIR filters are useful tools for digital image processing because they can achieve high compression ratios without sacrificing image quality by combining wavelet packet transform and adaptive filtering techniques.

Our proposed FIR filter design integrates two key aspects:

**Wavelet Packet Decomposition:** The image is decomposed into a set of wavelet subbands using WPT, allowing for selective filtering based on the frequency content of each subband.

**Adaptive FIR Filtering:** FIR filters with varying characteristics are applied to each wavelet subband based on its frequency content and compression requirements. This adaptive approach balances compression efficiency and image quality.

The following is how the work is structured. The fundamentals of Image compression techniques and the relation of wavelet filter are covered in Section II. The theoretical underpinnings of WPT and the implementation of WPT in filter are described in Section III. Section IV presents a comprehensive summary of the existing methods and current research work. Future research directions are provided in Section V, which wraps up the essay.

## II. EXISTING WORK

Discrete wavelet transforms (DWTs) are capable of performing multi-resolution signal analysis with both space (time) and frequency domain locality adjustments. DWT may be used to break down signals into different subbands with frequency and time information. The performance improvement in terms of image restoring capacity and clarity is better for Discrete Wavelet Transform than DCT. Furthermore, the compression ratio of DWT is high. As a result, DWT can be employed widely in signal and image processing applications such as JPEG2000, MPEG-4, and others. Subsampling followed by the use of FIR filters is the typical way that DWT is implemented. Due to its enormous computational load, numerous research projects aim to develop novel algorithms. Because a lifting scheme for DWT requires substantially fewer computations, it can be implemented easily. The wavelet

transform's spatial justification serves as the foundation for this entire procedure. It also possesses the capacity to generate new mother wavelets. Extensive advancement has been carried out in the context of DWT in the domain of VLSI in the form of DSP and FPGA implementation. Adaptive thresholding can remove more noise than traditional methods without sacrificing important signal features. The processing of such components can be realized with Multipliers. The processing speed is depending on clock rate of the proposed architecture. The number of multipliers required for a pipeline stage in the architecture related to clock rate of the system.

As per [1], the dispensation rate and number of multipliers present in the biggest obstacles of the hardware implementation of I-D DWT. However, the primary problem with 2-D DWT is memory, which also accounts for the majority of hardware complexity and cost. The cause is the power consumption and on-chip memory limitations. Nonetheless, the critical path has a  $T_m + T_a$ . In this case, the adder and multiplier delays are  $T_a$  and  $T_m$ , and the Effective folded architecture (EFA) computation takes a considerable amount of time.

Lin and Wu designed an DWT architecture using pipeline structure with a smaller number of delays reduces to  $T_m$  critical path. The designed pipeline structure has a temporal memory size has a limit of  $4N$  number of operations [2]. However, because scanning is done using a single input, single output method, processing speed cannot be increased. For [3] implement parallel 2-D DWT. The stated architecture follows pipeline method with 2 inputs and 1 output. Though this structure follows pipeline style, it requires 8 more pipeline stages to implement 1D-DWT. A flipping DWT architecture was proposed by [4]. Five pipeline stages with a single multiplier delay are used in this instance. However, a few pipelining stages can cause a considerable delay in the critical path and have a large temporal buffer. By recombining the intermediate values of the result, the number of pipeline stages and registers can be reduced. The shortcomings of earlier work can be addressed by the suggested lifting scheme, which also minimizes memory and logic sizes without sacrificing throughput. The critical path delay is  $T_m$  at this point, but it can be reduced to  $T_a$  by utilizing the shift add technique. Furthermore, the parallel scanning method is used to reduce the buffer size. As a result, our design can yield higher effectiveness.

The implementation of 2D-DWT concentrates on realizing small memory size with high-speed architectures. The separable approach is a technique that breaks down a group of wavelets into 1-D wavelets. This procedure will provide a simple way to implement the 2-D DWT. Even though this transform is simple to implement with a 1-D architecture, but it requires a large amount of memory space to be implemented [5]. Furthermore, processing an image with such an architecture would cause significant predicted misrepresentations. Filter architecture based on non-separable approach have been presented in [6] for overcome the aforementioned issues. Efficient architectures that optimize both area and time have been proposed in [7], utilizing a SIMD array or a parallel filter. Another architecture has been proposed in [8], which uses pipelines to provide high-speed, low-power performance based on a modified recursive pyramid algorithm. In addition to that, filter architecture designed using pipeline structure that will be performed parallelly for reducing the processing time [9]. A systolic array-based architecture for the multidimensional DWT that requires little hardware complexity has been proposed in [10]. Most non-separable 2-D architectures have been projected to deliver low hardware complexity. The low hardware complexity will be associated with little regard for computing time or throughput. These two parameters are two critical factors in an

architecture designed for DWT real-time applications. The Fourier basis, or complex exponentials, works well for smooth signals in most cases, but not so well for discontinuous signals or signals with both high- and low-frequency components. This is primarily due to the Fourier basis's subpar time resolution characteristics. Although the Short Time Fourier Transform (STFT) can help with this situation, it has a significant drawback. As the width of the window is constant, the high and low frequency portions are need to be captured. These activity causes issues with resolution. Wavelets were developed to address these constraints.

Wavelet basis is ideal for a variety of applications due to its flexibility in adapting to limited fluctuations in the signal. This is because broader windows can be used in the low frequency provinces of the signal and thinner windows for high frequency regions. Both types of windows have been used for allowing better resolution of the signal. Applications for wavelets include seismology, signal analysis, and image processing. Wavelet transform is widely used for image compression, offering notable enhancements in image quality at higher compression ratios compared to traditional methods. The Discrete Wavelet Transform is the transformation applied in JPEG 2000. The dual-tree complex wavelet transforms, which results in the Hilbert transform pair of wavelet bases. The wavelet bases can be used to get around some of the disadvantages of the discrete wavelet transform (DWT). The performance degradation is mainly due to lack of shift invariance and poor directional selectivity. A linear phase's condition is crucial for many filter bank applications. We require filters with symmetrical coefficients in order to achieve linear phase, and this cannot be done with compactly supported orthogonal wavelets. Several authors [11] and [12] have described designing bi-orthogonal wavelets that can form Hilbert transform pairs and yield symmetric filter coefficients. However, the author of [11] suggested using multipliers to implement a single level 1-D biorthogonal Hilbert transform pair on an FPGA. That implementation raises the cost and complexity of the hardware. This paper proposes an improved design that addresses this drawback.

### III. PROPOSED WORK

The Wavelet Algorithm Transform and the Discrete Cosine Transform (DCT) are two methods that can be used to compress images. DCT divides images into sections with different frequencies. The term "lossy" refers to the discarding of less significant frequencies during the step quantization, which is typically where part of the compression happens. The image compression process is then retrieved using only the most crucial frequencies. Because of this, there is some distortion in the reconstructed image; however, this distortion can be altered in the compression phase. The reconstructed image below shows some loss of quality, but it is still easily identifiable despite the removal of nearly 85% of the DCT coefficients. Images require a lot of storage space, high transmission bandwidths, and extended transmission times due to the amount of information they contain. As a result, it is critical to compress the image by saving only the data that is absolutely necessary for reconstructing it. An image is a matrix of pixels which contains the specific intensity level. In order to compress an image, it is important to take advantage of redundancies in the image, such as areas with little to no change in pixel values. The maximum area covered by the same colour represents large redundancies in images. While images with frequent and large colour changes produce less redundancy and are more difficult to compress.

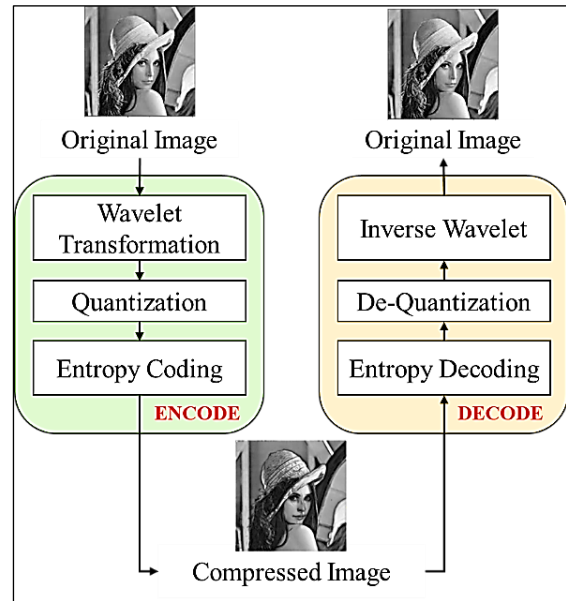


Figure 1: Block Diagram of Image compression and decompression using DWT.  
Source: Authors, (2024).

The DWT is generally consisting of three key stages: entropy coding, quantization, and transformation. The encoding and decoding procedures, which involve performing the stages in reverse to create a decoder, are shown in Figure 1. The decoding process involves only one distinct step, which is de-quantization, followed by an inverse transform to roughly recreate the original image. Wavelet analysis is a technique that can be used to separate an image's information into approximate and detailed sub-signals. These sub-signals can then be used to compress the image. The three important factors in the sub-signals represent the parallel, perpendicular, and oblique information or deviations in the image. However, the approximation sub-signal displays the overall trend of pixel values. If the factors are extremely small, the above-said factors can be set as zero without modify the given image. The threshold is the value below which information is deemed to be sufficiently small to be set to zero. The amount of condensation that can be accomplished upsurges with the number of zeros. The energy retained by an image is proportional to the sum of the squares of the pixel values. The energy represents the amount of information reserved by the image after condensation and decondensation.

A compression is referred to as lossless if all of the original energy is preserved, allowing for an exact reconstruction of the image. The information in the image has not changed means, the setting threshold value is zero. Lossy compression is the process of losing energy when any values are altered. While it is desirable to have the maximum number of zeros and energy retention during compression, it is essential to strike a balance between the two because the more zeros obtained, the more energy is lost.

#### III.1 WAVELET PACKET TRANSFORM (WPT)

Tree-structured filter banks are used to implement DWPT and DWT. The output of the low pass filter (LPF) is further administered to compute the subsequent stage coefficients. The output of the high pass filter (HPF) is taken into consideration as the outcome of the DWT computation. The outputs of the High pass and low pass filter play a vital role in computation of DWPT coefficients. The signal is broken down and down sampled using DWPT for multi-resolution analysis in order to produce



approximated. Also, the process includes detailed coefficients at each resolution level. The computation of the DWPT involves a three-level tree, as illustrates in Figure 2. The figure demonstrates that the frequency band obtained from the previous one is used for the decomposition at a level. The output of the low pass filter (LPF) yields the approximated coefficients at each level, while the output of the high pass filter (HPF) yields the detailed coefficients at each level 123. The signal flow graph (SFG) has used for matching the discrete wavelet packet transforms (DWPT) to a pipeline architecture. The SFG for mapping DWPT is similar to the SFG of the fast Fourier transform (FFT). The SFG's butterfly computes the level-specific high pass and low pass coefficients. Conversely, the tree-structured filter bank is directly mapped to a direct-mapped (DM) architecture.

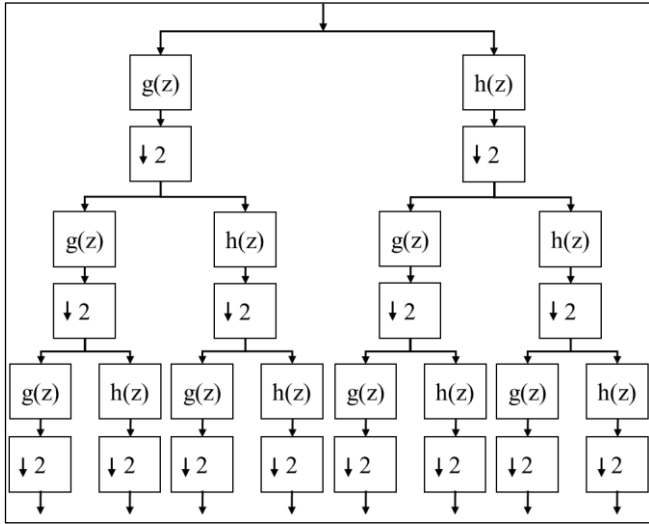


Figure 2: 3-Level Wallace Tree Structure. Source: Authors, (2024).

### III.2 ADAPTIVE THRESHOLD BASED WAVELET PACKET FILTERING

Swelden [13] introduced the lifting scheme. It is a productive way to calculate DWT/DWPT. As per [14], all category of filter coefficients can be factorized obsessed by a series of adaptive thresholding values. The polyphase matrix is factorized using the Euclidian algorithm. A diagonal normalization matrix consists a number of superior and inferior triangular matrices. They are the products of factorization. In this case,  $K$  is a constant and  $s_i(z)$  and  $t_i(z)$  are Laurent polynomials.

$$P(Z) = \begin{bmatrix} h_e(z) & g_e(z) \\ h_o(z) & g_o(z) \end{bmatrix}$$

$$\prod_{i=1}^m \begin{bmatrix} 1 & s_i(z) \\ 0 & 1 \end{bmatrix} \begin{bmatrix} 1 & 0 \\ t_i(z) & 1 \end{bmatrix} \begin{bmatrix} K & 0 \\ 0 & 1/K \end{bmatrix} \quad (1)$$

A highpass subband is produced by computing the superior triangular matrix. Similarly, a low pass subband is generated by processing the inferior triangular matrix. At last, the outputs are scaled by  $K$  and  $1/K$  in turn. The computational complexity of the DWPT/DWT is reduced by almost 50% with the polyphase factorization method compared to the convolution method [10].

Time and frequency analysis on the filter coefficients is very important for signal and image processing. The time and frequency analysis on filter coefficients can be computing by using the

discrete wavelet transform (DWT). A popular numerous-resolution method for characteristics abstraction, image condensation, and image de-noising is discrete wavelet decomposition. The input image is divided into four substitute bands by the standard discrete wavelet, which are LL, LH, HL, and HH. The LH, HL, and HH substitute bands provide the horizontal, vertical, and diagonal information of an image, respectively, while the LL substitute bands provides approximate coefficients, or the average image.

Figure 3 displays the DWT decomposition. The low-pass substitute bands in WPT following the initial level of decomposition is called the LL substitute bands. Stated differently, this substitute bands comprises the lowest frequencies present in the original signal. Since the LL substitute bands has the most significant information, it is frequently used as an approximation of the original signal. Since the LL subband is crucial for maintaining the image's visual quality, it is frequently used in image compression. The image can be compressed significantly with minimal loss of quality by removing the other substitute bands, which primarily contain noise and high-frequency information. The horizontal details of the original signal are contained in the LH sub-band, which is the horizontal detail sub-band. This indicates that it has data regarding the edges of the objects in the picture.

The vertical details of the original signal are contained in the HL sub-band, which is the vertical detail sub-band. This indicates that it has details regarding the textures of the image's objects. The diagonal details of the original signal are contained in the HH sub-band, which is the diagonal detail sub-band. This indicates that it has details about the edges and corners of the objects in the picture. Applications for the LL, LH, HL, and HH sub-bands are diverse. The most crucial sub-band for maintaining the image's visual quality is the LL sub-band. The picture can be greatly compressed with minimal quality loss by removing the other sub-bands, which are primarily composed of noise and high-frequency information. LL, LH, HL, and HH sub-bands can be applied to images to reduce noise. Since the noise in the image is usually concentrated in the higher-frequency sub-bands, the noise can be eliminated from the image by removing these sub-bands. You can use the LH, HL, and HH sub-bands to extract features from your photos. Subsequently, these characteristics can be applied to tasks related to image processing, such as object identification and classification.

LL 3	LH 3	LH2	LH1
HL 3	HH 3		
HL2		HH2	HH1
HL1			

Figure 3: Discrete Wavelet Transform Decomposition at the Third Level. Source: Authors, (2024).

Since the LL subband contains the majority of the important information, only the average coefficient, or DWT, is further broken down in pyramidal DWT. However, some of the dominant data might still be present in the HH, HL, and LH subbands. Due to the fact that the LH, HL, and HH subbands in an image contain

an object's contours in the horizontal, vertical, and diagonal directions [15]. Therefore, each subband is further broken down using a DWPT-based method. A generalization of discrete wavelet analysis, discrete wavelet packet transform (DWPT) analysis further breaks down the detail (LH, HL, and HH) and approximate

(LL) coefficients at each level. As a result, the DWPT offers the most comprehensive signal analysis and is better suited for feature extraction in multiple directions [13],[14]. A full tree produced by the DWPT is displayed in Figure 4.

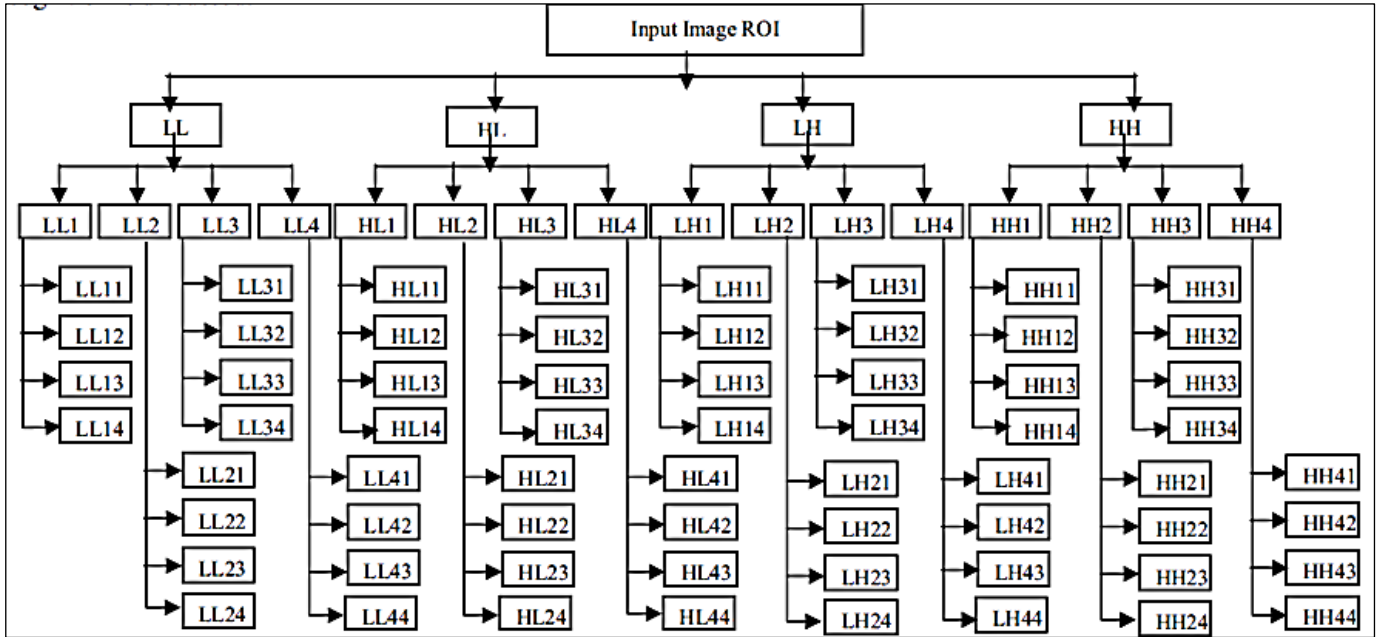


Figure 4: Complete Tree for Discrete Wavelet Packet Transform Decomposition. Source: Authors, (2024).

### III.3 FIR FILTER DESIGN

The signal and image processing applications relies on filter design for its operation. Generally, filter is frequently utilizing determinate impulse response (FIR) and detached wavelet transform (DWT). The N-tap FIR filter's associated equation is provided by equation (2).

$$Y(n) = \sum_{i=0}^{N-1} x(n-i)h(i) \quad (2)$$

The filter (h) consists of discrete filter coefficients X, and it includes the range {h(i): i=0,1,..., N-1}. Figure 1 depicts the traditional, straight-forward, and inverse FIR filter designs. In case the multiplier, adder tree delays and adder are Tm, Tat, and Ta, respectively. The parameter called critical path of the straight form filter is (Tm + Tad). Whereas the opposite form's critical path is (Tm + Ta). The basic DWT transform can be realized by employing convolution-based enactment with FIR-filters. At each transform level, the input discrete signal X(n) is filtered by a low-pass filter (h) and a high-pass filter (g). The low-pass subband YL and high-pass subband YH are then created by simply dropping the alternate output samples in each of the two output streams. The related equations (3) can be written [16].

$$y_L(n) = \sum_{i=0}^{\frac{N}{2}-1} h(2n-i)x(i), \quad y_H(n) = \sum_{i=0}^{\frac{N}{2}-1} g(2n-i)x(i) \quad (3)$$

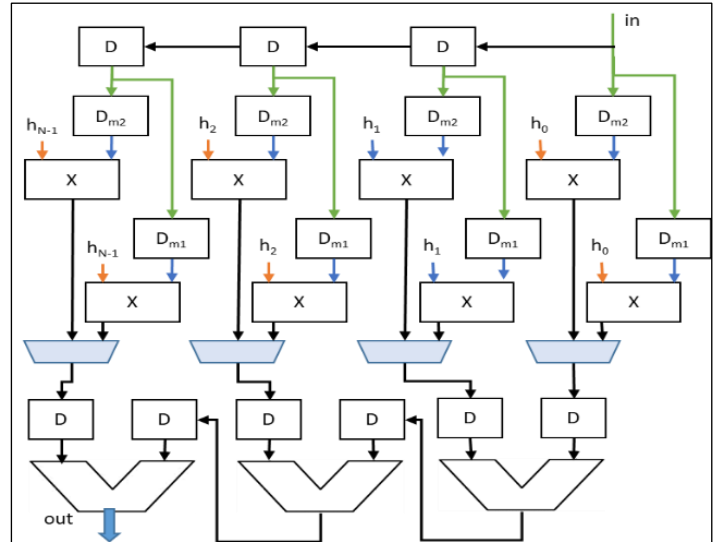


Figure 5: The proposed FIR Filter Architecture based on WPT. Source: Authors, (2024).

Our fundamentally new non-symmetric N-tap FIR filter architecture, which makes use of the alternate multiplication and D-latches distribution, is depicted in Figure 5. The suggested architecture's critical path is Tm/2 (assuming Ta < Tm/2) where Tm is the multiplier delay. By using symmetric FIR filters, an area-efficient architecture can be achieved, resulting in an extremely high processing rate. In this architecture, filter coefficients are multiplied in parallel with the input data samples. The multiplication results are then stored by the D-latches for a single clock cycle. The filter outputs are then produced by the new adder tree adding up all of the stored products [17].

### IV. RESULTS AND DISCUSSION

This section covers the design of the FIR filter using wavelets and the rectangular window method. For varying values of filter order, N, we compare the frequency response of the intended response with that of the designed filter. The two

parameters taken into consideration for our study are the mean square error and the percentage overshoot. The proposed design has been simulated in Xilinx Vivado suit and Modelsim. Figure 6 and 7 illustrates the simulation result of proposed WPT based FIR filter and its area utilization report.

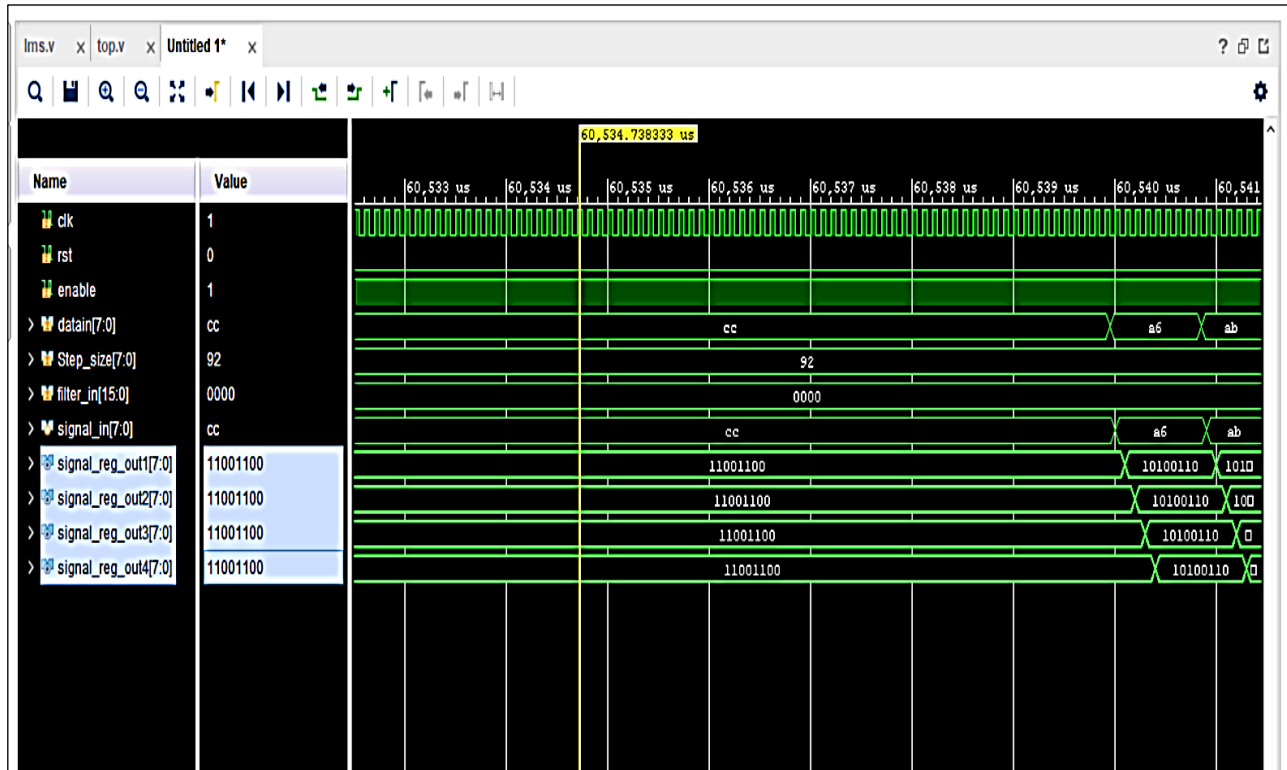


Figure 6: Simulation results for the proposed FIR filter using WPT. Source: Authors, (2024).

Resource	Estimation	Available	Utilization %
LUT	308	303600	0.10
FF	96	607200	0.02
DSP	4	2800	0.14
IO	51	600	8.50
BUFG	1	32	3.13

Figure 7: Area Utilization Report. Source: Authors, (2024).

Table 1: Comparative Analysis of the proposed work.

Parameters	[18]	[19]	This work
Area in $\mu m^2$	17654	18964	16763
Power in Watt	0.0237	0.0376	0.0187
Gate count	3167	3782	2478

Source: Authors, (2024).

Table I displays a comparison between the proposed circuit and a previously published circuit. According to [19] proposed an architecture which explains the initial computation regarding generalized wavelet packet tree. This type of architecture exhibits very flexible design for the generalized amendment on wavelet packet tree. From this observation, the output wavelet filter coefficients require double the amount of sample size of the memory. Since the proposed wavelet level module is utilized periodically in computation, it cannot be applied to an incessant

data flow. To the best of our knowledge, the architecture presented is the first register-based design that uses registers smaller than the sample size. This feasibility is very complicated to compute the comprehensive wavelet packet tree for continuous data flow. This one is very adaptable because it uses registers and multiplexers to support a generalized wavelet packet tree. The Virtex-7 FPGA (field-programmable gate array) was used to implement these circuits, and 250 MHz was used to calculate power. The Synopsys DC compiler with the 90-nm library is used to calculate area. As mentioned, when compared to the outcomes of the current methods, the area and power requirements of the proposed circuit are lowered to 10% and 20%, respectively.

### V. CONCLUSION

This brief designates a proposed architecture that uses bit exchange circuit and adaptive thresholding based bypassed wavelet filter to compute a generalized wavelet packet tree. The data flow that the filter processes is constant. This brief introduces the reordering mechanism and filter, which save a large number of memory elements and hardware, contributing to the architecture's high area- and power-efficiency. It is preferred over the previous architecture when calculating an arbitrary tree DWPT, as can be seen from a comparison. The DWPT coefficients for the continuous data flow are computed simultaneously by the suggested architecture.

## VI. AUTHOR'S CONTRIBUTION

**Conceptualization:** Author One, Author Two and Author Three.  
**Methodology:** Author Two and Author Three.  
**Investigation:** Author One and Author Two.  
**Discussion of results:** Author One, Author Two and Author Three.  
**Writing – Original Draft:** Author Two.  
**Writing – Review and Editing:** Author One and Author Two.  
**Resources:** Author Two.  
**Supervision:** Author One.  
**Approval of the final text:** Author One, Author Two and Author Three.

## VIII. REFERENCES

- [1] X. Zhang, "Design of FIR Halfband Filters for Orthonormal Wavelets Using Remez Exchange Algorithm," in *IEEE Signal Processing Letters*, vol. 16, no. 9, pp. 814-817, Sept. 2009, doi: 10.1109/LSP.2009.2025829.
- [2] V. Ďuriš, S. G. Chumarov, G. M. Mikheev, K. G. Mikheev and V. I. Semenov, "The Orthogonal Wavelets in the Frequency Domain Used for the Images Filtering," in *IEEE Access*, vol. 8, pp. 211125-211134, 2020, doi: 10.1109/ACCESS.2020.3039373.
- [3] B. Gopalan, A. Chilambuchelvan, S. Vijayan and G. Gowrison, "Performance Improvement of Average Based Spatial Filters through Multilevel Preprocessing using Wavelets," in *IEEE Signal Processing Letters*, vol. 22, no. 10, pp. 1698-1702, Oct. 2015, doi: 10.1109/LSP.2015.2426432.
- [4] K. Samantaray, P. J. Edavoor and A. D. Rahulkar, "A New Approach to the Design and Implementation of a Family of Multiplier Free Orthogonal Wavelet Filter Banks," in *IEEE Transactions on Circuits and Systems for Video Technology*, vol. 32, no. 4, pp. 1942-1954, April 2022, doi: 10.1109/TCSVT.2021.3092163.
- [5] N. Ansari and A. Gupta, "M-RWTL: Learning Signal-Matched Rational Wavelet Transform in Lifting Framework," in *IEEE Access*, vol. 6, pp. 12213-12227, 2018, doi: 10.1109/ACCESS.2017.2788084.
- [6] M. Mansouri Jam and H. Sadjedi, "Design and Evaluation of Optimal Orthogonal Wavelet With the Least Length of Wavelet Filters Using Spectral Matching," in *IEEE Access*, vol. 6, pp. 57414-57424, 2018, doi: 10.1109/ACCESS.2018.2873721.
- [7] N. N. Nagornov, P. A. Lyakhov, M. V. Valueva and M. V. Bergerman, "RNS-Based FPGA Accelerators for High-Quality 3D Medical Image Wavelet Processing Using Scaled Filter Coefficients," in *IEEE Access*, vol. 10, pp. 19215-19231, 2022, doi: 10.1109/ACCESS.2022.3151361.
- [8] W. Zhao, L. Ma, Y. Zhang, Y. He and Y. Sun, "Realization of Analog Wavelet Filter Using Hybrid Genetic Algorithm for On-Line Epileptic Event Detection," in *IEEE Access*, vol. 8, pp. 33137-33150, 2020, doi: 10.1109/ACCESS.2020.2973892.
- [9] J. Lin, "Reversible Integer-to-Integer Wavelet Filter Design for Lossless Image Compression," in *IEEE Access*, vol. 8, pp. 89117-89129, 2020, doi: 10.1109/ACCESS.2020.2993605.
- [10] Q. Wang, C. Meng and C. Wang, "Analog Continuous-Time Filter Designing for Morlet Wavelet Transform Using Constrained L2-Norm Approximation," in *IEEE Access*, vol. 8, pp. 121955-121968, 2020, doi: 10.1109/ACCESS.2020.3007254.
- [11] K. Samantaray, P. J. Edavoor and A. D. Rahulkar, "A Novel Design of Symmetric Daub-4 Wavelet Filter Bank for Image Analysis," in *IEEE Transactions on Circuits and Systems II: Express Briefs*, vol. 69, no. 9, pp. 3949-3953, Sept. 2022, doi: 10.1109/TCSII.2022.3174183.
- [12] P. Khatua and K. C. Ray, "VLSI Architecture of DCT-Based Harmonic Wavelet Transform for Time-Frequency Analysis," in *IEEE Transactions on Instrumentation and Measurement*, vol. 72, pp. 1-8, 2023, Art no. 6502108, doi: 10.1109/TIM.2023.3259023.
- [13] H. B. Seidel, M. M. A. da Rosa, G. Paim, E. A. C. da Costa, S. J. M. Almeida and S. Bampi, "Approximate Pruned and Truncated Haar Discrete Wavelet Transform VLSI Hardware for Energy-Efficient ECG Signal Processing," in *IEEE Transactions on Circuits and Systems I: Regular Papers*, vol. 68, no. 5, pp. 1814-1826, May 2021, doi: 10.1109/TCSI.2021.3057584.
- [14] K. Samantaray, P. J. Edavoor and A. D. Rahulkar, "Power-Efficient VLSI Architecture of a New Class of Dyadic Gabor Wavelets for Medical Image Retrieval," in *IEEE Transactions on Very Large Scale Integration (VLSI) Systems*, vol. 31, no. 1, pp. 104-113, Jan. 2023, doi: 10.1109/TVLSI.2022.3213186.
- [15] K. Samantaray, P. J. Edavoor and A. D. Rahulkar, "A New Approach to the Design and Implementation of a Family of Multiplier Free Orthogonal Wavelet Filter Banks," in *IEEE Transactions on Circuits and Systems for Video Technology*, vol. 32, no. 4, pp. 1942-1954, April 2022, doi: 10.1109/TCSVT.2021.3092163.
- [16] M. Singla, S. Azeemuddin and P. Sistla, "Accurate Fiducial Point Detection Using Haar Wavelet for Beat-by-Beat Blood Pressure Estimation," in *IEEE Journal of Translational Engineering in Health and Medicine*, vol. 8, pp. 1-11, 2020, Art no. 1900711, doi: 10.1109/JTEHM.2020.3000327.
- [17] D. Wang et al., "Improvement in EEG Source Imaging Accuracy by Means of Wavelet Packet Transform and Subspace Component Selection," in *IEEE Transactions on Neural Systems and Rehabilitation Engineering*, vol. 29, pp. 650-661, 2021, doi: 10.1109/TNSRE.2021.3064665.
- [18] T. Suzuki, "Wavelet-Based Spectral-Spatial Transforms for CFA-Sampled Raw Camera Image Compression," in *IEEE Transactions on Image Processing*, vol. 29, pp. 433-444, 2020, doi: 10.1109/TIP.2019.2928124.
- [19] D. Wang et al., "Improvement in EEG Source Imaging Accuracy by Means of Wavelet Packet Transform and Subspace Component Selection," in *IEEE Transactions on Neural Systems and Rehabilitation Engineering*, vol. 29, pp. 650-661, 2021, doi: 10.1109/TNSRE.2021.3064665.



ISSN ONLINE: 2447-0228



### RESEARCH ARTICLE

### OPEN ACCESS

## A REVIEW QUESTIONS CLASSIFICATION BASED ON BLOOM TAXONOMY USING A DATA MINING APPROACH

Sucipto<sup>1</sup>, Didik Dwi Prasetya<sup>2</sup>, Triyanna Widiyaningtyas<sup>3</sup>

<sup>1</sup> Department Information System, Universitas Nusantara PGRI Kediri, Kediri, Indonesia

<sup>2,3</sup> Department of Electrical Engineering and Informatics, Universitas Negeri Malang, Malang, Indonesia

<sup>1</sup><https://orcid.org/0000-0003-3412-002X> , <sup>2</sup><https://orcid.org/0000-0002-3540-2961> , <sup>3</sup><https://orcid.org/0000-0001-6104-6692> 

Email: [sucipto.2305349@students.um.ac.id](mailto:sucipto.2305349@students.um.ac.id), [didikdwi@um.ac.id](mailto:didikdwi@um.ac.id), [triyannaw.ft@um.ac.id](mailto:triyannaw.ft@um.ac.id)

### ARTICLE INFO

#### Article History

Received: July 16<sup>th</sup>, 2024

Revised: August 01<sup>th</sup>, 2024

Accepted: August 01<sup>th</sup>, 2024

Published: August 30<sup>th</sup>, 2024

#### Keywords:

Question,  
Taxonomy Bloom,  
Classification

### ABSTRACT

Bloom's taxonomy is used to categorize learning objectives into various cognitive levels. This study discusses the role of ontology in the classification of Bloom's taxonomy-based questions using a computer science approach in text mining. This research aims to review and analyze using a systematic ontology approach in cognitive level question classification techniques using Bloom's taxonomy with a text-mining scientific approach. Based on the prism method, 22 papers were analyzed from 490 articles from databases such as Scopus, ACM, IEEE, Springer, and Elsevier, published in 2016-2023. Meanwhile, qualified experts have not validated the main factors influencing the application of taxonomy-based question classification. Based on the evaluation results of using traditional, deep learning, and hybrid models in single-class question classification, it provides higher accuracy than in multiple classes in the case of bloom taxonomy. In various classification models, there is no significant difference in accuracy in the algorithm; the difference in results occurs due to data imbalance problems in multiple classes in the case of bloom taxonomy. This case provides a considerable opportunity to explore the topic of Bloom's taxonomy in the knowledge discovery database in KDD databases



Copyright ©2024 by authors and Galileo Institute of Technology and Education of the Amazon (ITEGAM). This work is licensed under the Creative Commons Attribution International License (CC BY 4.0).

### I. INTRODUCTION

Ontology is a branch of philosophy that studies the nature of reality or existing existence [1]. Ontology deals with what exists, its nature, and how it relates to each other. The role of ontology is very significant in scientific development [2]. Ontology studies the nature of setting the foundation for science, developing scientific theories, and solving problems scientifically [2]. In the scientific approach of computer science, ontology can help develop new information systems and technologies by knowing the fundamental nature of a system or technology [3]. The use of ontology is not only limited to philosophical scientific studies but also includes all studies of scientific aspects, including computer science [4].

Computer science is a science that studies everything related to computing, which includes hardware and software in which it is related to information governance and programming language

algorithms [5]. Computer science can support other sciences, such as education [6]. The development of educational science, especially regarding teaching materials, requires a valid strategy for conducting an analysis. Analysis of teaching materials One of them is in the classification of questions made by the teacher. The determination of questions used to maintain student learning outcomes needs to be standardized following the method of determining the classification of questions. One commonly used model is using the bloom taxonomy (BT) approach [7].

Bloom's Taxonomy is a learning classification framework with various levels. Bloom's Taxonomy was first developed by Benjamin Bloom in 1956 and revised several times, the last version published in 2001 [8]. Blomm's taxonomy has three domains: cognitive, affective, and psychomotor [9-11]. Bloom's domain taxonomy is presented in Figure 1.

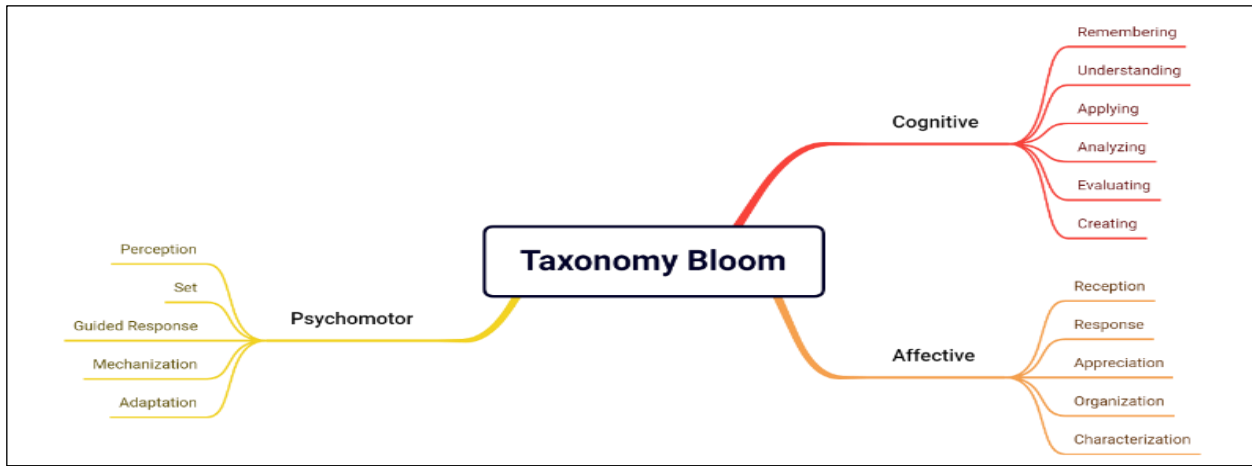


Figura 1: Taxonomy Bloom Domain.  
Source: Authors, (2024).

Bloom's taxonomy can be classified using a computer science scientific approach. Processing techniques in computer science are called Data Mining or knowledge discovery in databases (KDD) [12]. Several branches of data mining science are presented in Figure 2.

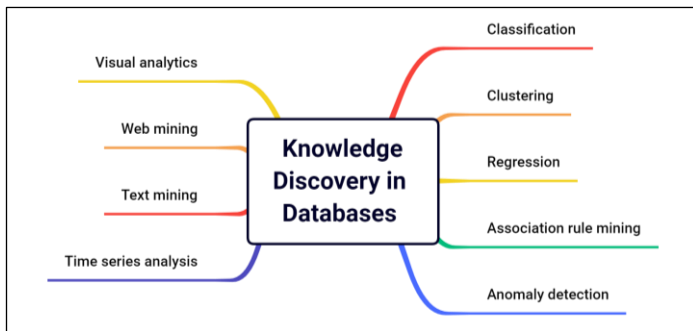


Figura 2: Knowledge Discovery in Databases.  
Source: Authors, (2024).

Ontology can provide the development of new understanding by combining two different sciences. In this case, with the classification questions in Bloom's taxonomy, optimization can be done with computer science, especially using knowledge discovery in databases. KDD is a computing-based big data processing. KDD is commonly used in various domains, such as business, finance, health, and education [13]. The KDD approach can efficiently classify questions in the domain of bloom taxonomy [14]. Research on the bloom taxonomy that has been extracted chiefly focuses on the cognitive domain. This cognitive focus is related to the student's thinking level, where six cognitive domains are divided into high-order thinking skills (HOTS) and low-order thinking skills (LOTS).

Learning question classification using Bloom's Taxonomy with the KDD approach in ontologies can be harmonized with the same techniques by adopting a formally structured knowledge model. In this case, an ontology defines important concepts and relationships between the fundamental scientific relationships of Bloom's taxonomy classification and classification in KDD [15]. Integral components for KDD ontologies, particularly classification techniques, include Knowledge Concepts, Classification methods, Data, Evaluation and Validation, Application Context, Relationships, Dependencies, and Technology.

Using ontologies in collaborative learning between Bloom's taxonomy and text classification in KDD is essential in improving our understanding of classification methods, facilitating data integration and analysis, and strengthening the development of intelligent systems capable of automating question classification in various application contexts [16]. The critical role of Ontology is essential to know the basis of classification determination in Bloom's taxonomy and fundamental determination in text classification techniques in KDD. Basic science knowledge can create novelty in classifying text questions in Bloom's taxonomy and understanding the basis of science based on existing research in the field of Bloom's taxonomy in the KDD text classification. Much research still needs to be done to facilitate classification with bloom taxonomy. Ontology was conducted to determine and investigate KDD classification techniques from an alternative perspective with comprehensive methods used with existing literature review analysis. This systematic review and validation ensures an intense exploration of topics within a new framework.

The question classification project on Bloom's taxonomy still needs to be studied in the KDD approach. In the literature review study, KDD analyzes the scientific base of text, such as news texts and social media. In question classification with taxonomy, the bloom has things that need to be explored with the KDD approach. This research was conducted by applying an Ontology-based Systematic Literature Review (SLR) by conducting a comprehensive survey of Scopus, ACM, IEEE, Springer, and Elsevier sources. The aim is to provide an optimal KDD use process and the novelty of KDD techniques to handle question classification with bloom taxonomy more accurately, including identifying areas where further research is needed or has been extensively researched for practitioners and research projects.

## II. LITERATURE REVIEW

### II.1 TRADITIONAL METHOD

This section discusses some research results on applying KDD to traditional algorithm models. Research conducted by Mohasseb examines the question answering classifying questions with a focus on BoW grammatical structure on the TREC 2007 dataset with DT, NB, SVM, and J48 algorithms. Optimal results were obtained J48 algorithm with 91% accuracy [17]. Another study conducted by Wang discussed the topic of text categorization, classified focusing on term-weighting with optimization of the chi-square test and information gain (entropy-

based) on KNN and SVM algorithms with private data. Optimal results were obtained using the KNN algorithm compared to SVM with a difference of less than 1% with an average accuracy of 98% [18]. Gani conducted another study on question classification in the Bloom taxonomy domain on private datasets on Term Weighting Unigram, TF-IDF with SVM, NB, and MLP algorithms. Optimal results on SVM and MLP algorithms [19]. Sangodiah conducted another study in the case of question classification in the domain of bloom taxonomy in the Reuters dataset. This research focuses on improving the TF-IDF1-3 Term Weighting using SVM and NB algorithms. Optimal results on SVM algorithm with 73.3% accuracy [20]. Another study was conducted by Mohammed in the same case as Sangodiah on private data. This research focuses on improving the extracted feature on TFPOS-IDF and word2vec using SVM, KNN, and LR algorithms—optimal results of the SVM algorithm with 89.7% accuracy [21].

## II.2 DEEP LEARNING METHOD

This section discusses some research results on the application of KDD in Deep Learning Algorithm models. Khilji's research examines question answering and optimizing the rule-based BERT algorithm on private data. Optimal DL accuracy results of 90% [22] Another study by Liang discussed the question answering with optimization on TF-IDF feature extraction on LSTM-CNN algorithm on private data. The optimal DL accuracy result of 94.2% [23]. Another study by Hung discussed question-answering optimizing word embeddings with the Bi-LSTM algorithm on private data. Optimal DL accuracy result of 94.36% [24]. SHAIKH conducted another study on question classification in the domain of bloom taxonomy on a private dataset. The focus of this research is improving word embedding with the LSTM algorithm. Optimal DL accuracy results of 87% [25]. Gani conducted another study on question classification in the domain taxonomy bloom on a private dataset. Focus on the case of word embedding with the CNN algorithm—optimal DL accuracy results of 86% [26].

## II.3 HYBRID METHOD

This section discusses some research results on the application of KDD in the Traditional Hybrid Algorithm model.

Razzaghnoori's research examines question answering and optimizing the TF-IDF feature extraction on the RNN algorithm. On UTQD.2016 data. Optimum accuracy results of 85% [27]. Another study conducted by Wu discussed question-answering optimizing hybrid classification using the CNN-SVM algorithm with Word2Vec on private data. Optimum accuracy result of 83.7%[28]. Hasmawati conducted another study on question classification in the bloom taxonomy domain on a private dataset with IndoBERT-SVM-NB optimization. Optimum accuracy results of 82%[29]. Gani conducted another study on question classification in the bloom taxonomy domain on a private dataset with ETFPOS-IDF optimization on ANN. Optimum accuracy result of 83.3% [30].

## II.4 RELATED SECONDARY RESEARCH

Research on SLR based on depth Ontology on classification using KDD on text data Most focused on general text [31-33]. Previous SLR research was conducted in the public domain with a target on single-class [34-36]. In the last literature review, it was known that the accuracy results in question classification in models using BT and non-BT had different accuracy. This is because the domain is a single class, and the BT classification uses multi-class cognitive domains. The results of using Traditional, Deep Learning, and Hybrid models are still in the results where there is no significant difference in outcomes [7]. The challenge of using BT in classification questions still has great opportunities for optimization with the application of pre-processing, feature extraction, and hybrid.

## III. MATERIALS AND METHODS

This study used the PRISMA (Preferred Reporting Items for Systematic Reviews and Meta-Analyses) method, including preliminary steps, methods, and results. This comprehensive method ensures a systematic and thorough review process, thereby increasing the reliability of the results. The method plot is presented in Figure 3.

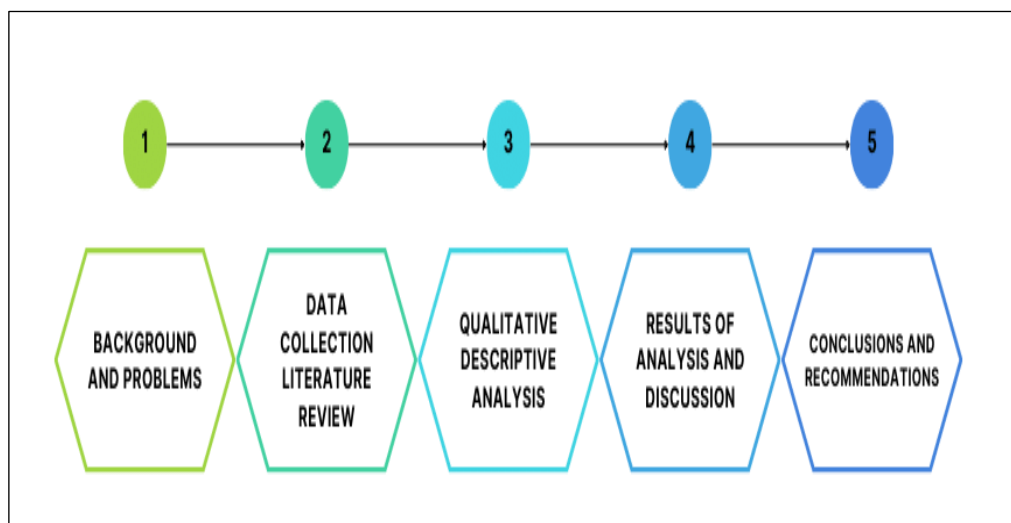


Figura 3: Research Methods.

Source: Authors, (2024).

This research searches metadata-based strings on digital databases such as Scopus, ACM, IEEE, Elsevier, and Springer,

processed using Mendeley Desktop and Xmind applications. Scopus is a database index that is a leading index database and is

famous for its comprehensive peer-reviewed literature database and is widely used in academic research. ACM, IEEE, Elsevier, and Springer are leading sources in the Scopus and WoS indexes for computer science and technology publications, offering an extensive collection of academic journals in various scientific fields, including Bloom's taxonomy and KDD. The articles collected in the database have undergone quality control and are validated by qualified experts.

This review aims to find answers to the literature review results based on data collected on current challenges in applying KDD learning in classifying questions within the scope of Bloom's taxonomy? Which type of traditional or deep learning algorithm is more effective in classifying question cases within Bloom's taxonomy? Which extract feature model is used for questions within the scope of bloom taxonomy?

#### IV. RESULTS AND DISCUSSIONS

The ontology of classification question learning in KDD refers to a formally defined knowledge model for understanding, describing, and compiling concepts, relationships, and entities involved in the question classification learning process on Bloom's taxonomy. The results of the literature search are presented in this chapter. The main components of the classification learning ontology are shown in Table 1.

Tabela 1: The Main Components of The Classification Learning Ontology.

Component	Description
Concepts and Terminology	The ontology contains definitions of essential concepts and terminology related to question classification in Bloom's taxonomy, such as sentiment analysis, question labeling, text summary, natural language inference, and so on [31], [36], [37]
Methods and Algorithms	Ontology of various descriptions Data mining algorithms are used to learn the rules of question classification using Bloom's taxonomy. Algortima is divided into two: traditional and deep learning [38], [39]
Data and Preprocessing	The ontology includes concepts related to data used in question classification using bloom taxonomy, such as feature extraction in traditional methods and LSTM in Deep Learning. Ontologies also describe how data is prepared before being applied in a text question classification model[26], [40], [41].
Data Source	Ontology describes various data sources used in the learning process of question classification using taxonomy bloomm. Some sources, such as DUC sources, come from private and open data [42], [43], [44].
Evaluation and Validation	Ontologies include definitions of evaluation metrics used to measure the accuracy of text classification models, including K-Fold cross-validation, confusion matrix, BLEU, and ROUGE[19], [45], [46]

Source: Authors, (2024).

Based on the definitions from Table 1, forecasting learning ontologies help understand and present the structured information needed to develop, apply, and understand the calcification process of the question using Bloom's Taxonomy. Trends regarding BT in the last five years, as shown in Figure 4, are still relevant to examine. BT topic data is taken from Google Trends.

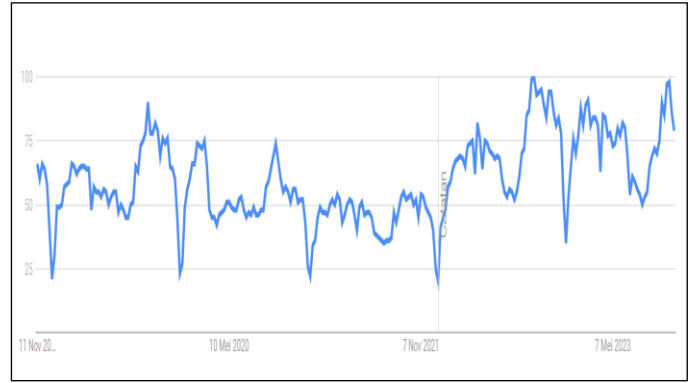


Figura 4: Interest over time “Taxonomy Bloom.”  
Source: Authors, (2024).

The distribution of data in Figure 5 on the trend topic of bloom taxonomy is spread across 145 areas. Some countries still focus on bloom taxonomy with a multi-scientific approach to export the science. As in the literature review, taxonomy is applied to questions in education and other fields such as news, novels, and general texts[25],[40].

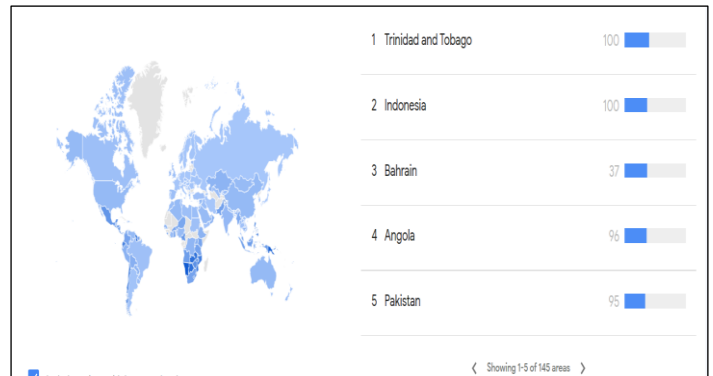


Figura 5: Interests by region “Taxonomy Bloom.”  
Source: Authors, (2024).

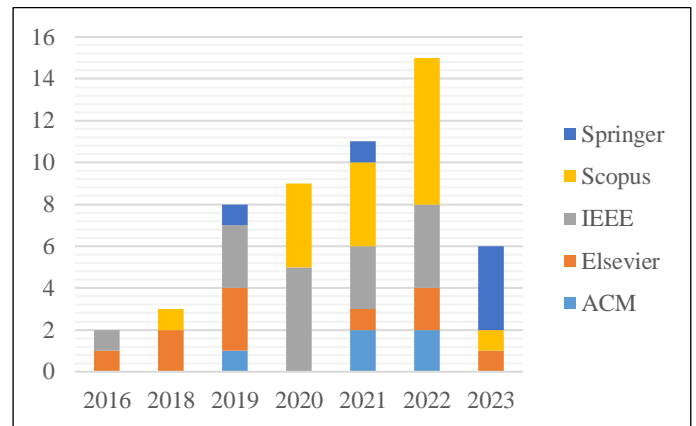


Figura 6: Selected paper database source.  
Source: Authors, (2024).

Figure 6 shows that the number of papers on Bloom's classification data mining focus on taxonomy has been collected and become literature in recent years, as reflected by the number of published articles in publishers. This data is collected from various databases included in the Scopus index. Figure 7 is an extract from Figure 6 on KDD classification using the bloom taxonomy domain.



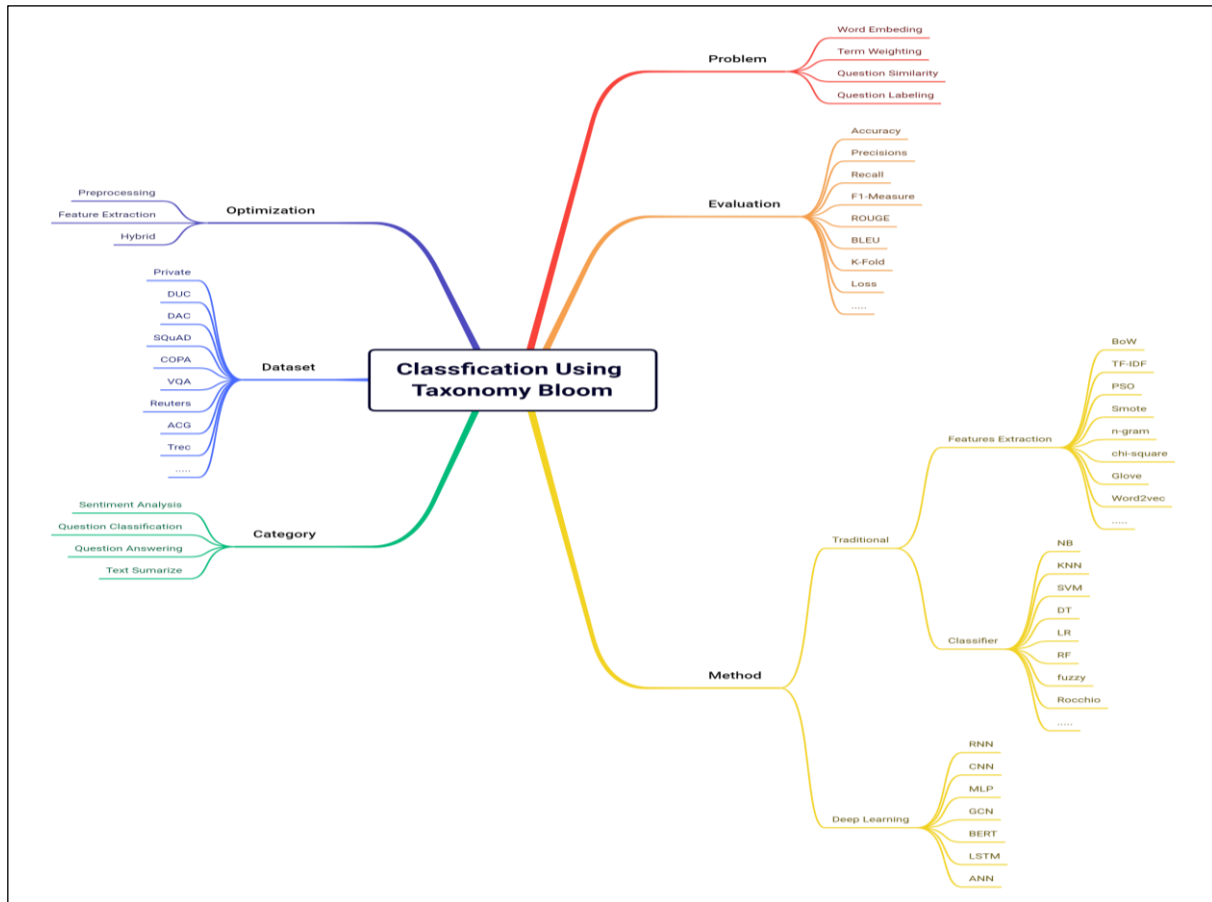


Figura 7: Components of Classification Question on Taxonomy Bloom.  
Source: Authors, (2024).

### III.1 CATEGORY

In the SLR data depicted in Figure 7, several categories apply question classification using Bloom Taxonomy. There are four discussions as follows:

Sentiment Analysis (SA) is a technique of analyzing points of view based on reviews, comments, or answers to a question textually. In general, SQ becomes divided into binary problems and plural class problems. Binary sentiment analysis classifies text into positive and negative classes, whereas plural class sentiment analysis classifies text into detailed labels or multi-level intensity. In the BT SA domain, it is a study in plural classes, one of which is about personality [47].

Question Answering (QA) is one method that can be used to access information widely to explore knowledge[48]. It can automatically return answers that have good accuracy based on the database collected and find out the essence of a short fact or long passage to a question asked by humans[47],[49]. There are two types of QA categories, namely extractive and generative. Extractive QA is TC's job: In the presence of questions and a series of candidate answers [42]. Generative QA is a text-generating task requiring quickly generating answers[48],[50],[51]. The data mining approach can classify each answer complexly based on candidates processed in a particular dataset as correct or no answers[42],[50],[51]. Bloom Taxonomy's approach in QA can provide knowledge by categorizing skills and understanding [15], [52].

Question Classification (QC) is a process that aims to categorize questions into specific classes or categories based on the nature or purpose of the question. One of the primary purposes of question classification is to find out the user's intention or the

purpose of the question so that the system can provide appropriate responses or actions. QC, in this case, uses the BT domain. Some of BT's research in data mining approaches in cognitive medicine [40],[53],[54]. Assessment is essential to achieve course objectives and improve the teaching and learning process. In any exam conducted in any academic or training field, it is necessary to ensure the quality of the question papers used to test various cognitive skills. Bloom's taxonomy with a data mining approach is famous for evaluating student learning ability [55]. Bloom's taxonomy can also help classify educational objectives into levels of specificity and complexity [40].

Text Summarize (TS) in data mining is the process of summarizing or rearranging information in text to produce a summary that shows the essence or essential points of the text [56]. This technique can cope with large volumes of text data and help users understand important information quickly [57]. TS can be used in question classification cases to make finding the essence of a question easier. Applying TS in question classification in the BT domain makes it easier to find keywords in the Bloom dictionary [41].

### III.2 PROBLEM

Several problems are raised in the classification using Bloom Taxonomy in the data mining approach. The following issues are discussed in Figure 7:

Word embedding (WE) is a processing technique representing words in vector form in high-dimensional space. The primary function of word embedding is to reveal semantic and syntactic relationships between words by assigning numerical vectors to each word-disclosure of word relationships to find word similarity. Applying classification models to textual data can be

converted into numerical measures to help embed comments. The selection of techniques in determining the proper embedding of the word plays a vital role in the classification [57]. Using WE in question classification improves the quality of questions according to the BT domain [26],[58],[59].

Term weighting (TW) is used in text processing and information retrieval. The term TW gives weight or importance to each word in the document or question. TW in question classification determines how relevant a word is in a question. TW is a technique close to traditional data mining methods [18]. TW is a fundamental problem in text classification of traditional data mining models and directly affects classification accuracy [30],[60],[61]. Researchers discuss the TW problem to improve existing methods into new techniques[30],[60],[62].

Question Labeling (QL) is a method used to mark questions based on a particular approach. QL on a data mining approach, assigning labels or categories to questions on data sets for data learning[8]. Labeling data on questions is used for classification or grouping questions based on data on specific topics; for example, in taxonomy [60, 63]—one of the ascetics QL is used as a method in BT. QL in BT uses a multi-class method [40],[64],[65].

Question Similarity (QS) is an idea that measures how similar questions consist of two or more questions that have a meaning or meaning of a particular purpose. The application of QS on the role of assessment in student learning in determining the leading indicators of student achievement in front of exam questions. QS challenges in categorizing exam questions automatically into learning levels using Bloom's taxonomy. Using a data mining

approach, this derivative rule makes it easier to analyze exam questions [41]. The Question Similarity mechanism is proposed to prevent the Question Answer system from asking irrelevant or unanswerable questions. This mechanism effectively finds irrelevant and unanswerable questions by incorporating human ways of thinking [48]. Another application of QS is used in automated essay grading systems, which can be beneficial in evaluating student learning outcomes as it allows them to demonstrate their knowledge [66].

### III.3 DATASET

In the application of question classification in data mining, several uses of datasets exist. Data sets are divided into two, namely private data and public data. The use of private datasets raises problems in data cleansing; this data cleansing problem can cause the accuracy of results in data mining to be reduced. Frequently used public datasets such as DUC [42],[56],[61], DAC [67], SQuAD [68],[48], COPA [15], VGA [52], Reuters [20], AQG [55], dan Trec [17],[69]. Some question classification studies use private datasets. Private data sets are used because they directly relate to the object under investigation [26],[40],[44],[50],[70]. Implementing question classification in datasets is associated with public data sets' quality and determining experts' labels. When the dataset pre-processing process is correct, it will get higher accuracy [21],[44],[63],[71].

### III.4 METHOD

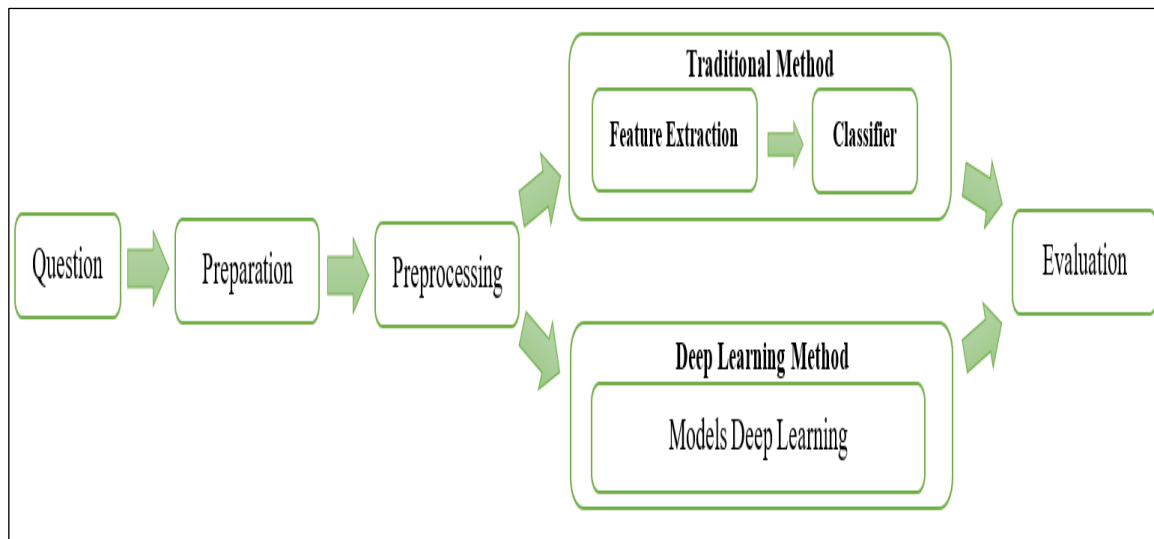


Figura 8: Classification Methods.  
Source: Authors, (2024).

The types of methods for calcification are divided into two, as presented in Figure 8. In this case, the classification stage consists of the dataset process in the form of questions, the preprocessing stage, and the classification and evaluation method stage. The discussion of the two is as follows:

#### III.4.1 TRADITIONAL

Applying the method to the question classification technique is still widely used. The application of this method is still used as it relates to the case methodology. Several classification methods are used, such as NB, KNN, SVM, DT, LR, RF, Fuzzy, Rocchio, etc. The use of a famous traditional method is KNN-SVM. The results of determining the popular method are obtained from

research that compares several methods. The best application of traditional methods in accuracy is by comparing several classification methods [18-20],[47],[72]. The KNN-SVM method provides better accuracy results compared to other methods. The application of improvements to traditional methods gets better results—improved classification method by improving pre-processing [17],[54],[60],[73].

#### III.4.2 Deep Learning

Applying Deep learning methods in question classification is quite a popular method. Deep learning methods were chosen because the process is shorter than traditional methods. The Deep Learning model includes an extraction feature in it. This method is

widely preferred because it is more practical [26],[52],[57],[67],[71]. Deep Learning Method research can also be modified in the extraction feature for better accuracy, such as adding n-gram and Word2Vec features[23],[26]. In the deep learning method, the CNN method is a popular algorithm, with some studies having good accuracy [22],[52],[57],[65],[69],[71].

### III.4.3 Optimization

Handling question classification in KDD has other options besides Traditional and Deep Learning. Another option is to do a Hybrid method on the Traditional Classification Method or a hybrid method on Deep Learning such as LTSM-CNN [23],[57],[71]. Hybrid methods can be applied to two or more classification or combination method models in both models. Hybrid models in both methods, such as SVM-CNN [28], and SVM-RNN [27]. The selection of this hybrid method aims to increase accuracy in classification.

### III.5 EVALUATION

In KDD, classification evaluation is critical because it allows an understanding of the classification model's ability to predict and understand text correctly. This helps determine whether the selected model adequately understands the text. Evaluation will enable inter-models to compare the performance of various classification models to determine which model is best suited for a given text data. It also helps select and use the model that offers the best results. Evaluation helps fine-tune and optimize model parameters; This makes it possible to try different configurations and parameters to improve model performance. In evaluation can understand what types of errors are often caused by the model by doing an evaluation. For example, whether the model tends to misclassify specific text or has problems understanding particular contexts. Evaluation helps in assessing whether the model that has been built can make sound predictions on never-before-seen data, ensuring the model can generalize to new data. With a good evaluation, we can understand more deeply how text in a particular domain or field can be processed and classified. Text classification results are usually used for decision-making. Proper evaluation results ensure that the predictions used in the decision-making process are reliable. With continuous evaluation, the model can be continuously improved as new data is added and changed. Thus, the model's performance can be improved on an ongoing basis.

Classification models are widely used in classification questions using the Confusion Matrix [25],[53],[74], K-Fold Validation [19],[46],[75], ROUGE [45],[67],[68], BLEU [44],[45],[68], and Loss [50],[65],[71],[73], [76]. Sometimes, the evaluation only focuses on accuracy and F1-Score [20],[30],[47],[59],[77],[78]. The selection of the evaluation model adjusts to the needs of the framework in question classification and is not limited by the use of traditional, Deep Learning, and Hybrid methods.

### V. CONCLUSIONS

This paper comprehensively reviews Ontology's approach to understanding Question Classification in Bloom's taxonomy model. The data used in this case can be categorized into private and public data. Most studies use private data. Using private data provides new opportunities for optimization in the data preparation stage. In this case, various models, such as traditional models, deep learning models, and hybrid models, tend to optimize in pre-processing and parameter optimization in algorithms. In the evaluation model, the accuracy model becomes popular, although other models allow giving different results. Based on the evaluation

results of using traditional, deep learning, and hybrid models in single class question classification provides higher accuracy than in multiple classes in the case of bloom taxonomy. In various classification models, there is no significant difference in accuracy in the algorithm; the difference in results occurs due to data imbalance problems in multiple classes in the case of bloom taxonomy. This case provides a considerable opportunity to explore the possibility of Bloom's taxonomy using KDD.

### VI. AUTHOR'S CONTRIBUTION

**Conceptualization:** Sucipto, Didik Dwi Prasetya and Triyanna Widiyaningtyas.

**Methodology:** Sucipto and Didik Dwi Prasetya.

**Investigation** Sucipto and Didik Dwi Prasetya.

**Discussion of results:** Author One, Didik Dwi Prasetya and Triyanna Widiyaningtyas.

**Writing – Original Draft:** Sucipto.

**Writing – Review and Editing:** Sucipto and Didik Dwi Prasetya.

**Resources:** Sucipto.

**Supervision:** Didik Dwi Prasetya and Triyanna Widiyaningtyas.

**Approval of the final text:** Sucipto, Didik Dwi Prasetya and Triyanna Widiyaningtyas.

### VII. ACKNOWLEDGMENTS

The author would like to thank the Directorate General of Higher Education, Research and Technology, Ministry of Education, Culture, Research and Technology of the Republic of Indonesia for providing financial support for this research through the 2024 Doctoral Dissertation research scheme Number: 0667/E5/AL.04 /2024.

### VIII. REFERENCES

- [1] D. D. Prasetya, A. P. Wibawa, and T. Hirashima, "The performance of text similarity algorithms," *International Journal of Advances in Intelligent Informatics*, vol. 4, no. 1, pp. 63–69, 2018, doi: <https://doi.org/10.26555/ijain.v4i1.152>.
- [2] J. D. Hathcoat, C. Meixner, and M. C. Nicholas, "Ontology and Epistemology," *Handbook of Research Methods in Health Social Sciences*, pp. 99–116, Jan. 2019, doi: 10.1007/978-981-10-5251-4\_56.
- [3] A. A. Salatino, T. Thanapalasingam, A. Mannocci, F. Osborne, and E. Motta, "The computer science ontology: A large-scale taxonomy of research areas," *Lecture Notes in Computer Science (including subseries Lecture Notes in Artificial Intelligence and Lecture Notes in Bioinformatics)*, vol. 11137 LNCS, pp. 187–205, 2018, doi: 10.1007/978-3-030-00668-6\_12/FIGURES/8.
- [4] A. A. Salatino, T. Thanapalasingam, A. Mannocci, A. Birukou, F. Osborne, and E. Motta, "The Computer Science Ontology: A Comprehensive Automatically-Generated Taxonomy of Research Areas," *Data Intell.*, vol. 2, no. 3, pp. 379–416, Jul. 2020, doi: 10.1162/DINT\_A\_00055.
- [5] D. D. Prasetya, A. Pinandito, Y. Hayashi, and T. Hirashima, "Investigating the Distribution of Knowledge Structure in Extended Concept Mapping," *Proceedings of the Business Innovation and Engineering Conference 2020 (BIEC 2020)*, vol. 184, pp. 74–79, Jul. 2021, doi: 10.2991/AEBMR.K.210727.013.
- [6] D. Arbian Sulistyio et al., "LSTM-Based Machine Translation for Madurese-Indonesian," *Journal of Applied Data Sciences*, vol. 4, no. 3, pp. 189–199, Sep. 2023, doi: 10.47738/JADS.V4I3.113.
- [7] H. Sharma, R. Mathur, T. Chintala, S. Dhanalakshmi, and R. Senthil, "An effective deep learning pipeline for improved question classification into bloom's taxonomy's domains," *Educ Inf Technol (Dordr)*, vol. 28, no. 5, 2023, doi: 10.1007/s10639-022-11356-2.
- [8] T. T. Goh, N. A. A. Jamaludin, H. Mohamed, M. N. Ismail, and H. S. Chua, "A Comparative Study on Part-of-Speech Taggers' Performance on Examination Questions Classification According to Bloom's Taxonomy," *J Phys Conf Ser*, vol. 2224, no. 1, p. 012001, Apr. 2022, doi: 10.1088/1742-6596/2224/1/012001.

- [9] S. Aisyah, Aripriharta, S. Wibawanto, K. Andajani, and Parlan, "The differences in learning outcomes of programmatic control systems between class with brainwriting models and scamper models on vocational school students," 4th International Conference on Vocational Education and Training, ICovET 2020, pp. 111–114, Sep. 2020, doi: 10.1109/ICOVET50258.2020.9230076.
- [10] Sutrisno, A. E. Winahyo, and M. A. Ichwanto, "The influence of open book strategy and Bloom's taxonomy comprehension on the achievement of higher-order thinking skill's multiple choice questions," AIP Conf Proc, vol. 2489, no. 1, Jun. 2022, doi: 10.1063/5.0094761/2826900.
- [11] D. Cooper and S. Higgins, "The effectiveness of online instructional videos in the acquisition and demonstration of cognitive, affective and psychomotor rehabilitation skills," British Journal of Educational Technology, vol. 46, no. 4, pp. 768–779, Jul. 2015, doi: 10.1111/BJET.12166.
- [12] A. Prasetya Wibawa, N. Susetyo, F. Putri, and P. Widiharso, "Letter Detection : An Empirical Comparative Study of Different ML Classifier and Feature Extraction," Signal and Image Processing Letters, vol. 5, no. 1, pp. 1–7, Mar. 2023, doi: 10.31763/SIMPLE.V5I1.45.
- [13] A. P. Wibawa, A. B. P. Utama, H. Elmunsyah, U. Pujianto, F. A. Dwiyanto, and L. Hernandez, "Time-series analysis with smoothed Convolutional Neural Network," J Big Data, vol. 9, no. 1, pp. 1–18, Dec. 2022, doi: 10.1186/S40537-022-00599-Y/TABLES/12.
- [14] Z. Wang, K. Manning, D. B. Mallick, and R. G. Baraniuk, "Towards Blooms Taxonomy Classification Without Labels," in Lecture Notes in Computer Science (including subseries Lecture Notes in Artificial Intelligence and Lecture Notes in Bioinformatics), 2021. doi: 10.1007/978-3-030-78292-4\_35.
- [15] P. Sahu, M. Cogswell, S. Rutherford-Quach, and A. Divakaran, "Comprehension Based Question Answering using Bloom's Taxonomy," in Repl4NLP 2021 - 6th Workshop on Representation Learning for NLP, Proceedings of the Workshop, 2021. doi: 10.18653/v1/2021.repl4nlp-1.3.
- [16] J. Huang et al., "Automatic Classroom Question Classification Based on Bloom's Taxonomy," ACM International Conference Proceeding Series, pp. 33–39, Oct. 2021, doi: 10.1145/3498765.3498771.
- [17] A. Mohasseb, M. Bader-El-Den, and M. Cocea, "Question categorization and classification using grammar based approach," Inf Process Manag, vol. 54, no. 6, pp. 1228–1243, Nov. 2018, doi: 10.1016/J.IPM.2018.05.001.
- [18] T. Wang, Y. Cai, H. fung Leung, R. Y. K. Lau, H. Xie, and Q. Li, "On entropy-based term weighting schemes for text categorization," Knowl Inf Syst, vol. 63, no. 9, 2021, doi: 10.1007/s10115-021-01581-5.
- [19] M. O. Gani, R. K. Ayyasamy, T. Fui, and A. Sangodiah, "USTW Vs. STW: A Comparative Analysis for Exam Question Classification based on Bloom's Taxonomy," Mendel, vol. 28, no. 2, 2022, doi: 10.13164/mendel.2022.2.025.
- [20] A. Sangodiah, T. J. San, Y. T. Fui, L. E. Heng, R. K. Ayyasamy, and N. B. A. Jalil, "Identifying Optimal Baseline Variant of Unsupervised Term Weighting in Question Classification Based on Bloom Taxonomy," Mendel, vol. 28, no. 1, 2022, doi: 10.13164/mendel.2022.1.008.
- [21] M. Mohammedid and N. Omar, "Question classification based on Bloom's taxonomy cognitive domain using modified TF-IDF and word2vec," PLoS One, vol. 15, no. 3, p. e0230442, 2020, doi: 10.1371/JOURNAL.PONE.0230442.
- [22] A. F. U. Rahman Khilji et al., "Question classification and answer extraction for developing a cooking QA system," Computacion y Sistemas, vol. 24, no. 2, 2020, doi: 10.13053/CyS-24-2-3445.
- [23] M. Liang and T. Niu, "Research on Text Classification Techniques Based on Improved TF-IDF Algorithm and LSTM Inputs," Procedia Comput Sci, vol. 208, pp. 460–470, Jan. 2022, doi: 10.1016/J.PROCS.2022.10.064.
- [24] B. T. Hung, "Vietnamese Question Classification based on Deep Learning for Educational Support System," Proceedings - 2019 19th International Symposium on Communications and Information Technologies, ISCIT 2019, pp. 317–321, Sep. 2019, doi: 10.1109/ISCIT.2019.8905237.
- [25] S. Shaikh, S. M. Daudpotta, and A. S. Imran, "Bloom's Learning Outcomes' Automatic Classification Using LSTM and Pretrained Word Embeddings," IEEE Access, vol. 9, pp. 117887–117909, 2021, doi: 10.1109/ACCESS.2021.3106443.
- [26] M. O. Gani, R. K. Ayyasamy, A. Sangodiah, and Y. T. Fui, "Bloom's Taxonomy-based exam question classification: The outcome of CNN and optimal pre-trained word embedding technique," Educ Inf Technol (Dordr), pp. 1–22, May 2023, doi: 10.1007/S10639-023-11842-1/FIGURES/10.
- [27] M. Razzaghnouri, H. Sajedi, and I. K. Jazani, "Question classification in Persian using word vectors and frequencies," Cogn Syst Res, vol. 47, pp. 16–27, Jan. 2018, doi: 10.1016/J.COGLSYS.2017.07.002.
- [28] E. H. K. Wu, S. E. Chen, J. J. Liu, Y. Y. Ou, and M. Te Sun, "A Self-Relevant CNN-SVM Model for Problem Classification in K-12 Question-Driven Learning," IEEE Access, vol. 8, pp. 225822–225830, 2020, doi: 10.1109/ACCESS.2020.3039531.
- [29] Hasmawati, A. Romadhony, and R. Abdurohman, "Primary and High School Question Classification based on Bloom's Taxonomy," 2022 10th International Conference on Information and Communication Technology, ICoICT 2022, pp. 234–239, 2022, doi: 10.1109/ICOICT55009.2022.9914842.
- [30] M. O. Gani, R. K. Ayyasamy, S. M. Alhashmi, A. Sangodiah, and Y. T. Fui, "ETFPOS-IDF: A Novel Term Weighting Scheme for Examination Question Classification Based on Bloom's Taxonomy," IEEE Access, vol. 10, pp. 132777–132785, 2022, doi: 10.1109/ACCESS.2022.3230592.
- [31] S. Minaee, N. Kalchbrenner, E. Cambria, N. Nikzad, M. Chenaghlu, and J. Gao, "Deep Learning--based Text Classification," ACM Computing Surveys (CSUR), vol. 54, no. 3, Apr. 2021, doi: 10.1145/3439726.
- [32] G. Sharma and D. Sharma, "Automatic Text Summarization Methods: A Comprehensive Review," 2023. doi: 10.1007/s42979-022-01446-w.
- [33] A. P. Widyassari et al., "Review of automatic text summarization techniques & methods," 2022. doi: 10.1016/j.jksuci.2020.05.006.
- [34] V. A. Silva, I. I. Bittencourt, and J. C. Maldonado, "Automatic Question Classifiers: A Systematic Review," IEEE Transactions on Learning Technologies, vol. 12, no. 4, pp. 485–502, Oct. 2019, doi: 10.1109/TLT.2018.2878447.
- [35] Q. Li et al., "A Survey on Text Classification: From Traditional to Deep Learning," ACM Transactions on Intelligent Systems and Technology (TIST), vol. 13, no. 2, p. 31, Apr. 2022, doi: 10.1145/3495162.
- [36] R. Zhang, J. Guo, L. Chen, Y. Fan, and X. Cheng, "A Review on Question Generation from Natural Language Text," ACM Transactions on Information Systems (TOIS), vol. 40, no. 1, Sep. 2021, doi: 10.1145/3468889.
- [37] R. Ferreira-Mello, M. André, A. Pinheiro, E. Costa, and C. Romero, "Text mining in education," Wiley Interdiscip Rev Data Min Knowl Discov, vol. 9, no. 6, p. e1332, Nov. 2019, doi: 10.1002/WIDM.1332.
- [38] K. Makhlof, L. Amouri, N. Chaabane, and N. El-Haggar, "Exam Questions Classification Based on Bloom's Taxonomy: Approaches and Techniques," 2020 2nd International Conference on Computer and Information Sciences, ICCIS 2020, Oct. 2020, doi: 10.1109/ICCIS49240.2020.9257698.
- [39] S. Masapanta-Carrión and J. Á. Velázquez-Iturbide, "Evaluating instructors' classification of programming exercises using the revised Bloom's taxonomy," Annual Conference on Innovation and Technology in Computer Science Education, ITiCSE, pp. 541–547, Jul. 2019, doi: 10.1145/3304221.3319748.
- [40] M. Jain, R. Beniwal, A. Ghosh, T. Grover, and U. Tyagi, "Classifying Question Papers with Bloom's Taxonomy Using Machine Learning Techniques," Communications in Computer and Information Science, vol. 1046, pp. 399–408, 2019, doi: 10.1007/978-981-13-9942-8\_38/COVER.
- [41] K. Jayakodi, M. Bandara, I. Perera, and D. Meedeniya, "WordNet and cosine similarity based classifier of exam questions using bloom's taxonomy," International Journal of Emerging Technologies in Learning, vol. 11, no. 4, 2016, doi: 10.3991/ijet.v11i04.5654.
- [42] Y. Chali, S. R. Joty, and S. A. Hasan, "Complex Question Answering: Unsupervised Learning Approaches and Experiments," Journal of Artificial Intelligence Research, vol. 35, pp. 1–47, May 2009, doi: 10.1613/JAIR.2784.
- [43] Q. Lang, X. Liu, and Y. Deng, "Multi-level retrieval with semantic Axiomatic Fuzzy Set clustering for question answering," Appl Soft Comput, vol. 111, Nov. 2021, doi: 10.1016/j.asoc.2021.107858.

- [44] B. D. Wijanarko, Y. Heryadi, H. Toba, and W. Budiharto, "Question generation model based on key-phrase, context-free grammar, and Bloom's taxonomy," *Educ Inf Technol (Dordr)*, vol. 26, no. 2, 2021, doi: 10.1007/s10639-020-10356-4.
- [45] H. Palivela, "Optimization of paraphrase generation and identification using language models in natural language processing," *International Journal of Information Management Data Insights*, vol. 1, no. 2, p. 100025, Nov. 2021, doi: 10.1016/J.JIMEI.2021.100025.
- [46] A. S. Callista, O. N. Pratiwi, and E. Sutoyo, "Questions Classification Based on Revised Bloom's Taxonomy Cognitive Level using Naive Bayes and Support Vector Machine," *Proceedings - 2021 4th International Conference on Computer and Informatics Engineering: IT-Based Digital Industrial Innovation for the Welfare of Society, IC2IE 2021*, pp. 260–265, 2021, doi: 10.1109/IC2IE53219.2021.9649187.
- [47] P. Wang et al., "Classification of Proactive Personality: Text Mining Based on Weibo Text and Short-Answer Questions Text," *IEEE Access*, vol. 8, pp. 97370–97382, 2020, doi: 10.1109/ACCESS.2020.2995905.
- [48] S. G. Aithal, A. B. Rao, and S. Singh, "Automatic question-answer pairs generation and question similarity mechanism in question answering system," *Applied Intelligence*, vol. 51, no. 11, 2021, doi: 10.1007/s10489-021-02348-9.
- [49] Y. Zhang et al., "A Question Answering-Based Framework for One-Step Event Argument Extraction," *IEEE Access*, vol. 8, pp. 65420–65431, 2020, doi: 10.1109/ACCESS.2020.2985126.
- [50] T. P. Sahu, R. S. Thummalapudi, and N. K. Nagwani, "Automatic Question Tagging Using Multi-label Classification in Community Question Answering Sites," *Proceedings - 6th IEEE International Conference on Cyber Security and Cloud Computing, CSCloud 2019 and 5th IEEE International Conference on Edge Computing and Scalable Cloud, EdgeCom 2019*, pp. 63–68, Jun. 2019, doi: 10.1109/CSCLOUD/EDGECom.2019.00-17.
- [51] B. Sun, Y. Zhu, Y. Xiao, R. Xiao, and Y. Wei, "Automatic Question Tagging with Deep Neural Networks," *IEEE Transactions on Learning Technologies*, vol. 12, no. 1, pp. 29–43, Jan. 2019, doi: 10.1109/TLT.2018.2808187.
- [52] A. Mishra, A. Anand, and P. Guha, "Dual Attention and Question Categorization-Based Visual Question Answering," *IEEE Transactions on Artificial Intelligence*, vol. 4, no. 1, pp. 81–91, Feb. 2023, doi: 10.1109/TAI.2022.3160418.
- [53] J. Zhang, C. Wong, N. Giacaman, and A. Luxton-Reilly, "Automated Classification of Computing Education Questions using Bloom's Taxonomy," *ACM International Conference Proceeding Series*, pp. 58–65, Feb. 2021, doi: 10.1145/3441636.3442305.
- [54] M. Mohammed and N. Omar, "Question classification based on bloom's taxonomy using enhanced tf-idf," *Int J Adv Sci Eng Inf Technol*, vol. 8, pp. 1679–1685, 2018.
- [55] R. T. Sairaj and S. R. Balasundaram, "Improving the Cognitive Levels of Automatic Generated Questions using Neuro-Fuzzy Approach in e-Assessment," *2020 IEEE 5th International Conference on Computing Communication and Automation, ICCCA 2020*, pp. 454–458, Oct. 2020, doi: 10.1109/ICCCA49541.2020.9250716.
- [56] A. P. Widyassari, E. Noersongko, A. Syukur, and Affandy, "An Extractive Text Summarization based on Candidate Summary Sentences using Fuzzy-Decision Tree," *International Journal of Advanced Computer Science and Applications*, vol. 13, no. 7, 2022, doi: 10.14569/IJACSA.2022.0130768.
- [57] P. Kathiria, U. Patel, and N. Kansara, "Document classification using deep neural network with different word embedding techniques," *International Journal of Web Engineering and Technology*, vol. 17, no. 2, 2022, doi: 10.1504/IJWET.2022.125654.
- [58] H. T. Nguyen, P. H. Duong, and E. Cambria, "Learning short-text semantic similarity with word embeddings and external knowledge sources," *Knowl Based Syst*, vol. 182, p. 104842, Oct. 2019, doi: 10.1016/J.KNOSYS.2019.07.013.
- [59] A. Sangodiah, Y. T. Fui, L. E. Heng, N. A. Jalil, R. K. Ayyasamy, and K. H. Meian, "A Comparative Analysis on Term Weighting in Exam Question Classification," *ISMSIT 2021 - 5th International Symposium on Multidisciplinary Studies and Innovative Technologies, Proceedings*, pp. 199–206, 2021, doi: 10.1109/ISMSIT52890.2021.9604639.
- [60] K. Chen, Z. Zhang, J. Long, and H. Zhang, "Turning from TF-IDF to TF-IGM for term weighting in text classification," *Expert Syst Appl*, vol. 66, pp. 245–260, Dec. 2016, doi: 10.1016/J.ESWA.2016.09.009.
- [61] A. Khurana and V. Bhatnagar, "Investigating Entropy for Extractive Document Summarization," *Expert Syst Appl*, vol. 187, p. 115820, Jan. 2022, doi: 10.1016/J.ESWA.2021.115820.
- [62] A. S. Alammery, "Arabic Questions Classification Using Modified TF-IDF," *IEEE Access*, vol. 9, pp. 95109–95122, 2021, doi: 10.1109/ACCESS.2021.3094115.
- [63] S. S. Haris and N. Omar, "Bloom's taxonomy question categorization using rules and N-gram approach," *J Theor Appl Inf Technol*, vol. 76, no. 3, 2015.
- [64] M. Wasim, W. Mahmood, M. N. Asim, and M. U. Khan, "Multi-Label Question Classification for Factoid and List Type Questions in Biomedical Question Answering," *IEEE Access*, vol. 7, pp. 3882–3896, 2019, doi: 10.1109/ACCESS.2018.2887165.
- [65] H. Sebbag and N. eddine El Faddouli, "MTBERT-Attention: An Explainable BERT Model based on Multi-Task Learning for Cognitive Text Classification," *Sci Afr*, vol. 21, p. e01799, Sep. 2023, doi: 10.1016/J.SCIAF.2023.E01799.
- [66] J. O. Contreras, S. Hilles, and Z. A. Bakar, "Essay question generator based on bloom's taxonomy for assessing automated essay scoring system," *2021 2nd International Conference on Smart Computing and Electronic Enterprise: Ubiquitous, Adaptive, and Sustainable Computing Solutions for New Normal, ICSCEE 2021*, pp. 55–62, Jun. 2021, doi: 10.1109/ICSCEE50312.2021.9498166.
- [67] A. A. AlArfaj and H. A. H. Mahmoud, "An Intelligent Tree Extractive Text Summarization Deep Learning," *Computers, Materials and Continua*, vol. 73, no. 2, 2022, doi: 10.32604/cmc.2022.030090.
- [68] M. Blšták and V. Rozinajová, "Automatic question generation based on sentence structure analysis using machine learning approach," *Nat Lang Eng*, vol. 28, no. 4, 2022, doi: 10.1017/S1351324921000139.
- [69] C. Mallikarjuna and S. Sivanesan, "Question classification using limited labelled data," *Inf Process Manag*, vol. 59, no. 6, p. 103094, Nov. 2022, doi: 10.1016/J.IPM.2022.103094.
- [70] T. T. Goh, N. A. A. Jamaludin, H. Mohamed, M. N. Ismail, and H. Chua, "Semantic Similarity Analysis for Examination Questions Classification Using WordNet," *Applied Sciences* 2023, Vol. 13, Page 8323, vol. 13, no. 14, p. 8323, Jul. 2023, doi: 10.3390/AP13148323.
- [71] M. D. Laddha, V. T. Lokare, A. W. Kiwelekar, and L. D. Netak, "Classifications of the summative assessment for revised bloom's taxonomy by using deep learning," *International Journal of Engineering Trends and Technology*, vol. 69, no. 3, 2021, doi: 10.14445/22315381/IJETT-V69I3P232.
- [72] J. Hartmann, J. Huppertz, C. Schamp, and M. Heitmann, "Comparing automated text classification methods," *International Journal of Research in Marketing*, vol. 36, no. 1, pp. 20–38, Mar. 2019, doi: 10.1016/J.IJRESMAR.2018.09.009.
- [73] M. Wasim, M. N. Asim, M. U. Ghani Khan, and W. Mahmood, "Multi-label biomedical question classification for lexical answer type prediction," *J Biomed Inform*, vol. 93, p. 103143, May 2019, doi: 10.1016/J.JBI.2019.103143.
- [74] N. Patil, O. Kulkarni, V. Bhujle, A. Joshi, K. Khanchandani, and M. Kambli, "Automatic Question Classifier," *Proceedings of 4th International Conference on Cybernetics, Cognition and Machine Learning Applications, ICCMLA 2022*, pp. 53–58, 2022, doi: 10.1109/ICCMLA56841.2022.9989066.
- [75] A. Aninditya, M. A. Hasibuan, and E. Sutoyo, "Text mining approach using TF-IDF and naive bayes for classification of exam questions based on cognitive level of bloom's taxonomy," *Proceedings - 2019 IEEE International Conference on Internet of Things and Intelligence System, IoTAIS 2019*, pp. 112–117, Nov. 2019, doi: 10.1109/IOTAIS47347.2019.8980428.
- [76] M. Ifham, K. Banujan, B. T. G. S. Kumara, and P. M. A. K. Wijeratne, "Automatic Classification of Questions based on Bloom's Taxonomy using Artificial Neural Network," *2022 International Conference on Decision Aid Sciences and Applications, DASA 2022*, pp. 311–315, 2022, doi: 10.1109/DASA54658.2022.9765190.

[77] S. Chotirat, P. Meesad, and H. Unger, "Question Classification from Thai Sentences by Considering Word Context to Question Generation," Proceedings - 2022 Research, Invention, and Innovation Congress: Innovative Electricals and Electronics, RI2C 2022, pp. 9–14, 2022, doi: 10.1109/RI2C56397.2022.9910313.

[78] S. Al Faraby, Adiwijaya, and A. Romadhony, "Educational Question Classification with Pre-trained Language Models," 2022 7th International Conference on Informatics and Computing, ICIC 2022, 2022, doi: 10.1109/ICIC56845.2022.10006957.



ISSN ONLINE: 2447-0228

# ITEGAM-JETIA

Manaus, v.10 n.48, p. 175-182. July/August., 2024.

DOI: <https://doi.org/10.5935/jetia.v10i48.1214>

RESEARCH ARTICLE

OPEN ACCESS

## EVALUATION OF DAM FOUNDATION GROUTABILITY USING SECONDARY PERMEABILITY INDEX AND ROCK QUALITY DESIGN (CASE STUDY IN JLANTAH DAM, INDONESIA)

\*Ilham F. Salam<sup>1</sup>, Yusep M. Purwana<sup>2</sup>, Galuh Chrismaningwang<sup>3</sup> and Dedi Saputra<sup>4</sup><sup>1,2,3</sup> Civil Engineering Department, Sebelas Maret University, Surakarta, Indonesia.<sup>4</sup> Mining Engineering Department, Islam Bandung University, Bandung, Indonesia.<sup>1</sup><http://orcid.org/0009-0005-4527-4560>, <sup>2</sup><https://orcid.org/0000-0002-6815-3033>, <sup>3</sup><http://orcid.org/000-0002-2768-0099><sup>4</sup><http://orcid.org/0009-0000-2867-2990>Email: <sup>1</sup> [ilhamfiksai97@student.uns.ac.id](mailto:ilhamfiksai97@student.uns.ac.id), <sup>2</sup> [ymuslih@staff.uns.ac.id](mailto:yumuslih@staff.uns.ac.id), <sup>3</sup> [galuh@ft.uns.ac.id](mailto:galuh@ft.uns.ac.id), <sup>4</sup> [Dedi.Saputrastsh233@gmail.com](mailto:Dedi.Saputrastsh233@gmail.com)

### ARTICLE INFO

#### Article History

Received: July 20<sup>th</sup>, 2024Revised: August 22<sup>th</sup>, 2024Accepted: August 15<sup>th</sup>, 2024Published: August 30<sup>th</sup>, 2024

#### Keywords:

Dam Foundation,  
Geological Conditions,  
Grouting,  
Rock Quality Design,  
Secondary Permeability Index.

### ABSTRACT

The dam is a building that functions to hold air by blocking the flow of river water. Seepage under the foundation can occur through pores so needs to be cement injection. This research was carried out based on the Secondary Permeability Index (SPI) method in grouting evaluation which still needs to be carried out. The foundation of the Jlantah dam rests on lapilli tuff, agglomerate and volcanic breccia with different characteristics. At this research location there are four relationships between RQD and SPI. Relationship with Type A which shows SPI with Class A to B1 (Very Good to Good) with a low RQD value, caused by the high intensity of interlocking discontinuity areas, and no need for foundation repairs which are rarely found. Type B, which shows RQD is directly proportional to SPI, is found second most frequently. Type C, which shows SPI with Class B2 and C (Fair to Poor) with low RQD due to the high intensity of interlocked discontinuity areas that require cement injection, is the first. Type D shows SPI with Classes C and D (Poor to Very Poor) with high RQD values caused by several faults with the 3rd largest wide opening found.



Copyright ©2024 by authors and Galileo Institute of Technology and Education of the Amazon (ITEGAM). This work is licensed under the Creative Commons Attribution International License (CC BY 4.0).

### I. INTRODUCTION

Dam is a building that functions as a water level rise and water storage area during the rainy season when river water flows in large quantities that exceed the need for irrigation, drinking water, industry, and others. Dam construction is built to hold back the rate of water into reservoirs, lakes, or tourist attractions [1]. The construction of this dam is carried out by calculating its stability so that construction failure does not occur [2]. Air seepage in the dam foundation is one of the critical factors in the calculation of the reservoir. Therefore, rock permeability is an important thing that needs to be considered in the replacement of foundation engineering so that leakage does not occur [3]. Calculating permeability values can be converted into Lugeon values (Lu), which can be divided into rock permeability levels [4]. This analysis was carried out based on compressed testing air on the rocks resulting in the degree of weathering of the airflow and its geometrical characteristics [5],[6]. The relationship between the airflow pattern and the injected semen has a relationship that results

in differences that can be divided into low and high categories [7], [8]. Earlier researchers have widely studied the relationship between the permeability value and the volume of semen injected, but there is still much debate about the relationship between these two aspects [9],[10]. In evaluating grouting, there is the development of methods that can relate or classify rock masses in terms of their secondary permeability values and divide them into soil treatment zones for dam foundations based on rock quality class, namely the secondary permeability index (SPI) method [11]. The Secondary Permeability Index (SPI) method was introduced based on this debate. It can relate or classify rock masses in their secondary permeability and create dam foundation zones based on rock quality classes [11]. This method was used by defining the rock mass's quality based on the discontinuity's permeability value in the pressure water test. The development of this method was applied in evaluating cement injection to study the groutability of

work results and planning foundation repairs with grouting at the Kamal-Saleh Dam [12].

Evaluation based on the cement injection value is related based on the Rock Mass Rating (RMR) value with the Geological Strength Index (GSI) to the Lugeon method, which was previously under debate, the results obtained show the intensity of the discontinuity area a direct relationship with the Lugeon value based on the secondary permeability value to the groutability value of the rock masses in the Ostur Dam [13]. the results obtained at the Ostur Dam correlated SPI and Lugeon values. The research was carried out again on the Nargesi and Cheshmeh-Assheg Dams using empirical equations in correlating secondary permeability index and the Lugeon method (SPI), an indication of rock quality, and collection of cement at the dam site showed that areas with a similar or close trend did not require treatment. In contrast, areas with opposite trends required large amounts of cement injection [14]. Developments in conducting evaluations to look for relationships between Lugeon values, SPI values, and RQD values based on mathematical observations [15], as well as linking cement injection volume with Q-system values, Lugeon values, SPI values, and connection holes for obtained an empirical relationship to the Bakhtiri Dam in Iran [15]. this method is carried out on igneous rock types with surface geotechnical investigations [16].

Foundation repair with grouting cement injection requires volume analysis in planning grouting work, estimated cement volume can be predicted by performing a statistical analysis of the gaps together with injection pressure and SPI by looking for this relationship using multiple linear and linear equations [17]. Evaluation of recommendations for handling cement injection based on Lu, SPI values, and cement injection was carried out on conglomerate rock types [18]. The injection volume is influenced by several factors that affect the amount of cement injection volume so that the value of the empirical equation can be taken based on the SPI value, RQD value, fracture opening, and Groutakes [19]. Determining foundation improvement using a soil treatment classification based on SPI values requires considering the factors between discontinuity field mapping and RQD values [20]. The relationship between the RQD value and the SPI value can be divided to look for some characteristics of rock properties to cracks and their permeability values which can be an evaluation of the use of cement grouting mixtures [21].

Grouting was first applied in Indonesia on the Jatiluhur Dam in 1961 to repair the dam foundation. Grouting was also used in the K-3 Dam project (Karangkates, Kali Konto, and Riam) in 1962. The Wlingi Dam was built in 1975 and inaugurated in 1977 using foundation repairs with grouting due to poor rock conditions and permeability values. The construction of large reservoirs in Indonesia is urgently needed to reduce flooding, the need for clean water, hydroelectric power, and others. Therefore, in 2005, Indonesia made guidelines for methods of using grouting so that it can be used as a reference for work and to improve the safety factor of dams. Evaluation of grouting can be seen from the Lugeon value parameters, SPI values, and cement injection to provide recommendations for soil management [18].

Foundation repair with cement grouting injection requires volume analysis in planning grouting work. Semen volume estimation can be predicted by performing statistical analysis of cracking, injection pressure, and SPI by looking for these relationships using multiple linear equations and linear equations [22]. Several factors that affect cement injection volume influence this volume so empirical equation values can be taken based on SPI values, RQD values, Joint Gaps, and Groutakes [19],[23].

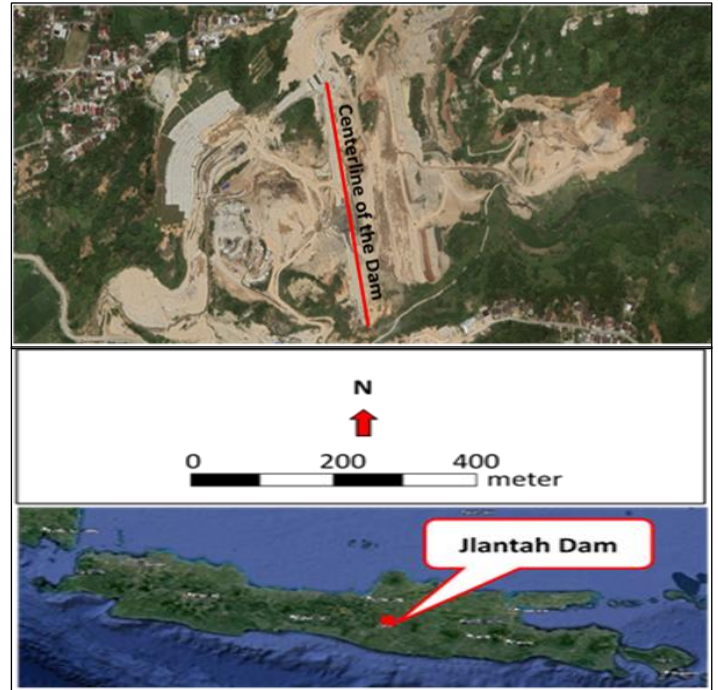


Figure 1: Location Map of Jlantah Dam (Accessed using Google Earth Pro on 11 August 2023 12.00 WIB).  
Source: Authors, (2024).

The method for determining foundation repairs using soil treatment classification based on SPI values must consider the factors between discontinuity field mapping and RQD values [20]. The relationship between the RQD value and the SPI value can be divided to look for some characteristics of rock properties to cracks and their permeability values that can be used to evaluate the use of cement grouting mixtures [21]. The analysis aims to determine the ground treatment by injection of cement using the secondary permeability index (SPI) method and to find a relationship between the RQD value and the SPI value, which can determine the composition of cement mixtures globally.

## II. MATERIALS AND METHODS

### II.1 RESEARCH METHODS

This research was conducted at the Center line of the Jlantah Dam, Karangsarai Village, Jatiyoso District, Karanganyar Regency, Central Java, Indonesia (Figure 1). The data used is from 22 drill points in the Pilot Hole (rock samples and water pressure tests) with a depth of 25 meters to 55 meters during the 2020 to 2023 data collection period. Data processing is carried out using statistical analysis to determine ground treatment zoning with cement injection to determine the relationship between the SPI value and the RQD and thematic analysis in correlating SPI and RQD values. In the first stage (processing of investigative data), at this stage a rock description is carried out to classify rock types, conduct an RQD assessment of each drilling sample and calculate the SPI value from the results of the water pressure test at 5 meters intervals for each test depth. The second stage (data analysis), At this stage, the data that has been obtained from the results of the initial investigation are in the form of rock types, Rock RQD values, and SPI values which are then correlated for each drill point to produce geological thematic cross sections, RQD and SPI. Data resulting from the RQD and SPI values are used to find the relationship between the two values in the resulting grouping of rock characteristics. The third stage (Evaluation), At this stage, the thematic correlation results show a ground treatment zoning that



requires foundation repair with cement injection. The ground treatment category includes needless, local, required, and extensive. Based on the thematic observations, the classification requires a suitable cement injection composition based on the results of rock characteristics obtained based on the relationship between RQD and SPI values. Evaluation based on thematic correlations and the relationship between RQD values and SPI can determine rock characteristics and describe the composition of the cement to be used.

### II.2 ROCK QUALITY DESIGN (RQD)

Rock Quality Designation (RQD) is a valuable calculation method for measuring rock mass quality in core logs based on the length of intact rock samples. RQD is also a measurement of intact rock samples with a length of more than 100 mm to the total length of the drilled sample [24]. This rock class marking has several limitations in the length of the drilling sample, which can be caused by damage during the drilling process, which causes a decrease in the quality value of the rock [14]. The rock mass quality of the Jlantah Dam was carried out at 22 drilling points on the dam axis.

The RQD value of rock can be known using the formula, which can be seen in equation (1).

$$RQD = \frac{\sum \text{Intact core cut length}}{\text{Total length of core retrieved}} \times 100\% \quad (1)$$

Table 1: Classification of rock quality design.

RQD-Value	Rock Classification
0 - 25%	Very poor
25 - 50%	Poor
50 - 75%	Fair
75 - 90%	Good
90 - 100%	Excellent

Source: [24].

The formula described in equation (1) shows the percentage of intact rock sample length greater than 10mm from the drill sample length taken. The results of these calculations are included in the rock quality classification. The classification of rock mass quality can be seen in Table 1.

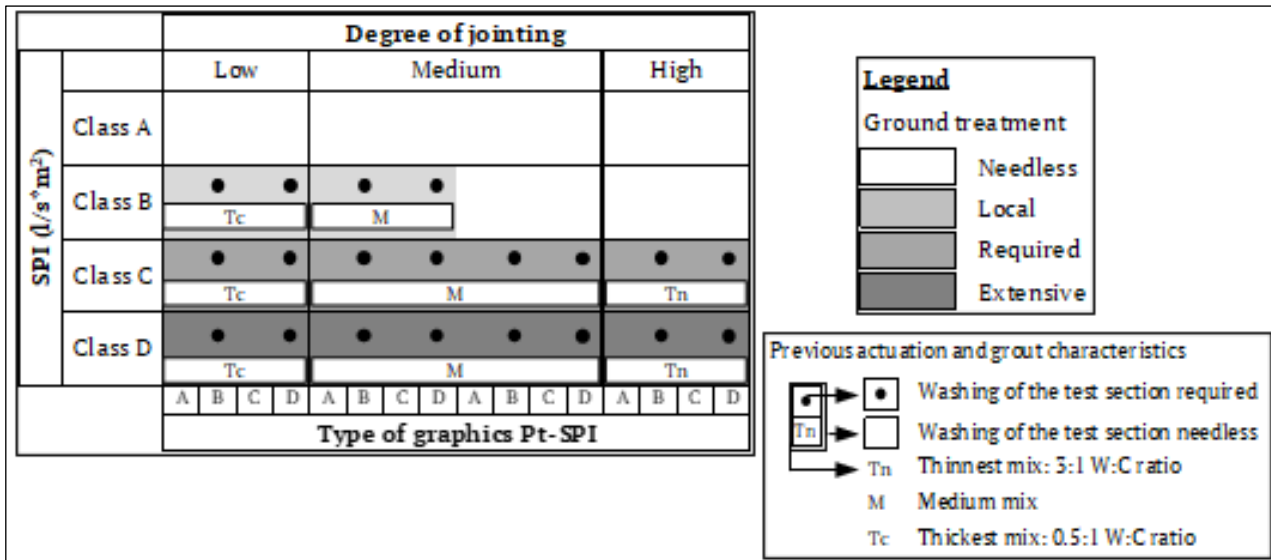


Figure 2: Ground treatment based on SPI value. Source: [11].

The results of SPI calculations can be applied to divide rock mass classes into different ground treatment zones. Table 2 shows the classification of SPI values, which are divided into class A, class B, class C, and class D based on the rock quality, and the classification of ground treatment types is divided into four classes based on the need for grouting cement injection [11]. Classification of Ground treatment based on SPI value can be seen in Figure 2.

Table 2: Modification of rock mass classification based on SPI value and soil treatment.

Rock Mass	SPI (l/s.m <sup>2</sup> )	Classification	Ground Treatment
A	< 2,16 x 10 <sup>-14</sup>	Excellent	Needless
B1	2,16 x 10 <sup>-14</sup> - 7,6 x 10 <sup>-14</sup>	Good	Needless
B2	7,6 x 10 <sup>-14</sup> - 1,7 x 10 <sup>-13</sup>	Fair	Local
C	1,7 x 10 <sup>-13</sup> - 1,7 x 10 <sup>-12</sup>	Poor	Required
D	> 1,7 x 10 <sup>-12</sup>	Very Poor	Extensive

Source: [11].

### II.3 SECONDARY PERMEABILITY INDEX (SPI)

The secondary permeability index (SPI) is a method for converting the results of the water pressure test (WPT) into a rock mass permeability value that can classify the rock mass into the type of ground treatment using injection cement grouting [11]. The formula for finding the secondary permeability index value can be seen in equation (2).

$$SPI = C \times L_n \times \frac{2le}{r+1} \times \frac{Q}{H} \quad (2)$$

The SPI value is the secondary permeability index (l/s.m<sup>2</sup>), and C is a constant on the viscosity with an assumed rock temperature of 10 °C = 1,49 x 10<sup>-10</sup> [25]. le is the length of the section being tested (m), r is the radius of the borehole (m), Q of water flow absorbed by the rock mass (liters), H total water pressure (m), t duration of test for each pressure level (s). The classification based on the SPI value is divided into classes which can be seen in Table 2. Class A indicates that foundation maintenance does not need to be carried out regarding the RQD, SPI, and Pt-SPI patterns. Class B indicates the presence of

treatment on the foundation locally at an RQD value of <50% with an SPI value of > 7,56 x 10<sup>-14</sup> l/s.m<sup>2</sup>. This local handling is based on the existence of a fracture with intensive activity. So, it is necessary to improve with a medium mixture with a ratio of 1:1 W/C at an RQD value of 25-50% or thick with a ratio of 0,5:1 W/C at an RQD value of <25%. For Pt-SPI patterns B and D, it is necessary to wash the test holes before cement injection. Classes C and D show moderately strong foundation damage. If the test section has a low fracture value, it indicates that at least one fracture has a very high conductivity. In this condition, use a viscous mixture with a ratio of 0.5:1 W/C. If the test section is very cracked with an RQD value < 25%, it is necessary to use a thin mixture ratio of 3:1 W/C [11].

**II.4 RELATIONSHIP BETWEEN RQD AND SPI VALUES**

The SPI value, in general, has similarities with the RQD value seen from the characteristics of the rock to the quality of the rock mass. Secondary permeability index values can be slammed with RQD. The better the quality of the rock, the permeability value of the rock is more impermeable. The relationship between the two values also shows a disproportionate relationship between the SPI and RQD. It can indicate abnormal conditions. Based on these differences, the relationship between these two values can be divided into several types of relationships. As in this study area, the low SPI values (Class A and Class B) and low RQD (Very Poor and Poor) may be due to the high intensity of interlocking discontinuities. SPI C and D classes with high RQD values (Excellent and Good) have areas of discontinuity with wide openings [21]. The relationship between SPI – RQD is shown in Table 3.

Table 3: Modification of the relationship between RQD and SPI values.

Type	Description	Ijection Cement
A	Class A SPI values with low RQD values are due to the high intensity of the discontinuity field	No need for foundation repair
B	The fracture intensity is proportional to the SPI value	Normal cement mixtures follow the SPI classification
C	Class B - C SPI values with low RQD values due to the high intensity of inter-locked discontinuity fields	Foundation repair with medium - the dilute mixture
D	Class C - D SPI values with high RQD values, there are areas of several fractures with wide openings	Foundation Repair with Thick mix

Source: [21].

Table 4: Example of the results of processing field studies and observations.

Hole Id	Stage	Top (m)	Bottom (m)	Rock Type	RQD (%)	Lu	Behavior	SPI
PH 1	1	0	5	Lapili tuff	24	29,5	Wash out	6,56E-13
	2	5	10	Lapili tuff	16	1,7	Lamination	3,74E-14
	3	10	15	Lapili tuff	16	5,9	Lamination	1,31E-13
	4	15	20	Volcanic breccia	70	1,7	Lamination	3,75E-14
	5	20	25	Volcanic breccia	50	1,4	Dilatation	3,17E-14
PH 2	1	0	5	Lapili tuff	15	29,9	Turbulent	6,64E-13
	2	5	10	Lapili tuff	43	29,0	Turbulent	6,44E-13
	3	10	15	Volcanic breccia	53	5,6	Lamination	1,24E-13
	4	15	20	Volcanic breccia	23	0,2	Lamination	4,92E-15
	5	20	25	Volcanic breccia	14	0,8	Lamination	1,72E-14
PH 3	1	0	5	Volcanic breccia	33,5	24,0	Turbulent	5,33E-13
	2	5	10	Volcanic breccia	15,1	9,7	Turbulent	2,16E-13
	3	10	15	Volcanic breccia	35	1,1	Lamination	2,40E-14
	4	15	20	Volcanic breccia	76	0,7	Lamination	1,49E-14

Source: Authors, (2024).

**III. RESULTS AND DISCUSSIONS**

**III.1 RESULTS**

Field observations were carried out in drill holes with a depth of 25 m and 55 meters each. The results of these observations are rock types, RQD values, Lugeon values, Lugeon values, and SPI values. An example of recording field data and observation results can be seen in Table 4. Correlation of rock types was carried out on the axis of the dam to surface appearance observations and samples from drilling results from PH drill holes of 22 points. The results of monitoring are shown in Table 4. Surface correlations were carried out to produce a geological map of the dam, as seen in Figure 3. The subsurface correlation results based on 22 drilling points can be seen in the geological cross-section of the Jlantah

dam in Figure 4. Figure 2 shows four types of lithology: alluvial deposits, tuff lapilli, agglomerates, and volcanic breccia. In Figure 3, alluvial deposits are not found in the geological correlation to the drill points as a result of the investigation. The gray color indicates alluvial deposits, the purple color indicates lapilli tuff, the orange indicates agglomerates, and the brown indicates volcanic breccia. The dotted line boundaries in the correlation are considered boundaries, and the groundwater table is indicated by the blue line in Figure 4. The RQD and SPI values indicate the water absorption level and grouting requirements, which can be determined based on the rock characteristics [21].

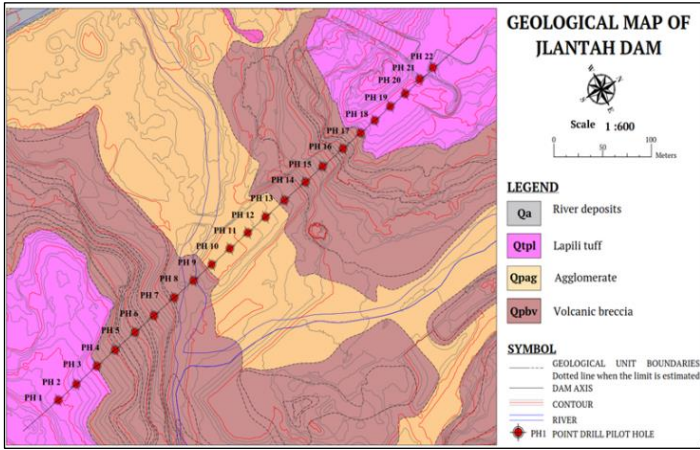


Figure 3: Geological Map of the Jlantah Dam Foundation.  
Source: Authors, (2024).

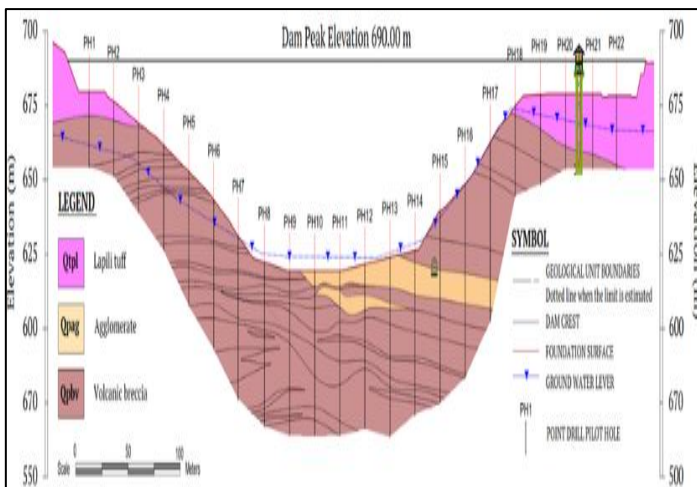


Figure 4: The geological cross-section of the Jlantah Dam.  
Source: Authors, (2024).

Interpretation of ground treatment is carried out based on the RQD value and SPI value. The relationship between the two values can be seen in the graphic pattern between the SPI-RQD values and the drill hole depth, presented at the drill hole points PH1, PH2, and PH3. The three drill holes can represent four types of relationships between SPI and RQD. The graph can be seen in Figure 4. Figure 4 shows three lithology types: gray, indicating alluvial deposits. Purple indicates lapilli tuff, orange indicates agglomerates, and brown indicates volcanic breccias. The dotted line boundaries in the correlation are considered boundaries, and the groundwater table is indicated by the blue line in Figure 4. Based on the RQD and SPI values, rock characteristics related to the degree of water absorption and the need for grouting can be determined [21]. This can show the composition of the mixture between cement and water to be used.

The RQD value of the SPI value proves the interpretation of ground treatment based on the SPI value. An example of a graphical relationship between SPI-RQD value and borehole depth is presented at borehole points PH1, PH2, and PH3, which can represent four types of relationships between SPI and RQD values.

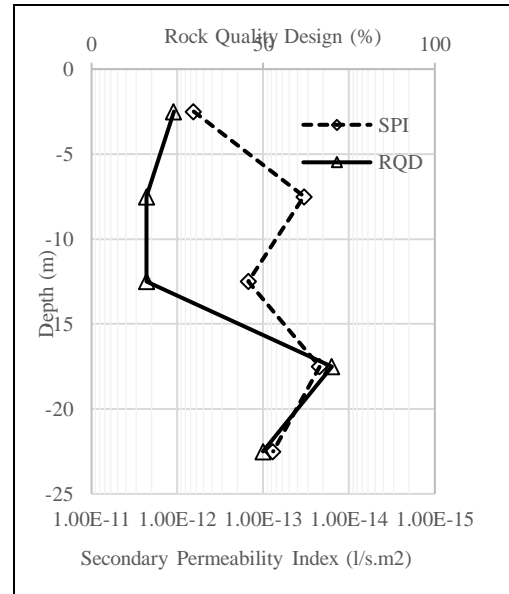


Figure 5: Relationship between SPI - RQD value and depth from Pilot Hole 1.  
Source: Authors, (2024).

Figure 5 shows the relationship between the SPI and the RQD in the pilot hole one. RQD and SPI values are calculated at 5 meters intervals. That location shows a type A connection that does not require cement injection repair at a depth of 15 to 20 meters. The relationship between type B and the SPI value with the RQD value is directly proportional to the depth of 0 to 5 meters and 20 to 25 meters, so cement injection uses a normal mixture based on this type. Type C relationship with class B2-C SPI values ( $7,6 \times 10^{-14}$  l/s.m<sup>2</sup> to  $1,7 \times 10^{-13}$  l/s.m<sup>2</sup>) has a low RQD value at a depth of 5 to 15 meters, so cement injection uses a fine mixture based on this type.

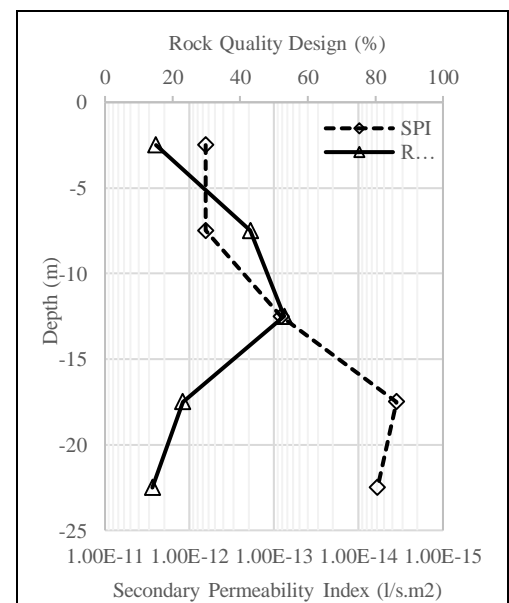


Figure 6: Relationship between SPI - RQD value and depth from Pilot Hole 2.  
Source: Authors, (2024).

Figure 6 shows the graph of RQD-SPI values against borehole depth at point PH2 with a total depth of 25 meters. This location represents a type A joint that does not require cement injection repair at a depth of 15 to 25 meters. At this depth, it has a

class A to B1 ( $<7,6 \times 10^{-14}$  l/s.m<sup>2</sup>) SPI value with a low RQD value, which indicates that many fractures are interlocked or fractures that are not connected so that water cannot flow through the gaps. The relationship between type B and the SPI value with the RQD value is directly proportional to the depth of 10 to 15 meters so cement injection uses a normal mixture based on this type. Type C relationship with class B2 to C SPI values ( $7,6 \times 10^{-14}$  l/s.m<sup>2</sup> to  $1,7 \times 10^{-13}$  l/s.m<sup>2</sup>) has a low RQD value at a depth of 1 to 5 meters, so cement injection uses a fine mixture based on this type. Type D relationship with class C to D ( $>1,7 \times 10^{-13}$  l/s.m<sup>2</sup>) SPI values with medium to high RQD values is found at depths of 5 to 10 meters, indicating the presence of at least extensive fractures. Type D requires a thick injection cement mix to fill wide fracture gaps.

Figure 7 shows the graph of RQD-SPI values against borehole depth at point PH3 with a total depth of 25m. This location represents a type A joint that does not require cement injection repair at a depth of 15 to 25 meters. At this depth, it has a class A to B1 ( $<7,6 \times 10^{-14}$  l/s.m<sup>2</sup>) SPI value with a low RQD value, which indicates that many fractures are interlocked or fractures that are not connected so that water cannot flow through the gaps. The relationship between type B and the SPI value with the RQD value is directly proportional to the depth of 0 to 5 meters so cement injection uses a normal mixture based on this type. Type C relationship with class B2-C SPI values ( $7,6 \times 10^{-14}$  l/s.m<sup>2</sup> to  $1,7 \times 10^{-13}$  l/s.m<sup>2</sup>) has a low RQD value at a depth of 5 to 10 meters, so cement injection uses a fine mixture based on this type.

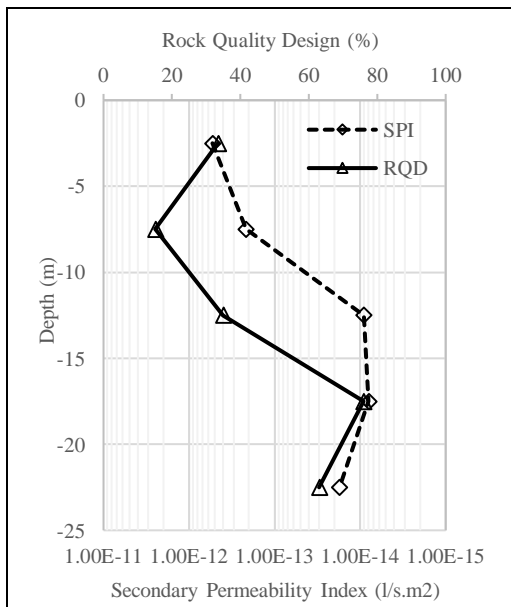


Figure 7: Relationship between SPI - RQD value and depth from Pilot Hole 3.  
Source: Authors, (2024).

The results of the percentage grouping of data obtained from the relationship between RQD and SPI can be seen in Table 5. There were 20 points with a type A relationship of 9,71 %, 51 points with a type B relationship of 24,76 %, 117 points with a type C of 56,80 %, and 10 points with a type D of 4,85 %. Based on these data, the type C relationship dominates the Jlantah Dam foundation.

The relationship between RQD and SPI values on the Jlantah Dam axis is dominated by type C. The correlation between SPI values and ground treatment using the cement grouting injection method is shown in Figure 8. The SPI values were correlated at 22 points of the pilot hole drill holes, which have their

respective depths. Each drill hole ranges from 25 m to 55 m with intervals of SPI values every 5 m.

The results are classified into four classes. Class A is shown in blue without the need for foundation repair, Class B in green with localized grouting, Class C in yellow, which is visible in sections requiring repair by grouting, and Class D in red requiring extensive grouting.

Table 5: Percentage of SPI-RQD types on the Jlantah Dam.

No	Type	Frequency	Percentage (%)
1	A	20	9,71
2	B	51	24,76
3	C	117	56,80
4	D	10	4,85

Source: Authors, (2024).

### III.2 DISCUSSIONS

The Jlantah Dam is located at 7o 42' 44,05" LS and 111o 4' 47,51" BT. Geologically, this dam is located in the Ponorogo Sheet Geology. The foundation of this dam is supported by Quaternary-aged rocks on the left and right abutments in the form of lapilli tuff and volcanic breccia, and the foundation area of the river bed is in the form of agglomerate and volcanic breccia. The weathering condition of the rocks is moderate to light, which is highly influenced by the high rainfall rate. No significant faults were observed during the investigation, and the geological characteristics were evaluated using drilling data and field observations. The subsurface correlation in Figure 4 is arranged from the oldest to the youngest based on the regional age comparison. During the Pliocene epoch, volcanic breccia was deposited, followed by agglomerate deposited by interfingering. During the Holocene epoch, lapilli tuff was deposited parallel with volcanic breccia.

The volcanic rock has poor grain uniformity, which can cause very porous permeability values. The agglomerate has a dominant appearance of rounded fragments with sizes ranging from 64 mm to 1000 mm, which allows water to flow easily through the gaps between the fragments. The composition of the rock causes differences in the permeability values. It is influenced by the boundaries between rock layers with a mutually supportive relationship and the fractures in each rock. One of the factors that can affect the value of very porous or impermeable permeability is the level of rock quality, as seen from the primary and secondary structure of the rock itself. The relationship between rock mass quality and secondary permeability index values can be observed and classified based on the relationship between the RQD value and the SPI value [21]. Figure 5 at a 0 m to 15 m depth shows a low RQD value (Very Bad) with SPI values ranging from  $2,16 \times 10^{-14}$  l/s.m<sup>2</sup> to  $1,7 \times 10^{-12}$  l/s. m<sup>2</sup> (Class B to C). This relationship belongs to Type-C, caused by the high intensity of the interconnected discontinuity fields. Cement grouting mixtures in this type of connection require a medium to a fine mixture.

Figure 6 shows that the RQD class values are better than the SPI class values at 5 m to 15 m depth. The graphic pattern relationship between RQD and SPI shows several cracks with wide openings, so the grouting cement mixture uses a thick mixture to fill the cracks with wide openings. The analysis results of the relationship between the RQD value and the SPI value can be categorized into the percentage of the presence of the left abutment, riverbed, and right abutment. This percentage can determine the need for cement for the grouting. In addition, a comparison of the volume of cement with the standard mixture to the need for the

cement mixture can be made based on the relationship between the RQD value and the SPI value.

This is useful in planning grouting work in calculating estimated cement requirements to be used. Figure 6 at a 0 m to 5 m depth shows a symmetrical pattern or value between the RQD value and the SPI value (Type A). This pattern indicates that the RQD value is directly proportional to the crack intensity, directly proportional to the secondary permeability value. The composition of the cement grouting mixture follows the composition specified in the ground treatment classification based on the SPI value. At a depth of 15 m to 20 m shows a low RQD value (Very Bad) with an SPI value of less than  $2,16 \times 10^{-14}$  l/s.m<sup>2</sup> (Class A). This relationship belongs to Type B, caused by the high intensity of the interconnected discontinuity fields. However, based on the SPI value in Class A, grouting is not required at that depth.

Table 5 shows the percentage of the type of relationship between the RQD value and the SPI value. Type A ranks second most from the entire area of the dam foundation by handling grouting cement injection using the same mixture ratio between cement and water. Type B is the smallest percentage of dam axis foundation locations that do not require grouting injection. Based on this, the volume of cement requirements can be estimated and compared with the grouting work plan, and all parts of the dam are dominated throughout dominated by Type C, so the use of cement grouting mixture using a medium-fine mixture to reduce the volume of cement needed. Finally, type D occupies the third highest order at the observation site. This type of ground treatment with grouting cement injection uses a thick cement mixture so that the volume of cement is more than the volume of water used. Therefore, cement requirements can be estimated and compared with the grouting work plan. The repair of the foundation was designed based on the RQD value and the SPI value, which were correlated to the axis cross-section of the Jlantah Dam (Figure 8). The results suggest that ground treatment in the Class A area of the Jlantah Dam does not require foundation repair.

Foundation repairs in Class C and D areas area urgently needed. Foundation repairs will be planned with a ratio of dam height to the grouting depth of 2/3 of the dam height, which refers to large dam construction standards. Cement injection blinds are urgently needed on riverbed foundations, which are dominated by Class C and D and require intensive repairs. On the right abutment area, which is dominated by Class B to C, local and thorough repairs are required. On the left abutments, which are seen to be dominated by Class A-B, some repairs are required on an ongoing basis, locally and slightly present at low depths at PH 1 to PH 3. The results of this study indicate similarities regarding the relationship between the RQD value and the SPI value, which has been carried out by modifying the relationship type boundaries that have been carried out by previous researchers [21]. This research was carried out on quaternary volcanic rocks. So, continuing previous research looks for a relationship between secondary permeability index values and rock quality design values to evaluate grouting on igneous rocks [16], conglomerates [18] and limestone [19].

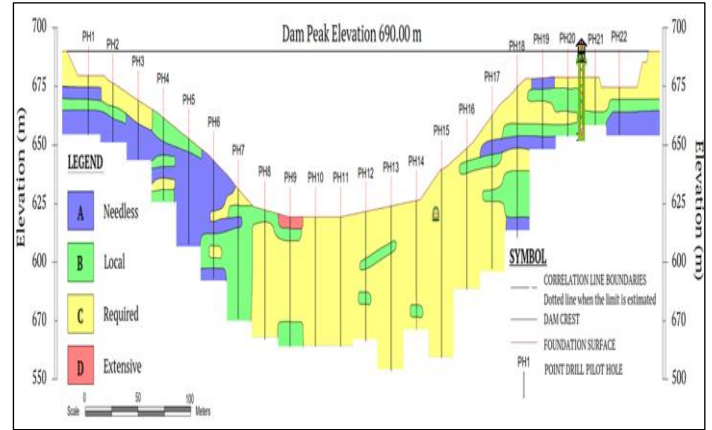


Figure 8: Cross section of the SPI-value axis Jlantah Dam.  
Source: Authors, (2024).

#### IV. CONCLUSIONS

The foundation of the Jlantah Dam rests on volcanic breccias, agglomerates, and lapilli tuffs with different rock characteristics. On the left and right abutments that rest on tuff lapilli at a depth of 15 m to 25 meters, SPI class B that required local repair was found, and SPI class A that did not require grouting cement injection. At a depth of 0 to 15 meters, it has an SPI Class C value requiring grouting cement injection. The left abutment, which rests on volcanic breccia rock, is dominated by SPI class A which does not require grouting cement injection. The location of the river bed, which is based on volcanic breccias and agglomerates, needs to be repaired by cement grouting injection seen from the SPI values, which are included in classes C and D. At this research location, there are four relationships between RQD and SPI. Relationship with type A, which shows RQD is directly proportional to the SPI, is found to be the 2nd most. Type B, which shows SPI with Class A (Excellent) with a low RQD value, is caused by the high intensity of interlocking discontinuity areas, and no foundation repairs are needed very rarely found. Type C showing SPI with Class B and C (Good-Fair-Poor) with low RQD due to the high intensity of interlocked discontinuity areas requiring cement injection was found to be the 1st. Type D showing SPI with Class C and D (Poor-Very Poor) with a high RQD value caused by several fractures with wide openings found the 3rd most.

#### V. AUTHOR'S CONTRIBUTION

**Conceptualization:** Ilham F. Salam, Yusep M. Purwana and Galuh Chrismaningwang.

**Methodology:** Ilham F. Salam, Yusep M. Purwana and Galuh Chrismaningwang.

**Investigation:** Ilham F. Salam, Yusep M. Purwana and Galuh Chrismaningwang.

**Discussion of results:** Ilham F. Salam, Yusep M. Purwana and Galuh Chrismaningwang.

**Writing – Original Draft:** Ilham F. Salam, Yusep M. Purwana and Galuh Chrismaningwang.

**Writing – Review and Editing:** Ilham F. Salam, Yusep M. Purwana, Galuh Chrismaningwang and Dedi Saputra.

**Supervision:** Ilham F. Salam, Yusep M. Purwana and Galuh Chrismaningwang.

**Approval of the final text:** Ilham F. Salam, Yusep M. Purwana, Galuh Chrismaningwang and Dedi Saputra.

## VII. ACKNOWLEDGMENTS

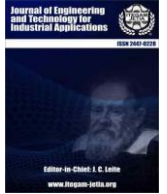
This research collaborated to support writing consultations and data analysis by postgraduate lecturers in the Department of Civil Engineering, Faculty of Engineering, Sebelas Maret University. BBWS Bengawan Solo supports the data used through PT Virama Karya in the Jlantah Dam construction project, Karangasari Village, Jatiyoso District, Karanganyar Regency, Central Java, Indonesia.

## VIII. REFERENCES

- [1] A. Sani, "Analisis Kapasitas Waduk dengan Metode Ripple dan Behaviour (Studi Kasus Pada Waduk Mamak Sumbawa)," Universitas Muhammadiyah Yogyakarta, 2008.
- [2] J. Yang, J. Hu, Y. Wu, and B. Zhang, "Numerical simulation of seepage and stability of tailing dams: A case study in Ledong, China," *Sustainability*, 2022, [Online]. Available: <https://api.semanticscholar.org/CorpusID:252653263>.
- [3] G. Kheiri, H. Javdanian, and G. Shams, "A numerical modeling study on the seepage under embankment dams," *Model Earth Syst Environ*, vol. 6, pp. 1075–1087, 2020, [Online]. Available: <https://api.semanticscholar.org/CorpusID:212718920>.
- [4] M. Lugeon, *Barrages et Géologie. Méthodes de recherches. Terrassement et Imperméabilisation*, 2nd ed. Pedrazzini, 1979. Accessed: Dec. 21, 2022. [Online]. Available: <https://www.worldcat.org/title/1069135491>.
- [5] F.-K. Ewert and U. Hungsberg, *Rock Grouting at Dam Sites*, vol. 1. Springer Cham, 2018. doi: 10.1007/978-3-319-64036-5.
- [6] R. Karagüzel and R. Kiliç, "The effect of the alteration degree of ophiolitic melange on permeability and grouting," *Eng Geol*, vol. 57, pp. 1–12, Sep. 2000, doi: 10.1016/S0013-7952(99)00124-6.
- [7] Heitfeld, Karl-Heinrich, and H. Breddin, *Hydro-und baugewissenschaftliche Untersuchungen über die Durchlässigkeit des Untergrundes an Talsperren des Sauerlandes Sonderdruck aus: Geologische Mitteilungen*, 5th ed. Aachen, Selbstverlag, 1965.
- [8] G. Lombardi, "Grouting of rock masses," in *3rd International Conference on Grouting and Grout Treatment*, Minosio, Oct. 2002.
- [9] E. Nonveiller, *Grouting Theory and Practice*, 1st ed. Elsevier, 1989. Accessed: Dec. 21, 2022. [Online]. Available: <https://books.google.com.cy/books?id=jcJPtQEACAAJ>.
- [10] G. Lombardi, "The Role of Cohesion in Cement Grouting of Rock," *15th ICOLD-Congress, Lausanne*, vol. 3, pp. 235–261, 1985.
- [11] A. Foyo, M. A. Sánchez, and C. Tomillo, "A proposal for a Secondary Permeability Index obtained from water pressure tests in dam foundations," *Eng Geol*, vol. 77, no. 1–2, pp. 69–82, Feb. 2005, doi: 10.1016/j.enggeo.2004.08.007.
- [12] A. Uromeihy and R. Farrokhi, "Evaluating groutability at the Kamal-Saleh Dam based on Lugeon tests," *Bulletin of Engineering Geology and the Environment*, vol. 71, no. 2, pp. 215–219, May 2012, doi: 10.1007/s10064-011-0382-7.
- [13] S. M. Sadeghiyeh, M. Hashemi, and R. Ajalloeian, "Comparison of permeability and groutability of ostur dam site rock mass for grout curtain design," *Rock Mech Rock Eng*, vol. 46, no. 2, pp. 341–357, Mar. 2012, doi: 10.1007/s00603-012-0282-6.
- [14] A. Azimian and R. Ajalloeian, "Permeability and groutability appraisal of the Nargesi dam site in Iran based on the secondary permeability index, joint hydraulic aperture and lugeon tests," *Bulletin of Engineering Geology and the Environment*, vol. 74, no. 3, pp. 845–859, Aug. 2015, doi: 10.1007/s10064-014-0675-8.
- [15] A. Sohrabi-Bidar, A. Rastegar-Nia, and A. Zolfaghari, "Estimation of the grout take using empirical relationships (case study: Bakhtiari dam site)," *Bulletin of Engineering Geology and the Environment*, vol. 75, no. 2, pp. 425–438, May 2016, doi: 10.1007/s10064-015-0754-5.
- [16] G. Barzegari, "Geotechnical evaluation of dam foundation with special reference to in situ permeability: A case study," *Geotechnical and Geological Engineering*, vol. 35, no. 3, pp. 991–1011, Jun. 2017, doi: 10.1007/s10706-016-0155-y.
- [17] A. Rastegar Nia, G. R. Lashkaripour, and M. Ghafoori, "Prediction of grout take using rock mass properties," *Bulletin of Engineering Geology and the Environment*, vol. 76, no. 4, pp. 1643–1654, Nov. 2017, doi: 10.1007/s10064-016-0956-5.
- [18] S. D. Mohammadi and A. Nooryazdan, "Evaluation of groutability in the pliocene conglomerate by SPI method for sealing (A Case Study)," *Scientific Quarterly Journal of Iranian Association of Engineering Geology*, vol. 11, no. 1, pp. 19–35, 2018, Accessed: Oct. 19, 2022. [Online]. Available: [http://www.jiraeg.ir/article\\_76906\\_en.html?lang=en](http://www.jiraeg.ir/article_76906_en.html?lang=en).
- [19] A. Kayabasi and C. Gokceoglu, "An assessment on permeability and grout take of limestone: a case study at Mut Dam, Karaman, Turkey," *Water (Switzerland)*, vol. 11, no. 12, Dec. 2019, doi: 10.3390/W11122649.
- [20] B. R. Jones, J. L. Van Rooy, and D. J. Mouton, "Verifying the ground treatment as proposed by the secondary permeability index during dam foundation grouting," *Bulletin of Engineering Geology and the Environment*, vol. 78, no. 3, pp. 1305–1326, Apr. 2019, doi: 10.1007/s10064-017-1219-9.
- [21] Y. Nikpeyman, F. Kargaranbafghi, M. Ghasemi, and M. Sedaghat, "Assessment of the groutability using secondary permeability index in an arid zone: A case study in Shitab Dam site, SE Iran," *Italian Journal of Engineering Geology and Environment*, vol. 19, no. 1, pp. 41–48, 2019, doi: 10.4408/IJEGE.2019-01.O-04.
- [22] A. Rastegarnia, G. R. Lashkaripour, M. Ghafoori, and S. S. Farrokhad, "Assessment of the engineering geological characteristics of the Bazoft dam site, SW Iran," *Quarterly Journal of Engineering Geology and Hydrogeology*, vol. 52, no. 3, pp. 360–374, Feb. 2019, doi: 10.1144/qjegh2017-042.
- [23] A. Kayabasi, N. Yesiloglu-Gultekin, and C. Gokceoglu, "Use of non-linear prediction tools to assess rock mass permeability using various discontinuity parameters," *Eng Geol*, vol. 185, pp. 1–9, Feb. 2015, doi: 10.1016/j.enggeo.2014.12.007.
- [24] D. U. Deere and D. W. Deere, "Rock Quality Designation (RQD) After Twenty Year," *New York*, Jun. 1989.
- [25] T. Snow David, "Rock fracture spacings, openings, and porosities," *Proceedings of the American Society of Civil Engineers*, vol. 94, pp. 73–91, 1968, [Online]. Available: <https://eurekamag.com/research/019/933/019933409.php>.



ISSN ONLINE: 2447-0228



## RESEARCH ARTICLE

## OPEN ACCESS

## ENVIRONMENTAL EFFECTS OF BIODIESEL ENGINES FUELLED BY WASTE COOKING OIL AND METAL NANO ADDITIVES

<sup>1</sup>K.Ch. Sekhar, <sup>2</sup>Ramyakalakapati, <sup>3</sup>Balaji Mugada, <sup>4</sup>Anusha Kalluri, <sup>5\*</sup>Raviteja Surakasi, <sup>6</sup>Iván Leandro Rodríguez Rico

<sup>1,3,4,5\*</sup>Department of Mechanical Engineering, Lendi Institute of Engineering and Technology, Jonnada, Vizianagaram, Andhra Pradesh, India – 535005

<sup>2</sup>Department of Mechanical Engineering, Anil Neerukonda Institute of Technology and Sciences (ANITS), Sangivalasa, Bheemunipatnam, Visakhapatnam, Andhra Pradesh – 531162, India

<sup>6</sup>Central University "Marta Abreu" of Las Villas, Cuba

<sup>1</sup><https://orcid.org/0000-0001-5603-1453>, <sup>2</sup><https://orcid.org/0000-0002-9159-673X>, <sup>4</sup><https://orcid.org/0000-0002-7046-9600>,

<sup>5</sup><https://orcid.org/0000-0002-0786-0105>, <sup>6</sup><https://orcid.org/0000-0003-1295-5368>,

Email: \* [sekhar.lendi@gmail.com](mailto:sekhar.lendi@gmail.com), [ramyapakalapati87@gmail.com](mailto:ramyapakalapati87@gmail.com), [balaji.lendi@gmail.com](mailto:balaji.lendi@gmail.com), [anu.k01101991@gmail.com](mailto:anu.k01101991@gmail.com), [ravitejasurakasi@gmail.com](mailto:ravitejasurakasi@gmail.com), [ivanl@uclv.edu.cu](mailto:ivanl@uclv.edu.cu).

## ARTICLE INFO

**Article History**

Received: July 02<sup>th</sup>, 2024

Revised: August 19<sup>th</sup>, 2024

Accepted: August 19<sup>th</sup>, 2024

Published: August 30<sup>th</sup>, 2024

**Keywords:**

Waste cooking oil, nano additive, transesterification, environmental pollution, methyl esters.

## ABSTRACT

The experiment yielded significant findings. Transesterification was used to turn waste cooking oil into biodiesel, a renewable energy source. The fuel mixture ratios were adjusted to measure engine performance and lower fossil fuel emissions. The study examined power generation, torque, consumption per hour, and emissions of unburnt hydrocarbons and carbon dioxide. The diesel engine's power output was 5.2 kilowatts. Biodiesel, derived from discarded leftover cooking oil, was synthesized by blending it with diesel fuel at a concentration of 20%. Engine performance tests revealed no statistically significant variations in power or torque across the various commercial diesel mixes. Notably, the consumption of diesel petroleum for commercial purposes increased by 15% and 20% per hour, respectively. The main advantage was the reduction in carbon dioxide emissions, which was 20% for all combinations of commercial fuel and biodiesel, compared to only commercial diesel.



Copyright ©2024 by authors and Galileo Institute of Technology and Education of the Amazon (ITEGAM). This work is licensed under the Creative Commons Attribution International License (CC BY 4.0).

## I. INTRODUCTION

In response to the growing need for oil, biodiesel has emerged as a practical and environmentally friendly substitute for conventional diesel fuel in ICEs, stoves, and other burners. Government policies in several nations have actively encouraged the production and widespread adoption of first-generation biodiesel, increasing usage within these countries. Many countries have encouraged the growth of oil palms for the production of biodiesel, which could potentially meet the energy needs of power plants [1]. It's important to note that first-generation biofuels come with drawbacks. They require a substantial amount of water during production, potentially impacting the food supply and competing with crops meant for human consumption. This sparks a discussion on the efficiency of utilizing food and energy obtained through these resources, which is crucial for developing creative strategies in certain countries. Due to these challenges, there is a growing focus on developing innovative solutions and materials [2]. The

development of biodiesel derived from non-food sources and its use has sparked diverse viewpoints about the potential for food and fuel production from these sources. Consequently, it is essential to thoroughly assess this aspect throughout the legislative procedures in different countries.

Researchers from various countries have conducted extensive studies on the effectiveness of internal combustion engines [3]. A thorough online investigation has been conducted on the process of producing biodiesel from non-edible vegetable oils, including comprehensive details on the properties and functionality of the fuel. Numerous plant oils have been investigated by scientists as possible sources of raw materials, including those obtained from cotton, tobacco, flax, jatropha, rubber, and jojoba trees. The cultivation of oil palms for biodiesel production has been advocated in many nations as a means to fulfill the need for this fuel source in electric generators [4]. First-generation biofuels include many drawbacks, such as the potential

for competing with food crops and their significant water use during manufacturing. Research has indicated that waste cooking oil has the potential to be transformed into biodiesel that meets global environmental standards and guidelines [5]. According to the study authors, a 98.1% transesterification conversion rate may be attained in producing this biofuel under ideal conditions. Recently, numerous scientists have been devoting considerable time and resources to exploring the viability of biodiesel as a fuel for internal combustion engines. Recent research has examined the efficiency of internal combustion engines concerning transportation [6].

## II. MATERIALS AND METHOD

### II.1 PRODUCTION OF BIODIESEL

According to the Food and Agriculture Organization (FAO), the first stage is extracting waste cooking oil by heating, which yields around 10 litres. This oil sample is specifically used to conduct acidity analysis. Understanding the acid number of a

triglyceride provides valuable insight into the presence of free fatty acids, allowing for an assessment of its acidity level. Potassium hydroxide is essential for titration, while acidity is determined using the acid number index. The oil's acid number will be determined by the investigation. A suitable operating condition free from problems is indicated by a computed result below or equivalent to 5. Nevertheless, it is not recommended to have an acidity index higher than 5 for manufacturing biodiesel because of the increased acid number. However, it is not ideal for biodiesel synthesis and is more beneficially utilized in other fields. To determine the acidity, we mixed a 5-gram sample with 50 millilitres of neutralized ethyl alcohol, heated to temperatures about 50 degrees Celsius. Afterward, an Erlenmeyer flask added a small amount of phenolphthalein to the amalgamation. Afterward, a solution of potassium hydroxide with a concentration of 0.1N was utilized to carry out the titration of the solution [7]. Figure 1 depicts the transesterification process.

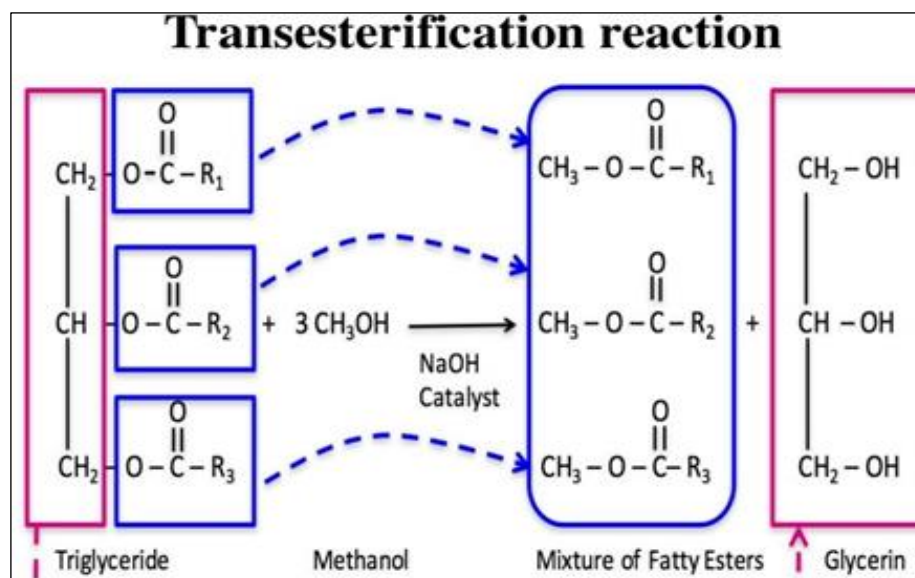


Figure 1: Transesterification process.

Source: Authors, (2024).

Through transesterification, plant and animal oils can be transformed into monoalkyl esters composed of long-chain fatty acids, which can be utilized multiple times. This method can also be applied to animal fats. Additionally, these oils are incorporated into the biodiesel production process. For the experiment, a container designated for this purpose was filled with 10 liters of waste cooking oil. After that, 20% (v/v) methanol was added to the bottle. The quantity of methanol utilized was roughly equivalent to the quantity of oil under examination. The total amount was increased by an equivalent value to the acid number to determine the required number of catalysts. A clear reaction occurred when 8 grams of potassium hydroxide (KOH) were added in equal amounts. Catalyst and methanol (methoxide) were combined before their addition to the sample for reaction. The mixture was agitated for approximately two hours at a temperature ranging from fifty to sixty degrees Celsius. The glycerin was separated through the process of decantation. After that, three to four washes with water were done. This was done because the amount of biodiesel

made varied. After this step [8], the steps of drying and filtering were done.

### II.2. FUEL SAMPLES

Using a magnetic stirrer, the mixture of 20 percent biodiesel and 80 percent diesel was thoroughly blended to create the waste cooking oil methyl ester blend (B20) for further evaluation. The process described above led to the creation of the final result. Zinc Oxide (ZnO) nanoparticles were evenly distributed in B20 fuel test samples using an ultrasonicator following the established procedure. Dosage levels of 50 and 100 ppm were used. Three different combinations of B20, B20 plus 50 ppm ZnO, and B20 plus 100 ppm ZnO were the starting materials employed in this experiment. Analyze the quality of all the fuels using the ASTM D 6751 test procedure, a widely accepted standard method for evaluating fuel properties. [9]



Table 1: Fuel blends Properties.

S. No	Properties	Diesel	Waste Cooking Oil (B20)	B20+ 50 ppm CuO	B20+100 ppm CuO
1	Kinetic viscosity cSt	3.05	4.78	4.76	4.73
2	Density kg/m <sup>3</sup>	830	889	891	893
3	Calorific value MJ/kg	44.5	39.2	37.4	37.8
4	Flashpoint °C	60	190	193	195
5	Cetane Number	40	43	46	49

Source: Authors, (2024).

### III. EXPERIMENTAL SET-UP

An engine with one cylinder, four strokes, compression ignition, and either a water-cooled or water-injected cooling system was used throughout the testing. To provide more details, the engine utilized in the trials was a Kirloskar, TV1-type engine. The engine in question was utilized to conduct experimental research. This engine can produce a remarkable power output of 5.2 kilowatts, even operating at maximum capacity while maintaining a consistent engine speed of 1500 rpm. This is the maximum power it can generate. Following the manufacturer's specifications, the fuel injection pressure was kept at 210 bar and the timing at 23 degrees before the top dead center (TDC). A constant 80 degrees Celsius coolant temperature was maintained throughout the operation. A system allowed continual coolant recirculation via the cylinder's water jackets. Our piezoelectric transducer was smoothly mounted on the vehicle's cylinder head to measure engine cylinder pressure correctly. Eddy current dynamometers were optionally installed to monitor engine torque. The experimental setup is depicted more compactly in Figure 2, showcasing an illustration of the schematic design.

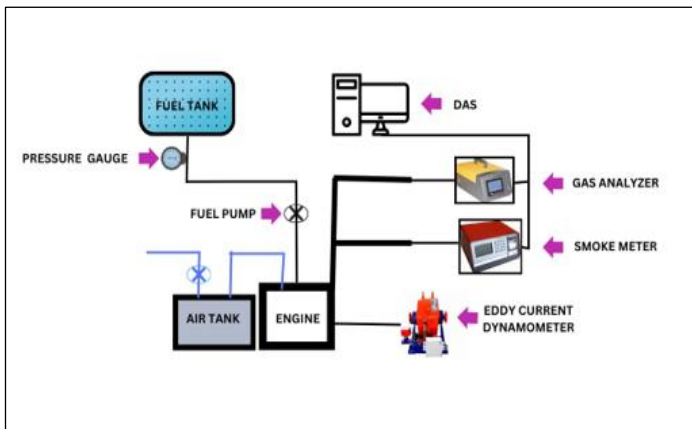


Figure 2: Experimental set-up.  
Source: Authors, (2024).

## IV. RESULTS AND DISCUSSIONS

### IV.1. POWER TEST

The engine's power output is shown in Figure 3 for each kind of fuel combination at 3600 rpm constant speed at four different loads, each of which was increased by 25%. As a point of reference for comparison, the amount of power produced by the B20 fuel mix, which also included 100 parts per million of ZnO, is utilized. There is no statistically significant difference between the power levels for each kind of mixing and the base power, with a mean difference of 0.01 kW. Figure 3 shows the results for each of the various loads placed on the engine and the various mixtures. The foundation's strength (B20) does not shift in any way since it is unaffected by external factors. Similarly, one may see that the

power shows a proportionate increase in coordination with the load, which exemplifies a recognizable connection often experienced [10].

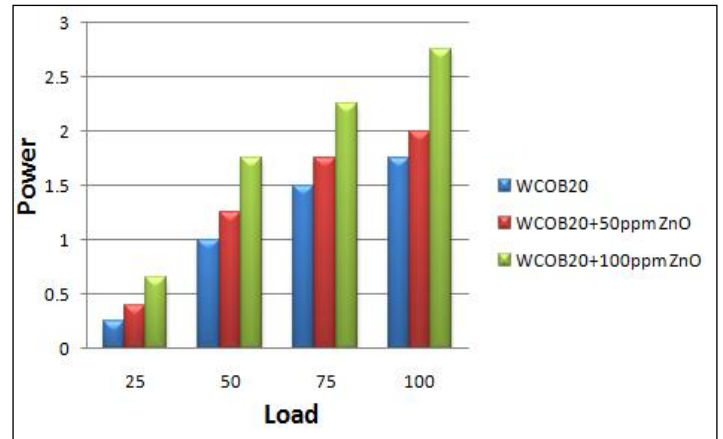


Figure 3: Power varying with an increase in load.  
Source: Authors, (2024).

### IV.2. TORQUE TEST

Figure 4 demonstrates that the values of the engine's torque are mostly the same regardless of the load group or the kind of mixture. displaying an almost linear upward tendency in conjunction with a rising trend as the load rises. The data in the picture demonstrate that the variety of gasoline used does not impact the engine's torque output [11]. This corresponds to each load applied to the engine, and the propensity for this to occur increases as the load-imposed increases (B20+100ppm ZnO), as the trend line demonstrates.

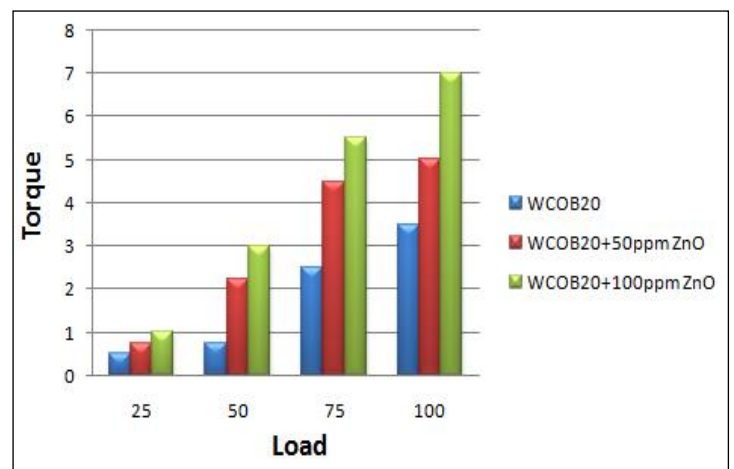


Figure 4: Torque varying with an increase in load  
Source: Authors, (2024).

### IV.3. CONSUMPTION TEST

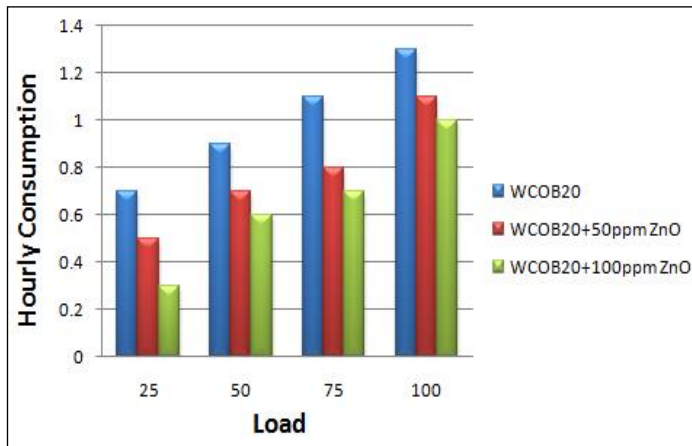


Figure 5: Hourly consumption varies with an increase in the load. Source: Authors, (2024).

The findings shown in Figure 5 indicate that the hourly consumption of commercial gasoline is consistently less than that seen with the blends throughout various load conditions [12]. Because biodiesel has a lower calorific value than B20, some have speculated that the increased usage of a combination of commercial gasoline and waste cooking oil biodiesel represents some compensation. The dependence of the hourly consumption curve on the combinations used, which depends on the loads adjusting to the anticipated characteristic, is shown in Figure 5 [13]. The biodiesel combination provides the least hourly usage. The use of all fuel types shows a decrease.

### IV.4. UHC EMISSION TEST

Figure 6 undeniably demonstrates the escalation in unburned hydrocarbons (UHC) emissions in both low-load and high-load conditions, culminating in maximum power [13]. According to the established theoretical framework, a restricted oxygen supply undeniably results in higher unburned hydrocarbon (UHC) emissions. The research unequivocally indicates that the fuel exhibits a higher richness than the fuel-air mixture ratio [14]. Figure 6 unequivocally portrays a consistent reduction in UHC emissions for all mixtures throughout the operational range. Furthermore, it is indisputable that the B20+100ppm ZnO combination exhibits even lower emissions than the B20 mixture [15].

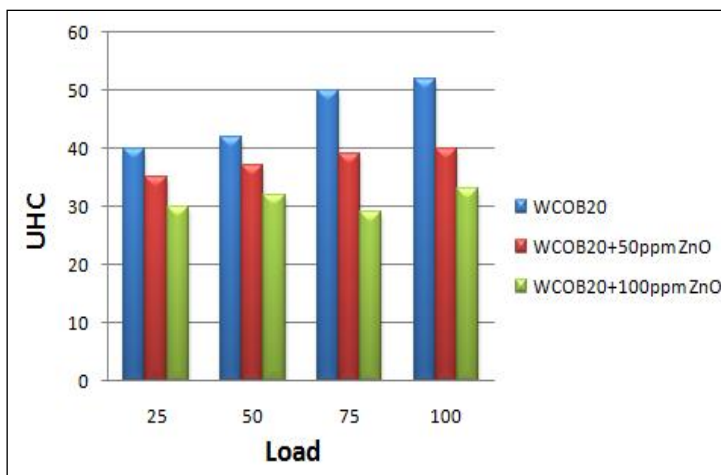


Figure 6: UHC varies with an increase in load. Source: Authors, (2024).

### IV.5. CO<sub>2</sub> EMISSION TEST

Based on the information provided in Figure 7, there appears to be a clear positive correlation between carbon dioxide (CO<sub>2</sub>) emissions and the increase in all loads. It's worth noting that incorporating leftover cooking oil biodiesel into the fuel mixture can lead to a substantial reduction of approximately 20% to 25% in total CO<sub>2</sub> emissions [16]. The data depicted in Figure 7 demonstrates the CO<sub>2</sub> emissions for different engine loads when using B20 fuel. Notably, the concentration of carbon dioxide (CO<sub>2</sub>) is highest in the general atmosphere, including the B20 blend combination [17]. Utilizing a B20 gasoline mix with 100 ppm of Zinc Oxide (ZnO) has the potential to diminish greenhouse gas emissions significantly.

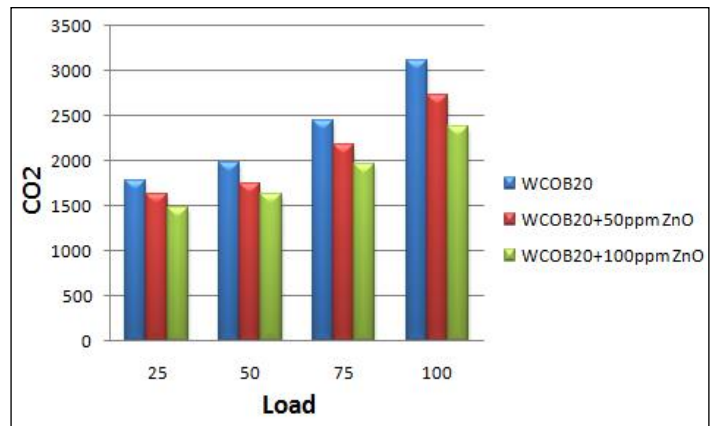


Figure 7: CO<sub>2</sub> varying with an increase in load. Source: Authors, (2024).

### V. CONCLUSION

Waste cooking oil is an important biodiesel feedstock. Residual cooking oil biodiesel is a third- or fourth-generation renewable fuel with little food security effect. Waste cooking oil biodiesel minimizes greenhouse gases. Energy-wise, waste cooking oil biodiesel beats diesel. ZnO nanoparticle-blended biodiesel outperforms B20 in power and emissions. The power of the base (B20) remains constant and does not undergo any changes. Similarly, it can be noticed that the power exhibits a proportional rise in tandem with the load, so illustrating a discernible relationship that is often encountered. To each load that is applied on the engine, and the propensity of this to occur increases as the load that is imposed torque increases (B20+100ppm ZnO), as the trend line demonstrates. The biodiesel combination provides the least hourly usage. The use of all fuel types shows a decrease. The UHC emission is consistently reduced for all mixtures. Furthermore, it is seen that the combination including B20+100ppm ZnO exhibits even lower emissions compared to the B20 mixture. It is seen that the aforementioned data demonstrates a significant decrease of around 20% to 25% in overall CO<sub>2</sub> emissions.

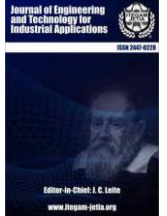
### VI. REFERENCES

- [1] Raviteja Surakasi, Yenda Srinivasa Rao, Sd. Abdul Kalam, Naziya Begum, "Emissions and Performance of Diesel Engines Correlated with Biodiesel Properties", *Journal of Engineering*, vol. 2023, Article ID 5274325, 4 pages, 2023. <https://doi.org/10.1155/2023/5274325>
- [2] SouadZighmi, SegniLadjel, Mohamed Bilal Goudjil, Salah EddineBencheikh, Renewable Energy from the Seaweed *Chlorella Pyrenoidosa* Cultivated in Developed Systems. *International Journal of Renewable Energy Research* Vol.7, No.1, 2017

- [3] M. Subramaniam, J. M. Solomon, V. Nadanakumar, S. Anaimuthu, and R. Sathyamurthy, "Experimental investigation on performance, combustion and emission characteristics of DI diesel engine using algae as a biodiesel," *Energy Reports*, vol. 6, pp. 1382–1392, 2020.
- [4] Thanikodi Sathish, Raviteja Surakasi, Lakshmana KishoreT, Saravanan Rathinasamy, Ümit Ağbulut, Saboor Shaik, Sung Goon Park, Asif Afzal, Waste to fuel: Pyrolysis of waste transformer oil and its evaluation as alternative fuel along with different nanoparticles in CI engine with exhaust gas recirculation, *Energy*, Volume 267, 2023, 126595, ISSN 0360-5442, <https://doi.org/10.1016/j.energy.2022.126595>
- [5] Li, Y., Jia, M., Xu, L., et al., 2020. Multiple-objective optimization of methanol/diesel dual-fuel engine at low loads: a comparison of reactivity controlled compression ignition (RCCI) and direct dual fuel stratification (DDFS) strategies. *Fuel* 262, 116673.
- [6] Ning, L., Duan, Q., Chen, Z., et al., 2020. A comparative study on the combustion and emissions of a non-road standard rail diesel engine fueled with primary alcohol fuels (methanol, ethanol, and n-butanol)/diesel dual fuel. *Fuel* 266, 117034.
- [7] K. Sunil Kumar, Raviteja Surakasi, S Gopal Krishna Patro, Nikhil Govil, M.K. Ramis, Abdul Razak, Prabhakar Sharma, Majed Alsubih, Saiful Islam, T.M.Yunus Khan, Naif Almakayeel, Sanjay Chintakindi, Performance, Combustion, and Emission analysis of diesel engine fuelled with pyrolysis oil blends and n-propyl alcohol-RSM optimization and ML modelling, *Journal of Cleaner Production*, Volume 434, 2024, 140354, ISSN 0959-6526, <https://doi.org/10.1016/j.jclepro.2023.140354>
- [8] Uyumaz, A., 2020. Experimental evaluation of linseed oil biodiesel/diesel fuel blends on combustion, performance and emission characteristics in a DI diesel engine. *Fuel* 267, 117150.
- [9] Raviteja Surakasi, Balakrishna Gogulamudi, Alla Naveen Krishna, Raja Ambethkar M, Pravin P. Patil, Pradeep Jayappa, "Optimization of the Process of Metal NanoCalcium Oxide Based Biodiesel Production through Simulation Using SuperPro Designer", *Journal of Engineering*, vol. 2022, Article ID 3473356, 6 pages, 2022. <https://doi.org/10.1155/2022/3473356>
- [10] Chen, C., Yao, A., Yao, C., et al., 2019a. Study of the characteristics of PM and the correlation of soot and smoke opacity on the diesel methanol dual fuel engine. *Applied Thermal Engineering* 148, 391-403.
- [11] Chen, Z., Chen, H., Wang, L., et al., 2020. Parametric study on effects of excess air/fuel ratio, spark timing, and methanol injection timing on combustion characteristics and performance of natural gas/methanol dual-fuel engine at low loads. *Energy Conversion and Management* 210, 112742.
- [12] Gong, C., Li, Z., Chen, Y., et al., 2019. Influence of ignition timing on combustion and emissions of a spark-ignition methanol engine with added hydrogen under lean-burn conditions. *Fuel* 235, 227-238.
- [13] Li, Z., Wang, Y., Geng, H., et al., 2019. Parametric study of a diesel engine fueled with directly injected methanol and pilot diesel. *Fuel* 256, 115882.
- [14] S. S. Reham, H. H. Masjuki, M. A. Kalam, I. Shancita, I. M. Rizwanul Fattah, and A. M. Ruhul, "Study on stability, fuel properties, engine combustion, performance and emission characteristics of biofuel emulsion," *Renewable and Sustainable Energy Reviews*, vol. 52, pp. 1566–1579, 2015.
- [15] Ning, L., Duan, Q., Kou, H., et al., 2020b. Parametric study on effects of methanol injection timing and methanol substitution percentage on combustion and emissions of methanol/diesel dual-fuel direct injection engine at full load. *Fuel* 279, 118424.
- [16] Surakasi Raviteja, Velivela Lakshmikanth Chowdary, "Liquid Fuels Derived from Microalgae: Physicochemical Analysis", *Journal of Engineering*, vol. 2022, Article ID 1293310, 5 pages, 2022. <https://doi.org/10.1155/2022/1293310>
- [17] Venu, H., Madhavan, V., 2017. Influence of diethyl ether (DEE) addition in ethanol-biodiesel-diesel (EBD) and methanolbiodiesel-diesel (MBD) blends in a diesel engine. *Fuel* 189,



ISSN ONLINE: 2447-0228



## xSMART INTERSECTION AND IoT: PRIORITY DRIVEN APPROACH TO URBAN MOBILITY

Okubanjo, Ayodeji A <sup>1,4</sup>, Odufuwa Bashir<sup>2</sup>, Akinloye Benjamin <sup>3</sup>, Okakwu Ignatius<sup>4</sup>

<sup>1,4</sup> Department of Electrical and Electronics Engineering, Olabisi Onabanjo University, Nigeria.

<sup>2</sup> Department of Urban and Regional Planning, Olabisi Onabanjo University, Ago-iwoye, Nigeria

<sup>3</sup> Department of Electrical and Electronics Engineering, Federal University of Petroleum Resources, Effurun, Nigeria.

<sup>1</sup><http://orcid.org/0000-0003-1908-0365> , <sup>2</sup><http://orcid.org/0000-0003-1876-073X> , <sup>3</sup><http://orcid.org/0000-0002-1571-0457> ,

<sup>4</sup><http://orcid.org/0000-0003-1252-9924>

Email: \* [okubanjo.ayodeji@oouagoiwoye.edu.ng](mailto:okubanjo.ayodeji@oouagoiwoye.edu.ng), [odufuwa.bashir@oouagoiwoye.edu.ng](mailto:odufuwa.bashir@oouagoiwoye.edu.ng), [akinloye.benjamin@fupre.edu.ng](mailto:akinloye.benjamin@fupre.edu.ng), [okakwu.ignatius@oouagoiwoye.edu.ng](mailto:okakwu.ignatius@oouagoiwoye.edu.ng)

### ARTICLE INFO

#### Article History

Received: November 23<sup>th</sup>, 2023

Revised: July 012<sup>th</sup>, 2024

Accepted: July 19<sup>th</sup>, 2024

Published: Month 30<sup>th</sup>, 2024

#### Keywords:

Intelligent Intersection,  
Arduino Controller,  
The Internet of Things (IoT),  
Priority-based Strategy,  
Mobility in Cities.

### ABSTRACT

The recent growth in car use and population have been identified as potential drivers of municipal traffic congestion, particularly in emerging nations with inadequate road networks. In Nigeria, for example, traffic wardens and traffic lights are prominent traffic control measures used to ease traffic congestion at major road intersections. However, stress, public anger, and rash traffic signal judgements restrict the effectiveness of these tactics, resulting in delayed mobility, decreased transit times, and a climate disaster. Recent solutions have emphasized emerging technologies like the Internet of Things (IoT), Artificial Intelligence (AI), and Artificial Neural Network (ANW). Consequently, an efficient use of these technologies can provide a sustainable future for city traffic management in Sub-Saharan African. This model seeks to develop a low cost internet-of-things traffic surveillance system to improve vehicles mobility on a Nigerian closed campus. The goal is to alleviate the academic community's problem of peak-hour traffic congestion by delivering real-time traffic updates.



Copyright ©2024 by authors and Galileo Institute of Technology and Education of the Amazon (ITEGAM). This work is licensed under the Creative Commons Attribution International License (CC BY 4.0).

### I. INTRODUCTION

Smart mobility has long been regarded as a critical driver of a country's economic progress. Global traffic issues are growing as urbanization [1], population expansion [2],[3], and vehicle numbers increase [4],[5]. For a variety of reasons, countries have begun to focus on strategies such as smart traffic management (STM) and traffic efficiency (TE), with a special emphasis on African countries. The major purpose of these initiatives is to close the supply-demand imbalance in the transportation network, making cities more sustainable in terms of vehicle mobility. This includes projects like a smart transport system (STS), which minimizes traffic while also giving real-time traffic updates. For decades, a significant difficulty for Nigeria's transport sector has been a lack of smart transport infrastructure, with bad road networks, inefficient public transport, and primitive traffic control systems dominating most cities. Efforts to revitalize the transportation sector have failed due to economic, political, and policy challenges. Unfortunately, as shown in Figure 1, traffic congestion has been increasing across the country, despite efforts

to relieve the situation by recruiting traffic wardens and utilizing the traditional traffic signal system. These efforts have not resulted in noticeable advances over time. Consequently, the number of automobiles on Nigerian roads has expanded dramatically, while traffic infrastructure has not kept up. As a result, traffic numbers have expanded dramatically, resulting in reduced mobility rates, shorter transit times, greater fuel prices, and higher carbon footprints. However, there is an increasing emphasis on using disruptive technology (IoT) to address this societal issue. Although IoT is not a new technology, its concept remains largely unexplored in several developing countries. The Internet of Things (IoT) is a revolutionary technology concept that has changed the way humans interact with devices and systems. It provides real-time internet connection between people and physical infrastructure in smart cities. This connection opens up new possibilities in a variety of applications, including, healthcare [6], smart energy meters [7], smart home automation [8], smart cities [9], smart libraries [10], smart bins [11-13], smart parking [5],[14],[15], and smart vehicles [16].



Figure 1: (i) Congestion in Lagos's metropolitan area caused by a traditional traffic light control system (b) The typical traffic pattern in a Nigerian city.  
Source: [17].

In recent years, a number of traffic control schemes have been presented that use various communication and surveillance technologies to automate and manage municipal traffic congestion and provide solutions to the limitations of traditional traffic signal systems. Firdous et al. developed a fuzzy logic-based traffic controller to reduce queue length and wait time. Dhingra [18], combines fog computing and IoT technology to reduce traffic congestion and detect accidents in real time. Hilmani employed a camera and an automated traffic system to measure traffic density and optimize traffic patterns. [19], presented an IoT-enabled vehicular traffic monitoring system for car sharing in smart cities. [20], also features a real-time traffic detection algorithm based on IoT sensors for different road users. The proposed strategy reduces vehicle density. Basil [21], developed an online traffic controller based on Raspberry Pi and IoT to monitor the traffic density and present users with the optimum path. Sarrab [22], presented an A-IoT-based traffic control scheme to improve vehicle mobility and emergency exits. The strategy employs several IoT devices to identify, monitor, control, and update traffic congestion as well as detect accidents in real time. [23-26], employed a bylnk web server application, IoT, and AI to prioritize emergency vehicles including fire trucks, ambulances, and armed cars, as well as deal with life-threatening occurrences. For [27], used an IoT-enabled traffic controller to monitor vehicle congestion. Infrared sensors are also built into the design to detect vehicle movement. According to [28], used an Internet of Things-enabled traffic monitoring system to track traffic congestion at an intersection. The model includes an SMS notification system based on an Android mobile application to keep clients aware of traffic conditions and to aid drivers in selecting the best route.

The main contributions of this study are summarized as follows.

- An IoT-based intelligent traffic surveillance system is proposed.
- Real-time monitoring of intersection traffic congestion is proposed.
- The proposed model uses web and mobile apps to inform drivers of regions with traffic congestion.
- The proposed model increases vehicle mobility and emergency response by giving real-time information.
- Real-time SMS alerts for traffic updates.

## II. MATERIALS AND METHODS

The proposed methodology for the system is structured into two main parts namely; system hardware and system software as shown in Fig.2.

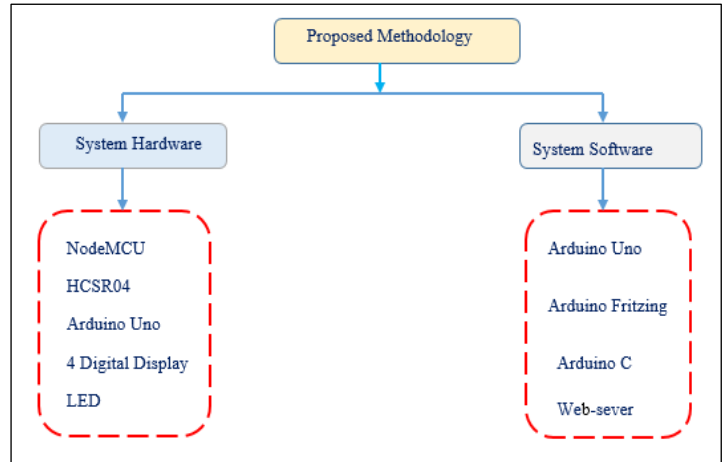


Figure 2. Proposed Design Methodology.  
Source: Authors, (2024).

As illustrated in Figure 3, the system hardware incorporates sensors, an Arduino controller, a Wi-Fi module, and light-emitting diodes (LEDs) to detect, automate, and establish communication between different levels of IoT. The Arduino controller serves as the primary controller, controlling all data communication and transmissions throughout the system, while the NodeMCU (ESP 8266), a system-on-chip, establishes a communication link between the sensor module and web server. This module improves real-time traffic data updates and data mining. The ultrasonic sensor (HCSR04) detects motion and estimates the distance based on sound waves. It is primarily used in this study as motion identification measurement. Three ultrasonic sensors strategically placed at the T-intersection detect automobile activity. Hence, the Arduino controller establishes data communication between the sensors to monitor traffic congestion at each junction. In addition, three LEDs are included in this design to convey traffic status via a digital display. A vehicle is a mobile machine made up of different model, used to transport passengers or payload. Vehicles are of different types including wagons, bicycles, motor cars, motorcycles, trucks, ambulance, and buses. The sensors identify levels of traffic congestion in these vehicles and wirelessly upload the data to a cloud server for traffic analysis.

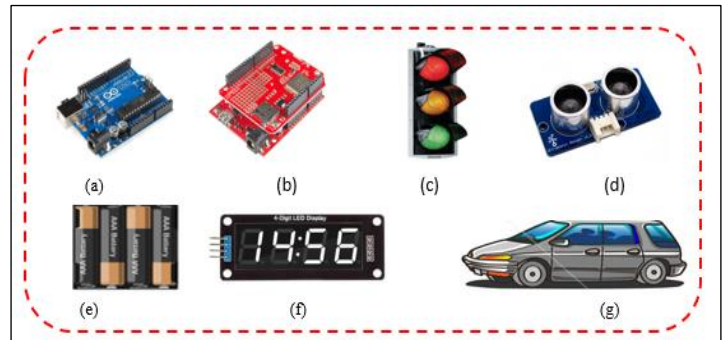


Figure 3. System hardware components (a) Arduino Uno, (b) NodeMCU, (c) Traffic light, (d) Ultrasonic sensor, (e) Battery, (f) 4 segment Display module, and (g) Vehicle.  
Source: Authors, (2024).

### II.1 SYSTEM SOFTWARE

The proposed model's core software includes an IDE, Arduino Fritzing, and a web-server application, and the proposed traffic mode code is written in the Arduino C language and runs on the Arduino integrated development environment (IDE). Furthermore, the entire system schematic diagram is built and simulated in Arduino fritzing software, which allows users to edit, change, and upload code straight to the Arduino board. The Arduino code implements the following commands: (a) writing Arduino C code for the ultrasonic sensors; (b) Automating traffic light signals; (c) establishing a communication link between the web server and the Wi-Fi module; (d) establishing a communication link between the Wi-Fi module and the sensor module; (e) developing Arduino C code for SMS notification; and (f) developing Arduino C code for the Arduino controller.

### II.2 METHOD

The proposed IoT traffic system (IoTTS) serves as a sustainable solution to address the issues of traffic congestion often experience daily at T-intersection at OOU campus.

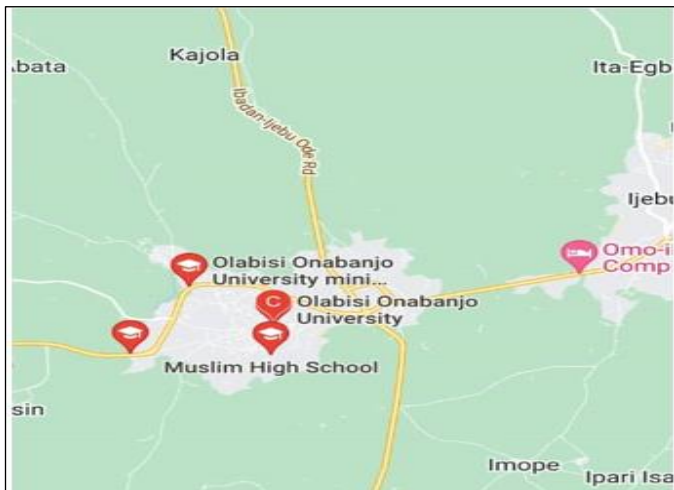


Figure 4: Location of Olabisi Onabanjo University. Source: Authors, (2024).

The system uses three ultrasonic sensors located at varied distances to determine traffic density at each junction. Each junction uses HCSR04 sensor to detect traffic levels. Furthermore, when a vehicle enters the detection zone, the sensor detects the vehicle movement and calculates the traffic level at each junction based on the predefined distance at each junction. The first sensor node is held at 15 meters, the second at 55 meters, and the third at 100 meters. Hence, the sensors at each intersection assess the traffic density inside the detection zone to ensure accurate traffic level monitoring; once the traffic exceeds the sensor detection zone's threshold, the Arduino checks the traffic density level to allocate priority to the high-traffic intersection. The Arduino controller assigns low when the first sensor output is low, medium when the second and third sensors are high, and high if all sensor outputs are high. The Arduino controller adjusts signal timing based on traffic density. Low, medium, and high traffic intensities are given periods of 15, 30, and 45 seconds, respectively. Table 1 depicts the traffic density of the three sensors' conditions. Furthermore, the traffic management authority uses the web to obtain information and regulate traffic flow in real time, allowing road users, particularly drivers, to receive real-time updates. The

traffic light and four-segment digital display show the traffic signal and timing. Figure 4 depicts the system schematic diagram.

Table 1: Sensor's Traffic Density.

Scenario	Sensors States at the junction			Traffic Level
	S <sub>1</sub>	S <sub>2</sub>	S <sub>3</sub>	
	J <sub>1</sub>	J <sub>2</sub>	J <sub>3</sub>	
A	1	0	0	L
B	1	1	0	M
C	1	1	1	H

L=Low, M= Medium, H= High  
Source: Authors, (2024).

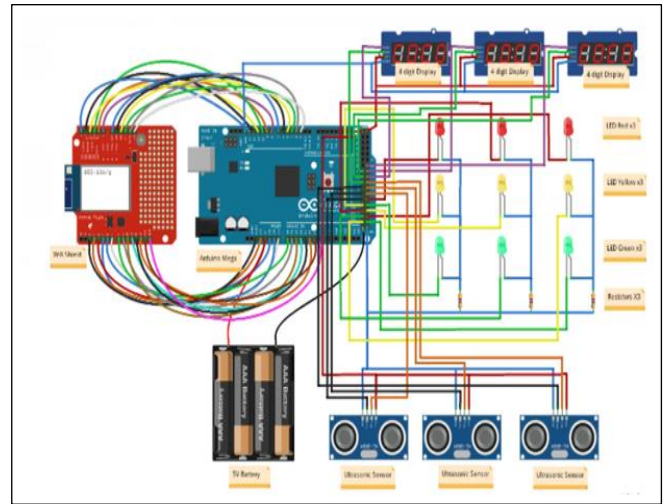


Figure 4: Proposed traffic surveillance system using IoT. Source: Authors, (2024).

### III. SYSTEM ARCHITETURE

Figure 5 displays the proposed system's three-tier Internet-of-Things infrastructure. The sensing layer detects and collects data via devices, sensors, and actuators. In this layer, the main controller communicates with the sensors and actuators to detect, collect, process, and transmit data via network connectivity. The network layer employs wireless technology to create a communication link between the sensing layer and the internet. The application layer handles data analysis and traffic congestion level processing. This layer is in charge of monitoring traffic congestion and updating traffic data.

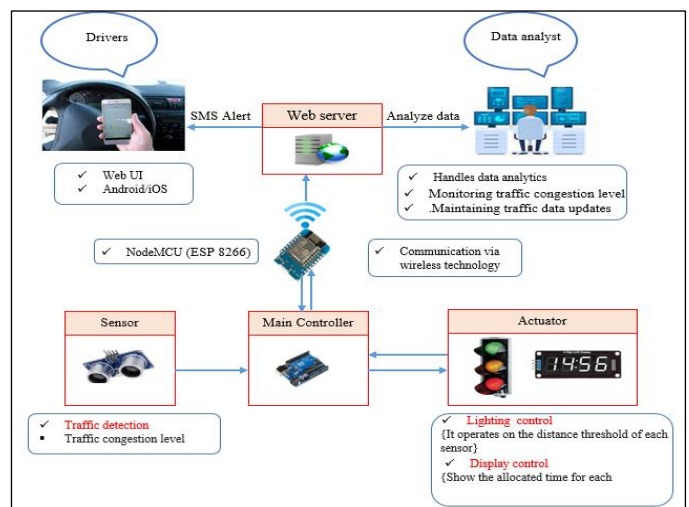


Figure 5: System Architecture. Source: Authors, (2024).

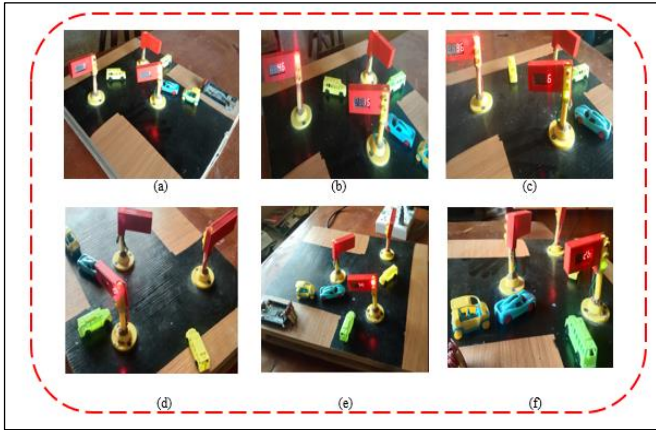


Figure 6: (a) Prototype set up test with sensor 1, (b) Prototype set up test with the sensor 2, (c) Prototype set up test with sensor 3, (d) Prototype set up test with sensor 3, (e) Prototype set up test with sensor 2, (f) Prototype set up test with sensor 1. Source: Authors, (2024).

#### IV. RESULTS AND DISCUSSIONS

Figure 6 depicts the model's prototype, which integrates several hardware and software components. These components were assembled, programmed, and tested to ensure their functionality.

Table 2: Traffic decision based on priority.

Case	J <sub>1</sub>	J <sub>2</sub>	J <sub>3</sub>	Traffic Decision			Junction sequence
				1 <sup>st</sup> P	2 <sup>nd</sup> P	3 <sup>rd</sup> P	
1	H	H	L	J <sub>1</sub>	J <sub>2</sub>	J <sub>3</sub>	J <sub>1</sub> J <sub>2</sub> J <sub>3</sub>
2	H	H	M	J <sub>1</sub>	J <sub>2</sub>	J <sub>3</sub>	J <sub>1</sub> J <sub>2</sub> J <sub>3</sub>
3	H	L	L	J <sub>1</sub>	J <sub>2</sub>	J <sub>3</sub>	J <sub>1</sub> J <sub>2</sub> J <sub>3</sub>
4	H	L	M	J <sub>1</sub>	J <sub>3</sub>	J <sub>2</sub>	J <sub>1</sub> J <sub>3</sub> J <sub>2</sub>
5	H	M	H	J <sub>1</sub>	J <sub>3</sub>	J <sub>2</sub>	J <sub>1</sub> J <sub>3</sub> J <sub>2</sub>
6	L	M	L	J <sub>2</sub>	J <sub>1</sub>	J <sub>3</sub>	J <sub>2</sub> J <sub>3</sub> J <sub>1</sub>
7	H	H	H	Normal			J <sub>1</sub> J <sub>2</sub> J <sub>3</sub>
8	M	M	M	Normal			J <sub>1</sub> J <sub>2</sub> J <sub>3</sub>
9	L	L	L	Normal			J <sub>1</sub> J <sub>2</sub> J <sub>3</sub>

Source: Authors, (2024).

Six independent prototype snapshots were shown to demonstrate system functionality at various levels. In addition, data from ultrasonic sensors are used to calculate traffic density. This data is saved on the cloud, shown in real time, and used to offer real-time updates to road users via text message. Table 2 depicts various traffic density levels and junction sequences. The traffic density rating ranges from 1 to 3 to represent the priority of the intersection. However, intersections with high traffic density are prioritized over others, whereas junctions with equal traffic density are treated equally. Furthermore, the ultrasonic

sensors transmit vehicle traffic density data to the main controller, allowing it to make traffic decisions based on junction priority. The standard mode indicates fixed timing for operating the conventional traffic light system CTS.

Table 3: Traffic evaluation of the IoTTS and C.

Traffic Modes	J <sub>1</sub>	J <sub>2</sub>	J <sub>3</sub>	Green light ON (sec)	Time Savings (%)
Congestion	H	H	H	135	25
Normal	H	M	L	90	50
busy	M	M	M	90	50
Free	L	L	L	45	75
Standard	All Levels			180	None

Source: Authors, (2024).

Table 3 compares the traffic performance of the proposed system to the current traffic system (CTS). Four traffic modes are compared to CTS's normal mode of operation. The CTS uses predetermined time for making traffic signal decisions. The integration of IoT with road intersection saves about 75% more time than the current traffic system. The time savings ranging from 25% to 75%. According to the findings, using IOTTS could save time. A 4-point Likert scale questionnaire with a score range of 1 to 4 was used as an additional statistical check to measure how well the proposed system performed. As shown in table 4, the highest scale indicates the number of people who strongly agree that the proposed system performed satisfactorily, while the lowest scale signifies the number of people who strongly disagree with the proposed system's performance. The questionnaire evaluation and user distribution rank are shown in Table 5. According to the assessment results, around 90% of the users were satisfied with the proposed system's design, while 5% were unsatisfied. IOTTS improves time management and minimizes road congestion, as seen by the system's 3.7 user rating average. Table 6 compares the proposed system's performance to previous studies. In addition, in terms of cost, we application, SMS notification, and traffic density monitoring, the proposed system improve previous solutions. It also features a priority-based decision-making strategy.

Table 4: 4-point likert scale.

Point	Scale range	Explanation
4	4.00 - 3.00	Strongly agree
3	2.99 - 2.00	Agree
2	1.99 - 1.00	Disagree
1	1.00 - 0.99	Strongly disagree

Source: Authors, (2024).

Table 5: Design Assessment Data.

Design Assessment Statement	4	3	2	1	Total	Sum	Average	Description
I found IOTTS more efficient and reliable in managing traffic congestion at the intersection than the existing traffic control system	40	10	0	0	50	190	3.8	Strongly agree
The developed system enhances the real time information update of traffic density	25	25	0	0	50	175	3.5	Strongly agree
The identification module is working perfectly within its detection zone	37	10	3	0	50	184	3.7	Strongly agree
Time management of the proposed system is optimal based on junction priority strategy	42	7	1	0	50	191	3.8	Strongly agree
Traffic data are easily accessible via webserver and sms notification	45	4	1	0	50	194	3.9	Strongly agree

Source: Authors, (2024).

Table 6: Performance evaluation of the proposed system with existing studies.

Performance metrics	Reference [29]	Reference [23]	Reference [16]	Reference [28]	Proposed System
System costs	Expensive	Cheap	Cheap	Cheap	Relatively Cheap
Technology	IoT	IoT	RFID	RFID	IoT
Web Application	No	No	No	No	Yes
SMS Notification	No	No	No	No	Yes
Network Connectivity	Wi-Fi	GSM	No	No	Wi-Fi
Traffic Density Monitoring Application	No	No	No	No	Yes
Junction Priority	No	No	No	No	Yes
Automation	Smart	Smart	Smart	Smart	Smart

Source: Authors, (2024).

#### IV.1 ECONOMIC ANALYSIS

The proposed system costs are assessed to determine their economic viability and to provide a clear roadmap for mass production of the model. The total system costs are shown in Table 6. The proposed unit price is (\$19.74), which translates to (N16,

576) in Nigerian currency. This suggests that the designed model is more cost-effective and budget-friendly than existing solutions.

Table 7: Table title.

System componenets	Unit price (\$)	Number of components	Amount (\$)
Arduino Uno	7.91	1	7.91
NodeMCU module	2.46	1	2.46
LEDs	0.03	9	0.27
Ultrasonic sensors	1.36	3	4.08
Battery	3.58	1	3.58
Display module	0.48	3	1.44
<b>Total</b>			<b>19.74</b>

Source: Authors, (2024).

#### V. FUTURE OUTLOOK

Recent advancements in artificial intelligence (AI) and machine learning have the potential to improve real-time traffic patterns and prediction. Such an AI system can be implemented into the prototype to aid in future decision-making. In the future, the proposed system could be upgraded with the cameras, global positioning system (GPS), radars, and other modern sensors to collect traffic congestion data. Furthermore, integrating the suggested system with public transportation will improve the smooth and efficient transportation network, accurate prediction times of the transit system, and reduced waiting times. A highly interesting future path of this work may be found in the energy-efficient and sustainable techniques of minimising the energy consumption of traffic signals and signs. Using renewable energy sources such as solar or hybrid systems, on the other hand, would boost efficiency and provide a more sustainable traffic management system. Furthermore, big data and data mining are emerging technologies that can help transportation planners optimise traffic routes by improving infrastructure monitoring.

#### V. CONCLUSIONS

This study proposes a priority-based technique for minimizing traffic congestion at road intersections. The proposed model seeks to develop a low-cost Internet of Things-enabled traffic surveillance system in order to increase vehicle mobility. The system uses a three-tier Internet of Things architecture to detect, collect, process, and transmit data via network connectivity. An Arduino Uno was utilized as a core controller to assign priorities and make traffic decision at the intersection. In addition, the system was linked to a web server to give real-time traffic data

and updates via smartphones and internet-enabled devices. The proposed strategy enables traffic management authorities to regulate traffic flow in real time while also providing road users with real-time updates, resulting in route optimization. Furthermore, economic and performance assessments highlight that the proposed system is superior to the current method in terms of mobility, efficiency, time management, and system costs. Therefore, shifting to intelligent, technologically driven traffic would help revolutionise the traffic management sector, especially in emerging nations.

#### VI. AUTHOR'S CONTRIBUTION

**Conceptualization:** Ayodeji A. Okubanjo.  
**Methodology:** Ayodeji A. Okubanjo. Odufuwa Bashir, Akinloye, Akinloye Benjamin, Okakwu Ignatius  
**Investigation:** Akinloye Benjamin, Okakwu Ignatius.  
**Discussion of results:** Ayodeji A. Okubanjo.  
**Writing – Original Draft:** Odufuwa Bashir, Akinloye, Akinloye Benjamin, Okakwu Ignatius.  
**Writing – Review and Editing:** Ayodeji A. Okubanjo,  
**Resources:** Ayodeji A. Okubanjo.  
**Supervision:** Odufuwa Bashir, Akinloye, Akinloye Benjamin  
**Approval of the final text:** Ayodeji A. Okubanjo. Odufuwa Bashir, Akinloye, Akinloye Benjamin, Okakwu Ignatius

#### VII. REFERENCES

- [1]Okubanjo A, Ofualagba G, Okandeji A, Oshevire O, Olufemi A, Olaluwoye O, et al. A Comprehensive Review of Energy Crisis in Nigeria and the contributing Role of Renewable Energy. Sci Forum (Journal Pure Appl Sci 2020;20:284. doi:10.5455/sf.89651.
- [2]Okubanjo A, Godswill O, Patrick O. Cost Optimization of Hybrid Solar/ Heat Pump Water Heating System : Model Formulation. 2022 IEEE Niger. 4th Int. Conf.



- Disruptive Technol. Sustain. Dev., IEEE; 2022, p. 1–5. doi:10.1109/NIGERCON54645.2022.9803094.
- [3]Sulaiman C, Abdul-Rahim AS. Population Growth and CO<sub>2</sub> Emission in Nigeria: A Recursive ARDL Approach. SAGE Open 2018;8:215824401876591. doi:10.1177/2158244018765916.
- [4]Maldonado Silveira Alonso Munhoz PA, da Costa Dias F, Kowal Chinelli C, Azevedo Guedes AL, Neves dos Santos JA, da Silveira e Silva W, et al. Smart Mobility: The Main Drivers for Increasing the Intelligence of Urban Mobility. Sustainability 2020;12:10675. doi:10.3390/su122410675.
- [5]Aydin M, Sorousbay C, Arslan H. Traffic Flow Pattern Based Approach to Predict Real Driving Emission Test Routes. Gazi Univ J Sci 2023;36:1339–49. doi:10.35378/gujs.1010216.
- [6]Okubanjo AA, Okandeji AA, Martins O, Ayoola O. Development of Patient Heartbeat and Temperature Monitoring System for Secured Health Using IoT. vol. 6. 2021.
- [7]Oyetola OK, Okubanjo AA, Okandeji AA, Olaluwoye OO, Alao PO, Ukagu SN. Internet ofThings ( IoT ) Cloud Based Model for Low Cost Demand Side Management Infrastructure. Arid Zo J Eng Technol Environ 2019;15:1082–91.
- [8]Okubanjo AA, Okandeji AA, Abolade OR, Alao OP. Development of GSM Based Home Automation System using Arduino Uno Microcontroller. FUW Trends Sci Technol Journal, WwwFtstjournalCom e-ISSN 2021;6:599–606.
- [9]Chandran M, Fadila Mahrom N, Sabapathy T, Jusoh M, Nasrun Osman M, Najib Yasin M, et al. An IoT Based Smart Parking System. J Phys Conf Ser 2019;1339:012044. doi:10.1088/1742-6596/1339/1/012044.
- [10]Okubanjo A, Okandeji A, Osifeko O, Onasote A, Olayemi M. Development of a Hybrid Radio Frequency Identification (RFID) and Biometric Based Library Management System. Gazi Univ J Sci 2021;35:567–84. doi:10.35378/gujs.834087.
- [11]Okubanjo A, Odufuwa B, Okandeji A, Daniel E. Smart Bin and IoT: A Sustainable Future for Waste Management System in Nigeria. Gazi Univ J Sci 2023;37:1–1. doi:10.35378/gujs.1254271.
- [12]N. S. A. H. T. K. R. S. G. S. Easy Clean – A Smart Solution for Garbage Finding and Collecting. Int J Comput Appl 2017;169:1–7. doi:10.5120/ijca2017914617.
- [13]Bano A, Ud Din I, Al-Huqail AA. AIoT-Based Smart Bin for Real-Time Monitoring and Management of Solid Waste. Sci Program 2020;2020:1–13. doi:10.1155/2020/6613263.
- [14]Rahman A, Ufiteyezu E. Smart Parking System for Green Computing. J Kejuruter 2023;35:923–8. doi:10.17576/jkukm-2023-35(4)-14.
- [15]Agarwal Y, Ratnani P, Shah U, Jain P. IoT based smart parking system. Proc - 5th Int Conf Intell Comput Control Syst ICICCS 2021 2021:464–70. doi:10.1109/ICICCS51141.2021.9432196.
- [16]Agarwal P, Matta P, Sharma S. Analysis based traffic flow control decision using IoT sensors. Mater Today Proc 2021;46:10707–11. doi:10.1016/j.matpr.2021.01.540.
- [17]Megaicon A. Traffic Wahala in Nigeria. Maga Icon Mag 2022.
- [18]Dhingra S, Madda RB, Patan R, Jiao P, Barri K, Alavi AH. Internet of things-based fog and cloud computing technology for smart traffic monitoring. Internet of Things (Netherlands) 2021;14:100175. doi:10.1016/j.iot.2020.100175.
- [19]Mihelj J, Kos A, Sedlar U. Source reputation assessment in an IoT-based vehicular traffic monitoring system. Procedia Comput Sci 2019;147:295–9. doi:10.1016/j.procs.2019.01.267.
- [20]Mahalakshmi S, Ragunthar T, Veena N, Sumukha S, Deshkulkarni PR. Adaptive ambulance monitoring system using IOT. Meas Sensors 2022;24:100555. doi:10.1016/j.measen.2022.100555.
- [21]Basil E, Sawant SD. IoT based traffic light control system using Raspberry Pi. 2017 Int. Conf. Energy, Commun. Data Anal. Soft Comput. ICECDS 2017, IEEE; 2018, p. 1078–81. doi:10.1109/ICECDS.2017.8389604.
- [22]Sarrab M, Pulparambil S, Awadalla M. Development of an IoT based real-time traffic monitoring system for city governance. Glob Transitions 2020;2:230–45. doi:10.1016/j.glt.2020.09.004.
- [23]Bali V, Mathur S, Sharma V, Gaur D. Smart Traffic Management System using IoT Enabled Technology. Proc. - IEEE 2020 2nd Int. Conf. Adv. Comput. Commun. Control Networking, ICACCCN 2020, 2020, p. 565–8. doi:10.1109/ICACCCN51052.2020.9362753.
- [24]Madisa MK, Joseph MK. Android and Cloud Based Traffic Control System. 2018 Int. Conf. Adv. Big Data, Comput. Data Commun. Syst., IEEE; 2018, p. 1–4. doi:10.1109/ICABCD.2018.8465443.
- [25]Mohandass MP, I K, R M, R V. IoT Based Traffic Management System for Emergency Vehicles. 2023 9th Int. Conf. Adv. Comput. Commun. Syst., IEEE; 2023, p. 1755–9.
- [26]Chowdhury A, Kaisar S, Khoda ME, Naha R, Khoshkholghi MA, Aiash M. IoT-Based Emergency Vehicle Services in Intelligent Transportation System. Sensors 2023;23:5324. doi:10.3390/s23115324.
- [27]LachiReddy P, Divya V, Swapna D, ChinmayiSrinija D, Rajesh M. Smart traffic controlling system. Mater Today Proc 2023;80:3702–4. doi:10.1016/j.matpr.2021.07.365.
- [28]Talukder MZ, Towqir SS, Remon AR, Zaman HU. An IoT based automated traffic control system with real-time update capability. 8th Int Conf Comput Commun Netw Technol ICCCNT 2017 2017:1–6. doi:10.1109/ICCCNT.2017.8204095.
- [29]Chilakala S, Renuka N, Mubeen S. Automation of traffic lights through IoT. 2020 7th Int. Conf. Smart Struct. Syst. ICSSS 2020, IEEE; 2020, p. 1–5. doi:10.1109/ICSSS49621.2020.9202275.



### RESEARCH ARTICLE

### OPEN ACCESS

## IOT-BASED REAL TIME GREENHOUSE MONITORING AND CONTROLLING SYSTEM

Yajie Liu<sup>1</sup>, Md Gapar Md Johar<sup>2</sup> and Asif Iqbal Hajamydeen<sup>3</sup>

<sup>1,2,3</sup> Cyber Security and Big Data Center, Management and Science University, Shah Alam, Selangor, Malaysia.

<sup>1</sup><https://orcid.org/0000-0001-6028-2298> , <sup>2</sup><https://orcid.org/0000-0001-7986-3834> , <sup>3</sup><https://orcid.org/0000-0002-5034-1781> 

Email: [2932028014@qq.com](mailto:2932028014@qq.com), [mdgapar@msu.edu.my](mailto:mdgapar@msu.edu.my), [asif@msu.edu.my](mailto:asif@msu.edu.my)

### ARTICLE INFO

#### Article History

Received: September 15<sup>th</sup>, 2023

Revised: July 22<sup>th</sup>, 2024

Accepted: August 18<sup>th</sup>, 2024

Published: August 20<sup>th</sup>, 2024

#### Keywords:

Automatic control,

ESP8266,

Intelligent greenhouse,

IoT,

Thingspeak.

### ABSTRACT

With the ongoing rise of social and economic levels, as well as people's living standards, the demand for out-of-season vegetables and fruits has increased in recent years. Nowadays, advanced scientific technologies are increasingly applied to traditional agricultural production. With the aid of Internet of Things (IoT) applications, intelligent greenhouses have helped cultivate growth. Intelligent greenhouses can produce a proper growing environment for crops, improve crop yields and quality, and achieve efficient production output. Temperature, humidity, and other elements are the key factors impacting crop development in greenhouses; how to effectively measure and control these environmental parameters is critical for farmers. In this study, an IoT-based, low-cost, intelligent agricultural production environment monitoring system is designed and developed. This system could monitor interior ambient temperature and humidity in real-time through the DHT22 sensor. Besides, monitored sensor data is uploaded and stored on the ThingSpeak cloud platform. In addition, a fan and a heating panel are utilized to control the inside environment. The results showed that the environment would be constantly adjusted and maintained at an ideal level for crop growth.



Copyright ©2024 by authors and Galileo Institute of Technology and Education of the Amazon (ITEGAM). This work is licensed under the Creative Commons Attribution International License (CC BY 4.0).

## I. INTRODUCTION

By 2030, the global population is expected to reach 8.6 billion, posing a significant challenge to adequate meat production and provision [1]. Due to world population expansion, industrialization, urbanization, climate change, and environmental pollution, agricultural land is continuously contaminated and decreasing. This results in new challenges to food supply and food security in the future [2]. The greenhouse is an emerging farming method that allows the environment to be controlled at a suitable level for crops to grow rapidly, in contrast with traditional planting methods [3]. The greenhouse is also called a controlled environment plant production system or controlled environment agriculture. With the development of agricultural facilities, greenhouses are becoming more critical to agricultural production. The use of greenhouses effectively reduces the harsh environment brought about by the external environment on the growth of agriculture and is one of the most effective ways to reduce the growth cycle and improve the yields of agriculture production. A greenhouse also reduces the amount of water and pesticides needed

for crop production, as well as minimizing labor costs. Additionally, greenhouses can be used to grow crops year-round, allowing for a more consistent supply of fresh produce. In traditional farming, vegetables and fruits are prone to diseases, pesticides are sprayed, and pesticide residues harm human health. By contrast, in the smart greenhouse, pesticides could be reduced or even avoided [4].

Traditionally, greenhouse planting management has been based primarily on experience. There is a low degree of intelligence, one cannot effectively measure and control the growth environment, there is a high labor input, a low level of labor efficiency, and a serious waste of resources, among other issues. With the utilization of intelligent computing technology in the agriculture field, the intelligent agriculture revolution came about. More and more countries are eager to construct modern, intelligent agriculture systems empowered by technology. Industry managers and scholars have drawn attention to intelligent agriculture systems as intelligent computing technologies have been rapidly developed and applied widely in recent years. Well-managed and controlled agriculture is more efficient, reliable, and cost-effective [5].

The use of intelligent monitoring and control systems could reduce the amount of time and manpower consumed by production. Providing farmers with more accurate and intelligent information allows them to make more informed decisions [6]. As the global economy and modern technology are developing rapidly, modern agriculture has also begun to gradually develop in the direction of intelligence. A variety of agricultural facilities are used to create a favorable environment for the growth of crops, among which smart greenhouses have become an important part of agricultural farming. At present, the degree of automation in traditional crop greenhouses is low, and the technology used to gather environmental data is relatively backward. The application of greenhouse has accelerated since modern technological developments like the big data, IoT, and machine learning [7-10].

Farmers could monitor the greenhouse in real-time remotely in the Industry Revolution (IR) 4.0 era. This allowed for greater efficiency in crop production as well as better use of resources. Automation in greenhouses has also been made smarter by artificial intelligence (AI), helping farmers save time and reduce costs [11]. As science and technology have advanced gradually, the imperative need for innovative solutions and emerging technologies to increase agricultural production efficiency has led to the implementation of IoT applications [12]. IoT technology plays a crucial role in precision agriculture management. IoT makes agriculture management more efficient, and all related data could be visualized and controlled as well. By 2030, the development and deployment of IoT technology in agriculture would create about a \$500 billion increase in GDP.

Farmers are able to take proactive steps to maximize their yields and minimize their losses [13]. As IoT technology becomes more popular in the modern world, it is utilized in a variety of fields of human life, including industry, healthcare, transportation, and agriculture. The greenhouse sector is facing new opportunities for productivity and efficiency improvement as a result of new technologies [14]. There are some other benefits of using IoT technology in the greenhouse field, such as reducing costs, increasing efficiency, improving product quality, easy resource management, aiding in disease and pest control, and enabling sustainable production [15].

Various communication methods are used to transmit data from sensors to user interfaces (UI) and controllers, such as wired communication, Controller Area Network (CAN), Bluetooth, General Packet Radio System (GPRS), System for Mobile Communications (GSM), and wireless networks [16]. The data collection, analysis, transmission, and control of greenhouse environmental parameters are of substantial significance in guiding agribusiness production and improving agricultural modernization. At present, most greenhouse control methods are achieved through short-distance communication, the sensor signal acquisition to the control host, the control host, and the host computer for communication, and through the host computer to realize the control information feedback regulation [17]. Temperature is one of the most significant factors that affects the growth and productivity of indoor agriculture [18].

Agriculture production requires environmental variables such as humidity, soil moisture, temperature, and carbon dioxide concentration to be at a suitable level. Monitoring these parameters is essential for optimal crop growth. Automated systems can be used to monitor these environmental parameters and adjust them accordingly. This can help to ensure optimal crop growth and reduce the risk of crop loss [19]. The gases emitted from the greenhouse affect the inside environment and further influence the growth of internal plants, animals, and even human health.

Therefore, it is necessary to maintain the greenhouse environment at an optimal level continuously and dynamically so that it facilitates healthy growth [20].

Technological advancements are critical in agricultural engineering, especially in greenhouses. These structures change the environment, allowing plants to be better managed and produce better outcomes. whereas there is still limited use of sophisticated IoT infrastructure in the agriculture industry, resulting in low production yields and profits [21].

## **II. THEORETICAL REFERENCE**

IoT technologies are applied in the greenhouse field to revolutionize and facilitate management solutions. It has been proven that the deployment of IoT in the greenhouse could improve production efficiency and profits. In this section, the latest work has been explained based on the communication methods between sensor data and user interfaces and controllers.

### **II.1 Wireless communication**

According to [22] proposed a low-cost, high-efficiency climatic behavior detection system based on the ESP8266 Node MCU microcontroller. This system could monitor the inside temperature, light intensity, content of soil water, and humidity in the greenhouse. Furthermore, water pumps, motors, lighting systems, and exhaust systems were utilized in order to automate the process. Farmers could access acquired data on their smartphones through wireless internet connections. For [23] developed an IoT-based intelligent hydroponic greenhouse system. In this system, Arduino Mega was used as the microcontroller, and DHT11, DS18B20, LDR module, and Ph4502C were incorporated to acquire humidity, temperature, light intensity, and water PH correspondingly. The collected data would be transmitted to the ThingSpeak cloud via ESP8266 wireless communication. And the data could be visualized on a smartphone APP through the Internet. Apart from that, relays and pumps were used to automatically control it to maintain the predefined environmental condition. The results showed that the system could ease farmers' workload and improve overall production. According to [24] proposed an intelligent IoT-based greenhouse system. Node MCU was used as the microcontroller, and DHT11 and LDR sensors were utilized to collect temperature, humidity, and brightness concentrations. The monitored data could be accessed through a Blynk application (APP) on mobile phones or via the Internet. Based on the collected data, a DC fan, DC motor, and bulb were used to adjust the environment.

This system could be deployed in real greenhouses to improve yield and save power as well. According to [25] demonstrated an illumination monitoring and automatic control system for the greenhouse. A Raspberry Pi 3 was used as the main microcontroller, allowing uniform lighting and satisfying plants' needs. With the help of Python and MySQL, the microcontroller extracted the values of nine light-sensitive TSL2561 sensors and stored them in a local database. A web application was created for accessing the data and remotely controlling the light intensity. Brightness management was autonomous or manual, using sensor data or user-chosen manual control. This IoT-based system optimizes lighting energy in greenhouses, reducing energy costs and improving tomato productivity and quality. The solar source could be used to supply power to the intelligent greenhouse system. In this way, it can reduce costs by reducing its reliance on power demand. Nouadjep et al. proposed a smart greenhouse monitoring and control system for year-round crop production using an

Arduino Mega controller. The system consisted of different sensors to gather room environment parameters like temperature, humidity, light intensity, soil humidity, and PH value. It also had a solar system to provide power for the whole system. Furthermore, an Android application allows displaying and analyzing parameters through the Internet. The system could reduce the exploitation of farm land and improving agricultural yields [26].

## II.2 Wired Network

An intelligent sensor network prototype for an automated urban greenhouse (AUG) was proposed based on an Arduino Pro microcontroller, which enabled automatic monitoring and control of heating, illumination, ventilation, and watering. Adafruit AM2302, Adafruit TSL2591, and Decagon Devices 10HS sensors were utilized for environmental humidity, temperature, soil water concentration, and light intensity parameter collection. The gathered data could be viewed from a web-based application via an Ethernet network [27].

## II.3 Bluetooth

Intelligent agriculture could solve global and regional agricultural issues. This research examined smart greenhouse agriculture using IoT technologies. A climate-programmed smart greenhouse prototype was built using an Arduino microcontroller. Environmental humidity and temperature, soil moisture, and illumination intensity were monitored and controlled. The smartphone-based application could be used to visualize and remotely control the greenhouse via an HC-06 Bluetooth connection. A test was conducted to compare the efficacy of traditional plant methods and smart plant methods in the same greenhouse. The results show that the smart greenhouse was proven to improve cucumber, tomato, pepper, and begonia growth. The smart greenhouse system saved 16.5% more water than the pot, and its manual and autonomous operation made greenhouse management easier [28].

## II.3 GSM

Aafreen, R. *et al.* [29] implemented a novel industrial greenhouse monitoring and control system based on IoT technology, utilizing the Blynk IoT platform. An Arduino Mega 2560 board was used as the main microcontroller. EVANA SM12, BH1750, and MQ135 sensors were employed to monitor soil water content, ambient light intensity, and CO<sub>2</sub> content, respectively. The system provided wireless data transmission in real-time, data visualization, and analysis on the central server of the ThingSpeak cloud. The fast and lightweight Blynk IoT platform was used for message transmission on the mobile app and control through GSM communication, enabling real-time irrigation needs. The experimental results demonstrated the system's effectiveness in energy-efficient smart farming in greenhouses. According to [30] presented an IoT-based intelligent greenhouse real-time monitoring and automatic control data logger system. Built-in sensors to monitor soil moisture, indoor temperature, humidity, carbon dioxide concentration (CO<sub>2</sub>), air pressure, soil pH value, illumination, and water level. A microcontroller to collect sensor data and send action commands. As part of the system, the GSM module and the GPRS communication protocol enabled wireless Internet access and data transmission. Implementing this smart agriculture service on the property enabled autonomous greenhouse control and increased production and efficiency.

The remaining of this writing is broken into the following parts: Section II is a literature review that summarizes the latest smart greenhouse-associated studies. Section III describes the required devices and experiment steps. Section IV discusses the results of this study. Section V summarizes the conclusion and future scope.

## III. MATERIALS AND METHODS

Applications based on the Internet of Things tend to make everything convenient and intelligent. In this undertaking, a smart, low-cost greenhouse real-time monitoring and control system is conceived and developed for agricultural planting. This section describes the system architecture and experimental prototype buildup for this research project.

### III.1 System Architecture

An intelligent agriculture environment monitoring system was developed to monitor the environmental temperature and humidity of the greenhouse. It adjusts the environment to an optimal level so that plants' health and growth can be maintained. In this system, there are six main workflow stages, including data gathering, data processing, data storage, data analysis, data response, and data visualization. Firstly, data collection involves collecting temperature and humidity values through a DHT22 sensor attached to a microcontroller. Then, data pre-processing is used to remove incomplete and invalid data gathered from the sensor. After that, the collected data is analyzed to check whether they are in a normal range or not at the data analysis stage. Following that, the data is uploaded and stored in the ThingSpeak cloud through the Internet. Next, stored data could be retrieved and visualized remotely by users through a smartphone or a webpage with an Internet connection. In the last, based on the results of data analysis, the corresponding electrical devices may be triggered to adjust and maintain the plant's growth environment. If the humidity or temperature is high, the ventilation fan will turn on automatically until it drops to a normal level. If the temperature is low, the heater will be turned on until it reaches normal. Besides, if environmental parameters are abnormal, an alarm would be triggered to alert farmers. The system can provide insight into the environment and suggest optimized strategies for improving crop growth. The proposed system architecture of this research project is illustrated in Figure 1.

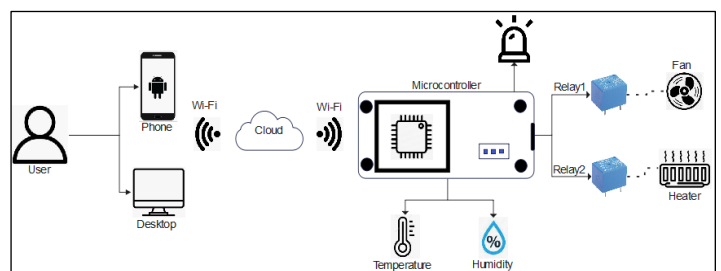


Figure 1: Proposed System Architecture.

Source: Authors, (2024).

### III.2 Experimental Setup

In this project, the NodeMCU ESP8266 is utilized as the primary microcontroller to control sensors and electrical devices via relays. It is a low-cost and cheap tool for developing IoT applications. In the programming part, the Arduino IDE is used to write the code. The ESP8266 environment is chosen for firmware development. The NodeMCU ESP8266 is programmed to communicate with the sensors, actuators, and central server. It also

monitors the system to ensure it works as expected. The gathered data is transmitted to the server for further analysis. The diagram of NodeMCU is shown in Figure 2.

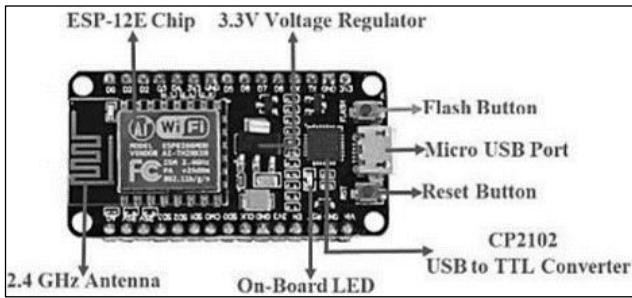


Figure 2: ESP8266 microcontroller.  
Source: Sunidhi Goel, (2022).

As the module for detecting humidity and temperature, the DHT22 sensor is utilized. There are four pins: DATA, VCC, GND, and NC. The standard voltage range for VCC is between 3 volts and 5 volts. The DHT22 sensor measures humidity and temperature values through an integrated capacitive humidity sensor and thermistor. Through the DATA port, data is transmitted to the microcontroller. The maximum operational current is 2.5 mA. Figure 3 illustrates the DHT22 picture.



Figure 3: DHT22 sensor.  
Source: Malika, N. Z., (2021).

A dual-channel relay is utilized to connect a fan and a heater so that they can be triggered later to maintain the ambient environment at a suitable level dynamically and constantly. This allows for efficient energy savings while providing optimal temperature and airflow. The dual-channel relay can be programmed to respond to changes in humidity and temperature, ensuring the environment is always kept at the desired level. It is utilized as a bridge to connect the controller to the heater panel and fan. The dual-channel relay diagram is shown in Figure 4.



Figure 4: Dual-channel relay.  
Source: Y. Liu, (2022).

The 16x2 LCD display is utilized to indicate the current monitoring parameter values. In addition, a buzzer is directly connected to the microcontroller. The connection diagram of different modules is described in Figure 5.

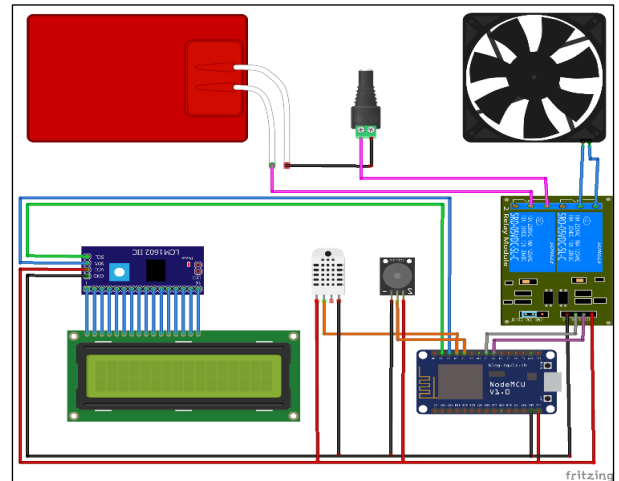


Figure 5: System scheme.  
Source: Authors, (2024).

The control flowchart of the proposed system is depicted in Figure 6. The procedure begins with system initialization, and then the microcontroller collects temperature and humidity data from the greenhouse. The data obtained by the DHT22 sensor will be processed further by the ESP8266 microcontroller and displayed on the LCD panel. The parameters will be checked by the microcontroller based on two situations. First, determine whether the temperature is less than 20 degrees Celsius; if so, a signal will be sent to relay 1 to activate the heating panel. Otherwise, no action will be taken. Second, determine whether the temperature is above 40 degrees Celsius or the humidity is above 80%. If this is the case, the activation signal will be delivered to relay 2 to activate the fan and speed up the ventilation process until the parameters return to normal. As a result, the greenhouse atmosphere can be dynamically modified within a preset range.

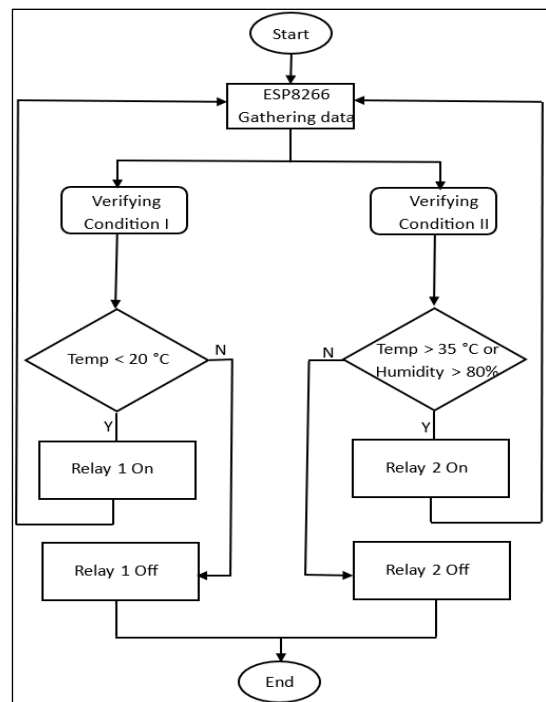


Figure 6: Flowchart of control.  
Source: Authors, (2024).

The proposed system prototype is designed and built, as demonstrated in Figure 7.



Figure 7: Prototype of proposed system.  
Source: Authors, (2024).

Overall, the system was developed to provide real-time ambient monitoring and automatic maintenance of the environment, which can facilitate plant growth and reduce farmer workload. The system is equipped with a temperature and humidity sensor to measure environmental conditions. The data collected from the sensor is then sent to the ThingSpeak cloud for storage and further analysis. The ESP8266 microcontroller acts as the brain of the proposed system, processing sensor data and controlling the other components. The ThingSpeak APP provides a user-friendly interface for interacting with the system, and the ESP8266 connects the system to the internet. An I2C interface connects the LCD display to the microcontroller. Two 18650 batteries are used as a power supply to deliver power to the system. Furthermore, a small greenhouse is constructed to test and verify the proposed system. The planting box measures 60 inches in height, 25 inches in width, and 30 inches in length. The planting box is placed on a shelf made of aluminum. In addition, four wheels are installed to facilitate movement. The indoor ambient temperature and humidity are monitored to ensure an optimal environment for the plants. Figure 8 shows the constructed greenhouse.



Figure 8: Constructed greenhouse.  
Source: Authors, (2024).

Additionally, a light lane is used to provide adequate light for the plants to perform photosynthesis. The temperature and

humidity in the greenhouse are closely monitored and controlled to simulate the environment of the actual growing space. With this setup, the performance of the prototype is evaluated to ensure it meets the desired requirements.

#### IV. RESULTS AND DISCUSSIONS

The collected data is uploaded and stored in the ThingSpeak cloud via a wireless network using a specific channel identification number. The stored data is not only directly retrieved using an HTTP request but can also be exported to a CSV format file, as shown in Figure 9.

	A	B	C	D
1	created_at	entry_id	field1	field2
40232	2023-07-29T1	40231	36.6	87.30
40233	2023-07-29T1	40232	37.2	83.20
40234	2023-07-29T1	40233	37.6	81.50
40235	2023-07-29T1	40234	37.8	80.60
40236	2023-07-29T1	40235	37.9	80.40
40237	2023-07-29T1	40236	38.1	79.80
40238	2023-07-29T1	40237	38.3	79.80
40239	2023-07-29T1	40238	38.3	79.20
40240	2023-07-29T1	40239	38.4	78.00

Figure 9: Data storage in CSV format.  
Source: Authors, (2024).

The monitoring data could be accessed not only through the smartphone APP but also on the ThingSpeak webpage with an Internet connection. Figure 10 shows the real-time monitoring results of the greenhouse on the webpage.

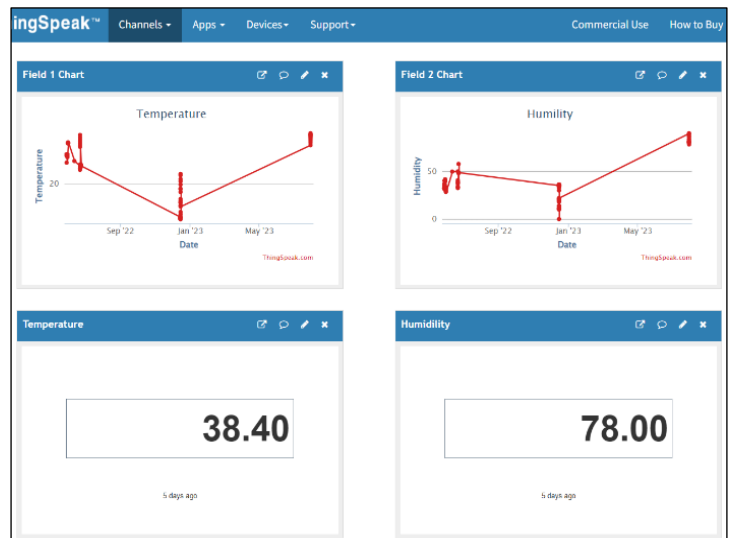


Figure 10: Webpage interface.  
Source: Authors, (2024).

On this page, temperature and humidity parameter values are displayed in a line diagram. The current values are also displayed below the diagram. Besides, the smartphone application provides the ability to access real time monitoring results by using a particular channel ID via the network, as seen in Figure 11.

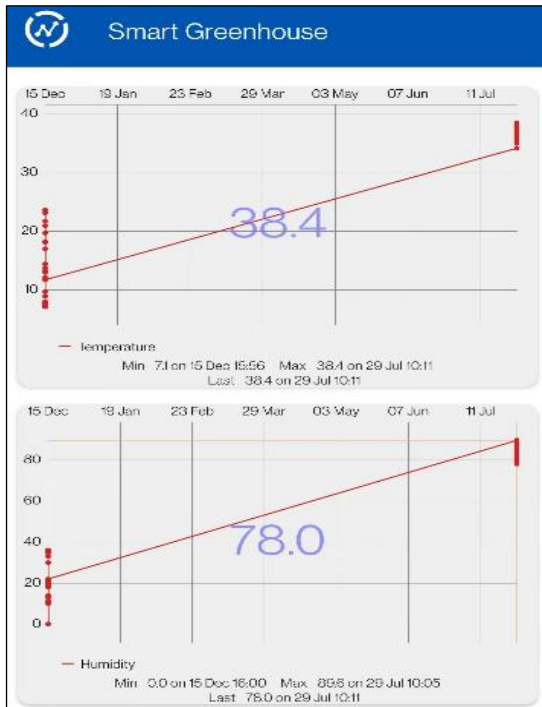


Figure 11: Phone interface.  
Source: Authors, (2024).

The cloud data is reloaded every fifteen seconds. The inside environment of the greenhouse is controlled and maintained at an appropriate level that has been predetermined.

## V. CONCLUSIONS

With the rapid development and deployment of modern science and technology in agriculture, as well as the increasing level of automation, intelligent greenhouse is becoming more and more popular in agricultural cultivation. Most traditional agricultural greenhouses rely on manual control, and their production efficiency is low. In this research, an IoT-based, low-cost intelligent greenhouse management system is designed and implemented to regulate the internal environment of the greenhouse and create an optimal growing environment for crops. In future work, more environmental monitoring parameters like light intensity, soil moisture, and carbon dioxide concentration may be further considered. Solar panels could be used as a source of power to save energy. Apart from that, machine learning technology could be applied to data analysis and predictions. Predictive analytics could forecast future weather and climatic changes. An alert system could be implemented to alert farmers of any potential weather changes. Finally, the data collected can be used to inform agricultural policy decisions and better manage natural resources.

## VI. AUTHOR'S CONTRIBUTION

**Conceptualization:** Liu Yajie.

**Methodology:** Md Gapar Md Johar and Asif Iqbal Hajamydeen.

**Investigation:** Liu Yajie and Md Gapar Md Johar.

**Discussion of results:** Liu Yajie, Md Gapar Md Johar and Asif Iqbal Hajamydeen.

**Writing – Original Draft:** Liu Yajie.

**Writing – Review and Editing:** Liu Yajie, Md Gapar Md Johar and Asif Iqbal Hajamydeen.

**Resources:** Md Gapar Md Johar.

**Supervision:** Md Gapar Md Johar and Asif Iqbal Hajamydeen.  
**Approval of the final text:** Liu Yajie, Md Gapar Md Johar and Asif Iqbal Hajamydeen.

## VII. ACKNOWLEDGMENTS

This work was supported by the Henan Vocational University of Science and Technology located in Zhoukou, China (Grant No.: HZDKYL2022--021).

## VIII. REFERENCES

- [1] F. Oecd, "OECD-FAO agricultural outlook 2022-2031," 2022, doi: <https://doi.org/10.1787/f1b0b29c-en>.
- [2] B. Ahmad *et al.*, "Evaluation of smart greenhouse monitoring system using raspberry-Pi microcontroller for the production of tomato crop," *Journal of Applied Research in Plant Sciences*, vol. 4, no. 01, pp. 452-458, 2023, doi: <https://dx.doi.org/10.5935/2447-0228.20200001>.
- [3] P. Srihari and M. Vibha, "A STUDY ON USE OF IOT TECHNOLOGY IN GREENHOUSE FARMING."
- [4] R. Geethamani and S. Jaganathan, "IoT Based smart greenhouse for future using node MCU," in *2021 7th International Conference on Advanced Computing and Communication Systems (ICACCS)*, 2021, vol. 1: IEEE, pp. 1615-1620, doi: <https://doi.org/10.1109/ICACCS51430.2021.9441708>.
- [5] H. Zhang and L. Zhang, "A Reliable Data-Driven Control Method for Planting Temperature in Smart Agricultural Systems," *IEEE Access*, vol. 11, pp. 38182-38193, 2023, doi: <https://doi.org/10.1109/ACCESS.2023.3267803>.
- [6] Y. Ji, "Design and Implementation of Monitoring and Controlling System for Greenhouse Plantation."
- [7] F. J. Adha, M. G. M. Johar, M. H. Alkawaz, A. I. Hajamydeen, and L. Raya, "IoT based Conceptual Framework for Monitoring Poultry Farms," in *2022 IEEE 12th Symposium on Computer Applications & Industrial Electronics (ISCAIE)*, 2022: IEEE, pp. 277-282, doi: <https://doi.org/10.1109/ISCAIE54458.2022.9794471>.
- [8] F. J. Adha, R. Ramli, M. H. Alkawaz, M. G. M. Johar, and A. I. Hajamydeen, "Assessment of Conceptual Framework for Monitoring Poultry Farm's Temperature and Humidity," in *2021 IEEE 11th International Conference on System Engineering and Technology (ICSET)*, 2021: IEEE, pp. 40-45, doi: <https://doi.org/10.1109/ICSET53708.2021.9612437>.
- [9] N. Z. Malika, M. G. M. Johar, M. H. Alkawaz, A. I. Hajamydeen, and L. Raya, "Temperature & humidity monitoring for poultry farms using IOT," in *2022 IEEE 12th Symposium on Computer Applications & Industrial Electronics (ISCAIE)*, 2022: IEEE, pp. 76-81, doi: <https://doi.org/10.1109/ISCAIE54458.2022.9794520>.
- [10] N. Z. Malika, R. Ramli, M. H. Alkawaz, M. G. M. Johar, and A. I. Hajamydeen, "IoT based Poultry Farm Temperature and Humidity Monitoring Systems: A Case Study," in *2021 IEEE 9th Conference on Systems, Process and Control (ICSPC 2021)*, 2021: IEEE, pp. 64-69, doi: <https://doi.org/10.1109/ICSPC53359.2021.9689101>.
- [11] K. Fatima, S. Hussain, S. A. Khan, M. A. Khan, S. R. Saleem, and S. Kanwal, "Digital Twin Greenhouse Technologies for Commercial Farmers," *Environmental*

- Sciences Proceedings*, vol. 23, no. 1, p. 33, 2023, doi: <https://doi.org/10.3390/environsciproc2022023033>.
- [12] V. K. Quy *et al.*, "IoT-enabled smart agriculture: architecture, applications, and challenges," *Applied Sciences*, vol. 12, no. 7, p. 3396, 2022, doi: <https://doi.org/10.3390/app12073396>.
- [13] C. Maraveas, D. Piromalis, K. Arvanitis, T. Bartzanas, and D. Loukatos, "Applications of IoT for optimized greenhouse environment and resources management," *Computers and Electronics in Agriculture*, vol. 198, p. 106993, 2022, doi: <https://doi.org/10.1016/j.compag.2022.106993>.
- [14] A. Kudratov, "INTERNET OF THINGS AS A TOOL FOR OPTIMIZING PROCESSES IN AGRICULTURE," *Modern Science and Research*, vol. 2, no. 6, pp. 813-818, 2023, doi: <https://doi.org/10.5281/zenodo.8041353>.
- [15] P. Cihan, "IoT Technology in Smart Agriculture," in *International Conference on Recent Academic Studies*, 2023, vol. 1, pp. 185-192, doi: <http://dx.doi.org/10.59287/icras.693>.
- [16] V. Lavanya, B. SriLatha, B. B. Sesank, S. Harshavardhan, and M. S. Shahsavara, "GREENHOUSE MONITORING AND CONTROLLING USIN IOT," *IJETMS*, vol. 6, no. 4, pp. 79-81, July, 2022, doi: <http://dx.doi.org/10.46647/ijetms.2022.v06si01.015>.
- [17] J. Zhao, S. Liu, and Z. Qiao, "Research and Implementation of Android-based Intelligent Greenhouse Environment Measurement and Control System," *Jiangsu Agricultural Science*, vol. 3, no. 44, pp. 394-397, 2016.
- [18] Z. Guo, Y. Shen, S. Wan, W.-L. Shang, and K. Yu, "Hybrid intelligence-driven medical image recognition for remote patient diagnosis in internet of medical things," *IEEE journal of biomedical and health informatics*, vol. 26, no. 12, pp. 5817-5828, 2021, doi: <https://doi.org/10.1109/JBHI.2021.3139541>.
- [19] J. Lv, W. Kong, Y. Shi, and H. Bao, "Design of Intelligent Greenhouse Management and Control System," *International Core Journal of Engineering*, vol. 7, no. 1, pp. 230-232, 2021, doi: [https://doi.org/10.6919/ICJE.202101\\_7\(1\).0030](https://doi.org/10.6919/ICJE.202101_7(1).0030).
- [20] F. A. Akomaye, E. I. Etim, and E. J. Ekanem, "Importance of Smart Farming Practices for Sustainable Agriculture," *International Contemporary Journal of Science Education and Technology*, vol. 2, no. 2, 2023.
- [21] G. Gebresenbet and S. A. Finecomess, "Assessment of the Smart Mechatronics Application in Agricultural: A Review," *Appl. Sci.*, no. 13, 2023, doi: <https://doi.org/10.20944/preprints202305.0169.v1>.
- [22] J. Sujin, R. Murugan, M. Nagarjun, and A. K. Praveen, "IOT based greenhouse monitoring and controlling system," in *Journal of Physics: Conference Series*, 2021, vol. 1916, no. 1: IOP Publishing, p. 012062, doi: 10.1088/1742-6596/1916/1/012062.
- [23] A. C. H. Austria, J. S. Fabros, K. R. G. Sumilang, J. Bernardino, and A. C. Doctor, "Development of IoT Smart Greenhouse System for Hydroponic Gardens," *arXiv preprint arXiv:2305.01189*, 2023, doi: <https://doi.org/10.48550/arXiv.2305.01189>.
- [24] S. Goel, N. Tyagi, A. Yadav, S. Goel, and G. Gupta, "Greenhouse Monitoring & Control System using Node MCU ESP 8266," in *IPEC*, 2022, vol. 1, p. 02.
- [25] A. Belkadi, D. Mezghani, and A. Mami, "IoT and lighting control for smart greenhouse," *Zenodo.*, vol. 3813434, 2019, doi: <http://doi.org/10.5281/zenodo>.
- [26] S. N. Nouadjep and H. F. Djouodjinang, "IoT and Arduino Based Design of a Solar, Automated and Smart Greenhouse for Vegetable," in *E3S Web of Conferences*, 2022, vol. 354: EDP Sciences, p. 01002, doi: <https://doi.org/10.1051/e3sconf/202235401002>.
- [27] K. Meah, J. Forsyth, and J. Moscola, "A smart sensor network for an automated urban greenhouse," in *2019 international conference on robotics, electrical and signal processing techniques (ICREST)*, 2019: IEEE, pp. 23-27, doi: <https://doi.org/10.1109/ICREST.2019.8644079>.
- [28] P. Kirci, E. Ozturk, and Y. Celik, "A novel approach for monitoring of smart greenhouse and flowerpot parameters and detection of plant growth with sensors," *Agriculture*, vol. 12, no. 10, p. 1705, 2022, doi: <https://doi.org/10.3390/agriculture12101705>.
- [29] R. Aafreen, S. Y. Neyaz, R. Shamim, and M. S. Beg, "An IoT based system for telemetry and control of Greenhouse environment," in *2019 International Conference on Electrical, Electronics and Computer Engineering (UPCON)*, 2019: IEEE, pp. 1-6, doi: <https://doi.org/10.1109/UPCON47278.2019.8980258>.
- [30] M. Djordjevic, V. Punovic, D. Dankovic, and B. Jovicic, "Smart autonomous agricultural system for improving yields in greenhouse based on sensor and IoT technology," *Journal of Applied Engineering Science*, vol. 18, no. 4, pp. 606-613, 2020, doi: <https://doi.org/10.5937/jaes0-26722>.





ISSN ONLINE: 2447-0228



### RESEARCH ARTICLE

### OPEN ACCESS

## A BIBLIOMETRIC OF FINANCIAL TECHNOLOGY QR CODE AND QRIS RESEARCH

Anisyah Vella<sup>1</sup>, Wihandaru Sotya Pamungkas<sup>2</sup> and Arni Surwanti<sup>3</sup>

<sup>1,2,3</sup> Yogyakarta Muhammadiyah University – Yogyakarta, Indonesia.

<sup>1</sup><http://orcid.org/0009-0001-4720-0283> , <sup>2</sup><http://orcid.org/0000-0001-6611-8309> , <sup>3</sup><http://orcid.org/0000-0003-2894-5674> 

Email: [anisyahvella00@gmail.com](mailto:anisyahvella00@gmail.com), [wihandaru@umy.ac.id](mailto:wihandaru@umy.ac.id), [arniumy@yahoo.com](mailto:arniumy@yahoo.com)

### ARTICLE INFO

#### Article History

Received: November 01<sup>th</sup>, 2023

Revised: July 22<sup>th</sup>, 2024

Accepted: August 13<sup>th</sup>, 2024

Published: August 30<sup>th</sup>, 2024

#### Keywords:

Fintech,  
QR code,  
QRIS.

### ABSTRACT

This study aims to determine the development of the use of technology-based financial transactions or Fintech, especially in QR codes and QRIS Fintech. This research discusses parameters related to many previous studies related to financial technology QR codes and QRIS. The bibliometric method identifies and analyzes publication patterns, the most productive authors, the journals that publish the most related articles, and research trends related to Fintech (QR Code and QRIS). Data collection was conducted in September 2023 on the Scopus database and data analysis using Rstudio, Biblioshiny, and VOSviewer applications. The results of this bibliometric analysis provide important insights into the development of research related to Fintech (QR Code and QRIS). It was found that the discussion of the two themes was still minimally researched as seen from the results of the QR Code theme 16 published documents and QRIS 7 published documents.



Copyright ©2024 by authors and Galileo Institute of Technology and Education of the Amazon (ITEGAM). This work is licensed under the Creative Commons Attribution International License (CC BY 4.0).

## I. INTRODUCTION

As time goes by, the world of technology is increasingly forced to continue to develop. This technological development extends to the world of finance which is currently known as financial technology [1,2]. So far, the usual use of financial transactions is using money in cash. but with the development of technology, there have been many financial transaction activities using technology or what is commonly known as Fintech [3]. Financial transactions using technology continue to experience an increase and interest from the public [4]. Until it affects the behavior of people who tend to always follow trends in financial transaction systems that are much easier and faster with the help of technology [5]. Technological developments also encourage people to have new habits and mindsets. At this time public demand for a financial system that can accommodate every need of the community is fast, guaranteed security, easy to use, and efficient, thus encouraging the development of financial system innovation very rapidly [6],[7].

Current financial developments require many non-cash financial transaction methods to be issued to facilitate the public in conducting financial transactions using transaction methods such

as QR codes Indonesia also publishes its own QR Code standard commonly known as QRIS (Quick Response Code Indonesian Standard). So, this study aims to determine the development of the use of technology-based financial transactions or Fintech, especially in QR Code and QRIS Fintech. This research discusses parameters related to many other studies related to financial technology QR codes and QRIS.

## II. THEORETICAL REFERENCE

### II.1 FINANCIAL TECHNOLOGY (FINTECH)

Fintech comes from the term Financial Technology or financial technology is the use of technology in the financial system that creates new products, services, and technology, or businesses that have an impact on the stability of the financial system, smoothness, and security of the payment system [6, 8]. Technological developments continue to provide innovations related to financial technology, to meet the needs of society [9]. Fintech is a combination of financial services with technology that originally had to be face-to-face transactions, then with the existence of technology can now make transactions remotely, anytime, and anywhere. The application of Fintech is a popular

method of financial transaction services in the digital era, this situation is then expected to encourage several people to have easier access to financial services [10].

## II.2 QUICK RESPONSE CODE (QR CODE)

Quick Response Code often called QR Code or QR Code is a kind of two-dimensional symbol developed by Denso Wave which is a subsidiary of Toyota, a Japanese company in 1994 [11]. The purpose of this QR Code is to convey information quickly and also get a response quickly [12]. At first, the QR Code was used for tracking vehicle parts for manufacturing. But now, it has been used for commercials aimed at cell phone users [13]. QR Code is the development of barcodes or bar codes that are only able to store information horizontally while QR Code can store more information, both horizontally and vertically [14].

## II.3 QUICK RESPONSE CODE INDONESIAN STANDARD (QRIS)

Quick Response Code Indonesian Standard commonly known as QRIS is a payment system launched or pioneered by Bank Indonesia and the Indonesian Payment System Association [15]. QRIS is a non-cash transaction application through a smartphone application [15]. QRIS is a shared delivery channel payment system similar to the operation of the QR code for non-cash resin payments which is part of payment transactions in the form and type of electronic money (e-money) [16],[17]. Therefore, QRIS becomes an electronic payment system that becomes the standard in all transactions[18]. Thus, each merchant only needs one QR code to make all transactions through any payment software [15].

## III. MATERIALS AND METHODS

In this study, a bibliometric approach was used to review the literature on Fintech (QR Code and QRIS). Bibliographic techniques are research methods that involve quantitative analysis of bibliographies or related documents. This method is used to analyze the volume, distribution, and characteristics of scientific publications, including the impact of journal articles, conferences, books, authors, journals, and keywords. The research data for this study are international journal searches in the Scopus database. Keywords used in Scopus research a) Fintech and QR code. (b) Quick Response Code Indonesian Standard. Data collection was carried out in September 2023. The procedure was used to obtain the results of data analysis using the Rstudio, Biblioshiny, and VOS viewer applications.

## IV. RESULTS AND DISCUSSIONS

### IV.1 QR CODE

#### IV.1.1 Main Information

Figure 1 provides an overview of the data sources used in the bibliometric analysis of this article. It is confirmed that 16 articles from 45 authors conducted research related to QR Code Fintech. Based on Figure 1 and Table 1, there are 16 research articles published from 2019 to 2023. In Table 1, the data from the annual Scientific Production results of the development of Fintech QR code-themed article production is still small, namely only 16 documents. QR code Fintech research was first discussed in 2019, so it can be said that there is still little research on QR code Fintech

in 2020 published 4 articles, in 2021 published 5 articles, in 2022 published 3 articles, and in 2023 published 2 articles.



Figure 1: Main information.  
Source: Authors, (2024).

Table 1: Annual Scientific Production.

Year	Articles
2019	1
2020	4
2021	6
2022	3
2023	2

Source: Authors, (2024).

#### IV.1.2 Three-Field Plot

Figure 2 three-pole graph characterizes the allocation by country (AU\_CO) on the left, Keyword (DE) in the middle, and Additional Keyword (ID) on the right. the three-pole graph was created to reflect the percentage of topics raised by previous researchers for each country related to QR Code Fintech. It can be seen that AU\_CO only has 6 countries that have recently researched Fintech QR codes, namely Ghana, Australia, India, Tanzania, USE, Korea, Malaysia, Canada, and North Macedonia. Looking at the DE and ID keywords that are often used for the development of this research are Fintech, mobile payments, digital transformation, crypto-exchanges, blockchain, mobile payments, disruption, 2fa, biometric fingerprint, QR Code, covid19, digital banking, digitalization, digital India, food supply, electronic money, authentication, blockings, competition, biometrics, codes (symbols), Chinese government, class diagrams, computer-aided instruction, business operation, computer programming, access control.

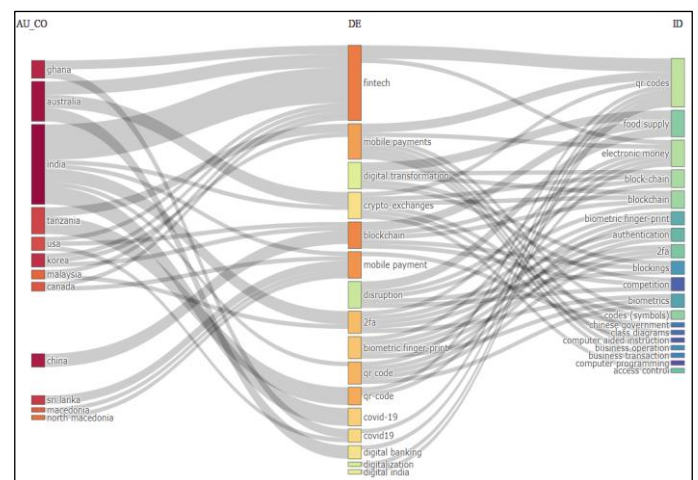


Figure 2: Three field plots.  
Source: Authors, (2024).

### IV.1.3 Most Relevant Sources

Figure 3 shows 10 sources or journals that have published research on Fintech QR Codes. It is said in Figure 1 that there are only 16 documents that have been published so Figure 3 Most Relevant Sources shows each journal there is only 1 article published about Fintech QR Code. It can be seen that the publication of articles about Fintech QR codes is published in conference journals, namely the 2021 9th International Conference on Reliability, the 2022 International Conference on Digital Transform, icacnis 2022-2022 International Conference on Ad, and proceedings- International Conference on communic. For journal publishing in 6 international journals, namely Internet fure, Global Social Welfare, International Journal on Recent and Innovation Tre, research anthology on small business strategies for, studies in systems decision and control, and technology in society.

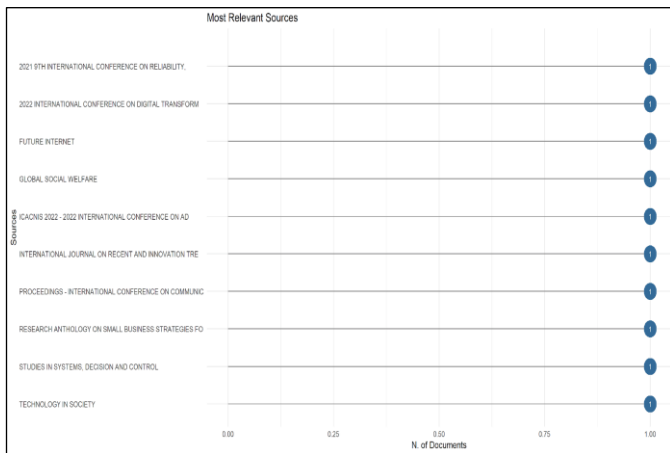


Figure 3: Most Relevant Sources. Source: Authors, (2024).

### IV.1.4 Countries' Scientific Production

Table 2 shows the countries that have published Fintech QR code articles. Seven countries have contributed to scientific publications about Fintech QR codes. Based on the acquisition of research data, India ranks first with the acquisition of 7 frequencies of scientific publication contributions related to the Fintech QR Code. Furthermore, followed by Australia and China have 3 frequencies, Ghana, South Korea, Sri Lanka, Tanzania, and the USA have 2 frequencies, while countries with low broadcast coverage include Canada, Malaysia, and North Macedonia each have 1 frequency. In Figure 4, the darker the color on the map, the higher the frequency of publishing articles from that country.

Table 2: Countries' Scientific Production.

Region	Freq
INDIA	7
AUSTRALIA	3
CHINA	3
GHANA	2
SOUTH KOREA	2
SRI LANKA	2
TANZANIA	2
USA	2
CANADA	1
MALAYSIA	1
NORTH MACEDONIA	1

Source: Authors, (2024).

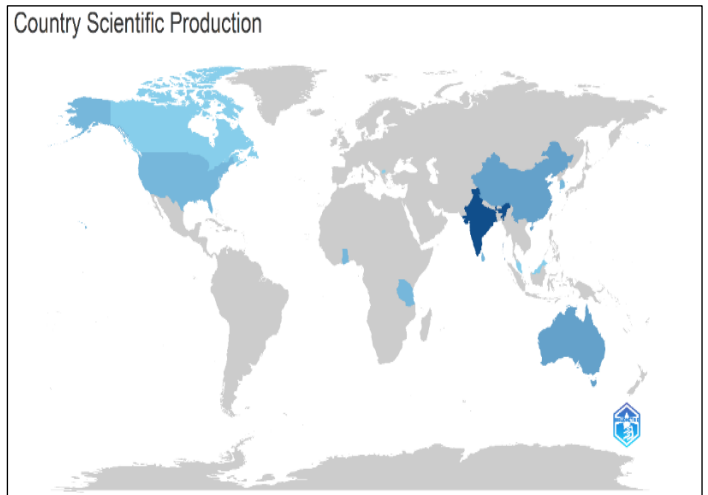


Figure 4: Countries' Scientific Production. Source: Authors, (2024).

### IV.1.5 Word Cloud and Tree Map

Figures 5 and 6 show the data visualization based on the most frequently used keywords on the keyword graph settings that the author has used before. The advantage of choosing these keywords is that they provide insight into the most important topics and research trends. Figure 5 is about the word cloud where it can be seen that the most visible keywords are food supply, block-chain, and QR codes. Figure 6 discusses keywords based on treemap illustrating the frequency of keyword users where the most frequently used words are QR codes 3 frequencies with a rate of 5%, Block-chain and food supply 2 frequencies with a rate of 4%.

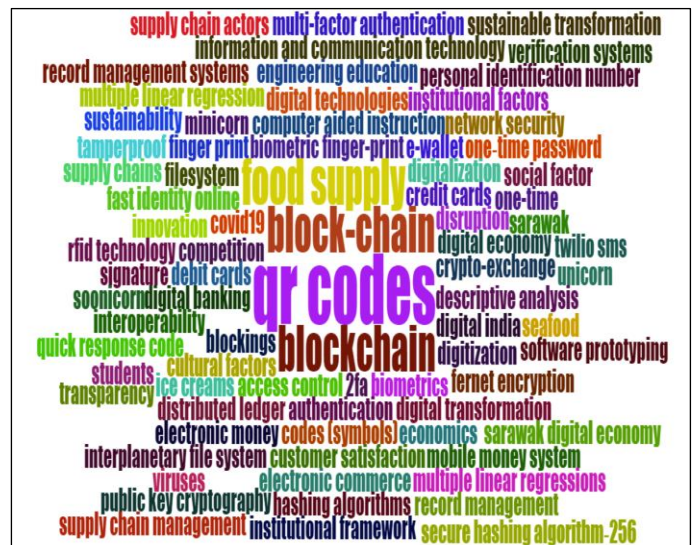


Figure 5: WordCloud. Source: Authors, (2024).

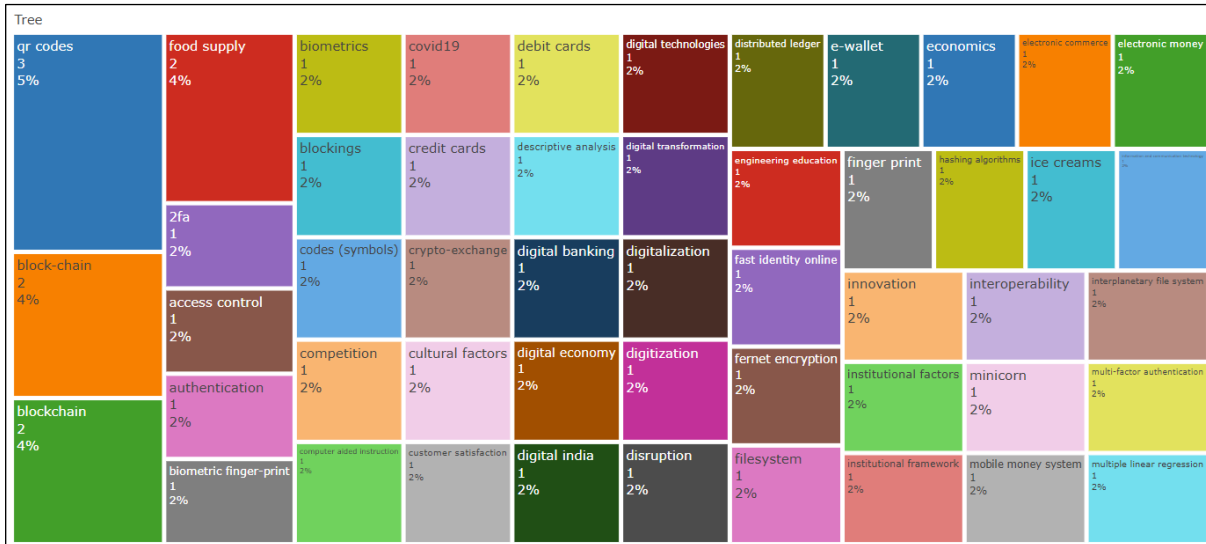


Figure 6: Tree Map.  
Source: Authors, (2023).

#### IV.1.6 VOSviewer

From 16 documents obtained based on Scopus search data, Figure 7 can provide an overview of the Co-occurrence network which displays words in colored form by considering whether there is a link between one word and another. The same round color shows the weight of the relationship between words. the darker the color results in the image, the longer the research discusses the topic. For the size of the circle in Figure 7, it shows the number of publications related to the word both in article titles, abstracts, and keywords, the larger the circle, the more the number of articles related to the term. It can be said in Figure 13 that every word that is connected means that the word is influential and significant whether the research on the word is positive or negative. Based on Table 2, there are 5 clusters and some gaps that are far enough between colors to get the results of the number of words there are 75 words

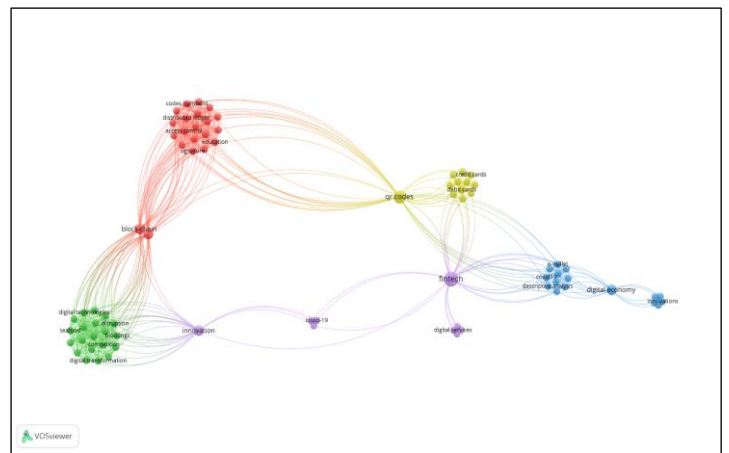


Figure 7: VOS viewers network visualization.  
Source: Authors, (2024).

Table 3: Clusters from VOS viewers.

Clusters	Items	Type
1	20 Red	Access control, blockchain, codes (symbols), computer-aided instruction, crypto-exchange, distributed ledger, education, engineering education, filesystem, interoperability, interplanetary file system, ipfs, network security, record management, record management systems, signature, students, tamper-proof, transparency, verification systems.
2	20 Green	Blockings, competition, digital technologies, digital transformation, digitization, disruption, electronic commerce, food, food supply, information and communication technology, institutional factors, institutional framework, seafood, social factors, supply chain, supply chain actors, supply chain management, sustainability, sustainable transformation.
3	16 Blue	COVID-19, descriptive analysis, digital economy, e-wallet, innovations, modern, multiple linear regression, payment instruments, payment market, payment systems, RFID technology, Sarawak, Sarawak digital economy, tam, technology acceptance model, viruses.
4	11 Yellow	Credit cards, customer satisfaction, debit cards, digital banking, digital India, digitalization, economics, mini corn, QR codes, soonicorn, unicorn.
5	8 Purple	Covid-19, digital services, disruption technology, financial inclusion, financial literacy, financial policy, Fintech, innovation, QR-code.

Source: Authors, (2024).

## IV.2 QUICK RESPONSE CODE INDONESIAN STANDARD (QRIS)

### IV.2.1 Main information

Figure 8 provides an overview of the Quick Response Code Indonesian Standard (QRIS) data sources used in bibliometric analysis. It is confirmed that 7 articles from 24 authors conducted research related to the Quick Response Code Indonesian Standard (QRIS). Based on Figure 8 and Table 4, there are 7 research articles published from 2021 to 2023. In Table 1, the data from the annual Scientific Production results of the development of the production of themed articles on the Quick Response Code Indonesian Standard (QRIS) is still small, namely only 7 documents. Research on the Quick Response Code Indonesian Standard (QRIS) was first discussed in 2021, so it can be said that there is still little research on the Quick Response Code Indonesian Standard (QRIS) In 2021, 2 articles were published, in 2022 4 articles were published, and in 2023 1 article was published.



Figure 8: Main information.  
Source: Authors, (2023).

Table 4: Annual Scientific Production.

Year	Articles
2021	2
2022	4
2023	1

Source: Authors, (2024).

### IV.2.2 Three-Field Plot

Figure 9 three-pole graph characterizes the allocation by country (AU\_CO) on the left, Keyword (DE) in the middle, and Additional Keyword (ID) on the right. the three-pole graph was created to reflect the percentage of topics raised by previous researchers for each country related to the Quick Response Code Indonesian Standard (QRIS). It can be seen that AU\_CO has 2 countries that research Quick Response Code Indonesian Standard (QRIS), namely Indonesia and the United Kingdom. The most research on the Quick Response Code Indonesian Standard (QRIS) is in Indonesia because QRIS is a Fintech QR code used by the country of Indonesia itself so it is said that Indonesia has several researchers who examine the development of the Quick Response Code Indonesian Standard (QRIS) itself. It can be seen that the DE and ID keywords that are often used for the development of this research are QRIS, e-wallet, technology acceptance model, perceived ease of use, intention to use, perceived usefulness, digital wallet, attitudes towards technology, in-store payment, m-payment, mobile technology acceptance model, trust, quick response code, Indonesia, medium enterprise merchant, quick response code Indonesian standard, electronic money, attitude towards technology, case studies, marketing sectors, micro, in-

store payment, e-wallet, ease of use, codes (symbols), and global system for mobile communications.

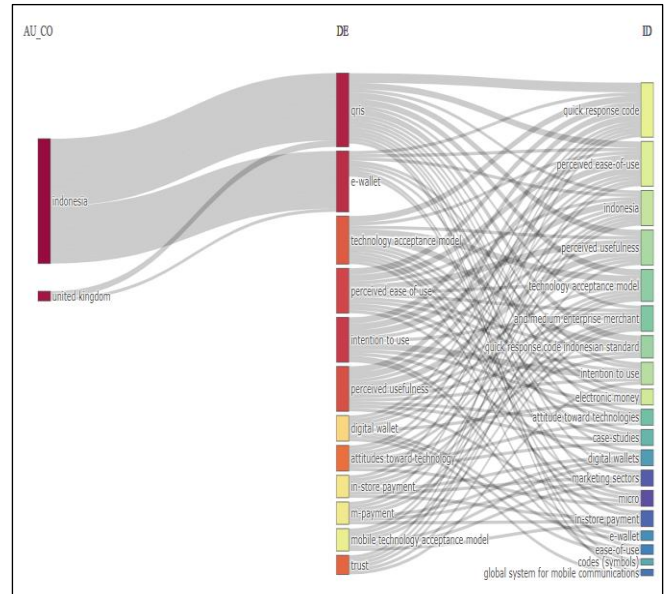


Figure 9: Three field plots.  
Source: Authors, (2024).

### IV.2.3 Most Relevant Sources

Figure 10 shows 7 sources or journals that have published research on the Quick Response Code Indonesian Standard (QRIS). It is said in Figure 8 that there are only 7 documents that have been published so that in Figure 10 Most Relevant Sources shows that each journal has only 1 article published about the Quick Response Code Indonesian Standard (QRIS). It can be seen that the publication of articles about the Quick Response Code Indonesian Standard (QRIS) is contained in 7 journals, namely the 2022 5th International Conference on Computers and, AIP conference proceedings, the International Journal of Economics and Management, Journal of Distribution Science, proceedings of 2021 6th international conference o, proceedings of 2021 international conference on in, proceedings of 2022 international conference on in.

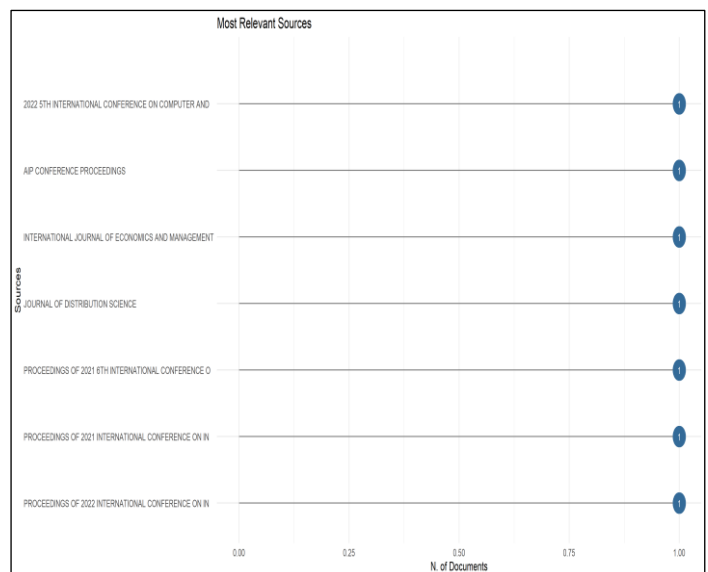


Figure 10: Most Relevant Sources.  
Source: Authors, (2024).

#### IV.2.4 WordCloud and TreeMap

Figures 11 and 12 show the data visualization based on the most frequently used keywords on the keyword graph settings that the author has used before. The advantage of choosing these keywords is that they provide insight into the most important topics and research trends. Figure 11 is about the word cloud where it can be seen that the most visible keywords are quick response code Indonesia standard, intention to use, perceived ease of use, quick response code, electronic money, Indonesia, perceived usefulness, and technology acceptance model. Figure 12 discussing keywords based on treemap illustrates the frequency of keyword users where the most frequently used words are quick response codes 4 frequencies with a level of 8%, perceived ease of use 3 frequencies with a level of 6%. At frequency level 2 there are six words, namely electronic money, Indonesian intention to use, perceived usefulness, quick response code Indonesian standard, and technology acceptance model.

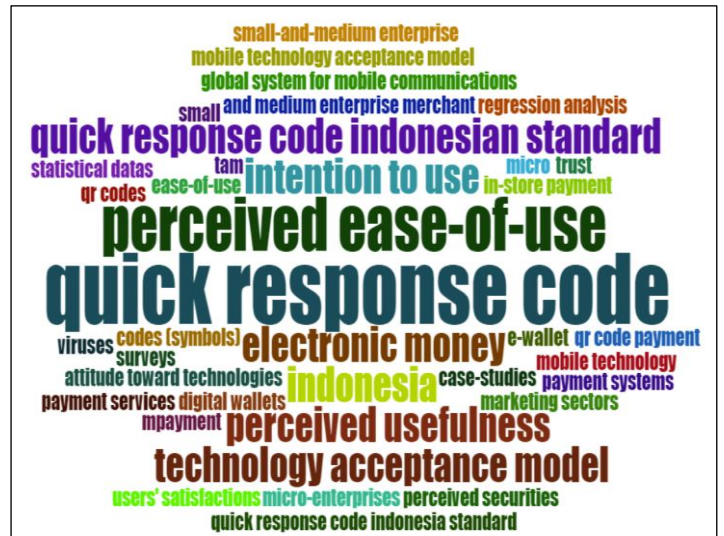


Figure 11: Word Cloud.  
Source: Authors, (2024).

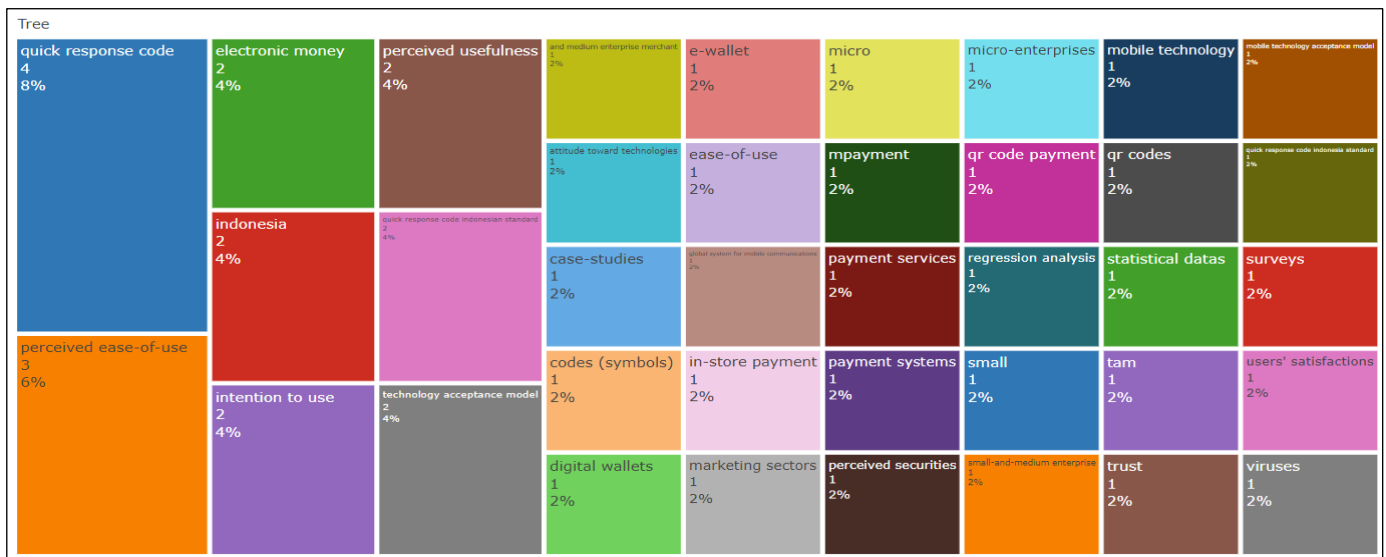


Figure 12: Tree Map.  
Source: Authors, (2024).

#### IV.2.5 VOS viewer

From 7 documents obtained based on Scopus search data, Figure 13 can provide an overview of the Co-occurrence network which displays words in colored form by considering whether there is a link between one word and another. The same round color shows the weight of the relationship between words. the darker the color results in the image, the longer the research discusses the topic. The size of the circle in Figure 13 shows the number of publications related to the word both in article titles, abstracts, and keywords the bigger the circle the more the number of articles there are related to the term. It can be said in Figure 13 that every word that is connected means that the word is influential and significant whether the research on the word is positive or negative. Based on Table 5, there are 5 clusters and some gaps that are far enough between colors to get the results of the number of words there are 48 words.

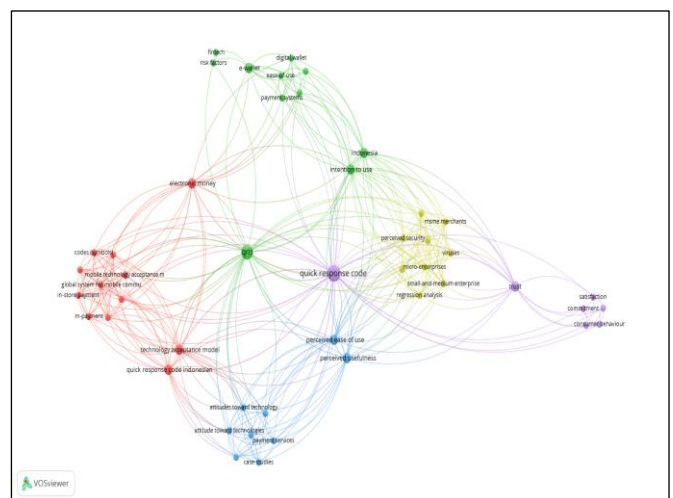


Figure 13: VOS viewers network visualization.  
Source: Authors, (2024).

Table 5: Clusters from VOSviewers.

Clusters	Items	Type
1	12 Red	codes (symbols), electronic money, global system for mobile communications, in-store payment, m-payment, mobile technology, mobile technology acceptance model, mpayment, QR code payment, QR codes, quick response code Indonesian standard, technology acceptance model.
2	11 Green	Digital wallet, e-wallet, ease of use, Fintech, Indonesia, intention to use, payment systems, QRIS, risk factors, tam, user satisfaction.
3	9 Blue	Attitude toward technologies, attitude toward technology, case studies, marketing sectors, payment services, perceived ease of use, perceived usefulness, statistical data, and surveys.
4	9 Yellow	Micro small and medium enterprise merchants, micro entrechats, MSME merchants, perceived securities, perceived security, quick response code Indonesia standard, regression analysis, small and medium enterprise, viruses.
5	7 Purple	Commitment, consumer behavior, customer loyalty, digital transaction, quick response code, satisfaction, trust.

Source: Authors, (2024).

## V. CONCLUSIONS

**QR Code:** The results of the analysis on Fintech QR Code research the development of Fintech QR code-themed article production is still small, namely only 16 documents from 2019-2023. Three-Field Plot and Countries' Scientific Production see that the dominating country is India. The results of the most dominating keywords based on the Three-Field Plot are Fintech and QR codes. There are different results on Word Cloud and Tree Map which are food supply, block-chain, and QR codes the dominating keywords. Most Relevant Sources The top 10 journals each only published 1 article topic. Vosviewer analysis there are 5 clusters and some gaps are far enough between colors to get the result of the number of words there are 75 words.

**QRIS:** The results of the QRIS research analysis of the development of QRIS-themed articles are only 7 documents published from 2021 to 2023. Based on the results of the Three-Field Plot and Countries' Scientific Production, it can be seen that the dominant country is Indonesia because this QR Code is used by the Indonesian people. For the results, the most dominating keywords based on the Three-Field Plot are QRIS, e-wallet, and quick response code. There are different results on Word Cloud and TreeMap which are quick response codes and perceived ease of use. Most Relevant Sources The top 7 journals each only published 1 article topic. Vosviewer analysis there are 5 clusters and some gaps that are far enough between colors to get the results of the number of words there are 48 words.

The conclusion of this research shows that the perception and issue of Fintech (QR Code and QRIS) has changed in each period. The discussion of these 2 themes is still minimally researched. Because this research is still minimal, it

is a good topic for further research to develop topics related to this research.

## VI. AUTHOR'S CONTRIBUTION

**Conceptualization:** Anisayah Vella.

**Methodology:** Anisayah Vella.

**Investigation:** Anisayah Vella.

**Discussion of results:** Anisayah Vella, Wihandaru Sotya Pamungkas, and Arni Surwanti.

**Writing – Original Draft:** Anisayah Vella.

**Writing – Review and Editing:** Anisayah Vella.

**Resources:** Anisayah Vella.

**Supervision:** Wihandaru Sotya Pamungkas, and Arni Surwanti.

**Approval of the final text:** Anisayah Vella, Wihandaru Sotya Pamungkas, and Arni Surwanti.

## VII. REFERENCES

- [1] J. R. Bhat, S. A. AlQahtani, and M. Nekovee, "FinTech enablers, use cases, and role of future internet of things," *J. King Saud Univ. - Comput. Inf. Sci.*, vol. 35, no. 1, pp. 87–101, 2023, doi: 10.1016/j.jksuci.2022.08.033.
- [2] K. B. Ooi and G. W. H. Tan, "Mobile technology acceptance model: An investigation using mobile users to explore smartphone credit card," *Expert Syst. Appl.*, vol. 59, pp. 33–46, 2016, doi: 10.1016/j.eswa.2016.04.015.
- [3] K. Mahmud, M. M. A. Joarder, and K. Sakib, "Customer Fintech Readiness (CFR): Assessing customer readiness for fintech in Bangladesh," *J. Open Innov. Technol. Mark. Complex.*, vol. 9, no. 2, p. 100032, 2023, doi: 10.1016/j.joitmc.2023.100032.
- [4] V. Murinde, E. Rizopoulos, and M. Zachariadis, "The impact of the FinTech revolution on the future of banking: Opportunities and risks," *Int. Rev. Financ. Anal.*, vol. 81, no. June 2021, 2022, doi: 10.1016/j.irfa.2022.102103.
- [5] K. P. Y. Lai and P. Langley, "Playful finance: Gamification and intermediation in FinTech economies," *Geoforum*, no. November 2022, p. 103848, 2023, doi: 10.1016/j.geoforum.2023.103848.
- [6] S. Bojjagani *et al.*, "The Use of IoT-based Wearable Devices to Ensure Secure Lightweight Payments in FinTech Applications," *J. King Saud Univ. - Comput. Inf. Sci.*, 2023, doi: https://doi.org/10.1016/j.jksuci.2023.101785.
- [7] M. Jucevski, A. Ghezzi, and N. Arvidsson, "Exploring the growth challenge of mobile payment platforms: A business model perspective," *Electron. Commer. Res. Appl.*, vol. 40, no. December 2019, p. 100908, 2020, doi: 10.1016/j.elerap.2019.100908.
- [8] M. Barroso and J. Laborda, "Digital transformation and the emergence of the Fintech sector: Systematic literature review," *Digit. Bus.*, vol. 2, no. 2, p. 100028, 2022, doi: 10.1016/j.digbus.2022.100028.
- [9] G. Ali, M. A. Dida, and A. E. Sam, "A secure and efficient multi-factor authentication algorithm for mobile money applications," *Futur. Internet*, vol. 13, no. 12, pp. 1–31, 2021, doi: 10.3390/fi13120299.
- [10] B. Hashan, Y. Abeyrathna, M. Kaluaratchi, A. Piyalath, and S. Thelijagoda, "VoiceNote: An Intelligent tool for monetary transactions with integrated voice support," *Proc. - IEEE Int. Res. Conf. Smart Comput. Syst. Eng. SCSE 2019*, pp. 119–125, 2019, doi: 10.23919/SCSE.2019.8842768.
- [11] E. Abad-Segura, M. D. González-Zamar, E. López-Meneses, and E. Vázquez-Cano, "Financial Technology: Review of trends, approaches, and management," *Mathematics*, vol. 8, no. 6, pp. 1–36, 2020, doi: 10.3390/math8060951.
- [12] J. Mookerjee, S. Chattopadhyay, T. Ahmed, and L. Addepalli, "Impact of QR-Codes as a Disruptive Technology during the Covid-19 Contagion," *Int. J. Recent Innov. Trends Comput. Commun.*, vol. 10, no. 1, pp. 284–289, 2022, doi: 10.17762/ijritcc.v10i1s.5850.
- [13] P. Escobedo *et al.*, "QRsens: Dual-purpose quick response code with built-in colorimetric sensors," *Sensors Actuators B Chem.*, vol. 376, no. November 2022, 2023, doi: 10.1016/j.snb.2022.133001.
- [14] H. Haxhimehmeti and A. Besimi, "Prototyping Micropayment Mobile Platform

using QR Codes,” *2020 9th Mediterr. Conf. Embed. Comput. MECO 2020*, pp. 8–11, 2020, doi: 10.1109/MECO49872.2020.9134150.

[15] W. Badrawani, “Measuring Central Bank’s Policy Effectiveness in Affecting Intention to Use New Payment Platform During The COVID-19 Pandemic,” *Int. J. Econ. Manag.*, vol. 16, no. 3, pp. 319–337, 2022, doi: 10.47836/ijeam.16.3.04.

[16] N. Nurhadi, M. Suhaidi, and L. Latip, “Implementasi Quick Response Code Indonesian Standard (Qris) Dalam Pembayaran Uji Kir Kendaraan Di Dinas Perhubungan Kota Dumai,” *Sebatik*, vol. 26, no. 2, pp. 557–564, 2022, doi: 10.46984/sebatik.v26i2.2007.

[17] E. Pravitasari and A. Fauziyah, “The Influence of Lifestyle, Perceived Convenience, And Promotion on The Decision to Use Quick Response Code Indonesian Standard (QRIS),” *Return Study Manag. Econ. Bussines*, vol. 2, no. 8, pp. 784–794, 2023, doi: 10.57096/return.v2i8.131.

[18] D. Wiryawan, J. Suhartono, S. E. Hiererra, S. D. A. Ambarwati, and A. Gui, “Factors influencing e-wallet users’ perception on payment transaction security: Evaluation on quick response Indonesia standard,” *AIP Conf. Proc.*, vol. 2508, no. March, 2023, doi: 10.1063/5.0114922.